



The enzymology of human drug and chemical glucosidation

by

Nuy Chau
BMedSci, BSc (Hons)

Thesis
submitted to Flinders University
for the degree of

Doctor of Philosophy

Clinical Pharmacology
College of Medicine and Public Health

August 2019

Table of Contents

LIST OF FIGURES.....	X
LIST OF TABLES.....	XIX
LIST OF EQUATIONS	XXIV
SUMMARY.....	XXV
DECLARATION.....	XXVII
ACKNOWLEDGEMENTS.....	XXVIII
PUBLICATIONS ARISING DIRECTLY FROM THIS THESIS.....	XXX
CONFERENCE ABSTRACTS AND AWARDS IN SUPPORT OF THIS THESIS.....	XXXI
ABBREVIATIONS	XXXIII
CHAPTER 1	1
UDP-GLYCOSYLTRANSFERASES AND THE GLUCOSIDATION PATHWAY	1
1.1 HUMAN DRUG METABOLISM AND CHEMICAL BIOTRANSFORMATION	1
<i>1.1.1 The UDP-glycosyltransferase superfamily.....</i>	<i>4</i>
<i>1.1.2 Human UGT evolution.....</i>	<i>5</i>
<i>1.1.3 Human UGT genes</i>	<i>6</i>

1.1.4	<i>Tissue specific expression of human UGTs</i>	9
1.1.5	<i>Substrate (aglycone) and inhibitor selectivities of human UGTs</i>	13
1.1.6	<i>UDP-sugar selectivity: glucosidation by mammalian UGTs</i>	18
1.2	STRUCTURE AND FUNCTION OF THE UGT MULTIGENE FAMILY	29
1.2.1	<i>Glycosyltransferases</i>	29
1.2.2	<i>Classification and catalytic mechanism of human UGTs</i>	32
1.2.3	<i>Subcellular localization and topology of human UGTs</i>	34
1.2.4	<i>Bacterial, baculoviral, invertebrate and plant UDP-glycosyltransferase evolution</i>	39
1.2.5	<i>Protein X-ray crystallography and homology modelling of human UGTs</i> . 41	
1.2.6	<i>The amino terminus (NT) of human UGTs</i>	49
1.2.7	<i>The carboxyl terminus (CT) of UGTs: role in UDP-glucuronic acid selectivity</i>	53
1.3	PHARMACOKINETICS AND ENZYME KINETICS	58
1.3.1	<i>Enzyme kinetics</i>	58
1.3.2	<i>Measurement of UGT activity in vitro</i>	69
1.4	EXPERIMENTAL AIMS.....	72
CHAPTER 2		73
MATERIALS AND GENERAL METHODS		73

2.1 MATERIALS	73
2.1.1 <i>Chemicals and reagents</i>	73
2.1.2 <i>Equipment</i>	77
2.1.3 <i>General stock solutions, buffers, media, broths and agar</i>	79
2.1.4 <i>Analytical and preparative kits</i>	84
2.1.5 <i>Enzymes</i>	85
2.1.6 <i>Antibodies</i>	86
2.1.7 <i>Plasmid DNA</i>	86
2.1.8 <i>Bacterial, insect and mammalian cells</i>	89
2.1.9 <i>Software for in silico chemistry, protein docking and data analysis</i>	89
2.2 GENERAL METHODS.....	90
2.2.1 <i>Molecular biology techniques</i>	90
2.2.2 <i>Tissue culture</i>	95
2.2.3 <i>Preparation of recombinant UGT enzymes</i>	98
2.2.4 <i>Western Blot</i>	99
2.2.5 <i>Human Livers</i>	101
2.2.6 <i>Protein content of enzyme sources</i>	102
2.2.7 <i>Confirmation of the activity of recombinant UGTs</i>	103
2.2.8 <i>Incubation and chromatography assay development and conditions</i>	104

2.3 DATA ANALYSIS	109
<i>Kinetic equations and constants</i>	109
<i>Statistical analysis</i>	109
CHAPTER 3	110
MORPHINE GLUCOSIDATION	110
3.1 INTRODUCTION.....	110
3.1.1 <i>Morphine and its metabolites</i>	110
3.1.2 <i>The further characterization of morphine glucosidation</i>	121
3.2 METHODS	124
3.2.1 <i>Incubation and assay conditions for glucosidation and glucuronidation</i>	124
3.2.2 <i>HPLC quantification of morphine and 4-MU glycosides</i>	128
3.2.3 <i>Human UGT2B7 cDNA</i>	130
3.3 RESULTS.....	131
3.3.1 <i>Morphine binding to HLM (\pm BSA)</i>	131
3.3.2 <i>Inhibition of HLM M-3-glucoside, M3G and M6G formation by UGT enzyme selective substrates/inhibitors</i>	133
3.3.3 <i>Fluconazole inhibition kinetics of morphine glucosidation and glucuronidation</i>	135
3.3.4 <i>Morphine glycosidation activity screening with single cofactors using SupersomesTM expressing UGT2B enzymes</i>	138

3.3.5 Control Supersomes TM (c-SUP) and UGT2B7 glucosidation kinetics \pm BSA	140
3.3.6 Morphine glycosidation activity screening with single cofactors by UGT enzymes expressed in HEK293T cells	142
3.3.7 Kinetics of morphine glycosidation by UGT2B7 expressed in HEK293T cells in the presence of separate and combined cofactors	144
3.3.8 Impact of the nonsynonymous UGT2B7 SNP (268His (*1) and 268Tyr (*2)) on morphine glucosidation activity	148
3.3.9 Characterization of the kinetics of human liver microsomal morphine glycosidation in the presence of combined cofactors (UDP-Glc and UDP-GlcUA), with and without BSA	152
3.3.10 Cofactor inhibition kinetics (\pm BSA)	157
3.4 DISCUSSION	160
CHAPTER 4	168
APPLICATION OF PROTEIN HOMOLOGY MODELLING TO IDENTIFY RESIDUES INVOLVED IN THE BINDING OF COFACTOR TO UDP-GLUCURONOSYLTRANSFERASE 2B7 (UGT2B7)	168
4.1 INTRODUCTION	168
4.1.1 Experimental plan and aims	170
4.2 METHODS	172

4.2.1 Identification of residues involved in UDP-sugar binding using the C-terminal X-ray crystal structure and homology model of human UGT2B7 using computational modelling	172
4.2.2 PCR site-directed mutagenesis of mutant UGT2B7 proteins	183
4.2.3 Expression of wild-type UGT2B7 and mutants in HEK293T cells.....	188
4.2.4 Incubation conditions and HPLC assays.....	191
4.3 RESULTS.....	193
4.3.1 UDP-sugar docking studies with the UGT2B7 C-terminal structure from X-ray crystallography (2O6L).....	193
4.3.2 UDP-sugar superpositioned with the human UGT2B7 homology model	196
4.3.3 UDP-sugar docking studies with the human UGT2B7 homology model .	201
4.3.4 Optimization of scale-up conditions for transient transfection of HEK293T UGT2B7 wild-type and mutant proteins.....	210
4.3.5 Immunoblotting of UGT2B7 wild-type and mutant proteins expressed in HEK293 cells.....	210
4.3.6 Effect of mutagenesis on UGT2B7 glucosidation and glucuronidation activities.....	220
4.4 DISCUSSION.....	227
Summary.....	236
CHAPTER 5	238

MYCOPHENOLIC ACID GLUCOSIDATION	238
5.1 INTRODUCTION.....	238
5.1.1 <i>Mycophenolic acid and its metabolites.....</i>	238
5.1.2 <i>Hypothesis.....</i>	249
5.1.3 <i>Experimental plan and aims</i>	249
5.2 METHODS.....	250
5.2.1 <i>Mycophenolic acid glycosidation HPLC assay conditions</i>	250
5.2.2 <i>MPA glycosidation assay.....</i>	251
5.2.3 <i>MPA glycosidation kinetics with combined cofactors (UDP-Glc and UDP-GlcUA) and HLM as the enzyme source.....</i>	252
5.2.4 <i>Cofactor kinetics at a fixed MPA concentration with HLM as the enzyme source.....</i>	252
5.2.5 <i>Cofactor inhibition kinetics</i>	252
5.2.6 <i>MPA glycosidation by recombinant UGT enzymes</i>	253
5.2.7 <i>Inhibition of human liver microsomal MPA glycoside formation by UGT enzyme selective substrates/inhibitors.....</i>	253
5.3 RESULTS.....	254
5.3.1 <i>Development of an HPLC assay for the characterization of MPA glycosidation.....</i>	254

5.3.2	<i>Characterization of the kinetics of human liver microsomal MPA glycosidation</i>	266
5.3.3	<i>Cofactor inhibition kinetics</i>	273
5.3.4	<i>Reaction phenotyping of MPA glycosidation</i>	276
5.4	DISCUSSION.....	280
CHAPTER 6		288
ENDOGENOUS GLUCOSIDATION CAPACITY OF <i>SPODOPTERA FRUGIPERDA</i> (SF9) AND <i>TRICHOPLUSIA NI</i> (HIGH FIVE™) CELLS TOWARDS DRUGS, NON-DRUG XENOBIOTICS AND HYDROXY STEROIDS.....		288
6.1	INTRODUCTION.....	288
6.1.1	<i>Expression of recombinant human UGT enzymes in insect cells</i>	288
6.1.2	<i>Hypothesis</i>	297
6.2	METHODS	298
6.2.1	<i>HPLC and LC-MS equipment, assay development and detection of xenobiotic glucosides</i>	298
6.2.3	<i>Preparation of uninfected Sf9 lysate and membranes</i>	299
6.2.2	<i>Xenobiotic glucosidation assays</i>	302
6.3	RESULTS.....	304
6.3.1	<i>Activity of Sf9 lysate and microsomal fractions</i>	304

6.3.2 <i>Xenobiotic glucosidation by Sf9 membranes and c-SUP</i>	305
6.3.3 <i>Verification of xenobiotic glucoside formation by uninfected Sf9 membranes and c-SUP using mass spectrometry</i>	311
6.3.4 <i>Kinetic characterization of MOR, 1-OHP, MPA and 4-MU glucosidation by Sf9 membranes and c-SUP</i>	313
6.4 DISCUSSION.....	316
CHAPTER 7	322
GENERAL SUMMARY AND CONCLUSION	322
APPENDIX 1: SUMMARY TABLE OF HPLC ASSAY CONDITIONS	329
APPENDIX 2: MPA KINETIC DATA FOR INDIVIDUAL LIVERS	335
BIBLIOGRAPHY	338

List of Figures

- Figure 1. 1: Glucuronidation reaction catalyzed by a UDP-glucuronosyltransferase (UGT). 3
- Figure 1. 2: Rooted phylogram of the four human UGT (1, 2, 3 and 8) gene families. Pseudogenes are indicated with the letter P added at the end of the gene name. Protein sequences were extracted from GenBank. Alignment and phylogram generated were performed with ClustalW. 8
- Figure 1. 3: Biosynthesis of UDP-hexoses, including UDP-Glc and UDP-GlcUA, in the cytoplasm. 25
- Figure 1. 4: Representative fold-types of GTs. 30
- Figure 1. 5: General metabolic pathway for xenobiotics and endogenous compounds within a cell (e.g. hepatocyte). 35
- Figure 1. 6: Sequence (170 amino acids) and protein secondary structure assignment for UGT2B7 C-terminus (CT) apo crystal structure (PDB code 2O6L). 44
- Figure 1. 7: Phylogenetic tree of human UGTs and a selection of the available X-ray crystal structures from plant, bacterial and human UGT2B7-CT from the PDB. 46
- Figure 1. 8: Amino acid alignment of UGT1A3, UGT1A4 and UGT1A5. The first 60 residues are shown. 51
- Figure 1. 9: Sequence alignment of the N-terminus (NT) of 22 human, plant (BpUGT94B1, UGT71G1, VvGT1), and bacterial (GtfA) UGTs. Catalytically important residues 33-35 and 151 (UGT2B7 numbering) are boxed with proposed UDP-GlcUA interacting residues marked with closed x

triangles. ClustalX 2.0.12 was used for multiple sequence alignment (Table 2.10)..... 52

Figure 1. 10: Sequence alignment of CT residues of selected GT1 family enzymes. 55

Figure 1.11: Plot of the rate of product formation (v) versus substrate concentration $[S]$ at a constant enzyme concentration for a single substrate reaction, derived from the Michaelis-Menten equation with (inset) the corresponding Eadie-Hofstee plot. 59

Figure 1. 12: Plot of the rate of product formation (v) versus substrate concentration $[S]$ at a constant enzyme concentration for a single substrate reaction, derived from the Hill equation, with (inset) the corresponding Eadie-Hofstee plots. In this example, $n = 0.5$ (A) for negative co-operativity and $n = 1.5$ (B) for autoactivation. 61

Figure 1. 13: Plot of the rate of product formation (v) versus substrate concentration $[S]$ at a constant enzyme concentration for a single substrate reaction, derived from the substrate inhibition equation, with (inset) the corresponding Eadie-Hofstee plot. 63

Figure 1. 14: Plot of the rate of product formation (v) versus substrate concentration $[S]$ at a constant enzyme concentration for a single substrate reaction (Michaelis-Menten kinetics) without inhibitor [zero], with a competitive inhibitor [comp], a non-competitive inhibitor [non-comp], and uncompetitive inhibitor [uncomp]. 65

Figure 1. 15: Dixon plots for competitive (A), non-competitive (B) and uncompetitive (C) inhibition at several different substrate concentrations ($[S]$). For each fixed $[S]$, inverse velocity ($1/V$) is plotted against the inhibitor concentration ($[I]$) and the

intersection point between these plots determines $[I] = -K_i$ for competitive (intersect in first quadrant) and non-competitive (intersect on x-axis in first quadrant) inhibition.	68
Figure 2. 1: Restriction map of UGT2B7 cDNA inserted into pBluescript II SK(+).	87
Figure 2. 2: Restriction map of UGT2B7 cDNA inserted into pEF-IRES-puro 5.	88
Figure 2. 3: Cell counting with a hemocytometer.	97
Figure 3. 1: Chemical structure of morphine with the phenolic (C3-) and enolic (C6-) hydroxyl groups numbered.	112
Figure 3. 2: Conjugation pathways for morphine elimination in humans.	115
Figure 3. 3: Inhibition of human liver microsomal M3G, M6G and M-3-glucoside formation by fluconazole (Fluc), hecogenin (Hec), niflumic acid (NFA) and zidovudine (AZT).	134
Figure 3. 4: Dixon plots for fluconazole inhibition of M-3-glucoside, M3G and M6G formation by HLM in the presence of single and combined (1:1) cofactors and BSA (2% w/v).	136
Figure 3. 5: Morphine glucosidation and glucuronidation by recombinant UGT2B enzymes expressed in Supersomes TM	139
Figure 3. 6: Velocity-substrate (A and C) and Eadie-Hofstee (B and D) plots for morphine-3-glucosidation by c-SUP and Supersomes TM expressing UGT2B7 (\pm BSA, 2% w/v).	141

Figure 3. 7: Morphine glucosidation and glucuronidation by recombinant UGT2B enzymes expressed in HEK293T cells.	143
Figure 3. 8: Eadie-Hofstee plots for morphine glycosdiation by UGT2B7 expressed in HEK293T cells in the presence of a single cofactor.....	145
Figure 3. 9: Eadie-Hofstee plots for morphine glycosdiation by UGT2B7 expressed in HEK293T cells in the presence of both UDP-Glc and UDP-GlcUA.	147
Figure 3. 10: Immunoblot of UGT2B7*1 and UGT2B7*2 stably expressed in HEK293T cells (n=3).	148
Figure 3. 11: Morphine glucosidation and glucuronidation by recombinant UGT2B7*1 and UGT2B7*2 expressed in HEK293T cells.....	150
Figure 3. 12: 4-MU glucosidation and glucuronidation by recombinant UGT2B7*1 and UGT2B7*2 expressed in HEK293T cells.....	151
Figure 3. 13: Eadie-Hofstee plots for morphine glycosidation by HLM (\pm BSA, 2% w/v) in the presence of combined cofactors (5 mM UDP-Glc and 5 mM UDP-GlcUA) and morphine as the variable substrate.	154
Figure 3. 14: Dixon plots for the inhibition of M-3-glucoside, M3G and M6G formation by UDP-Glc and UDP-GlcUA at a fixed morphine concentration (20 mM) in the absence and presence of BSA (2% w/v).....	158
Figure 4. 1: Comparison of labelled secondary structure (ribbon cartoon) of CT domains of plant VvGT1 superimposed with human UGT2B7-CT.....	175

Figure 4. 2: Major protonation species of UDP-Glc and UDP-GlcUA at biological pH 7.4 (2D planar structure).....	177
Figure 4. 3: Surface representation of the protomol cofactor binding pocket (globular green construction) of UGT2B7-CT and full length UGT2B7 homology model.	180
Figure 4. 4: Comparison of the full crystal structure of plant VvGT1 complexed with U2F and human UGT2B7 CT and full homology model protomol residue map.	181
Figure 4. 5: Residues within 3Å of UDP-Glc (A) and UDP-GlcUA (B) from superpositioning in the UGT2B7 homology model.....	200
Figure 4. 6: Residues within 3Å of UDP-Glc (A) and UDP-GlcUA (B) from superpositioning (green) compared to docking results (magenta and orange, respectively) in the UGT2B7 homology model.....	204
Figure 4. 7: Surface view of UGT2B7 with docked UDP-Glc (orange) and UDP-GlcUA (cyan) in white rectangular box (left panel).....	208
Figure 4. 8: UGT2B7 homology model docked with UDP-sugars.	209
Figure 4. 9: Immunoblots of wild-type and mutant UGT2B7 proteins showing relative expression from stable transfection in HEK293T cells.	214
Figure 4. 10: Raw densitometry results for the expression of UGT2B7 wild-type and mutant proteins.	215
Figure 4. 11: Relative densities (mean ± SD) of immunoblots.	216

Figure 4. 12: Immunoblot of wild-type and mutant UGT2B7 proteins showing relative expression from transient transfection of HEK293T cells.	218
Figure 4. 13: Relative mean densities of Western blots (from Figure 4.12) for transient transfections, based on the raw relative density data for 50µg of UGT2B7 protein. Data represent the mean of duplicate estimates.....	219
Figure 4. 14: Morphine 3-glucuronidation (M3G) activity of wild-type UGT2B7 and the C-terminal and N-terminal mutants.	221
Figure 4. 15: Morphine 6-glucuronidation (M6G) activity of wild-type UGT2B7 and the C-terminal and N-terminal mutants.	222
Figure 4. 16: Morphine 3-glucosidation (M3Glucoside) activity of wild-type UGT2B7 and th C-terminal and N-terminal mutants.	223
Figure 4. 17: 4-Methylumbelliferone glucuronidation (4-MUG) activity of wild-type UGT2B7 and the C-terminal and N-terminal mutants.	225
Figure 4. 18: 4-Methylumbelliferone glucosidation (4-MUGlucoside) activity of wild-type UGT2B7 and the C-terminal and N-terminal mutants.....	226
Figure 4. 19: Position of Arg 49 and 259 in relation to docked UDP-Glc and UDP-GlcUA in the UGT2B7 homology model.....	234
Figure 5.1: Chemical structure of mycophenolic acid (MPA), with the phenolic and carboxylic acid groups shown.	240
Figure 5. 2: Metabolism of the pro-drug mycophenolate mofetil (MMF) to mycophenolic acid (MPA), with phenolic hydroxyl and carboxyl functional	

groups labelled. MPA is metabolized to glucuronides and glucosides at both the phenolic and carboxylic acid functional groups before excretion into bile and urine.242

Figure 5. 3: Major charge species (-2 and -1) for MPAGlcUA and MPAGlc at pH 5.7.

The distribution of different species for MPAGlcUA and MPAGlc across the pH range (0-14) is shown directly below.256

Figure 5. 4: Major charge species (-1, -1, and 0) for AcMPAGlcUA, MPA and AcMPAGlc at pH 5.7. The distribution of different species for AcMPAGlcUA, MPA and AcMPAGlc across the pH range (0-14) is shown directly below.257

Figure 5. 5: UV absorption spectra: (A) 10mM ammonium acetate, 10% acetonitrile, pH 5.7 containing/ 1% methanol; and : (B) a 1% solution of MPA (50µM in methanol) in mobile phase (A).258

Figure 5. 6: HPLC mobile phase gradient composition for the separation of MPA glycosides259

Figure 5. 7: Representative chromatograms of MPA glycoside calibration standards (25µM) (Panel A) and incubations of HLM with MPA (100µM) and 5mM UDP-Glc (Panel B). MPAGlcUA eluted at 2.3min, MPAGlc at 4.5min, AcMPAGlcUA at 5.6min, MPA at 6.8min and AcMPAGlc at 7.4min. The total run time was 14min.261

Figure 5. 8: Representative calibration curves for MPAGlcUA (A), MPAGlc (B) and AcMPAGlcUA (C), respectively.262

Figure 5. 9: Eadie-Hofstee plots for MPAGlcUA (A and D), MPAGlc (B and E), and AcMPAGlcUA (C and F) formation by microsomes from 4 livers in the presence

of UDPGlcUA or UDPGlc separately (5mM each), and combined (1:1), respectively.....	268
Figure 5. 10: Eadie-Hofstee plots for MPA glycosidation by pooled HLM at a fixed MPA concentration (1mM) with UDP-Glc and UDP-GlcUA as the variable substrates.....	271
Figure 5. 11: Dixon plots for the inhibition of MPAGlcUA, MPAGlc and AcMPAGlcUA formation by UDP-Glc and UDP-GlcUA at a fixed MPA concentration (1mM) with HLM as the enzyme source.	274
Figure 5. 12: Formation of MPAGlcUA (Panel A), MPAGlc (Panel B), AcMPAGlcUA (Panel C) and AcMPAGlc (Panel D) by recombinant UGT enzymes at MPA concentrations of 100, 500 and 1500µM.	277
Figure 5. 13: Inhibition of human liver microsomal MPA (100µM) glycoside formation by selective UGT inhibitors: UGT1A9 (NFA, 2.5µM), UGT1A1/ 2B15 (NFA, 100µM), UGT1A4 (hecogenin) and UGT2B7/ 2B4 (fluconazole).....	279
Figure 6. 1: Chemical structures of aglycones used to investigate the glucosidation capacity by Control Supersomes TM (c-SUP) and uninfected <i>Spodoptera frugiperda</i> (Sf) 9 cell membranes. Arrows indicate the potential site(s) of glucosidation..	296
Figure 6. 2: Preparation of Sf9 cell membranes by homogenization and differential centrifugation. Sonication was included as an additional step for lysate preparation to increase protein yield.....	301
Figure 6. 3: Comparison of the 1-OHP glucosidation activity of Sf9 cell preparations (lysate, membranes and cytosol). The aglycone concentration was 40µM.	305

Figure 6. 4: Glucosidation of compounds containing a phenolic hydroxyl group at 4 substrate concentrations by Sf9 cell membranes and c-SUP (Control SupersomesTM): 1-hydroxypyrene (1-OHP) (A), 4-methylumbelliferone (4-MU) (B), morphine (MOR) (C), mycophenolic acid (MPA) (D), 1-naphthol (1-NAP) (E), and 4-nitrophenol (4-NP) (F). Bars represent the mean of duplicate measurements (<10% variance).....307

Figure 6. 5: Glucosidation of compounds containing an aliphatic hydroxyl group at 4 substrate concentrations by Sf9 cell membranes and c-SUP (Control SupersomesTM): 20-hydroxyecdysone (20-E) (A-C), 21-hydroxyprogesterone (21-OHP) (D), phenethyl alcohol (PE) (E), and zidovudine (AZT) (F). Bars represent the mean of duplicate measurements (<10% variance). 309

Figure 6. 6: Glucosidation of compounds containing either an amine- or carboxylic acid group at 4 substrate concentrations by Sf9 cell membranes and c-SUP (Control SupersomesTM): benzocaine (BZC) (A), lamotrigine (LTG) (B), trifluoperazine (TFP) (C), mycophenolic acid (MPA) (D), and S-naproxen (S-NAP) (E). Bars represent the mean of duplicate measurements (<10% variance).310

Figure 6. 7: Eadie-Hofstee plots for morphine 3-glucosidation (A and B), 1-hydroxypyrene (1-OHP) (C and D), mycophenolic acid (MPA) (E and F), and 4-methylumbelliferone (4-MU) (G and H) by c-SUP and Sf9 membranes, respectively. Points represent the means of duplicate measurements (<10% variance). 315

List of Tables

Table 1.1: Human tissue UGT mRNA and protein expression.	10
Table 1.2: Representative known selective substrates and inhibitors, and the preferred cofactors of human UGTs.....	15
Table 1.3: Drug glucosides detected in humans <i>in vivo</i>	19
Table 1.4: Compounds undergoing both glucuronidation and glucosidation <i>in vitro</i>	21
Table 1.5: UDP-sugar substrate selectivity and subcellular localization of representative human nucleotide UDP-sugar transporters.	28
Table 1. 6: Summary of UDP-glycosyltransferase X-ray crystal structures used as templates for homology modeling of human UGTs (RCSB PDB Ligand Explorer 3.8; Table 2.10).....	42
Table 1. 7: Summary of results from PSI-BLAST (first iteration) showing the closest structural relatives (search against PDB database) of human UGT1A4 protein sequence. X-ray crystal templates used previously for UGT homology modelling are in blue text and shaded in grey.	43
Table 1. 8: Characteristics of competitive, non-competitive and uncompetitive inhibition.....	65
Table 2. 1: Suppliers of the chemicals and reagents used in the biochemical and analytical procedures conducted in this thesis.....	73

Table 2. 2: Suppliers of chemicals and reagents used in the molecular biology procedures conducted in this thesis.	76
Table 2. 3: Equipment used in experimental procedures.	77
Table 2. 4: Stock solutions required for <i>in vitro</i> incubations and total protein determination.	79
Table 2. 5: Buffers, media, broths and agar used for molecular biology and protein techniques, including cloning, culturing (mammalian, insect and bacterial), gel electrophoresis and Western blotting.....	82
Table 2. 6: Analytical and preparative kits used in the experimental procedures.....	84
Table 2. 7: Enzymes used in the experimental procedures.	85
Table 2. 8: Primary and secondary antibodies used in the experimental procedures.	86
Table 2. 9: Cell lines used in experimental procedures.....	89
Table 2. 10: Molecular docking, kinetic modelling, statistical and chemistry software used in experimental procedures and data analysis.	89
Table 2. 11: Relevant clinical details of liver donors.....	102
Table 2. 12: Protein concentrations, incubation times and substrate (4-MU, LTG or COD) concentrations used for activity screening in UGTs.....	106
Table 2. 13: Mobile phase gradient timetable for HPLC quantification of 4-MUGlcUA, LTG-N2-GlcUA and COD-6-GlcUA.	107

Table 3. 1: Derived morphine glycosidation kinetic constants generated in the absence and presence of BSA (2% w/v).	118
Table 3. 2: Derived kinetic constants for morphine glycosidation generated in the absence and presence of BSA (2% w/v) with cofactor (UDP-Glc or UDP-GlcUA) as the variable substrate. Data are shown as the mean \pm SD of 4 replicates with pooled HLM.....	119
Table 3. 3: Binding of morphine to HLM (\pm BSA, 2% w/v). Data represent the means of duplicate measurements (<10% variance).....	131
Table 3. 4: Derived K_i values for fluconazole inhibition of M-3-glucoside, M3G and M6G by HLM in the presence of single and combined cofactors (1:1 UDP-Glc and UDP-GlcUA) and BSA (2% w/v).....	137
Table 3. 5: Derived kinetic constants for M-3-glucoside formation by Control (c-SUP) and UGT2B7-expressing Supersomes TM in the absence and presence of BSA.	141
Table 3. 6: Derived morphine glycosidation kinetic constants generated in the presence of a single cofactor (either UDP-Glc or UDP-GlcUA).	145
Table 3. 7: Derived morphine glycosidation kinetic constants generated in the presence of combined cofactors (UDP-Glc and UDP-GlcUA).	147
Table 3. 8: Derived microsomal kinetic constants for morphine glycosidation by HLM generated in the presence of combined cofactors, with and without BSA (2% w/v).	155

Table 3. 9: Derived cofactor inhibitor constants for inhibition of M-3-glucoside, M3G and M6G formation by UDP-Glc and UDP-GlcUA at a fixed morphine concentration (20 mM) in the absence and presence of BSA (2% w/v).....	159
Table 4. 1: Oligonucleotide primers used for site-directed mutagenesis. Mutagenic nucleotides are highlighted and underlined in red. Wild-type UGT2B7 (Accession NM_001074.2) was used as the parent template to generate all mutants.....	185
Table 4. 2: Residues within 3Å of UDP-Glc and UDP-GlcUA docked into the protomol site (threshold = 0.4, bloat = 1.0) of UGT2B7-CT minimized crystal structure compared to the superpositioned UGT2B7-CT data of Miley et al. (2007).....	195
Table 4. 3: Residues within 3Å of UDP-Glc and UDP-GlcUA superpositioned in the binding site of the UGT2B7 homology model based on the U2F/2C1Z crystal position compared to the superpositioned UGT2B7-CT data of Miley et al. (2007).	199
Table 4. 4: Residues within 3Å of UDP-Glc and UDP-GlcUA docked into protomol site (threshold = 0.4, bloat = 1.0) of the UGT2B7 homology model compared to the superpositioned UGT2B7-CT results of Miley et al. (2007).....	203
Table 4. 5: Residues within 3Å of UDP-Glc and UDP-GlcUA docked into the protomol site (threshold = 0.5, bloat = 2.0) of the UGT2B7 homology model compared to the superpositioned UGT2B7-CT data of Miley et al. (2007).....	207
Table 5. 1: Slopes and coefficients of determination (r^2) for MPAGlcUA, MPAGlc and AcMPAGlcUA measured on ten separate days.....	263

Table 5. 2: Derived mycophenolic acid (MPA) glycosidation kinetic constants generated using human liver microsomes as the enzyme source.	269
Table 5. 3: Derived cofactor kinetic constants for MPA glycosidation generated with cofactor (UDP-Glc or UDP-GlcUA) as the variable substrate.	272
Table 5. 4: Derived cofactor inhibitor constants for inhibition of MPAGlcUA, AcMPAGlcUA and MPAGlc formation by UDP-GlcUA and UDP-Glc at a fixed MPA concentration (1mM).....	275
Table 6. 1: Observed and expected m/z values (± 0.02 Da) for xenobiotic and steroidal glucosides formed by incubations of Sf9 membranes or c-SUP with UDP-glucose as cofactor.	312

List of Equations

Equation 1. 1: Single enzyme Michaelis-Menten equation (hyperbolic kinetics)	59
Equation 1. 2: Hill equation (positive (autoactivation) and negative co-operativity)	60
Equation 1. 3: Substrate inhibition (uncompetitive)	62
Equation 1. 4: Intrinsic clearance	63
Equation 1. 5: Maximal clearance	64
Equation 1. 6: Competitive inhibition	66
Equation 1. 7: Non-competitive inhibition.....	66
Equation 1. 8: Uncompetitive inhibition	67
Equation 2. 1: DNA concentration	93
Equation 2. 2: Quantity of cDNA insert for ligation.....	94
Equation 2. 3: Cell concentration	96
Equation 2. 4: Percentage of viable cells	97
Equation 2. 5: Viable cell concentration	98
Equation 2. 6: Total protein concentration.....	103
Equation 3. 1: Calculation of drug unbound fraction in incubations of HLM	130

Summary

Accumulating evidence indicates that conjugation with glucose ('glucosidation') is a more common metabolic pathway for drugs in humans than previously believed. The studies described in this thesis primarily aimed to characterize the enzymology of drug glucosidation.

Morphine (MOR) is known to be metabolized in humans via glucuronidation and glucosidation at the 3-position, and glucuronidation at the 6-position. Reaction phenotyping studies described in Chapter 3 demonstrated that UDP-glucuronosyltransferase (UGT) 2B7 catalyzes the formation of all three conjugates. Thus, glucuronidation and glucosidation occur as complementary metabolic pathways. Glucuronidation is the dominant pathway because the binding affinity of UDP-glucuronic acid (UDP-GlcUA) to UGT2B7 is higher than that of UDP-glucose (UDP-Glc). Kinetic studies with human liver microsomes (HLM) as the enzyme source showed that the relative formation of the three metabolites observed in humans *in vitro* was correctly predicted when incubations were performed in the presence of the combined (1:1 UDP-GlcUA/UDP-Glc) cofactors. However, kinetic data generated in the presence of the separated cofactors over-predicted MOR-3-glucoside formation.

Complementary experiments (Chapter 5) investigated the comparative enzymology of mycophenolic acid (MPA) glucuronidation and glucosidation. UGT1A9 and UGT2B7 were confirmed as the respective principle enzymes responsible for MPA phenolic- and acyl-glucuronidation. In contrast to the observations with MOR, multiple hepatic enzymes (UGT2B7, UGT1A1 and UGT1A9) catalyzed MPA phenolic glucosidation. Consistent with plasma and urinary metabolite excretion data in patients treated with MPA, human liver microsomal kinetic data generated in the presence of combined

cofactors (1:1 UDP-GlcUA/UDP-Glc) identified phenolic glucosidation as a minor metabolic pathway.

To rationalize the cofactor binding selectivity data, UDP-GlcUA and UDP-Glc were docked in a UGT2B7 protein homology model (Chapter 4). Both cofactors bound within the same C-terminal (CT) domain. Although binding interactions with the UDP-moiety were cofactor independent, residues involved in the binding of the sugar differed; Asp398 and Glu399 interact with glucose -OH groups of UDP-Glc, whereas Asn402 and Tyr33 bind to the carboxylate group of UDP-GlcUA. Site-directed mutagenesis of these residues and enzyme activity studies confirmed a role of these amino acids in cofactor binding.

Following the observation (Chapter 3) that Control SupersomesTM (c-SUP) express a native enzyme that glucosidates MOR, Chapter 6 characterized the glucosidation of c-SUP and membranes from uninfected *Spodoptera frugiperda* (Sf9) towards a series of aglycones with differing acceptor functional groups. Although both enzyme sources glucosidated phenolic substrates, differences were observed in the selectivities of the native UDP-glycosyltransferases towards aliphatic alcohols, carboxylic acids and amines. The results underscore the need to include control cell membranes in the investigation of drug and chemical glucosidation by UGT enzymes expressed in *Trichoplusia ni* (SupersomesTM) and Sf9 cells.

Declaration

I certify that this thesis does not incorporate without acknowledgement any material previously submitted for a degree or diploma in any university; and that to the best of my knowledge and belief, it does not contain any material previously published or written by another person except where due reference is made in the text.

Nuy Chau

Acknowledgements

“For a seed to achieve its greatest expression, it must come completely undone. The shell cracks, its insides come out and everything changes. To someone who doesn’t understand growth, it would look like complete destruction.” – Cynthia Ocelli

This thesis would not be possible without my support network of people and canines. Firstly, I would like to thank my supervisors; Professors John Miners and Peter Mackenzie. The wealth and breadth and depth of knowledge and experience between the two of you is astonishing. I have been extremely grateful for your generous guidance, sage advice, pragmatic approach, assistance and most of all, patience throughout this experience. I would like to also thank the Australian Government for funding this experience with the Australian Postgraduate Award and the Research Higher Degree team at Flinders University for administrative support. I have learnt a great deal about science, research and everything else in between that is unique to my personal and professional growth. I would like to thank all the people in the Department of Clinical Pharmacology, past and present, who have shaped my experience and provided the day-to-day support and growth promoting interactions. It takes a village to raise a child and it is the same to properly develop a research scientist. From my “village” I would like to specifically mention Kushari Burns, Dong Gui Hu, Anne Rogers, Robyn Meech, Kathleen Knights, Shane Spencer, David Elliott, Ben Lewis, Andrew Rowland, Pramod Nair, Verawan (Nu) Uchaipichat, Porntipa (Pa) Korprasertthaworn, Attarat Pattanawongsa, Leyla Kaya and Nitsupa (Tang) Wattanachai. Specifically, Ms. Kushari Burns has been a constant supportive rock since my early student days, and I would like to thank her for helping me with the

morphine cofactor inhibition kinetics. I realize I have lived more hours in those labs than in my own home during my PhD candidature, but I am confident knowing I gave it all that I had at the time.

To my dear and loving husband John, your endless patience is one of your greatest virtues but even that was sorely tested. It is all over now, and we now have our beautiful cheeky monkey Riley, whose role will be to endlessly test our patience. To my little furry children; Rusty, Millie and Ruben, you have from the beginning always greeted me enthusiastically at home, and unconditionally provided the distraction and comfort needed after long days in the lab. To my ever-generous parents, without your food I would not be as happy and full as I am. Thank you for cooking when I needed it most. Without your unconditional support, and your resilient, hard-working and survivalist nature (from what has been thrown at you in this life as refugees), I would literally not be where, or who, I am today. You may both never fully understand what this thesis is about but your brave decision to leave everything behind in Cambodia, and to start a new life in a strange new country for your children's future has shown me the sacrifices, blood, sweat and tears required to make something out of very little. To my brother Chouy, seeing you fulfil your life ambitions and goals provides such inspiration and restores my belief that dreams can manifest itself into something tangible. To my brother Vorng, thank you for your ever-gentle nature, artistic insight, technical help and advice with visual graphics. To all my other family members and friends, thank you for your moral support. And lastly, thank you to the childcare team for providing the time to write up this thesis.

“My mission in life is not merely to survive, but to thrive; and to do so with some passion, some compassion, some humour, and some style.” – Maya Angelou

Publications arising directly from this thesis

Chapter 3 and 4

Chau N, Elliot DJ, Lewis BC, Burns K, Johnston MR, Mackenzie PI and Miners JO, 2014, 'Morphine glucuronidation and glucosidation represent complementary metabolic pathways which are both catalyzed by UDP-glucuronosyltransferase 2B7: Kinetic, inhibition and molecular modelling studies', *Journal of Pharmacology and Experimental Therapeutics (JPET)*, 349 (1):126-137 (Highlighted publication).

Chapter 6

Chau N, Kaya L, Lewis BC, Mackenzie PI, and Miners JO, 2019, 'Drug and chemical glucosidation by Control SupersomesTM and membranes from *Spodoptera frugiperda* (Sf) 9 cells: Implications for the apparent glucuronidation of xenobiotics by UDP-glucuronosyltransferase 1A5', *Drug Metabolism and Disposition (DMD)*, 47 (3):271-278.

Conference Abstracts and Awards in support of this thesis

Drug and chemical glucosidation by untransfected SupersomesTM (u-SUP) and microsomes from *Spodoptera frugiperda* (Sf) 9 cells (oral and poster), ASCEPT Annual Scientific Meeting 2015, Hobart

Glucosidation and glucuronidation represent parallel metabolic pathways for the metabolism of mycophenolic acid and morphine by human UDP-glucuronosyltransferases (oral), FIPS-PSWC Scientific Meeting 2014, Melbourne
PSWC 2014 Student Award

The contribution of human UDP-glucuronosyltransferase enzymes to the glucosidation of mycophenolic acid (poster), ISSX International Scientific Meeting 2013, Toronto

Structure-function relationships of UDP-glucuronosyltransferase 2B7 (UGT2B7): Application of protein homology modelling, docking and mutagenesis to identify critical residues involved in cofactor binding, ComBio Joint Meeting, 2012, Adelaide

Glucosidation and glucuronidation of mycophenolic acid (MPA) by UDP-glucuronosyltransferase (UGT) enzymes (poster), ASCEPT Annual Scientific Meeting 2012, Sydney

Poster Prize in Drug Disposition and finalist for Neville Percy Prize (2012)

Application of protein homology modeling to identify critical residues involved in the binding of cofactor to UDP-glucuronosyltransferase 2B7 (poster), ASCEPT

Annual Scientific Meeting 2011, Perth

Poster Prize in Drug Disposition (2011)

UDP-glucuronosyltransferase 2B7 (UGT2B7) utilizes both UDP-glucuronic acid and UDP-glucose as cofactors in the metabolism of morphine (poster), ASCEPT Annual

Scientific Meeting 2010, Melbourne

In vitro characterization of human morphine glucosidation (poster), ASMR Annual

Scientific Meeting 2010, Adelaide

Abbreviations

Abbreviation	Full Description
Å	angstrom
AcMPAGlc	acyl mycophenolic acid glucoside
AcMPAGlcUA	acyl mycophenolic acid glucuronide
Ala (A)	alanine
Arg (R)	arginine
Asn (N)	asparagine
Asp (D)	aspartic acid
AZT	zidovudine
BBB	blood-brain barrier
BSA	bovine serum albumin
BZC	benzocaine
C	concentration
°C	degrees Celsius
C α	alpha-carbon atom
cDNA	complementary deoxyribonucleic acid
CDS	coding sequence
CL	clearance
CL_{int}	intrinsic (endobiotic/xenobiotic) clearance
CL_{max}	maximal clearance
cm	centimetre
CNS	central nervous system
COD	codeine
c-SUP	Control Supersomes TM

Abbreviation	Full Description
CT	C-terminus
CV	coefficient of variation
CYP	cytochrome P450
Cys (C)	cysteine
3-D	3-dimensional
Da	daltons
DMSO	dimethyl sulfoxide
E	enzyme
E. coli	Escherichia coli
ER	endoplasmic reticulum
ES-complex	enzyme-substrate – complex
Fluc	fluconazole
$f_{u(mic)}$	fraction unbound in microsome
g	gram
g	gravitational force
GAG	glycosaminoglycan
Glc	glucose (i.e. UDP-Glc) or glucoside (i.e. 4-MUGlc)
GlcUA	glucuronic acid (i.e. UDP-GlcUA) or glucuronide (i.e. 4-MUGlcUA)
Gln (Q)	glutamine
Glu (E)	glutamic acid
Gly (G)	glycine
HDCA	hyodeoxycholic acid
HEK293	human embryonic kidney 293 epithelial cells
HEK293T	human embryonic kidney 293 epithelial cells containing the SV40 T-antigen

Abbreviation	Full Description
Hi5	High Five TM insect cell line (BTI-Tn-5B1-4) derived from <i>Trichoplusia ni</i>
His (H)	histidine
HLM	human liver microsomes
HPLC	high performance liquid chromatography
HPLC-FLD	high performance liquid chromatography with fluorescence detection
HPLC-UV	high performance liquid chromatography with ultraviolet detection
HMM	hidden Markov model
hr	hour(s)
HRP	horseradish peroxidase
Ile (I)	isoleucine
IU	international units
kb	kilobases
kDa	kilodaltons
K_i	inhibition constant for inhibition kinetics
K_m	Michaelis constant
K_{si}	inhibition constant for substrate inhibition kinetics
L	litre
LB	Lauria-Bertani broth or agar
LC	liquid chromatography
LC/MS	liquid chromatography coupled mass spectrometry
Leu (L)	leucine
Lys (K)	lysine
LTG	lamotrigine
M-3-glucoside	morphine 3-glucoside

Abbreviation	Full Description
M3G	morphine 3-glucuronide
M6G	morphine 6-glucuronide
M	moles per litre
mA	milliamps
Met (M)	methionine
mg	milligram
min	minute(s)
mL	millilitre
μ L	microlitre
mM	millimolar
mm	millimetre
μ M	micromolar
μ m	micrometer
MM	Michaelis-Menten
MPA	mycophenolic acid
MPAGlc	phenolic mycophenolic acid glucoside
MPAGlcUA	phenolic mycophenolic acid glucuronide
MOPS	3-morpholino propane sulfonic acid
mRNA	messenger ribonucleic acid
4-MU	4-methylumbelliferone
4-MUGlc	4-methylumbelliferone glucoside
4-MUG	4-methylumbelliferone glucuronide
1-NAP	1-naphthol
4-NP	4-nitrophenol
n	Hill coefficient

Abbreviation	Full Description
ng	nanogram
nM	nanomolar
NFA	niflumic acid
N/OFQ	nociceptor/orphanin FQ receptor
NMR	nuclear magnetic resonance
NSB	non-specific binding
NST	nucleotide sugar transporter
NT	N-terminus
20-E	20-hydroxyecdysone
21-OHP	21-hydroxyprogesterone
1-OHP	1-hydroxypyrene
OD	optical density
P450	cytochrome P450
PAGE	polyacrylamide gel electrophoresis
PDB	RCSB protein databank
PE	phenethyl alcohol
PCR	polymerase chain reaction
Phe (F)	phenylalanine
pmol	picomole
Pro (P)	proline
RMSD	root mean square deviation
rpm	revolutions per minute
R-value	statistical measure of fit
r^2	coefficient of determination
RT	retention time

Abbreviation	Full Description
RVM	rostral ventromedial medulla
S	Substrate
S_{50}	substrate concentration at which $V = \frac{1}{2} V_{\max}$
SCR	sequence conserved region
SD	standard deviation
SDS PAGE	sodium dodecyl sulfate polyacrylamide gel electrophoresis
sec	second(s)
Ser (S)	serine
S-NAP	S-naproxen
SNP	single nucleotide polymorphism
SBD	Schneckenbecken dysplasia
SE	standard error
SLC35	solute carrier family 35
SMILES	Simplified Molecular Input Line Entry Specification
TBS	tris-buffered saline
TBST	TBS + Tween-20
TEA	triethylamine
TFA	trifluoroacetic acid
TFP	trifluoroperazine
Thr (T)	threonine
Trp (W)	tryptophan
Tyr (Y)	tyrosine
U	Units
UDCA	ursodeoxycholic acid
UDP	uridine diphosphate

Abbreviation	Full Description
UDP-Gal	UDP-galactose
UDP-Glc	UDP-glucose
UDP-GlcNAc	UDP-N-acetylglucosamine
UDP-GlcUA	UDP-glucuronic acid
UDP-Xyl	UDP-xylose
UGT	UDP-glycosyltransferase
UTP	uridine triphosphate
UV	ultraviolet
V	volume (L)
Val (V)	valine
v/v	volume per volume
Vis	visible
V	velocity of metabolite formation
V_{\max}	maximum velocity of an enzyme reaction
W	watts
w/v	weight per volume
w/w	weight per weight

Chapter 1

UDP-glycosyltransferases and the glucosidation pathway

1.1 Human drug metabolism and chemical biotransformation

Metabolism, or biotransformation, is defined as the chemical modification of a drug or other compound by the body. In general, metabolism facilitates the elimination (clearance) and detoxification of hydrophobic (lipophilic) compounds, including drugs and non-drug xenobiotics (dietary, environmental and industrial chemicals).

Drug metabolism reactions may be classified as either 'functionalization' or 'conjugation' (Rowland, Miners & Mackenzie 2013). Functionalization involves the addition or 'unmasking' of a polar functional group (hydroxyl (-OH), carboxyl (CO₂H) or amino (-NR₂)) within the molecule primarily through oxidation, reduction or hydrolytic reactions. Although functionalization and conjugation reactions are also referred to as 'phase I' and 'phase II' reactions, respectively, this classification is a misnomer with a sequential order implied which, not infrequently, is not necessarily the case (Di 2014; Josephy, Guengerich & Miners 2005; Rowland, Miners & Mackenzie 2013). The addition of functional groups typically alters the biological properties of the drug, and generally increases water solubility to some extent (Gonzalez, Coughtrie & Tukey 2011). Conjugation reactions are characterized by the covalent linkage of a suitable functional group (e.g. hydroxyl (-OH), carboxyl (CO₂H), sulfuryl (-SH) or amino (-NR₂)) on the substrate to a polar endogenous compound. With the exception of N-acetylation, conjugation reactions serve to produce more water-soluble metabolites to enhance their urinary excretion. Metabolites formed via conjugation are typically inactive (detoxification pathway), but occasionally the

conjugate is pharmacologically and/or toxicologically active (bioactivation pathway) (Obach 2013; Sallustio 2008). Both functionalization and conjugation reactions are catalyzed by enzymes. The most important functionalization and conjugation enzymes involved in drug and chemical metabolism are cytochrome P450 (CYP) and UDP-glycosyltransferase (UGT), respectively (Di 2014; Evans & Relling 1999; Miners & Mackenzie 1991; Rowland, Miners & Mackenzie 2013; Tripathi et al. 2013). Together, these enzymes contribute to the metabolism of more than 75% of drugs cleared by biotransformation.

The focus of this thesis is the role of UGT in facilitating the metabolism of drugs, non-drug xenobiotics, and endogenous compounds by catalyzing the transfer of the sugar moiety from a nucleotide sugar, such as UDP-glucuronic acid (UDP-GlcUA), to an acceptor functional group (Figure 1.1). Notably, drugs from almost all therapeutic classes undergo glucuronidation, for example non-steroidal anti-inflammatory drugs (NSAIDs) and opioids (Miners & Mackenzie 1991). Consistent with the ability to metabolize such a structurally diverse range of compounds, UGTs exist as a ‘superfamily’ of enzymes, each of which exhibits a distinct, but somewhat overlapping, substrate (aglycone) selectivity (see further in Section 1.1.5).

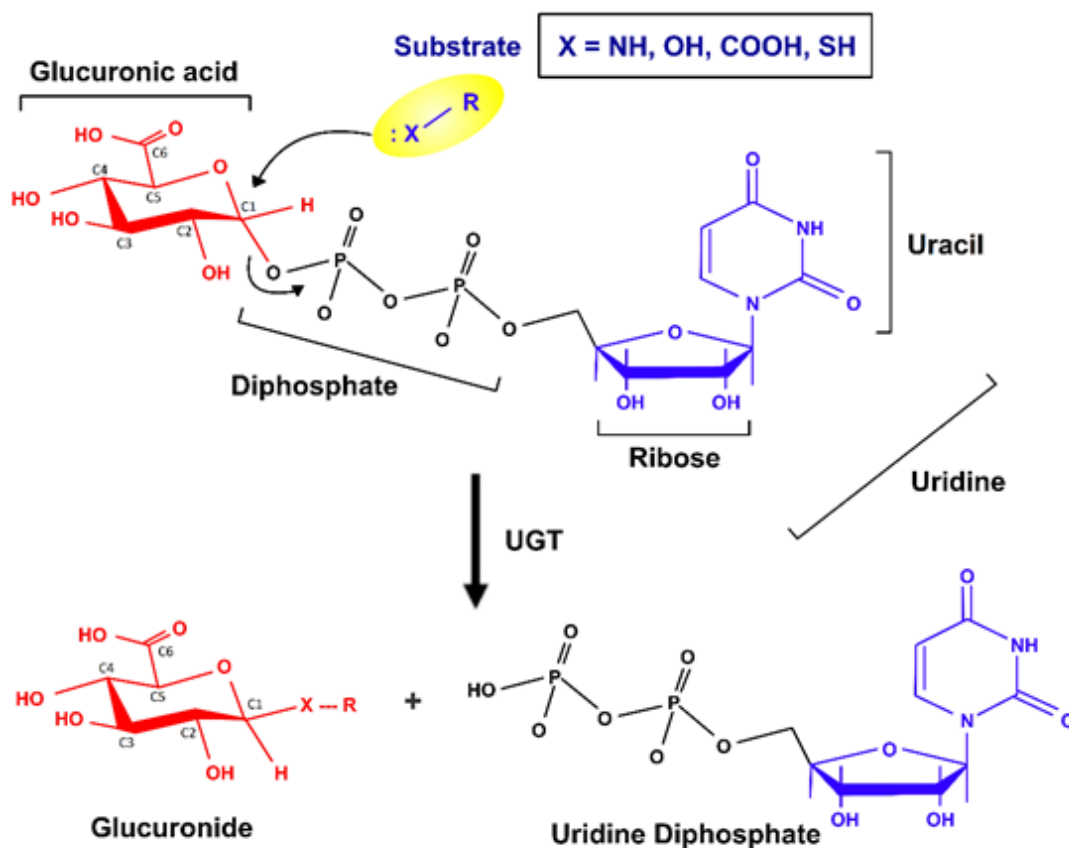


Figure 1. 1: Glucuronidation reaction catalyzed by a UDP-glucuronosyltransferase (UGT).

R=substrate (aglycone), X= nucleophilic acceptor functional group on substrate. Adapted with permission from Zhou, J & Miners, JO 2014, 'Enzyme Kinetics of Uridine Diphosphate Glucuronosyltransferases (UGTs)', in *Enzyme Kinetics in Drug Metabolism: Fundamentals and Applications*, eds S Nagar, UA Argikar & DJ Tweedie, Springer, New York. Copyright (2014) Springer Nature.

The human UGT superfamily comprises four gene families, designated UGT1, UGT2, UGT3 and UGT8 (Mackenzie et al. 2005) (Figure 1.2). Nineteen functional human UGT enzymes in the UGT1A, UGT2A and UGT2B subfamilies that utilize UDP-GlcUA as cofactor have been identified to date (Mackenzie et al. 2005; Miners et al. 2004). Additionally, however, other UDP-sugars including UDP-glucose (UDP-Glc), UDP-xylose (UDP-Xyl) and UDP-galactose (UDP-Gal) may potentially be used as the sugar donor by these enzymes (see Section 1.1.6). The more recently identified

UGT3A family consists of just two enzymes that variably utilize UDP-N-acetylglucosamine (UDP-GlcNAc) (UGT3A1), UDP-Glc and UDP-Xyl (UGT3A2) as the cofactor, while UDP-Gal is the cofactor for the only member of the UGT8 family (UGT8A1) (Mackenzie et al. 2011; Mackenzie et al. 2008; Meech & Mackenzie 2010).

1.1.1 The UDP-glycosyltransferase superfamily

UDP-Glycosyltransferases belong to a superfamily of enzymes found in animals, plants, fungi, baculoviruses and bacteria (Ahn et al. 2014; Ahn, Vogel & Heckel 2012; Bock 2015; Mackenzie et al. 2005; Offen et al. 2006; Osmani, Bak & Moller 2009). The UDP-glycosyltransferase proteins are characterized by similar protein structure and fold, and a ‘signature sequence’ of 44 amino acids localized in the carboxyl terminal (CT) half that binds the UDP-moiety of the nucleotide sugar (Mackenzie et al. 2005; Mackenzie, Gardner-Stephen & Miners 2010; Mackenzie et al. 1997). In contrast to lower organisms such as plants and invertebrates, which mainly catalyze glucosidation reactions utilizing UDP-Glc as the cofactor, vertebrates such as mammals mainly catalyze glucuronidation reactions using UDP-GlcUA as the cofactor (Meech et al. 2012a). The reason for this difference in UDP-sugar selectivity is unknown, but may be related to the development of anionic glucuronide transporters for the efficient elimination of charged conjugates as opposed to the storage of glucoside conjugates in the vacuoles of plants (Bock 2015).

UGT genes are classified in families and subfamilies. Families (denoted by a number) and subfamilies (denoted with a letter) are distinguished by the amino acid sequence identity of the encoded protein. UGT proteins with sequence identities >45% and >60% are classified in the same family and subfamily, respectively. Families 1-50 are reserved for animals, 51-70 for fungi/ yeast, 71-100 for plants, and 101-200 for

bacteria (<http://prime.vetmed.wsu.edu/resources/udp-glucuronosyltransferase-homepage/current-nomenclature>). Within the ‘animals’ category, mammalian enzymes are classified in families 1-8, nematodes in families 9-27, and insects in families 31-50 (Bock 2015). Three families (UGT31, UGT32 and UGT305) related to the insect order Lepidoptera are unique to baculoviruses (Ahn, Vogel & Heckel 2012).

1.1.2 Human UGT evolution

Throughout the time course of human biological adaptation, it has been proposed that UDP-glycosyltransferase heterogeneity has occurred as an evolutionary response to changes in chemical exposure. These chemical ‘drivers’ include: the complex human diet and dietary shifts, migration and expansion into new environments, and increased exposure to environmental chemicals (Gonzalez & Nebert 1990; Marciniak & Perry 2017; Weyrich et al. 2017). In evolutionary terms, it has been proposed that drug metabolism by CYP is a late acquired function in comparison to homeostatic roles such as maintaining steady-state levels of endogenous compounds (steroids, fatty acids) involved in the control of various basic cellular functions (growth, differentiation, apoptosis) (Nebert & Gonzalez 1987). Given their broadly similar function in metabolism and detoxification, this is also likely with the UDP-glycosyltransferases (Meech et al. 2019).

As with invertebrate UDP-glycosyltransferases, the human UGT superfamily evolved by two rounds of gene duplication (Meech et al. 2012a). An example of this adaptive evolutionary response is provided by the unusual structure of the human *UGT1* gene locus whereby each *UGT1* transcript is encoded by a unique exon 1 spliced to a set of exons 2-5 that are shared in common (Owens & Ritter 1995). Exon 1 corresponds to the variable aglycone binding amino terminal (NT) domain while common exons 2-5

correspond to the invariable UDP-sugar binding CT domain. Splicing of each of the unique exons to the four common exons results in the translation of proteins with differing substrate selectivities (Li & Wu 2007; Mackenzie et al. 2005; Radominska-Pandya et al. 1999).

As noted previously, human UGT1 and UGT2 family enzymes most commonly conjugate endobiotics and xenobiotics with GlcUA (Miners & Mackenzie 1991). To reflect this function, human UDP-glycosyltransferases are generally referred to as ‘UDP-glucuronosyltransferases’, abbreviated as ‘UGT’. More recently, however, it has been shown that other members of the human UGT family (viz. UGT3 and UGT8) typically utilize UDP-sugars other than UDP-GlcUA as the cofactor (Mackenzie et al. 2011; Mackenzie et al. 2008; Meech & Mackenzie 2010; Meech et al. 2015). Hence, the recommended nomenclature of ‘UDP-glycosyltransferase’ will be employed in this thesis (Mackenzie et al. 2005; Magdalou, Fournel-Gigleux & Ouzzine 2010; Meech et al. 2012a), with ‘UGT’ as the abbreviation. Of note, there is increasing evidence human UGT1 and UGT2 family enzymes may additionally utilize cofactors other than UDP-GlcUA (see Section 1.1.6).

1.1.3 Human UGT genes

Human UGT1 family

The *UGT1* gene locus is located on chromosome 2q37 and comprise a single subfamily (Mackenzie et al. 2005). As indicated previously, a unique first exon is spliced to the shared exons 2-5, giving rise to 13 individual transcripts (Figure 1.2). Nine transcripts, *UGT1A1*, *UGT1A3*, *UGT1A4*, *UGT1A5*, *UGT1A6*, *UGT1A7*, *UGT1A8*, *UGT1A9*, and *UGT1A10*, encode functional proteins, whereas four are pseudogenes (*UGT1A2P*, *UGT1A11P*, *UGT1A12P* and *UGT1A13P*).

Human UGT2 family

By contrast, the *UGT2* gene family, which is located on chromosome 4q13 comprises two subfamilies; *UGT2A* and *UGT2B* (Mackenzie et al. 2005). Each gene includes six exons, whereby exons 1-2 encode the NT. The exons are unique to each gene, except for *UGT2A1* and *UGT2A2*. These two members share identical CT sequences (exons 2-5), much like the *UGT1* family, with a unique first exon. There are three members of the *UGT2A* subfamily; *UGT2A1*, *UGT2A2* and *UGT2A3*. The *UGT2B* subfamily consists of twelve members (Figure 1.2), seven of which encode active proteins (viz. *UGT2B4*, *UGT2B7*, *UGT2B10*, *UGT2B11*, *UGT2B15*, *UGT2B15*, *UGT2B28*). The remaining five are pseudogenes (*UGT2B24P-UGT2B27P* and *UGT2B29P*).

Human UGT3 family

The *UGT3* gene, which is located on chromosome 5p13.2, comprises just two members, *UGT3A1* and *UGT3A2* (Figure 1.2) (Mackenzie et al. 2005). Each consists of seven exons, which exhibit substantial sequence variability (30-40% sequence identity) compared to the *UGT1* and *UGT2* family (Meech & Mackenzie 2010).

Human UGT8 family

The *UGT8* family consists of a single member, *UGT8A1*. The *UGT8A1* gene is located on the chromosome 4q26 and comprises five exons (Figure 1.2) (Mackenzie et al. 2005).

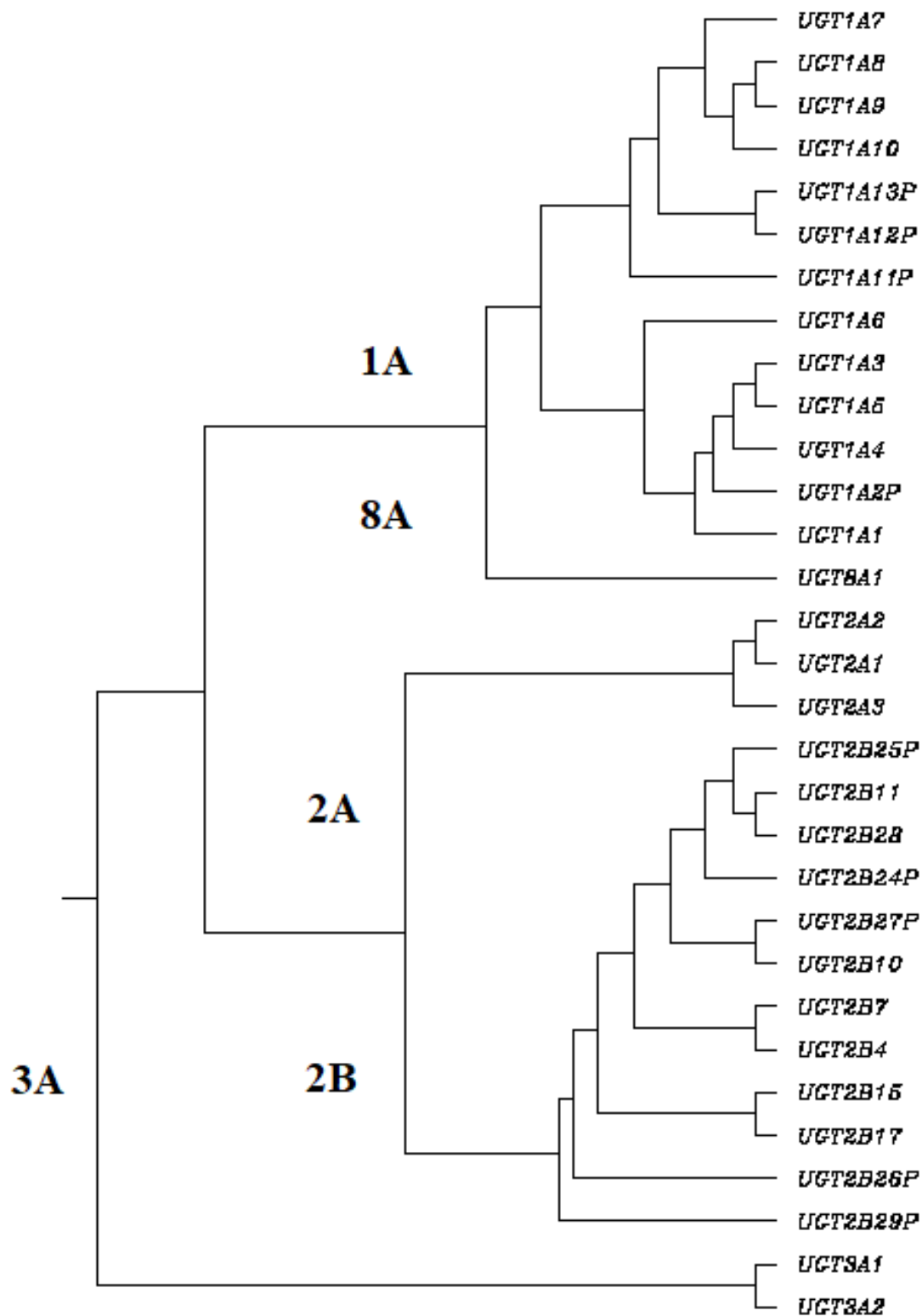


Figure 1. 2: Rooted phylogram of the four human UGT (1, 2, 3 and 8) gene families. Pseudogenes are indicated with the letter P added at the end of the gene name. Protein sequences were extracted from GenBank. Alignment and phylogram generated were performed with ClustalW.

1.1.4 Tissue specific expression of human UGTs

The liver, kidney and gastrointestinal tract (GIT) are considered the main sites of drug and chemical glucuronidation in humans, although enzyme activity is variably observed in other tissues (Radomska-Pandya et al. 1998; Ritter 2007; Rowland, Miners & Mackenzie 2013). Indeed, UGT mRNA is expressed in most tissues, with evidence of tissue-selective expression (Table 1.1). However, recent proteomic studies, using liquid chromatography-mass spectrometry (LC-MS) have shown that mRNA expression is poorly predictive of protein expression (Table 1.1). In particular, UGT1A9, UGT2B7 and UGT1A6 are the only proteins expressed in human kidney (Knights et al. 2016; Margaillan et al. 2015a). UGT2B7 is the most abundant human hepatic UGT protein, followed by UGT1A1, UGT1A4, UGT2B4, and UGT2B15 (Fallon et al. 2013; Margaillan et al. 2015b). The next tier of hepatic UGT proteins of similar abundance consist of UGT1A9, UGT1A6, UGT1A3, UGT2B10 and UGT2B17. A more recent study by Bhatt et al. (2019) demonstrated age-dependent changes in protein abundance and activity of six hepatic UGTs: UGT2B15 is the major enzyme expressed in neonates; UGT2B7 in infants; UGT1A4 and UGT2B7 in early and middle childhood; while by adolescence and adulthood both UGT2B7 and UGT1A4 are the predominant enzymes with relatively similar ratios of UGT2B15, UGT1A1, UGT1A9, and UGT1A6. The adult hepatic protein expression data are in general agreement with the earlier quantitative proteomic studies. All UGT1A proteins and some UGT2B subfamily proteins have been detected in the GIT although variability in expression was apparent between studies (Harbourt et al. 2012; Nakamura et al. 2016; Rouleau et al. 2017). This is most likely due to segmental differences in the distribution of UGT proteins along the length of the GIT (Drozdik et al. 2018; Iswandana et al. 2018).

Table 1.1: Human tissue UGT mRNA and protein expression.

UGT subfamily	UGT member	Tissue		Reference
		mRNA	Protein	
UGT1	A1	Liver, bile ducts, stomach, colon, small intestine	Liver, intestine	Bhatt et al. (2019); Fallon et al. (2013); Margaillan et al. (2015b); Nakamura et al. (2016); Ohno and Nakajin (2009); Rouleau et al. (2017); Tukey and Strassburg (2000)
	A3	Liver, bile ducts, stomach, colon, small intestine	Liver, intestine	
	A4	Liver, bile ducts, colon	Liver, intestine	Bhatt et al. (2019); Fallon et al. (2013); Margaillan et al. (2015b); Rouleau et al. (2017); Tukey and Strassburg (2000)
	A5	Gastrointestinal tract (small intestine, colon), kidney, oesophagus, liver, prostate, placenta, cervix, trachea, brain, thymus, testes, lung, bladder	Intestine	Finel et al. (2005); Ohno and Nakajin (2009); Rouleau et al. (2017)
	A6	Liver, bile ducts, stomach, colon, brain, small intestine, adrenal, trachea, kidney, bladder	Liver, kidney, intestine	Bhatt et al. (2019); Fallon et al. (2013); King et al. (1999); Knights et al. (2016); Margaillan et al. (2015a); Margaillan et al. (2015b); Nakamura et al. (2016); Ohno and Nakajin (2009); Rouleau et al. (2017); Tukey and Strassburg (2000)

UGT subfamily	UGT member	Tissue		Reference
		mRNA	Protein	
	A7	Oesophagus, stomach, liver, small intestine, colon, cervix, trachea, kidney	Intestine	Bhatt et al. (2019); Fallon et al. (2013); Harbourt et al. (2012); Knights et al. (2016); Margaillan et al. (2015a); Margaillan et al. (2015b); Ohno and Nakajin (2009); Rouleau et al. (2017); Tukey and Strassburg (2000)
	A8	Oesophagus, ileum, jejunum, colon, adrenal, trachea, bladder	Intestine	
	A9	Liver, colon, kidney, oesophagus, small intestine, adrenal, bladder	Liver, kidney, intestine	
	A10	Oesophagus, stomach, bile ducts, small intestine, colon, adrenal, trachea	Intestine	
UGT2	A1	Olfactory epithelium, brain, foetal lung		Tukey and Strassburg (2000)
	A2	Nasal mucosa		Sneitz et al. (2009)
	A3	Liver, small intestine, adipose tissue, colon, pancreas, kidney, stomach, testis		Court et al. (2008)
	B4	Liver, oesophagus, thymus, testis, breast, lung, prostate, heart, trachea, kidney, placenta, adipose tissue, skin, adrenal	Liver	Bhatt et al. (2019); Fallon et al. (2013); King et al. (1999); Knights et al. (2016); Levesque et al. (1999); Margaillan et al. (2015a); Margaillan et al. (2015b); Nakamura et al. (2016); Ohno and Nakajin (2009); Tukey and Strassburg (2000); Turgeon et al. (2001)
	B7	Oesophagus, liver, small intestine, mammary gland, colon, brain, kidney, pancreas, lung	Liver, kidney, intestine	
	B10	Oesophagus, liver, kidney, mammary gland, prostate, lung, spleen, small intestine, testis, placenta	Liver	
	B11	Liver, kidney, mammary gland, prostate, adrenal, skin, adipose tissue, lung		Beaulieu et al. (1998); Ohno and Nakajin (2011)

UGT subfamily	UGT member	Tissue		Reference
		mRNA	Protein	
	B15	Oesophagus, liver, prostate, stomach, small intestine, colon, breast, testis, trachea, lung, placenta, adipose tissue, skin, uterus, kidney	Liver	Beaulieu et al. (1996); Bhatt et al. (2019); Fallon et al. (2013); Levesque et al. (1997); Margaillan et al. (2015b); Nakamura et al. (2016); Ohno and Nakajin (2009); Tukey and Strassburg (2000)
	B17	Prostate, liver, stomach, small intestine, colon, brain, thymus, breast, testis, ovary, cervix, placenta, lung, trachea, kidney, spleen, adipose tissue, skin, uterus, adrenal	Liver, intestine	
	B28	Breast, adipose tissue, liver		Levesque et al. (2001); Ohno and Nakajin (2011)
UGT3	A1	Liver, kidney, stomach, duodenum, colon, testes		Meech and Mackenzie (2010)
	A2	Thymus, testes, kidney		Mackenzie et al. (2011); Meech and Mackenzie (2010)
UGT8	A1	Brain, colon, small intestine, kidney, spleen, testis, thyroid, trachea, adipose tissue, bladder, breast, oesophagus, ovary, prostate, thymus		Meech et al. (2015)

1.1.5 Substrate (aglycone) and inhibitor selectivities of human UGTs

As discussed earlier, human UDP-glycosyltransferases have distinct aglycone and cofactor binding domains localized within the NT and CT, respectively, although individual amino acids within the alternate domain may contribute to cofactor and substrate binding (Mackenzie 1990). As would be expected from these distinct functional domains, amino acid sequence identity is more highly variable in the NT. In the past, UDP-glycosyltransferases have been labelled ‘promiscuous’ in nature due to their acceptance of a wide range of structurally unrelated compounds (e.g. bulky steroids, bilirubin, planar aryl polycyclic hydrocarbons, short- and long-chain aliphatic compounds) (Lin & Wong 2002; Magdalou, Fournel-Gigleux & Ouzzine 2010). However, while most UGTs are able to glucuronidate low molecular weight phenols and aliphatic alcohols (Sorich et al. 2004; Uchaipichat et al. 2004), enzyme substrate selectivity increases with increasing structural and chemical complexity of the aglycone, primarily due to steric, electrostatic, and hydrophobic interactions (Miners, Mackenzie & Knights 2010). Thus, UGTs have distinct but overlapping substrate and inhibitor selectivities. Some substrates may be glucuronidated by multiple UGTs (e.g. paracetamol, which is glucuronidated by UGT1A6, UGT1A1, UGT1A9 and UGT2B15) (Miners et al. 2011), whereas others may be metabolized by a single UGT (e.g. bilirubin by UGT1A1 and zidovudine (AZT) by UGT2B7). The ability to accommodate substrates of diverse structure and size within UGT enzyme active sites is most likely due to structural flexibility or ‘plasticity’, whereby ligand binding induces conformational changes to accommodate each structural class of substrate/inhibitor (Nair, McKinnon & Miners 2016). As will be discussed later, the unique abilities of UGT1A4 and UGT2B10 to glucuronidate tertiary amines arises from

Chapter 1: UDP-glycosyltransferases and glucosidation

substitution of the near conserved His (at position 39 in UGT1A1) that occurs in most UGT1A and UGT2B proteins with Pro and Leu, respectively.

The UGT-enzyme selectivity observed for many substrates and inhibitors provides the basis for reaction phenotyping (discussed later), that is identification of the UGT enzyme(s) contributing to the metabolism of any given drug or other chemical (Miners, Mackenzie & Knights 2010). Although UGT-enzyme-selective inhibition is the most powerful reaction phenotyping approach, there are only a very limited number of identified selective inhibitors compared to selective substrates (aglycone) (Table 1.2).

Table 1.2: Representative known selective substrates and inhibitors, and the preferred cofactors of human UGTs.

Note some UGT enzymes are able to utilize multiple different cofactors but only the preferred known UDP-sugar is listed here.

UGT subfamily	UGT member	Substrates	Inhibitors	Cofactor	Reference
UGT1	A1	Bilirubin, β -estradiol, ethinylestradiol, etoposide, niflumic acid (NFA), SN-38, raloxifene, raltegravir	Atazanavir, sorafenib, regorafenib	UDP-GlcUA	Bosma et al. (1994); Hanioka et al. (2001b); Kassahun et al. (2007); Kemp, Fan and Stevens (2002); Kiang, Ensom and Chang (2005); Lepine et al. (2004); Mano, Usui and Kamimura (2006); Miners et al. (2011); Miners et al. (2017); Park et al. (2010); Watanabe et al. (2003)
	A3	Fimasartan, hexafluoro-1 α , 5-dihydroxyvitamin D, telmisartan			Ieiri et al. (2011); Jeong et al. (2015); Miners, Mackenzie and Knights (2010)
	A4	Amitriptyline, trifluoperazine, lamotrigine, olanzapine, posaconazole, 1'-hydroxymidazolam	Hecogenin		Ghosal et al. (2004); Linnet (2002); Rowland et al. (2006); Uchaipichat et al. (2006a); Williams et al. (2004); Zhu et al. (2008)
	A6	Deferiprone, 5-hydroxytryptamine (serotonin), paracetamol			Benoit-Biancamano et al. (2009); King et al. (1999); Krishnaswamy et al. (2003); Miners et al. (2011)
	A9	Canaglifozin, dapagliflozin, edaravone, frusemide, mycophenolic acid, phenylbutazone, propofol, regorafenib, sorafenib, sulfinpyrazone	Digoxin, NFA, tranilast		Bernard and Guillemette (2004); Francke et al. (2015); Gaganis et al. (2007); Kerdpin et al. (2006); Kerdpin et al. (2008); Lapham et al. (2012); Ma et al. (2012); McGurk, Brierley and Burchell (1998); Miners et al. (2017); Miners et al. (1997); Nishiyama et al. (2006); (Pattanawongsa et al. 2015); Peer et al. (2012); Picard et al. (2005)

UGT subfamily	UGT member	Substrates	Inhibitors	Cofactor	Reference
	B4	Codeine	Fluconazole	UDP-GlcUA	Raungrut et al. (2010)
	B7	Aldosterone, chloramphenicol, codeine, clofibric acid, 5,6-dimethylxanthenone-4-acetic acid (DMXAA), efavirenz, epirubicin, fenofibrate, gemfibrozil, 6 α -hydroxyprogesterone, 21-hydroxyprogesterone, morphine, naloxone, NSAIDs (ibuprofen, flurbiprofen, ketoprofen, diclofenac, naproxen), valproic acid, zidovudine,	Fluconazole		Barbier et al. (2000b); Bowalgaha et al. (2007); Bowalgaha et al. (2005); Chen et al. (2010); Coffman et al. (2001); Coffman et al. (1998); Coffman et al. (1997); Court (2005); Court et al. (2002); Court et al. (2003); Ethell, Anderson and Burchell (2003); Innocenti et al. (2001); Knights et al. (2009); Kuehl et al. (2005); Mano, Usui and Kamimura (2007); Miners et al. (1997); Raungrut et al. (2010); Sten et al. (2009); Stone et al. (2003); Tojcic et al. (2009); Uchaipichat et al. (2006b); Williams et al. (2004)
	B10	Cotinine, desloratadine, ketoconazole, medetomidine, midazolam, nicotine, olanzapine, tricyclic antidepressants (TCA) (amitriptyline, clomipramine, imipramine, trimipramine), tamoxifen	Desloratadine, nicotine		Pattanawongsa et al. (2016)
	B15	Lorazepam, R-methadone, S-oxazepam			Court (2005); Court et al. (2002); Morrish, Foster and Somogyi (2006)
	B17	Dihydrotestosterone (DHT), testosterone, vorinostat			Foti, Fisher and Lyubimov (2012); Kang et al. (2010); Sten et al. (2009)
UGT3	A1	Ursodeoxycholic acid (UDCA)			UDP-GlcNAc

UGT subfamily	UGT member	Substrates	Inhibitors	Cofactor	Reference
	A2			UDP-Glc/UDP-Xyl	
UGT8	A1	Bile acids (deoxycholic acid, chenodeoxycholic acid, cholic acid, hyodeoxycholic acid (HDCA), UDCA)		UDP-Gal	Meech et al. (2015)

1.1.6 UDP-sugar selectivity: glucosidation by mammalian UGTs

Glucosidation, arising from the transfer of glucose to a substrate, has received relatively little attention as a metabolic pathway in humans. Xenobiotic glucosidation was first reported as a metabolic pathway in mammals in 1969, when 4-nitrophenol (4-NP) glucoside was identified with mouse liver microsomes as the enzyme source (Tang 1990). The first drug glucoside conjugate (of a triazole xanthine oxidase inhibitor) was detected in the bile of dogs in the mid 1970's (Duggan et al. 1974). Since then, various other drug glucosides have been detected in human biological samples (Table 1.3). Furthermore, the formation of glucosides of endogenous aglycones, for example bilirubin (Burchell & Blanckaert 1984; Senafi, Clarke & Burchell 1994), hyodeoxycholic acid (HDCA) (Mackenzie, Little & Radomska-Pandya 2003; Radomska et al. 1993) and various other bile acids ('trihydroxy', cholic and chenodeoxycholic acid; Wietholtz et al. (1991)) has been reported *in vivo* and/or *in vitro*.

With the exception of the barbiturates amobarbitone and phenobarbitone (17-30%), the formation of drug glucosides in humans typically represents a small fraction (<10%) of the drug dose. Interestingly, as with the barbiturates, sulfonamides and 5-aminosalicylic acid undergo glucosidation but apparently not glucuronidation indicating glucoside conjugation can occur as the sole glycosidation pathway (Meech et al. 2012a; Tang 1990; Tjornelund, Hansen & Cornett 1989). Overall, glucosidation is generally considered to be a minor metabolic pathway compared to glucuronidation, which is presumably why few studies have been conducted to investigate the extent and contribution of this pathway to overall drug clearance. Furthermore, the enzyme(s) responsible for the formation of these glucosides have generally not have been elucidated.

Table 1.3: Drug glucosides detected in humans *in vivo*.

Drug (aglycone)	Percentage ^a	Biological fluid	Reference
Sulfamethazine	1.5-2.5%	Urine	Ahmad and Powell (1988)
Sulfamerazine	2%		
Sulfamethoxazole	2.7%		
5-aminosalicylic acid	~27% ^b	Plasma	Tjornelund, Hansen and Cornett (1989)
Amobarbitone	17-23%	Urine	Tang, Inaba and Kalow (1975); Tang, Kalow and Grey (1978)
Phenobarbitone	24-30%	Urine	Tang, Kalow and Grey (1979)
Morphine	1.4-5.0%	Urine	Chen, Zhao and Zhong (2003)
Mycophenolic acid	<1% ^c	Plasma	Picard et al. (2005); Shipkova et al. (1999a)
Varenicline	3.5% ^d	Plasma	Obach et al. (2006)
Hydromorphone	<10% ^e	Plasma	Toyama et al. (2015)

^aAmount of glucoside formed as percentage of drug dose

^bConcentration relative to drug concentration, only trace amounts detected in urine due to decomposition

^cCalculated based on reported normalized glycoside: MPA AUC_{0-12hr} ratios.

^dObserved in blood but not in urine

^eCalculated as percentage of sum of three compounds (hydromorphone (H), H-3-glucuronide and H-3-glucoside)

Inter-species differences in xenobiotic glucosidation are evident, which is not surprising given species differences in metabolic enzymes and drug transporters between humans and other mammals such as mice and rats are well documented (Chu, Bleasby & Evers 2013; Fujiwara, Yoda & Tukey 2018; Gu, Tingle & Wilson 2011; Meech et al. 2012b). While phenobarbitone is only glucosidated in humans, it is both glucosidated and glucuronidated in mice (Neighbors & Soine 1995; Paibir et al. 2004; Tang, Kalow & Grey 1979). Although humans, dogs and cats both glucuronidate and glucosidate mycophenolic acid (MPA), phenolic glucosidation is the predominant pathway in cats whereas phenolic glucuronidation predominates in other species (Slovak, Mealey & Court 2017). Another drug with known differences in conjugation

with UDP-Glc or UDP-GlcUA between species is FYX-05, a novel xanthine oxidoreductase inhibitor developed for the treatment of hyperuricemia (Nakazawa et al. 2006). The main urinary metabolites were triazole N₁- and N₂-glucosides in dogs, while only N₁- and N₂-glucuronides were detected in humans and monkeys. As reviewed by Tang (1990), drug glucosides have been detected in the urine of various other mammalian species, including: oxepinac acid in mouse (21%); zinc pyridinethione in dog (21%), monkey (11%), rabbit (5%) and rat (<1%); and hypothernate in dog (4.2%). To further demonstrate the large differences in glucosidation capacity between species, the first drug glucoside (the xanthine oxidase inhibitor FXY) detected in the bile of dogs was found to be extensively (62%) glucosidated (Duggan et al. 1974).

Although N-glucosidation is an important clearance pathway for phenobarbitone and amobarbitone in humans, the enzyme/s catalyzing this reaction are unknown. Like the N-glucosidation site for these barbiturates, AS-3201, a potent aldose reductase inhibitor, is glucosidated at the nitrogen atom of a succinimide ring (Toide et al. 2004). It was shown that rates of amobarbitone N-glucosidation by human liver microsomes (HLM) correlated well ($r=0.964$) with AS-3201 N-glucosidation activity. AS-3201 N-glucosidation was shown to be catalyzed by UGT 1A1, 1A3, 1A4, 2B4, 2B7, 2B15 expressed in insect cells (SupersomesTM). (No N-glucosidation activity was detected in Control SupersomesTM; see Chapter 6). Use of the relative activity factor (RAF) approach suggested that UGT2B15 and UGT2B4 were the major enzymes involved in the N-glucosidation of AS-3201 and, by inference, possibly the N-glucosidation of amobarbitone. Interestingly, the barbituric acid derivative of the novel NSAID bucolome does not form an N-glucoside; rather, only an N-glucuronide formed with HLM as the enzyme source (Kanoh et al. 2011).

Unlike the barbiturates, however, AS-3201 is additionally N-glucuronidated by UGT 1A9, 1A4, 1A3 and 1A1, although this pathway constitutes <4% the hepatic intrinsic clearance predicted for N-glucosidation (Toide et al. 2004). N-Glucuronides and N-glucosides are also reportedly formed by varenicline, mianserin, cyclizine and naronapride (ATI-7505) (Table 1.4). Rates of formation of both glycosides by UGT2B10 were comparable for mianserin, whereas the rate of formation of cyclizine N-glucoside was higher than that of the glucuronide (Lu et al. 2018). Interestingly, only breast cancer resistance protein (BCRP) excreted the N-glucosides whereas the N-glucuronides were excreted by both BCRP and multidrug resistance protein 4 (MRP4). Many other compounds with a variety of different functional groups are also known to be glucuronidated and glucosidated. Acyl glucuronides and glucosides are formed by ibuprofen, bilirubin and an endothelin ET_A antagonist. Phenolic and enolic glucosides and glucuronides are formed by morphine; phenolic and acyl conjugates by the immunosuppressant drug mycophenolic acid; and aliphatic glucosides and glucuronides by bile acids (hyodeoxycholic acid, cholic acid, and chenodeoxycholic acid) (Table 1.4).

Table 1.4: Compounds undergoing both glucuronidation and glucosidation *in vitro*

Substrate	Glucuronide(s)	Glucosides(s)	UGT	References
AS-3201 (aldose reductase inhibitor)	N-	N-	Many	Toide et al. (2004)
Cyclizine	N-	N-	2B10	Lu et al. (2018)
Mianserin	N-	N-		
Varenicline	N-	N-	2B7 ^a	Obach et al. (2006)
Naronapride (ATI-7505)	N-	N-	-	Bowersox et al. (2011)
Ibuprofen	Acyl	Acyl	2B7	Buchheit et al. (2011)

Endothelin ET _A antagonist	Acyl	Acyl	Many	Tang et al. (2003)
Bilirubin ^b	Acyl	Acyl	1A1	Senafi, Clarke and Burchell (1994)
Morphine	Phenolic, enolic	Phenolic, enolic	-	Chen, Zhao and Zhong (2003)
Mycophenolic acid	Phenolic, acyl	Phenolic, acyl	Many ^a	Shipkova et al. (2001)
	-	-	3A2	Mackenzie et al. (2011)
Hyodeoxycholic acid	Aliphatic –OH	Aliphatic –OH	2B7	Mackenzie, Little and Radominska-Pandya (2003)
Bile acids	Aliphatic –OH	Aliphatic –OH	-	Wietholtz et al. (1991)

^aOnly N-glucuronidation investigated with recombinant protein/s

^bConjugation with UDP-xylose also detected

Other interesting novel drug glucosides formed include those of tamoxifen and ARQ 501. The investigational anti-cancer drug ARQ 501 was found to undergo both glucosidation and sulfation to form a novel glucosylsulfate conjugate in humans during Phase II clinical trials (Savage et al. 2008). Analysis of plasma samples from patients treated with tamoxifen (≤ 4 months) for breast cancer were analyzed using high-resolution full scan (HR-FS) mass spectrometry (MS), identified 37 metabolites including 3 glucoside conjugates (Dahmane et al. 2014). Although the formation of these glucoside conjugates was minor, low abundance does not necessarily correlate with the importance or relevance of a metabolite, particularly if they are bioactive (e.g. morphine 6-glucuronide (M6G) and mycophenolic acid acyl glucuronide (AcMPAGlcUA)). It is interesting to note that synthetic morphine 6-glucoside exhibits significant antinociceptive activity in a mouse hotplate model (2 and 4mg/kg dose level), and has a marginally higher affinity for the μ_1 receptor ($K_i=0.28\text{nM}$) relative to morphine ($K_i=0.78\text{nM}$) and M6G ($K_i=1.5\text{nM}$) (Stachulski et al. 2003).

Other bioactive glucosides with potential therapeutic effects include 4-demethylpicropodophyllotoxin 7'-O-beta-D-glucopyranoside (4DPG) (Qi et al. 2005; Zhang et al. 2005), D-19575 (glufosfamide: β -D-glucosylisophosphoramidate mustard) (Shimizu et al. 2010) and physcion 8-O-beta-glucopyranoside (PG), which both have anti-cancer properties *in vitro*. The stilbene derivative 2,3,5,4'-tetrahydroxystilbene-2-O- β -D-glucoside (TSG) is under investigation for its cardio- and neuro-protective effects (Dong et al. 2016; Wang et al. 2009; Zhang et al. 2017; Zhang et al. 2012b; Zhang et al. 2008; Zhao et al. 2016; Zhao et al. 2014), as well as its downregulation of several UGTs which may inhibit emodin (anthraquinone) glucuronidation (Ma et al. 2013; Yu et al. 2017). Consequently, the increase in emodin concentration may be the cause of the hepatotoxicity associated with the herbal tonic *Polygoni Multiflori Radix* (PMR).

It is important to characterize new metabolites and metabolic pathways because it contributes to the overall understanding of the total clearance of a compound, pharmacokinetic (PK) variability, and in the identification of potentially pharmacologically active/toxic metabolites. Although glucosidation appears to be a less efficient clearance pathway compared to glucuronidation, this may change with the increasing sensitivity of analytical equipment and the number of new chemical entities relying on non-CYP enzymes for clearance (Gan, Ma & Zhang 2016). For example, *in vitro* work with an ET_A antagonist showed that its clearance via glucosidation was just as significant as glucuronidation by UGT2B7 (Tang et al. 2003).

The synthesis of uridine diphosphate glucuronic acid (UDP-GlcUA) from uridine diphosphate glucose (UDP-Glc) and uptake into the lumen of the ER and Golgi apparatus

The synthesis of nucleotide sugars (UDP-hexoses) requires glucose, which is the main monosaccharide and energy source for many organisms (Figure 1.3). Glucose is the precursor for UDP-glucose (UDP-Glc), which is synthesized from glucose 1-phosphate and uridine triphosphate (UTP) via UDP-glucose pyrophosphorylase. UDP-Glc is an essential metabolite in many cellular processes, for example the synthesis of glycogen (Csala et al. 2007; Flores-Diaz et al. 1997). UDP-GlcUA is synthesized from UDP-Glc by a two-stage NAD⁺ dependent reaction catalyzed by UDP-glucose dehydrogenase (UGDH) (Freeze & Elbein 2009). UDP-GlcUA is mainly utilized in glycosaminoglycan (GAG) synthesis in the Golgi and in the metabolism of drugs, xenobiotics and endogenous compounds (Csala et al. 2007).

Glycosylation takes place in the lumen of the ER and the Golgi apparatus by type II transmembrane proteins with luminal facing catalytic domains. The ER and Golgi apparatus are sealed vesicles and this compartmentalization ensures that intracellular reactions are carried out with high efficiency, with little interference from other cellular processes (Song 2013). The lipid bilayer membrane acts as a barrier for polar substrates that need to enter or exit these organelles, and hence transporters are required for cofactor translocation (Csala et al. 2007; Freeze & Elbein 2009). Nucleotide sugar transporters (NSTs) transfer specific nucleotide sugars into the ER and Golgi apparatus from the cytoplasm and nucleus, where synthesis occurs. NSTs are energy-independent antiporters belonging to solute carrier family 35 (SLC35). The SLC35 family has been divided into six subfamilies (A-F), four of which have known functions (A-D) (Nishimura et al. 2009). The electroneutral simultaneous exchange

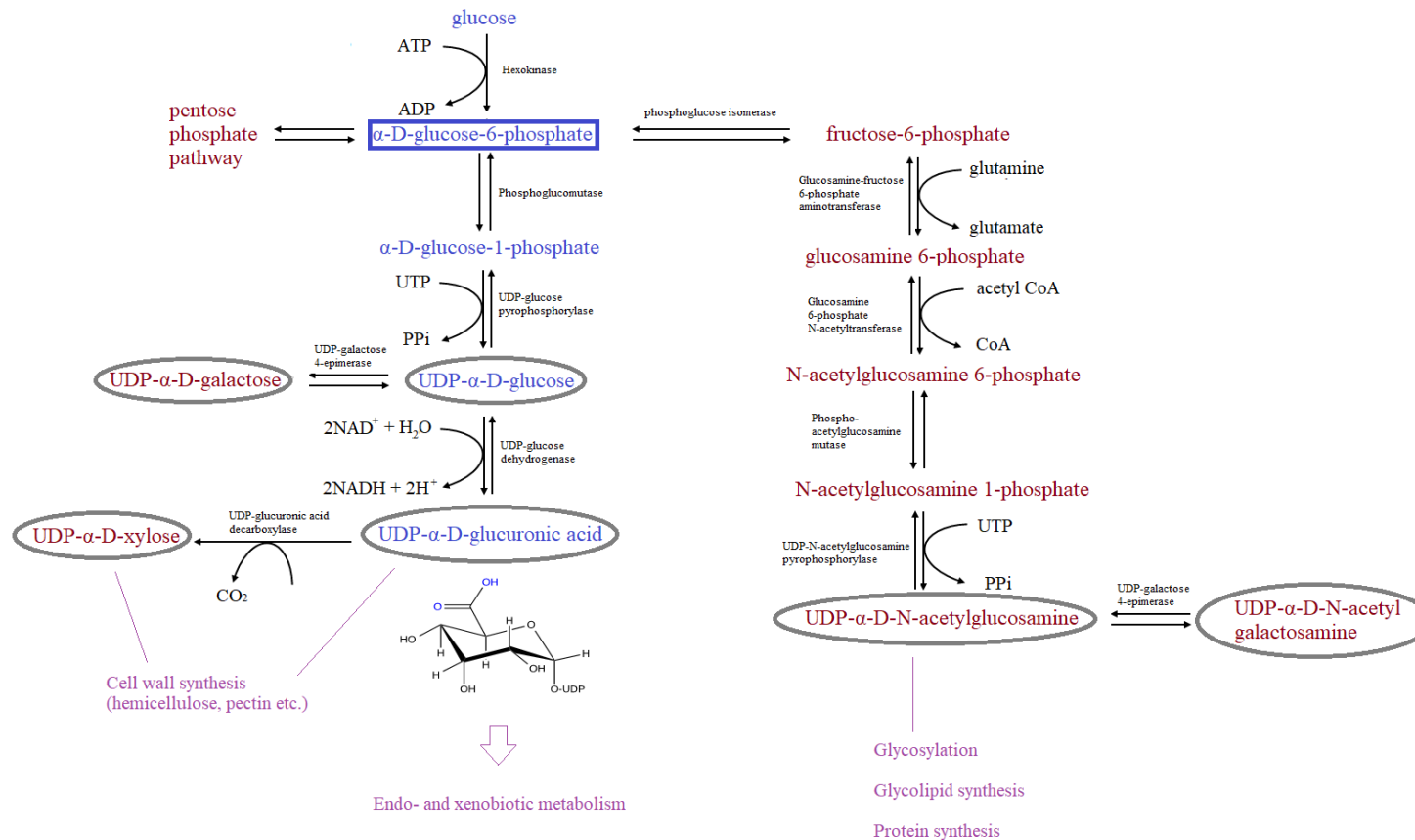


Figure 1. 3: Biosynthesis of UDP-hexoses, including UDP-Glc and UDP-GlcUA, in the cytoplasm.

Abbreviations: UTP, uridine triphosphate; PPi, pyrophosphate; ATP, adenine triphosphate; ADP, adenine diphosphate; NAD^+ , oxidized nicotinamide adenine dinucleotide; NADH , reduced nicotinamide adenine dinucleotide.

of a negatively charged nucleotide sugar from the cytosol with an equally charged luminal monophosphate (generated from UDP by uridine diphosphatase) couples the rate of utilization with import (Freeze & Elbein 2009; Hirschberg, Robbins & Abeijon 1998). Little is known about the exact structure of NSTs due to difficulties associated with crystallizing membrane proteins. As a result, a 3-dimensional (3-D) structure of a NST is yet to be elucidated (Hadley et al. 2014).

The eight essential sugars transported into the ER and/ or Golgi that are required by the body for optimal cell function and synthesis of biomacromolecules are: CMP-sialic acid, UDP-Gal, UDP-GlcNAc, UDP-GlcUA, UDP-Glc, GDP-fucose and UDP-Xyl (Song 2013). Available evidence demonstrates the existence of a specific human transporter(s) for each of these nucleotide sugars, apart from an ER UDP-Glc transporter (Table 1.5) (Hadley et al. 2014; Meech et al. 2012a; Song 2013). More recently, it has been shown that human liver microsomal UDP-GlcUA uptake displays biphasic kinetics, consistent with the involvement of high ($K_d=13 \mu\text{M}$) and low affinity ($K_d=374\mu\text{M}$) uptake transporters. Additionally, UDP-GlcUA uptake was inhibited by certain drugs, UDP-sugars, and glucuronide conjugates (Rowland, Mackenzie & Miners 2015). Nucleotides and nucleotide sugars transported into the ER/Golgi lumen can reach concentrations up to 20- to 50-fold higher than those of the cytoplasm or reaction medium (Hirschberg, Robbins & Abeijon 1998; Sesma et al. 2009).

Estimates of the ratio of UDP-GlcUA to UDP-Glc present in rat hepatocytes range from approximately 0.6 to 2 with one study reporting an approximate 1:1 ratio (Alary et al. 1992; Aw & Jones 1982; Linster & Van Schaftingen 2003). In humans, the ratio of UDP-GlcUA to UDP-Glc, and the relative distribution of UDP-GlcUA and UDP-Glc transporters in the ER is unknown. However, it is reported that the relative

distribution of nucleotide transporters for UDP-GlcUA in the ER and Golgi (in mammals) is approximately unity, while for UDP-Glc (in mammals and plants) it is 4-fold greater in the ER compared to the Golgi (Hirschberg, Robbins & Abeijon 1998). The concentration of UDP-GlcUA in human liver is higher than in extrahepatic tissues (280 μ M versus <20 μ M) including kidney, small intestine, and lung (Lin & Wong 2002). Rat hepatic UDP-GlcUA concentrations are similarly higher than those of extrahepatic tissues (275-400 μ M versus 25-120 μ M) (Bossuyt & Blanckaert 1994; Lin & Wong 2002). Interestingly, the rates of synthesis of UDP-Glc and UDP-GlcUA in rat liver are approximately 100nmol/min/g of liver, with most of the UDP-Glc produced directed towards UDP-GlcUA synthesis (Dills, Howell & Klaassen 1987). This study did not analyze the relative expression of the two precursor enzymes important in the synthesis of UDP-GlcUA (UDP-glucose pyrophosphorylase and UDP-glucose dehydrogenase) in the rat liver tissue, or any extrahepatic tissue. However, in mice UDP-glucose pyrophosphorylase mRNA is highly expressed in the liver, kidney, stomach, large intestine and heart while UDP-glucose dehydrogenase mRNA was highly expressed in the gastrointestinal tract (GI) (stomach, duodenum, jejunum, ileum, and large intestine) (Buckley & Klaassen 2007).

Table 1.5: UDP-sugar substrate selectivity and subcellular localization of representative human nucleotide UDP-sugar transporters.

Transporter	UDP-sugar(s) transported	Subcellular localization	Reference
SLC35A1	CMP-sialic acid	Golgi	Ng et al. (2017); Riemersma et al. (2015)
SLC35A2	UDP-Gal UDP-GlcNAc	Golgi and/or ER	Hara et al. (1993); Kimizu et al. (2017); Kodera et al. (2013); Kumamoto et al. (2001)
SLC35A3	UDP-GlcNAc	Predominantly Golgi	Edmondson et al. (2017); Edvardson et al. (2013)
SLC35A4	Putative UDP-Gal	Predominantly Golgi	Sosicka et al. (2017)
SLC35B4	UDP-Xyl UDP-GlcNAc	Golgi and ER	Siegel et al. (2013); Wex et al. (2018)
SLC35C1	GDP-fucose	Golgi	Lühn et al. (2001)
SLC35D1	UDP-GlcUA UDP-GalNAc	Exclusively ER	Hiraoka et al. (2007)
SLC35D2	UDP-GlcNAc UDP-Glc	Exclusively Golgi	Ishida et al. (2005); Suda et al. (2004)

Abbreviations: solute carrier, SLC; UDP-galactose, UDP-Gal; UDP-N-acetylglucosamine, UDP-GlcNAc; UDP-xylose, UDP-Xyl; UDP-glucuronic acid, UDP-GlcUA; UDP-N-acetylgalactosamine, UDP-GalNAc.

1.2 Structure and function of the UGT multigene family

1.2.1 Glycosyltransferases

The ubiquitous glycosyltransferases (GTs) catalyze the transfer of sugars to an acceptor functional group, a reaction that is biologically important in prokaryotes and eukaryotes (Breton & Imberty 1999). Glycosylation is a highly coordinated, orchestrated, and directed process involving several hundred genes. As noted previously, most eukaryotic GTs are membrane proteins that primarily localize to the ER and the Golgi apparatus (Breton, Mucha & Jeanneau 2001; Spiro 2002). At the time of writing (January 2019), there are 106 GT families classified in the CAZY (Carbohydrate Active enZYmes) database (<http://www.cazy.org/GlycosylTransferases.html>). The diversity of glycosyl-products and their numerous cellular functions reflects the ability of GTs to utilize a large number of nucleotide sugar donors and a myriad of saccharide and non-saccharide aglycones (proteins, lipids, steroids, nucleic acids, antibiotics and small molecules) (Coutinho et al. 2003; Lairson et al. 2008). Although there are a myriad of GTs in existence, the focus of this thesis is on the uridine diphosphate (UDP)-glycosyltransferases (UGTs) from insect species and humans that preferentially conjugate small molecules (Mackenzie et al. 1997).

Surprisingly, the functionally diverse nature of GTs, as demonstrated by the structurally diverse repertoire of donor and acceptor substrates, is accommodated by only two types of folds, making these two structural templates “one of the most ingenious and versatile scaffolds in nature” (Breton et al. 2006; Coutinho et al. 2003). Two folds, referred to as GT-A and GT-B, have been observed in all structures of nucleotide-sugar-dependent GTs solved (up to 2008), with the majority of GTs likely

evolving from a small number of ancestral sequences with the requirement for at least one nucleotide-binding domain of the Rossmann fold type (Lairson et al. 2008). The GT-A fold comprises two closely adjoining $\beta/\alpha/\beta$ Rossmann domains (sometimes described as a single domain fold), while the GT-B fold consists of two $\beta/\alpha/\beta$ Rossmann domains that face each other and are flexibly linked, forming a cleft that contains the active site (Coutinho et al. 2003) (Figure 1.4). As with the GT-A fold, the separate domains are associated with the donor and acceptor substrate binding sites. It should be noted, however, that not all enzymes that possess a GT-A or GT-B fold are GTs.

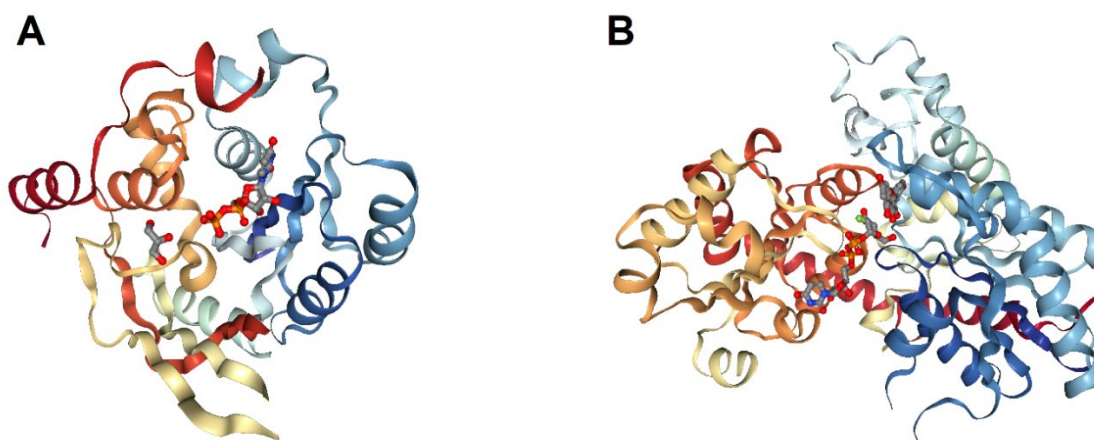


Figure 1. 4: Representative fold-types of GTs.

The two domains are represented by ‘warm’ (red/orange/yellow) and ‘cool’ (navy/sky-blue/pale blue) coloured ribbons of α -helices and β -sheets.

The GT-A fold (A) is from the enzyme SpsA of *Bacillus subtilis* (PDB code: 1QGQ), and the GT-B fold (B) is from enzyme VvGT1 of *Vitis vinifera* (PDB code: 2C1Z). 3-D images are taken from <https://www.rcsb.org/structure>.

Nucleotide sugar-dependent GTs are often referred to as Leloir enzymes, after Luis F. Leloir, who discovered the first sugar nucleotide and was awarded the Nobel Prize for Chemistry in 1970 (Lairson et al. 2008). All GTs utilize an activated donor sugar

containing a (substituted) phosphate leaving group. Donor sugar substrates are most commonly activated by formation of nucleotide diphosphates (e.g. UDP-, GDP-) although nucleotide monophosphate (e.g. UMP-, CMP-) sugars, lipid phosphates (e.g. dolichol phosphate oligosaccharides), and unsubstituted phosphates are also utilized (Lairson et al. 2008). It is known that the most conserved motifs in GTs are involved in catalytic activity and substrate binding (Breton & Imberty 1999). The glycosyl transfer reaction often occurs at the nucleophilic oxygen of a hydroxyl group of the acceptor but can also occur at nitrogen (e.g. N-linked glycoproteins), sulfur (e.g. thioglycosides), and carbon (e.g. C-glycoside antibiotics) nucleophilic centers. Glycoside bond formation results in one of two possible conformations; either the retained or inverted anomeric configuration, with respect to the donor sugar (Breton, Mucha & Jeanneau 2001). Among the GT-A and GT-B superfamilies, the fold-type or topology of the enzyme does not determine the stereochemical configuration of the product that is formed (i.e. either retained or inverted product stereochemistry exist for both fold types).

1.2.2 Classification and catalytic mechanism of human UGTs

Human UGTs belong to the GT1 family of inverting enzymes with a GT-B fold. This hierarchical classification system of GTs, proposed by Coutinho et al. (2003), places human UGTs into clan II (combination of GT-B fold and inverting mechanism; inverting GTs with GT-A fold belong to clan I). Many GT-B fold-inverting enzymes have a His as the catalytic base (Lairson et al. 2008). The proposed ‘critical’ residues in human UGTs involved in aglycone binding are located in the NT (Li et al. 2007; Miley et al. 2007; Patana et al. 2008; Radomska-Pandya et al. 1999). When both substrates (UDP-sugar and aglycone) bind, glycosidation proceeds with the release of a polar glycoside metabolite and UDP (Figure 1.1). Most commonly, the glucuronidation reaction proceeds via a second order nucleophilic substitution (S_N2) mechanism whereby a base (His) accepts a proton from a hydroxyl group on the aglycone, ‘activating’ the acceptor aglycone for nucleophilic attack on the UDP-sugar donor (at C1; Figure 1.1). An acidic residue (Asp/Glu) stabilizes the protonated His through a ‘charge-relay’ type mechanism (Battaglia et al. 1994; Patana et al. 2008; Radomska-Pandya et al. 1999). As a result of this mechanism, the conjugate formed has the β -D configuration due to inversion of configuration at the C-1 atom of the sugar moiety (from α to β form) (Gonzalez, Coughtrie & Tukey 2011; Magdalou, Fournel-Gigleux & Ouzzine 2010; Ouzzine et al. 2014). This mechanism relates to the glucuronidation of aglycones containing an –OH or –SH group. A similar mechanism accounts for the UGT1A9 catalyzed glucuronidation of aglycones (e.g. phenylbutazone and sulfinpyrazone) with an acidic carbon atom (adjacent to two electron withdrawing substituents) to form a C-glucuronide (Kerdpin et al. 2006; Nishiyama et al. 2006). However, the mechanism by which UGTs catalyze the acyl glucuronidation of most carboxylic acids, which are mainly charged at physiological

Chapter 1: UDP-glycosyltransferases and glucosidation

pH, is unknown (Kerdpin et al. 2009). The catalytic His (at position 40 and 34, respectively) is not conserved in human UGT 1A4 (Pro) and 2B10 (Leu), which mainly catalyze the N-glucuronidation of tertiary amines (Kaivosaaari, Finel & Koskinen 2011; Kerdpin et al. 2009; Kubota et al. 2007; Patana et al. 2008).

1.2.3 Subcellular localization and topology of human UGTs

Human UGTs (50-60 kDa in size) are type I integral membrane proteins of the ER and nuclear compartment of cells (Bossuyt & Blanckaert 1997; Gaganis et al. 2007; Higy, Junne & Spiess 2004; Meech & Mackenzie 1997a; Radomska-Pandya et al. 1999; Tukey & Strassburg 2000). It should be noted that the ER membrane is continuous with the outer nuclear membrane. Nuclear expression of UGTs may provide a mechanism to regulate nuclear receptor interactions (Radomska-Pandya et al. 2002). Unlike the cytosolic facing CYP enzymes (Kida et al. 1998), available evidence indicates that all of the NT and most of the CT domain are located on the luminal side of the ER membrane (Meech & Mackenzie 1998; Radomska-Pandya et al. 1999) (Figure 1.5). Two functional motifs are important in mammalian UGT topology; a NT signal sequence that is cleaved upon integration into the ER compartment, and a short transmembrane domain (17 residues) at the CT anchors the enzyme to the membrane (Meech & Mackenzie 1998; Radomska-Pandya et al. 2005). Apart from the CT transmembrane domain, a hydrophobic region(s) of the NT may also interact with the ER membrane. In particular, the NT of UGT1A6 was shown to contain a hydrophobic internal topogenic element (residues 140-240) of buried α -helices that may act as a membrane-embedded domain to facilitate the access of lipophilic aglycones to the active site of the enzyme (Ouzzine et al. 1999). The problems associated with solubilization and crystallization of membrane-bound proteins due to their interactions with the lipid bilayer contribute to the difficulties in obtaining a full-length mammalian UGT suitable for X-ray crystallography.

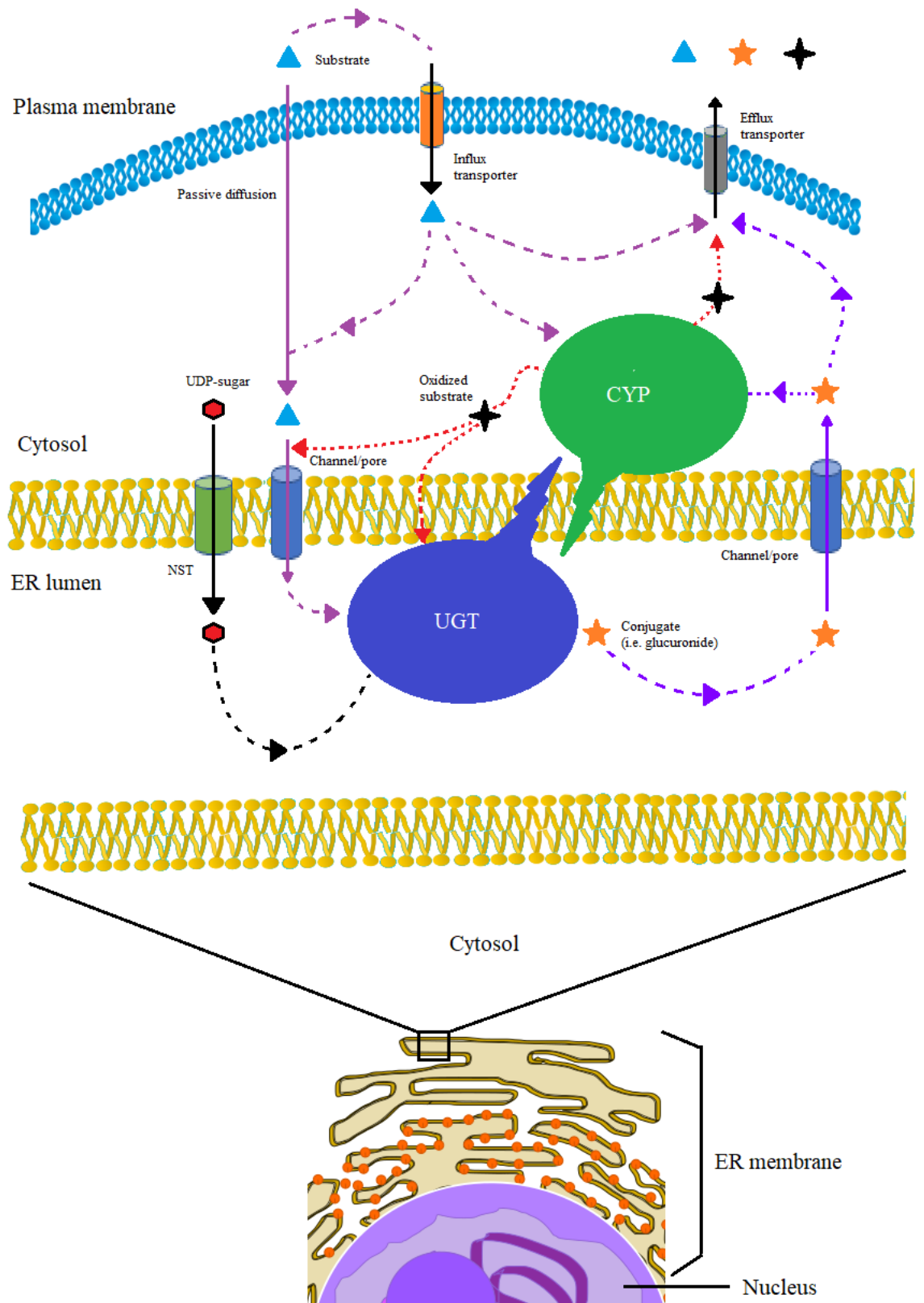


Figure 1. 5: General metabolic pathway for xenobiotics and endogenous compounds within a cell (e.g. hepatocyte).

Accumulating evidence supports UGT homo- and hetero-dimerization, as well as possible proximity and/or interaction (protein-protein) with other ER-residing drug metabolizing enzymes, giving rise to the metabolosome concept (Fujiwara & Itoh 2014; Fujiwara, Yokoi & Nakajima 2016; Lewis, Mackenzie & Miners 2011; Rowland, Miners & Mackenzie 2013). Evidence for UGT oligomerization has been demonstrated using several techniques; co-immunoprecipitation (Fremont, Wang & King 2005; Fujiwara & Itoh 2014; Kurkela et al. 2004; Lewis, Mackenzie & Miners 2011), cross-linking studies (Ikushiro, Emi & Iyanagi 1997), fluorescence resonance energy transfer (FRET) (Operana & Tukey 2007; Yuan et al. 2016; Yuan et al. 2015), gel-filtration (Marschall et al. 1992), and functional complementation/inhibition of UGT mutants (Meech & Mackenzie 1997b). All UGT1A proteins are believed to form oligomers. A putative UGT2B7 dimerization domain of 18 amino acids (positions 183-200) has been proposed based on chimeragenesis, enzyme kinetic, and homology modelling data. The proposed dimerization signature motif (positions 189-199) is present in all UGT2B enzymes (Lewis, Mackenzie & Miners 2011). It is possible that functional diversification occurs as a result of dimerization; for example, altered reaction rates, binding affinities, and/ or substrate selectivity. Indeed, dimerization provides a mechanistic explanation for the observed atypical (non-Michaelis-Menten) kinetics of several substrates of UGT2B7 and potentially other enzymes (Stone et al. 2003; Uchaipichat et al. 2008).

Studies over 50 years ago demonstrated that intact microsomal preparations from mammalian liver displayed latency, such that optimal UGT-catalyzed glucuronidation activity did not occur unless the membrane was chemically (detergents or pore forming agents) or physically (sonication or freeze-thawing cycles) disrupted (Liu & Coughtrie 2017). It was proposed that this latency was due to the intra-vesicular (luminal)

localization of the active site in the ER membrane (Figure 1.5). It is now standard practice to include the pore-forming peptide alamethicin in incubations of HLM to fully 'activate' UGT activity (Boase & Miners 2002; Fisher et al. 2000). UDP-sugar transport into, and glycoside metabolite transport out of, the ER lumen across the lipophilic membrane barrier is now well established, and transport proteins may also facilitate the transluminal movement of polar conjugates (Csala et al. 2007; Lin & Wong 2002; Meech & Mackenzie 1997a; Meech et al. 2012b; Radomska-Pandya et al. 1999). As indicated earlier, the ER-residing NST SLC35D1 transports both UDP-GlcUA and UDP-GalNAc from the cytoplasm into the luminal ER space. An ER-specific UDP-Glc transporter remains unidentified. It has been suggested that a low-selectivity channel or pore (i.e. a translocon protein channel) could also mediate the transmembrane flux (Lizák et al. 2008) (Figure 1.5).

In comparison, more is known about the movement of substrates (aglycone) and metabolites across the plasma membrane via passive diffusion and/or active transport (Chu et al. 2018; Zamek-Gliszczyński et al. 2018) (Figure 1.5). Of major importance to drug safety and efficacy, membrane transporters expressed in the intestine, kidney, liver, and blood-brain barrier (BBB) and other tissues belonging to the ATP-binding cassette (ABC) and solute carrier (SLC) superfamilies are well characterized (Giacomini et al. 2010). Some of these membrane transporters (e.g. organic anion-transporting polypeptide (OATP), breast cancer resistance protein (BCRP), and multidrug resistance-associated proteins (MRPs)) are known to be involved in the transport of drug glucuronides (Hirouchi et al. 2009; Järvinen et al. 2017; Zhang et al. 2016), although only BCRP has been identified as a N-glycoside transporter (Lu et al. 2018). The simplified scheme shown in Figure 1.5 summarizes the localization,

Chapter 1: UDP-glycosyltransferases and glucosidation

surrounding network, and complex interplay of different components of chemical biotransformation (i.e. conjugation and functionalization) and clearance in the cell.

1.2.4 Bacterial, baculoviral, invertebrate and plant UDP-glycosyltransferase evolution

The conserved 44 amino acid residue signature motif ‘consensus sequence’ in plants responsible for recognition and binding of the UDP-moiety of a nucleotide sugar is known as the ‘plant secondary product glucosyltransferase’ (PSPG) box (Offen et al. 2006; Owens & McIntosh 2009). Plants, like invertebrates, mainly use UDP-Glc as the activated sugar donor in the biotransformation of hormones, secondary metabolites, and biotic and abiotic environmental toxins to more hydrophilic compounds, which may impact on the regulation of plant hormones, growth and cellular homeostasis, in facilitating storage of reactive and toxic aglycones into more stable and non-reactive forms, and inter- and intracellular transport (Offen et al. 2006; Paquette, Moller & Bak 2003; Wang 2009). Although not as common, plant UDP-glycosyltransferases are known to utilize UDP-glucuronic acid (UDP-GlcUA) in the conjugation of some chemicals; for example the flavonoids baicalein, scutellarein, wogonin, apigenin, and cyanidin (Nagashima, Hirotsu & Yoshikawa 2000; Noguchi et al. 2009; Osmani et al. 2008; Sawada et al. 2005).

As noted previously, mammalian and insect UDP-glycosyltransferases, both from the animal kingdom, have an NT signal sequence and CT transmembrane domain that facilitates membrane binding (Ahn et al. 2014; Bock 2015; Huang et al. 2008; Jensen et al. 2011; Kannangara et al. 2017; Ross et al. 2001). By contrast, plant and bacterial UDP-glycosyltransferases lack a transmembrane binding domain and consequently are localized in the cytosol. The lack of membrane binding renders the cytosolic enzymes more readily amenable to crystallization. Indeed, there are many examples of complete X-ray crystal structures of plant and bacterial UDP-glycosyltransferases. In comparison, there are no X-ray crystal structures of insect UGTs, and only a partial

structure of a mammalian UGT (see Table 1.6). Of note, cleavage of the transmembrane domain of human CYP enzymes is typically required for successful crystallization (Barnaba et al. 2017).

Phytoalexins (e.g. quercetin glucuronide, stilbene derivatives such as resveratrol glucoside, and glucosinolate-derived isocyanates) provide a chemical defence mechanism used by plants against herbivores. The compounds, which are also known as secondary metabolites or allelochemicals, are 'stored' as glycosides (Bock 2015; Gonzalez, Coughtrie & Tukey 2011; Kimura 2003; Meech et al. 2012a; Wang 2009). Phytoalexins act as insect attractant pigments in plants and have been suggested to possess antioxidative, anti-inflammatory and chemoprotective properties in humans (Bock 2015). The ingestion of these compounds by herbivores (i.e. insects) is thought to be the major molecular or chemical driving force in the evolution and expansion of UDP-glycosyltransferase families as part of the plant-animal warfare or co-evolution, as herbivores respond by producing new enzymes to detoxify these compounds (Bock 2015; You et al. 2013). This hypothesis was originally proposed for another ubiquitous superfamily of metabolizing enzymes, the cytochromes P450 (Gonzalez & Nebert 1990), but would appear to be equally applicable to the UDP-glycosyltransferases as lineage-specific expansions of some insect UDP-glycosyltransferase families are driven by diversification in the NT aglycone binding domain, increasing the range of compounds that could be detoxified or regulated by glycosidation (Ahn et al. 2014; Ahn, Vogel & Heckel 2012).

1.2.5 Protein X-ray crystallography and homology modelling of human UGTs

Despite technological advances for high-throughput structure determination by X-ray crystallography, generation and expression of a protein that provides diffraction-quality crystals can be experimentally challenging. For example, ER membrane-anchored human cytochromes P450 were crystallized by shortening the NT membrane-binding helix and modifying residues associated with aggregation, with the exception of just one enzyme, CYP19A1 (Ghosh et al. 2010; Johnson & Stout 2005; Johnson & Stout 2013). Nevertheless, many high resolution ($\leq 2\text{\AA}$) crystal structures have been solved for plant and bacterial glycosyltransferases which utilize UDP sugars other than UDP-GlcUA as cofactor (Table 1.6). Although most share low sequence identity (20-30%) with human UGTs (Table 1.7 and Figure 1.7), accumulating evidence indicates remarkable structural similarities exist between diverse glycosyltransferases across species (Hu & Walker 2002). As described previously, human UGTs are proteins membrane bound and localized in the smooth ER and nuclear compartment of cells (Meech & Mackenzie 1997a; Radomska-Pandya et al. 1999). This has made structural determination difficult, especially in relation to their overexpression, solubilization, and purification (with retention of activity) despite much effort (Meech & Mackenzie 1998; Radomska-Pandya et al. 2010). To date, only the apo-crystal CT domain of UGT2B7 which has been successfully crystallized and the structure determined to a resolution of 1.8\AA (Miley et al. 2007). The X-ray crystal structure is of a region encompassing 170 residues (positions 285-451) that is composed of 7 α -helices and 6 β -sheet strands (Figure 1.6).

Table 1. 6: Summary of UDP-glycosyltransferase X-ray crystal structures used as templates for homology modeling of human UGTs (RCSB PDB Ligand Explorer 3.8; Table 2.10).

Protein	Species		Reference	Human UGT Modelled	PDB	UDP-sugar ligand	Resolution (Å)
	Name	Type					
UGT2B7-CT	<i>Homo sapiens</i>	human	Miley et al. (2007) ⁱ	2B7 ^f	2O6L	-	1.80
UGT72B1	<i>Aribidopsis thaliana</i>	plant	Brazier-Hicks et al. (2007) ⁱ Laakkonen and Finel (2010)	1A1 ^a	2VCE	U2F ^h (W346)	1.90
					2VCH	UDP	1.45
					2VG8	UDP	1.75
VvGT1	<i>Vitis vinifera</i>	plant (grape)	Offen et al. (2006) ⁱ Takaoka et al. (2010) Lewis, Mackenzie and Miners (2011)	1A1 ^c 2B7 ^e	2C1X	UDP	1.90
					2C1Z	U2F ^h (W332)	1.90
					2C9Z	UDP	2.10
UGT71G1	<i>Medicago truncatula</i>	plant	Shao et al. (2005) ⁱ Locuson and Tracy (2007) Li and Wu (2007) Patana et al. (2007)	1A1 ^d 1A1 ^b 1A6 ^g	2ACV	UDP	2.00
					2ACW	UDP-Glc ^h (W339)	2.60
GtfA	<i>Amycolatopsis orientalis</i>	bacteria	Mulichak et al. (2003) ⁱ Fujiwara et al. (2009)	1A8,1A9	1PN3	TDP, Glc	2.80

^a based on multiple templates: NT (2VCE, 1HIR, 2IYA), CT (2O6L) and UDP-Glc (2VCE) crystal analogue extracted

^b based on comparative analysis and homology modelling (crystal structure of UGT71G1 + sequence analysis of 91 UGT1 and 35 UGT2 GT-B proteins) and docking of UDP-GlcUA

^c based on multiple templates: NT (2C1Z, 2ACV) and CT (2O6L)

^d based on multiple templates: 2ACV and 1RRV. Docked UDP-GlcUA molecule constructed in SYBYL (version 7.2) with formal charge of -3

^e based on multiple templates: NT (2C1X, 2C1Z, 2C9Z, 2ACV, 2ACW) and CT (2O6L)

^f NT and CT based on full crystal of 'VvGT1' complexed with quercetin and UDP-Glc (PDB not disclosed but likely 2ACW which is UGT71G1)

^g based on multiple templates: CT only (2C1X, 2C1Z, 2C9Z, 2ACV, 2ACW)

^h pi- or -ring stacking interactions observed between uracil ring of UDP-sugars and benzene rings of Trp (W), Phe (F) and Tyr (Y) residues

ⁱ X-ray crystal structure deposition authors

Table 1. 7: Summary of results from PSI-BLAST (first iteration) showing the closest structural relatives (search against PDB database) of human UGT1A4 protein sequence. X-ray crystal templates used previously for UGT homology modelling are in blue text and shaded in grey.

PDB	Protein	Analysis results						Species	
		Score (bits)	% UGT1A4 coverage	% Identity	% Similarity (Positive matrix score)	% Gaps	E-value	Name	Type
2O6L	UGT2B7	199	31	55	71	0	3E-51	<i>Homo sapiens</i>	human
3HBF	UGT78G1	67.8	26	32	48	10	1E-11	<i>Medicago truncatula</i>	plant
2C1X 2C1Z 2C9Z	VvGT1	65.9	39	25	42	12	4E-11	<i>Vitis vinifera</i>	plant (grape)
2PQ6	UGT85H2	64.3	27	28	43	10	1E-10	<i>Medicago truncatula</i>	plant
2IYA	Macrolide GT	60.8	20	34	54	7	1E-9	<i>Streptomyces antibioticus</i>	bacteria
2IYF	Macrolide GT	55.5	29	24	42	4	5E-8	<i>Streptomyces antibioticus</i>	bacteria
2VCE	UGT72B1	52.8	16	30	47	18	4E-7	<i>Aribidopsis thaliana</i>	plant
2ACV 2ACW	UGT71G1	51.6 51.6	26 26	23 23	43 43	10 10	7E-7 8E-7	<i>Medicago truncatula</i>	plant
3IA7	CalG4	45.4	25	27	47	5	6E-5	<i>Micromonospora echinospora</i>	bacteria

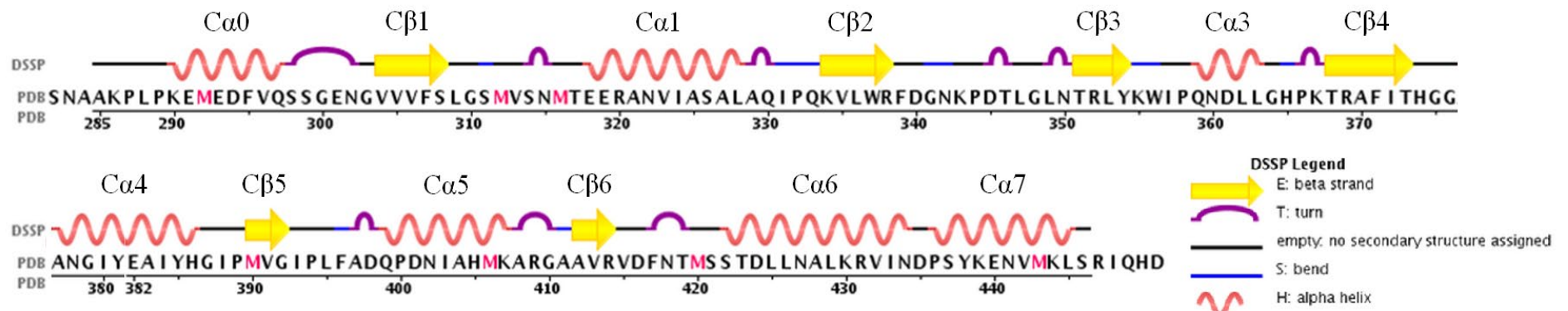


Figure 1. 6: Sequence (170 amino acids) and protein secondary structure assignment for UGT2B7 C-terminus (CT) apo crystal structure (PDB code 2O6L).

Annotated secondary structure features by dictionary of protein secondary structure (DSSP) showing 7 α -helices (38% or 66 residues) and 6 β -sheet strands (15% or 26 residues). Image sourced from PDB website (Table 2.10) and labelled according to Miley et al. (2007).

As indicated in Section 1.2.2, sequence comparison places human UGTs within the GT1 family of glycosyltransferases with a GT-B inverting type fold. All contain two Rossmann-like domains that associate to form the catalytic cleft at the interface between the NT and CT domains (Breton et al. 2006; Miley et al. 2007). Furthermore, comparison of the X-ray crystal structures of two plant glycosyltransferases, UGT71G1 (Shao et al. 2005) and VvGT1 (Offen et al. 2006), and the CT domain of human UGT2B7 reveals high structural homology despite having only 19% sequence identity (Miley et al. 2007). Hence, apart from the low sequence overlap, the plant and bacterial X-ray crystal structures are currently the closest available complete templates (both NT and CT domains; Figure 1.7 and Tables 1.6 and 1.7) for human UGT homology modelling studies (Dong et al. 2012). This can be demonstrated with human UGT1A4, using Position Specific Iteration – Basic Local Alignment Search Tools (PSI-BLAST), as an example (N. Chau, unpublished data). A pairwise comparison search using the full length UGT1A4 protein sequence (534 amino acids; accession no. AAG30422) as a query for the closest (3-D) structural templates from the PDB database retrieved mostly plant and bacterial X-ray crystal structures, of which approximately half of the top hits shown had already been used previously for homology modelling of human UGTs (Table 1.7). Unsurprisingly, the human UGT2B7 CT X-ray crystal structure has the greatest alignment score with human UGT1A4. The amino acid sequence identity between full length UGT1A4 and UGT2B7 is only 43% (at 94% coverage), while it is increased to 55% between UGT1A4 and the UGT2B7 CT X-ray crystal structure (31% coverage) (Table 1.7).



Figure 1. 7: Phylogenetic tree of human UGTs and a selection of the available X-ray crystal structures from plant, bacterial and human UGT2B7-CT from the PDB.

X-ray crystal structures are boxed in red while human UGT protein sequences are boxed in blue. The plant and bacterial UGT crystal structures are clearly separated early from the human UGTs. The phylogenetic tree was generated using the neighbour-joining clustering method (ClustalW; Table 2.10). Abbreviations: *Homo sapiens* (hs), *Vitis Vinifera* (vv), *Medicago truncatula* (mt), *Aribidopsis thaliana* (at), *Streptomyces antibioticus* (sa), *Amycolatopsis orientalis* (ao), and *Eschericia coli* (ec).

It should be noted that this is due to the bias towards the UGT2B7 CT structure (Figure 1.6) and its high conservation across all UDP-glycosyltransferases between species, in contrast to the NT. When a PSI-BLAST search was conducted with only the variable NT of UGT1A4, currently available crystal templates used so for UGT homology modelling (Tables 1.6 and 1.7) were not selected. The observed low sequence identity between human UGTs and existing plant and bacterial X-ray crystal templates is due mainly to the highly variable aglycone NT domain having greater sequence divergence between UGT members in comparison to the highly conserved cofactor CT domain (Meech & Mackenzie 1997a).

In the absence of a full X-ray crystal structure, comparative homology modelling can provide valuable insights into protein structure-function relationships when a homologous protein of known structure is available (Barcellos et al. 2008). These 3-D structures, in conjunction with kinetic data, lay the foundation for more detailed analysis of catalytic mechanisms and specificity (Offen et al. 2006). However, even with the availability of the partial crystal structure of human UGT2B7-CT, there are few computer-aided molecular modelling studies that have investigated the structural properties of human UGTs. Furthermore, all have used different approaches and modelling software (see footnote to Table 1.6) which is not surprising given there is no universally accepted method (Floudas et al. 2006; Reddy et al. 2006). Of the eight studies listed in Table 1.6 utilizing homology models of human UGTs, only three incorporated the partial crystal structure of human UGT2B7-CT (PDB code 2O6L) as a template, while only half of these studies supported the structural insights gained from homology modelling with experimental (site-directed mutagenesis) data (Fujiwara et al. 2009; Miley et al. 2007; Patana et al. 2007; Takaoka et al. 2010). Meaningful models can be generated when the percentage identity of the template with

the target sequence is as low as 25-32% (Qu et al. 2009; Reddy et al. 2006). However, the ideal situation would be to have a template structure that has at least 50% sequence identity to the target protein, as a higher percentage identity between the template and protein of interest results in better resolution (i.e. RMSD of C α \sim 1Å). In addition, models should ideally consider the quality of X-ray crystallographic data (e.g. completeness of structure, 3-D resolution, quality of structure data or R-factor), especially when sequence identity is low.

1.2.6 The amino terminus (NT) of human UGTs

There is overwhelming evidence demonstrating that aglycone selectivity is associated with the NT of UGT enzymes. Greater amino acid sequence variability in the NT reflects the diversity in aglycone selectivity. Early chimeragenesis studies with both rat and human UGT2B enzymes (UGT2B2 and UGT2B3, and UGT2B4 and UGT2B7, respectively) provided experimental evidence of the NT domain being linked to aglycone binding (Mackenzie 1990; Ritter et al. 1992). UGT2B7 is the major enzyme in the metabolism of morphine, catalyzing the formation of both morphine 3-glucuronide (M3G) and morphine 6-glucuronide (M6G) (Coffman et al. 1997; Stone et al. 2003). Nuclear magnetic resonance (NMR) spectroscopy showed an opioid binding site within the first 119 residues (84-118) of UGT2B7, with the mutant Asp99Ala greatly reducing morphine binding (Coffman et al. 2003; Coffman et al. 2001). Site-directed mutagenesis of Tyr33 present in UGT 2B4 and 2B7 indicated that this residue, which is thought to be close to the catalytic site, is important for activity and aglycone selectivity (Barre et al. 2007). Furthermore, construction of UGT2B7-UGT2B15 chimeras demonstrated that residues 158-194 of UGT2B7 are involved in substrate binding of phenolic compounds such as 4-MU, while residues 61-194 of UGT2B15 were responsible for substrate binding of phenols, anthraquinones and flavonoids (Lewis et al. 2007). Interestingly, a putative dimerization domain present in all UGT2B enzymes (residues 183-200) partially overlaps these substrate binding regions with a proposed signature motif (residues ¹⁸⁹FPPSYVPVMS¹⁹⁹) providing some insight into the mechanism of atypical glucuronidation kinetics for substrates of UGT enzymes (Lewis, Mackenzie & Miners 2011). A single amino acid, Ser121, in UGT2B17 is required for the glucuronidation of 3 α - but not 17 β -hydroxy C₁₉ steroids,

while Tyr121 of UGT2B15 is required for glucuronidation activity more generally (Dubois et al. 1999).

Photo-affinity labelling, mass spectrometry and site-directed mutagenesis of UGT1A10 have revealed the role of two Phe residues at positions 90 and 93 (part of the ⁹⁰FMVF⁹⁰ motif) in phenol- and estrogen binding (Starlard-Davenport et al. 2007; Xiong et al. 2006). Mutagenesis of Phe90 of UGT1A10 abolished estrone and 16 α -hydroxyestrone 3-glucuronidation, while some mutants of Phe93 (Phe93Gly) were still active and able to increase 16 α -hydroxyestrone 3-glucuronidation but not estrone 3-glucuronidation (Kallionpaa, Jarvinen & Finel 2015). Additionally, substitution of Ile for Thr at position 211 of UGT1A10 resulted in activity loss towards several substrates, including mycophenolic acid (Martineau, Tchernof & Bélanger 2004). As discussed below, other mutagenesis studies regarding substrate selectivity within the UGT1A family include UGT 1A1, 1A3, 1A4, 1A6 and 1A9.

Although the NT is highly variable, there are only 35 amino acid differences between the NT sequences of UGT 1A3 and 1A4. Reciprocal site-directed mutagenesis demonstrated that Thr36 and Pro40 of UGT1A4 are essential for the N-glucuronidation of tertiary amine substrates. By contrast, UGT1A3, which has Ile and His at positions 36 and 40 (Figure 1.8), respectively, preferentially catalyzes the O-glucuronidation of planar phenols such as 4-methylumbelliferone (4-MU) and 1-naphthol (1-NAP) (Kubota et al. 2007; Li et al. 2007). Additionally, substitution of His39 of UGT1A1, His38 of UGT1A6, and His37 of UGT1A9 with Pro (as in UGT1A4) resulted in the loss of glucuronidation activity towards phenols and naproxen (a carboxylic acid). Furthermore, all of the Pro mutants were able to glucuronidate the tertiary amine lamotrigine (Kerdpin et al. 2009; Li et al. 2007).

Similarly, mutagenesis of His37 in UGT1A9 abolished glucuronidation activity towards all substrates tested, except for the amine retigabine (Korprasertthaworn et al. 2012).

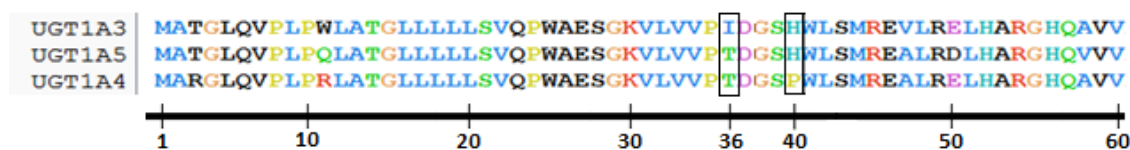


Figure 1. 8: Amino acid alignment of UGT1A3, UGT1A4 and UGT1A5. The first 60 residues are shown.

Site-directed mutagenesis of Arg52 and His54 greatly decreased the activity of human UGT1A6 (Senay et al. 1997). The His54Gln substitution abolished 4-MU glucuronidation, while the Arg52Ala and His54Ala mutations resulted in a 75-80% decrease in the V_{max} for 4-MU glucuronidation. Interestingly, Senay et al. (1997) showed that Arg52 in UGT1A6 (corresponding to Arg49 in UGT2B7; Figure 1.9) is highly conserved in many UDP-glycosyltransferases. An exception is the ecdysteroid glucosyltransferase where the conserved Arg is substituted with Leu, which utilizes UDP-Glc as the cofactor in the glucosidation of ecdysteroids (O'Reilly & Miller 1989).

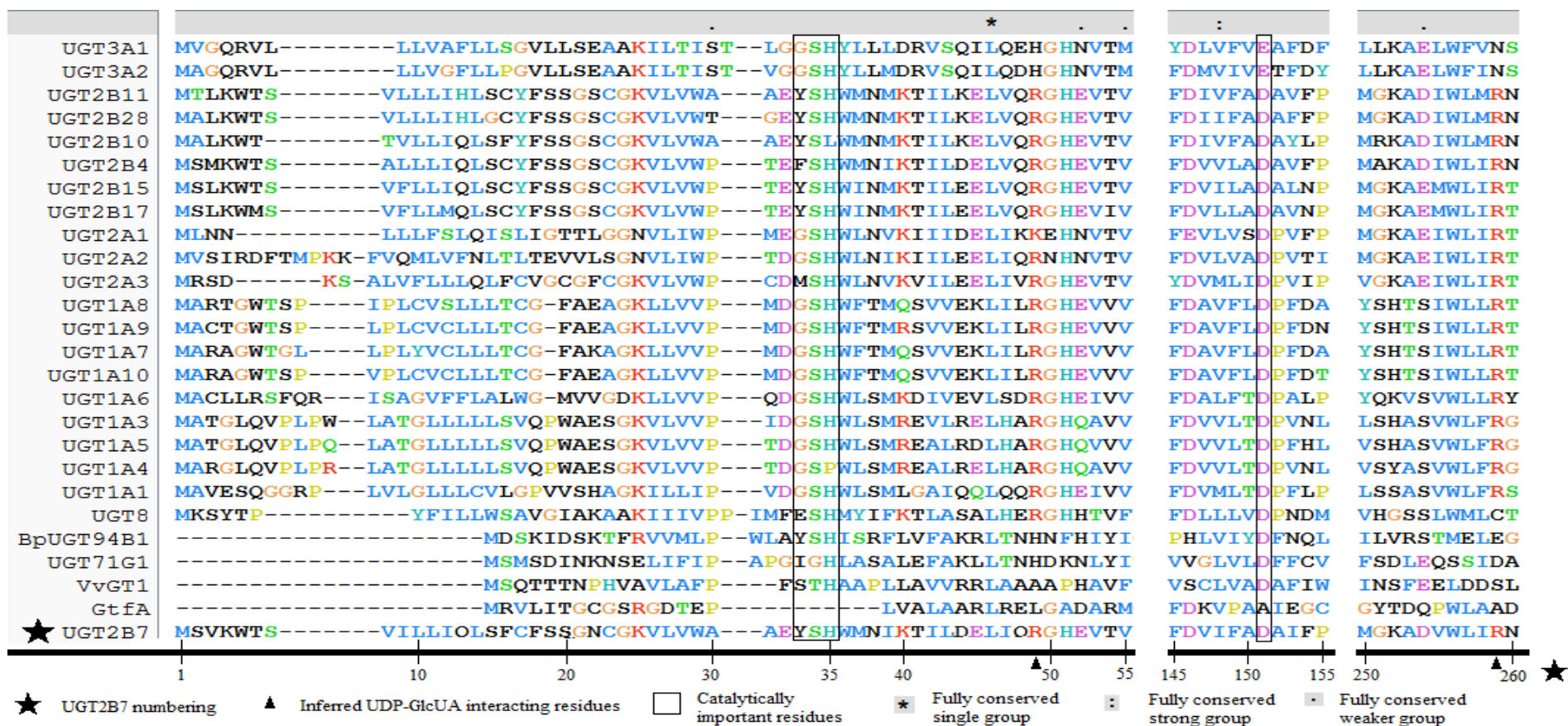


Figure 1. 9: Sequence alignment of the N-terminus (NT) of 22 human, plant (BpUGT94B1, UGT71G1, VvGT1), and bacterial (Gtfa) UGTs. Catalytically important residues 33-35 and 151 (UGT2B7 numbering) are boxed with proposed UDP-GlcUA interacting residues marked with closed triangles. ClustalX 2.0.12 was used for multiple sequence alignment (Table 2.10)

1.2.7 The carboxyl terminus (CT) of UGTs: role in UDP-glucuronic acid selectivity

As described previously, compared to the NT, the CT is highly homologous across all species (Mackenzie et al. 1997). The existence of a CT ‘signature’ sequence that recognizes the UDP-moiety of UDP-sugars across species is well established (Miley et al. 2007; Patana et al. 2007; Radomska-Pandya et al. 2010; Xiong et al. 2008). While most enzymes have a preferred cofactor, many UDP-glycosyltransferases can utilize multiple UDP-sugars. The molecular basis for this lack of specificity of human UGTs is poorly understood (Meech et al. 2015; Meech et al. 2012b; Nair et al. 2015). Several questions relating to the lack of specificity remain unanswered: why vertebrates and lower organisms utilize different cofactors (UDP-GlcUA vs. UDP-Glc) in the conjugation of small lipophilic compounds; whether glucuronidation is an evolutionary selective adaptive response (‘gain of function’), and when did this occur on the evolutionary timescale; and is there a functional role of glucoside conjugates in humans and/ or is glucosidation a redundant conjugation pathway in humans. It is possible that the chemical and molecular drivers of gene expansion in the more variable NT aglycone binding domain may also have induced changes in UDP-sugar donor recognition/specificity (Noguchi et al. 2009). For example, the preference for UDP-GlcUA in one plant species has been shown to be due to an NT residue (Arg25), even though the large majority of residues interacting with sugar donors reside within the CT (Osmani et al. 2008; Osmani, Bak & Moller 2009). In all probability, both domains are likely to be involved in the binding selectivity of the aglycone and UDP-sugar to some extent (Kurkela et al. 2004; Radomska-Pandya et al. 2010). However, the degree of involvement from each domain remains to be fully characterized, highlighting the need for further structure-function studies.

In addition to the concept of the UDP-sugar donor mainly interacting with residues of the CT domain, Radomska-Pandya et al. (2010) proposed that the NT residues Arg49 and Arg259 of UGT2B7 may confer selectivity for UDP-GlcUA by interacting with the negatively charged 6'-carboxylate group of this cofactor. This proposal is based on two studies (Osmani, Bak & Moller 2009; Pedersen, Darden & Negishi 2002) that identified involvement of Arg25 (NT domain) in the UDP-GlcUA selectivity of the plant enzyme BpUGT94B1, but Arg156 (NTP-sugar domain) in the UDP-GlcUA selectivity of the human UDP-glycosyltransferase enzyme 1,3-glucuronosyltransferase (GlcAT-I). Additionally, using site-directed mutagenesis and homology modelling, Noguchi et al. (2009) demonstrated that Arg350 located in the 'plant secondary product glucosyltransferase' (PSPG) box of the CT of Lamiales F7GAT (a plant UGT) was the primary residue determining sugar donor selectivity, since the Arg350Trp substitution caused a shift towards UDP-Glc utilization. This suggests both the NT and CT domains can be involved in UDP-GlcUA selectivity, but the consensus remains that an Arg residue plays an important role in this selective recognition of the anionic carboxylate of the glucuronic acid moiety.

Arg49 and Arg259 (UGT2B7 numbering) are highly conserved throughout the human UGT1 and UGT2 families, but not in UGT3 (at both positions) and UGT8 (at position 259) proteins, which are known to utilize UDP-sugars other than UDP-GlcUA (Figure 1.9) (Meech & Mackenzie 2010; Meech et al. 2015). *In silico* modelling of UGT2B7 and UGT1A5 suggest the involvement of Arg259 in UDP-GlcUA selectivity (Nair et al. 2015; Yang et al. 2018). However, this hypothesis remains to be experimentally verified *in vitro*. Alternatively, Arg338 in the CT is also highly conserved in the human UGT1, UGT2 and UGT8 families but not in UGT3 proteins (Figure 1.10). Mutagenesis and homology modelling studies with UGT2B7 indicate that this residue

is involved with UDP-GlcUA binding, where it interacts with the nucleotide moiety, and that this interaction is substrate dependent (Miley et al. 2007).

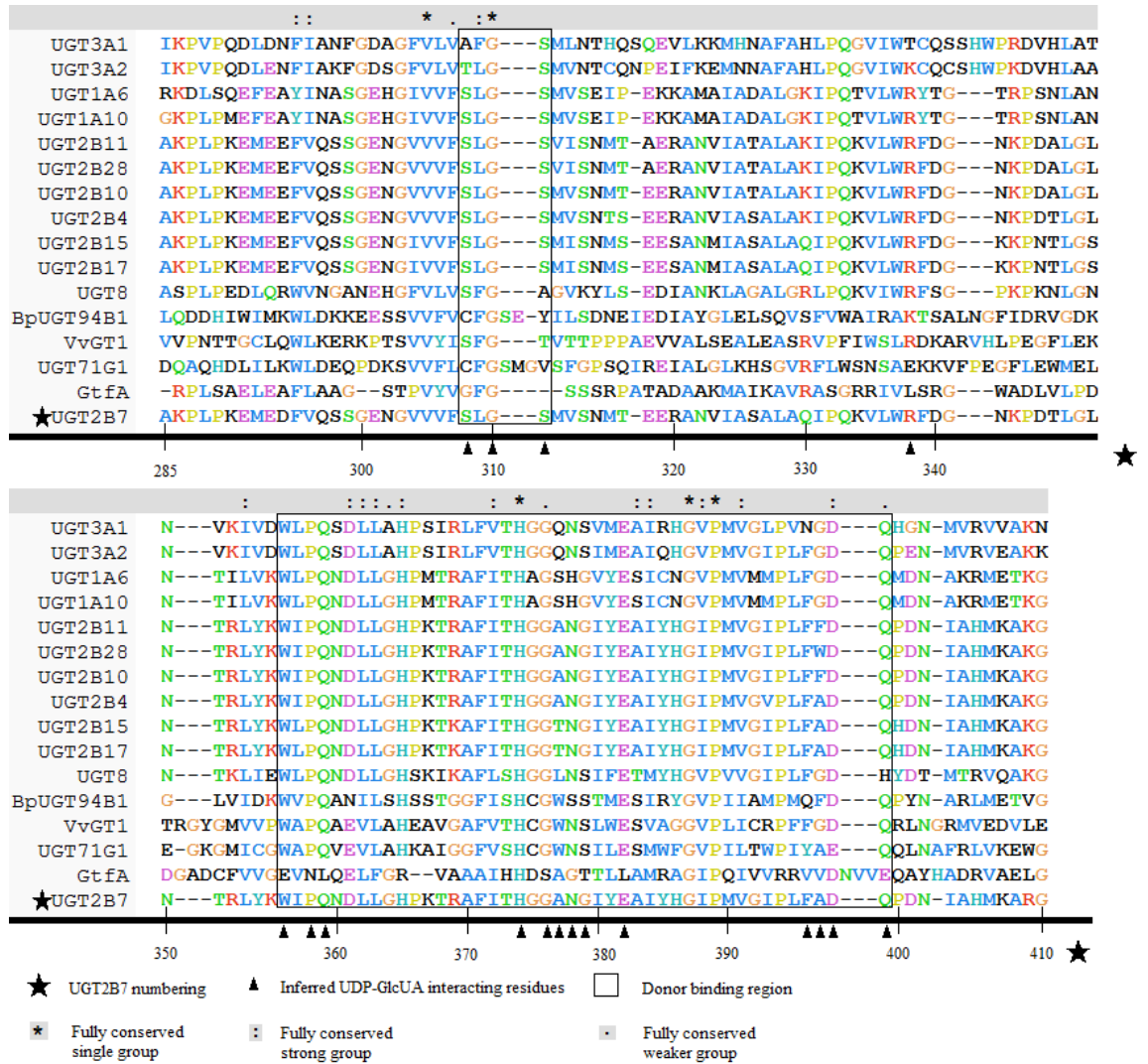


Figure 1. 10: Sequence alignment of CT residues of selected GT1 family enzymes.

Donor binding residues 308-311 (DBR₂) and 356-399 (DBR₁) (UGT2B7 numbering) are boxed, with the proposed UDP-GlcUA interacting residues marked with closed triangles. The UGT signature sequence (44 residues) resides within DBR₁ (371-399; UGT2B7 numbering) (Mackenzie et al. 1997). ClustalX 2.0.12 was used for multiple sequence alignment (Table 2.10). UGT1A6 and UGT1A10 are shown as representative members of the UGT1A family and have shared CT domain sequences. All enzymes are human, except for BpUGT94B1 (plant), VvGT1 (plant), UGT71G1 (plant) and GtfA (bacteria).

Residues interacting with the sugar moiety of UDP-Glc and UDP-GlcUA

As discussed previously, a wealth of experimental (e.g. chimeragenesis, site-directed mutagenesis) and computational studies indicate that the UDP-GlcUA binding site in human UGTs is located within the CT domain (Laakkonen & Finel 2010; Lewis et al. 2007; Li & Wu 2007; Locuson & Tracy 2007; Miley et al. 2007; Patana et al. 2007; Xiong et al. 2008). Importantly, the cofactor binding domain is highly conserved between glycosyltransferases and includes the 44 residue UGT ‘signature sequence’, which encompasses residues 371-399 (UGT2B7 numbering), which is part of one of two donor binding regions (DBR) (Figure 1.10) (Mackenzie et al. 2005; Mackenzie et al. 1997). DBR₂ (residues 308-311, UGT2B7 numbering) is highly conserved except in UGT3A1 and UGT8, which have Ala at positions 308 and 311, respectively, instead of Ser (Figure 1.10). This region is thought to interact with the UDP-moiety of UDP-sugars (Laakkonen & Finel 2010; Miley et al. 2007), although *in silico* modelling indicates that it may form part of a flexible C1 loop that contributes to UDP-sugar binding selectivity (Nair et al. 2015). DBR₁ (residues 356-399, UGT2B7 numbering) is the larger of the two DBR. DBR₁ includes a highly conserved DQxD motif (positions 398-401, UGT2B7 numbering) in human UGT 1A and 2B subfamily proteins, but not in UGT 3A or 8 proteins (Figure 1.10). The first section of DBR₁ is thought to be important for interactions with uracil and the ribose ring; the middle section in binding to the phosphate backbone; and the last section, including the DQxD motif, in the binding of the sugar moiety of UDP-GlcUA (Miley et al. 2007; Nair et al. 2015; Xiong et al. 2008). Studies with UGT 3A1 and 3A2, which do not utilize UDP-GlcUA as the cofactor, demonstrate that the highly conserved Phe391 (which corresponds to Phe396 in UGT2B7) favors UDP-Glc binding in UGT3A2, while the unique residue Asn391 in UGT3A1 is required for UDP-N-acetylglucosamine (UDP-

GlcNAc) utilization (Meech et al. 2012b). Furthermore, localization of the cofactor binding site in the CT domain is consistent with X-ray crystal structures of plant and bacterial UGTs complexed with various UDP-sugars (Bolam et al. 2007; Brazier-Hicks et al. 2007; Ha et al. 2000; Hu et al. 2003; Mulichak et al. 2003; Offen et al. 2006; Shao et al. 2005) (Table 1.6). A consistent feature of the X-ray crystal structures is the π -stacking interactions between the aromatic rings of Trp, Phe or Tyr residues with the uracil ring of the UDP-sugar (see Table 1.6) (Bolam et al. 2007; Brazier-Hicks et al. 2007; Hu et al. 2003; Offen et al. 2006; Osmani et al. 2008; Osmani, Bak & Moller 2009; Pedersen, Darden & Negishi 2002; Shao et al. 2005). Trp332, Trp339, Tyr84 and Phe244 in the X-ray crystal structures of 2C1Z, 2ACW, 1KWS, and 1NLM are all located approximately 3.5Å from the uracil ring of the UDP-sugar. Another consistent feature is the hydrogen bonding network of typically 4-5 residues in the vicinity of the sugar moiety ($\leq 3.3\text{Å}$) of UDP-sugars. Most commonly, these include (in descending order of frequency of occurrence): Gln, Asp, Thr and Trp. Further, Asn, Ala, Glu, Arg and His may also contribute to hydrogen bonding interactions.

1.3 Pharmacokinetics and enzyme kinetics

Pharmacokinetics describes how the body ‘handles’ the drug as opposed to what the drug does to the body (pharmacodynamics). Pharmacokinetics provides a quantitative description of the time course of drug concentration in the body (Birkett 2002), and includes the processes of absorption, distribution, metabolism and excretion (also known as ADME). In addition to ADME, clinical response to a drug may depend on many factors such as genetics, gender, ethnicity, weight, disease states, and concomitant medications, to name a few (Rawlins 1974; Turner, Park & Pirmohamed 2015; Wilkinson 2005; Wilson et al. 2001). The pharmacokinetic parameter of greatest relevance to this project is clearance as it provides a measure of the efficiency of the irreversible elimination of a drug, either by an organ, by a metabolic pathway, or by the whole body (Birkett 2002).

1.3.1 Enzyme kinetics

Glucuronidation is a bi-substrate reaction as it involves the primary substrate (aglycone) and a co-substrate/cofactor (UDP-GlcUA). However, if the UDP-GlcUA concentration is saturating (3- to 5-times the K_m) it may be assumed that it is not rate-limiting for product formation (Lin & Wong 2002; Miners et al. 2010). Hence, the use of the Michaelis-Menten equation (Equation 1.1) for bi-substrate reactions is valid under these conditions. UDP-Glc is also a cofactor for UGTs, and hence similar kinetic considerations hold for glucosidation reactions.

Single enzyme Michaelis-Menten (hyperbolic) kinetics

The Michaelis-Menten equation and corresponding Eadie-Hofstee plot (Figure 1.11) describes the dependence of the rate of an enzyme reaction on substrate concentration when the relationship between substrate concentration ($[S]$) and rate of product

formation (v) is hyperbolic. The Michaelis-Menten equation is given in Equation 1.1. Hence, V_{\max} is the maximum velocity and K_m (the Michaelis constant) is the substrate concentration at half V_{\max} . As this model is empirical in nature, the K_m should not be assigned any mechanistic meaning except for the definition already given. However, the K_m reflects the binding affinity of the substrate; the lower the K_m , the higher the binding affinity. K_m is independent of the amount of enzyme present but V_{\max} changes as a function of the enzyme protein concentration.

Equation 1. 1: Single enzyme Michaelis-Menten equation (hyperbolic kinetics)

$$\text{Rate } (v) = \frac{V_{\max} \times [S]}{K_m + [S]}$$

An assumption of the Michaelis-Menten equation is that the substrate-interaction occurs at only one site per enzyme and that each site operates independently from the others (Houston & Kenworthy 2000).

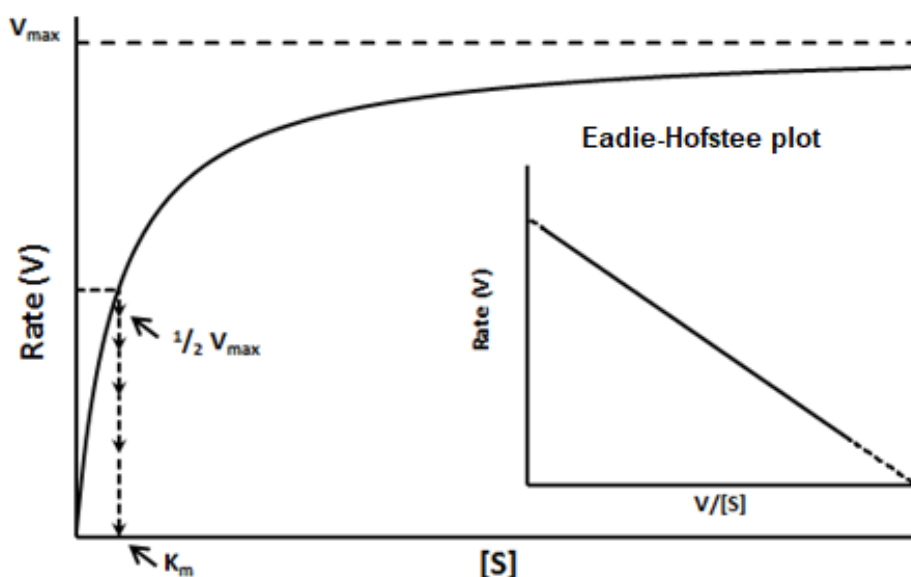


Figure 1.11: Plot of the rate of product formation (v) versus substrate concentration [S] at a constant enzyme concentration for a single substrate reaction, derived from the Michaelis-Menten equation with (inset) the corresponding Eadie-Hofstee plot.

Atypical kinetics

Hill equation

Cooperativity arises from interactions between multiple substrate binding sites (Palmer 1995). The Hill equation is useful for describing the data for a single substrate but does not provide any mechanistic explanation of the interactions between multiple substrates (Houston, Kenworthy & Galetin 2003). Positive cooperativity occurs when the binding of one molecule of a substrate *increases* the affinity of the protein for the same (homotropic) or different (heterotropic) substrate. Negative cooperativity is the reverse – when binding of one molecule of substrate *decreases* the affinity of the protein for other molecules (either homo- or hetero-tropic).

Both negative and positive cooperativity can be described empirically by the Hill equation (Equation 1.2). Here, V_{\max} is the maximal velocity, S_{50} is the concentration at half V_{\max} (analogous to K_m), n is the Hill coefficient reflecting the deviation from hyperbolic kinetics, and $[S]$ is the substrate concentration (Houston, Kenworthy & Galetin 2003). When $n=1$ then the equation simplifies to the Michaelis-Menten equation. Values of $n>1$ give sigmoidal rate versus $[S]$ plots and convex Eadie-Hofstee plots, which describe positive cooperativity or ‘autoactivation’ (Figure 1.12B). Values of $n<1$ result in a concave Eadie-Hofstee plot, which reflects negative cooperativity (Figure 1.12A).

Equation 1. 2: Hill equation (positive (autoactivation) and negative cooperativity)

$$\text{Rate } (v) = \frac{V_{\max} \times [S]^n}{S_{50}^n + [S]^n}$$

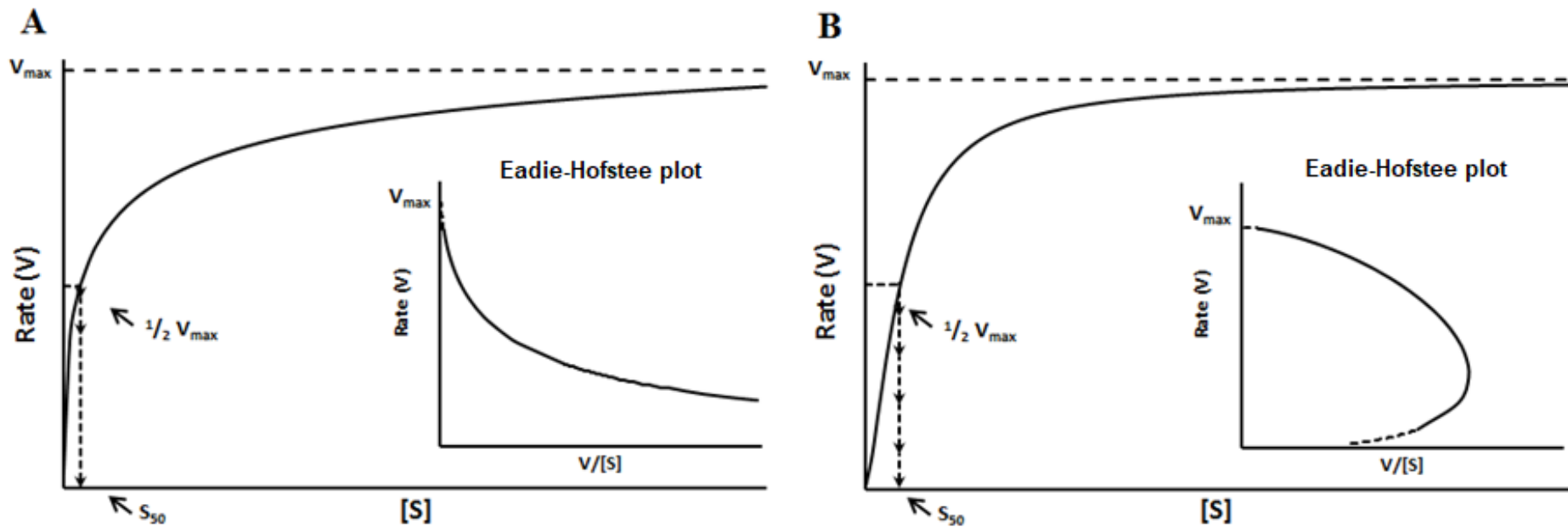


Figure 1. 12: Plot of the rate of product formation (v) versus substrate concentration [S] at a constant enzyme concentration for a single substrate reaction, derived from the Hill equation, with (inset) the corresponding Eadie-Hofstee plots. In this example, $n = 0.5$ (A) for negative co-operativity and $n = 1.5$ (B) for autoactivation.

Substrate inhibition

Apart from positive and negative co-operativity, non-hyperbolic (or ‘atypical’) kinetics may arise from substrate inhibition (Equation 1.3). At low substrate concentrations, a hyperbolic relationship is observed, but the rate decreases from that expected at higher substrate concentrations (Figure 1.13). The Eadie-Hofstee plot is convex and it is apparent that the true V_{\max} is not attained for the reaction due to inhibition at high substrate concentrations (Houston, Kenworthy & Galetin 2003). Ignoring the inhibition observed at high concentrations can lead to incorrect estimates of kinetic parameters (Houston, Kenworthy & Galetin 2003; Miners, Mackenzie & Knights 2010). Substrate inhibition can be considered analogous to an uncompetitive type of inhibition mechanism where V_{\max} is the maximal velocity, K_m is the Michaelis constant ($[S]$ at half V_{\max}), K_{si} is the constant describing the inhibition interaction, and $[S]$ is the substrate concentration (Houston & Kenworthy 2000).

Equation 1. 3: Substrate inhibition (uncompetitive)

$$\text{Rate } (v) = \frac{V_{\max}}{1 + \frac{K_m}{[S]} + \frac{[S]}{K_{si}}}$$

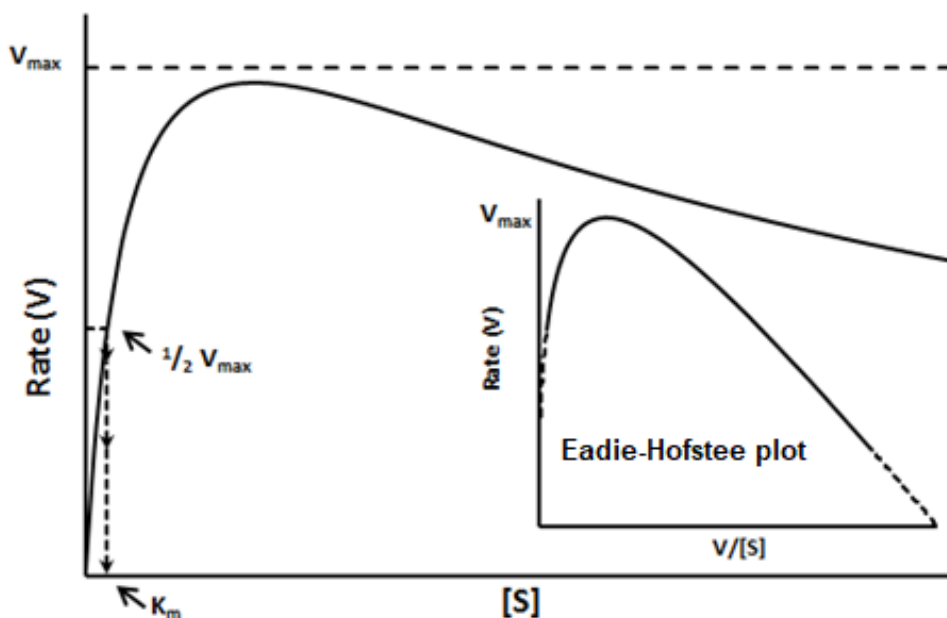


Figure 1.13: Plot of the rate of product formation (v) versus substrate concentration $[S]$ at a constant enzyme concentration for a single substrate reaction, derived from the substrate inhibition equation, with (inset) the corresponding Eadie-Hofstee plot.

In vitro clearance

Intrinsic clearance (CL_{int}) is the parameter employed for describing the efficiency of drug metabolism. For compounds exhibiting Michaelis-Menten and substrate inhibition kinetics, CL_{int} is given as Equation 1.4.

Equation 1.4: Intrinsic clearance

$$CL_{int} = \frac{V_{max}}{K_m}$$

Autoactivation (positive cooperativity, described by the Hill equation with $n > 1$) is characterized by the dependence of clearance on the substrate concentration and requires an alternative to CL_{int} (Houston, Kenworthy & Galetin 2003). Maximal clearance (CL_{max} ; Equation 1.5) provides an estimation of the highest clearance

attained (Houston & Kenworthy 2000). It is derived by differentiating the Hill equation (Equation 1.2) with respect to [S] (Houston & Kenworthy 2000).

Equation 1. 5: Maximal clearance

$$CL_{max} = \frac{V_{max}}{S_{50}} \times \frac{n-1}{n(n-1)^{1/n}}$$

This approach is not applicable to negative co-operativity ($n < 1$). Hence, in this thesis CL_{int} for reactions following negative co-operative kinetics is calculated as the ratio of V_{max} to S_{50} . Clearly, when n approaches 1, S_{50} approximates K_m , and calculation of CL_{int} as V_{max}/S_{50} is valid.

Inhibition kinetics

An inhibitor is a substance that can reduce the rate of an enzyme catalyzed reaction. Inhibition can be reversible or irreversible; only the former is considered here. The most common forms of inhibition are competitive, non-competitive and uncompetitive. Characteristics of each type of inhibition are given in Table 1.8 and shown graphically in Figure 1.14 (Palmer 1995; Segel 1993).

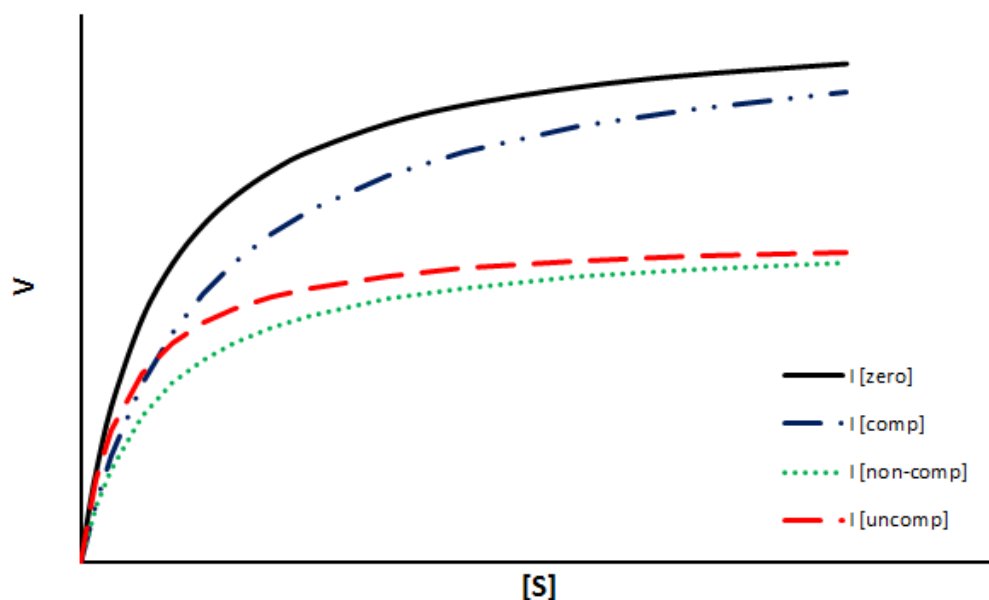


Figure 1. 14: Plot of the rate of product formation (v) versus substrate concentration $[S]$ at a constant enzyme concentration for a single substrate reaction (Michaelis-Menten kinetics) without inhibitor [zero], with a competitive inhibitor [comp], a non-competitive inhibitor [non-comp], and uncompetitive inhibitor [uncomp].

Table 1. 8: Characteristics of competitive, non-competitive and uncompetitive inhibition.

Inhibition type	Inhibitor binding and complexes formed	Effect observed	
		K_m^a	V_{max}
Competitive	Inhibitor competes with substrate for binding in the active site, forming an EI complex	increased	unchanged
Non-competitive	Inhibitor binds at sites distinct to that of the substrate, forming EI and EIS complexes	unchanged	decreased
Uncompetitive	Inhibitor binds to the substrate-bound enzyme (but not to the enzyme itself), forming an EIS complex	decreased	decreased

^a decrease in number reflects an increase enzyme binding 'affinity' and vice versa

E = enzyme, S = substrate, I = inhibitor

EI = enzyme-inhibitor complex

ES = enzyme-substrate complex

EIS = enzyme-inhibitor-substrate complex

Competitive inhibition is the simplest form of reversible inhibition and can be described by Equation 1.6, where $[S]$ is the substrate concentration, V_{max} the maximum

velocity, K_m (Michaelis constant) is the substrate concentration at half V_{max} , $[I]$ is the inhibitor concentration, and K_i the inhibitor constant or the dissociation constant between E and I (when the inhibitor dissociates from the enzyme at equilibrium). As its name suggests, competitive inhibitors compete with the substrate for binding on the enzyme, either at the substrate binding site or elsewhere, rendering the substrate unable to bind to the enzyme due to EI complex formation. This results in decreased enzyme binding affinity for the substrate (apparent as an increase in K_m) without a change in the maximal velocity (V_{max}).

Equation 1. 6: Competitive inhibition

$$\text{Rate } (v) = \frac{V_{max} \times [S]}{K_m \times \left(1 + \frac{[I]}{K_i}\right) + [S]}$$

Non-competitive inhibition can be described mathematically by Equation 1.7 with kinetic parameters as described for Equation 1.6. Non-competitive inhibitors bind randomly at sites distinct to that of the substrate, forming EI and EIS complexes. The total free enzyme concentration is reduced by the inhibitor resulting in decreased maximal velocity (V_{max}), whereas K_m is unaffected.

Equation 1. 7: Non-competitive inhibition

$$\text{Rate } (v) = \frac{V_{max} \times [S]}{\left(1 + \frac{[I]}{K_i}\right) \times (K_m + [S])}$$

Uncompetitive inhibition can be described mathematically by Equation 1.8, with kinetic parameters also as described for Equation 1.6. Unlike competitive or non-competitive inhibitors, uncompetitive inhibitors do not bind to the free enzyme. Binding occurs only to the ES complex, forming the inactive EIS complex. However,

since inhibitor binding is reversible, the EIS complex can dissociate to ES. Thus, both K_m and V_{max} are decreased to the same extent.

Equation 1. 8: Uncompetitive inhibition

$$\text{Rate } (v) = \frac{V_{\max} \times [S]}{K_m + [S] \times \left(1 + \frac{[I]}{K_i}\right)}$$

Dixon plots

Like Eadie-Hofstee plots, Dixon plots are a valuable diagnostic ‘tool’ as they provide a visual means to distinguish between the different inhibition mechanisms (Figure 1.15). At a fixed substrate concentration ($[S]$), a plot of $1/V$ against the inhibitor concentration ($[I]$) is linear. When several plots at different substrate concentrations are combined, the intersection point gives $[I] = -K_i$ for competitive and non-competitive inhibition, but not for uncompetitive inhibition (Figure 1.15).

Other types of inhibitor mechanisms

Sometimes inhibitors do not act by the above mechanisms. Examples include mixed inhibition, partial inhibition, allosteric inhibition, and irreversible inhibition. These types of inhibition mechanisms are beyond the scope of this thesis and will not be discussed further.

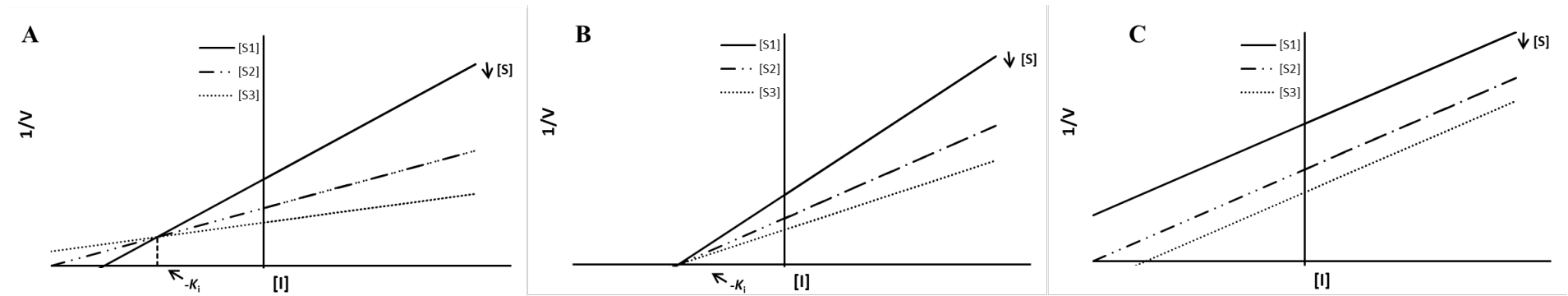


Figure 1. 15: Dixon plots for competitive (A), non-competitive (B) and uncompetitive (C) inhibition at several different substrate concentrations ($[S]$). For each fixed $[S]$, inverse velocity ($1/V$) is plotted against the inhibitor concentration ($[I]$) and the intersection point between these plots determines $[I] = -K_i$ for competitive (intersect in first quadrant) and non-competitive (intersect on x-axis in first quadrant) inhibition.

1.3.2 Measurement of UGT activity *in vitro*

Techniques for predicting *in vivo* drug clearance from *in vitro* kinetic data (*in vitro-in vivo* extrapolation; IV-IVE) are well established in humans and in animal species (Houston & Kenworthy 2000; Miners, Mackenzie & Knights 2010). However, CL_{int} determined *in vitro* frequently under predicts *in vivo* hepatic clearance for both drugs metabolized by CYP and UGT (Boase & Miners 2002; Galetin, Gertz & Houston 2010; Houston & Aleksandra 2008; Miners et al. 2006). For drugs metabolized by UGTs, factors that contribute to the variable predictivity of IV-IVE include the lipophilic membrane environment, the intraluminal localization of UGT proteins, and the need to translocate both cofactor and aglycone across this membrane to the catalytic site for the bi-substrate reaction to occur. Therefore, it is important to understand the various experimental factors that can affect the accuracy of predicting glucuronidation reactions *in vitro*, including; enzyme source (i.e. latency of microsomal UGTs and the need for chemical or physical disruption of the microsomal membrane); the dependence of UGT activity on pH, buffer type, ionic strength, and organic solvents; the stability of glucuronide conjugates, especially acyl glucuronides; cofactor concentration (should be saturating); and the non-specific membrane binding of the substrate (Miners et al. 2010).

Reliable estimates of enzyme kinetic parameters can be affected by other experimental factors. In particular, K_m values for drugs metabolized by UGT1A9, UGT2B4, UGT2B7, and UGT2B10 catalyzed glucuronidation are characteristically overestimated when HLM and recombinant proteins (expressed in HEK293 cells or in insect cells) are used as the enzyme source (Miners et al. 2010). As a consequence of the overestimation of K_m , CL_{int} is underestimated (Equation 1.4). It is now known that

overestimation of K_m arises, at least in part, from an experimental artifact, whereby long chain unsaturated fatty acids released from membranes during the course of an incubation act as potent competitive inhibitors of UGT1A9, UGT2B4, UGT2B7 and several cytochromes P450 (Rowland et al., 2007; Rowland et al., 2008a; Rowland et al., 2008b; J.O. Miners, unpublished data). The inhibitory effect can be reversed by supplementation of incubations with bovine serum albumin (BSA), which sequesters the inhibitory fatty acids. Thus, K_m and CL_{int} values generated in the presence of BSA represent ‘true’ hepatocellular values (Rowland et al. 2008a; Rowland et al. 2007; Rowland et al. 2008b). As drug glucosidation is a less well characterized pathway, it was not known until more recently if and/or how the addition of BSA would impact on this glycosidation pathway and estimates of kinetic parameters (Chau et al. 2014). These are important experimental considerations when conducting reaction phenotyping experiments to identify the enzyme(s) involved in the metabolism of a given compound, particularly when characterizing novel metabolites and/or pathways (Miners, Mackenzie & Knights 2010; Miners et al. 2010; Zientek & Youdim 2015). Similar considerations apply to the determination of the inhibition constant (K_i) *in vitro*, that is the non-specific binding of the inhibitor to the enzyme source and ‘competing’ inhibition by long chain unsaturated fatty acids should be accounted for (Miners et al. 2010).

Reaction phenotyping

As indicated above, the *in vitro* identification of the enzyme(s) involved in the metabolism of a given compound requires careful consideration of many factors. The protein source of choice utilized are HLM or hepatocytes as they express the full range of hepatic enzymes (UGTs and CYPs). Several approaches are available (Miners, Mackenzie & Knights 2010):

- 1) Reduction in the metabolism (i.e. glucuronidation) of the test compound by an enzyme-selective chemical and antibody inhibitor/s.
- 2) Inhibition (competitive) of metabolism (i.e. glucuronidation) with an enzyme-selective substrate by the test compound with K_i matching its known K_m .
- 3) Significant correlation between rates of metabolism (i.e. glucuronidation) of the test compound and the immunoreactive enzyme content or activity in microsomes/hepatocytes from a panel of human livers.
- 4) Screening for metabolism by a range of recombinant enzymes (i.e. UGTs) with comparison of the K_m values for metabolism (i.e. glucuronidation) by the individual enzymes and HLM/hepatocytes.

The reduction in metabolism (i.e. glucuronidation) of any given compound by enzyme-selective chemical inhibitors is the most powerful approach for selective identification of the UGT enzyme(s) responsible for conjugation, with the extent of the decrease giving the contribution of that enzyme to overall metabolism. Furthermore, combining several approaches together (e.g. complementing approach (2) with UGT enzyme-selective inhibitors and (4) by screening activity with a battery of recombinant UGTs) is considered the most definitive approach for reaction phenotyping glucuronidation reactions (Miners, Mackenzie & Knights 2010). This method provides strong evidence for the involvement of specific UGT enzyme(s) and, therefore, allows identification of the UGT enzyme(s) responsible for the metabolism of a compound with greater certainty. However, as previously mentioned, there are only a limited number of UGT enzyme-selective inhibitors identified compared to probe substrates (Section 1.1.5 and Table 1.2). Thus, it is generally necessary to combine multiple approaches to the reaction phenotyping of drug and chemical glucuronidation (and glucosidation).

1.4 Experimental Aims

Glucosidation is a poorly characterized metabolic pathway in humans. Knowledge gained from further studies of drug glucosidation will contribute to increasing the overall understanding of drug and chemical metabolism pathways in humans and how glucosidation might contribute to population variability in drug elimination, and in turn, potentially influence the therapeutic efficacy and safety of drug treatment in patients. Although drug glucosidation is an under characterized drug metabolism pathway in comparison to glucuronidation, there are an increasing number of studies demonstrating the relevance of this pathway in the metabolism of novel and ‘old’ drugs. The central hypothesis drawn from the review of the literature is that human glucosidation and glucuronidation are complementary pathways carried out by common UGT enzymes. Thus, the overarching aim of this thesis is to characterize the enzymology of human drug and chemical glucosidation. This aim will be achieved in three Parts.

Part I: Characterization of the enzymology of morphine (Chapter 3) and mycophenolic acid (Chapter 5) glucosidation. Morphine and mycophenolic acid are widely used drugs; the former an analgesic, the latter as an immunosuppressant. It is hypothesized that UGT2B7 and UGT1A9 are the main enzymes involved in both the glucuronidation and glucosidation morphine and mycophenolic acid. **Part II:** Elucidation of the molecular mechanism of cofactor (UDP-GlcUA and UDP-Glc) binding to UGT2B7 using automated *in silico* docking with a 3-D homology model, and validation by site-directed mutagenesis (Chapter 4). **Part III:** Investigation of the ability of the native UDP-glycosyltransferases of insect cell lines commonly used to express recombinant human UDP-glycosyltransferases to catalyze drug and chemical glucosidation (Chapter 6).

Chapter 2

Materials and general methods

2.1 Materials

2.1.1 Chemicals and reagents

In vitro incubations and protein determination

Table 2.1 and 2.2 lists the suppliers of the chemicals and reagents used in the experiments described in this thesis.

Table 2. 1: Suppliers of the chemicals and reagents used in the biochemical and analytical procedures conducted in this thesis.

Chemical or Reagent	Supplier
Acetic acid (glacial)	BDH Laboratory Supplies, Poole, UK
Acetonitrile (HPLC grade)	Merck KGaA, Darmstadt, Germany
Alamethicin (from <i>Trichoderma viride</i>)	A.G. Scientific, Inc., San Diego, California, USA
Ammonium acetate	Merck KGaA, Darmstadt, Germany
Ascorbic acid	AJAX Finechemicals, Sydney, NSW, Australia
Benzocaine	Toronto Research Chemicals, North York, Ontario, Canada
Benzocaine N- β -D-glucoside	Dalton Pharma Services, Toronto, Ontario, Canada
Bovine serum albumin	Sigma Aldrich, Sydney, NSW, Australia
Calcium chloride	AJAX Finechemicals, Sydney, NSW, Australia
Codeine	Sigma Aldrich, Sydney, NSW, Australia
Codeine 6- β -D-glucuronide	Toronto Research Chemicals, North York, Ontario, Canada

Chemical or Reagent	Supplier
Copper sulfate pentahydrate	BDH Laboratory Supplies, Poole, UK
Deoxycorticosterone 21- β -D-glucoside (21-hydroxyprogesterone β -D-glucoside)	Sigma Aldrich, Sydney, NSW, Australia
Dimethyl sulfoxide (DMSO)	Merck KGaA, Darmstadt, Germany
Di- Potassium hydrogen orthophosphate	Chem Supply, Gillman, SA, Australia
Di-Sodium hydrogen orthophosphate	AJAX Finechemicals, Sydney, NSW, Australia
Fluconazole	Pfizer Australia, Sydney, NSW, Australia
Hecogenin	Sigma Aldrich, Sydney, NSW, Australia
Hydrochloric acid	BDH Laboratory Supplies, Poole, UK
20-Hydroxyecdysone	Selleckchem, Houston, USA
21-Hydroxyprogesterone	Sigma Aldrich, Sydney, NSW, Australia
1-Hydroxypyrene	Sigma Aldrich, Sydney, NSW, Australia
1-Hydroxypyrene β -D-glucuronide	Toronto Research Chemicals, North York, Ontario, Canada
Lamotrigine	The Wellcome Foundation Ltd, London, UK
Lamotrigine N2- β -D-glucuronide	The Wellcome Foundation Ltd, Beckenham, UK
Magnesium chloride (hexahydrate)	BDH Laboratory Supplies, Poole, UK
Magnesium sulphate	Merck KGaA, Darmstadt, Germany
Manganese chloride	Astral Scientific, Sydney, NSW, Australia
Methanol	Sigma Aldrich, Sydney, NSW, Australia
4-Methylumbelliferone	Sigma Aldrich, Sydney, NSW, Australia
4-Methylumbelliferone β -D-glucoside	Sigma Aldrich, Sydney, NSW, Australia
4-Methylumbelliferone β -D-glucuronide	Sigma Aldrich, Sydney, NSW, Australia
Morphine hydrochloride	GlaxoSmithKline, Melbourne, Vic, Australia
Morphine 3- β -D-glucuronide	Sigma Aldrich, Sydney, NSW, Australia
Morphine 6- β -D-glucuronide	Salford Ultrafine Chemicals, Manchester, UK

Chemical or Reagent	Supplier
Mycophenolic acid	Toronto Research Chemicals, North York, Ontario, Canada
Mycophenolic acid acyl β -D-glucoside	Toronto Research Chemicals, North York, Ontario, Canada
Mycophenolic acid acyl β -D-glucuronide	Roche, gift from Dr. Betty Sallustio (The Basil Hetzel Institute, The Queen Elizabeth Hospital)
Mycophenolic acid phenolic β -D- glucoside	Toronto Research Chemicals, North York, Ontario, Canada
Mycophenolic acid phenolic β -D- glucuronide	Roche Colorado Corporation, Boulder, Colorado, USA
1-Naphthol	Toronto Research Chemicals, North York, Ontario, Canada
1-Naphthol β -D-glucuronide	Sigma Aldrich, Sydney, NSW, Australia
S-Naproxen	Sigma Aldrich, Sydney, NSW, Australia
Niflumic acid	E.R. Squibb & Sons, Inc., Princeton, New Jersey, USA
4-Nitrophenol	Toronto Research Chemicals, North York, Ontario, Canada
4-Nitrophenyl β -D-glucoside	Molekula Limited, Gillingham, Dorset, UK
1-Octanesulfonic acid sodium salt (98%)	Sigma Aldrich, Sydney, NSW, Australia
Orthophosphoric acid (85%)	Merck KGaA, Darmstadt, Germany
Perchloric acid (70%)	Sigma Aldrich, Sydney, NSW, Australia
Phenethyl alcohol	Toronto Research Chemicals, North York, Ontario, Canada
Phenethyl β -D-glucoside	Toronto Research Chemicals, North York, Ontario, Canada
Potassium acetate	AJAX Finechemicals, Sydney, NSW, Australia
Potassium chloride	BDH Laboratory Supplies, Poole, UK
Potassium di-hydrogen orthophosphate	Chem Supply, Gillman, SA, Australia

Chemical or Reagent	Supplier
Potassium hydroxide	AJAX Finechemicals, Sydney, NSW, Australia
Sodium chloride	Chem Supply, Gillman, SA, Australia
Sodium carbonate	Chem Supply, Gillman, SA, Australia
Sodium hydrogen carbonate	Chem Supply, Gillman, SA, Australia
Sodium hydroxide	BDH Laboratory Supplies, Poole, UK
Sodium tartrate dihydrate	BDH Laboratory Supplies, Poole, UK
Triethylamine	Sigma Aldrich, Sydney, NSW, Australia
Trifluoroperazine	Sigma Aldrich, Sydney, NSW, Australia
Trifluoroacetic acid	Sigma Aldrich, Sydney, NSW, Australia
UDP-Glucose (disodium salt) from <i>Saccharomyces cerevisiae</i>	Sigma Aldrich, Sydney, NSW, Australia
UDP-Glucuronic acid (trisodium salt)	Sigma Aldrich, Sydney, NSW, Australia
Zidovudine	Sigma Aldrich, Sydney, NSW, Australia
Zidovudine β -D-glucuronide	Sigma Aldrich, Sydney, NSW, Australia

Molecular biology and cell/tissue culture

Table 2. 2: Suppliers of chemicals and reagents used in the molecular biology procedures conducted in this thesis.

Chemical or Reagent	Supplier
Bioline dNTP Set (dATP, dGTP, dCTP, dTTP)	Astral Scientific, Taren Point, NSW, Australia
1kb DNA Ladder	New England Biolabs, United Kingdom
Puromycin, ammonium persulphate (APS), β -mercaptoethanol (BME), ColorBurst™ Electrophoresis protein marker, ethidium bromide, Tris-base, trypan blue, Tween-20, N-Z-Amine® (casein hydrolysate), 4-morpholinepropanesulfonic acid (MOPS), glucose, glycine	Sigma-Aldrich, Sydney, NSW, Australia
30% Acrylamide/bis solution 19:1 (5% C), bromophenol blue, Trans-Blot® Transfer nitrocellulose, Precision Plus Protein™ WesternC™ Standards, Coomassie Brilliant Blue R-250	BIO-RAD, Life Science, Sydney, NSW, Australia

Chemical or Reagent	Supplier
HyClone SFX-Insect Cell Culture Medium (serum free), foetal bovine serum	HyClone Laboratories Inc., Logan, UT, USA
Bacto-agar, bacto-tryptone, yeast extract	US Biologicals, Salem, MA, USA
Ethylenediaminetetraacetic (EDTA), sodium dodecyl sulphate (SDS)	Merck (BDH), Kilsyth, Vic, Australia
Dulbecco's Modified Eagle Medium (DMEM), Lipofectamine™ 2000, MEM non-essential amino acids, MEM sodium pyruvate, peptone, Opti-MEM PLUS reagent, Penicillin Streptomycin (Pen Strep)	Invitrogen, Mount Waverley, VIC, Australia
Rubidium chloride (RbCl), tetramethylethylenediamine (TEMED), ampicillin, glycerol, agarose	Amresco, Cleveland, OH, USA
Sucrose	Chem Supply, Gillman, SA, Australia
BM Chemiluminescence Blotting Substrate (POD)	Roche Diagnostics Deutschland GmbH, Mannheim, Germany
Xylene cyanol FF	Pharmacia, Rydalmere, NSW, Australia
Skim milk powder	Bonland Dairies, Rowville, Vic, Australia

2.1.2 Equipment

Table 2.3 lists the equipment and the respective manufacturers used to perform the experimental procedures conducted in this thesis.

Table 2. 3: Equipment used in experimental procedures.

Equipment and Model	Manufacturer
Series 1100 HPLC; auto sampler, degasser, quaternary pump, thermostat column compartment, fluorescence detector	Agilent Technologies, Mulgrave, Vic, Australia
Series 1200 HPLC; auto sampler, degasser, quaternary pump, thermostat column compartment, UV detector	Agilent Technologies, Mulgrave, Vic, Australia
Column: C18 Waters Nova-Pak 4µm (3.9×150mm)	Waters Corporation, Milford, MA, USA

Equipment and Model	Manufacturer
Column: Phenomenex Synergi HydroRP C18 4 μ m (3.0 \times 150mm)	Phenomenex Inc., Lane Cove, NSW, Australia
Column: Zorbax Eclipse XDB-C8 5 μ m (4.6 \times 150mm)	Agilent Technologies, Mulgrave, Vic, Australia
Column: Beckman Ultrasphere ODS 5 μ m (4.6 \times 250mm)	Beckman Instruments, Fullerton, CA, USA
Waters ACQUITY™ Ultra Performance Liquid Chromatography (UPLC™) system coupled to a Waters Micromass Q-TOF Premier™ mass spectrometer	Waters Corporation Micromass UK Ltd., Manchester, UK
Column: ACQUITY UPLC® HSST3 1.8 μ m (2.1 \times 100 mm)	Waters Corporation, Milford, MA, USA
Microfuge® 18 bench top centrifuge	Beckman Instruments, Krefeld, Germany
Sigma 4K15 refrigerated table top centrifuge	Sigma Laborzentrifugen GmbH, Osterode am Harz, Germany
J2-21M/E centrifuge, L8-70M Ultracentrifuge	Beckman Instruments, Krefeld, Germany
Innova™ 4330 refrigerated incubator shaker	New Brunswick Scientific Co Inc., Edison, NJ, USA
Thermomixer Comfort 96-well plate shaker	Eppendorf South Pacific Pty. Ltd., Macquarie Park, NSW, Australia
Plate incubator (agar; 37°C)	Scientific Equipment Manufacturers Pty. Ltd., Magill, SA, Australia
Inverted microscope (CK2)	OLYMPUS, Macquarie Park, NSW, Australia
Hy-Lite Haemocytometer	Hausser Scientific, Horsham, PA, USA
Gene Genius Bio Imaging System and GeneSnap software (version 6.04)	SYNGENE, Cambridge, UK
LAS-400 Imager (Chemiluminescence) and Multi Gauge software	Fujifilm, Brookvale, NSW, Australia
Cary 300 UV-VIS spectrophotometer	Varian Australia Pty. Ltd., Mulgrave, Vic, Australia
Pharmacia Biotech GeneQuant II	GE Healthcare, Amersham, UK
ABI 3130-XL DNA sequencer	Applied Biosystems, Mulgrave, Vic, Australia
Perkin Elmer 3000 fluorescence spectrophotometer	Perkin Elmer, Waltham, MA, USA
Mini-Protean® III Cell (PAGE), Mini-Sub® Cell GT (AGE)	BIO-RAD Laboratories Pty. Ltd., Gladesville, NSW, Australia
Robocycler® Gradient 96 PCR machine	Stratagene, La Jolla, CA, USA

Equipment and Model	Manufacturer
DNA Thermal Cycler 480	Perkin Elmer Inc, Waltham, Massachusetts, USA
Vibra Cell VCX 130 Ultrasonics Processor	Sonics and Materials, Newton, CT, USA
Shimaden incubator	ADELAB SCIENTIFIC, Thebarton, SA, Australia
Ratek Instruments orbital shaker and incubator	ADELAB SCIENTIFIC, Therbarton, SA, Australia
SANYO CO ₂ Incubator (MCO-18AIC)	VWR International Pty Ltd, Tingalpa, QLD, Australia

2.1.3 General stock solutions, buffers, media, broths and agar

In vitro incubations and protein determination

Stock solutions were prepared according to Table 2.4 and diluted as required for *in vitro* incubations and total protein determination according to Lowry et al. (1951).

Table 2. 4: Stock solutions required for *in vitro* incubations and total protein determination.

Stock solutions	Preparation
40mM Magnesium chloride	8.13mg MgCl ₂ / ml distilled water
1M Potassium hydroxide	56.11mg KOH/ ml distilled water
1M di-Potassium hydrogen orthophosphate	228.23mg K ₂ HPO ₄ .3H ₂ O/ ml distilled water
1M Potassium dihydrogen orthophosphate	136.09mg KH ₂ PO ₄ .3H ₂ O/ ml distilled water
1M Phosphate buffer pH 6.8	49.7% 1M K ₂ HPO ₄ with 50.3% 1M KH ₂ PO ₄
1M Phosphate buffer pH 7.4	80.2% 1M K ₂ HPO ₄ with 19.8% 1M KH ₂ PO ₄
Lowry solution A	4g NaOH and 30g Na ₂ CO ₃ in 1L distilled water
Lowry solution B	16g sodium tartrate.2H ₂ O in 1L distilled water
Lowry solution C	8g CuSO ₄ .5H ₂ O in 1L distilled water
Lowry reagent	Solutions A, B and C in ratio 100:1:1
10mM Niflumic acid	2.822mg NFA/mL DMSO
1mM Hecogenin	0.4306mg Hec/mL methanol

Stock solutions	Preparation
25mM Fluconazole	7.656mg Fluc/mL 25mM H ₃ PO ₄ /distilled water
100μM Morphine 3-glucoside	0.044 mg M3Glc/mL distilled water
20μM Morphine 6-glucuronide	0.0092 mg M6G/mL distilled water
10mM 4-Methylumbelliferone	1.982mg 4MU/mL distilled water
1mM 4-Methylumbelliferone glucoside	0.338mg 4MUGlc/mL distilled water
4-Methylumbelliferone glucuronide	0.352mg 4MUGlcUA/mL distilled water
50mM Trifluoperazine	24.020mg TFP/mL distilled water
30mM Lamotrigine	7.682mg LTG/mL 10% acetonitrile/1M H ₃ PO ₄ /distilled water
1mM Lamotrigine N-glucuronide	0.436mg LTG-GlcUA/mL distilled water
20mM Codeine	5.987mg COD/mL 88.2mM H ₃ PO ₄ /0.1M phosphate buffer pH 7.4
1mM Codeine 6-glucuronide	0.475mg COD-GlcUA/mL distilled water
50mM S-Naproxen	12.610mg S-NAP/mL distilled water
50mM Zidovudine	13.362mg AZT/mL distilled water
1mM Zidovudine glucuronide	0.443mg AZT-GlcUA/mL distilled water
250mM 1-Naphthol	36.042mg 1-NAP/mL DMSO/water (50/50)
1mM 1-Naphthol glucuronide	0.342mg 1-NAP/mL distilled water
50mM 4-Nitrophenol	6.955mg 4-NP/mL methanol
10mM 4-Nitrophenol glucoside	3.012mg 4-NPGlc/mL methanol
50mM Phenethyl alcohol	6.108mg PE/mL distilled water
1mM Phenethyl glucoside	0.2843mg PEGlc/ ml distilled water
500mM 21-Hydroxyprogesterone	165.23mg 21-OHP/mL methanol
10mM 21-Hydroxyprogesterone glucoside	4.926mg 21-OHPGlc/mL methanol
4mM 1-Hydroxypyrene	0.873mg 1-OHP/mL DMSO
2mM 1-Hydroxypyrene glucuronide	0.78868mg 1-OHPGlcUA/mL DMSO
100μM 1-Hydroxypyrene glucuronide	diluted with 10% DMSO in distilled water from 2mM 1-OHPGlcUA stock
10mM 20-Hydroxyecdysone	4.806mg 20-E/mL methanol
50mM Benzocaine	8.259mg BZC/mL methanol
10mM Benzocaine N-glucoside	3.273mg BZCGlc/mL methanol
1mM Mycophenolic acid phenolic glucoside	0.482mg MPAGlc/mL distilled water
1mM Mycophenolic acid phenolic glucuronide	0.496mg MPAGlcUA/mL distilled water

Chapter 2: Materials and general methods

Stock solutions	Preparation
2.5mM Mycophenolic acid acyl glucoside	1.206mg AcMPAGlc/mL methanol
2.5mM Mycophenolic acid acyl glucuronide	1.241mg AcMPAGlcUA/mL methanol
200mM Mycophenolic acid	64.068mg MPA/mL DMSO

Molecular biology and cell/tissue culture

Buffers, media and broths were prepared according to Table 2.5 and used as required for molecular biology techniques. Sterile buffers and solutions (either by autoclaving at 121 °C or ultra-filtration through 0.2-0.45µm filters) were prepared according to the methods outlined by Sambrook and Russell (2001).

Table 2. 5: Buffers, media, broths and agar used for molecular biology and protein techniques, including cloning, culturing (mammalian, insect and bacterial), gel electrophoresis and Western blotting.

Solutions	Preparation
1 x Phosphate-buffered saline (PBS) pH 7.4	137mM/8g NaCl 2.7mM/0.2g KCl 10mM/1.44g Na ₂ HPO ₄ 2mM/0.24g KH ₂ PO ₄ 800mL distilled water (pH 7.4, HCl) then top up with additional 200mL (total 1L)
6 x DNA gel loading dye buffer	0.25% (w/v) bromophenol blue 0.25% (w/v) xylene cyanol FF 30% (v/v) glycerol
1 x Tris-acetate EDTA (TAE) buffer	10mM Tris-HCl, pH 7.5 1mM EDTA
1 x Tris-acetate EDTA (TAE) electrophoresis buffer	40mM Tris-acetate 1mM EDTA
1% (w/v) agarose gel (+ 0.25 µg/mL EtBr)	0.4g agarose 40mL TAE buffer 1µL ethidium bromide (10mg/mL)
DMEM incomplete media	133.7 g DMEM powder 37g NaHCO ₃ 200mL Penicillin (+5,000 Units/mL)/ Streptomycin (+5,000 µg/mL) 100mL MEM Non-essential amino acids (100x) 100mL MEM sodium pyruvate (100mM;100x) 10L distilled water in conical flask pH 7.4 (HCl if required) then filter sterilize
DMEM complete media	900mL DMEM incomplete media 100mL FBS
HEK293T frozen cell stock solution	5mL/10% DMSO 45mL/90% FBS
SFX insect complete media	930mL SFX insect media (serum-free) 50mL FBS

Solutions	Preparation
	20mL Penicillin (+5,000 Units/mL)/ Streptomycin (+5,000 µg/mL)
Insect media for frozen cell stock	30mL/60% SFX insect media (serum-free) 15mL/30% FBS 5mL/10% DMSO
Lauria-Bertani (LB) broth	10g bacto-tryptone 5g yeast extract 5g NaCl 1g sucrose 1L distilled water, pH 7.0 (10mM NaOH)
Lauria-Bertani (LB) agar	1L LB broth 14g bacto-agar
NZY ⁺ amine broth	10g NZ amine (casein hydrolysate) 5g yeast extract 5g NaCl 1L distilled water, pH 7.5 (10mM NaOH)
RF1 buffer pH 5.8	100mM rubidium chloride 50mM manganese chloride 30mM potassium acetate 10mM calcium chloride 15% w/v glycerol
RF2 buffer	10mM MOPS 10mM rubidium chloride 75mM calcium chloride 15% w/v glycerol
Western Blot	
1.5 M Tris-HCl pH 8.8	27.23g Tris-base, pH 8.8 (1M HCl) with 80mL distilled water then top up with additional 70mL (total 150mL)
0.5 M Tris-HCl pH 6.8	6g Tris-base, pH 6.8 (1M HCl) with 60mL distilled water then top up with additional 40mL (total 100mL)
10% (w/v) SDS	1g SDS, 10mL distilled water
10% (w/v) APS	0.1g APS, 1mL distilled water
Sample buffer	4mL distilled water 1mL 0.5M Tris-HCl pH 6.8 0.8mL glycerol 1.6mL 10% (w/v) SDS 0.4mL 2-β-mercaptoethanol 0.2mL 0.05% (w/v) bromophenol blue
4% Stacking gel (set of 2 x 1.5mm thick)	6mL distilled water 2.5mL 0.5M Tris-HCl pH 6.8 100µL 10% (w/v) SDS 1.34mL 30% Acrylamide/Bis Solution (19:1) 50µL 10% (w/v) APS 24µL TEMED

Solutions	Preparation
10% Separating gel (set of 2 x 1.5mm thick)	8mL distilled water 5mL 1.5M Tris-HCl pH 8.8 200µL 10% (w/v) SDS 6.72mL 30% Acrylamide/Bis Solution (19:1) 100µL 10% (w/v) APS 80µL TEMED
Running buffer	25mM/12.11g Tris-base 192mM/57.65g glycine 3.5mM/4.05g SDS 4L distilled water
Transfer buffer	25mM/12.11g Tris-base 192mM/57.65g glycine 800mL 20% methanol 3.2L distilled water
Tris-buffered saline (TBS)	50mM/24.22g Tris-base 37.5mM/8.76g NaCl 4L distilled water pH 7.4 (1M HCl)
Tris-buffered saline + Tween20 (TBST)	1L TBS, 2mL Tween20
3% Membrane blocking solution	1.5g skim milk powder, 50mL TBS
2% Antibody incubation solution	1g skim milk powder, 50mL TBST
Coomassie gel-stain	0.1% Coomassie Blue (R250) 45% methanol 10% acetic acid water
Coomassie gel-destain	45% methanol 10% acetic acid water

2.1.4 Analytical and preparative kits

Table 2.6 shows the analytical and preparative kits used in this thesis, together with the respective suppliers.

Table 2. 6: Analytical and preparative kits used in the experimental procedures.

Kit	Supplier
QIAprep® Spin Miniprep Kit, QIAquick® Gel Extraction Kit, QIAquick® PCR Purification Kit, Plasmid Midi and Maxi Kit	QIAGEN Pty. Ltd., Chadstone, Vic, Australia

Bioline ISOLATE DNA Kit	Astral Scientific, Taren Point, NSW, Australia
QuikChange® II Site-Directed Mutagenesis Kit	Stratagene, La Jolla, CA, USA

2.1.5 Enzymes

Table 2.7 shows the commercial enzymes used in this thesis and their respective suppliers. All enzymes were supplied free of nucleases.

Table 2. 7: Enzymes used in the experimental procedures.

Enzyme	Buffer	Supplier
Antarctic phosphatase	AP unique	New England Biolabs, Ipswich, MA, USA
<i>XbaI</i> + <i>XhoI</i> (double)	#4	
<i>XbaI</i> , <i>XhoI</i> , <i>DpnI</i>	#4	
T4 DNA Ligase	T4	Promega Corporation, Madison, WI, USA
<i>Pfu</i> Ultra II Hot Start Fusion Polymerase	<i>Pfu</i> Ultra HS II	Stratagene, La Jolla, CA, USA

2.1.6 Antibodies

Table 2.8 shows the antibodies used in this thesis and their respective suppliers.

Table 2. 8: Primary and secondary antibodies used in the experimental procedures.

Antibody	Supplier
Rabbit anti-human UGT2B7 (polyclonal) primary antisera ('MACK 3')	Department of Clinical Pharmacology, Flinders University (Kerdpin et al. 2009)
ImmunoPure [®] Antibody goat anti-Rabbit IgG (H+L) secondary HRP-conjugated IgG	ImmunoPure, Thermo Scientific, MA, USA

2.1.7 Plasmid DNA

The shuttle and mammalian expression vectors, pBluescript II SK(+) (Agilent Technologies, Santa Clara, CA, USA) and pEF-IRES-puro 5 (Clontech Laboratories, Inc., CA, USA), respectively, were used to clone and express human wild-type and mutant UGT2B7 cDNAs (Figure 2.1 and 2.2). Both vectors confer ampicillin resistance and hence selection was achieved with 100µg/mL ampicillin.

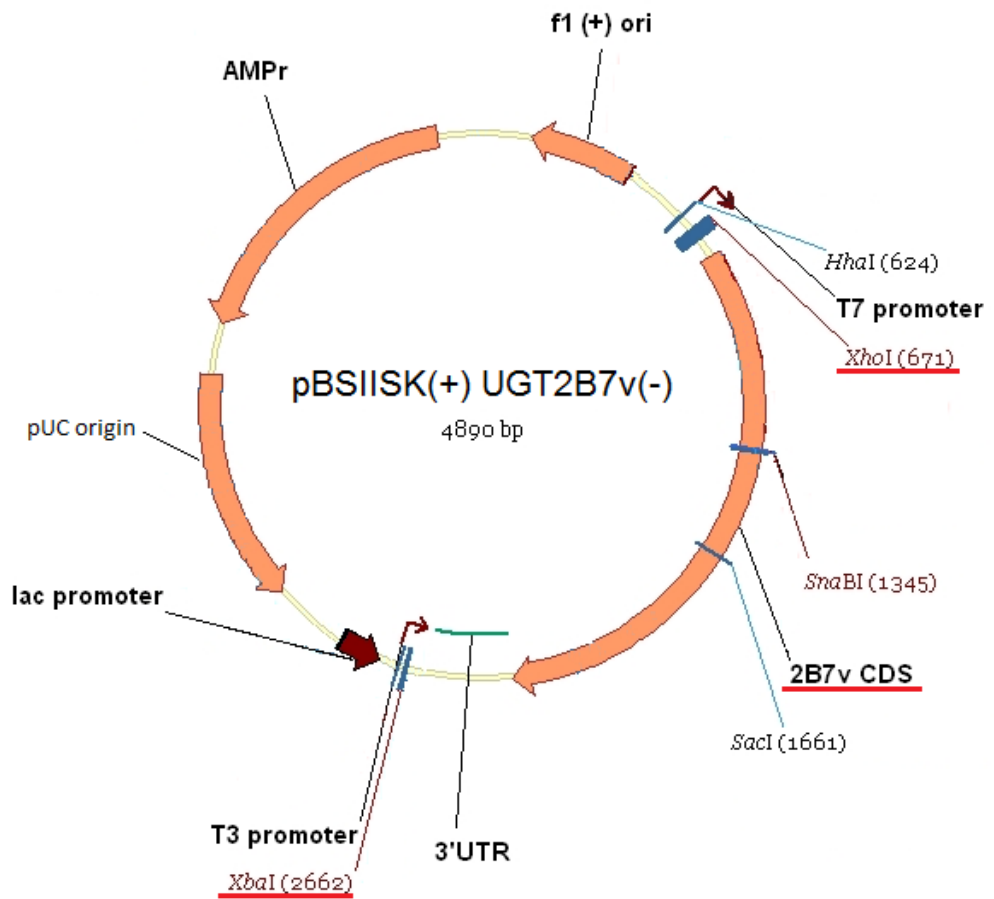


Figure 2. 1: Restriction map of UGT2B7 cDNA inserted into pBluescript II SK(+).

Relevant restriction sites (*XbaI* and *XhoI*) used during cloning. UGT2B7 cDNA, *XbaI* and *XhoI* are underlined in red.

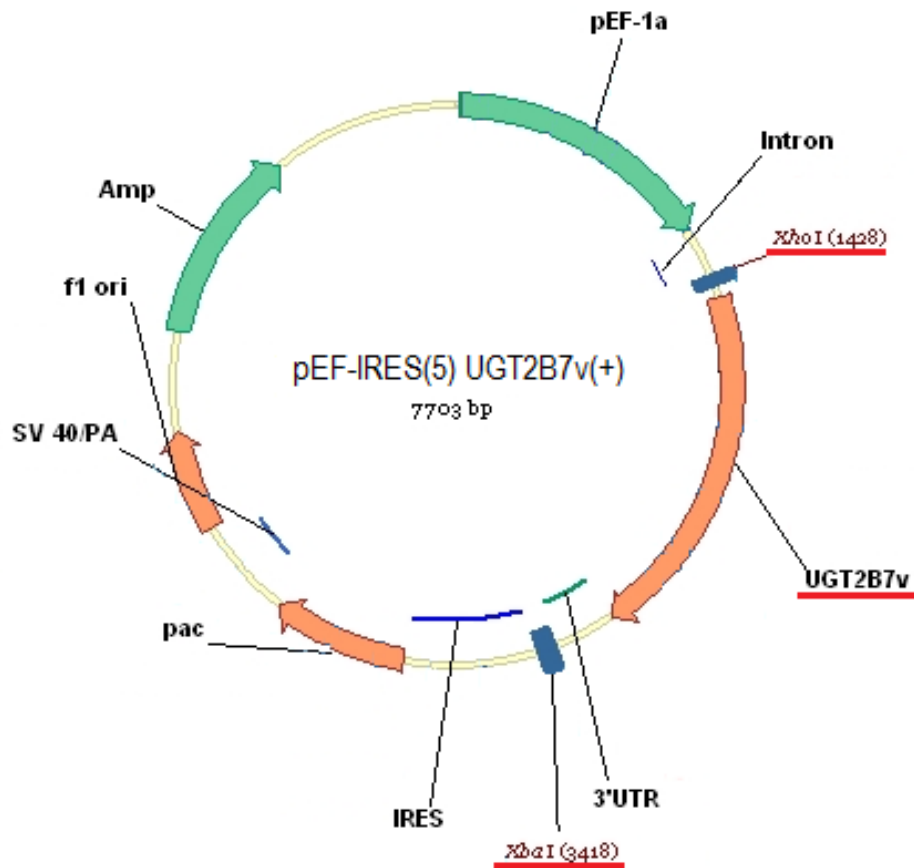


Figure 2. 2: Restriction map of UGT2B7 cDNA inserted into pEF-IRES-puro 5.

Relevant restriction sites (XbaI and XhoI) used during cloning. UGT2B7 cDNA, XbaI and XhoI are underlined in red.

Human UGT2B7 cDNA

The UGT2B7 cDNA used in this thesis refers to UGT2B7*2 (GenBank accession no. NM_001074.2) where a C to T transversion at nucleotide 802 (802C>T) translates to a tyrosine (Y) at position 268 (Bhasker et al. 2000; Jin et al. 1993). UGT2B7(*2) was cloned initially in this laboratory (Jin et al. 1993).

2.1.8 Bacterial, insect and mammalian cells

Table 2.9 shows the cell lines used in this thesis and their respective suppliers. DH5 α cells are a K-12 strain of *E. coli* while Sf9 cells are clonal isolates from the parent insect *Spodoptera frugiperda* cell line IPLB-Sf-21-AE, which is commonly used for the expression of recombinant proteins using the baculovirus expression vector system (BEVS). HEK293T cells (ATCC® CRL-3216™) are derived from human embryonic kidney epithelial cells containing the SV40 T-antigen, which makes it competent for replicating vectors carrying the SV40 region of replication such as with pEF-IRES-puro 5.

Table 2. 9: Cell lines used in experimental procedures.

Cell line	Supplier
DH5 α	Life Technologies, Mulgrave, VIC, Australia
Sf9	Life Technologies, Mulgrave, VIC, Australia
HEK293T	American Type Culture Collection, Manassas, VA, USA

2.1.9 Software for in silico chemistry, protein docking and data analysis

Table 2.10 shows all software programs used in this thesis and their respective suppliers. All molecular docking, kinetic modelling, statistical and chemistry software was licensed according to the conditions relating to use by an academic institution.

Table 2. 10: Molecular docking, kinetic modelling, statistical and chemistry software used in experimental procedures and data analysis.

Program	Developer
Vector NTi v9.0	Invitrogen, Mt Waverley, Vic, Australia
Marvin View 5.3.8	Chem Axon, Budapest, Hungary
ChemSketch 12.0	Advanced Chemistry Development, Inc., Toronto, ON, Canada

Program	Developer
SYBYL-X 1.1.2 Surflex-Dock	Tripos, St Louis, MO, USA
EnzFitter®	Biosoft, Cambridge, UK
SPSS v19.0	SPSS Inc., Chicago, IL, USA
RCSB PDB Ligand Explorer 3.8	www.rcsb.org/pdb/ , Berman et al. (2000)
ClustalX 2.0.12	www.clustal.org , Larkin et al. (2007)
ClustalW2	www.ebi.ac.uk/Tools/phylogeny/clustalw2_phylogeny/

2.2 General Methods

2.2.1 Molecular biology techniques

Bacterial strains

Freshly prepared DH5 α competent cells (Hanahan 1985) were used for routine DNA manipulation of UGT2B7 wild-type and mutant constructs for their heterologous expression in HEK293 cells. Briefly, DH5 α cells were streaked from a 40% glycerol stock onto a Lauria-Bertani (LB) agar plate (antibiotic-free; Table 2.5) and incubated overnight at 37°C. A single colony was isolated and subcultured in 5mL NZY⁺ broth (antibiotic-free; Table 2.5) with orbital shaking (220rpm; InnovaTM 4330, Table 2.3) at 37°C for 16hr. The subculture was then used to inoculate pre-warmed 100mL LB broth (antibiotic-free; Table 2.5) at 1:100 dilutions in 500mL conical flasks. Cultures were grown to an optical density of 0.3-0.5AU at 600nm, transferred to sterile falcon tubes and placed on ice for 10min prior to centrifugation at 1,610g (Sigma 4K15; Table 2.3) for 10min at 4°C. The supernatant fraction was decanted and the cell pellet resuspended in 30mL of RF1 buffer pH 5.8 (Table 2.5), followed by incubation on ice for 45min. Cells were then pelleted at 3,007g (Sigma 4K15; Table 2.3) for 10min at 4°C, the supernatant fraction decanted, and the cell pellets resuspended in RF2 buffer (Table 2.5) to a final volume of 8mL. The cell suspension was incubated on ice for

Chapter 2: Materials and general methods

10min and then aliquoted (100 μ L) into sterile 1.5mL tubes. All tubes were snap frozen in a bath of dry ice and ethanol and stored at -80°C.

Transformation of competent *E. coli* cells

DH5 α competent cells were thawed on ice and a 40 μ L aliquot transferred to a pre-chilled sterile 1.5mL tube. Whole plasmids (0.5 μ L; ~25ng), nicked plasmids (2 μ L; <200ng), or ligation reaction products (2-3 μ L) were added to the cells and gently mixed by swirling with a pipette tip, and then incubated on ice for 30min. Uptake of plasmid DNA was induced by heating the competent cell/DNA solution to 42°C in a water bath for 50sec. The transformation stock was then cooled on ice for 2min before being transferred into a 13mL round bottom aerobic subculture tube containing 400 μ L of pre-warmed (42°C, 5min) NZY+ amine broth. Transformations were subsequently incubated at 37°C with shaking (220rpm; InnovaTM 4330, Table 2.3) for 1h. A 50 μ L aliquot of the transformation stock was plated onto LB agar plates containing the desired antibiotic (100 μ g/mL ampicillin for UGT2B7 in pBluescript II SK (+) or pEF-IRES-puro 5) for plasmid selection and incubated overnight at 37°C.

Plasmid amplification by bacterial subculture

Single colonies of pBluescript II SK (+) UGT2B7 or pEF-IRES-puro 5 UGT2B7 plasmids transformed in DH5 α were isolated from agar plates and individually used to inoculate 5mL LB subcultures to amplify the number of plasmids. LB subcultures contained the desired antibiotic for plasmid selection which was ampicillin (100 μ g/mL) for pBluescript II SK (+) and pEF-IRES-puro 5. Subcultures were incubated at 37°C with shaking (200rpm) for 12-16hr. For larger plasmid preparations (Plasmid Midi and Maxi Kit; Table 2.6), 1mL of the overnight LB subculture was used as the starter culture or inoculate for a 100mL culture with the desired antibiotic.

Chapter 2: Materials and general methods

Cultures were incubated at 37°C with shaking (200rpm; Innova™ 4330, Table 2.3) for 12-16hr.

Digestion and identification of plasmid DNA

The QIAprep Spin Miniprep Kit or Plasmid Midi and Maxi Kit was used to purify plasmid DNA from the bacterial subculture according to the manufacturer's instructions (Table 2.6). Plasmid DNA (pBluescript II SK (+) and pEF-IRES-puro 5) was digested with restriction enzymes (*XhoI* and *XbaI*; Table 2.7) to resolve the fragmentation pattern specific to the size of each plasmid containing the UGT2B7 cDNA. The restriction digests were prepared by mixing 1µL of plasmid DNA (~50-200ng), 1µL buffer (10x NEB 4), 0.1µL BSA (100x), 0.25µL of restriction enzyme(s) and water to a final volume of 10µL. Digests were incubated for 60min at 37°C, followed by agarose gel electrophoresis to visualize plasmid fragmentation.

Agarose gel electrophoresis of restriction digests

Resolution of relative size/mobility of digestion products (DNA fragments and plasmids) was routinely performed by mixing 10µL of the sample with 2µL of 6x DNA loading dye buffer (Table 2.5) and loading 10µL of this mixture into the wells of a 1% (w/v) agarose gel (Table 2.5) bathed in Tris-acetate EDTA (TAE) electrophoresis buffer (Table 2.5). Electrophoresis was carried out at 100V for 20min in a Mini-Sub® Cell GT electrophoresis system (Table 2.3). DNA bands were analysed with a Gene Genius imaging system (Table 2.3). The sizes and quantity of the DNA bands in each lane were estimated by comparison with a set of DNA molecular weight markers (NEB 1kb DNA ladder; Table 2.2) at 0.3µg DNA per lane.

DNA extraction by gel purification

After agarose gel electrophoresis separation of DNA bands was achieved, extraction or excision from agarose gels was performed under low-intensity UV light irradiation (365nm). The agarose gel slice was transferred into a microcentrifuge tube and the DNA extracted using the QIAquick® Gel Extraction Kit (Table 2.6), using a modified version of the manufacturer's instructions. Briefly, the gel slice was dissolved by adding 3x volume of QG™ buffer (v/w) to the gel with subsequent heating at 42°C for ~5min. After the gel had dissolved completely, 1x gel volume of isopropanol (v/w) was added and the sample loaded on the QIAquick column. The column was centrifuged for 1min (18,000g; Beckman Microfuge® 18, Table 2.3) and the eluent discarded. The DNA was washed with Buffer QG™ (500µL; 1x 1min) and with PE™ buffer (750µL; 1x 1min). The column was dried by centrifugation at 18,000g for 1min and the DNA then eluted into a clean tube by the addition of water (50µL) to the column and subsequent centrifugation at 18,000g for 1min.

Determination of DNA concentration and purity

Spectrophotometry (optical density or absorbance at 260nm versus 280nm) was used to determine the concentration and purity of DNA samples. Pure double stranded DNA at a concentration of 0.05µg/µL in water has an absorbance of 1.0 at 260nm. A Pharmacia Biotech GeneQuant II or Cary 300 UV-VIS spectrophotometer (Table 2.3) was used to measure the absorbance at 260nm to determine the DNA concentration of a 1:50 dilution of DNA sample (in water) according to Equation 2.1:

Equation 2. 1: DNA concentration

DNA concentration (µg/µL) = Absorbance @ 260nm × 0.05 µg/µL × 50 (dilution factor)

Quality and purity of DNA can be calculated by determining the relative ratio of absorbance at 260:280nm. Clean DNA with minimal contaminants (proteins, RNA, organic compounds, salt carry-over) will have a ratio range 1.7-2.0. DNA concentration and purity can also be assessed by measurement against a set of known standards/molecular markers after agarose gel electrophoresis, as described previously.

Ligation

T4 DNA Ligase (3 Weiss units per reaction; Promega; Table 2.7) was used for ligation reactions. T4 DNA Ligase catalyzes the combination of two strands of DNA between the terminal 5'-phosphate and the 3'-hydroxyl groups of adjacent nucleotides. The optimal ligation molar ratio of pEF-IRES-puro 5 vector (5.7kb) to UGT2B7 cDNA insert (2kb) was 1:2 or 1:3 based on Equation 2.2.

Equation 2. 2: Quantity of cDNA insert for ligation

$$(\text{ng}) \text{ of insert} = \frac{(\text{ng}) \text{ vector} \times (\text{kb}) \text{ size of insert}}{(\text{kb}) \text{ size of vector}} \times \text{molar ratio} \frac{\text{insert}}{\text{vector}}$$

All ligation reactions were conducted at 8°C overnight (DNA Thermal Cycler; Table 2.3) followed by heat inactivation of the enzyme at 70°C for 10min prior to transformation.

Generation of human UGT2B7 mutants

Mutagenesis, primer design and PCR conditions

Mutants were generated by site-directed mutagenesis using the wild-type UGT2B7 cDNA in pBluescript II SK (+) as the template. Partially overlapping oligonucleotide primers were employed for mutagenesis (see Chapter 4 for details). All mutations were confirmed on both strands by DNA sequencing using an Applied Biosystems 3130xl

Chapter 2: Materials and general methods

Genetic Analyser with Big Dye Terminator v3.1 Chemistry (Applied Biosystems, Foster City, CA, USA). Refer to Chapter 4 for details of PCR conditions.

2.2.2 Tissue culture

General maintenance of cell lines

Mammalian HEK293T cells

HEK293T cells were cultured in a monolayer under sterile conditions in DMEM (0.1mM non-essential amino acids and 1mM sodium pyruvate) supplemented with 10% (v/v) foetal bovine serum and penicillin-streptomycin (100µg/mL; Table 2.5). Cells were grown in a humidified incubator (37°C) with an atmosphere of 5% CO₂ and routinely passaged at approximate 80% confluency. Trypsin digestion was not required to release and disperse HEK293T cells from the surface of the flask (NuncTM; ThermoFisher Scientific, Scoresby, Vic, Australia) for re-plating; rather vigorous pipetting sufficed. Cell cultures were replaced from frozen cell stocks after 10-15 passages. Cell stocks were preserved in foetal bovine serum with 10% (v/v) DMSO (Table 2.5) and stored in liquid nitrogen.

Spodoptera frugiperda (Sf9) cells

Sf9 cells were grown as a suspension culture at 28°C in modified SFX insect medium (filter sterilized) containing penicillin-streptomycin (100µg/mL) and 5% fetal bovine serum (Table 2.5) in a non-humidified incubator (Shimaden and Ratek; Table 2.3). Starter cultures (75-100mL) in sterile plastic disposable Erlenmeyer baffled flasks (Corning®, New York, USA) were placed in a 28°C incubator with an orbital shaker rotating at ~140rpm (Ratek; Table 2.3). A one litre M/C spinner flask with magnetic paddled impeller (Bellco Glass, Inc., NJ, USA) was used for larger cultures (250mL)

and placed in a 28°C incubator with a magnetic stirrer at a speed of ~140rpm (Shimaden; Table 2.3). Sf9 cells were seeded at 3×10^5 viable cells/mL, which then approximately doubled to 7.3×10^5 cells/mL over three days. After two days the density reached log phase (approximately 2×10^6 cells/mL), ready for passaging or harvest. Cell cultures were replaced from frozen cell stocks after 10-15 passages. Cell stocks were preserved in 60% serum free SFX-Insect medium, 30% foetal bovine serum and 10% DMSO (v/v) (Table 2.5) at a particular cell density for optimal recovery (5×10^7 viable cells/mL) and stored in liquid nitrogen.

Cell counting to determine density and viability

Cell counting was conducted using a haemocytometer (Hy-Lite; Table 2.3). Trypan blue stain solution (0.4% in buffered isotonic salt solution (PBS), pH 7.2-7.3) was additionally added to determine cell viability at the start of every culture, or before passaging in order to calculate seeding density or monitor growth rate.

The haemocytometer chamber is divided into nine 1.0mm squares (Figure 2.3). The chamber of the hemocytometer was filled with a homogenous cell suspension (10 μ l) by capillary action beneath a coverslip. The total number of cells in three central gridded 1.0mm squares was counted using a Clay Adams cell counter (BD, NSW, Australia) and averaged. The concentration or number of cells per milliliter (mL) was determined using Equation 2.3.

Equation 2. 3: Cell concentration

$$\text{number of cells/ mL} = \text{average number of cells} \times 10^4$$

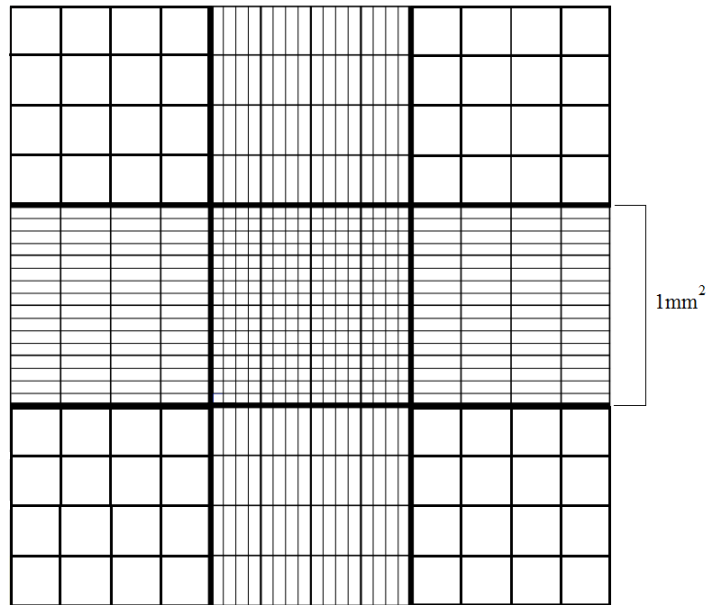


Figure 2. 3: Cell counting with a hemocytometer.

The coverslip supported over the hemocytometer ensures the total volume over each 1.0mm square is $1 \times 10^{-4} \text{ cm}^3$ (length x width x height; $0.1 \text{ cm} \times 0.1 \text{ cm} \times 0.01 \text{ cm}$).

To determine cell viability, Trypan blue dye exclusion or staining was used to discriminate the viable cells from the dead. The blue dye is excluded by membranes of viable cells while they readily enter dead cells. A homogenous cell suspension ($500 \mu\text{L}$) was mixed with 0.4% Trypan blue solution ($50 \mu\text{L}$) in a sterile microfuge tube, and then loaded ($10 \mu\text{L}$) into the haemocytometer chamber and counted as previously. The percentage of viable cells can be determined according to Equation 2.4.

Equation 2. 4: Percentage of viable cells

$$\% \text{ viable cells} = \left[1 - \left(\frac{\text{number of dead blue cells}}{\text{total number of cells}} \right) \right] \times 100$$

In order to accurately calculate the concentration of cells/mL, multiply the number of viable cells by 1.1 as shown in Equation 2.5, which takes into account the dilution factor with Trypan blue.

Equation 2. 5: Viable cell concentration

$$\text{viable cells/ mL culture} = \text{number of viable cells} \times 10^4 \times 1.1 \text{ (dilution factor)}$$

2.2.3 Preparation of recombinant UGT enzymes

Recombinant human UGTs from the 1A family (1A1, 1A3, 1A4, 1A6, 1A7, 1A8, 1A9 and 1A10) were individually stably expressed in the human embryonic kidney 293 (HEK293) cell line and lysates were prepared according to Uchaipichat et al. (2004). In brief, cDNA encoding each individual UGT enzyme was amplified from various human cDNA libraries by the polymerase chain reaction (PCR) and the identity of the coding region was confirmed by sequence analysis. Each of the cDNAs was then cloned separately into the pEF-IRES-puro6 expression vector before transfection into HEK293 cells (see Section 4.2.3 for further details on transfections). After transfection, cells were grown at 37°C in DMEM containing puromycin (1.5mg/L) and 10% fetal bovine serum in a humidified incubator with an atmosphere of 5% CO₂. The cells were harvested and washed in phosphate-buffered saline once they had grown to at least 80% confluency. Cells were subsequently lysed by sonication with four 2-sec ‘bursts’, each separated by 1min cooling on ice, using a Vibra Cell VCX 130 Ultrasonics Processor (Table 2.3). The lysate was centrifuged at 12,000g for 1min at 4°C to remove cellular debris and the supernatant fractions separated and stored in phosphate buffer (0.1M, pH 7.4) at -80°C until use.

Recombinant human UGTs from the 2B family (2B4, 2B7, 2B15 and 2B17) were purchased from BD Biosciences (BD Biosciences, North Ryde, NSW, Australia) as BD Supersomes™. Human UGT2B cDNA was cloned into a baculovirus expression system, and microsomes were prepared from baculovirus infected insect cells (BTI-TN-5B1-4 or High-Five) expressing each UGT2B enzyme. Supersomes™ were used

here as a source of UGT2B enzymes since they exhibit higher activities than the corresponding UGT2B enzymes expressed in HEK293 cells. Expression of the UGT1A enzymes was demonstrated by immunoblotting with a commercial UGT1A antibody (BD Gentest, Woburn, MA, USA) and a non-selective UGT antibody raised against purified mouse Ugt (Uchaipichat et al. 2004), together with measurement of enzyme activities (see Section 2.2.7).

2.2.4 Western Blot

Polyacrylamide gel electrophoresis (PAGE)

Equal amounts of total protein from each recombinant enzyme preparation were subjected separately to SDS PAGE (Laemmli 1970). Protein extracts (50µg) were combined with denaturing sample buffer (5µL; Table 2.5) and made up to a final volume of 20µL with sterile water. Samples were denatured by heating at 95°C for 5min, loaded (20µL) onto 4% stacking gels (Table 2.5) with Precision Plus Protein WesternC Standard (5µL; Table 2.2), and electrophoresed at 100V (150W/150mA) until the samples passed through the stacking gel (~30min). Samples were then separated on 10% polyacrylamide running gels (Table 2.5) at 170V (150W/150mA) until the solvent front eluted from the base of the gel (~60min). SDS PAGE was conducted in running buffer (Table 2.5) using the BIORAD Mini-PROTEAN® III Electrophoresis Cell (Table 2.3).

Protein transfer

Following PAGE, proteins were transferred to Trans-Blot® Transfer Medium pure nitrocellulose membrane (BIORAD; 0.45µm) using the BIORAD Mini-PROTEAN® III Electrophoresis Cell at 90V (150W/150mA). Transfer was performed at 4°C with stirring for 2hr in pre-chilled (4°C) transfer buffer (Table 2.5). Membranes were

Chapter 2: Materials and general methods

initially washed in tris-buffered saline + Tween-20 (TBST) (3x 2min; Table 2.5) to remove any residual methanol that contributes to background staining, followed by a rinse in tris-buffered saline (TBS) (2x 30sec; Table 2.5). Immunodetection of UGT2B7 proteins was achieved by sequential incubations at room temperature with gentle agitation on a reciprocal shaker (Thermomixer; Table 2.3). Incubations were performed as follows:

- i. Membrane blocking was achieved in 3% blocking solution (Table 2.5) overnight at 4°C (without shaking) followed by rinsing in TBS (2x 60mL).
- ii. Incubation of rabbit anti-human UGT2B7 (polyclonal) primary antisera (MACK3; Table 2.8) diluted 1:2000 in 2% antibody incubation solution (Table 2.5) was performed for 2hr at room temperature with shaking followed by washing in TBST (3x 10 min). Membranes were gently rinsed in TBS (2x 60mL).
- iii. Incubation of ImmunoPure[®] Antibody goat anti-rabbit IgG (H+L) secondary HRP-conjugated IgG (Table 2.8) diluted 1:1000 in 2% antibody incubation solution for 1h at room temperature with shaking, followed by washing in TBST (3x 10min). Membranes were placed in TBS until exposure to chemiluminescence substrates.

Immunodetection detection of proteins

Immunoreactivity was detected using the BM Chemiluminescence Blotting Substrate (POD; Table 2.2). Blots were visualized with a Fujifilm LAS-4000 imaging system (Table 2.3) and band intensities were measured using Multi Gauge software. Relative

UGT2B7 protein levels represent the mean of duplicate measurements. Western blot analysis and activity assays were performed using the same batch of cell lysate.

2.2.5 Human Livers

Human liver tissue from five donors (H7, H10, H12, H13 and H40; Table 2.11) was used to prepare microsomes for use in the *in vitro* kinetic experiments. Liver tissue, stored at -80°C, was procured from the tissue ‘bank’ of the Department of Clinical Pharmacology. Ethics approval for the use of human liver tissue in xenobiotic metabolism studies was obtained from the Southern Adelaide Clinical Research Ethics Committee.

Table 2. 11: Relevant clinical details of liver donors.

Liver	Age (years)	Sex	Smoking history	Alcohol history	Drug treatment prior to death
H7	44	Female	Non-smoker	Social ^a	Dexamethasone
H10	67	Female	Non-smoker	Social ^a	Dopamine Morphine Frusemide Midazolam
H12	66	Male	Non-smoker	Moderate ^b	Insulin
H13	61	Female	Non-smoker	Social ^a	Metoprolol Methyclothiazide Bethanechol
H40	54	Female	Non-smoker	Unknown	Dexamethasone Dopamine

^a Less than one standard drink per day

^b Two to three standard drinks per day

Preparation of human liver microsomes (HLM)

HLM were prepared by centrifugation, according to the procedure of Bowalgaha et al. (2005). Microsomes from each of the five livers were used separately and ‘pooled’. The pooled sample contained equal protein concentrations of microsomes from each liver, providing a mixed protein source representative of all five livers. This approach was previously validated and is useful in certain circumstances as the need for human liver (a limited resource) and the time required performing kinetic experiments multiple times with different livers is reduced.

2.2.6 Protein content of enzyme sources

The protein content of each enzyme source (microsomes, lysates and SupersomesTM) was determined using the method of Lowry et al. (1951). Briefly, protein samples were first diluted 1 in 10 in distilled water. A 25µl aliquot of the diluted sample was mixed with 475µl of distilled water and treated with 2ml of Lowry reagent (Lowry solutions A, B and C mixed in ratio 100:1:1; Table 2.3). Samples were vortex-mixed and left to stand at room temperature for 10min. A 250µl aliquot of Folin’s reagent was added to each sample and the reaction was allowed to proceed for 15min. Samples were

analyzed in triplicate. Unknown protein concentrations were determined from a standard curve using BSA as the standard. The absorbance of all samples and standards was determined at 660nm using a Varian Cary 300 UV-Vis spectrophotometer (Table 2.3). The spectrophotometer was zeroed with a ‘blank’ sample containing distilled water in place of protein.

Calculation of protein content by Lowry method

A plot of protein amount (µg of BSA) versus absorbance at 660nm was used to obtain the slope of the BSA calibration curve, which was then employed to calculate the protein concentration of samples (mg/mL) according to Equation 2.6:

Equation 2. 6: Total protein concentration

$$[\text{Protein}]_{\text{mg/mL}} = \left[\frac{\text{Absorbance of sample @ 660nm}}{\text{Slope of calibration curve}} \right] \times \frac{1}{\text{Sample volume aliquoted}} \times \text{Dilution factor}$$

2.2.7 Confirmation of the activity of recombinant UGTs

The non-selective substrate 4-methylumbelliferone (4-MU) was used to confirm the catalytic activity of the majority of the UGT enzymes expressed in HEK293 and insect cells (SupersomesTM), including UGT 1A1, 1A3, 1A6, 1A7, 1A8, 1A9, 1A10, 2B7, 2B15 and 2B17 according to the procedure of Lewis et al. (2007). UGT1A4 and UGT2B4 activities were measured using lamotrigine and codeine as the respective substrates (Raungrut et al. 2010; Rowland et al. 2006), given the low or absent 4-MU glucuronidation activities of these enzymes.

2.2.8 Incubation and chromatography assay development and conditions

HPLC-UV and FL

The various reversed-phase HPLC (UV and FL detection) assays used in this thesis were either fully or previously developed and will be acknowledged in detail in following Chapters. Most of the assays are capable of the simultaneous identification and separation of both glucuronide and glucoside conjugates formed by incubations of human liver microsomes, recombinant human UGTs, and insect microsomes (refer to Appendix 1 for a detailed summary of the HPLC conditions). However, the following assays were also used for the general quantification of glucuronidation activity referred to in Section 2.2.7.

Quantification of 4-MU glucuronidation (4-MUGlcUA)

As indicated above, 4-methylumbelliferone (4-MU) is a nonselective substrate for the majority of the human UGT1A and UGT2B enzymes (viz. UGT 1A1, 1A3, 1A6, 1A7, 1A8, 1A9, 1A10, 2B7, 2B15, and 2B17) and quantification of the 4MU-glucuronide conjugate was used to confirm catalytic activity for these enzymes according to Lewis et al. (2007).

In brief, incubations, in a total volume of 200 μ L, contained phosphate buffer (0.1M, pH 7.4), MgCl₂ (4mM), recombinant UGT protein (Table 2.12 for protein amount), 4-MU (Table 2.12 for substrate concentration) and UDP-GlcUA (5mM). UDP-GlcUA was added to initiate the reaction after a 5min pre-incubation at 37°C in a shaking water bath and incubations were performed for varying times depending on the UGT enzyme (see Table 2.12). Reactions were terminated by the addition of perchloric acid (11.6M; 2 μ L) and cooling on ice for 10min. Samples were subsequently centrifuged (5000g for 10min), and an aliquot of the supernatant fraction was analysed by HPLC.

Chapter 2: Materials and general methods

The mobile phase, delivered at a flow rate of 1.0 mL/min, consisted of two solutions mixed according to a gradient timetable: phase A (100% HPLC grade acetonitrile) and phase B (aqueous 10mM TEA, pH 2.5 (HClO₄) with 10% acetonitrile) (Table 2.13). Analytes were separated using a NovaPak C18 column (Table 2.3) and detected by UV detection at a wavelength of 316nm. Under these conditions the retention times for 4-MUGlcUA and 4-MU were 3.5 and 5.8min, respectively. An analysis time of 8min was required to achieve adequate separation of 4-MUGlcUA and parent 4-MU. 4-MUGlcUA quantification by HPLC was achieved using authentic standard with calibration curves generated for 3 to 5 concentrations in the range 0.5-40 μ M.

Table 2. 12: Protein concentrations, incubation times and substrate (4-MU, LTG or COD) concentrations used for activity screening in UGTs.

UGT Enzyme	[Protein] mg/mL	Incubation Time (min)	[Substrate] μM
1A1	0.33	120	100 (4-MU)
1A3	0.167	75	2400 (4-MU)
1A6	0.0025	30	100 (4-MU)
1A7	0.0083	10	15 (4-MU)
1A8	0.05	30	750 (4-MU)
1A9	0.025	15	10 (4-MU)
1A10	0.0208	30	30 (4-MU)
2B7	0.2	90	350 (4-MU)
2B15	0.83	120	300 (4-MU)
2B17	0.5	120	1000 (4-MU)
1A4	0.5	75	1500 (LTG)
2B4	1	120	2000 (COD)

Table 2. 13: Mobile phase gradient timetable for HPLC quantification of 4-MUGlcUA, LTG-N2-GlcUA and COD-6-GlcUA.

Assay	Time	% Mobile Phase A	% Mobile Phase B
4-MUGlcUA	0	4	96
	3	4	96
	3.1	30	70
	4.1	30	70
	4.2	4	96
	8	4	96
LTG-N2-GlcUA	0	4	96
	3	4	96
	7	13	87
	8	13	87
	9	50	50
	9.5	4	96
	14	4	96
COD-6-GlcUA	0	0	100
	15	0	100

Quantification of lamotrigine-N2-glucuronidation (LTG-N2-GlcUA)

4-MU glucuronidation by human UGT1A4 activity is low or absent and therefore, lamotrigine (LTG) was used as the substrate. LTG-N2-GlcUA formation was measured according to Rowland et al. (2006). In brief, incubations, in a total volume of 200 μ L, contained KOH (1M, 37.2 μ L), MgCl₂ (4mM), UGT1A4 (HEK293 cell lysate protein 0.5mg/mL), LTG (1500 μ M; dissolved in 1M H₃PO₄ and 10% acetonitrile) and UDP-GlcUA (5mM). Note that phosphate buffer (0.1M, pH 7.4) was generated *in situ* by the addition of KOH with the LTG solution. Reactions were initiated by the addition of UDP-GlcUA after a 5min pre-incubation at 37°C in a shaking water bath and then continued for 75min (see Table 2.12). Reactions were terminated by the addition of perchloric acid (11.6M; 2 μ L) and cooling on ice for 10min. Samples were centrifuged (5000g for 10min), and an aliquot of the supernatant fraction was analysed by HPLC.

Chapter 2: Materials and general methods

The mobile phase, delivered at a flow rate of 1.0 mL/min, consisted of two solutions mixed according to a gradient timetable: phase A (100% HPLC grade acetonitrile) and phase B (25mM phosphate buffer, pH 7.4 with 5% acetonitrile and 0.02% TEA) (Table 2.13). Analytes were separated using a Zorbax Eclipse XDB-C8 column (Table 2.3) and measured by UV detection at a wavelength of 254nm. Under these conditions the retention times for LTG-N2-GlcUA and LTG were 5.2 and 10.3min, respectively. The analysis time was 14min. Quantification by HPLC was achieved using an authentic standard with calibration curves generated using 3 to 5 concentrations ranging from 2.5-10 μ M.

Quantification of codeine glucuronidation (COD-6-GlcUA)

Similarly, 4-MU glucuronidation by human UGT2B4 is also low and hence codeine (COD) was used to determine glucuronidation activity according to Raungrut et al. (2010). In brief, incubations, in a total volume of 200 μ L, contained phosphate buffer (0.1M, pH 7.4), MgCl₂ (4mM), UGT2B4 (SupersomesTM protein 1mg/mL), COD (2000 μ M) and UDP-GlcUA (5mM). Reactions were initiated by the addition of UDP-GlcUA after a 5min pre-incubation at 37°C in a shaking water bath and then continued for 120min (see Table 2.12). Reactions were terminated by the addition of perchloric acid (11.6M; 2 μ L) and cooling on ice for 10min. Samples were centrifuged (5000g for 10min), and a 120 μ L aliquot of the supernatant fraction was added to a new tube containing KOH (4M; 2 μ L) before analysis by HPLC.

The mobile phase, which was delivered isocratically at a flow rate of 1.0mL/min, consisted of 2mM TEA, pH 2.7 (adjusted with HClO₄) and 13.5% acetonitrile (Table 2.13). Analytes were separated using a Phenomenex Synergi HydroRP C18 column (Table 2.3) and measured by UV detection at a wavelength of 205nm. Under these

conditions the retention times for COD-6-GlcUA and COD were 1.9 and 2.7min, respectively. The analysis time was 15min. Quantification by HPLC was achieved using authentic standard with calibration curves generated using 3 to 5 concentrations in the range 2.5-10 μ M.

2.3 Data analysis

Kinetic equations and constants

Several equations describing various kinetic models (Equations 1.1-1.3 and 1.6-1.8) used to generate kinetic data have been shown in Chapter 1. These equations were fitted to untransformed experimental data using the program Enzfitter (Table 2.10) to generate kinetic parameters. Transformed data are represented by Eadie-Hofstee (velocity versus velocity/ [substrate]) and Dixon plots, provide useful visual tools to determine the goodness of fit of equations. Goodness of fit was assessed by the coefficient of determination (r^2), F- statistic, and standard error of the parameter fit. The computer generated (Enzfitter) kinetic parameters are given as the parameter value \pm standard error (SE) of the parameter estimate.

Statistical analysis

Statistical analysis was performed using SPSS 19.0 (Table 2.10). The Shapiro-Wilk Test of normality was used to assess the distribution of data before using parametric independent and paired t-tests to analyze morphine kinetic data from five individual livers and pooled HLM, with and without BSA supplementation of incubations. p values < 0.05 were considered significant.

Chapter 3

Morphine glucosidation

Published in part as: Chau N, Elliot DJ, Lewis BC, Burns K, Johnston MR, Mackenzie PI and Miners JO, 2014, 'Morphine glucuronidation and glucosidation represent complementary metabolic pathways which are both catalyzed by UDP-glucuronosyltransferase 2B7: Kinetic, inhibition and molecular modelling studies', *Journal of Pharmacology and Experimental Therapeutics*, 349 (1): 126-137.

Reproduced with the permission of the American Society for Pharmacology and Experimental Therapeutics.

3.1 Introduction

3.1.1 Morphine and its metabolites

History, chemistry and metabolism

Pain is a very complex trait which exhibits high variability between individuals, in both experience and perception. A myriad of genetic and environmental factors contribute to this variability, with epigenetics potentially providing the bridging link in the gene-environment interaction (Belfer 2013; Lotsch & Geisslinger 2005; Lotsch, Geisslinger & Tegeder 2009; Somogyi, Barratt & Coller 2007). The opioids provide one of the earliest and successful treatments for pain. Morphine, named after the Greek god of dreams *Morpheus*, has been used as a drug globally for centuries with references to opium as early as the third century B.C. (Gutstein & Akil 2006). Indeed, morphine remains the most widely prescribed analgesic for the treatment of moderate to severe pain and is additionally employed for the relief of severe dyspnoea, as an adjunct in

Chapter 3: Morphine glucosidation

general anaesthesia, and for the treatment of acute pulmonary oedema (Field et al. 2012; Jennings et al. 2002; Milne, Nation & Somogyi 1996; Sear et al. 1989).

Morphine is an opioid receptor agonist which is still obtained from opium, as stereoselective synthesis is difficult. The milky juice from the unripe seed capsules of the poppy plant, *Papaver somniferum*, is extracted and the juice dried and powdered. More than 20 alkaloids are obtained from the extract, the most prevalent being morphine (10%), codeine (0.5%), thebaine (0.2%), noscapine (6%) and papaverine (1%) (Gutstein & Akil 2006). Moreover, Poeaknapo et al. (2004) demonstrated the *de novo* biosynthesis of morphine from distant precursors in human cells and trace amounts of 'endogenous' morphine have been detected in human tissue and biological fluid (Matsubara et al. 1992; Mikus et al. 1994; Zhu et al. 2001).

Morphine is a weak base due to its tertiary amino group and it is relatively water soluble with 4 hydrophilic hetero atoms. The structure of morphine is shown in Figure 3.1. Morphine is metabolically reactive due to three functional groups; C3 phenolic, C6 enolic alcohol (cyclohexenol), and a tertiary amine (N-methyl piperidine) (Christrup 1997). Glucuronidation at the 3- and 6- positions, to form morphine-3- β -D-glucuronide (M3G) and morphine-6- β -D-glucuronide (M6G), respectively, are the major metabolic pathways of morphine in humans. M3G, M6G and unchanged drug account on average for 55%, 10%, and 8% of the urinary recovery, respectively, of an intravenous dose of morphine in humans along with trace amounts of normorphine, morphine-3-sulfate and morphine-3,6-diglucuronide (Hasselstrom & Sawe 1993; Milne, Nation & Somogyi 1996). Morphine glucuronidation occurs primarily in the liver, but also takes place to a lesser extent in the kidney and brain (King et al. 1999; Knights et al. 2016). The principal enzyme contributing to morphine glucuronidation

is UGT2B7, which has been shown to catalyze the conversion of morphine to both M3G and M6G (Coffman et al. 1997). Stone et al. (2003) reported that several UGTs expressed in HEK293 cells additionally had the capacity to form M3G (viz. UGT1A1, 1A3, 1A6, 1A8, 1A9, 1A10, and 2B7) but, as indicated above, UGT2B7 was the dominant enzyme involved in this pathway. By contrast, only UGT2B7 was found to catalyze M6G formation. Ohno, Kawana and Nakajin (2008) subsequently reported M6G formation by recombinant human UGT1A1 and UGT1A8 from baculovirus-infected insect cells at low substrate concentration, although activity of these enzymes was low. Interestingly, mRNA of the extrahepatic UGT1A8 and UGT1A10 have been detected in hepatocytes (Li, Bratton & Radominska-Pandya 2007), although there is no evidence of protein expression.

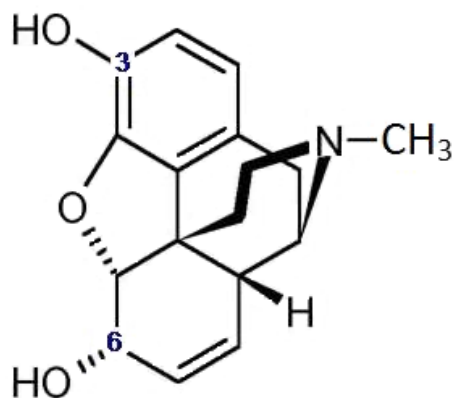


Figure 3. 1: Chemical structure of morphine with the phenolic (C3-) and enolic (C6-) hydroxyl groups numbered.

Adapted with permission from Wang, X, Loram, LC, Ramos, K, de Jesus, AJ, Thomas, J, Cheng, K, Reddy, A, Somogyi, AA, Hutchinson, MR, Watkins, LR & Yin, H 2012, 'Morphine activates neuroinflammation in a manner parallel to endotoxin', Proceedings of the National Academy of Sciences, vol. 109, no. 16, pp. 6325. Copyright (2012) Proceedings of the National Academy of Sciences of the United States of America (PNAS).

Chapter 3: Morphine glucosidation

As glucuronides, M3G and M6G are considered polar hydrophilic metabolites. However, they are known to cross the blood-brain barrier (BBB) and exert significant pharmacological effects. M6G is a more potent opioid μ -receptor agonist than morphine itself (Christrup 1997; Frances et al. 1992; Milne, Nation & Somogyi 1996; Osborne et al. 1990). It remains unclear, especially in humans, whether this ability to cross the BBB is due to lipid-mediated free diffusion (compounds <400Da with <8 hydrogen bonds), facilitated or active transport (carrier-/receptor-mediated), or both as the majority of the studies have been performed *in vitro* or *in vivo* in laboratory animals. Thus, species differences may occur (Bourasset & Scherrmann 2006; De Gregori et al. 2012; Ohtsuki & Terasaki 2007; Pardridge 2012; Sawchuk & Elmquist 2000; Somogyi, Barratt & Coller 2007). Most of the evidence for transport suggests the involvement of ATP binding cassette (ABC) efflux and solute carrier (SLC) influx transporters. Also of note, however, M3G and M6G are surprisingly lipophilic. Log k_i (isocratic capacity factor) values for M6G and M3G are only 0.5 and 1.0 k_i units lower than that of morphine at physiological pH (Carrupt et al. 1991). Carrupt et al. (1991) suggested that M3G and M6G may exist in conformational equilibrium between folded and extended forms which act as 'molecular chameleons'; polar groups are exposed when the conformation is extended in polar media such as water but masked in the folded conformation in low polarity media such as biological membranes.

Either way, M6G and morphine are pharmacologically active as analgesics. Both bind to opioid μ -receptors and act as agonists in the CNS (Milne, Nation & Somogyi 1996). In addition, morphine has a role as an endogenous key signaling molecule in downregulating physiological responses (neural and immune) mediated through the putative μ_3 receptor subtype and the release of nitric oxide (Stefano et al. 2000). Although pharmacological classification historically suggested more than one sub-

type of opioid μ -receptors (μ_1 and μ_2), molecular biology has since only uncovered one μ -receptor gene which undergoes extensive alternative splicing, therefore generating multiple splice variant proteins that may also interact with one another, or with other receptors and signaling molecules to potentially elicit the varied pain responses observed clinically (Dietis, Rowbotham & Lambert 2011; Feng et al. 2012; Pasternak & Pan 2011). In contrast, M3G lacks analgesic activity as it has low binding affinity for the μ opioid receptor. Rather, M3G is neuroexcitatory, and is believed to evoke excitatory behaviours such as allodynia, myoclonus, seizures, and cause adverse effects such as hyperalgesia and the development of tolerance and dependence via unknown cellular mechanisms (Milne, Nation & Somogyi 1996; Smith 2000). A possible non-neuronal mechanism that may explain how M3G can mediate these effects is through the activation of toll-like receptor 4 (TLR4) signaling, which releases proinflammatory products including interleukin-1 in the CNS (Due et al. 2012; Hutchinson et al. 2010; Lewis et al. 2010).

More recently, and as indicated in Chapter 1, novel morphine metabolites were detected in the urine of five terminal stomach cancer patients taking morphine (60mg/day) for the treatment of severe pain. Using LC with multi-stage mass spectrometry Chen, Zhao and Zhong (2003) identified morphine-3- β -D-glucoside (M-3-glucoside) and morphine-6- β -D-glucoside (M-6-glucoside). M3G, M6G and normorphine 3- and 6-glucuronide were also detected. The mean relative ratios of morphine and metabolites formed compared to M3G (as 100 arbitrary units) were: M6G (21.9), morphine (14.2), M-3-glucoside (3.47), normorphine 6-glucuronide (0.44), M-6-glucoside (0.40), and normorphine 3-glucuronide (0.11) (Chen, Zhao & Zhong 2003). Thus, M-3-glucoside may contribute to the deficit in metabolite recovery observed in earlier studies. Besides the previously reported analgesic potential of M-

6-glucoside in a mouse model (Stachulski et al. 2003), it is unknown whether the morphine glucosides, like M6G and M3G, are pharmacologically active in humans or whether they also form in healthy subjects. The relative ratio of M3G to M6G was approximately 5:1, consistent with previous studies in both healthy subjects and cancer patients (Chen, Zhao & Zhong 2003; Fladvad et al. 2013; Hasselstrom & Sawe 1993; Holthe et al. 2002; Milne, Nation & Somogyi 1996; Osborne et al. 1990). Based on the data reported by Chen, Zhao and Zhong (2003), the relative ratio of M-3-glucoside to M-6-glucoside present in urine was is approximately 8:1. Thus, like glucuronidation, glucosidation is favoured at the 3-position. Although inter-individual M3G: M6G ratios remain relatively consistent at 5: 1, M3G: MOR and M6G: MOR ratios can vary between individuals by 16 to 42-fold (Holthe et al. 2002). The three major pathways for morphine conjugation are shown in Figure 3.2.

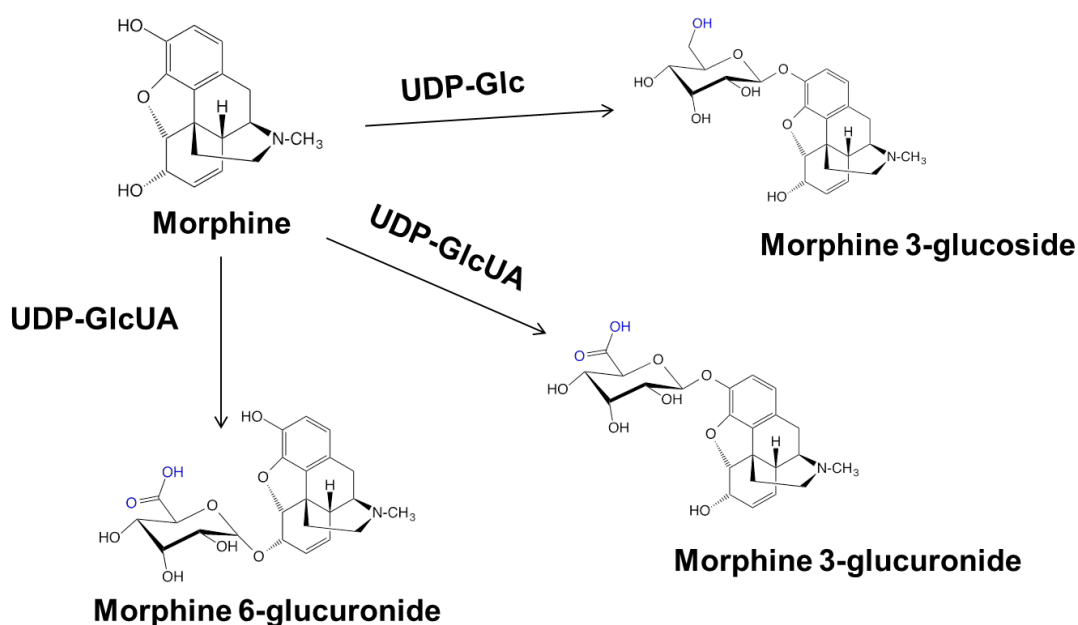


Figure 3. 2: Conjugation pathways for morphine elimination in humans.

Summary of previous findings

This chapter builds upon results generated previously as part of a BSc (Hons) project, whereby an HPLC assay was developed for the separation and quantification of M-3-glucoside, M3G and M6G. (It should be noted that formation of M-6-glucoside was not detected with HLM as the enzyme source, consistent with preferential glycosidation at the 3-position). The earlier study used morphine as the model substrate to characterize the relative formation of glucosides and glucuronides by HLM to demonstrate that glucosidation and glucuronidation occur as complementary metabolic pathways in humans (Figure 3.2). In addition, morphine glucosidation and glucuronidation kinetics were characterized separately with respect to morphine as the substrate (Table 3.1), and then with respect to both cofactors; UDP-Glc and UDP-GlcUA (Table 3.2). This was performed in the absence and presence of bovine serum albumin (BSA). Key results from the earlier study, published in Chau et al. (2014), are summarized below.

In all 5 livers, M-3-glucosidation kinetics with morphine as the variable substrate (at fixed cofactor concentration of 5mM) characterized in the absence and presence of BSA (2% w/v) exhibited Michaelis-Menten kinetics, while M3G formation followed negative cooperative kinetics. M6G formation followed negative co-operative kinetics in the absence of BSA but exhibited weak substrate inhibition ($K_m \gg K_{si}$) in the presence of BSA (see Table 3.1 for derived kinetic constants). There was an 89% decrease ($p < 0.01$) in the mean K_m for M-3-glucoside formation and an 88% decrease ($p < 0.01$) in mean S_{50} or K_m for both M3G and M6G formation when incubations were performed in the presence of BSA. Despite significant (albeit minor to moderate) changes in V_{max} there were still significant increases in the mean CL_{int} in the presence of BSA; 8.5-fold ($p < 0.01$), 6.7-fold ($p < 0.01$), 6.8-fold ($p < 0.01$) for M-3-glucosidation,

Chapter 3: Morphine glucosidation

morphine 3-glucuronidation and 6-glucuronidation, respectively. CL_{int} values for M-3-glucosidation were 2- to 2.5-fold greater than those for M6G formation in both the presence and absence of BSA.

Cofactor kinetics were characterized using HLM as the enzyme source with UDP-GlcUA and UDP-Glc as the variable substrates at a fixed, saturating morphine concentration (20mM). Experiments were performed in the presence and absence of BSA. Negative cooperative kinetics were observed for both cofactors. The S_{50} values for UDP-GlcUA were similar with respect to both M3G and M6G formation (Table 3.2). However, the S_{50} for UDP-Glc, measured with respect to M-3-glucoside formation, was approximately 3 to 6-fold higher than the values for UDP-GlcUA. While the S_{50} for UDP-Glc was unaffected by BSA, addition of BSA to incubations resulted in a 40% to 60% reduction in the S_{50} for UDP-GlcUA (Table 3.2).

Table 3. 1: Derived morphine glycosidation kinetic constants generated in the absence and presence of BSA (2% w/v).

Morphine was used as the variable substrate with either UDP-Glc or UDP-GlcUA (5mM each). Data are shown as the mean \pm SD for experiments (n=4) from HLM from 5 separate livers.

Glycoside	Cofactor	Without BSA				With BSA			
		K_m or S_{50} (mM)	V_{max} (pmol/min/mg)	CL_{int} (μ l/min/mg)	n	K_m or S_{50} (mM)	V_{max} (pmol/min/mg)	CL_{int} (μ l/min/mg)	n
M-3-glucoside	UDP-Glc	5.56 \pm 1.03	1581 \pm 631	0.30 \pm 0.14	-	0.63 \pm 0.12 ^b	1536 \pm 580	2.54 \pm 1.29 ^b	-
M3G	UDP-GlcUA	3.63 \pm 1.11	2803 \pm 599	0.82 \pm 0.24	0.86 \pm 0.03	0.45 \pm 0.09 ^b	2429 \pm 588 ^a	5.74 \pm 2.32 ^b	0.83 \pm 0.04
M6G^c	UDP-GlcUA	2.88 \pm 1.21	387 \pm 79	0.15 \pm 0.05	0.89 \pm 0.03	0.36 \pm 0.07 ^b	353 \pm 96	1.03 \pm 0.41 ^b	-

^a $p < 0.05$, comparisons for each glycoside \pm BSA.

^b $p < 0.01$; comparisons for each glycoside \pm BSA.

^c K_{si} for M6G formation in presence of BSA = 62 \pm 6mM

Table 3. 2: Derived kinetic constants for morphine glycosidation generated in the absence and presence of BSA (2% w/v) with cofactor (UDP-Glc or UDP-GlcUA) as the variable substrate. Data are shown as the mean \pm SD of 4 replicates with pooled HLM.

Cofactor (glycoside)	Without BSA				With BSA			
	S_{50} (mM)	V_{max} (pmol/min/mg)	CL_{int} (μ l/min/mg)	n	S_{50} (mM)	V_{max} (pmol/min/mg)	CL_{int} (μ l/min/mg)	n
UDP-Glc (M-3-glucoside)	1.98 \pm 0.19	1701 \pm 48	0.86	0.82 \pm 0.02	2.02 \pm 0.17	2186 \pm 85 ^b	1.08 ^a	0.74 \pm 0.01 ^b
UDP-GlcUA (M3G)	0.64 \pm 0.05 ^c	2696 \pm 104 ^c	4.19 ^c	0.75 \pm 0.02	0.39 \pm 0.02 ^{b, c}	2981 \pm 133 ^{b, c}	7.61 ^{b, c}	0.72 \pm 0.02
UDP-GlcUA (M6G)	0.56 \pm 0.06 ^c	378 \pm 15 ^c	0.67	0.77 \pm 0.03	0.32 \pm 0.04 ^{a, c}	356 \pm 15 ^c	1.13 ^b	0.76 \pm 0.02

^a $p < 0.05$; comparisons for each cofactor with and without BSA (i.e. across rows)

^b $p < 0.01$; comparisons for each cofactor with and without BSA (i.e. across rows).

^c $p < 0.01$; UDP-GlcUA compared to UDP-Glc (i.e. down columns)

Chapter 3: Morphine glucosidation

In summary, the previous work demonstrated that hepatic morphine 3-glucosidation *in vitro* occurs as a complementary, parallel pathway to glucuronidation. In contrast to Chen, Zhao and Zhong (2003), kinetic data generated with the separate cofactors suggests 3-glucosidation may be a significant pathway since the CL_{int} was higher than that for M6G formation. Furthermore, kinetic characterization of these pathways (\pm BSA, 2% w/v) provided mechanistic insights into substrate and cofactor binding. The BSA or ‘albumin effect’, as indicated by a large decrease in K_m/S_{50} (89% reduction), was observed with morphine kinetic experiments but not with the cofactor kinetic experiments with respect to UDP-Glc. There was, however, a decrease in S_{50} with UDP-GlcUA (40-60% reduction). These data suggest distinct cofactor and substrate (aglycone) binding site(s). This observation is consistent with long-chain unsaturated fatty acids acting as alternate substrates that access the aglycone binding site and not the cofactor binding site as they are known to undergo glucuronidation (Jude et al. 2001a; Jude et al. 2001b; Jude et al. 2000; Rowland et al. 2007; Turgeon et al. 2003). In this regard, several long-chain unsaturated fatty acids are known to be potent inhibitors of UGT2B7 and UGT1A9 activities (Tsoutsikos et al. 2004). If a single UGT enzyme catalyzes both the glucosidation and glucuronidation of morphine, it is tempting to speculate that UDP-Glc and UDP-GlcUA occupy the same cofactor domain, especially given the similarities in their structures. In HLM, the finding that BSA has little or no effect on the binding of UDP-Glc but UDP-GlcUA binding is slightly improved in the presence of BSA further suggests overlapping binding modes within the cofactor binding domain. It is also interesting to note that BSA (0.1%) did not affect the K_m of UDP-GlcUA with recombinant UGT1A9 and entacapone as the substrate but did so with 4-MU (Manevski et al. 2011). However, the low BSA

concentration used by these authors was almost certainly sub-optimal for sequestration of inhibitory long-chain unsaturated fatty acids.

It is postulated that the enzyme involved in morphine glucuronidation and glucosidation is UGT2B7, since this enzyme is known to be the major UGT involved in morphine glucuronidation (Coffman et al. 1998; Coffman et al. 1997; Stone et al. 2003), activity is enhanced by BSA (Gill, Houston & Galetin 2012; Manevski et al. 2011; Rowland et al. 2007; Rowland et al. 2008b), and UGT2B7 is capable of glucosidating HDCA and ibuprofen (Buchheit et al. 2011; Mackenzie, Little & Radomska-Pandya 2003). However, confirmation of this hypothesis is required.

3.1.2 The further characterization of morphine glucosidation

As indicated above, available evidence indicates UGT2B7 is involved in the glucosidation and glucuronidation of morphine. However, a contribution of other UGTs cannot be discounted. Reaction phenotyping of human liver microsomal drug glucuronidation reactions is possible given the availability of substrate and/or inhibitor ‘probes’ for most hepatic drug metabolizing UGTs, with additional confirmation using recombinant enzymes (Miners, Mackenzie & Knights 2010). Characterization of all clearance pathways is essential to understand sources of variability in morphine clearance and response, and its potential clinical significance. Therefore, the main aim for this chapter will be to fully characterize the morphine glycosidation pathways to assess the relative contributions of glucuronidation and glucosidation to morphine elimination.

Genetic polymorphism can affect the activity of an enzyme involved in the metabolism of a compound (endogenous or exogenous), and potentially therapeutic outcome. In relation to morphine glucuronidation, the most studied UGT2B7 gene variants are

Chapter 3: Morphine glucosidation

UGT2B7*1 (His268) and UGT2B7*2 (Tyr268) in exon 2, which are expressed at near identical frequencies (viz. 51:49) (Bhasker et al. 2000; Coffman et al. 1998; Court et al. 2003; Holthe et al. 2002; Madadi et al. 2009; Sawyer et al. 2003). It remains unknown whether the single nucleotide polymorphisms (SNP) at residue 268 effect on the formation of M-3-glucoside, as has been reported for ibuprofen acyl glucoside (Buchheit et al. 2011).

A potentially important experimental variable that could influence morphine glycosidation *in vitro* is whether the pathways are characterized separately or combined. Given the observation that both UDP-Glc and UDP-GlcUA most probably bind within the same cofactor domain, competition between cofactors is likely. In the previous study (Table 3.1), each glucosidation and glucuronidation pathway was characterized separately in HLM. However, the endogenous cellular environment within the cytosol of hepatocytes (and potentially the ER) consists of an approximately equal amount of both UDP-Glc and UDP-GlcUA (see Chapter 1). It is unknown if the availability of both cofactors *in vitro*, as occurs *in vivo*, affects the relative formation of M-3-glucoside, M3G and M6G. Characterization of morphine glycosidation kinetics in the presence of both cofactors along with cofactor inhibition studies will provide insights into the mechanism by which glucuronidation dominates over glucosidation (Table 3.2).

Hypotheses

1. A human UGT enzyme(s) both glucosidates and glucuronidates morphine, with UGT2B7 the most likely candidate.
2. In human liver, glucosidation is a less dominant pathway since the binding affinity of UDP-Glc is lower than that of UDP-GlcUA.

Experimental plan and aims

The specific aims were to:

1. Characterize the binding of morphine to HLM (\pm BSA) to ascertain whether correction for non-specific binding to incubation constituents is necessary for the calculation of morphine kinetic parameters *in vitro*.
2. Identify the UGT enzyme(s) responsible for morphine glucuronidation and glucosidation by investigating M3G, M6G and M-3-glucoside formation by a panel of recombinant human UGT enzymes, and the effects of UGT enzyme-selective inhibitors on the formation of each metabolite with HLM as the enzyme source.
3. If Aim (2) confirms that UGT2B7 is the enzyme responsible for morphine glycosidation, compare the formation of each metabolite by UGT2B7*1 and UGT2B7*2 to investigate whether morphine glycosidation varies with genotype.
4. Determine the kinetics of morphine glucosidation and glucuronidation by HLM in the presence of UDP-Glc plus UDP-GlcUA (1:1), in the absence and presence of BSA.
5. Investigate mutual inhibition of cofactor (UDP-GlcUA and UDP-Glc) binding with morphine as the fixed substrate with HLM (\pm BSA) as the enzyme source.

3.2 Methods

3.2.1 Incubation and assay conditions for glucosidation and glucuronidation

Binding assay

Binding of morphine to HLM and 2% (w/v) BSA was investigated using equilibrium dialysis according to the method of McLure, Miners and Birkett (2000). Binding measurements were performed using a Dianorm equilibrium dialysis apparatus comprising TeflonTM dialysis cells (capacity of 1.2mL per side) separated into two compartments with Sigma Aldrich (Sydney, NSW, Australia) dialysis membrane (molecular mass cut off 12kDa). One side of the dialysis cell was loaded with a solution (1mL) of morphine (0.1 to 10mM) in phosphate buffer (0.1M, pH 7.4), and the other with 1ml of either a suspension of HLM (0.5mg/mL) in phosphate buffer (0.1M, pH 7.4), or HLM (0.5mg/mL) plus BSA (2% w/v) in phosphate buffer (0.1M, pH 7.4). The dialysis cell assembly was immersed in a water bath maintained at 37°C and rotated at 12rpm for 4hr. After this time, a 200µL aliquot was collected from each compartment, treated with ice-cold methanol containing 4% glacial acetic acid (200µL), and cooled on ice. Samples were subsequently centrifuged at 4000g for 10 min at 10°C and an aliquot of the supernatant fraction (5µL) was analysed by HPLC for quantification of morphine (Section 3.2.2). Control experiments were also performed with phosphate buffer or HLM (0.5mg/mL) and BSA (2% w/v) on both sides of the dialysis cells at low and high concentrations of morphine to ensure that equilibrium was attained.

Morphine 3- and 6-glycosidation assay

(i) *Human liver microsomes (HLM) as the enzyme source*

The method employed to measure the formation of M3G, M6G and M-3-glucoside was a modification of the procedure for the quantification of morphine 3- and 6-glucuronidation (Uchaipichat et al. 2011), as reported by Chau et al. (2014). HLM (Section 2.2.5) were activated by pre-incubation on ice (30min) with alamethicin (50µg/mg protein), a pore forming peptide, as described by Boase and Miners (2002). Briefly, incubations, in a total volume of 200µL, contained phosphate buffer (0.1M, pH 7.4), MgCl₂ (4mM), alamethicin-activated HLM (0.1mg), morphine, UDP-GlcUA and/or UDP-Glc (5mM, unless specified otherwise), with or without BSA (2% w/v). After a 5min pre-incubation at 37°C in a shaking water bath, reactions were initiated by the addition of cofactor (UDP-Glc and/or UDP-GlcUA) and performed for 30min. Reactions were terminated by the addition of perchloric acid (11.6M; 2µL, or 8µL for incubations containing BSA) and cooling on ice. Samples were centrifuged (5000g for 10min), and a 10 µL aliquot of the supernatant fraction was analysed by HPLC (Section 3.2.2). Rates of M-3-glucoside, M3G and M6G formation were linear with respect to protein concentration and incubation time under these conditions. Blank incubations, which excluded cofactor, were performed to confirm the absence of interfering peaks in the HPLC chromatograms.

(ii) *Recombinant human UGTs as the enzyme source*

Recombinant UGTs were prepared or purchased as described in Section 2.2.3. Incubations with recombinant UGTs expressed in HEK293T cells were as described for HLM, except for altered protein concentration (0.4mg of HEK293T cell lysate or 0.1mg of SupersomesTM protein), incubation time (120min) and omission of alamethicin. (The sonication procedure used to lyse HEK293T cells results in full

activation of expressed UGTs. Supersomes™ similarly do not require alamethicin activation (Miners, Mackenzie & Knights 2010; Walsky et al. 2012)). Incubations with Supersomes™ employed a lower incubation volume (100µL), and hence reactions were terminated with 1µL of perchloric acid and a 10µL aliquot of the supernatant fraction was analysed by HPLC. Initially, experiments with recombinant UGT2B enzymes were conducted with Supersomes™ expressing UGT2B4, UGT2B7, UGT2B15 and UGT2B17 due to the relatively low glucuronidation activity of these enzymes expressed in HEK293T cells. However, later experiments also utilized meted UGT2B proteins expressed in HEK293T cells following the observation that insect (Hi5) cells expressed a native UDP-glycosyltransferase (see Section 3.3.6).

Inhibition of human liver microsomal M-3-glucoside, M3G and M6G formation by UGT enzyme selective substrates/inhibitors

The effect of UGT enzyme selective inhibitors and/or substrates on M-3-glucoside, M3G and M6G formation with HLM as the enzyme source was investigated to confirm the involvement of specific hepatic UGTs in M-3-glucoside formation. Compounds screened for inhibition included niflumic acid, hecogenin, fluconazole and AZT. Concentrations of each inhibitor, with the enzyme(s) inhibited in parenthesis, were: niflumic acid, 5µM (UGT1A9); niflumic acid, 100µM (UGT 1A1 and 2B15); hecogenin, 10µM (UGT1A4); and fluconazole, 2.5mM (UGT 2B7 and 2B4) (Miners, Mackenzie & Knights 2010). Inhibition by AZT (5mM), which is a selective substrate of UGT2B7, was also characterized. The morphine concentration used in the inhibition studies was 4mM, which is between the mean K_m/S_{50} values for M-3-glucoside (5.56mM), M3G (3.63mM) and M6G (2.88mM) formation (Table 3.1).

Kinetics of fluconazole inhibition of human liver microsomal M-3-glucoside, M3G and M6G formation

Since fluconazole is known to inhibit UGT2B7 activity *in vitro* and *in vivo* (Sahai et al. 1994; Uchaipichat et al. 2006b), the inhibition kinetics of M3G, M6G and M-3-glucoside formation by this compound were characterized. Experiments were performed in the presence of BSA (2% w/v) using pooled HLM (n=5) and four fluconazole concentrations (100, 400, 700 and 1000 μ M) at each of the three morphine concentrations (300, 600, 1500 μ M) spanning the K_m for M-3-glucoside, M3G and M6G measured in the presence of BSA (Table 3.1). Fluconazole inhibition of morphine glucosidation and glucuronidation in the presence of combined cofactors, UDP-Glc plus UDP-GlcUA (1:1) was additionally investigated.

Recombinant UGT morphine and 4-MU activity and kinetics

Recombinant UGT 1A1, 1A3, 1A4, 1A6, 1A7, 1A8, 1A9 and 1A10 (expressed in HEK293T cells), and 2B4, 2B7, 2B15 and 2B17 (expressed in HEK293 cells and as SupersomesTM) were used in activity screening experiments to identify enzymes with the capacity to catalyze morphine glucuronidation and glucosidation. The activity screening experiments were conducted at three morphine concentrations; 1, 5 and 10mM. In addition to UGT2B7 (268Tyr), the variant UGT2B7*1 (268His) was also screened for glycosidation activity at these morphine concentrations and at 4-MU concentrations of 100, 350 and 1000 μ M.

Morphine glycosidation kinetic experiments with recombinant Control SupersomesTM (c-SUP) and UGT2B7-expressing SupersomesTM in the absence and presence of BSA (2% w/v) followed the same experimental protocol as for HLM as the enzyme source apart from incubation time and protein (60min and 1mg/mL, respectively). Morphine

Chapter 3: Morphine glucosidation

glycosidation kinetic experiments in the presence of single and combined (1:1) cofactors with UGT2B7 expressed in HEK293T cells employed a longer incubation time (150min) and higher protein concentration (2mg/mL).

Morphine glucosidation by HLM kinetics with combined cofactors (UDP-Glc and UDP-GlcUA)

As with morphine kinetic experiments in the presence of a single cofactor (UDP-Glc or UDP-GlcUA; Table 3.1), morphine kinetics in the presence of combined cofactors (UDP-Glc and UDP-GlcUA) in a 1:1 ratio (5mM each) were performed using 11 morphine concentrations ranging from 0.1-10mM. Experiments were performed in the absence and presence of BSA (2% w/v).

Cofactor inhibition kinetics

Inhibition of M-3-glucoside formation by UDP-GlcUA (five concentrations in the range 0.2 – 1mM) at each of three UDP-Glc concentrations (1, 1.5 and 2.5mM) was investigated in the absence and presence of BSA at a fixed saturating, morphine concentration (20mM). Additionally, inhibition of M3G and M6G formation by UDP-Glc (five concentrations in the range 1 – 3mM) was investigated at each of three UDP-GlcUA concentrations (0.25, 0.5 and 1mM) in the absence and presence of BSA at a fixed, saturating morphine concentration (20mM).

3.2.2 HPLC quantification of morphine and 4-MU glycosides

Morphine-3-glucoside, M3G and M6G formation

Briefly, M3G, M6G and M-3-glucoside formation were measured simultaneously by reversed-phase HPLC using an Agilent 1100 series instrument (Table 2.3) comprising an auto-injector, a quaternary solvent delivery system and a fluorescence detector

Chapter 3: Morphine glucosidation

(1200 series). Analytes were separated on a Nova-Pak C18 column (Table 2.3). The mobile phase, delivered at a flow rate of 1mL/min, consisted of two solutions combined according to a gradient timetable (refer to Appendix 1 for details). The identity of individual peaks was confirmed by co-chromatography with authentic standards. Quantification of M3G, M6G and M-3-glucoside was achieved by reference to standard curves generated using authentic standards of each of the three analytes over the concentration range 0.5 – 80 μ M.

4-MU-glucoside (4-MUGlc) and glucuronide (4-MUG) formation

The method employed to measure the formation of 4-MUGlc and 4-MUG was as reported by Lewis et al. (2007) for 4-MUG formation. Details are given in Appendix 1. Briefly, 4-MUGlc and 4-MUG formation were measured simultaneously by reversed-phase HPLC using an Agilent 1100 series instrument (Table 2.3) comprising an auto-injector, a quaternary solvent delivery system and a UV detector. Analytes were separated on a Nova-Pak C18 column (Table 2.3). The mobile phase, delivered at a flow rate of 1 mL/min, consisted of two solutions mixed according to a gradient timetable. The identity of individual peaks was confirmed by co-chromatography with authentic standards (Table 2.1). Quantification of 4-MUGlc and 4-MUG was achieved by reference to calibration curves generated using authentic standards of each of the analytes over the concentration range 1 – 20 μ M.

Quantification of morphine binding to HLM and BSA

Morphine present in dialysate samples was measured using the HPLC instrument and column described for the morphine glycosides. Separation was achieved using an isocratic mobile phase comprising of acetonitrile (5%) and glacial acetic acid (1%) in distilled water at a flow rate of 1mL/min. The retention time for morphine under these

conditions was 2.8min. Morphine concentrations in dialysis samples were determined by comparison of peak areas to those of a morphine calibration curve prepared over the concentration range 0.1 to 10mM. The lower limit of quantitation (assessed arbitrarily as 5 times the limit of detection) for morphine was 0.15 μ M.

Calculation of fluconazole binding to HLM

In addition to determining morphine binding to HLM in the presence of BSA, fluconazole binding ($f_{u(mic)2}$) at 0.5mg/mL (C_2) of HLM (conditions used in this thesis) was calculated using Equation 3.1 (McLure et al. 2011).

Equation 3. 1: Calculation of drug unbound fraction in incubations of HLM

$$f_{u(mic)2} = \frac{1}{\frac{C_2}{C_1} \left(\frac{1-f_{u(mic)1}}{f_{u(mic)1}} \right) + 1}$$

Where C_1 and C_2 are the two concentrations of HLM and $f_{u(mic)1}$ and $f_{u(mic)2}$ are unbound fractions at the two HLM concentrations. The calculated $f_{u(mic)2}$ was 0.850, based on $f_{u(mic)1}$ value of 0.919 for binding fluconazole to HLM (0.25mg/mL) (Uchaipichat et al. 2006b). Despite the expected increase in binding at the higher HLM concentration, binding is still considered low and hence fluconazole concentrations were not corrected for binding to HLM in the calculation of kinetic parameters.

3.2.3 Human UGT2B7 cDNA

The UGT2B7 cDNA used in this thesis encodes Tyr268 (see Section 2.1.7). The alternate variant UGT2B7*1 (His268) has also been cloned previously in this laboratory (Bhasker et al. 2000). Both variant cDNAs were transfected, cultured, harvested and analyzed by Western Blot as described in Section 2.2.

3.3 Results

3.3.1 Morphine binding to HLM (\pm BSA)

To accurately measure the *in vitro* K_m (or S_{50}) of UGT2B7 substrates, BSA (2% w/v) is typically added to incubations of HLM to sequester inhibitory long-chain unsaturated fatty acids. Thus, any binding of the typically lipophilic aglycone (substrate) needs to be corrected for in the calculation of kinetic parameters. The binding of morphine to HLM and BSA was determined by equilibrium dialysis and calculated as the concentration of morphine in the buffer compartment divided by the concentration of morphine in the protein compartment (HLM \pm BSA). Binding data are shown as the fraction unbound in the incubation mixture ($f_{u(mic)}$). As shown in Table 3.3, binding to both HLM (0.5mg/mL) and HLM with BSA (2% w/v) was negligible (<10%) across the morphine concentration range investigated (0.1 – 10mM). Hence, there was no requirement for the correction of morphine concentrations due to binding to incubation constituents (HLM and/or BSA) in the calculation of kinetic parameters.

Table 3. 3: Binding of morphine to HLM (\pm BSA, 2% w/v). Data represent the means of duplicate measurements (<10% variance).

	Sample	$f_u(\text{mic})$
Controls	Buffer + HLM + BSA	0.00
	0.1mM MOR + Buffer	0.97
	10mM MOR + Buffer	0.98
	0.1mM MOR in HLM + BSA	0.93
	10mM MOR in HLM + BSA	0.98
HLM	0.1mM MOR + HLM	0.98
	1mM MOR + HLM	0.99
	10mM MOR + HLM	1.03
HLM + BSA	0.1mM MOR + HLM + BSA	0.91
	1mM MOR + HLM + BSA	0.96
	10mM MOR + HLM + BSA	0.95

3.3.2 Inhibition of HLM M-3-glucoside, M3G and M6G formation by UGT enzyme selective substrates/inhibitors

AZT, fluconazole, hecogenin and niflumic acid were screened as inhibitors of morphine glucosidation and glucuronidation with pooled HLM (n=5 livers) as the enzyme source. Fluconazole, a relatively selective inhibitor of UGT2B7/2B4 (Raungrut et al. 2010; Uchaipichat et al. 2006b), and AZT, a selective substrate of UGT2B7 (Court et al. 2003), reduced M-3-glucoside, M3G and M6G formation by 80%, 66% and 69%, respectively (Figure 3.3). The extent of inhibition of morphine glycosidation by fluconazole (2.5mM) observed here is typical of the effect of this compound on glucuronidation reactions catalyzed by recombinant UGT2B7 (Raungrut et al. 2010; Uchaipichat et al. 2006b). Hecogenin, a selective inhibitor of UGT1A4 (Uchaipichat et al. 2006a), and niflumic acid, which inhibits UGT1A1, 1A9 and 2B15 at concentrations ranging from 2.5 to 100 μ M (Miners et al. 2011), had no effect on morphine conjugate formation.

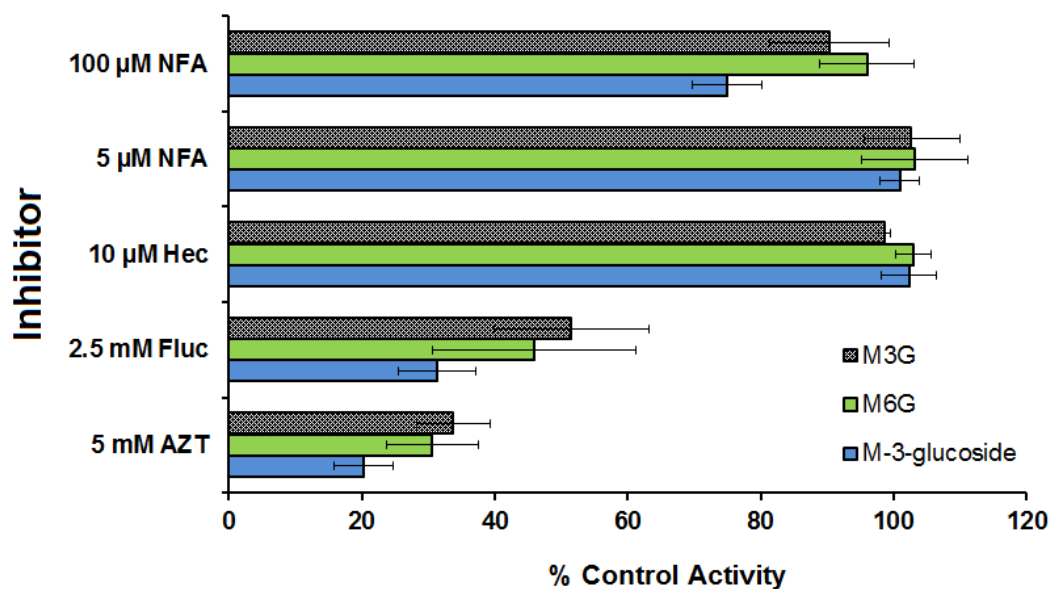


Figure 3. 3: Inhibition of human liver microsomal M3G, M6G and M-3-glucoside formation by fluconazole (Fluc), hecogenin (Hec), niflumic acid (NFA) and zidovudine (AZT).

Bars represent the mean \pm SD of quadruplicate measurements.

3.3.3 Fluconazole inhibition kinetics of morphine glucosidation and glucuronidation

Dixon plots for inhibition of M-3-glucoside, M3G and M6G formation by fluconazole in the presence of BSA are shown in Figure 3.4 and kinetic data in Table 3.4. Fluconazole (0, 0.1, 0.4, 0.7, 1.0mM) was varied as the inhibitor at three different concentrations of morphine (0.3, 0.6 and 1.5mM) as the substrate. This was repeated in the presence of combined (1:1) cofactors (5mM each). Fluconazole inhibition was investigated in the presence of a fixed and saturated concentration of UDP-Glc and UDP-GlcUA separately and combined (1:1) (5mM each). Fluconazole inhibited the formation of all three morphine glycosides in the presence of the separate and combined cofactors. Fluconazole competitively inhibited M-3-glucoside formation with K_i values of $0.11 \pm 0.003\text{mM}$ (parameter \pm SD) and $0.24 \pm 0.007\text{mM}$ in the presence of UDP-Glc and combined cofactors, respectively (Figures 3.4A and B). The approximate doubling of K_i in the presence of the combined cofactors was statistically significant ($p < 0.01$). K_i values for fluconazole inhibition of M3G formation were close in value, although statistically significantly different ($p < 0.05$); $0.24 \pm 0.016\text{mM}$ and $0.20 \pm 0.012\text{mM}$ in the presence of UDP-GlcUA and combined cofactors, respectively (Figures 3.4C and D). K_i values for fluconazole inhibition of M6G formation were also close in value and close to those determined for the inhibition of M3G formation; $0.20 \pm 0.021\text{mM}$ and $0.17 \pm 0.016\text{mM}$ in the presence of UDP-GlcUA and combined cofactors, respectively (Figures 3.4E and F). In contrast to fluconazole inhibition of M3G formation, the difference in the K_i values for fluconazole inhibition of M6G formation was not statistically significant.

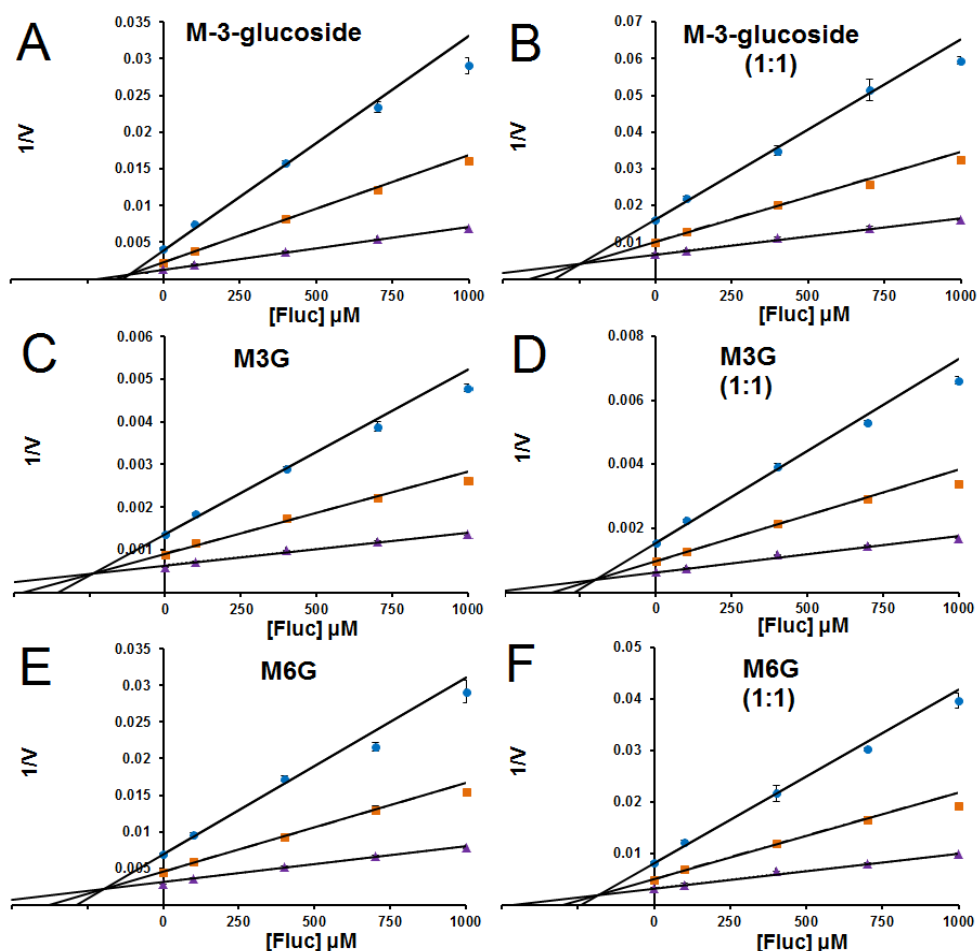


Figure 3. 4: Dixon plots for fluconazole inhibition of M-3-glucoside, M3G and M6G formation by HLM in the presence of single and combined (1:1) cofactors and BSA (2% w/v).

(A) Inhibition of M-3-glucoside formation by fluconazole at morphine concentrations of 0.3mM (●), 0.6mM (■), and 1.5mM (▲) in the presence of 5mM UDP-Glc. (B) Inhibition of M-3-glucoside formation by fluconazole at morphine concentrations of 0.3mM (●), 0.6mM (■), and 1.5mM (▲) in the presence of 5mM UDP-Glc and UDP-GlcUA (1:1).

(C) Inhibition of M3G formation by fluconazole at morphine concentrations of 0.3mM (●), 0.6mM (■), and 1.5mM (▲) in the presence of 5mM UDP-GlcUA. (D) Inhibition of M3G formation by fluconazole at morphine concentrations of 0.3mM (●), 0.6mM (■), and 1.5mM (▲) in the presence of 5mM UDP-Glc and UDP-GlcUA (1:1).

(E) Inhibition of M6G formation by fluconazole at morphine concentrations of 0.3mM (●), 0.6mM (■), and 1.5mM (▲) in the presence of 5mM UDP-GlcUA. (F) Inhibition of M6G formation by fluconazole at morphine concentrations of 0.3mM (●), 0.6mM (■), and 1.5mM (▲) in the presence of 5mM UDP-Glc and UDP-GlcUA (1:1).

Points represent the mean of quadruplicate measurements (\pm SEM error bars).

Table 3. 4: Derived K_i values for fluconazole inhibition of M-3-glucoside, M3G and M6G by HLM in the presence of single and combined cofactors (1:1 UDP-Glc and UDP-GlcUA) and BSA (2% w/v).

Pathway	$K_i \pm SD$ (mM)	$K_i \pm SD$ (mM)
	UDP-Glc <u>or</u> UDP-GlcUA	Combined UDP-Glc <u>and</u> UDP-GlcUA (1:1)
M-3-glucoside	0.11 \pm 0.003	0.24 \pm 0.007 ^b
M3G	0.24 \pm 0.016	0.20 \pm 0.012 ^a
M6G	0.20 \pm 0.021	0.17 \pm 0.016

Data are shown as the mean \pm SD for experiments (n=4) using pooled HLM (from 5 livers).

K_i : inhibition constant

^a $p < 0.05$, comparisons for each glycoside between single and combined cofactor experiments.

^b $p < 0.01$; comparisons for each glycoside between single and combined cofactor experiments.

3.3.4 Morphine glycosidation activity screening with single cofactors using SupersomesTM expressing UGT2B enzymes

Initial screening experiments with recombinant UGT2B enzymes were conducted with commercially sourced SupersomesTM expressing UGT2B4, UGT2B7, UGT2B15 and UGT2B17 due to the relatively low activity of these enzymes expressed in HEK293 cells. The four UGT2B enzymes expressed in SupersomesTM all formed M-3-glucoside (Figure 3.5A). UGT2B4 (minor) and UGT2B7 (major) also formed M3G and M6G (Figures 3.5B and C). Additionally, UGT2B15 exhibited very low morphine 3-glucosidation activity. Interestingly, however, Control SupersomesTM (c-SUP) formed substantial amounts of M-3-glucoside (Figure 3.5A). When the endogenous glucosidation activity was taken into account, only UGT2B7 had significant remaining M-3-glucosidation activity. The M-3-glucoside: M3G: M6G ratio for SupersomesTM UGT2B7 ranged from approximately 3.7: 6: 1 at the lowest (1mM) to 7: 6.5: 1 at the highest (10mM) morphine concentration. The concentration-dependent increase in M-3-glucoside formation is presumably due to combined human UGT/ native insect UDP-glycosyltransferase enzyme activities.

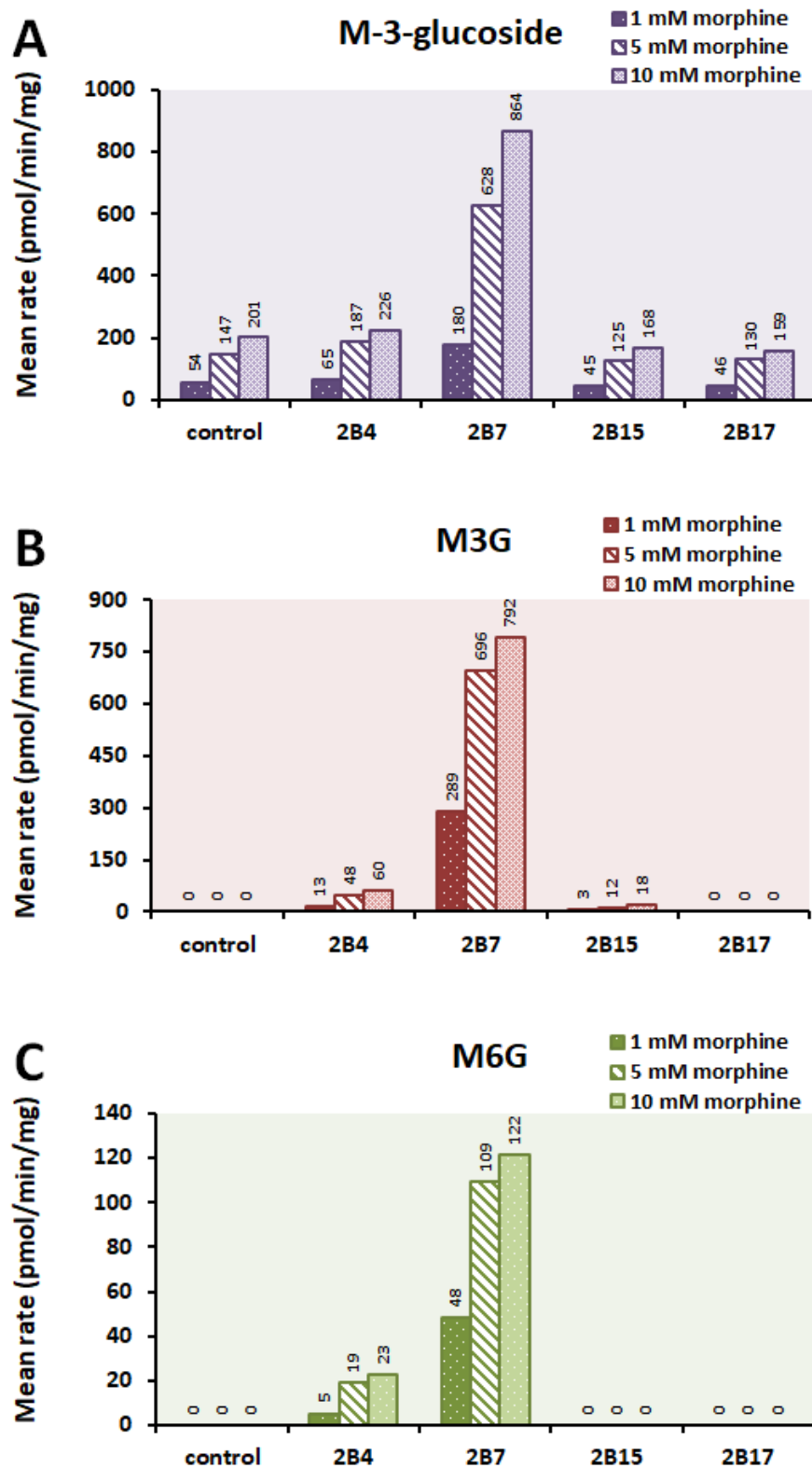


Figure 3. 5: Morphine glucosidation and glucuronidation by recombinant UGT2B enzymes expressed in Supersomes™.

Control refers to Control Supersomes™ (c-SUP). Bars represent the means of duplicate measurements (<10% variance).

3.3.5 Control SupersomesTM (c-SUP) and UGT2B7 glucosidation kinetics \pm BSA

To further understand the contribution of the endogenous UDP-glycosyltransferase to M-3-glucoside formation, the kinetics of morphine-3-glucosidation by c-SUP and SupersomesTM expressing UGT2B7 were compared in experiments using UDP-Glc as the sole cofactor. Velocity-substrate and Eadie-Hofstee plots for M-3-glucoside formation by c-SUP and UGT2B7-expressing SupersomesTM are shown in Figure 3.6 and derived kinetic parameters in Table 3.6. M-3-glucoside formation by both enzyme sources exhibited Michaelis-Menten kinetics. As expected, a higher maximal velocity was observed with UGT2B7-expressing SupersomesTM compared to c-SUP in the absence (Figures 3.6A and B) and presence of BSA (Figures 3.6C and D). This difference was approximately 5-fold, both for experiments with and without BSA (Table 3.5). Addition of BSA to incubations reduced the K_m for M-3-glucosidation by approximately 75% (5.28 to 1.45mM), but only for UGT2B7-expressing SupersomesTM. Hence, intrinsic clearance was increased nearly 4-fold for UGT2B7-expressing SupersomesTM. Interestingly, BSA had little to no effect on any of the kinetic parameters with c-SUP as the enzyme source.

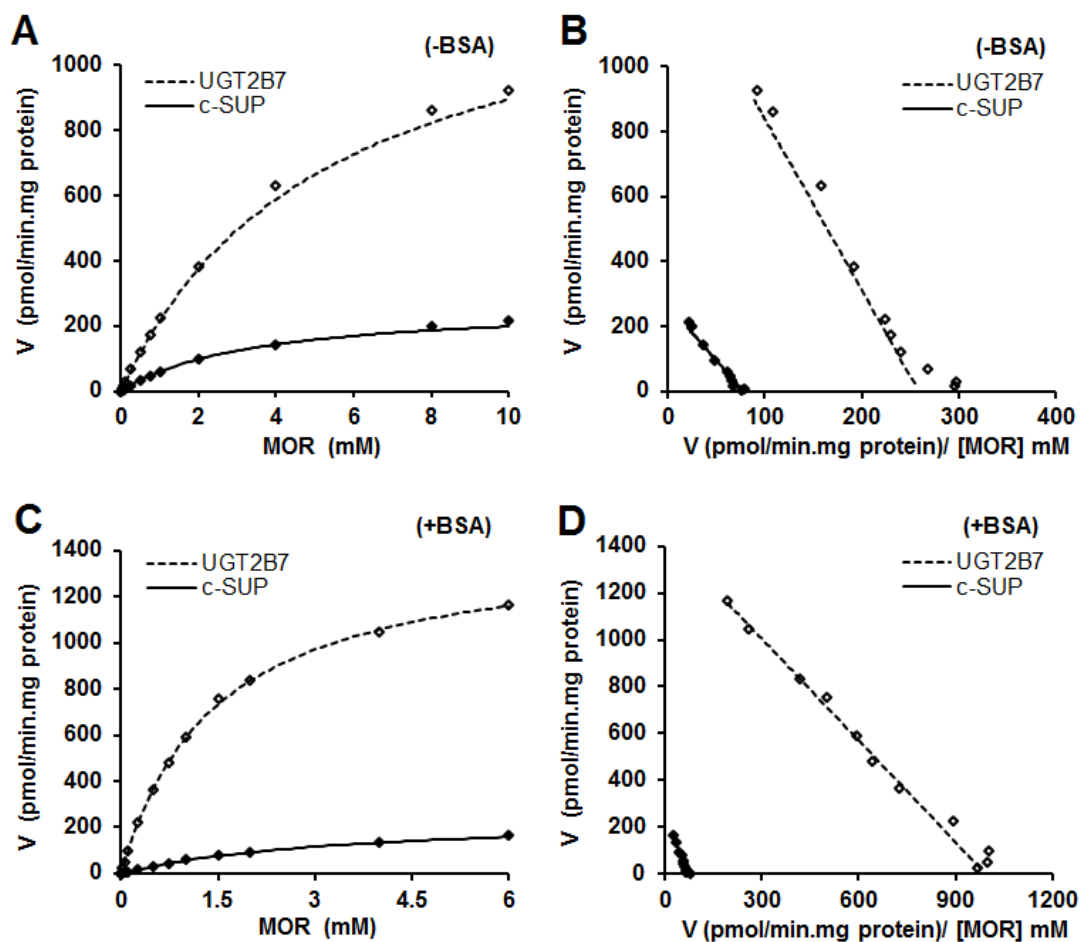


Figure 3. 6: Velocity-substrate (A and C) and Eadie-Hofstee (B and D) plots for morphine-3-glucosidation by c-SUP and Supersomes™ expressing UGT2B7 (± BSA, 2% w/v).

Points represent mean values from duplicate experiments.

Table 3. 5: Derived kinetic constants for M-3-glucoside formation by Control (c-SUP) and UGT2B7-expressing Supersomes™ in the absence and presence of BSA.

	Enzyme source	$K_m \pm SE$ (mM)	$V_{max} \pm SE$ (pmol/min.mg)	CL_{int} (μ l/min/mg)
- BSA	UGT2B7	5.28 ± 0.089	1368 ± 10.54	0.259
	c-SUP	3.42 ± 0.001	266 ± 0.06	0.078
+ BSA	UGT2B7	1.45 ± 0.032	1440 ± 12.76	0.993
	c-SUP	3.41 ± 0.009	247 ± 0.41	0.072

Data are shown as the mean \pm SE of parameter fit from duplicate experiments.

3.3.6 Morphine glycosidation activity screening with single cofactors by UGT enzymes expressed in HEK293T cells

Due to the native glucosidation background activity of insect cells, human UGT1A, UGT2B and UGT3A2 enzymes expressed in HEK293T cells were screened for morphine glucosidation and glucuronidation. Data for UGT2B and UGT3A2 enzymes are shown (Figure 3.7). As indicated in Section 3.2.1, the activity of UGT2B enzymes expressed in HEK293T cells is low compared to the enzymes expressed in SupersomesTM. Consistent with previous data from this laboratory employing UGT enzymes expressed in HEK293T cells (Stone et al. 2003), only UGT2B7 formed M6G and rates of M3G formation by UGT2B7 were 15-fold greater than for UGT1A9, the only hepatically expressed UGT1A enzyme that metabolized morphine (data not shown). The extrahepatically expressed UGT1A10 metabolized morphine with rates of M3G formation 2 to 3-fold higher than for UGT2B7 (data not shown). High levels of M3G formation by UGT1A10 have been reported previously for this enzyme expressed in insect cells (Troberg et al. 2017) and HEK293 cells (Stone et al. 2003). Rates of M3G and M6G formation by UGT2B7 expressed in HEK293T cells were approximately 80% lower than with UGT2B7 expressed in SupersomesTM (cf. Figure 3.5) at a morphine concentration of 10mM. Interestingly, UGT3A2 also catalyzed M-3-glucosidation, but rates of M-3-glucoside formation by UGT3A2 were very low (~ 1 to 2pmol/min.mg). The ratio of the M-3-glucoside: M3G: M6G maximal velocities was approximately 1.4: 5.7: 1 across the morphine concentration range (1-10mM) catalyzed by UGT2B7 (expressed in HEK293T cells).

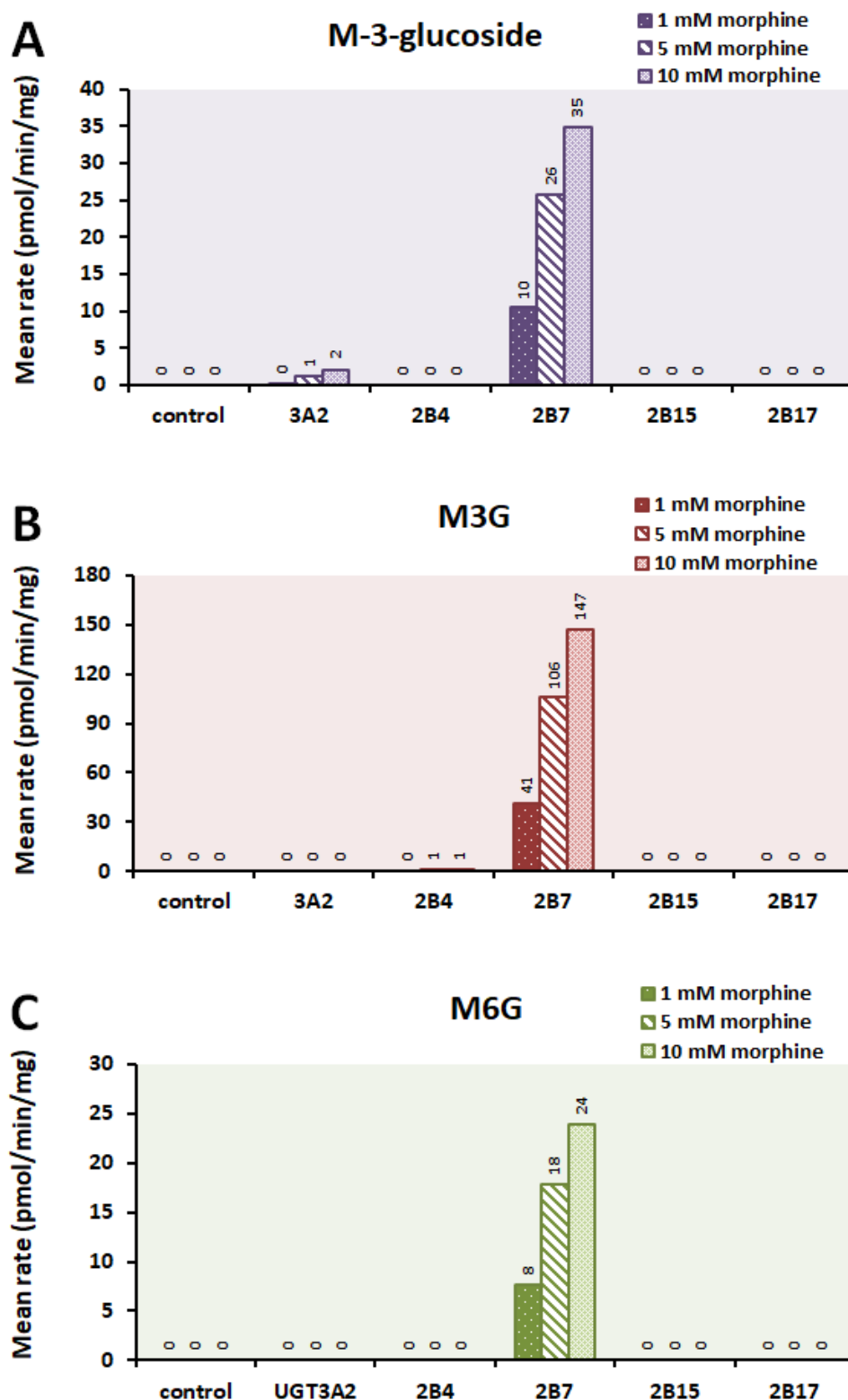


Figure 3. 7: Morphine glucosidation and glucuronidation by recombinant UGT2B enzymes expressed in HEK293T cells.

Control refers to untransfected HEK293T cells. Bars represent the means of duplicate measurements (<10% variance).

3.3.7 Kinetics of morphine glycosidation by UGT2B7 expressed in HEK293T cells in the presence of separate and combined cofactors

Given the background glucosidation activity detected in Supersomes™, HEK293T cells expressing recombinant human UGT2B7 were used to characterize the kinetics of morphine glucosidation and glucuronidation in the presence of separate (UDP-Glc and UDP-GlcUA), and combined cofactors.

Single cofactor kinetic studies (UDP-Glc or UDP-GlcUA)

Eadie-Hofstee plots for M-3-glucoside, M3G and M6G formation by human UGT2B7 expressed in HEK293T cells are shown in Figure 3.8, and kinetic parameters are given in Table 3.6. M-3-glucoside and M3G formation exhibited negative cooperative kinetics, with very similar S_{50} values (5.91 and 5.97mM, respectively) and n -values (~ 0.9), while M6G formation followed hyperbolic (Michaelis-Menten) kinetics with a K_m value of 4.16mM. Highest maximal velocity was observed with M3G (~ 143 pmol/min.mg), followed by M-3-glucoside (~ 64 pmol/min.mg) and M6G (~ 21 pmol/min.mg). The intrinsic clearance ratio for M-glucoside: M3G: M6G was 2: 4.8: 1. This is consistent with HLM data in the presence of single cofactors (cf. Table 3.1), where a similar ratio was observed (2: 5.5: 1).

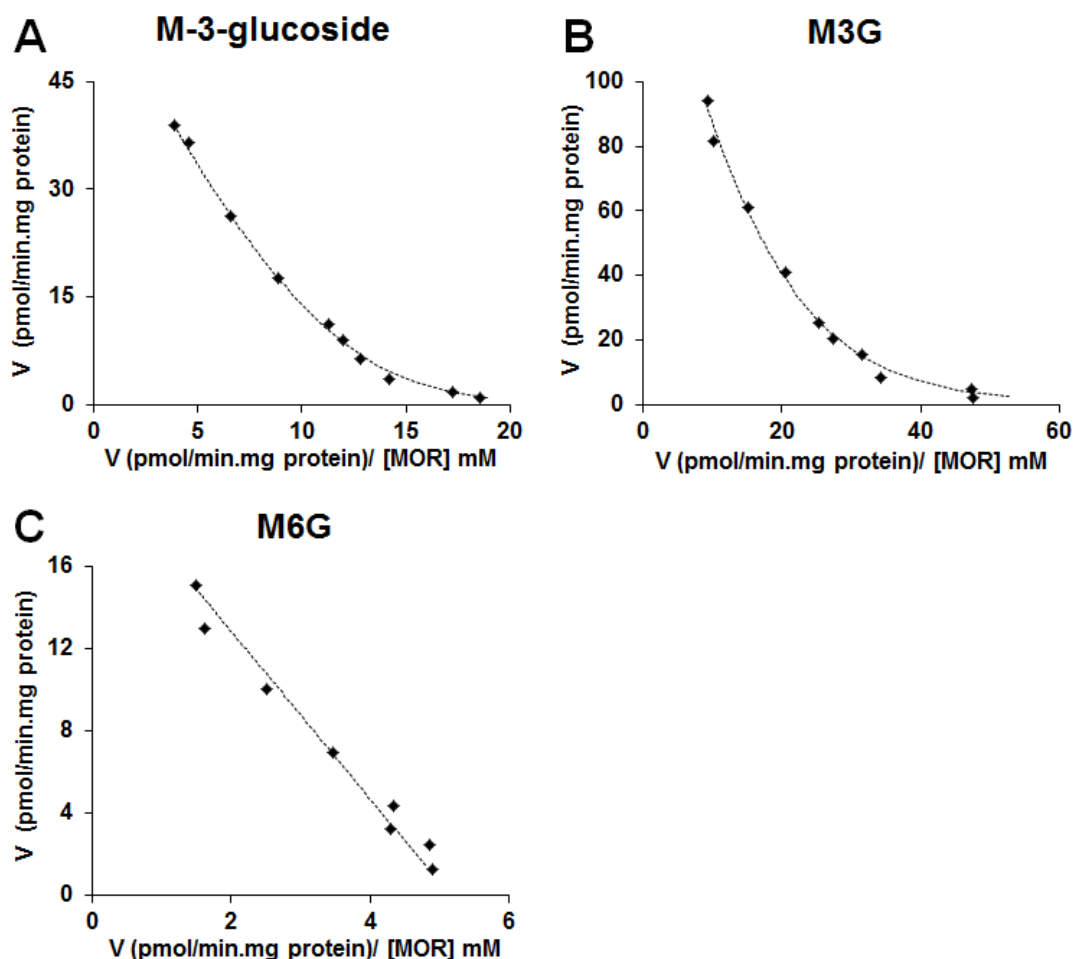


Figure 3. 8: Eadie-Hofstee plots for morphine glycosidation by UGT2B7 expressed in HEK293T cells in the presence of a single cofactor.

UDP-Glc (5mM) (A) or UDP-GlcUA (5mM) (B and C) were the respective cofactors for the glucosidation and glucuronidation reactions. Points represent the mean values of quadruplicate experiments.

Table 3. 6: Derived morphine glycosidation kinetic constants generated in the presence of a single cofactor (either UDP-Glc or UDP-GlcUA).

Glycoside	$S_{50}/K_m \pm SD$ (mM)	$V_{max} \pm SD$ (pmol/min.mg)	$n \pm SD$	CL_{int} (μ l/min/mg)
M-3-glucoside	5.91 ± 0.96	64 ± 6	0.88 ± 0.02	0.0108
M3G	5.97 ± 3.39	143 ± 32	0.89 ± 0.06	0.0239
M6G	4.16 ± 1.55	21 ± 3	-	0.0050

Data are shown as the mean \pm SD for quadruplicate experiments

Combined cofactor (UDP-Glc and UDP-GlcUA in 1:1 ratio) kinetic studies

M-3-glucoside, M3G and M6G formation by UGT2B7 expressed in HEK293T cells displayed Michaelis-Menten kinetics. Eadie-Hofstee plots are shown in Figure 3.9 and kinetic parameters are given in Table 3.7. Compared to the kinetic studies with separate cofactors, the mean K_m values for M-3-glucoside (2.87mM), M3G (3.18mM) and M6G (2.41mM) were decreased by 51, 47 and 43%, respectively, in the presence of the combined cofactors. The highest maximal velocity was observed with M3G (106pmol/min.mg), followed by M-3-glucoside and M6G (both ~19pmol/min.mg). Compared to the 70% decrease (from ~64 to 19pmol/min.mg; cf. Table 3.6) in the V_{max} values observed for M-3-glucoside formation in the presence of combined cofactors, the V_{max} values for M3G and M6G showed only a modest (25%) or no decrease, respectively. The intrinsic clearance ratio for M-glucoside: M3G: M6G formation was 0.85: 4.2: 1.

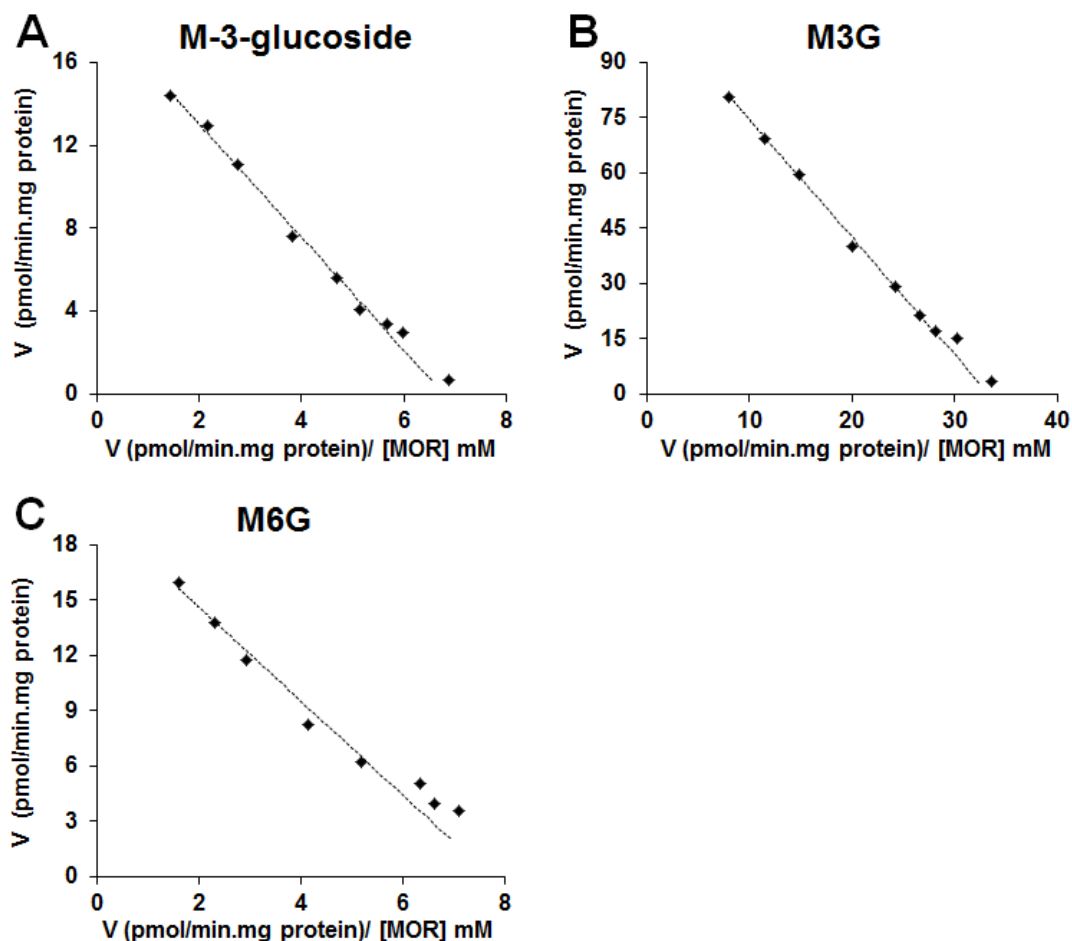


Figure 3. 9: Eadie-Hofstee plots for morphine glycosidation by UGT2B7 expressed in HEK293T cells in the presence of both UDP-Glc and UDP-GlcUA.

UDP-Glc (5mM) and UDP-GlcUA (5mM) were both present in incubations. Points represent the mean values of quadruplicate experiments.

Table 3. 7: Derived morphine glycosidation kinetic constants generated in the presence of combined cofactors (UDP-Glc and UDP-GlcUA).

Glycoside	$K_m \pm SD$ (mM)	$V_{max} \pm SD$ (pmol/min.mg)	CL_{int} (μ l/min/mg)
M-3-glucoside	2.87 ± 0.28	19 ± 2	0.0067
M3G	3.18 ± 0.38	106 ± 11	0.0334
M6G	2.41 ± 0.12	19 ± 2	0.0079

Data are shown as the mean \pm SD for quadruplicate experiments.

3.3.8 Impact of the nonsynonymous UGT2B7 SNP (268His (*1) and 268Tyr (*2)) on morphine glucosidation activity

Since UGT2B7 is the major hepatic enzyme implicated in both the glucosidation and glucuronidation of morphine, and UGT2B7*1 and UGT2B7*2 are the most studied UGT2B7 variants in relation to morphine glucuronidation, the impact of this nonsynonymous SNP on morphine glucosidation was investigated.

*HEK293T UGT2B7*1 and UGT2B7*2 protein expression*

The UGT2B7*1 and UGT2B7*2 cDNAs were stably expressed in HEK293T cells, harvested and analyzed by Western blotting according to Section 2.2 (Figure 3.10). The mean (\pm SD) density measurements (n=3) for expression of the UGT2B7*1 and UGT2B7*2 proteins were 1.01 ± 0.18 and 0.95 ± 0.09 , respectively. This factor was used to normalize subsequent morphine glucosidation and glucuronidation activity screening data with morphine and 4-MU as the substrates.

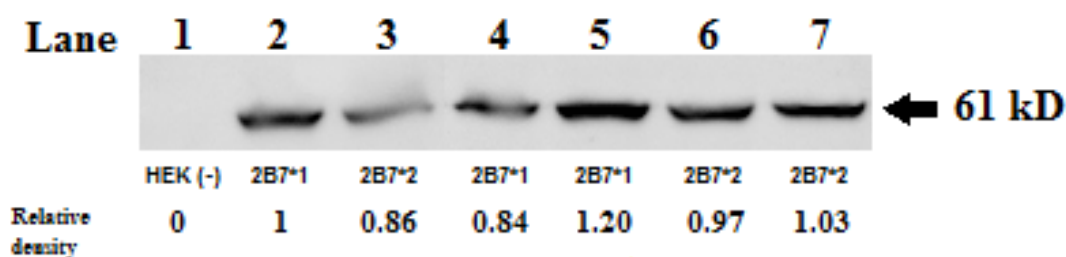


Figure 3. 10: Immunoblot of UGT2B7*1 and UGT2B7*2 stably expressed in HEK293T cells (n=3).

Lysate protein preparations (50 μ g) were resolved by SDS-PAGE, transferred to nitrocellulose, and probed with anti-human UGT2B7 antisera. Immuno-reactive bands are present at 61 kDa. Lane 1 was loaded with untransfected HEK293T (negative control), Lanes 2, 4, and 5 with UGT2B7*1 and Lanes 3, 6, and 7 with UGT2B7*2.

HEK293T UGT2B7*1 and UGT2B7*2 activity

UGT2B7*1 and UGT2B7*2 were incubated with UDP-Glc and UDP-GlcUA independently. Both variant enzymes glucosidated and glucuronidated morphine to form M-3-glucoside (Figure 3.11A), M3G (Figure 3.11B) and M6G (Figure 3.11C) in a substrate concentration dependent manner. UGT2B7*1 had consistently greater M-3-glucoside (40 - 46%), M3G (52 - 78%) and M6G (51 - 74%) formation rates than UGT2B7*2. However, there was no significant change in the ratio of M-3-glucoside to M3G and M6G (boxed numbers above bars). The ratio of the rates of M-3-glucoside: M3G: M6G formation remained consistent (~1.7: 6.5: 1) for the two variants across the morphine concentration range (1-10mM).

Experiments with 4-MU as the substrate resulted in very low rates of formation of 4-MU-glucoside, but relatively high rates of formation of 4-MUG for both UGT2B7*1 and UGT2B7*2 (Figure 3.12). Although 4-MU-glucoside formation was low, substrate concentration dependent increases in rates of product formation were evident (Figure 3.12A). As with morphine, UGT2B7*1 demonstrated somewhat higher (11 - 35%) 4-MU glucosidation activity compared to UGT2B7*2. This effect was larger with 4-MUG formation, where UGT2B7*1 exhibited approximately twice the activity of UGT2B7*2 (at 100 and 350 μ M 4-MU) (Figure 3.12B). Compared to morphine, 4-MU is a poor substrate for glucosidation with both UGT2B7 variants.

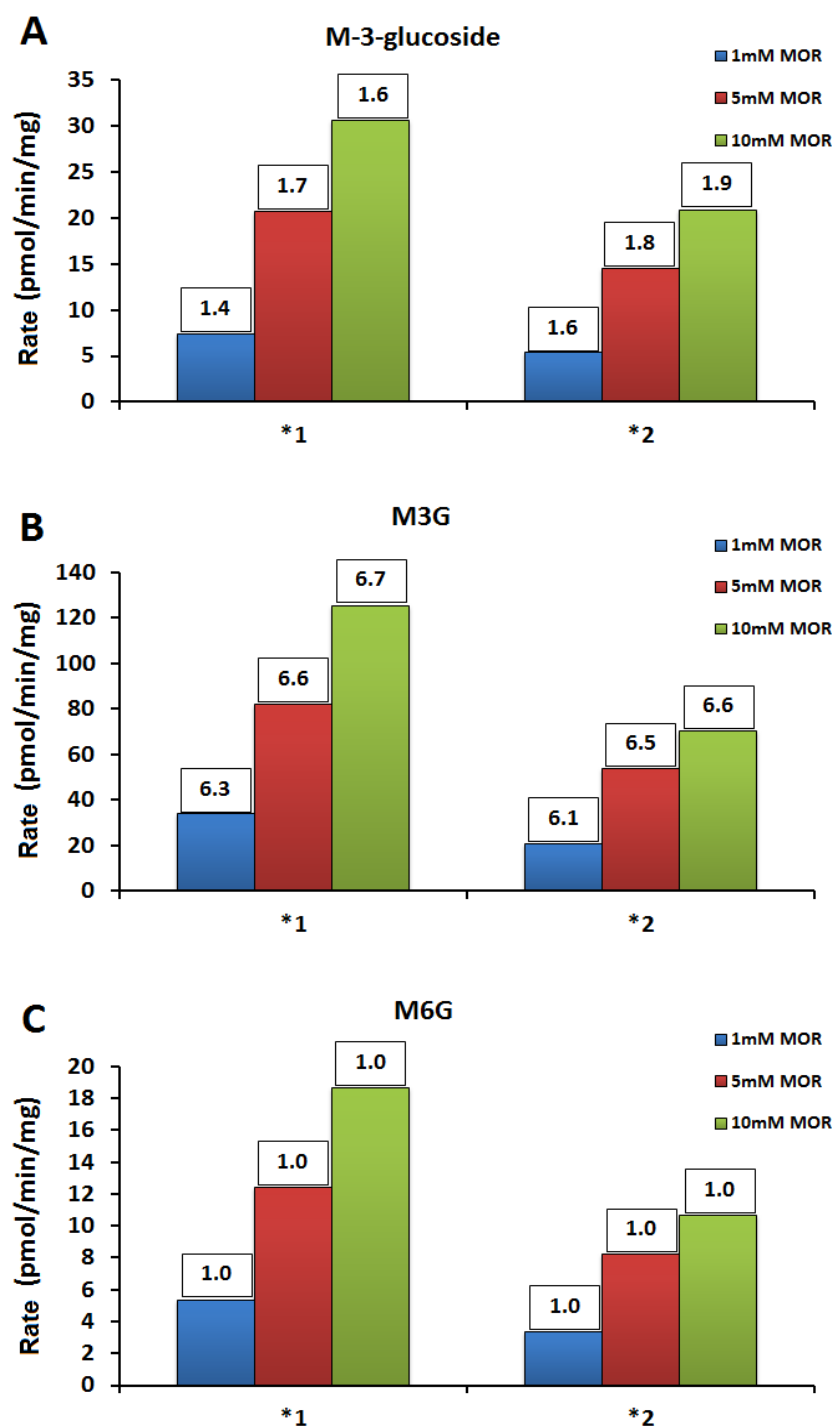


Figure 3. 11: Morphine glucosidation and glucuronidation by recombinant UGT2B7*1 and UGT2B7*2 expressed in HEK293T cells.

M-3-glucoside (A), M3G (B) and M6G (C) formation by UGT2B7*1 and UGT2B7*2. Boxed numbers above each bar represents the ratio for the rate of formation of each metabolite compared to M6G at each substrate (morphine) concentration. Untransfected HEK293T cells were used as controls (data not shown). Bars represent the means of duplicate measurements (<10% variance).

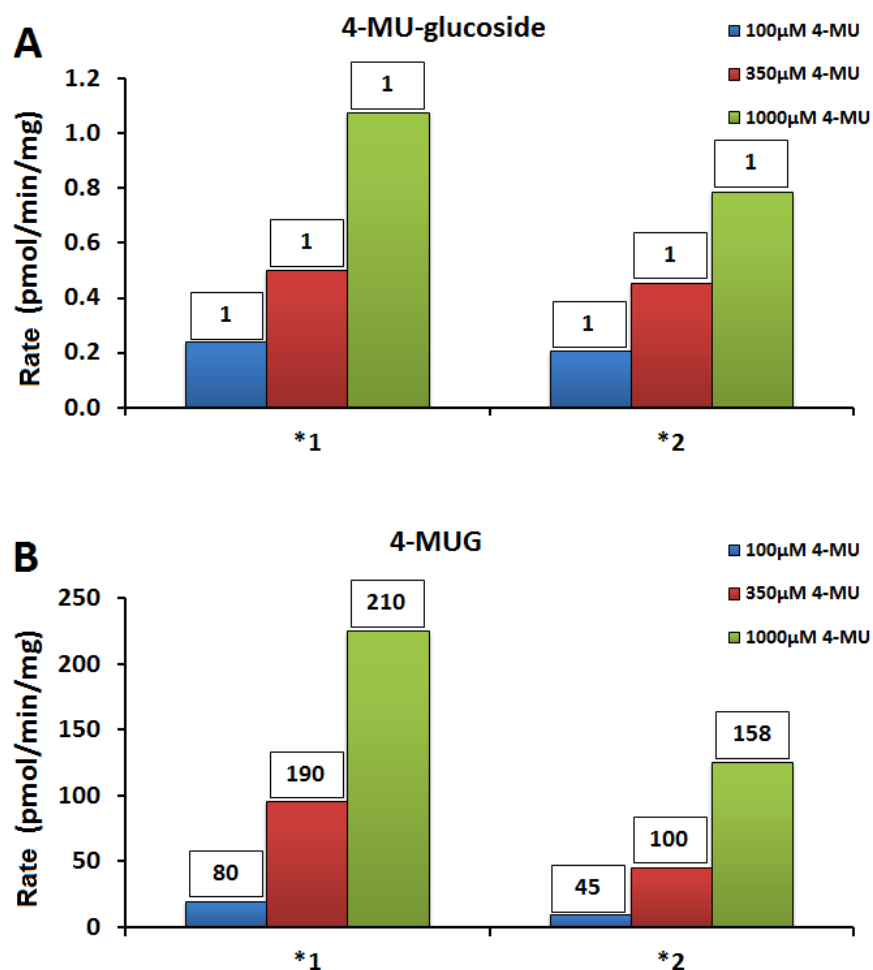


Figure 3. 12: 4-MU glucosidation and glucuronidation by recombinant UGT2B7*1 and UGT2B7*2 expressed in HEK293T cells.

4-MU-glucoside (A) and 4-MUG (B) formation by UGT2B7*1 and UGT2B7*2. Boxed numbers above each bar represents the ratio of the rate of formation of each metabolite compared to 4-MU-glucoside at each substrate (4-MU) concentration. Untransfected HEK293T cells were used as controls (data not shown). Bars represent the means of duplicate measurements (<10% variance).

3.3.9 Characterization of the kinetics of human liver microsomal morphine glycosidation in the presence of combined cofactors (UDP-Glc and UDP-GlcUA), with and without BSA

The kinetics of morphine glycosidation by HLM in the presence of UDP-GlcUA and UDP-Glc in a ratio reflective of the endogenous intracellular concentrations of cofactors were characterized. As indicated previously, the ratio of UDP-Glc: UDP-GlcUA in rat hepatocytes is estimated to be approximately 1:1 (Aw & Jones 1982). Thus, the kinetics of morphine glycosidation in the presence of combined cofactors presumably reflects physiological conditions more accurately than incubations performed in the presence of single cofactors.

In the presence of both UDP-Glc and UDP-GlcUA, 5mM each (\pm BSA, 2% w/v), there were statistically significant ($p < 0.05$ and < 0.01 ; Table 3.8) changes in all M-3-glucoside kinetic parameters compared to data previously generated in the presence of UDP-Glc alone (see Table 3.1). Whereas M-3-glucoside formation kinetics exhibited negative cooperativity in the presence of both cofactors plus BSA, Michaelis-Menten kinetics were observed in the absence of BSA (Figure 3.13A). The combination of cofactors resulted in modest changes (\sim 30-40% increase or decrease) in the mean K_m or S_{50} for M-3-glucoside formation but large decreases in V_{max} (ca. 85%) and intrinsic clearance (77% to 89%), both in the absence and presence of BSA. As observed in the presence of UDP-Glc alone, addition of BSA to incubations resulted in a significant decrease in the mean K_m (or S_{50}) for M-3-glucoside formation (by 77%) without an effect on V_{max} in the presence of the combined cofactors (Table 3.8).

Like M-3-glucoside formation, addition of the second cofactor, in this case UDP-Glc, altered the mean K_m or S_{50} values for M3G and M6G formation (35% to 64%

Chapter 3: Morphine glucosidation

increases), both in the absence and presence of BSA (Table 3.1 and 3.8; Figures 3.13B and C). However, in contrast to the 3-glucosidation pathway, changes in V_{\max} values for M3G and M6G in the presence of both cofactors were minor. As observed in the single cofactor experiments (Table 3.1), BSA decreased the mean K_m and S_{50} values for M3G and M6G formation (by 88%) in the presence of the combined cofactors, without significantly affecting V_{\max} (Table 3.8).

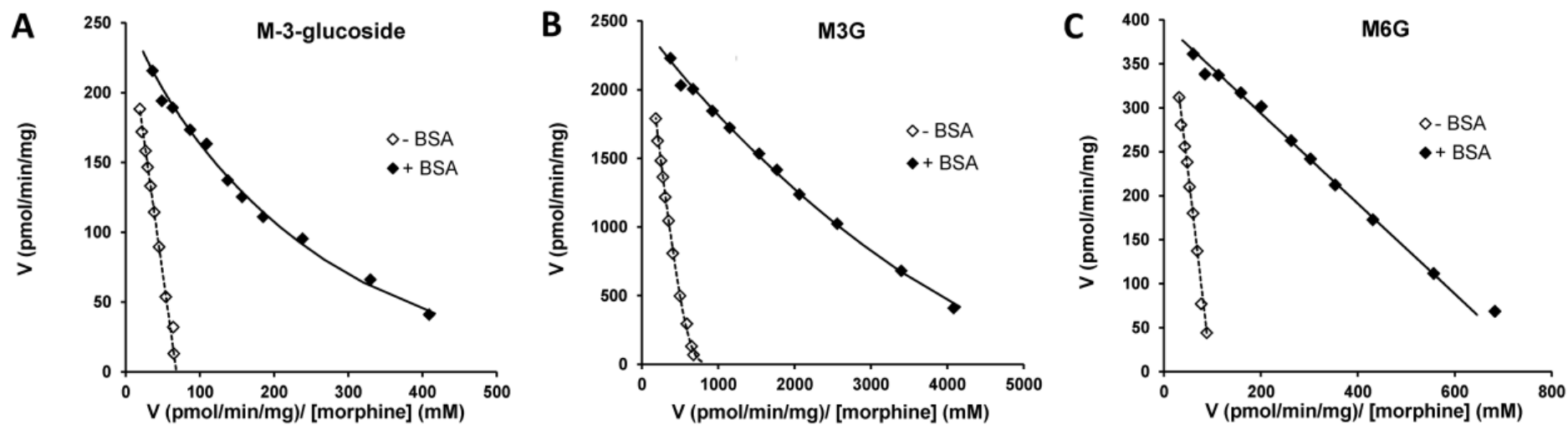


Figure 3. 13: Eadie-Hofstee plots for morphine glycosidation by HLM (\pm BSA, 2% w/v) in the presence of combined cofactors (5 mM UDP-Glc and 5 mM UDP-GlcUA) and morphine as the variable substrate.

(A) M-3-glucoside formation with combined cofactors; (B) M3G formation with combined cofactors; and (C) M6G formation with combined cofactors. Points represent the mean values of quadruplicate experiments which used pooled HLM (n=5 livers).

Table 3. 8: Derived microsomal kinetic constants for morphine glycosidation by HLM generated in the presence of combined cofactors, with and without BSA (2% w/v).

Morphine was used as the variable substrate with a 1:1 combination of UDP-Glc and UDP-GlcUA (5mM each).

Pathway	Cofactor	Without BSA				With BSA			
		K_m or S_{50} (mM)	V_{max} (pmol/min/mg)	CL_{int} (μ l/min/mg)	n	K_m or S_{50} (mM)	V_{max} (pmol/min/mg)	CL_{int} (μ l/min/mg)	n
M-3-glucoside	1:1	3.82 \pm 0.26 ^c	260 \pm 25 ^d	0.07 \pm 0.01 ^d	-	0.89 \pm 0.14 ^{b,c}	265 \pm 18 ^d	0.30 \pm 0.03 ^{b,d}	0.77 \pm 0.01
M3G	1:1	5.07 \pm 0.29 ^c	2747 \pm 163	0.54 \pm 0.02 ^c	0.93 \pm 0.02	0.61 \pm 0.09 ^{b,c}	2500 \pm 134	4.14 \pm 0.35 ^b	0.89 \pm 0.03
M6G	1:1	4.72 \pm 0.43 ^c	460 \pm 40	0.10 \pm 0.02 ^c	-	0.51 \pm 0.08 ^{b,c}	396 \pm 20	0.78 \pm 0.08 ^b	-

Data are shown as the mean \pm SD for experiments (n=4) using pooled HLM (from 5 livers).

^a $p < 0.05$, comparisons for each glycoside \pm BSA.

^b $p < 0.01$; comparisons for each glycoside \pm BSA.

^c $p < 0.05$, comparisons for each glycoside between single (see Table 3.1) and combined cofactor experiments.

^d $p < 0.01$; comparisons for each glycoside between single (see Table 3.1) and combined cofactor experiments.

Chapter 3: Morphine glucosidation

In the presence of a single cofactor, the ratio of the CL_{int} values of M-3-glucoside: M3G: M6G was approximately 2: 5.5: 1 (Table 3.1). With the combined UDP-sugars, the CL_{int} for M-3-glucoside formation was reduced by approximately 80% such that the CL_{int} ratios became (0.4 to 0.7): 5.5: 1, depending on the presence or absence of BSA. In contrast, the changes in kinetic parameters for M3G and M6G were minor. Hence, the clearance ratio of M-3-glucoside: M3G: M6G generated in the presence of both UDP-sugars more closely reflects that observed with UGT2B7 combined cofactor kinetics (0.85: 4.2: 1) and *in vivo* (0.16: 4.57: 1), with M-3-glucoside formation less than that of M6G (Chen, Zhao & Zhong 2003). As with previous data, the effect of BSA on kinetic parameters was consistent across M-3-glucoside and both morphine glucuronides (Table 3.1).

3.3.10 Cofactor inhibition kinetics (\pm BSA)

As demonstrated in the previous section, the presence of combined cofactors resulted in a 77-88% reduction in the CL_{int} for M-3-glucosidation (compared to 28-34% and 25-33% for M3G and M6G, respectively). In addition, comparison of cofactor kinetics with UDP-Glc and UDP-GlcUA demonstrated a 3- to 6-fold higher S_{50} for UDP-Glc (M-3-glucosidation) (Table 3.2) compared to UDP-GlcUA (M3G and M6G pathways). This suggests a higher affinity for UDP-GlcUA binding. To quantify the relative binding of each cofactor, inhibition kinetics (K_i measurement) with each cofactor as the co-substrate and the other as the inhibitor were performed in the absence and presence of BSA (2% w/v).

Dixon plots for the inhibition of M-3-glucoside formation by UDP-GlcUA and inhibition of M3G and M6G formation by UDP-Glc in the absence and presence of BSA at a fixed, saturating morphine concentration (20mM) are shown in Figure 3.14 and kinetic data in Table 3.9. UDP-GlcUA competitively inhibited M-3-glucoside formation with K_i values of 0.15 ± 0.01 mM (parameter \pm SE of parameter fit) and 0.18 ± 0.01 mM in the absence and presence of BSA, respectively (Figure 3.14A and D). Likewise, UDP-Glc was a competitive inhibitor of both M3G and M6G formation. K_i values with respect to M3G were 2.27 ± 0.13 mM and 1.73 ± 0.27 mM in the absence and presence of BSA, respectively (Figure 3.14B and E), while K_i values with respect to M6G were 2.49 ± 0.19 mM and 1.63 ± 0.25 mM in the absence and presence of BSA, respectively (Figure 3.14C and F).

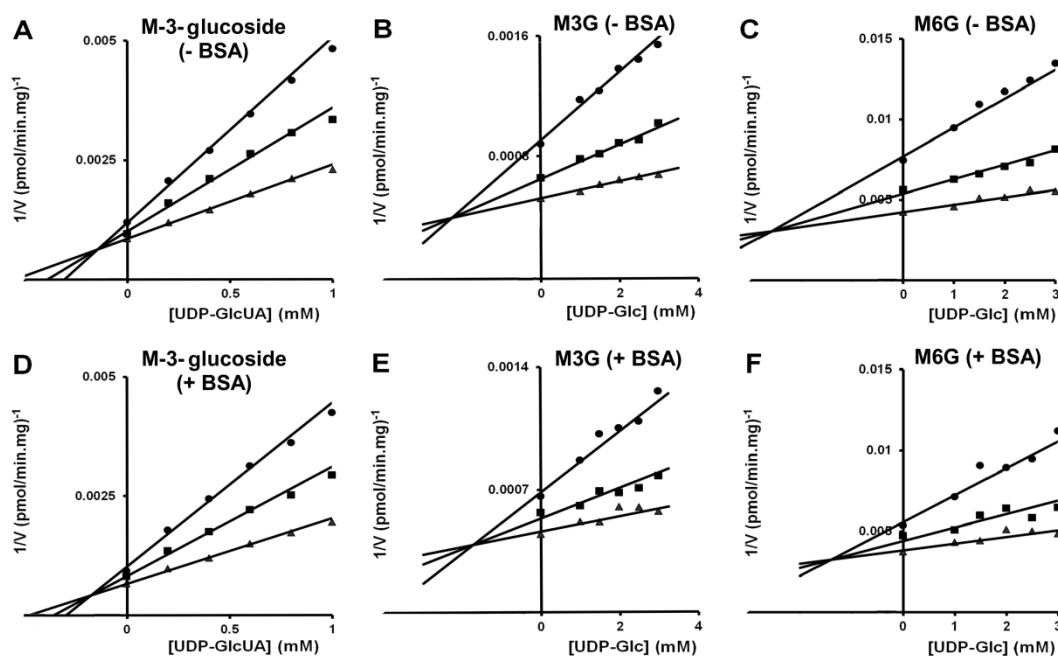


Figure 3.14: Dixon plots for the inhibition of M-3-glucoside, M3G and M6G formation by UDP-Glc and UDP-GlcUA at a fixed morphine concentration (20 mM) in the absence and presence of BSA (2% w/v).

(A) Inhibition of M-3-glucoside formation by UDP-GlcUA at 1 mM (●), 1.5mM (■), and 2.5mM (▲) UDP-Glc in the absence of BSA. (B) Inhibition of M3G formation by UDP-Glc at 0.25mM (●), 0.5mM (■), and 1mM (▲) UDP-GlcUA in the absence of BSA. (C) Inhibition of M6G formation by UDP-Glc at 0.25mM (●), 0.5mM (■), and 1mM (▲) UDP-GlcUA in the absence of BSA.

(D) Inhibition of M-3-glucoside formation by UDP-GlcUA at 1mM (●), 1.5mM (■), and 2.5mM (▲) UDP-Glc in the presence of BSA. (E) Inhibition of M3G formation by UDP-Glc at 0.25mM (●), 0.5mM (■), and 1mM (▲) UDP-GlcUA in the presence of BSA. (F) Inhibition of M6G formation by UDP-Glc at 0.25mM (●), 0.5mM (■), and 1mM (▲) UDP-GlcUA in the presence of BSA.

Points represent the mean of duplicate measurements (< 5% variance).

Table 3. 9: Derived cofactor inhibitor constants for inhibition of M-3-glucoside, M3G and M6G formation by UDP-Glc and UDP-GlcUA at a fixed morphine concentration (20 mM) in the absence and presence of BSA (2% w/v).

UDP-GlcUA concentration was varied as the inhibitor with three different concentrations of UDP-Glc as the substrate while morphine was fixed at an excess concentration (20mM). Reciprocal experiments investigated UDP-Glc as the inhibitor.

Pathway	Co-substrate	Inhibitor	$K_i \pm SE$ (mM)	
			Without BSA	With BSA
M-3-glucoside	UDP-Glc	UDP-GlcUA	0.15 ± 0.01	0.18 ± 0.01
M3G	UDP-GlcUA	UDP-Glc	2.27 ± 0.13	1.73 ± 0.27
M6G	UDP-GlcUA	UDP-Glc	2.49 ± 0.20	1.39 ± 0.25

K_i : inhibition constant

3.4 Discussion

Morphine is the most important and widely used opioid analgesic, with known active metabolites. In particular, M6G is considered a more potent analgesic than the parent compound. Hence, any novel morphine metabolites should be investigated, whether minor or major, to better understand morphine pharmacokinetics and response. Although it is unknown if M-3-glucoside possesses pharmacological activity, characterization of its potential contribution to morphine elimination is warranted.

Fluconazole (a selective UGT2B7 inhibitor) and zidovudine (a selective UGT2B7 substrate) inhibited M-3-glucoside formation by HLM whereas hecogenin and niflumic acid, which selectively inhibit UGT1A4 and UGT1A9/1A1/2B15, respectively, did not. Together, this strongly suggests that UGT2B7 (with perhaps some involvement of UGT2B4) is involved in both the glucosidation and glucuronidation of morphine as fluconazole inhibited all glycosidation pathways of morphine. Furthermore, the UGT2B7 substrate AZT also inhibited morphine glycosidation, which suggests competition at the substrate (aglycone) binding site as morphine is a well-established substrate of UGT2B7. Importantly, both fluconazole and AZT inhibited morphine glucosidation and glucuronidation to similar extents; differences between pathways were not statistically significantly different (Figure 3.3). It should be noted that fluconazole and AZT at the concentrations employed incompletely inhibit the glucuronidation of UGT2B7 probe substrates with both HLM and recombinant UGT2B7 as the enzyme sources (Uchaipichat et al. 2006b).

Since fluconazole is known to cause drug-drug interactions *in vivo* with AZT and K_i values determined *in vitro* in the presence (but not absence) of BSA predicted an interaction *in vivo*, these conditions were replicated to assess the potential inhibition of morphine glucosidation and glucuronidation by fluconazole *in vitro*. Fluconazole

inhibited M-3-glucoside, M3G and M6G formation to a similar extent with HLM (+BSA) as the enzyme source, with K_i values ranging from 0.17 - 0.24mM in the presence of combined cofactors. This K_i range is similar to the K_i value obtained for fluconazole inhibition of the UGT2B7 substrates AZT (0.145mM) and codeine (0.202mM) with HLM (+BSA) as the enzyme source (Raungrut et al. 2010; Uchaipichat et al. 2006b). Other compounds (e.g. methadone, ketoconazole, tamoxifen, diclofenac, tricyclic antidepressants (clomipramine, amitriptyline) and benzodiazepines (oxazepam, diazepam)) have been shown to inhibit morphine glucuronidation *in vitro*, and it is reasonable to assume they will also inhibit morphine-3-glucosidation (Hara et al. 2007; Morrish, Foster & Somogyi 2006; Takeda et al. 2006). As observed with HLM- and recombinant UGT2B7-catalyzed morphine glycoside formation, the presence of UDP-GlcUA in the incubation reduced the potency of fluconazole inhibition of M-3-glucosidation by approximately 50%; the K_i for inhibition of M-3-glucosidation increased from 0.11 vs 0.24mM. This doubling of the K_i produced comparable K_i 's for all pathways. Hence, as recommended for the measurement of glucoside formation for substrates that also undergo glucuronidation due to the involvement of a common enzyme (see later Discussion), the kinetic characterization of inhibitors should also be performed in the presence of both UDP-sugars.

Complementing the selective UGT inhibition experiments in HLM, and consistent with the 'albumin effect' observed for M-3-glucoside formation, experiments with recombinant UGT enzymes of the 1A and 2B subfamilies demonstrated that only UGT2B7 glucosidates morphine. The UGT enzyme activity studies further confirmed the major contribution of UGT2B7 to morphine 3- and 6- glucuronidation. Interestingly, of the UGT 1A and 2B enzymes expressed in HEK293T cells only

Chapter 3: Morphine glucosidation

UGT2B7 glucosidated morphine, whereas SupersomesTM expressing UGT 2B4, 2B7, 2B15 and 2B17 all formed M-3-glucoside. By contrast, M3G and M6G formation was observed only with SupersomesTM expressing UGT2B7 (major) and UGT2B4 (minor). Importantly, Control SupersomesTM (c-SUP) exhibited high M-3-glucosidation activity but, when corrected for endogenous glucosidation activity, M-3-glucoside formation occurred with just UGT2B7. Apart from morphine, the enzyme present in SupersomesTM has the capacity to glucosidate a structurally diverse range of xenobiotics that are metabolized by glucuronidation (see Chapter 6). Further, the kinetic characterization of M-3-glucosidation by c-SUP demonstrated the lack of a 'BSA effect'; no reduction in K_m was observed as was the case with HLM and SupersomesTM-expressed UGT2B7. This indicates that the activity of the endogenous UDP-glycosyltransferase present in Hi5 cells (used for the generation of SupersomesTM) is not inhibited by long-chain unsaturated fatty acids, presumably because the native UDP-glycosyltransferases in SupersomesTM do not metabolize long-chain unsaturated fatty acids as does human UGT2B7.

It was previously shown that HLM supplemented with UDP-GlcUA alone formed both M3G and M6G (Table 3.1 and Chau et al. (2014)). The ratios of the mean CL_{int} values for M3G to M6G (viz. 5.5: 1), in both the presence and absence of BSA (2% w/v), are consistent with the relative formation of these metabolites in humans (Hasselstrom & Sawe 1993; Milne, Nation & Somogyi 1996; Osborne et al. 1990). The mean CL_{int} values for M-3-glucosidation by incubations of HLM with UDP-Glc as cofactor (\pm BSA) were approximately twice those for M6G formation (with UDP-GlcUA as cofactor), suggesting that the 3-glucosidation pathway could account for about 20% of morphine elimination (Table 3.1). Broadly consistent with this, the ratio of M-3-glucoside: M3G: M6G formation by UGT2B7 expressed in HEK293T cells ranges

from approximately 1.25: 5: 1 at the lowest (1mM) to 1.45: 6: 1 at the highest (10mM) morphine concentration. This is a much tighter range of ratios for M-3-glucosidation than observed with SupersomesTM-expressed UGT2B7, which ranged from 3.7 to 7-fold greater than M6G. This narrower range of ratios is more consistent with human liver microsomal data (2: 5.5: 1). Thus, SupersomesTM as an expression system is not suitable for characterizing human glucosidation as it expresses a glucosidating enzyme (see Chapter 6). In addition, the present study showed that while the M3G to M6G CL_{int} ratio remained close to 5.5: 1 when human liver microsomal kinetic studies were performed in the presence of a 1:1 mixture of cofactors, reflecting the estimated ratio that occurs in hepatocytes (Aw & Jones 1982), mean CL_{int} values for M-3-glucoside formation were lower than those of M6G (Table 3.9) indicating a lesser role for glucosidation in morphine metabolism. This is consistent with the *in vivo* data of Chen, Zhao and Zhong (2003), based on urine metabolite ratios in cancer patients. The relatively lower CL_{int} for M-3-glucosidation in the presence of combined cofactors (1:1) was also observed when recombinant UGT2B7 expressed in HEK293T cells was used as the enzyme source. Hence, as noted previously characterization of complementary, parallel pathways by a common enzyme should be performed in the presence of both UDP-sugar cofactors.

With regards to UGT2B7 genetic polymorphism, M-3-glucosidation *in vitro* activity was found here to be modestly greater (40-46%) with UGT2B7*1 compared to UGT2B7*2. The same trend was also observed with M3G and M6G formation (51-78%). However, the ratios of M3G and M-3-glucoside formation relative to M6G did not differ between variants. In contrast, Coffman et al. (1998) observed the opposite trend with morphine glucuronidation, namely modestly (7-40%) higher M3G and M6G formation by recombinant UGT2B7*2 compared to UGT2B7*1. Bhasker et al.

(2000) and Court et al. (2003) reported that morphine glucuronidation activity (M3G and M6G), along with the glucuronidation of several other substrates (viz. androsterone, menthol, AZT and codeine), did not differ between HLM genotyped for UGT2B7*1 and UGT2B7*2. *In vivo* studies that have investigated relationships between UGT2B7 genotype (*1 and *2) and serum concentrations of morphine glucuronides are generally inconclusive with respect to an effect of genotype on morphine glucuronidation (Fujita et al. 2010; Holthe et al. 2002; Holthe et al. 2003; Sawyer et al. 2003). The reason(s) for the difference in M3G and M6G formation by recombinant UGT2B7*1 and UGT2B7*2 reported here and by Coffman et al. (1998) remain unclear. Although data were normalized for UGT2B7 protein expression (from Western blotting) in both studies, this may not reflect active protein. Taken together, however, the *in vitro* and *in vivo* studies tend to suggest that any effect of UGT2B7 polymorphism at position 268 (His/Tyr) on morphine glucuronidation activity is relatively minor.

Several lines of evidence suggest that UDP-GlcUA binds with higher affinity to UGT2B7 than does UDP-Glc, at least with morphine as the aglycone. Firstly, S_{50} values obtained from previous studies with UDP-GlcUA as the variable substrate were close in value for both the M3G and M6G pathways and 70% to 83% lower than the S_{50} for UDP-Glc, which was measured with respect to M-3-glucoside formation (Table 3.2). Secondly, K_i values for UDP-GlcUA inhibition of M-3-glucosidation (\pm BSA) were 0.15 - 0.18mM, whereas K_i values for UDP-Glc inhibition of morphine 3- and 6-glucuronidation in the absence and presence of BSA were an order of magnitude higher, ranging from 1.63 to 2.49mM (Table 3.2). Lastly, the CL_{int} values for M-3-glucoside formation in the presence of the combined cofactors (\pm BSA) were lower than those measured in the previous study performed with UDP-Glc alone. This was

primarily due to an approximate 85% reduction in V_{\max} . By contrast, V_{\max} values for the morphine glucuronidation pathways did not differ significantly between the single (i.e. UDP-GlcUA) and combined cofactor experiments (cf. Table 3.1 and 3.9). This presumably arises from the preferential binding of UDP-GlcUA to UGT2B7.

Tang et al. (2003) previously observed mutual competitive inhibition by UDP-Glc and UDP-GlcUA in the acyl glucosidation and glucuronidation of an endothelin ET_A antagonist by HLM and recombinant UGT2B7. K_m and K_i values for each cofactor - enzyme source combination were both approximately 0.6mM, which is similar to the S_{50} found here for UDP-GlcUA but lower than the value found here for UDP-Glc (viz. 2.0mM). Subsequent experiments by the same group with diclofenac glycosidation found a K_i for UDP-Glc similar to the S_{50} and K_i values (ca. 2.0mM) reported here with morphine as the aglycone, but a lower K_m (ca. 0.1mM) for UDP-GlcUA (Tang & Ma 2005). Differing cofactor K_m values for AS-3201 glucuronidation and glucosidation by HLM and hyodeoxycholic acid glucuronidation and glucosidation by HLM and UGT2B7 have also been reported (Mackenzie, Little & Radomska-Pandya 2003; Radomska et al. 1993; Toide et al. 2004). Tang and Ma (2005) suggested that the selectivity and binding affinity of UDP-sugars may be aglycone dependent, due possibly to enzyme conformational changes that occur upon aglycone binding. Minor formation of 4-MU-glucoside compared to M-3-glucoside seems to support this hypothesis. While this may provide an explanation for the differing results between studies most, but not all, bi-substrate kinetic investigations of the glucuronidation reaction suggest that UDP-GlcUA binding to UGT occurs first (Luukkanen et al. 2005; Manevski, Yli-Kauhaluoma & Finel 2012; Patana et al. 2007). It should be noted, however, that the interpretation of glucosidation studies with recombinant UGT

enzymes expressed in insect cells, as used by Ma and colleagues, may be confounded by the expression of an endogenous UDP-glycosyltransferase, as reported here.

In summary, the present study has demonstrated that morphine 3- and 6-glucuronidation and morphine 3-glucosidation occur as complementary metabolic pathways catalyzed by a common enzyme, namely UGT2B7. Moreover, *in vitro* kinetic data from experiments with the individual cofactors, UDP-Glc and UDP-GlcUA, appear to over-estimate the contribution of glucosidation to morphine elimination whereas data generated in the presence of both UDP-GlcUA and UDP-Glc are consistent with *in vivo* observations. Lower M-3-glucoside formation occurs due to the higher binding affinity of UDP-GlcUA to UGT2B7, resulting in competitive displacement of UDP-Glc. Further studies will provide insights into the cofactor binding domain of UGT2B7 (Chapter 4). In addition, the combined cofactor approach resulted in measurement of a K_i for fluconazole inhibition of morphine glucosidation that was in the same range as for inhibition of morphine glucuronidation (and other UGT2B7 substrates). A higher K_i compared to glucuronidation when characterized separately was unexpected, and presumably reflects the more complex inhibition process that involves both displacement of the aglycone (by fluconazole) and the cofactor (UDP-GlcUA displacement of UDP-Glc). Although greater glucuronidation activity is an advantage offered by the SupersomesTM insect expression system, glucosidation cannot be accurately measured using this enzyme source due to native UDP-glycosyltransferase activity. Thus, other expression systems such as HEK293 cells or fission yeast cells (Buchheit et al. 2011; Yang et al. 2018) are recommended. Glucosidation is a relatively minor pathway for morphine compared to glucuronidation, accounting for less than 10% of elimination. However, given the involvement of UGT2B7 in both glycosidation reactions, understanding of factors that

Chapter 3: Morphine glucosidation

affect activity of this enzyme are critical for assessing variability in response. The nonsynonymous SNP at position 268 leading to the variants UGT2B7*1(His) and UGT2B7*2(Tyr) appears not to affect *in vitro* morphine glucosidation to an appreciable extent, which is consistent with most previous *in vitro* and *in vivo* observations with morphine glucuronidation.

Chapter 4

Application of protein homology modelling to identify residues involved in the binding of cofactor to UDP-Glucuronosyltransferase 2B7 (UGT2B7)

Published in part as: Chau N, Elliot DJ, Lewis BC, Burns K, Johnston MR, Mackenzie PI and Miners JO, 2014, 'Morphine glucuronidation and glucosidation represent complementary metabolic pathways which are both catalyzed by UDP-glucuronosyltransferase 2B7: Kinetic, inhibition and molecular modelling studies', *Journal of Pharmacology and Experimental Therapeutics*, 349 (1): 126-137.

Reproduced with the permission of the American Society for Pharmacology and Experimental Therapeutics.

4.1 Introduction

Previously published data from this laboratory (Chau et al. 2014) and results presented in Chapter 3 indicate that UGT2B7 catalyzes both the glucuronidation and glucosidation of morphine, and several other substrates (e.g. HDCA, ibuprofen) have also been shown to be metabolized by UGT2B7 via these dual pathways (Buchheit et al. 2011; Mackenzie, Little & Radomska-Pandya 2003). Further, the mutual competitive inhibition observed between the separate cofactors for glucuronidation and glucosidation (viz. UDP-GlcUA and UDP-Glc) is strongly suggestive of a common cofactor binding domain. As reviewed in Chapter 1, there is much evidence to support the link between the CT with cofactor binding and the NT with aglycone

binding in human UGTs (Kubota et al. 2007; Lewis et al. 2007; Magdalou, Fournel-Gigleux & Ouzzine 2010; Miley et al. 2007; Patana et al. 2007; Radomska-Pandya et al. 2010; Tripathi et al. 2013; Xiong et al. 2008).

Despite the importance of UGTs in drug and chemical metabolism, experimentally derived physical models of human UGTs are limited. Indeed, an X-ray crystal structure for an entire UGT protein is lacking. However, Miley et al. (2007) have reported a partial apo crystal structure of the UDP-GlcUA binding domain (170 residues; 282-451) of UGT2B7. The domain consists of seven α -helices and six β -strands (Figure 1.8). Based on this structure and several X-ray crystal structures of non-mammalian glycosyltransferases, homology models of human UGT proteins have been generated (see Table 1.6; see Chapter 1.2). For UGT2B7, comparative homology modelling and site-directed mutagenesis data suggest that Asn378 is a key residue involved in binding the glucuronic acid moiety, along with the demonstrated and highly conserved Asp398 and Gln399 (Figure 1.10) (Miley et al. 2007). In contrast, little is known about the residues likely to be important for the binding of UDP-Glc to human UGT2B7.

Improved high throughput ADME screening activities for identifying CYP oxidative clearance over the last few decades have likely improved drug attrition rates due to poor pharmacokinetics, but one consequence of ‘designing out’ this capacity for oxidative clearance from new drug entities is the increased involvement of non-CYP enzymes in drug clearance pathways (Boyd & Lalonde 2007; Foti, Fisher & Lyubimov 2012; Gan, Ma & Zhang 2016). The design of new drug molecules in current years has gravitated towards entities which are larger, more complex and lipophilic, and with more hydrogen bonding donor and acceptor groups, resulting in compounds that are ‘less drug-like’ than previous ‘typical’ drugs on the market (Walters et al. 2011).

Glucuronidation as a drug clearance pathway is listed as the second most common pathway after CYP-mediated oxidative metabolism for the top 200 drugs reviewed by Williams et al. (2004), with UGT2B7 listed as the most commonly listed enzyme followed by UGT1A4 and UGT1A1, respectively. Since human UGT2B7 is involved in the glucuronidation of many important drugs (Miners, Mackenzie & Knights 2010) and is implicated in more clinically relevant drug-drug interactions (DDIs) than other UGTs (Kiang, Ensom & Chang 2005; Miners et al. 2010; Rowland, Miners & Mackenzie 2013), glucuronidation and glucosidation catalyzed by UGT2B7 (and other enzymes) may become more important clearance pathways for new drugs given the current trends in drug discovery.

Thus far, studies identifying the donor/acceptor binding site residues of human UGTs have focused on UDP-GlcUA as the cofactor, except with the UGT3 and UGT8 families because they are known to utilize UDP-sugars other than UDP-GlcUA (Meech et al. 2015; Meech et al. 2012b; Nair et al. 2015). As such, the UGT1 and UGT2 family are generally viewed as mainly utilizing UDP-GlcUA in the conjugation of lipophilic drugs and xenobiotics. However, there is *in vitro* evidence to suggest that UDP-sugars other than UDP-GlcUA may be utilized by these UGTs. Since a partial UGT2B7 crystal CT structure exists (UGT2B7-CT), and UGT2B7 has been shown to catalyze both the glucosidation and glucuronidation of morphine and other compounds, this enzyme provides a good model to study the structural determinants of UDP-sugar selectivity of a human UGT.

4.1.1 Experimental plan and aims

The general aim of experiments described in this chapter was to identify residues that confer cofactor binding selectivity of UGT2B7 using automated *in silico* docking with

Chapter 4: Application of UGT2B7 protein homology modelling

a 3-D homology model of UGT2B7, and model validation by site-directed mutagenesis and enzyme activity studies. This study employed computational techniques established in the Department of Clinical Pharmacology, using an existing homology model of UGT2B7 (Lewis, Mackenzie & Miners 2011).

Specific aims were to:

1. Separately dock UDP-GlcUA and UDP-Glc in the energy minimized structures of UGT2B7-CT and the entire UGT2B7 protein generated by homology modelling.
2. Determine whether UDP-GlcUA, which contains a negatively charged carboxylate group at C6 of the sugar moiety, and UDP-Glc have distinct binding poses in the structures of UGT2B7-CT and the full length UGT2B7 protein.
3. Identify the residues that confer cofactor binding selectivity from hydrogen bonding interactions with the sugar moieties of UDP-Glc and UDP-GlcUA.
4. Validate the observations from the docking experiments by site-directed mutagenesis and enzyme activity studies.

4.2 Methods

4.2.1 Identification of residues involved in UDP-sugar binding using the C-terminal X-ray crystal structure and homology model of human UGT2B7 using computational modelling

UDP-Glc and UDP-GlcUA were separately docked into the active site of the UGT2B7-CT crystal structure (PDB code 2O6L) (Miley et al. 2007) and full length UGT2B7 homology model (Lewis, Mackenzie & Miners 2011) using the SYBYL-X 1.1.2 Surflex-Dock program (Table 2.10). The Surflex-Dock program (Jain 2003) uses an empirical scoring function and search engine (Jain 1996) to dock ligands into the protein active site, whereby docking is guided by the 'protomol'. Additionally, superpositioning analysis (structural overlay and comparison) of both UDP-sugars was also performed with the full length UGT2B7 homology model before docking studies to demonstrate that a full protein structure containing both the C- and N-termini may provide more information on potential binding residues for UDP-Glc and UDP-GlcUA.

Preparation of UGT2B7 protein model

Preparation of the UGT2B7 C-terminal structure for model generation

The Surflex-Dock docking procedure requires that the 3-D structure of the protein has hydrogens atoms, which need to be added to the X-ray crystal templates, and an active site free of co-crystallized ligand. UGT2B7-CT (PDB code 2O6L) was crystallised as two monomers; Chain A and B. Backbone alignment of the two monomers shows that they have a root mean square deviation (RMSD) of 1.25Å, indicating that the structures have crystallized with similar secondary structure. However, there were some minor differences between the two monomers with Chain A missing residues at the N- (282-

284) and C- (447-451) terminus ends, while Chain B had missing residues from positions 311-314. Chain A was chosen for model generation because missing residues were simpler to model than joining two parts of a monomer. Once residues were checked for correct atom typing, hydrogen atoms were added to all residues, and water molecules were removed from the structures. Amino acid sidechains were progressively energy minimized using the AMBER7_FF99 force field (recommended for biopolymers), and Powell method, which is the fastest and most efficient method for small and large molecules. Maximum iterations were set at 1,000 (Powell 1977; Tripos™ 2010b,d). As noted earlier, UGT2B7-CT was crystallised without bound cofactor. The UGT2B7 homology model (Lewis, Mackenzie & Miners 2011) was prepared using the same process described for UGT2B7-CT.

Preparation of cofactors (UDP-glucose and UDP-glucuronic acid) as ligands

UDP-Glc and UDP-GlcUA ligand preparation for superpositioning

Following the method of Miley et al. (2007), the energy minimized UGT2B7-CT (Figure 4.1; orange ribbon) was superpositioned (sequence alignment and structural overlay) on the CT of the plant UDP-glucose:flavanoid 3-O-glycosyltransferase (VvGT1) structure (Figure 4.1; blue ribbon, PDB code 2C1Z) co-crystallized with UDP-2-deoxy-2-fluoro-glucose (U2F) (Offen et al. 2006) (Figure 4.1). These two CT domains share 23.9% sequence identity. The RMSD over the carbon atom backbone (C^{α}) of 162 residues was 3.28Å, with high structural homology observed between the structures. The non-minimized crystal structure of UGT2B7-CT (Figure 4.1; green ribbon and missing residues due to poor electron density) was also superpositioned on the VvGT1 structure to gauge how much the structural minimization and preparation process affected the structure of the protein. The RMSD was 3.49Å which is close to

that observed for the energy minimized UGT2B7-CT. Sequence identity was 25.3% over 155 residues (due to missing residues, as previously described). Although Miley et al. (2007) reported an RMSD of 1.77Å between VvGT1 and the UGT2B7-CT, the alignment spanned only 147 residues.

Despite the difference in RMSD, the domains align very well, particularly at C α 3, C α 4, and C β 5 where the UDP-sugar UDP-2-deoxy-2-fluoro glucose (U2F) is in close contact (Figure 4.1). Hence, the U2F position and 3-D co-ordinates were used as the reference point for superposition of UDP-Glc and UDP-GlcUA into the human UGT2B7 homology model. These co-ordinates were also used for optimizing the protocol for docking into both the human UGT2B7-CT minimized structure and UGT2B7 homology model. The following chemical modifications were made to U2F: fluorine was removed at C2 and replaced with a hydroxyl group to form UDP-Glc, and then from this structure the C6 hydroxyl group was replaced with a carboxylate group to produce UDP-GlcUA. No additional positional optimization was undertaken with the UDP-sugars and UGT2B7 homology model structure after this step.

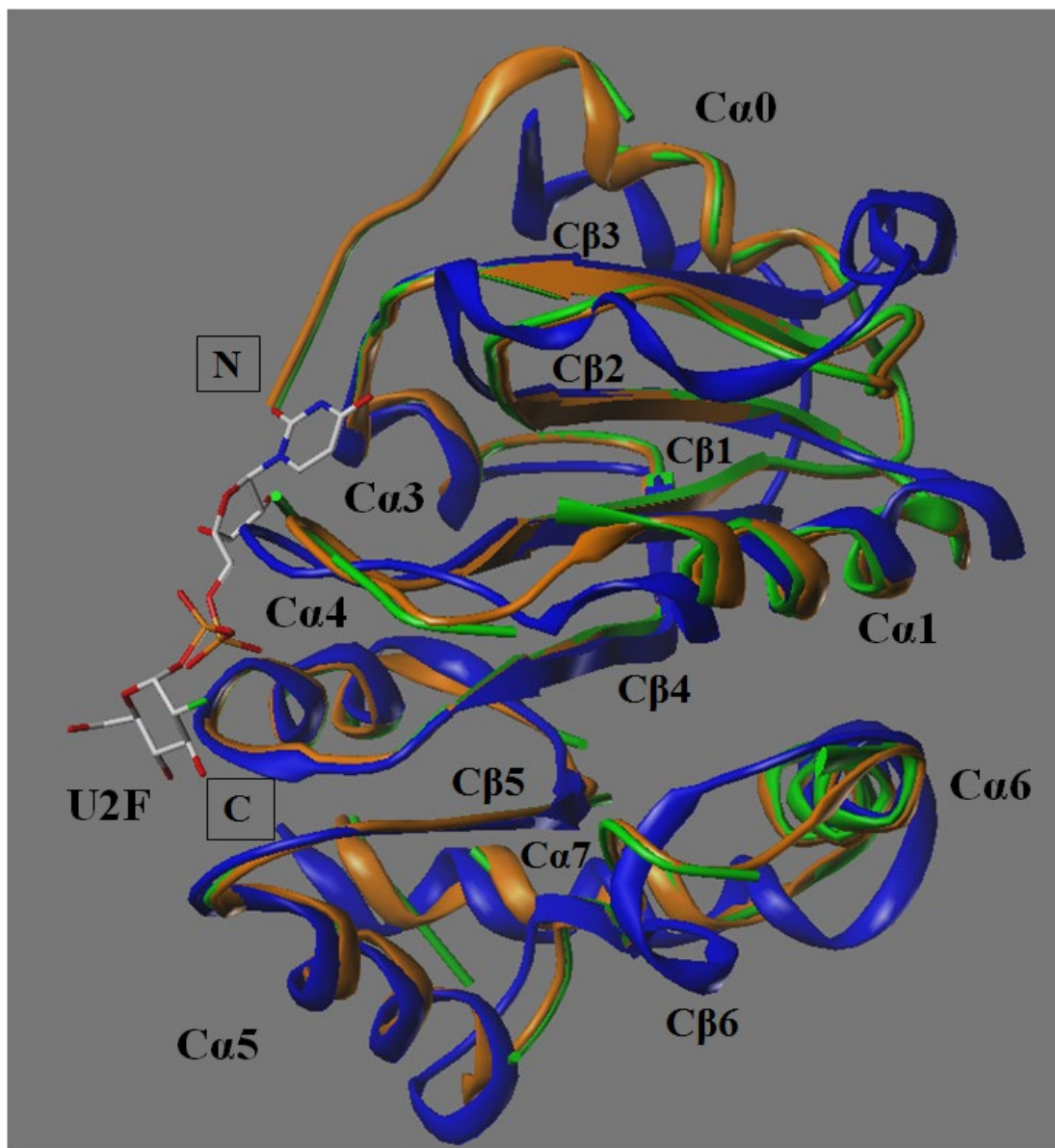


Figure 4. 1: Comparison of labelled secondary structure (ribbon cartoon) of CT domains of plant VvGT1 superimposed with human UGT2B7-CT.

The reference structure VvGT1 (blue; PDB code 2C1Z) was aligned over 162 residues with the energy minimized UGT2B7-CT structure (orange) and over 155 residues with the non-minimized UGT2B7-CT (green; PDB code 2O6L). The RMSD and sequence identity for energy minimized UGT2B7-CT were 3.28Å and 23.9%, respectively, while the RMSD and sequence identity for non-minimized UGT2B7-CT were 3.49Å and 25.3%, respectively. The plant VvGT1 co-crystallized UDP-sugar, U2F, is shown as a reference for the binding region and surrounding secondary structures. The amino-(N) and carboxyl-(C) terminal ends of the protein structure are labelled and boxed.

UDP-Glc and UDP-GlcUA ligand optimisation for docking

The 3-D structures of UDP-Glc and UDP-GlcUA were prepared using the planar structure information with a canonical SMILES file available from the PubChem website (<http://www.ncbi.nlm.nih.gov/pccompound>; chemical identification numbers 8629 and 17473, respectively). This structure input file was subsequently used to generate an energy minimized 3-D structure in the SYBYL mol2 file format ready for docking. Partial atomic charges were determined using the Gasteiger-Huckel method (TriposTM 2010a) with energy minimization performed using the same process as described for UGT2B7-CT and homology models, but with the Tripos force field as this is more suitable for small molecules (TriposTM 2010b).

Surflex-Dock requires ligands to be 3-D, atoms properly typed (into a file format recognised by the SYBYL dictionary) and with attached hydrogens (TriposTM 2010a,c). Certain functional groups such as carboxylate, which can be typed in more than one way (aromatic or Kékulé), may produce different results due to electrostatic differences. Tripos recommends using the aromatic (delocalised) form of the carboxylate. Tripos also required that the oxygens in a phosphate group be typed the same way. This resulted in 2 (phosphate backbone) and 3 (phosphate backbone and carboxylate) aromatic-like sites on UDP-Glc and UDP-GlcUA, respectively. It was also recommended that ligands are in the relevant protonation state at biological pH. Hence, Marvin View 5.3.8 (Table 2.10) was used to determine the major species of UDP-Glc and UDP-GlcUA at pH 7.4 (Figure 4.5). UDP-Glc and UDP-GlcUA have charges of -2 (phosphate backbone) and -3 (phosphate backbone and carboxylate), respectively. Hence, the carboxylate ion of UDP-GlcUA was docked.

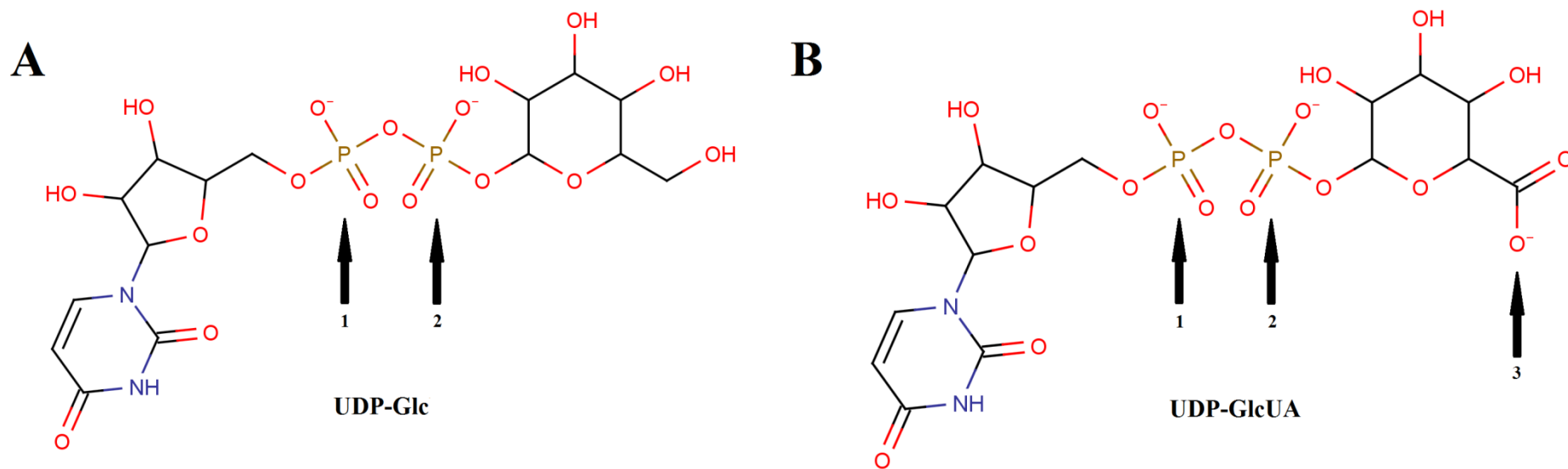


Figure 4. 2: Major protonation species of UDP-Glc and UDP-GlcUA at biological pH 7.4 (2D planar structure).

UDP-Glc (A) has a charge of -2 due to the two negatively charged phosphate groups (arrows 1 and 2) on the UDP-sugar backbone while UDP-GlcUA (B) has a charge of -3 due to the extra carboxylate group on C6 of the glucuronic acid sugar moiety (arrow 3), in addition to the two phosphate groups (arrows 1 and 2) as with UDP-Glc.

Preparation of the binding site for docking

UGT2B7 protomol binding site optimization

A protomol is a computational representation of an intended binding site to which putative ligands are aligned and placed initially during the docking process (Ruppert, Welch & Jain 1997). It is not designed to be an absolute docking envelope and the docked ligands are scored in the context of the protein. The protomol can be generated automatically (the largest cavity is selected), or defined based on a similar or related ligand, or a known active site. The constructed protomol is a pocket of ‘sticky spots’ of probes (steric hydrophobic CH₄, hydrogen bond donor N-H, and hydrogen bond acceptor C=O) complementary to the active site surface of the protein. The protomol is biased towards the protein’s interior hydrophobic regions (Figure 4.3) as hydrophobic interactions play a large part in the binding of ligands (TriposTM 2010c).

The UGT2B7 homology model protomol threshold (volume and depth parameter) and bloat (inflation parameter) conditions were optimised based on existing location and orientation data from the red grape UDP-glucose:flavanoid 3-O-glycosyltransferase (VvGT1) X-ray crystal structure (PDB code 2C1Z) with the co-crystallized ligand U2F (Offen et al. 2006) (Figure 4.4A). The threshold parameter (between 0.01 and 1.0) indicates the extent or depth that the protomol can be buried in the protein, where a default setting of 0.5 is considered adequate in most circumstances. Increasing this number decreases the volume of the binding site. The bloat parameter (0 - 10Å) is used to inflate or expand the protomol in 3-D. A smaller protomol is generally preferred as it provides a more defined space. The residues covered within the generated protomol space in both UGT2B7-CT and the homology model (Figure 4.3) were mapped in different sections (N- vs. C-terminus), and are colour coded in the two UGT2B7

Chapter 4: Application of UGT2B7 protein homology modelling

structures (CT and full-length homology model) shown in Figure 4.4B. Based on the plant VvGT1 crystal complexed with U2F (Figure 4.4A), docking occurs in the expected domain of each UGT2B7 structure.

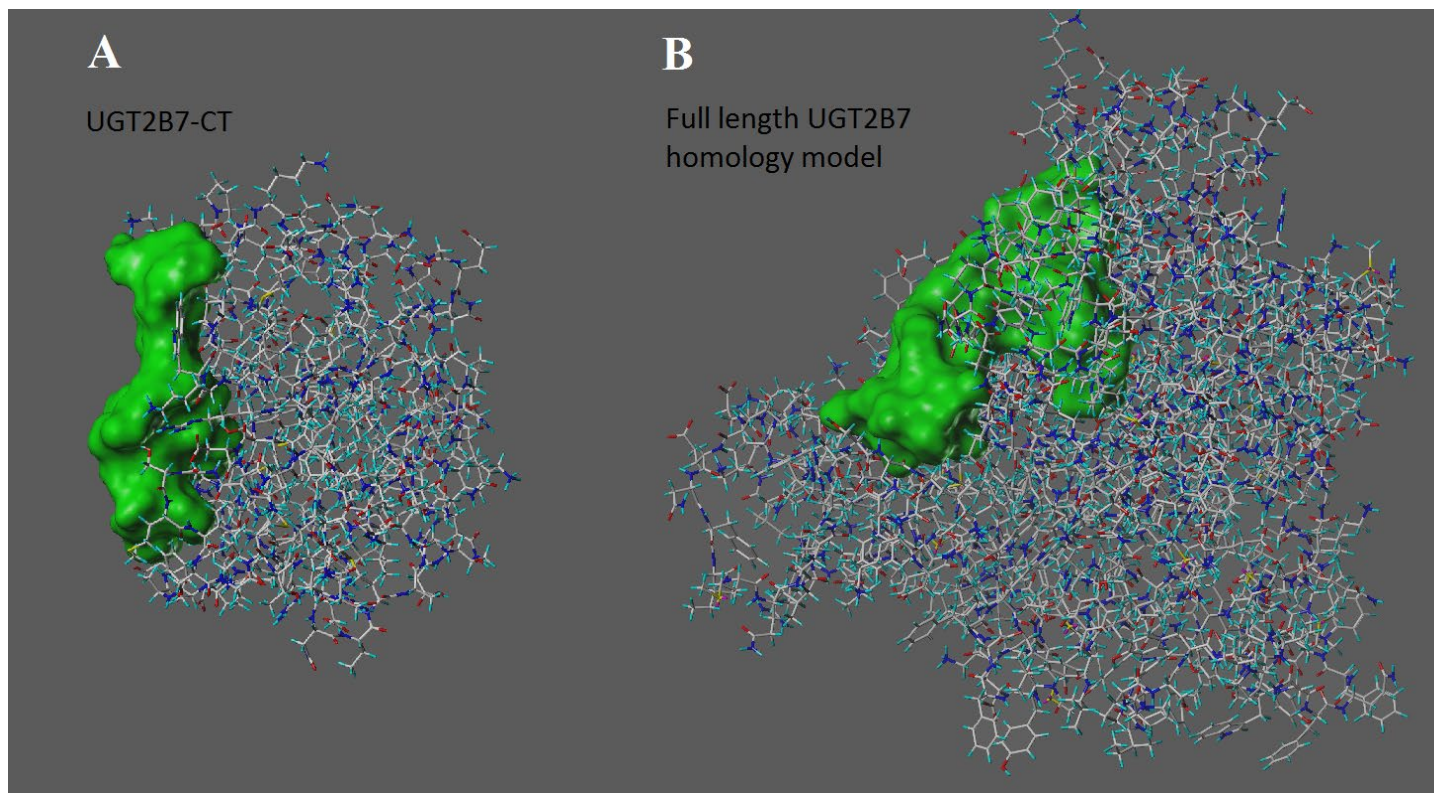


Figure 4. 3: Surface representation of the protomol cofactor binding pocket (globular green construction) of UGT2B7-CT and full length UGT2B7 homology model.

The protomol was generated at threshold and bloat parameters of 0.2 and 2.0, respectively for both UGT2B7-CT (A) and the full length UGT2B7 homology model (B). Both structures are oriented with the C-terminus on its side facing forward. The N-terminus of the homology model is therefore protruding back into to page (B). Atoms of residues are presented as capped sticks in grey (carbon), cyan (hydrogen), blue (nitrogen), yellow (sulfur) and red (oxygen).

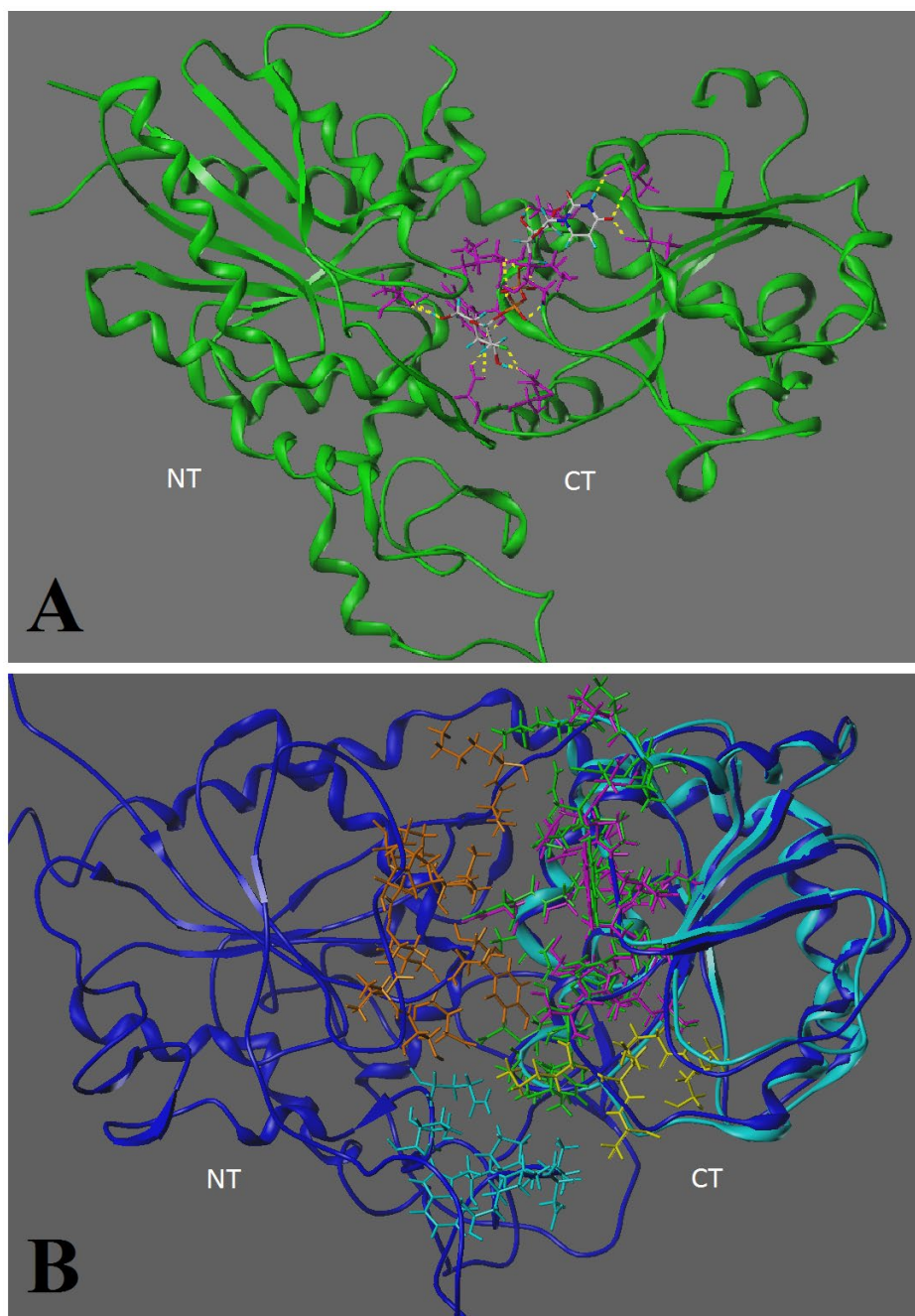


Figure 4. 4: Comparison of the full crystal structure of plant VvGT1 complexed with U2F and human UGT2B7 CT and full homology model protomol residue map.

Ribbon cartoon representation of secondary structure of VvGT1 (green) with U2F hydrogen bonded (yellow dotted lines) to residues within a 3 Å radius (magenta) (A). Ribbon cartoon representation of the secondary structure of UGT2B7-CT (cyan) and full homology model (dark blue) superpositioned with mapped residues of the protomol (threshold 0.2, bloat 2.0) in green (UGT2B7-CT only), orange and cyan (top and bottom NT of model, respectively), and magenta and yellow (top and bottom CT of model, respectively) (B).

Docking and scoring poses

Surflex-Dock uses the Hammerhead procedure to ‘dock’ or screen for the binding of flexible molecules in a ligand binding domain (Welch, Ruppert & Jain 1996). Briefly, ligand fragments are generated, the geometrically favoured top scoring ‘head’ fragments are rigidly aligned onto the protomol probes, and then the rest of the fragments are ‘docked’ or aligned and refined starting with the head fragment. ‘Head’ fragments are the top scoring lead fragments that align well with the protomol probes and do not penetrate excessively into the protein (TriposTM 2010c). As indicated earlier, docked ligands are scored in the context of the protein and not in the context of the protomol. Three factors were considered when assessing which docking results are ‘sensible’ or ‘reasonable’ as hypotheses worthy of testing experimentally. Poses generated from docking were initially evaluated based on two scoring functions: a consensus score (CScore) and the Surflex-Dock scoring function (Total score) (Jain 1996). The highest scoring poses based on a combination of these two scores were then visually inspected and poses selected based on the number (the higher the better) of hydrogen bonding interactions ($\leq 2.8\text{\AA}$, default setting) with the sugar moiety and the distance of the anomeric carbon (C1) from His35, the proposed catalytic base involved in proton abstraction during conjugation of a hydroxylated aglycone with the UDP-sugar (Battaglia et al. 1994; Kubota et al. 2007; Li et al. 2007; Miley et al. 2007; Patana et al. 2008). Thirdly, the orientation and distance (π - or ring stacking interaction potential) of the uracil group of the UDP-sugar from Trp356 was determined. Once the best docked poses for each UDP-sugar was selected, residues close enough ($\leq 2.8\text{\AA}$) to hydrogen bond with the sugar moiety of the UDP-sugar were identified as targets for site-directed mutagenesis.

By default, Surflex-Dock scores are sorted from best to worst (decreasing values), first by CScore (Consensus score) and then by Total score. CScore combines many scoring functions (Total score, Chem score, G-score, D-score and PMF-score) to more accurately rank ligand binding to the active sites and is computed from the sum of several 'good' results for each ligand in each scoring function. The range of scores for each scoring function are determined, normalized (ranging from 0-1), and all values above the cut-off threshold are considered 'good'. The maximum CScore attainable is 5, as there are 5 scoring functions. The Total score is the Surflex-Dock score, an empirically derived scoring function based on the binding affinity of protein-ligand complexes and hence, expressed as $-\log_{10}(K_d)$ units to reflect binding affinities.

4.2.2 PCR site-directed mutagenesis of mutant UGT2B7 proteins

Based on the results of the docking experiments (see Results) and previously published data, mutants were generated at positions 33 (Tyr33Phe and Tyr33Leu), 378 (Asn378Ala, Asn378Leu, Asn378His and Asn378Gln), 398 (Asp398Ala and Asp398Leu), 399 (Gln399Ala and Gln399Leu), and 402 (Asn402Ala, Asn402His, Asn402Leu and Asn402Gln) by site-directed mutagenesis using the wild-type UGT2B7 cDNA in pBluescript II SK (+) as the template (Figure 2.1).

Primer design

The primer design method described by Zheng, Baumann and Reymond (2004) was used to minimize primer hetero-dimerization by ensuring priority of primer-template annealing over primer self-pairing (thereby improving amplification efficiency) during PCR. All oligonucleotides were prepared using a partial overlapping primer design. The following criteria were applied to primer design: at least eight non-overlapping bases should be introduced at the 3' terminus of the primer; the targeted mutation(s)

Chapter 4: Application of UGT2B7 protein homology modelling

should be included in both primers; and at least one G or C should be placed at the end of each terminus. An advantage of this protocol is that it allows more of the sequence to be spanned without having to increase the primer length and the mutation can be introduced as early as four bases away from the 5'-terminus and at least 6-8 bases from the 3'-terminus. All oligonucleotides were synthesized by Sigma-Genosys (Sigma-Aldrich, NSW, Sydney, Australia) and purified by PAGE gel electrophoresis. Oligonucleotide primers employed for mutagenesis are shown in Table 4.1.

Table 4. 1: Oligonucleotide primers used for site-directed mutagenesis. Mutagenic nucleotides are highlighted and underlined in red. Wild-type UGT2B7 (Accession NM_001074.2) was used as the parent template to generate all mutants.

Mutant	Primer Overlap (5' forward to 5' reverse)	ΔG° of Heterodimerisation (kcal/mol)
Y33F	5' GGCAGCAGAAT <u>T</u> CAGCCATTGGATG 3' 3' CACACCCGTCGTCTTA <u>A</u> GTCGG 5'	-50.13
Y33L	5' GCAGCAGAA <u>CT</u> CAGCCATTGGATG 3' 3' CACACCCGTCGTCTT <u>GA</u> GTCGG 5'	-46.58
N378A	5' GAGCC <u>GCT</u> TGGCATCTACGAGGCAATC 3' 3' CC GAAAATATTGAGTACCACCTCGG <u>CG</u> ACCG 5'	-64.21
N378L	5' GAGCC <u>CT</u> TGGCATCTACGAGGCAATCT 3' 3' CCGAAAATATTGAGTACCACCTCGG <u>GA</u> ACCG 5'	-62.47
N378H	5' GAGCC <u>CAT</u> TGGCATCTACGAGGCAATCT 3' 3' CCGAAAATATTGAGTACCACCTCGG <u>G</u> TACCG 5'	-62.35
N378Q	5' GAGCC <u>CAG</u> GGCATCTACGAGGCAATCT 3' 3' ATATTGAGTACCACCTCGG <u>GT</u> CCGTAG 5'	-55.73
D398A	5' GTTTGCCG <u>C</u> TCAACCTGATAACATTGC 3' 3' CCCTAAGGTAACAAACGGC <u>G</u> AGTTG 5'	-52.94

Mutant	Primer Overlap (5' forward to 5' reverse)	ΔG° of Heterodimerisation (kcal/mol)
D398L	5' GTTTGCC <u>CT</u> TCAACCTGATAACATTGCTC 3' 3' CCTAAGGTAACAAACGG <u>GA</u> AGTTGGAC 5'	-54.38
Q399A	5' GCCGAT <u>GC</u> ACCTGATAACATTGCTCAC 3' 3' CCTAAGGTAACAAACGGCTA <u>CG</u> TGGAC 5'	-55.10
Q399L	5' GCCGAT <u>CT</u> ACCTGATAACATTGCTCAC 3' 3' CCTAAGGTAACAAACGGCTA <u>GA</u> TGGAC 5'	-52.19
N402A	5' CCTGAT <u>GC</u> CATTGCTCACATGAAGGCC 3' 3' CAAACGGCTAGTTGGACTA <u>CG</u> GTAACG 5'	-55.17
N402L	5' CCTGAT <u>CT</u> CATTGCTCACATGAAGGCC 3' 3' CAAACGGCTAGTTGGACTA <u>GA</u> GTAACG 5'	-51.75
N402H	5' CTGAT <u>C</u> ACATTGCTCACATGAAGGCCA 3' 3' CAAACGGCTAGTTGGACTA <u>G</u> TGTAACG 5'	-51.88
N402Q	5' CTGAT <u>CAG</u> ATTGCTCACATGAAGGCCA 3' 3' CAAACGGCTAGTTGGACTA <u>GT</u> <u>CT</u> AACG 5'	-51.82

Polymerase Chain Reaction (PCR)

The QuickChange® II Site-Directed Mutagenesis kit (Table 2.5) was employed for PCR. Reactions, in a total volume of 50µL, contained 100ng of DNA template (Figure 2.1), 125ng of forward and reverse oligonucleotide primers, 0.2mM of each dNTP (Table 2.2), DMSO (5%, v/v), and 2.5U *PfuUltra*® II Fusion HS DNA Polymerase (Table 2.7). Reaction mixtures were prepared in *PfuUltra*® II Hot Start reaction buffer. A master mix of all reagents (template and polymerase) was used to reduce the variation between reactions. An aliquot (47µL) of the mastermix was delivered into each microfuge tube containing the DNA template (2µL) and then *PfuUltra*® II Fusion HS DNA Polymerase (1µL) was added before vortex mixing and centrifugation of the contents. Tubes were covered with mineral oil (2 drops) to reduce evaporation during thermal cycling. Negative control reactions (without DNA template) were included to monitor contamination by template or reaction components. PCR was performed using a RoboCycler Gradient 96 temperature cycler (Table 2.3). Cycling parameters were: 3min at 95°C, followed by 16 cycles of 1min at 95°C for denaturation, 1 min at 52°C for primer annealing and 10min at 68°C for extension, with a final extension of 60min at 68°C.

PCR products were purified using the QIAquick PCR Purification Kit (Table 2.6). The PCR product was digested with 20U of *DpnI* (Table 2.7; 37°C for 60min) to cleave the methylated circular template plasmid, and then heat inactivated at 80°C for 20min. *DpnI* digestion is a crucial step in order to improve the transformation efficiency of the linear unmethylated mutagenesis product. After transformation into DH5α cells and purification (Section 2.2.1), all mutations were confirmed by DNA sequencing of both strands (Section 2.2.1) using the universal primers M13pUC-fwd (5'-GTAAAACGACGGCCAGT-3') and M13pUC-rev (5'-

CAGGAAACAGCTATGACC-3') (purchased from Sigma-Genosys; Sigma-Aldrich, Sydney, NSW, Australia). Wild-type and mutant UGT2B7 coding sequences were then ligated into the mammalian vector pEF-IRES-puro 5.

Ligation of UGT2B7 cDNA from pBluescript II SK(+) to pEF-IRES-puro 5

Before wild-type and mutant human UGT2B7 cDNA from pBluescript II SK(+) could be ligated into pEF-IRES-puro 5 according to the method described in Section 2.2.1, separate but parallel double digestions of both plasmids with *Xho*I and *Xba*I was carried out, followed by diagnostic and quantitative agarose gel electrophoresis. UGT2B7 cDNA was then extracted by gel purification, while pEF-IRES-puro 5 was heat inactivated (65°C for 20min) after digestion, further purified using the QIAquick PCR Purification Kit (Table 2.6) and eluted with distilled water (47µL). The linear pEF-IRES-puro 5 digest was subsequently treated with 10U Antarctic phosphatase (Table 2.7; 37°C for 60min) to prevent plasmid recircularization before ligation. Ligation was then performed as described in Chapter 2 (Section 2.2.1).

4.2.3 Expression of wild-type UGT2B7 and mutants in HEK293T cells

Human UGT2B7 wild-type and mutant constructs in pEF-IRES-puro 5 were transfected in HEK293T cells and both stably and transiently expressed. As 14 mutants were investigated, this process was divided into two groups of experiments, with 8 and 6 mutants in the first and second groups, respectively. The first group of mutants comprised of Tyr33Phe, Tyr33Leu, Asp398Ala, Asp398Leu, Gln399Ala, Gln399Leu, Asn402Ala, and Asn402Leu. There was an unexpected issue with protein stability, mostly with the CT mutant UGT2B7 proteins (see Results). Thus, transient transfection was undertaken to ensure the synthesis of active proteins. Once conditions for transient transfection and expression were optimized, the first set of 8 mutants were

Chapter 4: Application of UGT2B7 protein homology modelling

re-expressed, followed by the second group; Asn378Ala, Asn378Leu, Asn378His, Asn378Gln, Asn402His, and Asn402Gln.

Stable Transfections

Plasmid mini-preparations

pEF-IRES-puro 5 plasmid with UGT2B7 and mutant cDNAs were required for stable transfections in HEK293T cells (see mini-preparation protocol, Section 2.2.1). Small (5mL) cultures typically yielded between 14 - 27 μ g DNA (concentration range 270 - 540ng/ μ L), with a DNA purity ratio of 1.7 - 2.0.

Cell transfection and selection

UGT2B7 and mutant cDNAs were stably expressed in HEK293T cells following the procedure of Uchaipichat et al. (2004), with minor modifications. Cells were plated at a density of 6×10^5 cells/mL in each separate well of a 6-well NuncTM plate. Cells were ready for transfection 24hr later (approximately 60 - 70% confluent). Plasmid DNA (2 μ g), OptiMEM[®] (0.25mL per complex x 2), and LipofectamineTM 2000 (4 μ L) were mixed and incubated (20min) according to the LipofectamineTM 2000 (Table 2.2) guidelines. Duplicate wells were transfected for each protein. Twelve hours later, the duplicate wells were re-suspended and pooled into fresh complete DMEM media (20mL) in a T175 flask. Cells were grown for up to 48hr post-transfection, after which time fresh complete DMEM and puromycin (1 μ g/mL) were used to initiate selection.

Cell harvesting

Cells were harvested as described previously (Section 2.2.3). Harvested cells were washed in phosphate-buffered saline once they had grown to at least 80% confluency. Cells were subsequently lysed by sonication with four 1-sec 'bursts', each separated

Chapter 4: Application of UGT2B7 protein homology modelling

by 1min with cooling on ice, using a Vibra Cell VCX 130 Ultrasonics Processor (Table 2.3). The lysate was centrifuged at 12,000g for 1min at 4°C to remove cellular debris and the supernatant fractions separated and stored in phosphate buffer (0.1M, pH 7.4) at -80°C until use.

Transient Transfections

Plasmid Midi-preparations

An increased amount of pEF-IRES-puro 5 plasmid with UGT2B7 and mutant cDNAs were required for a large transient transfection scale-up (Section 2.2.1). Large (100mL) cultures typically yielded between 120-250µg DNA (concentration ranging 404 - 860ng/µL), with a DNA purity ratio between 1.70 - 1.98.

Cell transfection and harvest

UGT2B7 and mutant cDNAs were transiently expressed in HEK293T cells. The cells were plated at a density of 6×10^6 cells/10mL in a medium T75 Nunc™ flask. Cells were ready for transfection 24hr later (80% confluent). Plasmid DNA (24µg), OptiMEM® (1.5mL per complex x 2), and Lipofectamine™ 2000 (60µL) were mixed and incubated (20min) according to the Lipofectamine™ 2000 (Table 2.2) guidelines, for each T75 flask. Duplicate T75 flasks were transfected with each UGT2B7 protein, which were re-suspended and pooled into fresh media in a large T175 flask 24hr after transfection. Transfected cells in the T175 flask were left to grow to 80-90% confluency and harvested 36 - 38hr later (i.e. 60 - 62hr post-transfection). Cells were harvested as described above for the stable cell line expression of UGT2B7 and mutant proteins. Lysates from transient expression were used immediately (same day of harvest) for activity experiments and Western blot analysis.

Western blotting

UGT2B7 wild-type and mutant expression was confirmed by immunoblotting protein from both stable and transient transfections according to the method described in Section 2.2.4. The total protein content of lysates was determined by the method of Lowry et al. (1951) (Section 2.2.6). Proteins (50 μ g) were resolved by SDS-PAGE. The separated proteins were transferred onto nitrocellulose, and then probed with rabbit anti-human UGT2B7 (polyclonal) primary antisera (1:2000 dilution) and goat anti-rabbit HRP-conjugated IgG (H+L) (1:1000 dilution) as the secondary antibody (Table 2.8). Untransfected HEK293T lysate (50mg) was used as a negative control. Membrane-bound peptides conjugated with HRP were detected by BM Chemiluminescence (Table 2.2) at 61 kDa.

4.2.4 Incubation conditions and HPLC assays

Incubations of recombinant UGT2B7

Incubation mixtures containing phosphate buffer (0.1M, pH 7.4), MgCl₂ (4mM), UDP-Glc (5mM) or UDP-GlcUA (5mM), 4-methylumbelliferone (4-MU) or morphine, and HEK cell lysate expressing recombinant UGT2B7 or mutant enzyme (2mg/mL) in a total volume of 200 μ L were performed at 37°C for 120min. Reactions were terminated by the addition of 2 μ L HClO₄ (11.6M). After centrifugation, supernatant fractions were analyzed by HPLC for quantification of morphine and 4-MU glucoside and glucuronide conjugate formation (Section 3.2.2).

Recombinant UGT activities were screened at three substrate concentrations: morphine, 1, 5 and 10mM; and 4-MU, 0.1, 0.35 and 1mM. Incubations at each morphine and 4-MU concentration were performed in duplicate. Duplicate estimates invariably differed by less than 10%. UDP-Glc and UDP-GlcUA were omitted from

Chapter 4: Application of UGT2B7 protein homology modelling

‘blank’ incubations. Analytical conditions for the quantification of the morphine and 4-MU glycosides are given in Appendix 1 table and Section 3.2.1 - 3.2.2.

4.3 Results

4.3.1 UDP-sugar docking studies with the UGT2B7 C-terminal structure from X-ray crystallography (2O6L)

The UGT2B7-CT structure, prepared as described in Section 4.2.1, was used for docking studies with UDP-Glc and UDP-GlcUA. Optimal threshold and bloat settings were determined by sequential modification of these parameters, with initial settings of 0.4 and 1.0, respectively. It was found that protomol threshold and bloat settings of 0.5 and 2.0, respectively, resulted in UDP-Glc and UDP-GlcUA docking poses within the predicted binding region, and also satisfied the criteria detailed in Section 4.2.1.

Docking results

Selected poses generated from docking into the UGT2B7-CT structure at threshold and bloat settings of 0.4 and 1.0, respectively, for UDP-Glc and UDP-GlcUA are given in Table 4.2. The poses were selected based on the criteria detailed in Section 4.2.1. Residues within a 3Å radius of the nucleotide sugar pose were identified and compared to those amino acids selected for mutagenesis by Miley et al. (2007) based on superpositioning of UDP-GlcUA into the UGT2B7-CT structure.

The docking results demonstrate that both UDP-Glc and UDP-GlcUA attained the maximum CScore of 5, with UDP-Glc achieving a greater binding affinity than UDP-GlcUA (5.36 compared to 3.68 $-\log_{10}(K_d)$ units, respectively). Many of the residues within a 3Å radius of the nucleotide sugars were consistent with residues deemed important for UDP-GlcUA binding within UGT2B7-CT from superpositioning (Miley et al. 2007), apart from Ser308 and Thr373. Amino acids identified from docking experiments that were not chosen for mutagenesis by Miley et al. (2007) include Ile357, Gly376, Ala377, Phe396, Ala397 and Asn402.

Two residues in VvGT1, Asp374 and Gln375, that interact directly with the glucose moiety are also conserved in human UGTs (Asp398 and Gln399 – UGT2B7 numbering). These residues are located on a short loop that connects C^{α5} and C^{β5} (Figure 4.1) and are involved in hydrogen bonding (Figure 4.4A). This is consistent with the docking results (Table 4.2) which indicate that the protomol conditions used are optimal for docking in the correct binding pocket region for UDP-sugars. However, based on the plant crystal VvGT1 complexed with U2F (Figure 4.4A) and other human, bacterial and plant UDP-glycosyltransferase crystal structures, it is obvious that NT residues are also involved in nucleotide sugar binding. As shown in Figure 4.3 and 4.4B, the protomol area is shallower, or not as deep, and residue coverage is much less in the UGT2B7-CT structure compared to the full protein homology model of UGT2B7. To fully understand and rationalise the docking results, the full protein structure, would seem a more valid starting reference point than the half protein structure, even if the other half is a modelled structure relying on plant X-ray crystal templates. In fact, Miley et al. (2007) were only able to identify His35 and Asp151 as critical residues for catalysis once a homology model of UGT2B7 was analyzed (Table 4.2). Hence, further docking experiments utilized the full UGT2B7 homology model prepared in Section 4.2.1 after superpositioning analysis (Section 4.3.2) was carried out.

Table 4. 2: Residues within 3Å of UDP-Glc and UDP-GlcUA docked into the protomol site (threshold = 0.4, bloat = 1.0) of UGT2B7-CT minimized crystal structure compared to the superpositioned UGT2B7-CT data of Miley et al. (2007).

Superpositioned	Docked	
CScore	5	5
Total score	5.36	3.68
Miley et al. (2007)	UDP-Glc	UDP-GlcUA
His35*		
Asp151*		
Ser308		
Arg338	Arg338	Arg338
Trp356	Trp356	Trp356
	Ile357	Ile357
Gln359	Gln359	Gln359
Thr373		
His374	His374	His374
	Gly376	Gly376
	Ala377	Ala377
Asn378	Asn378	Asn378
Gly379	Gly379	Gly379
	Phe396	
	Ala397	Ala397
Asp398	Asp398	Asp398
Gln399	Gln399	
	Asn402	

*Identified from analysis of UGT2B7 homology model which contains the NT

4.3.2 UDP-sugar superpositioned with the human UGT2B7 homology model

The UGT2B7-CT crystal structure and homology model generated as described in Section 4.2.1 was used for superpositioning studies with UDP-Glc and UDP-GlcUA. A protomol was not generated since docking with UDP-Glc and UDP-GlcUA was not required. Instead, the superpositioning process described for the 3-D co-ordinate extraction of U2F from the VvGT1 crystal structure into the UGT2B7-CT minimized structure was performed with the full human UGT2B7 homology model. The homology model was superpositioned with the energy minimized UGT2B7-CT structure over 162 C^α residues with a RMSD of 1.2Å, with high structural homology observed between the structures (Figure 4.4B). Unlike the relatively more ‘flexible’ docking process, where the UDP-sugar pose was determined by building fragments of the ligand in the context of the interaction between the protein binding site and the ligand, no structural or positional changes were introduced into the UDP-Glc and UDP-GlcUA poses.

Superpositioned results

As expected, the full homology model provides additional information about the NT residues that are in close contact with the nucleotide sugar, unlike the partial UGT2B7-CT structure (cf. Table 4.3 and 4.2). His35 was identified as a nearby ($\leq 3\text{\AA}$) residue that hydrogen bonded ($\leq 2.8\text{\AA}$) to the C6 hydroxyl and carboxylate group of UDP-Glc and UDP-GlcUA, respectively. By contrast, Asp151 was not identified as an interacting residue. The homology model employed by Miley et al. (2007) to predict involvement of His35 as the catalytic base and Asp151 as the stabilizing acid was based on the NT sequence of the plant proteins VvGT1 (PDB code 2C1Z) and UGT71G1 (PDB codes 2ACV/2ACW) and their proposed serine hydrolase-like

catalytic triad mechanism. The sequence of human UGT2B7 aligned well with the corresponding proposed catalytic residues His20 and Asp119 of VvGT1 (Offen et al. 2006) and His22 and Asp121 of UGT71G1 (Shao et al. 2005). In the VvGT1 crystal structure, His20 is approximately 3.6Å and Asp119 approximately 6.6Å from U2F (RCSB PDB Ligand Explorer 3.8; Table 2.10). This is consistent with the superpositioning results (Table 4.3) which did not identify Asp151 as a ‘close’ ($\leq 3\text{\AA}$) residue. In contrast, His22 in the UGT71G1 crystal structure is approximately 4.7Å, and Asp121 approximately 3.0Å away from UDP-Glc (Shao et al. 2005). Mutagenesis was performed with His22 and Asp121 of UGT71G1. His20 of VvGT1 was shown to be a critically important residue, with mutagenesis resulting in loss of activity (Offen et al. 2006). Although important for catalysis, these residues are not suspected to be involved UDP-sugar selectivity.

In the homology model, the CT residues ($\leq 3\text{\AA}$) surrounding the superpositioned UDP-Glc and UDP-GlcUA are identical for the two nucleotide sugars. These CT residues are similar to those observed from docking into UGT2B7-CT (cf. Table 4.2 and 4.3). The identical pose for both UDP-Glc and UDP-GlcUA is not surprising because they have been modelled on the same static U2F ligand scaffold with no positional optimization (Figure 4.5). However, since the sugar moieties of UDP-Glc and UDP-GlcUA differ (-CH₂OH vs. CO₂H) at position 6, some differences in the interactions with binding site residues might be expected. ‘Strong’ hydrogen bonding ($\leq 2.8\text{\AA}$) interactions between CT residues to the uracil, ribose and phosphate moieties of the nucleotide sugars were observed, but not to the sugar moiety. There were, however, many residues between positions 377-402 that were within 3Å of the sugar moiety. As indicated above, the only residue within ‘strong’ hydrogen bonding distance ($\leq 2.8\text{\AA}$) to the sugar moiety was the NT residue His35 (to the C6 functional group of each

nucleotide sugar). With the VvGT1 crystal structure, a distance of approximately 5.7Å was observed between the catalytic base (His20) and the donor ligand (U2F C1) (RCSB PDB Ligand Explorer 3.8 (Table 2.10)), but there was contact (2.7Å) between His20 and the acceptor substrate (i.e. aglycone kaempferol (KMP)), which is expected given the role of the catalytic base in catalysis. Interestingly, and of note, Ser18 of the VvGT1 structure (equivalent to Tyr33 of human UGT2B7) is also in hydrogen binding distance to kaempferol. Similarly, the pose of UDP-Glc and UDP-GlcUA in the UGT2B7 homology model was superpositioned near the catalytic base as expected (4.11Å from His35 nitrogen to UDP-sugar C1).

Since the same superpositioning method was used with the same ligand scaffold, the orientation and pose of UDP-GlcUA (Figure 4.5B), and hence UDP-Glc, was very similar to that shown in Figure 5 of Miley et al. (2007), and to Figure 4 shown in Xiong et al. (2008) and Radomska-Pandya et al. (2010). The C6 carboxylate of UDP-GlcUA faces towards Ala377, although the sugar moiety was further from Asp398/Gln399 (making no hydrogen bonding contact) when superpositioned in the homology model. Consistent with Miley et al. (2007), no π - π or ring stacking was observed between Trp356 and the uracil ring, which was not a favourable orientation despite being within 3Å. This contrasts to the parallel displaced π - π or ring stacking demonstrated between Trp332 and the uracil ring in the VvGT1 crystal structure.

Table 4. 3: Residues within 3Å of UDP-Glc and UDP-GlcUA superpositioned in the binding site of the UGT2B7 homology model based on the U2F/2C1Z crystal position compared to the superpositioned UGT2B7-CT data of Miley et al. (2007).

Superpositioned				
Miley et al. (2007)	UDP-Glc		UDP-GlcUA	
	Tyr33		Tyr33	
	Ser34	H-bond to phosphate	Ser34	H-bond to phosphate
His35*	His35	H-bond to sugar C6-OH	His35	H-bond to sugar C6-COO⁻
	Met37		Met37	
Asp151*				
	Ser173		Ser173	
	Phe174		Phe174	
Ser308				
Arg338	Arg338		Arg338	
Trp356	Trp356		Trp356	
	Ile357	H-bond to uracil	Ile357	H-bond to uracil
Gln359	Gln359		Gln359	
	Asn360	H-bond to ribose	Asn360	H-bond to ribose
Thr373				
His374				
	Gly376		Gly376	
	Ala377	Within 3Å of sugar C4-OH	Ala377	Within 3Å of sugar C4-OH
Asn378	Asn378	Within 3Å of sugar C2-OH	Asn378	Within 3Å of sugar C2-OH
Gly379	Gly379	H-bond to phosphate	Gly379	H-bond to phosphate
	Ala397	Within 3Å of sugar C3-OH	Ala397	Within 3Å of sugar C3-OH
Asp398				
Gln399	Q399	Within 3Å of sugar C3-OH	Gln399	Within 3Å of sugar C3-OH
	Asn402	Within 3Å of sugar C4-OH	Asn402	Within 3Å of sugar C4-OH
	4.11Å between His35 (N) and C1 of sugar		4.11Å between His35 (N) and C1 of sugar	

* Identified from analysis of UGT2B7 homology model which contains NT

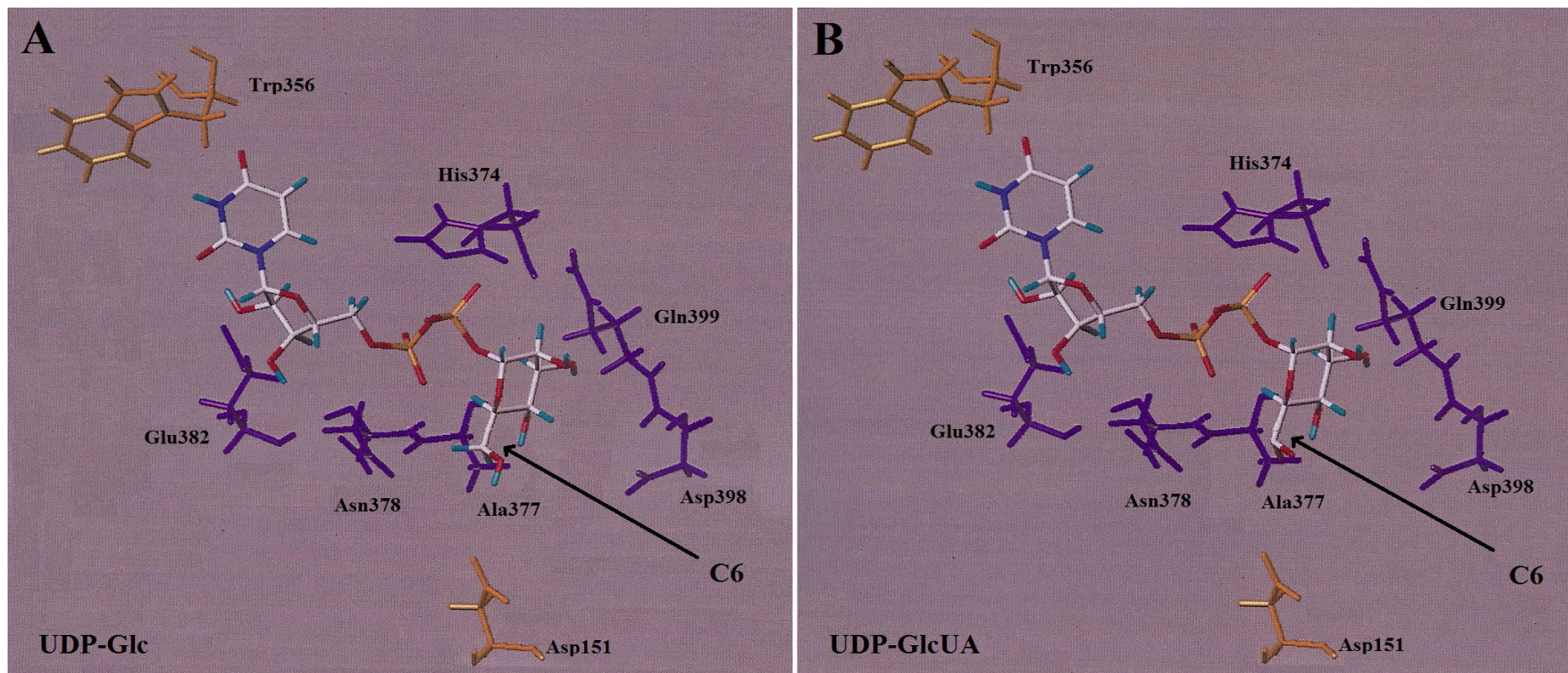


Figure 4. 5: Residues within 3Å of UDP-Glc (A) and UDP-GlcUA (B) from superpositioning in the UGT2B7 homology model.

Poses for UDP-Glc (A) and UDP-GlcUA (B) are identical (except C6 functional group) as they are both based on the extracted complexed U2F donor ligand from the VvGT1 crystal. Residues depicted in Figure 4 (Xiong et al. 2008) are shown here in purple for comparison and residues in orange are shown as reference points for contextual purposes. His35 (not shown) is located between Ala377 and Asp151 within 2.8Å of C6.

4.3.3 UDP-sugar docking studies with the human UGT2B7 homology model

The UGT2B7 homology model prepared as described in Section 4.2.1 was used for docking studies with UDP-Glc and UDP-GlcUA. The initial protomol generated for docking studies used threshold and bloat settings of 0.4 and 1.0 (Table 4.4), respectively, based on previous docking studies with the UGT2B7-CT crystal structure (Section 4.3.1). However, the final protomol generated was optimized at threshold and bloat settings of 0.5 and 2.0 (Table 4.5), respectively, prior to docking with UDP-Glc and UDP-GlcUA. These settings gave poses with greater binding affinity (Total score) measurements due to the increased number of hydrogen bonding interactions observed around the sugar moiety of both UDP-Glc and UDP-GlcUA (see red highlighted sections and Total score in Table 4.4 and 4.5). This increase in both threshold and bloat parameters decreased the depth that the protomol is buried in the protein and increased the volume of the protomol to 2Å, providing greater flexibility for binding within the active site pocket. The same 3-D structures of UDP-Glc and UDP-GlcUA as those described in Section 4.3.1 were docked.

As indicated above, initial protomol docking parameters for the full UGT2B7 homology model were set at threshold and bloat settings of 0.4 and 1.0, respectively, based on docking into the UGT2B7-CT model (Section 4.3.1 and Table 4.2). The results are shown in Table 4.4. The CScore for both UDP-Glc and UDP-GlcUA was 4, while binding affinities (Total score) were 4.92 and 7.09 $-\log_{10}$ (K_d) units, respectively. The results demonstrate that both UDP-sugars bind within the same pocket as the rigid superpositioned poses, with the backbone of the UDP-moiety aligning in a similar conformation. However, the sugar moieties differ from the superpositioned structures and from one another (Figure 4.6). Firstly, both sugar moieties no longer hydrogen bond to the catalytic base (His35) and the distance from

Chapter 4: Application of UGT2B7 protein homology modelling

C1 is further for UDP-Glc (5.63Å), although not for UDP-GlcUA (4.10Å). However, the angle and change in orientation of UDP-GlcUA is more favourable for hydrogen bonding interactions with the conserved DQ (398Asp-399Gln) residues and Asn402, resulting in a greater Total score than what was obtained for UDP-Glc (Table 4.4). Hydrogen bonding of UDP-Glc was only observed with Asp398. The protomol threshold and bloat parameters were optimized further to investigate whether the Total score for UDP-Glc could be improved, as these initial settings were based on optimal docking into UGT2B7-CT.

Table 4. 4: Residues within 3Å of UDP-Glc and UDP-GlcUA docked into protomol site (threshold = 0.4, bloat = 1.0) of the UGT2B7 homology model compared to the superpositioned UGT2B7-CT results of Miley et al. (2007).

Superpositioned	Docked			
CScore	4		4	
Total score	4.92		7.09	
Miley et al.(2007)	UDP-Glc		UDP-GlcUA	
	Tyr33			
	Ser34	H-bond to phosphate	Ser34	H-bond to phosphate
His35*			His35	Within 3Å of sugar C2-OH
	Trp106	Within 3Å of sugar C4-OH	Trp106	Within 3Å of sugar C3-OH
D151*				
			Phe174	
Ser308	Ser308	H-bond to uracil	Ser308	H-bond to uracil
	Gly310			
Arg338	Arg338		Arg338	
Trp356	Trp356		Trp356	
	Ile357	H-bond to uracil	Ile357	H-bond to uracil
Gln359	Gln359		Gln359	H-bond to ribose
	Asn360	H-bond to ribose	Asn360	
Thr373				
His374	His374		His374	
	Gly376		Gly376	
Asn378	Asn378		Asn378	
Gly379	Gly379		Gly379	
	Glu382	H-bond to ribose	Glu382	H-bond to ribose
	Phe396	Within 3Å of sugar C2/C3-OH	Phe396	
	Ala397		Ala397	
Asp398	Asp398	H-bond to sugar C6-OH	Asp398	H-bond to sugar C6-COO⁻/ sugar C4-OH
Gln399	Gln399		Gln399	
	Asn402		Asn402	H-bond to sugar C6-COO⁻
	5.63Å between His35 (N) and C1 of sugar		4.10Å between His35 (N) and C1 of sugar	

* Identified from analysis of UGT2B7 homology model which contains NT

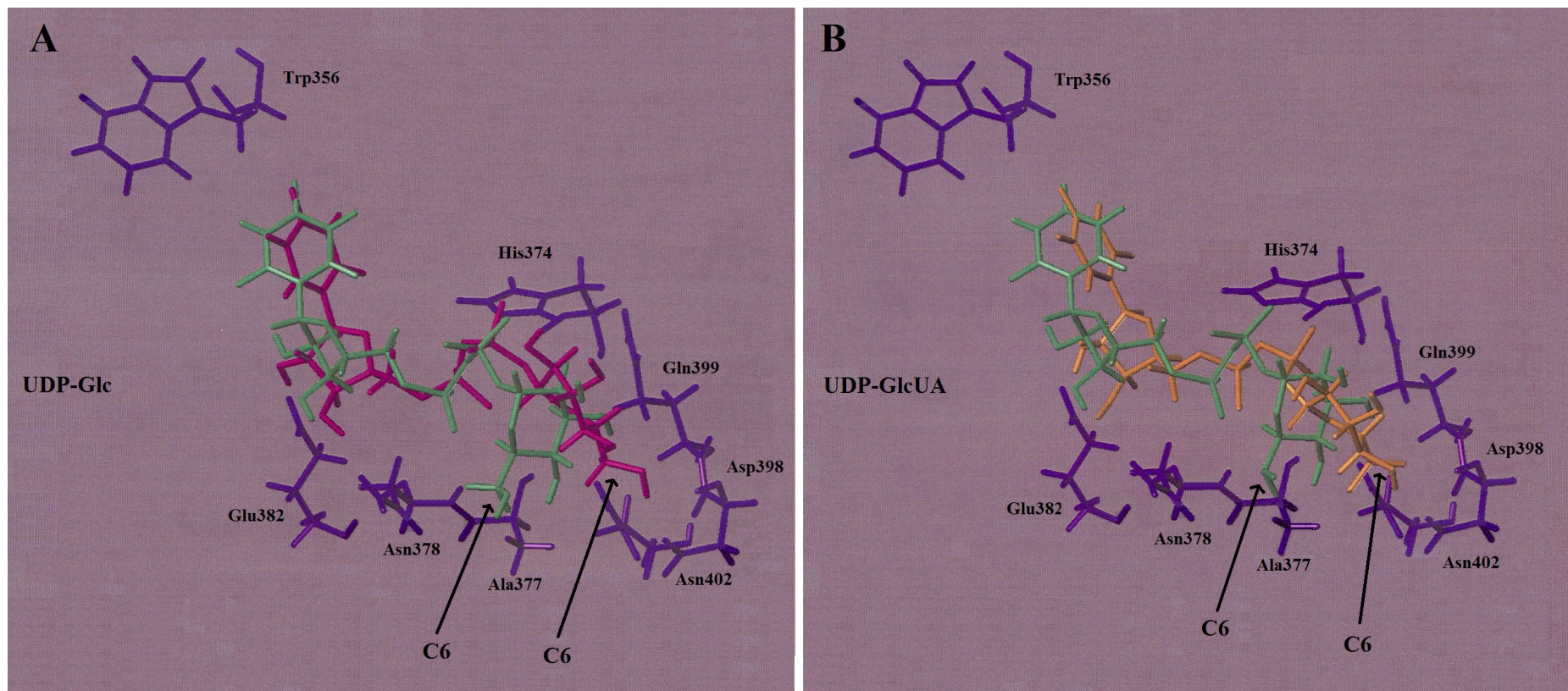


Figure 4. 6: Residues within 3Å of UDP-Glc (A) and UDP-GlcUA (B) from superpositioning (green) compared to docking results (magenta and orange, respectively) in the UGT2B7 homology model.

Superpositioning poses from Figure 4.5 (green) are aligned with docking poses (UDP-Glc in magenta and UDP-GlcUA in orange) at threshold and bloat bloat settings 0.4 and 1.0, respectively.

Subsequent docking experiments with the UGT2B7 homology model using threshold and bloat settings of 0.5 and 2.0, respectively, demonstrated that both UDP-Glc and UDP-GlcUA bind within the same domain of the CT of UGT2B7 and binding interactions of the UDP moiety are cofactor-independent (Table 4.5 and Figure 4.7). However, residues involved in the binding of the sugar differed (Table 4.5); Asp398 and Gln399 hydrogen bonded with the O6' and O3' of glucose, respectively (Figure 4.8A and B). In contrast, hydrogen bonding occurred between Asn402 and Tyr33 with O6' and O2' of glucuronic acid, respectively (Figure 4.8C and D). The anomeric carbons (C1) of both cofactors are within 5Å of His35, namely 4.75 and 4.99Å for UDP-Glc and UDP-GlcUA, respectively (Table 4.5). This is more consistent with what was observed with the X-ray crystal structure of plant VvGT1, with a distance of 5.7Å measured between His20 and C1 of U2F.

The CScore for both UDP-Glc and UDP-GlcUA was 4, while binding affinities (Total score) were 7.99 and 8.17 $-\log_{10}(K_d)$ units, respectively. Thus, the change in threshold and bloat parameter settings increased the binding affinities for both nucleotide sugars, providing similar values for this parameter. Overall, important residues surrounding and interacting with the docked UDP-sugars correlate well (Table 4.5), matching 14 out of 17 (or 82%) of the inferred CT UDP-GlcUA interacting residues (between Ser308-Gln399) shown in Figure 1.11.

Site-directed mutagenesis studies were divided into two separate 'sets', so that the work could be more conveniently performed. The first set of UGT2B7 mutants investigated was Tyr33Phe, Tyr33Leu, Asp398Ala and Asp398Leu, Gln399Ala and Gln399Leu, Asn402Ala, Asn402Leu. Selection of these mutants was based on the residues observed to be in hydrogen bonding contact with the sugar moiety of either

UDP-Glc or UDP-GlcUA (Tyr33, Asp398, Gln399 and Asn402) from docking experiments (Table 4.5). The Tyr residue present at position 33 of wild-type UGT2B7 was substituted with the smaller, neutral Leu and with Phe, which is of comparable size to Tyr but lacks the phenolic -OH group. The polar Asp (charged/acidic), Gln (neutral/polar), and Asn (neutral/polar) residues at positions 398, 399, and 402, respectively, of wild-type UGT2B7 were substituted with Ala (small, neutral and non-polar) and Leu, which is of similar size to Asp and Asn but is neutral/non-polar. Although Gln has an additional methylene side chain group compared to Asn, Leu was the closest non-polar residue in size and shape to Gln.

The second set of mutants generated comprised Asn378Ala, Asn378Leu, Asn378His, Asn378Gln, Asn402His, and Asn402Gln. Since the docking studies implicated Asn402 in the binding of the carboxylate group of UDP-GlcUA, this residue was additionally substituted with the chemically related amino acid Gln in a further attempt to differentiate residues involved in the binding of UDP-GlcUA and UDP-Glc. In the first set of mutations, Ala and Leu could be considered ‘drastic’ mutational changes from Asn as the chemistry and structure are very different. Further, Asn378 was selected for mutagenesis since Miley et al. (2007) predicted a role for this residue in the binding of the carboxylate group of UDP-GlcUA based on superpositioning studies with the X-ray crystal structure of the CT domain of UGT2B7. In addition to the amino acids substituted at other positions investigated, the Asn378His mutant was generated as Asn occurs at the equivalent position in all UGT1A subfamily proteins. Wild-type UGT2B7 was included as the control in both sets of experiments, during cloning, expression and the measurement of enzyme activity.

Table 4. 5: Residues within 3Å of UDP-Glc and UDP-GlcUA docked into the protomol site (threshold = 0.5, bloat = 2.0) of the UGT2B7 homology model compared to the superpositioned UGT2B7-CT data of Miley et al. (2007).

Superpositioned	Docked			
CScore	4		4	
Total score	7.99		8.17	
Miley et al. (2007)	UDP-Glc		UDP-GlcUA	
	Tyr33		Tyr33	H-bond to sugar C2-OH
	Ser34	H-bond to phosphate	Ser34	H-bond to phosphate
His35*				
	Met37		Met37	
Asp151*				
Ser308	Ser308	H-bond to uracil	Ser308	H-bond to uracil
Arg338	Arg338		Arg338	
W356				
	Ile357	H-bond to uracil	Ile357	H-bond to uracil
Gln359	Gln359		Gln359	
	Asn360	H-bond to ribose	Asn360	H-bond to ribose
Thr373				
His374	His374		His374	
	Gly376		Gly376	
	Ala377	H-bond to phosphate	Ala377	H-bond to phosphate
Asn378	Asn378	H-bond to phosphate	Asn378	H-bond to phosphate
Gly379			Gly379	
	Glu382	H-bond to ribose	Glu382	H-bond to ribose
	Phe396		Phe396	
	Ala397		Ala397	
Asp398	Asp398	H-bond to sugar C6-OH		
Gln399	Gln399	H-bond to sugar C3-OH	Gln399	
	Asn402		Asn402	H-bond to sugar C6-COO⁻
	4.75Å between His35 (N) and C1 of sugar		4.99Å between His35 (N) and C1 of sugar	

* Identified from analysis of UGT2B7 homology model which contains NT

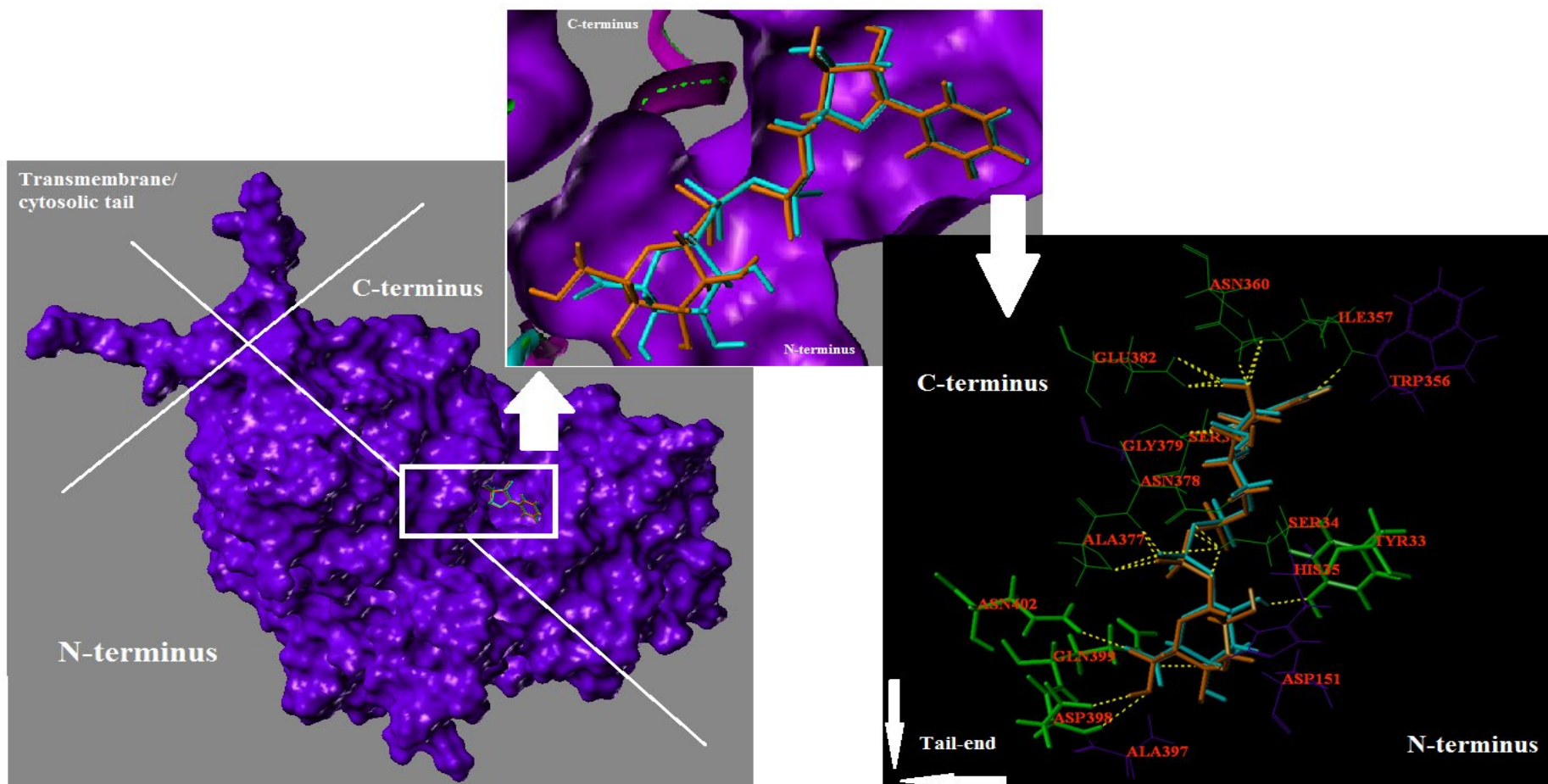


Figure 4. 7: Surface view of UGT2B7 with docked UDP-Glc (orange) and UDP-GlcUA (cyan) in white rectangular box (left panel).

Close up view of the UGT2B7 C-terminus binding pocket (middle panel). Residues with hydrogen bonding interactions (dotted yellow line) are in green while other residues within 3Å are in purple (right panel).

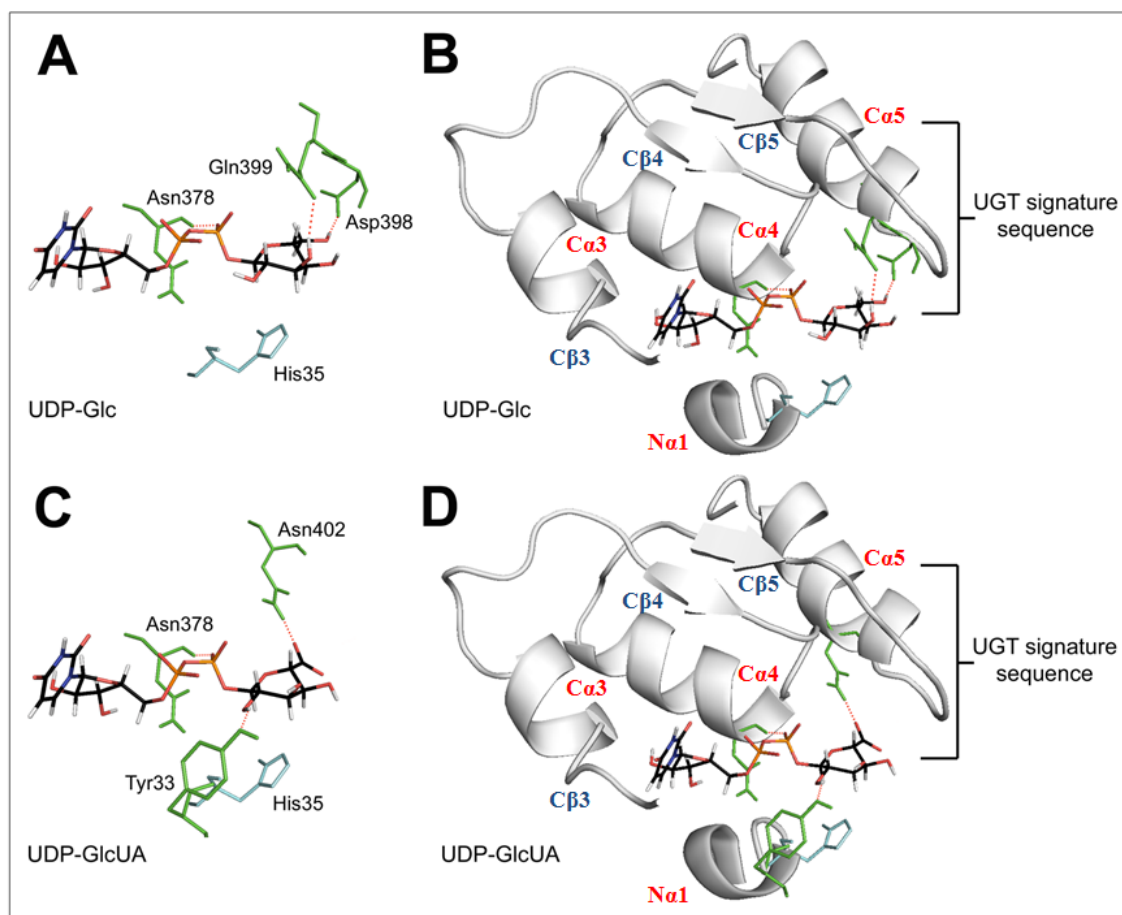


Figure 4. 8: UGT2B7 homology model docked with UDP-sugars.

Docking of UDP-Glc and UDP-GlcUA (as the carboxylate anion) in the UGT2B7 homology model. The catalytic base (His35 resides at the start of $N^{\alpha 1}$; cyan) and Asn378 (resides on $C^{\alpha 4}$; green) are shown as reference points. (A) Asp398 and Gln399 (green) hydrogen bond to the glucose moiety of UDP-Glc, part of the UGT signature sequence sitting at the beginning of $C^{\alpha 5}$ (B). (C) Tyr33 and Asn402 (green) hydrogen bond with the glucuronic acid moiety of UDP-GlcUA. Asn402 is located on $C^{\alpha 5}$ just outside the UGT signature sequence while Tyr33 is located on the $N^{\alpha 1}$ loop just before $N^{\alpha 1}$, near the catalytic base His35 (D).

4.3.4 Optimization of scale-up conditions for transient transfection of HEK293T UGT2B7 wild-type and mutant proteins

Unlike the stable transfection and expression protocol, the transient transfection and expression protocol required optimization since this approach was not established in the laboratory. With transient transfection there is only one harvesting opportunity to acquire sufficient protein for each experiment, as variations will occur between batches. Since 14 mutants were investigated, wild-type UGT2B7 was expressed at the same time as each mutant as a control and for ‘benchmark’ comparison across expressions.

Scale-up was initially based on the Lipofectamine™ 2000 (Table 2.2) transfection guidelines for transfection in a 6-well plate. Mock transfections were carried out at both lower (2×10^6 cells) and higher (6×10^6 cells) plating densities, with and without Lipofectamine™ 2000, to account for the cytotoxicity from the transfection agent. It was found that plating at the higher density was optimal for transfection in a T75 flask as there was less cytotoxicity (70-80% confluent vs. 30% confluent 24hr post-transfection). The final optimized protocol was as described in Section 4.2.3.

4.3.5 Immunoblotting of UGT2B7 wild-type and mutant proteins expressed in HEK293 cells

Stable Transfections

Wild-type UGT2B7 and the Tyr33Phe, Tyr33Leu, Asp398Ala, Asp398Leu, Gln399Ala, Gln399Leu, Asn402Ala, and Asn402Leu mutants were initially stably expressed in HEK293T cells. Total protein, estimated using the Lowry method, did not vary greatly between wild-type UGT2B7 and each mutant. Mean total protein was in the range of 10-12mg/mL for both wild-type and mutant enzymes, except for

Chapter 4: Application of UGT2B7 protein homology modelling

Asp398Leu and Gln399Ala, where expression was 15-18mg/mL. Total protein expression of all mutants was similar to, or higher than, that obtained for the wild-type. Repeated total protein measurement of the same sample batches over 8 weeks provided consistent results with a percent coefficient of variation (CV) range of 4.7-19.3%.

Despite the similarities in total protein expression, Western blotting over a 2-week period showed that relative expression of UGT2B7 apoprotein varied between wild-type and mutants (Figure 4.9). The first and second Western blots shown in Figures 4.9A and B are repeat experiments performed 5 days apart. In all the immunoblots shown, untransfected HEK293T lysate was used as the negative (-) control (Lane 1; L1) while transfected wild-type UGT2B7 was used as the reference protein band (L2). The CT mutants of UGT2B7 (at positions 398, 399, and 402) are shown in the first row (R1) of immune-reactive bands at 61kDa. The NT mutants (at position 33) are shown in the second row (R2) of immune-reactive bands, also at 61kDa. Although expression based on band density is less obvious with the first replicate (cf. Figure 4.9A and B), relative expression of CT mutant proteins to wild-type (R1) is greater in the second blot based on densitometry data (cf. Figure 4.10A and B). However, this was not the case when comparing the N-terminal mutants (R2) (cf. Figure 4.10A and B), as the relative density to wild-type remained consistent. In the second blot, the decrease in relative density to wild-type for the C-terminal mutants was approximately half that of the first blot, indicating a large decline in UGT2B7 protein between the first and second blots.

To more clearly visualise the bands for the C-terminal mutant proteins, the third blot (Figure 4.9C; R1) was loaded with less wild-type UGT2B7 (25µg; L2) with matching negative control (25µg; untransfected HEK293T in L1) and more of the C-terminal

mutant proteins (100µg; L3-8) with matching negative control (100µg; untransfected HEK293T in L9). Even with a 4-fold greater (4:1) amount of mutant protein compared to wild-type UGT2B7, the C-terminal mutant proteins were barely visible, consistent with normalized densitometry data indicating that expression was a tenth of that of the wild-type reference loaded at 25µg (Figure 4.10C; Row 1). This set of densitometry data was normalized to the same amount of total protein as previous blots (60µg) for comparison. The normalized results indicate further decline, by approximately half, relative to the second immunoblot (cf. Row 1 of Figure 4.10B and 4.10C). In comparison, the third immunoblot of the N-terminal mutants relative to UGT2B7 wild-type (60µg) was visibly 'denser' (Figure 4.9C; R2), and the densitometry data showed a consistent ratio of mutant relative to the reference wild-type UGT2B7 (Figure 4.10C; Row 2).

Analysis of the densitometry data from the 3 blots (Figure 4.11) show that the mean relative density range for the C-terminal mutants was between 0.22 to 0.47 with standard deviations (SD) ranging from 0.14 to 0.36. The very large deviations in comparison to the mean were reflected in the extremely large percent coefficient of variation (CV), which ranged from 60.8-77.1%. This is consistent with the observed decrease in band density of the UGT2B7 mutant proteins with each subsequent blot performed. In contrast, the N-terminal mutants were more stable with mean (\pm SD) relative densities of 0.69 ± 0.05 (Tyr33Phe) and 0.44 ± 0.06 (Tyr33Leu), with CVs of 7.11% and 12.61%, respectively.

To understand whether the cause of the instability of the C-terminal mutants was due to the freeze-thaw process, a fourth Western blot (Panel D in Figure 4.9) was generated with 25µg of UGT2B7 wild-type and 100µg of HEK293T and UGT2B7 mutant lysate.

Chapter 4: Application of UGT2B7 protein homology modelling

Data for UGT2B7 wild-type and the C-terminal mutants are shown for freeze-thawed (a) and freshly thawed (b) samples. Both conditions provided a similar result with no specific UGT2B7 protein band present in the C-terminal mutant lysate samples, even as freshly thawed samples. Wild-type UGT2B7 was the only sample with an immunodetectable band under both conditions. This indicates that the multiple freeze-thaw process is not the probable cause of instability in the C-terminal mutants, especially since the UGT2B7 wild-type density was unaffected by this treatment.

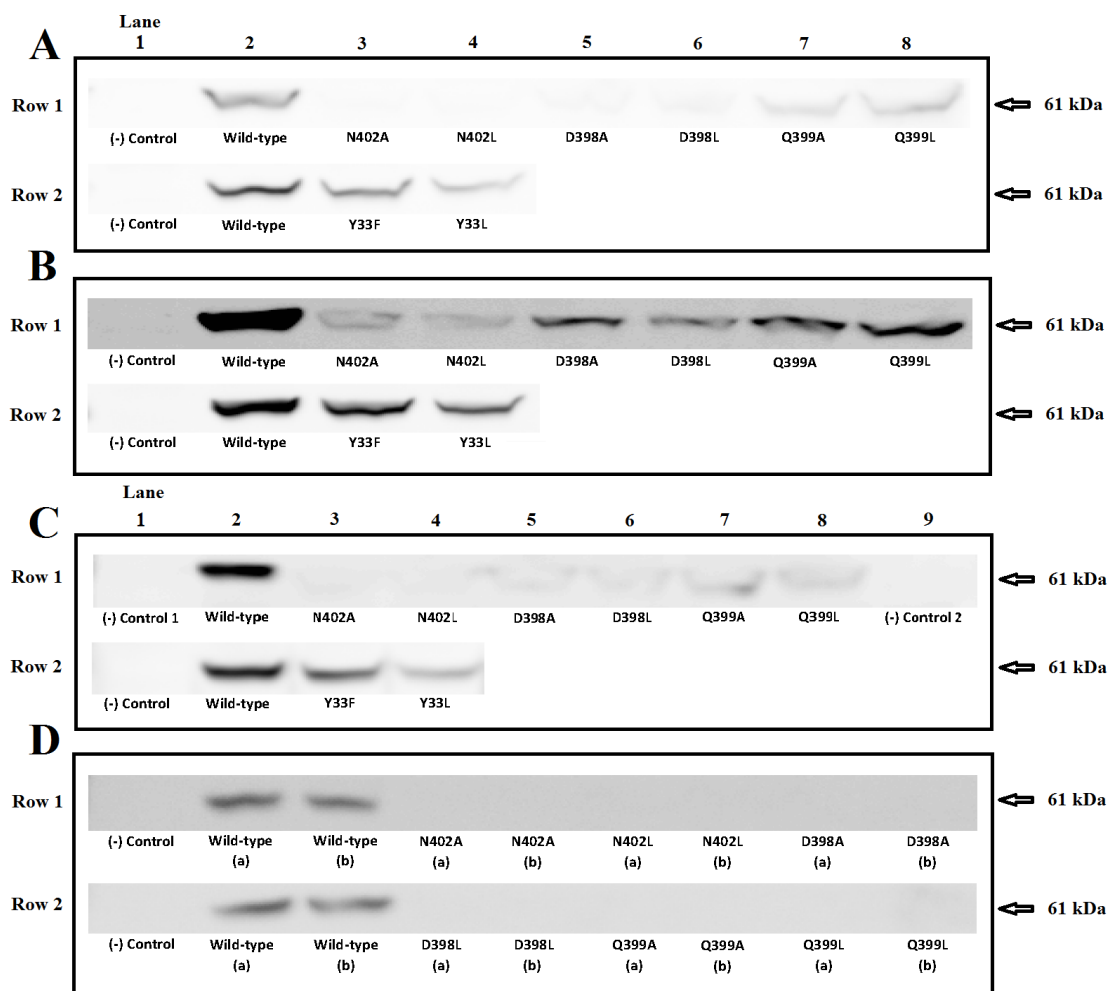


Figure 4. 9: Immunoblots of wild-type and mutant UGT2B7 proteins showing relative expression from stable transfection in HEK293T cells.

Lysate protein preparations (60µg) were resolved by SDS-PAGE, blotted to nitrocellulose, and probed with anti-human UGT2B7 antisera. Immuno-reactive bands are present at 61 kDa. Panel A and B: negative control (untransfected HEK293T) (L1; R1-2), UGT2B7-WT (L2; R1-2), C-terminal mutant proteins (N402A, N402L, D398A, D398L, Q399A, Q399L: L3-8; R1), and N-terminal mutants (Y33F and Y33L: L3-4; R2).

Panel C; negative control (untransfected HEK293T) (L1; R1 (25µg) and R2 (60µg); L9; R1 (100µg)), UGT2B7-WT (L2; R1 (25µg), L2; R2 (60µg)), 100µg of C-terminal mutants (N402A, N402L, D398A, D398L, Q399A, Q399L: L3-8; R1) and 60µg of N-terminal mutants (Y33F and Y33L: L3-4; R2).

Panel D compared repeated freeze-thawed (5x) samples (a) versus freshly thawed (1x) samples (b); negative control (100µg untransfected HEK293T) (L1; R1-2), 25µg UGT2B7-WT (L2-3; R1-2), and 100µg of C-terminal mutants (N402A, N402L, D398A, D398L, Q399A, Q399L: L4-9; R1-2).

Code: A, Ala; D, Asp; F, Phe; L, Leu; N, Asn; Q, Gln; Y, Tyr.

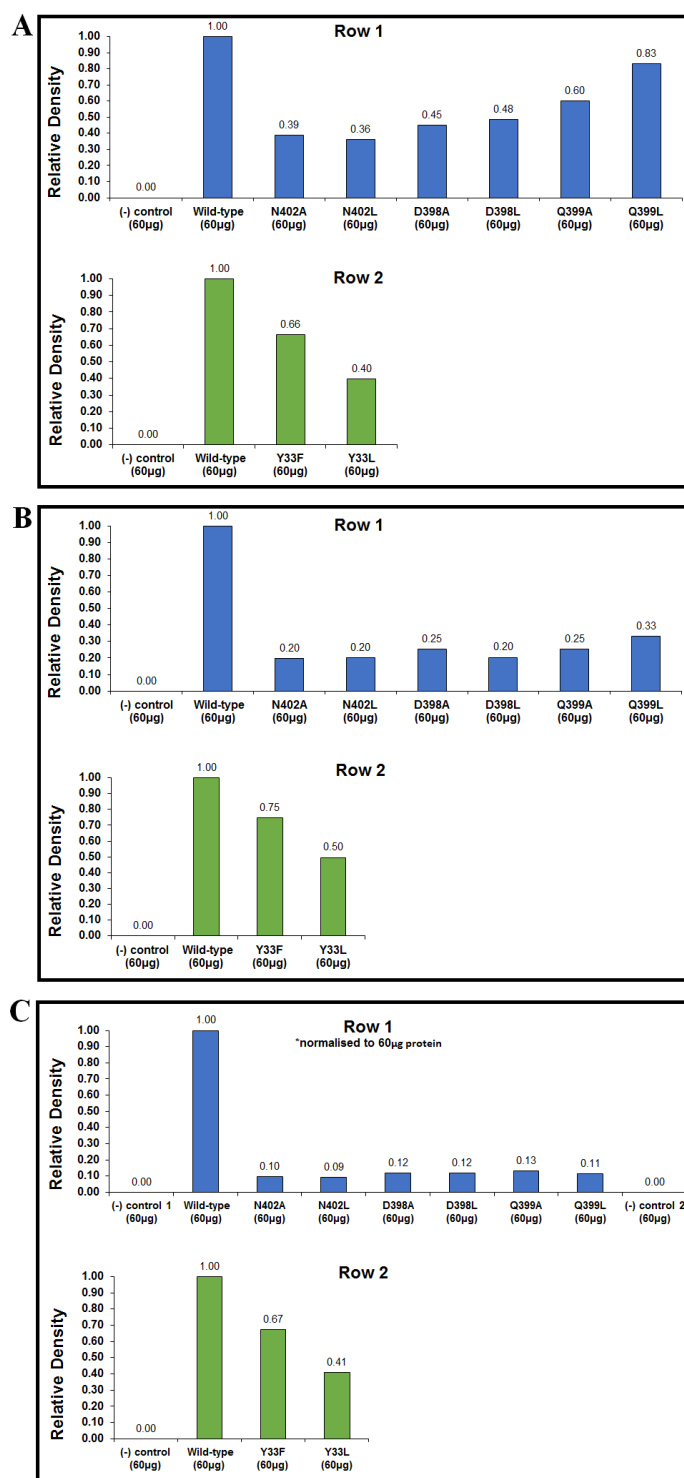


Figure 4. 10: Raw densitometry results for the expression of UGT2B7 wild-type and mutant proteins.

Relative expression levels of UGT2B7 proteins from Western blots in Figure 4.9A (panel A), 4.9B (panel B) and 4.9C (panel C). Results are shown for experiments using 60µg of protein.

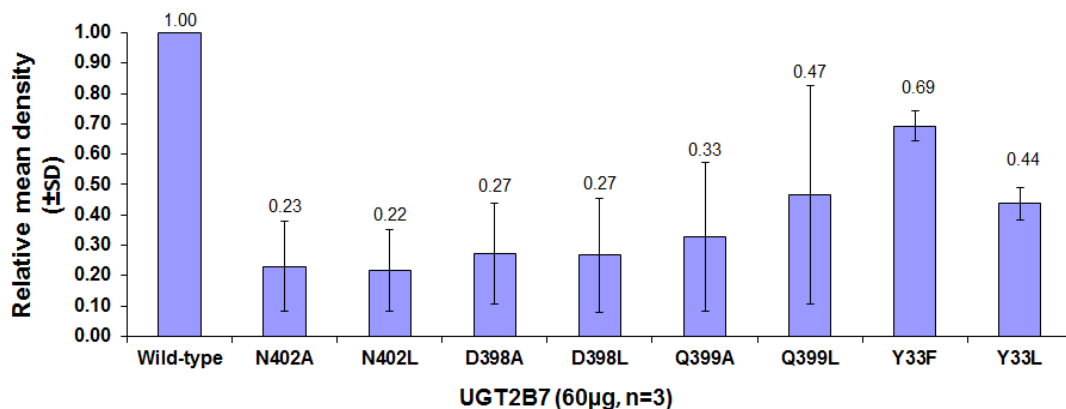


Figure 4. 11: Relative densities (mean ± SD) of immunoblots.

The raw and normalized relative density data shown on Figure 4.10A-C for UGT2B7 (60µg) based on Western blots (n=3; Figure 4.9A-C) were analyzed to show the relative variability of each protein sample.

Transient Transfections

Given the instability observed for the ‘stably’ expressed proteins, wild-type UGT2B7 and the Tyr33Phe, Tyr33Leu, Asp398Ala, Asp398Leu, Gln399Ala, Gln399Leu, Asn402Ala, Asn402Leu, Asn402His, Asn402Gln, Asn378Ala, Asn378Leu, Asn378His, and Asn378Gln mutants were transiently expressed in HEK293T cells. As with stable expression, the total protein content of transiently expressed UGT2B7 enzymes did not vary greatly between wild-type UGT2B7, and each mutant within each batch of transfections, although variability was observed between batches. Mean total protein was 10-13, 20-25 and 25-30mg/mL for both wild-type and mutant UGT2B7, across three separate transfections. Like stable expression, total protein expression of all mutants was similar to, or higher than that obtained for wild-type UGT2B7.

However, unlike stable expression, Western blotting showed that relative UGT2B7 expression was consistent (Figure 4.12; 50µg protein) between wild-type and mutants. As indicated previously, cells were harvested in the morning, lysed, and used immediately for activity assays and immunoblotting. Mean densitometry data (Figure 4.13) support consistent expression of UGT2B7 proteins from transient transfections, with relative density ratios close to 1:1 (wild-type: mutant), except for Asn378His/Gln and Asn402His/Gln (Figure 4.13, Row 3). However, given the lack of activity observed (Section 4.3.6), the variability in relative expression for mutations at positions 378 and 402 was inconsequential.

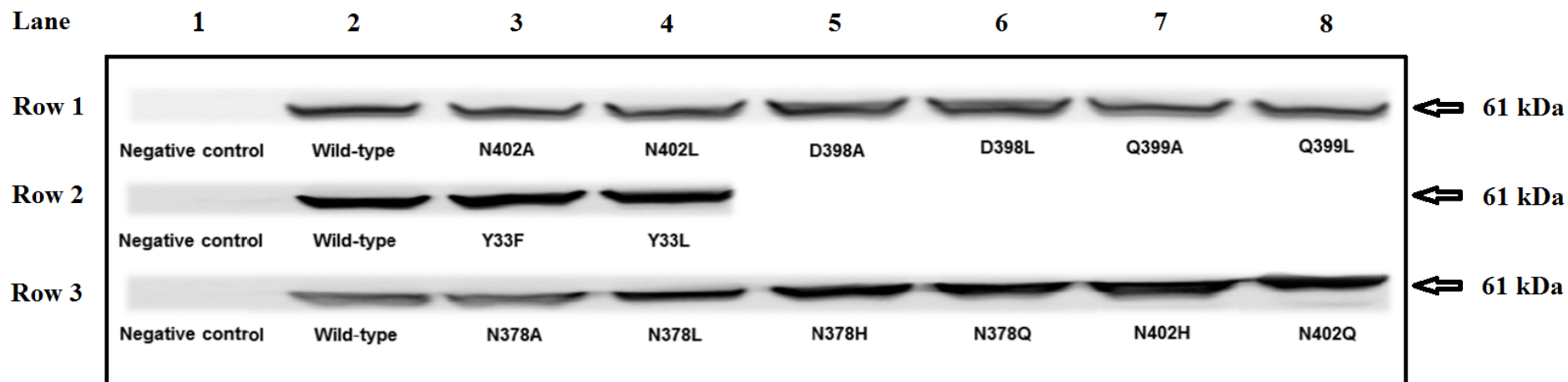


Figure 4. 12: Immunoblot of wild-type and mutant UGT2B7 proteins showing relative expression from transient transfection of HEK293T cells.

Lysate protein preparations (50µg) were resolved by SDS-PAGE, blotted to nitrocellulose, and probed with anti-human UGT2B7 antisera. Negative control (untransfected HEK293T) (L1; R1-3), UGT2B7-WT (L2; R1-3), N402A (L3; R1), N402L (L4; R1), D398A (L5; R1), D398L (L6; R1), Q399A (L7; R1), Q399L (L8; R1), Y33F (L3; R2), Y33L (L4; R2), N378A (L3; R3), N378L (L4; R3), N378H (L5; R3), N378Q (L6; R3), N402H (L7; R3), N402Q (L8; R3). Immuno-reactive bands are present at 61 kDa.

Code: A, Ala; D, Asp; F, Phe; L, Leu; N, Asn; Q, Gln; Y, Tyr.

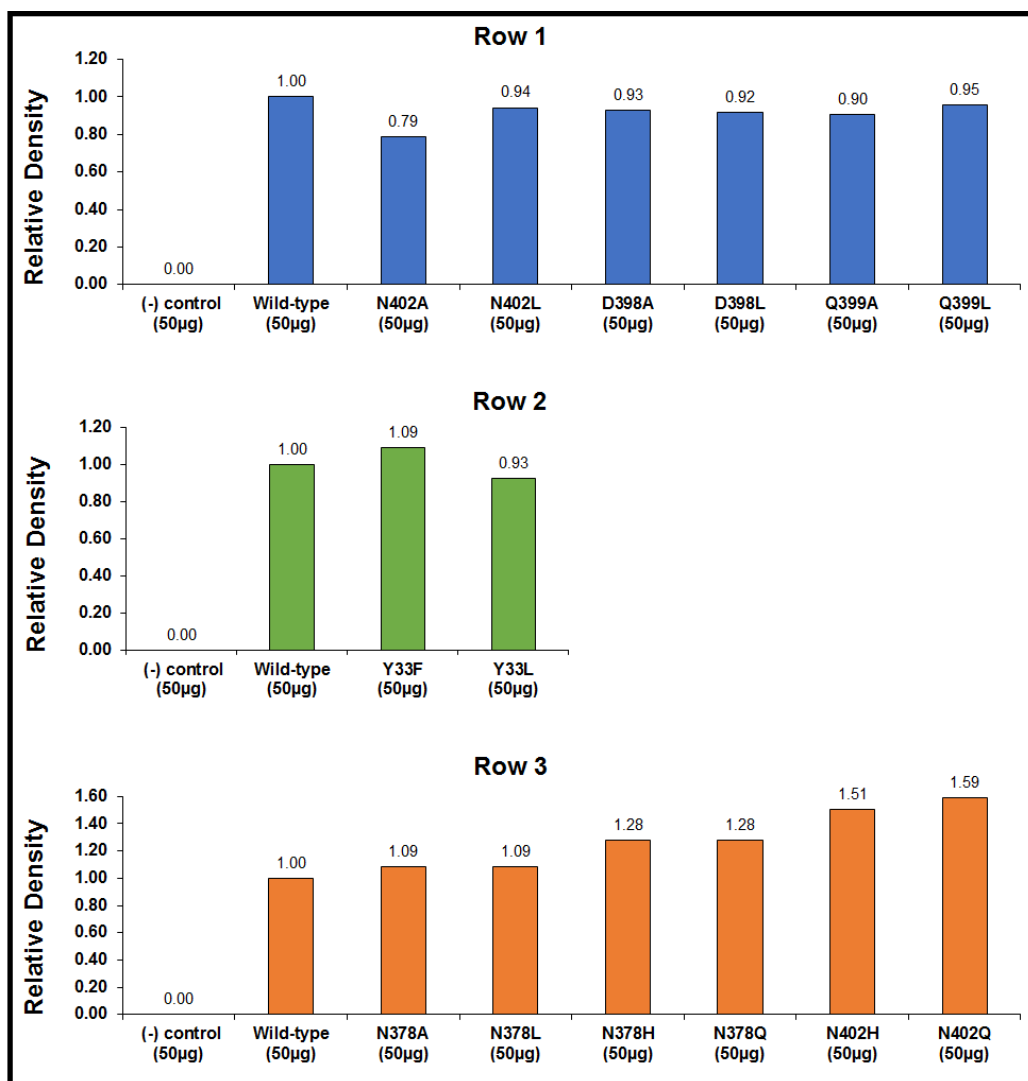


Figure 4. 13: Relative mean densities of Western blots (from Figure 4.12) for transient transfections, based on the raw relative density data for 50µg of UGT2B7 protein. Data represent the mean of duplicate estimates.

4.3.6 Effect of mutagenesis on UGT2B7 glucosidation and glucuronidation activities

Morphine glycosidation

Lysates from transient expression of UGT2B7 wild-type and mutants in HEK293T cells were used for activity screening with UDP-Glc and UDP-GlcUA as the cofactor and morphine (1, 5 and 10mM) as the aglycone, as described in Section 4.2.4. The CT mutants (at positions 398, 399 and 402) and Tyr33Leu lacked glucosidation and glucuronidation activity. Minor M3G formation was observed with Asn378His (1.5 - 5.2 pmol/min.mg; Figure 4.14) and very low (<1pmol/min/mg) morphine 3-glucosidation with Asn378Ala and Asn378His (Figure 4.16).

Substantial activity was observed only with Tyr33Phe (Figures 4.14-4.16), with M3G formation ranging from 53 to 144 pmol/min.mg and 62 to 185 pmol/min.mg for wild-type UGT2B7 and the Tyr33Phe mutant, respectively. Rates of M6G formation ranged from 9 to 27 pmol/min.mg and 12 to 35 pmol/min.mg for wild-type UGT2B7 and the Tyr33Phe mutant, respectively. By contrast, rates of M-3-glucoside formation were higher for the wild-type UGT2B7 than for the Tyr33Phe mutant; 11 – 39 pmol/min.mg vs. 7 – 29 pmol/min.mg. The substitution of Tyr for Phe favoured a modest increase (15-25%) in glucuronidation rates but a decrease in glucosidation activity with morphine as the substrate.

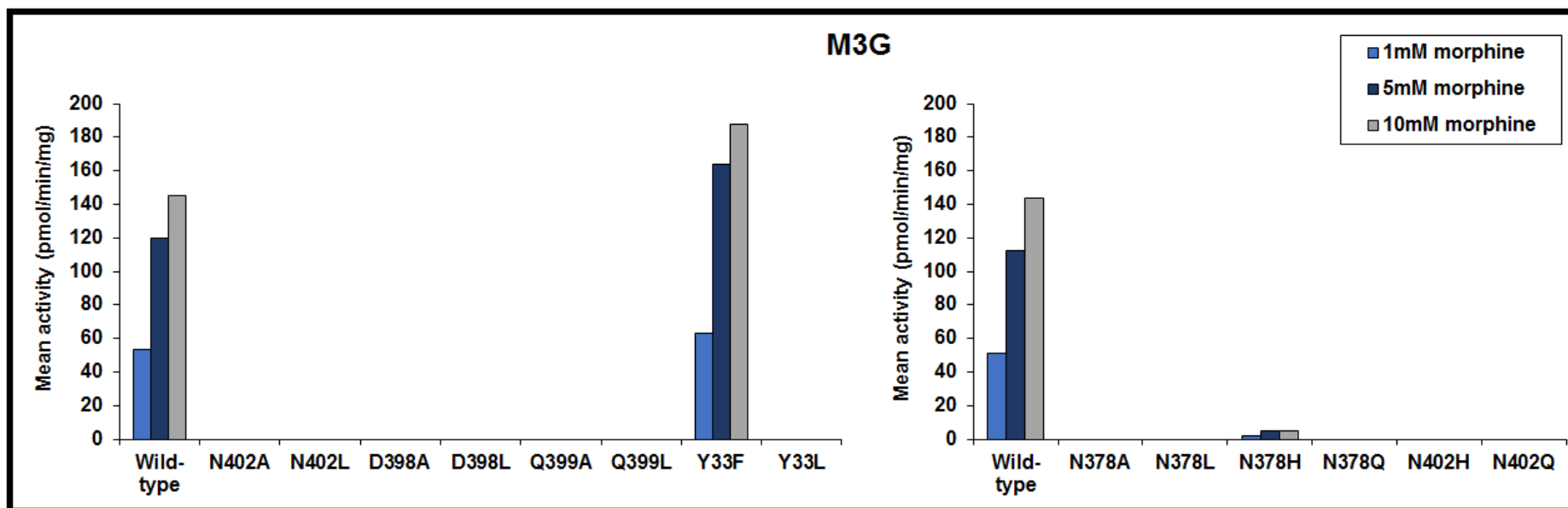


Figure 4. 14: Morphine 3-glucuronidation (M3G) activity of wild-type UGT2B7 and the C-terminal and N-terminal mutants.

Proteins were transiently expressed in HEK293T cells. Lysates (2mg/mL) were incubated for 2hr with 1, 5, and 10mM morphine and UDP-GlcUA (5mM).

Code: A, Ala; D, Asp; F, Phe; L, Leu; N, Asn; Q, Gln; Y, Tyr.

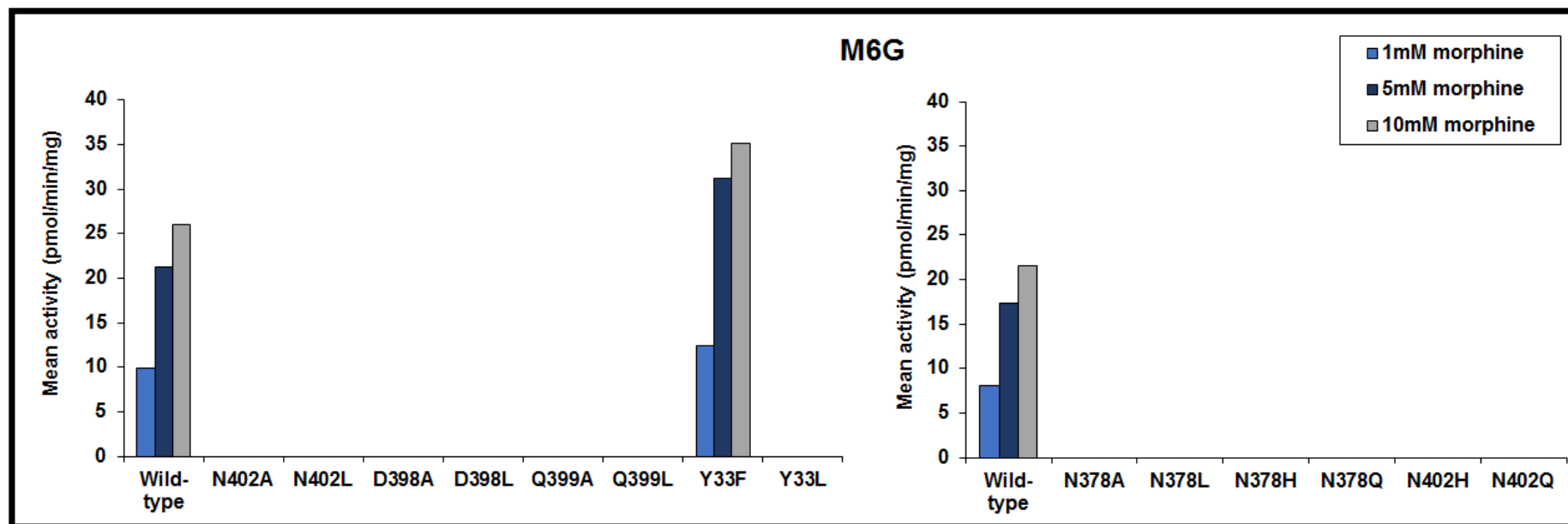


Figure 4. 15: Morphine 6-glucuronidation (M6G) activity of wild-type UGT2B7 and the C-terminal and N-terminal mutants.

Proteins were transiently expressed in HEK293T cells. Lysates (2mg/mL) were incubated for 2hr with 1, 5, and 10mM morphine and UDP-GlcUA (5mM).

Code: A, Ala; D, Asp; F, Phe; L, Leu; N, Asn; Q, Gln; Y, Tyr.

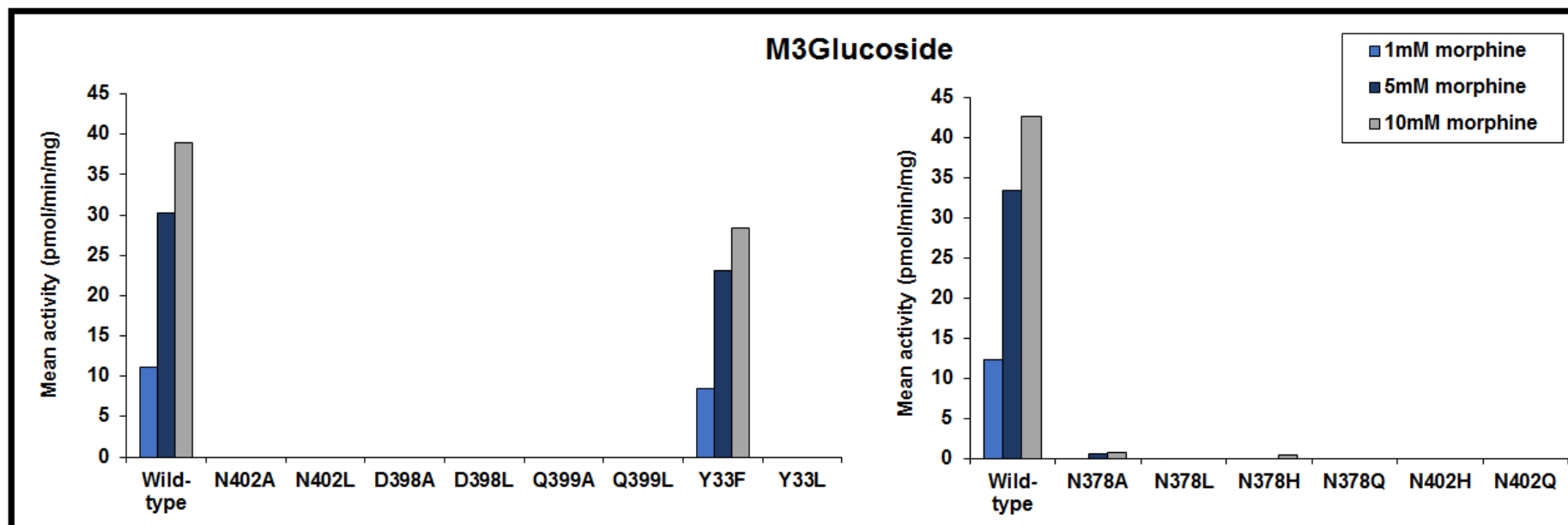


Figure 4. 16: Morphine 3-glucosidation (M3Glucoside) activity of wild-type UGT2B7 and th C-terminal and N-terminal mutants.

Proteins were transiently expressed in HEK293T cells. Lysates (2mg/mL) were incubated for 2hr with 1, 5, and 10mM morphine and UDP-Glc (5mM).

Code: A, Ala; D, Asp; F, Phe; L, Leu; N, Asn; Q, Gln; Y, Tyr.

4-MU glycosidation

Lysates from transient expression of UGT2B7 wild-type and mutants in HEK293T cells were additionally screened with UDP-Glc and UDP-GlcUA as the cofactors and 4-MU (100, 350 and 1000 μ M) as the aglycone, as described in Section 4.2.4. Similar to the results with morphine as the substrate, the CT mutants (at positions 378, 398, 399 and 402) and Tyr33Leu lacked appreciable activity towards 4-MU. Although trace amounts of 4-MU glucoside and glucuronide were observed for these mutants, the rates were <1pmol/min/mg, except for 4-MUG formation by Tyr33Leu and Asn378His (0.4 - 7 pmol/min.mg and 1.5 - 20 pmol/min.mg, respectively) (Figure 4.17 and 4.18).

As with morphine, substantial glucuronidation and activity was observed only with Tyr33Phe (Figures 4.17). 4-MUG formation ranged from 17 - 213 pmol/min.mg and 27 - 406 pmol/min.mg for wild-type UGT2B7 and the Tyr33Phe mutant, respectively. This moderate increase in glucuronidation activity (37 - 47%) observed for the Tyr33Phe mutant was consistent with the morphine glucuronidation data. By contrast, rates of 4-MU glucoside formation were similar for wild-type UGT2B7 and for the Tyr33Phe mutant, albeit <1pmol/min/mg (Figure 4.18).

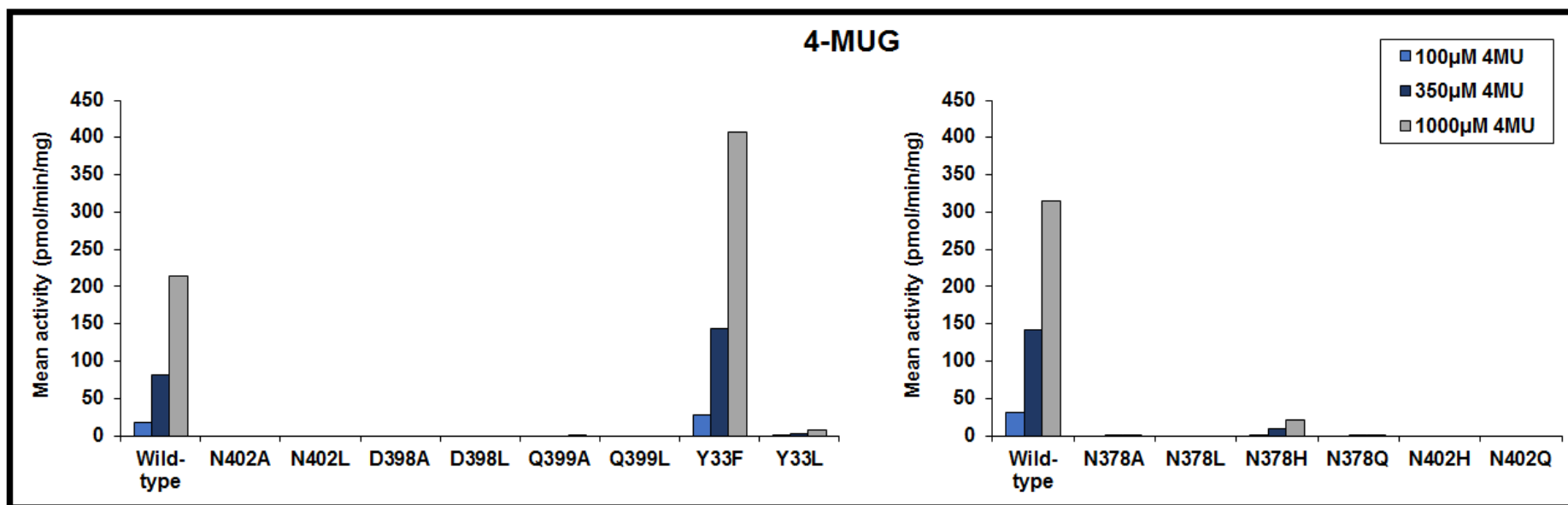


Figure 4. 17: 4-Methylumbelliferone glucuronidation (4-MUG) activity of wild-type UGT2B7 and the C-terminal and N-terminal mutants.

Proteins were transiently expressed in HEK293T cells. Lysates (2mg/mL) were incubated for 2hr with 100, 350, and 1000µM 4-MU and UDP-GlcUA (5mM).

Code: A, Ala; D, Asp; F, Phe; L, Leu; N, Asn; Q, Gln; Y, Tyr.

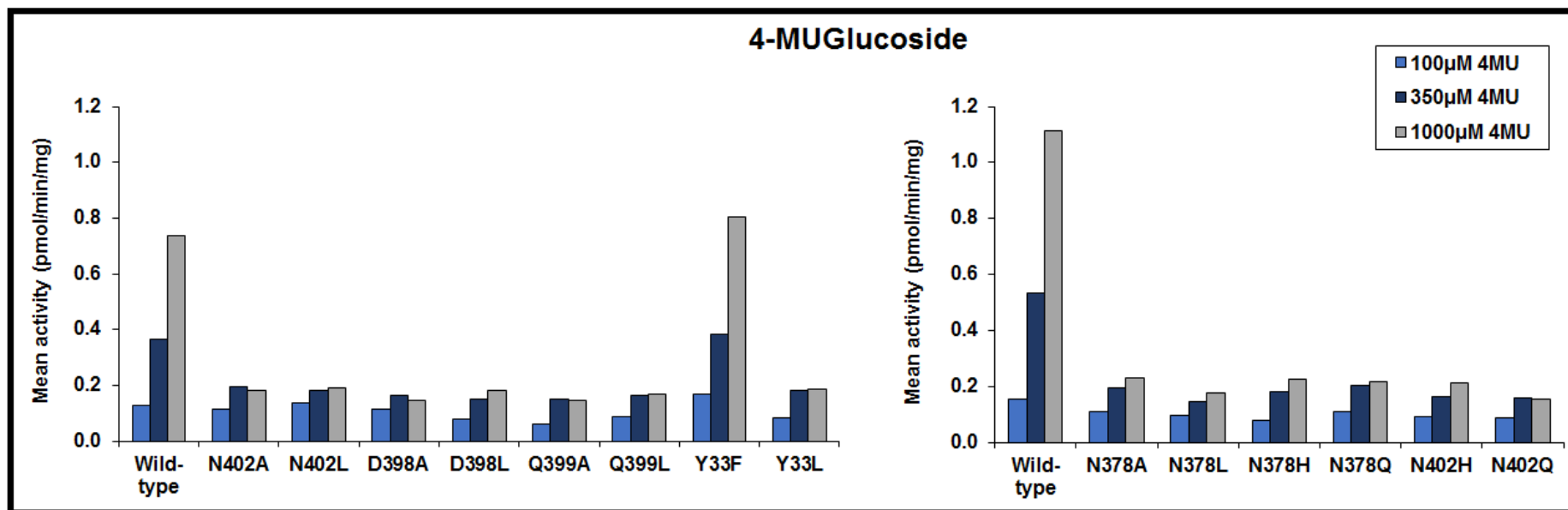


Figure 4. 18: 4-Methylumbelliferone glucosidation (4-MUGlucoside) activity of wild-type UGT2B7 and the C-terminal and N-terminal mutants.

Proteins were transiently expressed in HEK293T cells. Lysates (2mg/mL) were incubated for 2hr with 100, 350, and 1000μM 4-MU and UDP-Glc (5mM).

Code: A, Ala; D, Asp; F, Phe; L, Leu; N, Asn; Q, Gln; Y, Tyr.

4.4 Discussion

Molecular modelling and site-directed mutagenesis studies were employed to identify the amino acids involved in the selective binding of the sugar moieties of UDP-Glc and UDP-GlcUA to the cofactor binding domain of UGT2B7. Docking experiments in the CT structure of UGT2B7 identified residues within a 3Å radius of both nucleotide sugars that were generally consistent with previous residues deemed important in UDP-GlcUA binding within the UGT2B7 CT (Miley et al. 2007; Radomska-Pandya et al. 2010; Wang, Yuan & Zeng 2011). Although the CT mainly interacts with the UDP-sugar donor and the NT with the aglycone, cross talk between the domains is likely to occur during catalysis as UGT2B7 belongs to the GT-B fold family with an active catalytic site sandwiched between two Rossmann-like folds ($\alpha/\beta/\alpha$). Hence, the absence of an NT domain may potentially limit insights into the role of the NT residues, should any occur, in the UDP-sugar selectivity of UGT2B7.

As indicated above, docking experiments with the full length UGT2B7 homology model performed here demonstrated that both UDP-Glc and UDP-GlcUA bind within the same domain of the CT of UGT2B7 and binding interactions of the UDP moiety are cofactor independent. However, residues involved in the binding of the sugar differed with hydrogen bonding interactions between Asp398 (O6' hydroxyl) and Glu399 (O3' hydroxyl) identified with the glucose moiety, and Asn402 (O6'/carboxylate) and Tyr33 (O2' hydroxyl) with the glucuronic acid moiety. These results demonstrate that the docking approach could deliver different docking conformations, and interactions between amino acids and functional groups of the sugar moiety of the two UDP-sugars. Based on the UGT2B7-CT X-ray crystal structure, Miley et al. (2007) further predicted a role for Asn378 in the selective binding of the carboxylate group of UDP-GlcUA, but did not experimentally verify

this hypothesis. This differs to the docking results generated here, which suggests Asn402 is involved in the selective binding of UDP-GlcUA. To the best of my knowledge, Asn402 has not previously been predicted or tested for its interaction with UDP-GlcUA, or any other UDP-sugar. Asn402 is just one amino acid distal to the highly conserved DQxD motif (at the end of DBR1) previously reported to interact with the O2'/O3'/O4' hydroxyl groups of UDP-GlcUA of UGT2B7, UGT1A10 and UGT1A6 (Miley et al. 2007; Patana et al. 2007; Xiong et al. 2008). The docking studies performed here predicted that the NT residue Tyr33 additionally interacted with the glucuronic acid moiety of UDP-GlcUA. Mutation of Tyr33 of UGT2B7 has previously only been studied in relation to an interaction with aglycones, not the UDP-sugar (Barre et al. 2007).

Thus, the Tyr33Phe, Tyr33Leu, Asn378Ala, Asn378Leu, Asn378Gln, Asn378His, Asp398Ala, Asp398Leu, Gln399Ala, Gln399Leu, Asn402Ala, Asn402Leu, Asn402His, and Asn402Gln mutants were generated by site-directed mutagenesis. Although all mutant proteins were transiently expressed to a similar level in HEK293T cells, 'significant' morphine glucuronidation and glucosidation activity was observed only with wild-type UGT2B7 and the Tyr33Phe mutant. Similarly, 4-MU glucuronidation activity was observed only with wild-type UGT2B7 and the Tyr33Phe mutant, while rates of 4-MU glucosidation were very low (less than 1 pmol/min/mg) with all mutants and wild-type UGT2B7.

Degradation of the stably expressed CT mutant proteins occurred even when stored at -80°C. Since NT mutant and wild-type UGT2B7 protein was harvested, processed and stored under the same conditions as the CT mutant proteins, but wild-type UGT2B7 was relatively stable in comparison, the reduced stability of the CT mutant proteins is

most likely due to changes in the secondary and/or tertiary structures of the mutant proteins. The amino acids at positions 378, 398, 399, and 402 are highly conserved and are in, or close to, the UGT signature sequence (also known as ‘donor binding region’ or DBR1) in the CT domain (residue 356-399 in UGT2B7). The high degree of conservation infers an important intrinsic functional role of this region in protein structure and function. Thus, mutagenesis or single nucleotide polymorphisms (SNPs) in this region may be deleterious (Hao, Xiao & Chen 2010; Thomas & Kejariwal 2004), making the protein more susceptible to degradation over time. For this reason, activity studies were performed with transiently expressed enzymes immediately after harvesting.

A modest increase in morphine (~20%) and 4-MU (~40%) glucuronidation activity and a modest decrease in morphine glucosidation (~20%) were observed with the NT domain mutant Tyr33Phe. The data suggest that either a Phe or Tyr amino acid at position 33 is required for both glucuronidation and glucosidation, as the Leu mutation abolished morphine and 4-MU glycosidation activity. Although, glucosidation activity was too low with 4-MU as the aglycone to be considered reliable for a trend comparison with morphine glucosidation, glucuronidation of 4-MU and morphine may be compared. A study by Barre et al. (2007) investigating the effect of this mutation on the glucuronidation of 16 aglycones found substrate dependent changes, with increases in the glucuronidation of some substrates (e.g. hyodeoxycholic acid, 4-hydroxyestrone and 17-epiestriol) but not for others. It was therefore suggested that Tyr33 has a vital role in aglycone selectivity. However, an effect of the mutation on cofactor binding was not investigated.

Due to its proximity to the putative catalytic base, His35, it would seem likely that Tyr33 is involved in both aglycone and sugar donor binding as this is the region where both the NT and CT domains can interact to form a cleft. However, as the differential effect on glycosidation activity was only modest with the Phe33 mutation, the role of the benzene ring (on Phe and Tyr) may serve more towards alignment, rather than participating in UDP-sugar hydrogen bonding, of the aglycone and/or UDP-sugar in the active site. It is interesting to note that Ser18 in the plant VvGT1 crystal structure (equivalent to Tyr33 in UGT2B7) participates hydrogen bonding interactions with both the aglycone and sugar donor (Nair et al. 2015; Offen et al. 2006), suggesting a potential dual binding role for Tyr33. Mutation of Arg25 in the bifunctional plant BpUGT94B1 demonstrated clear cofactor selectivity; glucuronidation was essentially abolished, with only 0.5-2.5% of wild-type activity remaining, while glucosidation displayed a 3-fold increase in activity (Osmani et al. 2008). A dual binding/alignment role would be consistent with the observation in this study of an inverse activity relationship with morphine glucuronidation (increase) and glucosidation (decrease) following the Tyr33Phe mutation. However, the effect size was minor in comparison to the much greater inverse activity relationship effect observed with BpUGT94B1.

The molecular modelling and mutagenesis work presented here is consistent with previous studies showing the importance of Asp398 and Gln399 (part of the DQxD motif) in DBR1 and its interaction with the sugar moiety of UDP-GlcUA in human UGT2B7. Previous studies by Miley et al. (2007) and Wang, Yuan and Zeng (2011) demonstrated that mutagenesis of these highly conserved residues drastically decreased the capacity of UGT2B7 to glucuronidate a number of substrates (androsterone, hyodeoxycholic acid (HDCA), tetrachlorocatechol (TCC), flurbiprofen). Studies by Patana et al. (2007) and Xiong et al. (2008) also corroborate

this observation for the equivalent residues of UGT1A6 and UGT1A10, respectively. Data presented here also demonstrate that Asp398 and Gln399 are important for UDP-Glc binding.

Asn378 and Asn402 were both assessed for a selective interaction with UDP-GlcUA, but mutagenesis at these positions abolished both glucuronidation and glucosidation. Based on these observations, neither Asn378 nor Asn402 are selective residues for UDP-GlcUA binding to human UGT2B7. Rather, Asn402, which lies just outside the UGT signature sequence and is highly conserved among the human and plant UGTs (except UGT8), is apparently involved in the binding of the sugar moiety of both UDP-GlcUA and UDP-Glc. Most likely, Asn402 binds to hydroxyl groups on the sugar moiety that are common to both cofactors, that is the O2', O3' and/ or O4' hydroxyls. Additionally, binding to the carboxyl group on the glucuronic acid moiety cannot be discounted. Like Asn402, Asn378 appears to be involved in both UDP-Glc and UDP-GlcUA binding. This role is consistent with docking results from this work that demonstrated Asn378 hydrogen bonds to the phosphate backbone of UDP, a common moiety shared between UDP-GlcUA and UDP-Glc (Table 4.5 and Figure 4.2).

It has been proposed, based on a number of different structure-function studies of UDP-glycosyltransferases (human and plant) utilizing UDP-GlcUA as a cofactor (Osmani et al. 2008; Pedersen, Darden & Negishi 2002; Senay et al. 1997), that the positively charged side chain of an Arg residue is able to interact electrostatically with the negatively charged carboxylate ion of the glucuronic acid moiety, thereby conferring specificity for UDP-GlcUA (discussed further in Section 1.2.7). Two highly conserved positively charged arginines in human UGT1A and UGT2B (Arg49 and Arg259) (Figure 1.9) proteins were proposed to stabilize binding of the negatively

charged carboxylate ion (Radomska-Pandya et al. 2010). Inspection of the NT domain of the homology model generated here with docked UDP-Glc and UDP-GlcUA showed that Arg49, residing on a helix (N α 1), was approximately 25Å from the docked UDP-sugar, while Arg259 (N13 loop) was located at a distance of approximately 22Å (Figure 4.19). This distance is clearly too large for an electrostatic interaction with the carboxylate group of UDP-GlcUA. However, there is no human UGT crystal structure for the NT, which is highly variable, making homology modelling a challenge and a less than ideal for detailed assessment of structure-function relationships.

It is acknowledged that the homology model generated here was intended primarily for docking experiments with UDP-sugars in the CT and was based on the crystal structure of human UGT2B7-CT (PDB code 2O6L). In contrast, the NT domain was based on X-ray crystal templates from two plant species, *Vitis vinifera* (VvGT1) and *Medicago truncatula* (UGT71G1) (Lewis, Mackenzie & Miners 2011). This approach has previously been used to construct several homology models of human UGT enzymes (see Chapter 1; Table 1.6). Alternatively, the NT domain could be modelled using multiple plant UGT X-ray crystal structures as templates. This approach was adopted by Nair et al. (2015), who used 3 templates from the same two plant species for modelling UGT2B7. Nair et al. (2015) observed differences in the location of the catalytic base (His35) on the secondary structure depending on the template used (on the N1 loop with template 2C1X (PDB code) but on N α 1 with templates 2ACW and 2PQ6). This shows greater variability in secondary structure in the NT compared to the CT, consistent with the known greater variability in NT sequence identity compared to CT domain.

Also noted by Nair et al. (2015), details of whether a residue is situated on a flexible structure, such as a loop, or on a well-defined structure, such as a helix, is important for determining the preferred conformation of an amino acid. Importantly, Tyr33 in the UGT2B7 homology model (equivalent to Ser18 in VvGT1) generated here resides on the N1 loop, consistent with the model by Nair et al. (2015), which was also based on the VvGT1 template (PDB code 2C1Z). Molecular dynamic simulations performed by Nair et al. (2015) predicted significant flexibility in this loop. Such flexibility within the binding site could conceivably facilitate aglycone and sugar donor binding that would be optimal. As discussed previously, Arg49 and Arg259 were predicted to be $\sim 20\text{\AA}$ from the docked UDP-sugar in the homology model developed in this thesis. The position of Arg49 was confirmed by Nair et al. (2015) who reported this residue was located at the end of N α 1, towards the outer surface of the protein. By contrast, Arg259, which resides on a flexible loop in both models, was found by Nair et al. (2015) to be much closer to the catalytic site ($\sim 4.5\text{\AA}$ from UDP-sugar binding site), potentially allowing it form a salt bridge with UDP-GlcUA. Arg259 has additionally been implicated in the enhanced binding of UDP-GlcUA to UGT1A5*8 compared to wild-type UGT1A5 (which has Gly at this position) (Yang et al. 2018). Overall, these data highlight how less reliable homology modelling of the NT of human UGT enzymes is compared to the CT.

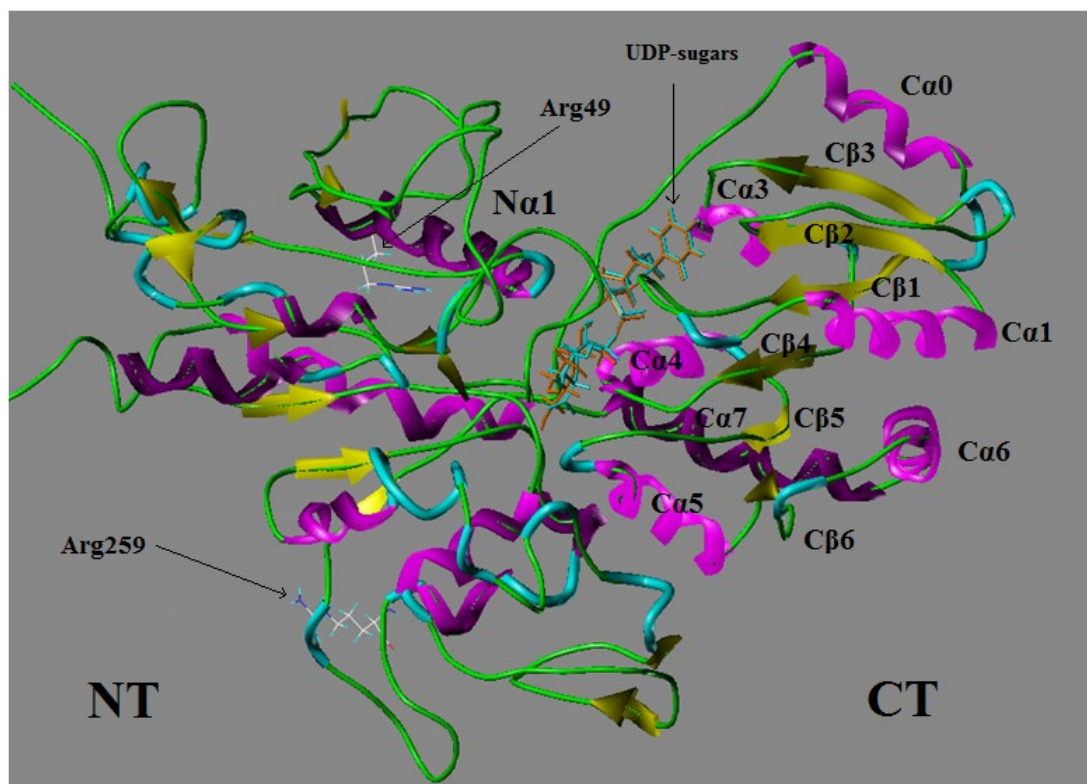


Figure 4. 19: Position of Arg 49 and 259 in relation to docked UDP-Glc and UDP-GlcUA in the UGT2B7 homology model.

The secondary structure of the UGT2B7 homology model with UDP-glucose (orange) and UDP-glucuronic acid (cyan) docked mainly in the CT end. The α -helices are represented by magenta ribbons, β -sheets by yellow arrow strands, and the loops by green/cyan tubes. Arg49 and Arg259 (stick structures) are shown towards the top and bottom end of the NT, respectively. Arg49 is part of a helix ($N\alpha 1$) that faces towards the surface of the protein while Arg259 is part of a very long loop (N13), also facing towards the outer surface of UGT2B7.

Although the UGT2B7 homology model did not predict Arg49 or Arg259 as potential ($>20\text{\AA}$ distance from docked site) residues for stabilizing the binding of the carboxylate ion of UDP-GlcUA, this does not necessarily preclude a role of these amino acids in UDP-GlcUA binding given the limitations of modelling the NT (discussed above). These positively charged amino acids may still be selective for UDP-GluUA binding. However, in agreement with the UGT2B7 homology model of Nair et al. (2015), Arg259 is the more likely candidate based on sequence analysis.

Figure 1.10 shows that Arg49 or Arg259 are highly conserved in the UGT 1A, 2A (except 2A1, which has Lys49) and 2B subfamily proteins that mainly utilize UDP-GlcUA as the sugar donor. In comparison, Arg49 and Arg259 (UGT2B7 numbering) are not conserved in the UGT3A (His49 and Asn250) or UGT8 (Cys243) family proteins which utilize UDP-sugars other than UDP-GlcUA (Mackenzie et al. 2011; Mackenzie et al. 2008; Meech & Mackenzie 2010; Meech et al. 2015; Meech et al. 2012b). In addition, although UGT8 has an Arg at position 49, it only utilizes UDP-galactose, not UDP-GlcUA (Figure 1.10) (Meech et al. 2012b). With respect to position 49 (UGT2B7 numbering), it is noted that Arg, Lys and His are all positively charged bases with similar chemistry, albeit with differing sidechain lengths and structure. On the other hand, position 259 (UGT2B7 numbering) consists of the conserved basic and charged Arg for all UGT members except for UGT3A and UGT8 with the polar Asn and Cys, respectively. Hence, at this position compared to residue 49, there is less conservation for positively charged bases across the UGT subfamilies utilizing different UDP-sugars. Therefore, Arg259 would be more consistent with the hypothesis of a selective base residue for the negatively charged UDP-GlcUA by all the UGT members that utilize UDP-GlcUA as the main cofactor.

A number of limitations of the docking approach followed here are acknowledged. These include: the ‘static’ nature of the model, when UGTs are almost certainly dynamic proteins (Nair et al. 2015); the low sequence identity of the plant UGTs used as templates; and the lack of an aglycone positioned (either docked or co-crystallized) within the model, as this could affect cofactor binding. The modelling work performed here in the absence of a docked aglycone suggested differences in UDP-sugar binding, but this was not reflected in the mutagenesis and activity data. Nevertheless, modelling suggests that each of the CT residues mutated is appears to be critical for cofactor

binding. It is likely that mutations in DBR1 have a deleterious effect on cofactor binding due to changes in secondary and tertiary structure, which may additionally affect stability.

Summary

The project has elucidated further insight into the structural basis for UDP-sugar binding in human UGT2B7. Docking UDP-Glc and UDP-GlcUA into the static homology model of UGT2B7 has suggested that the binding site is within the same pocket for both sugar donors but that their inherently different chemistry has resulted in different residue binding towards the sugar moieties. The low sequence homology but highly conserved structural plant/bacterial UGT crystal templates, along with the experimental mutagenesis work have been an invaluable source of information for helping to construct new insight into human UGT sugar selectivity. Collectively, these data indicate that Asn378, Asp398, Glu399, and Asn402 are essential for the binding of both UDP-GlcUA and UDP-Glc. This is consistent with work already published in the literature with respect to UDP-GlcUA binding in UGT2B7, but no study has previously investigated the binding of UDP-Glc. Overall, it appears an aromatic amino acid (present in both wild-type and Tyr33Phe) at position 33 is important for retaining both glucosidation and glucuronidation activity with morphine.

Future experimental studies should focus on the NT residues with respect to identifying selective UDP-cofactor residues to support comparative homology modelling studies which are currently not as robust, and therefore, not as informative for the NT of human UGTs due to the lack of a highly homologous (>50% sequence identity) crystal templates for this region. Incorporating MD simulations into the analysis could provide useful insights in comparison with rigid and static models but

Chapter 4: Application of UGT2B7 protein homology modelling

again, this relies on having high resolution and highly homologous template scaffolds to begin with.

Chapter 5

Mycophenolic acid glucosidation

5.1 Introduction

5.1.1 Mycophenolic acid and its metabolites

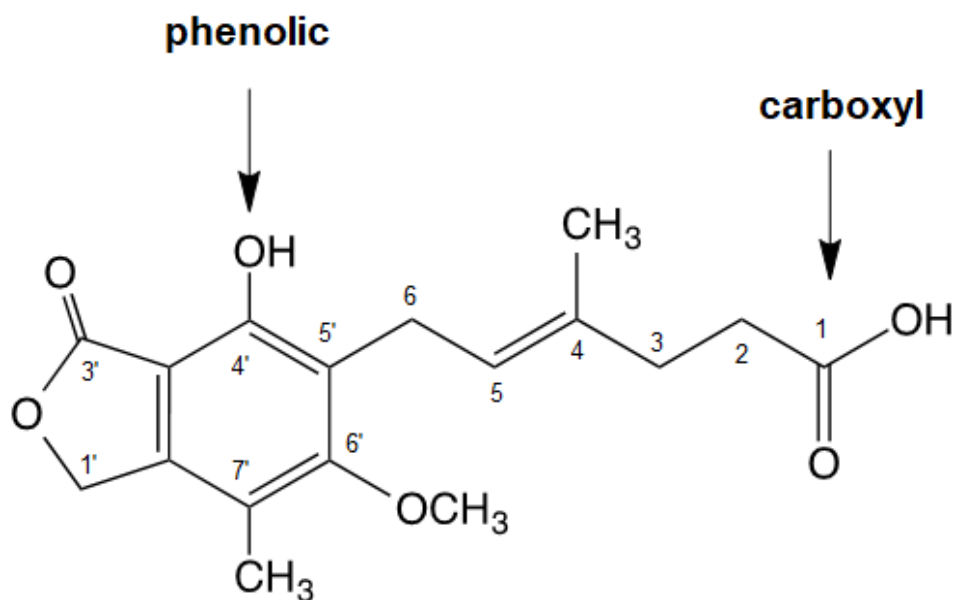
History, chemistry and pharmacology

Mycophenolic acid (MPA) was first discovered in 1896 as a metabolic product of several *Penicillium* species (*P. glaucum*, *P. brevicompactum* and *P. stoloniferum*) (Barta 2002; Park 2011; Shaw & Nowak 1995). A preliminary chemical structure was proposed in 1933, then modified in 1948 (Birkinshaw, Raistrick & Ross 1952). Although MPA is not useful clinically as an antibiotic, it was the first antibiotic to be crystallized from a mold and has antifungal properties (Lipsky 1996). It is also used as an antineoplastic agent and immunosuppressive agent for the treatment of several autoimmune diseases (viz. rheumatoid arthritis and psoriasis), although it is employed most commonly for the prevention of organ transplant rejection (Abd Rahman, Tett & Staatz 2013; Jones et al. 1975; Lipsky 1996; Sherwin et al. 2011b). Mechanistically, MPA is a potent uncompetitive, selective inhibitor of inosine monophosphate dehydrogenase (IMPDH). MPA acts by binding to IMPDH and replacing the nicotinamide portion of the nicotinamide adenine dinucleotide cofactor (NADH) after NADH is released (Sintchak et al.). This prevents the oxidation of inosine-5'-monophosphate (IMP) to xanthosine-5'-monophosphate (XMP) in the *de novo* guanosine nucleotide biosynthesis pathway needed by B and T lymphocytes for proliferation in response to mitogen or antigen (Allison et al. 1975,1977).

The systematic name for MPA is (E)-6-(4'-hydroxy-6'-methoxy-7'-methyl-3'-oxo-1H-2-benzofuran-5-yl)-4-methylhex-4-enoic acid

(https://pubchem.ncbi.nlm.nih.gov/compound/mycophenolic_acid) (Figure 5.1). The semi-synthetic mycophenolate mofetil (MMF), the morpholinyl ethyl ester of MPA, is a pro-drug synthesized to increase MPA bioavailability (Bullingham, Nicholls & Kamm 1998; Lee et al. 1990; Park 2011). The oral bioavailability of MPA when administered as MMF is high (80.8 - 94%) (Lipsky 1996; Park 2011; Staatz & Tett 2007). MMF is rapidly de-esterified by cleavage of the morpholinyl ethyl ester bond by carboxylesterases (likely CES1 and 2) (Figure 5.2), which are found in numerous human tissues including the gastrointestinal tract and liver (Fujiyama et al. 2009).

MPA is metabolized mainly via glucuronidation at the phenolic hydroxy group, forming MPA phenolic glucuronide (MPAGlcUA), and at the carboxyl group, forming the minor MPA acyl glucuronide (AcMPAGlcUA) (Bullingham, Nicholls & Kamm 1998; Shipkova et al. 1999a) (Figure 5.2). In healthy individuals, urinary excretion of MPAGlcUA and unchanged MPA account for 76% and 17% of the administered dose, respectively. Recovery of a radioactive dose of MMF in faeces was 5.5% (Bullingham, Nicholls & Kamm 1998). MPA and AcMPAGlcUA are pharmacologically active as inhibitors of IMPDH, while MPAGlcUA is not (Shipkova et al. 1999a). Interestingly, the literature reports the major phenolic glucuronide (MPAGlcUA) as the 7-O-glucuronide but according to the systematic nomenclature, it should be the 4'-O-glucuronide since conjugation occurs at the 4'-hydroxyl group of the benzofuran structure (Figure 5.1). For simplicity, this thesis refers to the phenolic MPA glucuronide as MPAGlcUA.



(E)-6-(4-hydroxy-6-methoxy-7-methyl-3-oxo-1H-2-benzofuran-5-yl)-4-methylhex-4-enoic acid

Figure 5.1: Chemical structure of mycophenolic acid (MPA), with the phenolic and carboxylic acid groups shown.

MPA can also be glucosidated at both the phenolic and carboxyl functional groups forming MPA phenolic glucoside (MPAGlc) and MPA acyl glucoside (AcMPAGlc) (Shipkova et al. 1999a; Shipkova et al. 2001) (Figure 5.2). Just as MPAGlcUA can be hydrolyzed by β -glucuronidase, MPAGlc can be hydrolyzed by β -glucosidase and both AcMPAGlcUA and AcMPAGlc are also susceptible to alkaline (NaOH) hydrolysis (Picard et al. 2005; Shipkova et al. 1999a; Shipkova et al. 2001). Like MPAGlcUA, MPAGlc does not inhibit IMPDH-II (Schutz et al. 1999).

In contrast, no loss of pharmacological activity was observed due to modification of the carboxyl group since, as noted previously AcMPAGlcUA demonstrated IMPDH-II inhibition efficiency similar to that of MPA. It is not known whether this effect also

translates to AcMPAGlc. The minor glycoside metabolites, MPAGlc and AcMPAGlcUA, were first observed in the plasma of kidney, liver and heart transplant recipients receiving immunosuppressive therapy with MMF; the area under the plasma concentration (AUC)-time curve for each of these minor metabolites was approximately 10% of the AUC observed for MPA. The mean AUC ratio of MPAGlc to AcMPAGlcUA was 1: 1.18 (Schutz et al. 1999; Shipkova et al. 1999b). Picard et al. (2005) similarly reported that the mean AUC values of AcMPAGlcUA and MPAGlc that were 6.2% and 5.4%, respectively, of the average MPA AUC_{0-12hr}. Thus, it appears that the phenolic MPA glucoside (MPAGlc) may be as abundant as the acyl glucuronide (AcMPAGlcUA) in plasma. Both glucoside conjugates of MPA have been detected in urine (Picard et al. 2005), but relative abundance data were not provided. MPAGlc and AcMPAGlc have variably been reported to be formed by incubations of MPA with HLM, human kidney microsomes (HKM), and human intestinal microsomes (HIM) (Picard et al. 2005; Shipkova et al. 2001). Shipkova et al. (2001) reported that the intrinsic clearance (CL_{int}) for MPAGlc formation was ~15.4-fold greater in HKM than in HLM and that only HKM formed AcMPAGlc. In comparison, Picard et al. (2005) was able to detect both glucosides and glucuronides of MPA in incubations of HLM, HKM and HIM. The rank order of CL_{int} values for MPAGlc and AcMPAGlc was HLM>HKM>HIM. A fourth minor metabolite, 6-O-desmethyl-MPA, was detected in trace amounts in human plasma and HLM. Studies with recombinant enzymes confirmed a role for CYP3A4 and, to a lesser extent, CYP3A5 in the formation of this compound (Picard et al. 2004; Shipkova et al. 1999a).

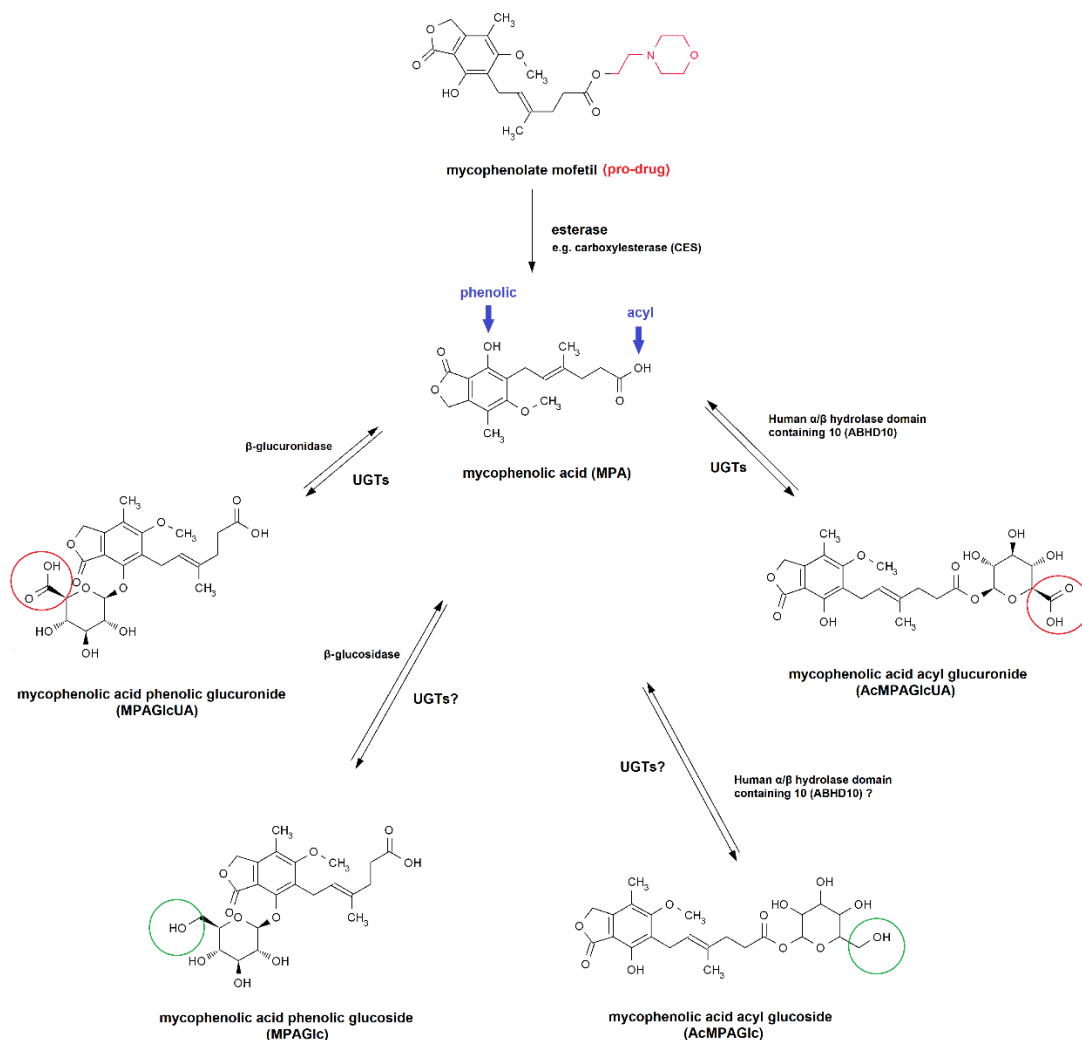


Figure 5. 2: Metabolism of the pro-drug mycophenolate mofetil (MMF) to mycophenolic acid (MPA), with phenolic hydroxyl and carboxyl functional groups labelled. MPA is metabolized to glucuronides and glucosides at both the phenolic and carboxylic acid functional groups before excretion into bile and urine.

In addition to hydrolysis by esterases and presumed glycosidation by UGT enzymes, another key feature of MPA pharmacokinetics is the ‘secondary’ peaks detected in the MPA plasma concentration-time profiles (4-12hr post-dose), which represent extensive (~40%, with a range of 10-60%) enterohepatic cycling (EHC) of MPAGlcUA followed by de-glucuronidation by enterobacteria and subsequent intestinal reabsorption of MPA (Bernard & Guillemette 2004; Bullingham, Nicholls & Kamm 1998; Picard et al. 2005; Shaw et al. 2003; Shaw & Nowak 1995; Sherwin et al. 2011a). The multidrug resistance protein 2 (MRP2) appears to mediate the biliary transport of MPAGlcUA. However, the *in vitro* evidence for AcMPAGlcUA transport is contradictory. One study suggested a role for MRP2 along with an unidentified transporter, whereas another study excluded MRP2 involvement (Patel, Ogasawara & Akhlaghi 2013; Westley et al. 2006). The impact of EHC on MPA pharmacokinetics is somewhat unpredictable, as it is influenced by host (i.e. co-medication, genetic variability, disease states) and external (i.e. diet, time of food intake) factors (Bullingham, Nicholls & Kamm 1998; Roberts et al. 2002; Sherwin et al. 2011a).

It is clear thus far that the metabolism of MPA is relatively complex, involving several pathways and enzymes. Transport and EHC further influence MPA exposure and pharmacokinetics. Significant within- (up to 10-fold) and between-subject pharmacokinetic variability has resulted in the need to optimize MPA therapy (de Winter et al. 2011; Kuypers et al. 2010; Shaw et al. 2007; Sherwin et al. 2011a; Staatz & Tett 2007; Tredger & Brown 2006). The optimal exposure target, indicated by the area under the plasma drug concentration-time curve (AUC_{0-12hr}), is 35-60 μ g.hr/mL which appears to maximize efficacy and minimize toxicity (Bennett 2003). The recommended target AUC_{0-12hr} for lupus nephritis is somewhat lower, 35-45 μ g.hr/mL (van Gelder, Berden & Berger 2015). Numerous factors are known to influence MPA

Chapter 5: Mycophenolic acid glucosidation

response (Kuypers et al. 2010; Sherwin et al. 2011a; Tredger & Brown 2006), most of which relate to pharmacokinetic variability (e.g. genetic polymorphism, altered renal and hepatic function, EHC, drug-drug interactions).

MPA metabolism by recombinant UGT enzymes

Early UGT activity screening studies indicated that the extrahepatic enzymes UGT 1A8 and 1A10 are able to form the phenolic and acyl glucuronides of MPA. Both UGT enzymes exhibited similar activities, which were approximately half of those observed with HLM as the enzyme source. Of the hepatic and renally expressed enzymes, only UGT1A9 catalyzed the phenolic glucuronidation of MPA, although activity was low (Mackenzie 2000; Mojarrabi & Mackenzie 1997). Other recombinant UGT enzymes (UGT 1A1, 1A3, 1A4, 1A6, 2B7, 2B10 and 2B11) expressed in COS-7 cells were reported not to glucuronidate MPA. In contrast, Shipkova et al. (2001) demonstrated MPAGlcUA formation by UGT 1A1, 1A3, 1A4, 1A6, 1A7, 1A9, 1A10, 2B4, 2B7 and 2B15 expressed in insect (Sf9) cells. K_m (115-276 μ M) and V_{max} (29-106pmol/min/mg protein) values spanned a relatively narrow range. AcMPAGlcUA was detected in all incubations, but only in trace amounts. Glucosidation of MPA by these recombinant enzymes was not investigated, even though both the glucosidation and glucuronidation of MPA by human liver (HLM), kidney (HKM) and intestinal (HIM) microsomes were characterized.

Building on these studies, Picard et al. (2005) investigated the UGTs involved in the formation of MPAGlcUA and AcMPAGlcUA using commercially sourced SupersomesTM expressing human UGTs. Again, only glucuronidation was investigated. At an MPA concentration of 0.1mM, the rank order of MPAGlcUA formation was UGT 1A9>1A7>1A8>1A10>1A1, with lesser contributions of UGT

1A6, 2B4 and 2B7. MPAGlcUA kinetics were characterized for several UGTs, but the K_m and V_{max} ranges were wider than reported by Shipkova et al. (2001), and differences in kinetic parameters between different UGT enzymes were larger. UGT1A9 catalyzed MPAGlcUA formation with K_m and V_{max} values of 160 μ M and 11,820pmol/min/mg, respectively. Bernard and Guillemette (2004) additionally reported that UGT 1A8 and 1A9 exhibited highest MPA phenolic glucuronidation activity, with minor contributions from UGT 1A1, 1A7 and 1A10. Overall, these data indicate that, of the hepatically expressed UGTs 1A9 is the main enzyme involved in MPAGlcUA formation.

By contrast, UGT2B7 was shown to be the predominant enzyme involved in the formation of the acyl glucuronide (AcMPAGlcUA) (Picard et al. 2005). Minor contributions of UGT 1A1 and 2B4 to AcMPAGlcUA formation were also demonstrated. The *in vitro* intrinsic clearances for AcMPAGlcUA formation by UGT2B7 and UGT1A1 were 1.08 and 0.08 μ L/mg/min, respectively. Consistent with the initial studies of Mackenzie and colleagues, Basu et al. (2004) reported the extrahepatic enzymes UGT 1A7, 1A8 and 1A10 glucuronidated MPA at both the acyl and phenolic positions. The rank order of the combined intrinsic clearances (i.e. CL_{int} for MPAGlcUA + CL_{int} for AcMPAGlcUA) was UGT 1A7>1A8>1A10. Comparison of data between studies is difficult when recombinant UGTs are used as the enzyme source, since expression of active UGT protein cannot be normalized, as is the case with cytochrome P450 (as spectral P450 content).

Pharmacogenetics of MPA metabolism

In vivo studies

Due to the variability in MPA elimination, a number of *in vivo* studies investigating the impact of UGT (1A1, 1A7, 1A8, 1A9 and 2B7) genetic polymorphism on MPA pharmacokinetics have been published (reviewed by Stingl et al. (2014)). Consistent with the dominant role of UGT1A9 in MPA glucuronidation, it was recommended that Caucasian heterozygous carriers of the UGT1A9*3 allele should receive ~70% of the average MPA dose, while carriers of the UGT1A9*1 *l,n,v,w* genotype may need higher than average doses. UGT1A9*1 *l,n,v,w* is a promoter variant (-275 T>A, -2152 C>T) functionally linked to increased (~two-fold) expression and activity with HLM as the enzyme source (using propofol and MPA as the substrates) (Girard et al. 2004). In comparison, HLM expressing UGT1A9*3 have been shown to have a similar level of protein expression to wild-type UGT1A9, but decreased glucuronidation activity (~50%) with the same aglycones (Girard et al. 2004), indicating that this polymorphism may be associated with decreased glucuronidation activity. Kuypers et al. (2005) reported that 3 out of 95 renal allograft recipients (3.1%) heterozygous for the UGT1A9*3 allele had significantly higher MPA exposure (AUC_{0-12hr}) compared to non-carriers (78.7 vs. 42.5mg.h/L for 1g/day dose MMF group; 73.82 vs. 57.13mg.h/L in 2g/day MMF dose group). Levesque et al. (2007) further found that healthy subjects carrying the UGT1A9*3 allele had significantly higher MPA and AcMPAGlcUA AUC_{0-12hr} values (by 30% and 85%, respectively, compared to wild-type) while the MPAGlcUA AUC_{0-12hr} value was not altered to a statistically significant extent. Urinary excretion of AcMPAGlcUA also increased significantly (~71%) over the 12hr period. Additionally, van Schaik et al. (2009) found that kidney

transplant patients with the UGT1A9*3 genotype had 49% and 54% higher MPA exposure measured as AUC_{0-12hr} .

In vitro studies

In vivo studies also strongly suggest that genetic polymorphism of the hepatically expressed enzyme UGT1A9 may contribute to the interindividual variability observed in MPA clearance in patients receiving this drug (Kuypers et al. 2005; Levesque et al. 2007). *In vitro* studies have largely focused on altered MPA phenolic glucuronidation by UGT1A9*3 (Met33Thr). A comprehensive study was conducted by Korprasertthaworn et al. (2012). The Met33Thr substitution resulted in statistically significant decreases in the *in vitro* intrinsic clearances for 4-MU, propofol, sulfinpyrazone, S-naproxen and retigabine glucuronidation, whereas the CL_{int} value for frusemide was increased. Although the Met33Thr substitution increased the K_m (3.8-fold) for MPAGlcUA formation, there was a compensatory increase in V_{max} (3.9-fold) such that CL_{int} was unchanged. The Met33Thr substitution additionally resulted in a change of kinetic mechanism from hyperbolic to weak substrate inhibition ($K_{si}=1,774\mu M$). As noted previously, Girard et al. (2004) reported decreased glucuronidation activity by HLM expressing the UGT1A9*3 allele with both propofol (~52%) and MPA (~55%) as substrates, while Bernard and Guillemette (2004) found a similar 40% decrease in the CL_{int} for MPAGlcUA formation by recombinant UGT1A9*3. As with Korprasertthaworn et al. (2012), Bernard and Guillemette (2004) showed that the Met33Thr substitution increased the K_m (2.5-fold) and V_{max} (1.4-fold) for MPAGlcUA formation but the increase in V_{max} was not compensatory (less than K_m). Therefore, the CL_{int} decreased.

Chapter 5: Mycophenolic acid glucosidation

Collectively, the *in vitro* and *in vivo* data (kinetic, reaction phenotyping and pharmacogenetic) indicate that UGT1A9 is primarily responsible for the phenolic glucuronidation of MPA in liver, while UGT2B7 is apparently the major enzyme involved in AcMPAGlcUA formation. However, the enzyme(s) responsible for MPA glucosidation are unknown.

5.1.2 Hypothesis

Similar to morphine glucosidation and glucuronidation, MPA glucosidation and glucuronidation occur as complementary metabolic pathways catalyzed by common enzymes (viz. UGT1A9, and possibly UGT2B7).

5.1.3 Experimental plan and aims

1. Develop an HPLC assay for the quantification of the glucuronide and glucoside conjugates of MPA formed by incubations of HLM and recombinant UGT enzymes.
2. Characterize the (aglycone and cofactor) kinetics for MPA glucosidation and glucuronidation by HLM in the presence of single and combined cofactors (UDP-Glc and UDP-GlcUA).
3. Characterize mutual competitive inhibition of the MPA glycosidation pathways with respect to the cofactors UDP-GlcUA and UDP-Glc, with MPA as the fixed substrate and HLM as the enzyme source.
4. Confirm the UGT enzyme(s) responsible for MPA glucuronidation and glucosidation (MPAGlcUA, MPAGlc, AcMPAGlcUA and AcMPAGlc formation) using a panel of recombinant human UGT enzymes.
5. Determine the effect of UGT enzyme-selective inhibitors on the formation of MPAGlcUA, MPAGlc, AcMPAGlcUA and AcMPAGlc with HLM as the enzyme source to complement Aim (4).

5.2 Methods

5.2.1 Mycophenolic acid glycosidation HPLC assay conditions

HPLC equipment

MPAGlcUA, MPAGlc, AcMPAGlcUA and AcMPAGlc formation were measured simultaneously by reversed-phase HPLC using an Agilent 1100 series instrument (Agilent Technologies, Sydney, Australia) comprising an auto-injector, a quaternary solvent delivery system and a UV detector (1200 series). Analytes were separated on a Nova-Pak C18 column (4 μ m particle size, 3.9 \times 150mm; Waters Corporation, Milford, MA, USA).

Chromatography conditions for the quantification of MPA glucoside and glucuronide formation using HPLC-UV

The mobile phase, delivered at a flow rate of 1mL/min, consisted of two solutions mixed according to a gradient timetable: phase A (100% HPLC grade acetonitrile) and phase B (10mM ammonium acetate and acetonitrile (10%) in distilled water, adjusted to pH 5.7 with glacial acetic acid). Initial conditions were 5% phase A - 95% phase B held constant for 1min followed by a linear gradient over 10min to 60% phase A - 40% phase B, returning to initial conditions over 3min (see Figure 5.5 in Results). The optimal absorbance wavelength (250nm) for the MPA conjugates was confirmed by spectrophotometry (Section 5.3.1). The retention times for MPAGlcUA, MPAGlc, AcMPAGlcUA, MPA and AcMPAGlc were 2.3, 4.5, 5.6, 6.7 and 7.4min, respectively (Figure 5.6).

Quantification of the formation of MPA glycosides

The identity of individual peaks was confirmed by co-chromatography with authentic standards (Table 2.1). Quantification of MPAGlcUA, MPAGlc, AcMPAGlcUA and

AcMPAGlc was achieved by reference to standard curves generated using authentic standards of each of the four analytes over the concentration range 2.5 – 25 μ M.

5.2.2 MPA glycosidation assay

(iii) Human liver microsomes (HLM) as the enzyme source

Incubations, in a total volume of 200 μ L, contained phosphate buffer (0.1M, pH 6.8), MgCl₂ (4mM), alamethicin-activated HLM (0.04mg), MPA, and UDP-GlcUA and/or UDP-Glc (5mM). After a 5min pre-incubation at 37°C in a shaking water bath, reactions were initiated by the addition of cofactor (UDP-Glc and/or UDP-GlcUA) and performed for 15min. Reactions were terminated by the addition of perchloric acid (11.6M; 2 μ L) and cooling on ice. Samples were centrifuged (5000g for 10min), and a 20 μ L aliquot of the supernatant fraction was analyzed by HPLC. Control incubations, which excluded cofactor, were performed to confirm the absence of interfering peaks in the HPLC chromatograms. Under these conditions, rates of MPAGlcUA, MPAGlc, AcMPAGlcUA and AcMPAGlc formation were linear with respect to protein concentration and incubation time ($r^2 \geq 0.93$; Section 5.3.1).

(iv) Recombinant human UGTs as the enzyme source

Recombinant UGTs were prepared as described in Section 2.2.3. Incubations with recombinant UGTs expressed in HEK293T cells in kinetic experiments were as described for HLM, except for protein concentration (0.03mg of HEK293T cell lysate), incubation time (20min) and omission of alamethicin. Due to the expression of native glucosyltransferase(s) in Control SupersomesTM (c-SUP) (Chapter 3), recombinant UGTs expressed in High FiveTM cells were not used for screening experiments in this Chapter but were investigated further in Chapter 6.

5.2.3 MPA glycosidation kinetics with combined cofactors (UDP-Glc and UDP-GlcUA) and HLM as the enzyme source

As with MPA kinetic experiments in the presence of a single cofactor (UDP-Glc or UDP-GlcUA; Figure 5.8 and Table 5.2), MPA kinetics in the presence of combined cofactors (UDP-Glc and UDP-GlcUA) in a 1:1 ratio (5mM each) were performed with MPA concentrations ranging from 25-800 μ M.

5.2.4 Cofactor kinetics at a fixed MPA concentration with HLM as the enzyme source

UDP-Glc and UDP-GlcUA kinetics were characterized separately at a saturating MPA concentration (1mM), which is approximately 5- to 7- times the K_m values (121-214 μ M) observed for MPAGlcUA, MPAGlc, and AcMPAGlcUA formation with MPA as the variable substrate (Table 5.3). Kinetic experiments were performed in triplicate, using 1-20mM and 0.1-2.5mM of UDP-Glc and UDP-GlcUA, respectively.

5.2.5 Cofactor inhibition kinetics

Inhibition of phenolic MPA glucoside (MPAGlc) formation by UDP-GlcUA (five concentrations in the range 400 – 1600 μ M) at each of three UDP-Glc concentrations (800, 1600 and 2500 μ M) was investigated at a fixed, saturating MPA concentration (1mM). Additionally, inhibition of MPAGlcUA and AcMPAGlcUA formation by UDP-Glc (five concentrations in the range 800 – 2500 μ M) was investigated at each of three UDP-GlcUA concentrations (400, 800 and 1600 μ M) at an MPA concentration of 1mM.

5.2.6 MPA glycosidation by recombinant UGT enzymes

Recombinant UGT 1A1, 1A3, 1A4, 1A6, 1A7, 1A8, 1A9, 1A10, 2B4, 2B7, 2B15 and 2B17 (expressed in HEK293T cells) were used in activity screening experiments to identify enzymes with the capacity to catalyze MPA glucuronidation and glucosidation. The activity screening experiments were conducted at three MPA concentrations (100, 500 and 1500 μ M) for 120min at an HEK293T protein lysate concentration of 1mg/mL and in the presence of a single cofactor.

5.2.7 Inhibition of human liver microsomal MPA glycoside formation by UGT enzyme selective substrates/inhibitors

The effect of UGT enzyme selective inhibitors and/or substrates on MPAGlcUA, MPAGlc, AcMPAGlcUA and AcMPAGlc formation with HLM as the enzyme source was investigated to confirm the involvement of specific hepatic UGTs involved in the formation of MPAGlc and AcMPAGlc. Compounds screened for inhibition included niflumic acid (NFA), hecogenin, and fluconazole. Concentrations of each inhibitor, with the enzyme(s) inhibited in parenthesis, were: NFA, 2.5 μ M (UGT1A9); NFA, 100 μ M (UGT 1A1 and 2B15); hecogenin, 10 μ M (UGT1A4); and fluconazole, 2.5mM (UGT 2B7 and 2B4) (Miners et al. 2011; Miners, Mackenzie & Knights 2010; Raungrut et al. 2010; Uchaipichat et al. 2006a; Uchaipichat et al. 2006b). The MPA concentration used in the inhibition studies was 100 μ M, which is close to the K_m values for MPAGlcUA (121 μ M), MPAGlc (155 μ M) and AcMPAGlcUA (154 μ M) formation (Table 5.2). These experiments were performed in the presence of a single cofactor.

5.3 Results

5.3.1 Development of an HPLC assay for the characterization of MPA glycosidation

The first aim of this Chapter was to develop and validate an HPLC assay for the simultaneous detection and quantification of MPA and its glucuronide and glucoside conjugates. Previous published assays for measuring MPA glucuronidation and glucosidation *in vitro* and *in vivo* were based on HPLC-UV and LC-MS/MS procedures (Bernard et al. 2006; Dostalek et al. 2011; Levesque et al. 2007; Picard et al. 2005; Shipkova et al. 2001). However, the HPLC-UV methods were not developed to simultaneously detect both the glucuronide and glucoside conjugates. MPA glucosides were measured by LC-MS/MS due to the lack of commercially available MPA (acyl and phenolic) glucoside standards at the time.

The assay used for the simultaneous measurement of MPA glycosides was a modification of an HPLC-UV procedure based on a triethylamine (TEA)-containing mobile phase developed previously in this laboratory to detect MPAGlcUA and MPA (Korprasertthaworn et al. 2012). While the TEA mobile phase, acidified with perchloric acid (pH 2.5), enables the facile separation of MPAGlcUA and MPA, it is not suitable for the more complicated separation and detection of multiple glycosides with varying chemistries. Comparison of the major charge species as a function of pH (Figures 5.3a and 5.3b) suggests the optimal pH range for simultaneously detecting each conjugate is 4.8-6.0, as this spans the maximal distribution of a single charged species for each of the four MPA glycosides and MPA itself. The solvent environment should promote the presence of one species of a compound, if possible, for resolution of analytes. Ammonium acetate buffer has a pH range of 3.8-5.8, which largely

Chapter 5: Mycophenolic acid glucosidation

encompasses the desired pH range of 4.8-6.0. Hence, this study employed ammonium acetate buffer (10mM), pH 5.7 for assay development. MPAGlcUA, MPAGlc, AcMPAGlcUA, MPA and AcMPAGlc have charges of -2, -1, -1, -1 and 0, respectively, at this pH (Figure 5.3 and 5.4).

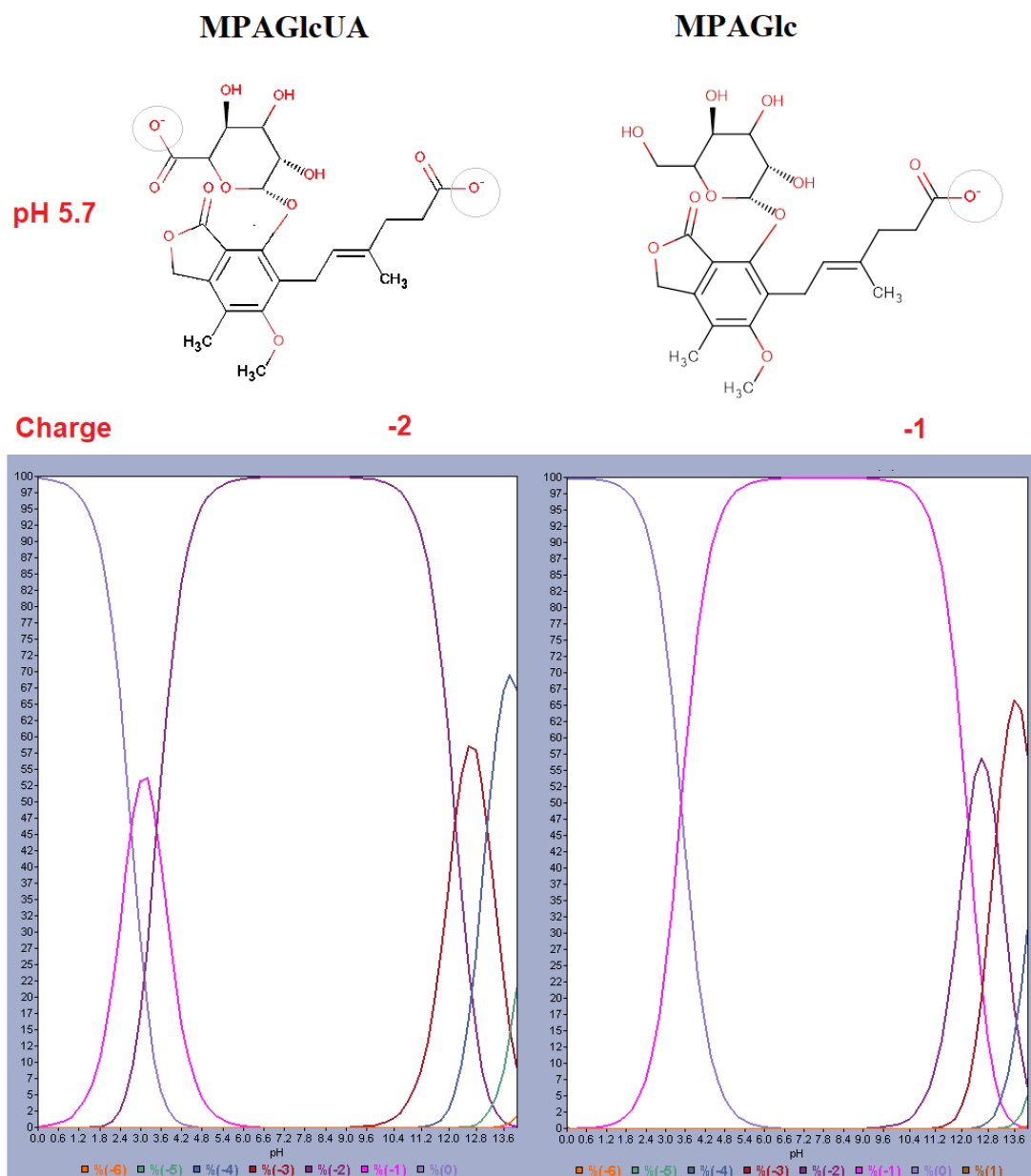


Figure 5. 3: Major charge species (-2 and -1) for MPAGlcUA and MPAGlc at pH 5.7. The distribution of different species for MPAGlcUA and MPAGlc across the pH range (0-14) is shown directly below.

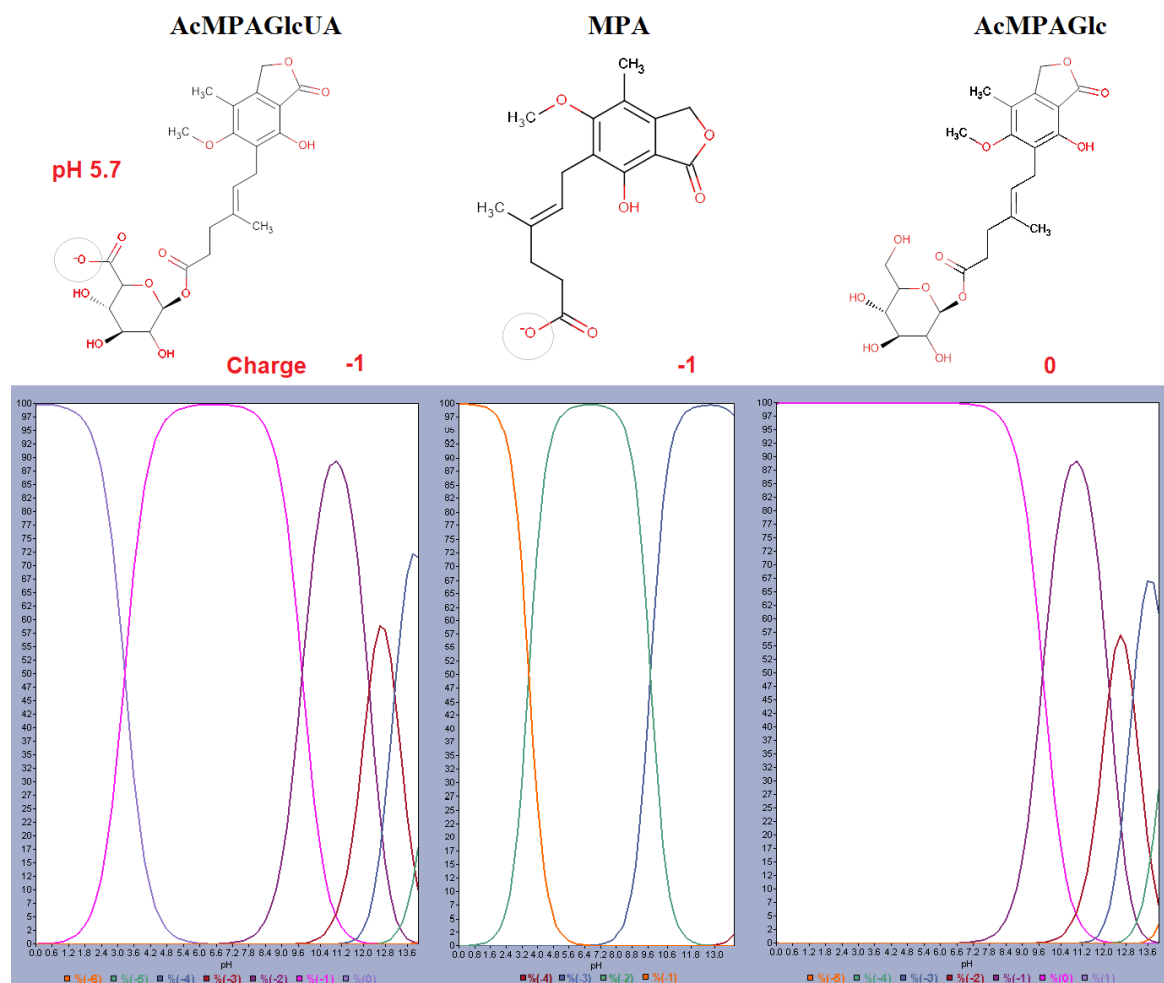


Figure 5. 4: Major charge species (-1, -1, and 0) for AcMPAGlcUA, MPA and AcMPAGlc at pH 5.7. The distribution of different species for AcMPAGlcUA, MPA and AcMPAGlc across the pH range (0-14) is shown directly below.

Ultraviolet (UV) spectra of MPA and glycosides

The absorbance wavelengths for UV detection were optimized for MPA, MPAGlcUA, MPAGlc, AcMPAGlcUA and AcMPAGlc. The UV-visible spectrum of MPA (from 200-450nm) exhibited absorption maxima at 213, 250, and 304nm (Figure 5.5B), while a solution of mobile phase and methanol (1% v/v) exhibited no peaks in this region (Figure 5.5A). The spectra for the MPA glycosides were the same as that of MPA (data not shown). A wavelength of 250nm was subsequently selected for analyte detection as background ‘noise’ was high at 213nm and absorbance was lower at 304nm.

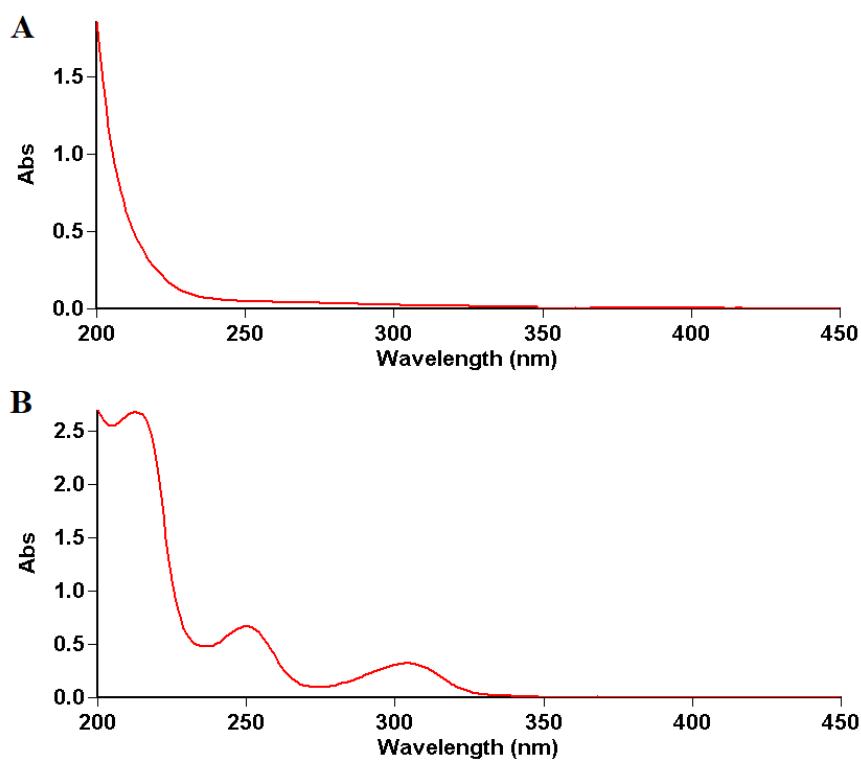


Figure 5. 5: UV absorption spectra: (A) 10mM ammonium acetate, 10% acetonitrile, pH 5.7 containing/ 1% methanol; and : (B) a 1% solution of MPA (50 μ M in methanol) in mobile phase (A).

Mobile phase gradient composition for separation of MPA glycosides

The reversed-phase HPLC assay developed was capable of simultaneously identifying and separating MPA and the four conjugates. Figure 5.6 gives the stepwise mixing of the two phases; phase A (100% HPLC grade acetonitrile) and phase B (10mM ammonium acetate, acetonitrile (10%) and glacial acetic acid in distilled water, adjusted to pH 5.7). An analysis time of 14min was required to achieve adequate separation of the MPA conjugates.

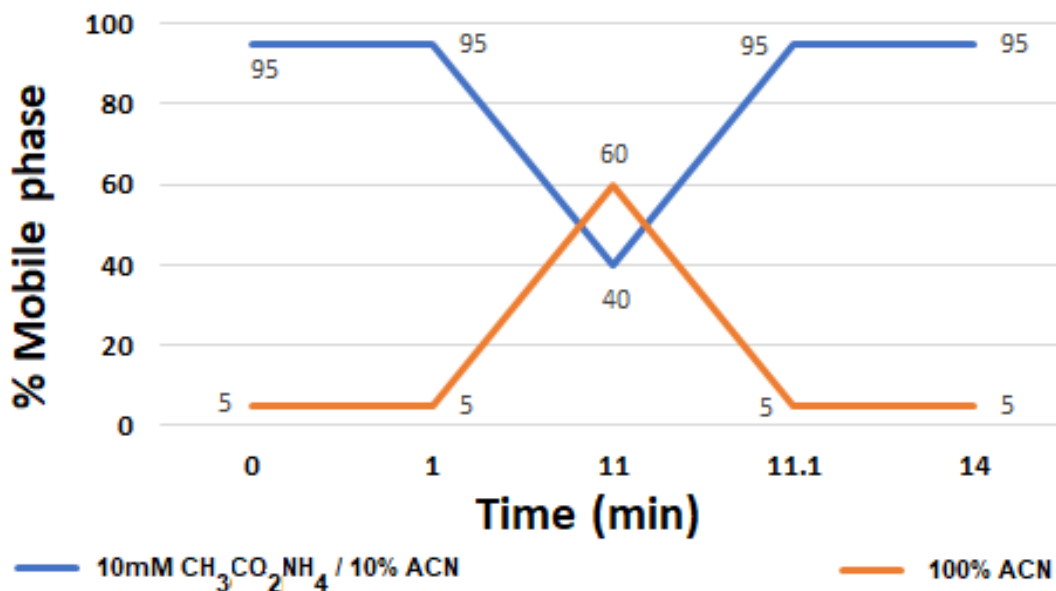


Figure 5. 6: HPLC mobile phase gradient composition for the separation of MPA glycosides

Identification of the peaks for MPA, MPAGlcUA, MPAGlc, AcMPAGlcUA and AcMPAGlc in chromatograms

As recommended by the commercial provider, AcMPAGlc was dissolved in methanol, a polar protic solvent, rather than water to avoid hydrolysis of this acyl glycoside. However, the AcMPAGlc provided by Toronto Research Chemicals (TRC) was not pure. Two peaks with respective retention times of 6.8min (parent MPA) and 7.4min were observed (Figure 5.7A). LC-MS identified the latter peak as AcMPAGlc (data not shown). By contrast, AcMPAGlcUA dissolved in methanol was relatively stable. The purity of AcMPAGlcUA was estimated as 98%. Both the phenolic MPAGlcUA and MPAGlc were stable when dissolved in water (i.e. no peak corresponding to parent MPA was observed).

The commercial availability of MPAGlcUA, MPAGlc, AcMPAGlcUA and AcMPAGlc permitted confirmation of the identity of these conjugates in chromatograms (Figure 5.7). Five well-resolved peaks corresponding to MPAGlcUA, MPAGlc, AcMPAGlcUA, MPA and AcMPAGlc were observed with retention times of 2.3, 4.5, 5.6, 6.8 and 7.4min, respectively (Figure 5.7A). Incubations of MPA and UDP-Glc with pooled HLM as the enzyme source showed peaks corresponding to MPAGlc and AcMPAGlc (Figure 5.7B). Although the peak corresponding to AcMPAGlc was considerably smaller than that of MPAGlc, the acyl glucoside was nevertheless detectable (2.1 peak area units). Incubations (200 μ L) were terminated by the addition of 2 μ L of perchloric acid (11.6M). Termination of reactions with glacial acetic acid (4%) in methanol (200 μ L) distorted the shape of the MPAGlcUA peak (data not shown).

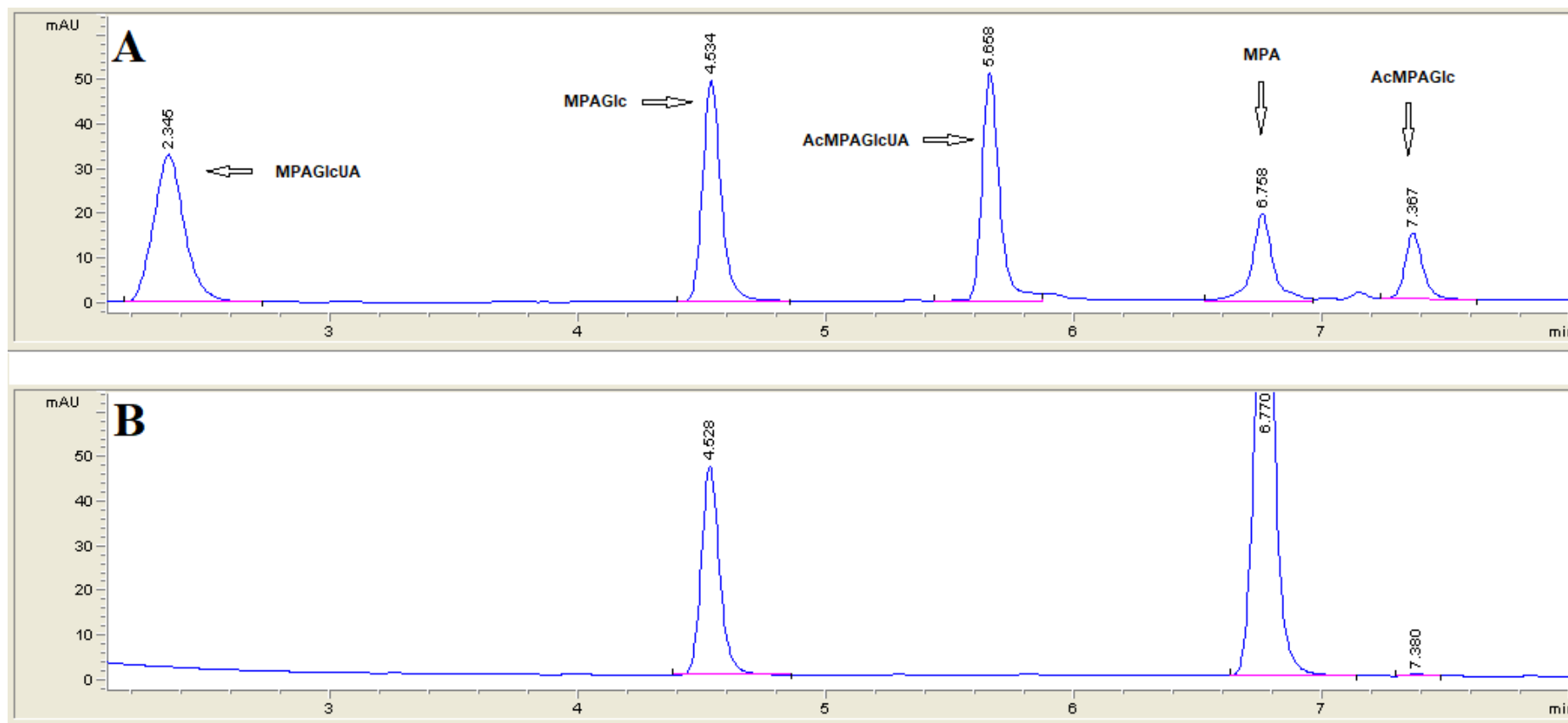


Figure 5. 7: Representative chromatograms of MPA glycoside calibration standards (25 μ M) (Panel A) and incubations of HLM with MPA (100 μ M) and 5mM UDP-Glc (Panel B). MPAGlcUA eluted at 2.3min, MPAGlc at 4.5min, AcMPAGlcUA at 5.6min, MPA at 6.8min and AcMPAGlc at 7.4min. The total run time was 14min.

Calibration curve linearity and between-day reproducibility

Calibration curves for MPAGlcUA, MPAGlc, AcMPAGlcUA, and AcMPAGlc were linear over the concentration range 0-25 μM (Figure 5.8A-C). Coefficients of determination (r^2) for 10 calibration curves for each of the MPA glycosides were >0.99 (Table 5.1). The coefficients of variation for 10 slopes of MPAGlcUA, MPAGlc, and AcMPAGlcUA standard curves were 2.39%, 3.31%, and 5.98% respectively, indicating acceptable between day variability. It should be noted that the calibration curve slope for MPAGlcUA, MPAGlc, and AcMPAGlcUA were essentially identical but different to that for AcMPAGlc due to issues with the purity of the AcMPAGlc authentic standard. Given the lack of purity of the AcMPAGlc standard, this metabolite was quantified using the standard curve for AcMPAGlcUA.

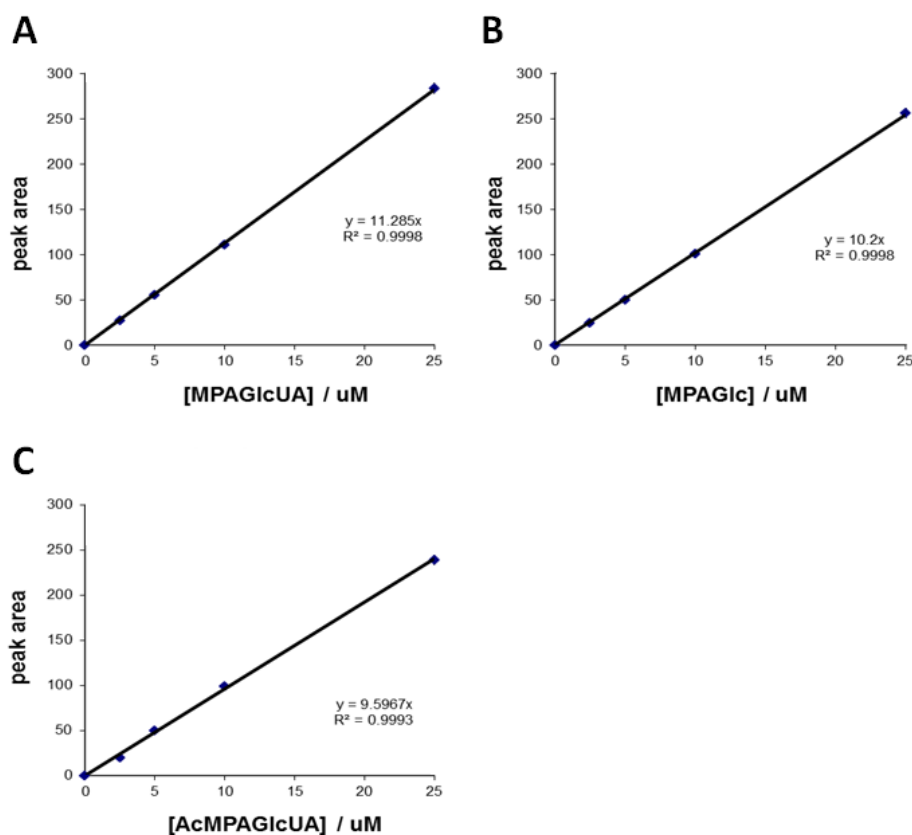


Figure 5. 8: Representative calibration curves for MPAGlcUA (A), MPAGlc (B) and AcMPAGlcUA (C), respectively.

Table 5. 1: Slopes and coefficients of determination (r^2) for MPAGlcUA, MPAGlc and AcMPAGlcUA measured on ten separate days.

Day	MPAGlcUA		MPAGlc		AcMPAGlcUA	
	Slope	r^2	Slope	r^2	Slope	r^2
1	10.89	1.00	9.36	1.00	10.46	1.00
2	10.78	1.00	9.43	1.00	10.50	1.00
3	11.33	1.00	9.97	1.00	9.87	1.00
4	11.70	0.99	10.22	1.00	9.43	1.00
5	11.29	1.00	10.20	1.00	9.18	1.00
6	11.43	1.00	10.22	1.00	8.64	1.00
7	11.39	1.00	10.21	1.00	9.66	1.00
8	11.20	1.00	10.20	1.00	9.34	1.00
9	11.06	1.00	10.10	1.00	9.56	1.00
10	11.28	1.00	10.10	1.00	10.12	0.99
Mean	11.23	1.00	10.00	1.00	9.68	1.00
SD	0.27	0.00	0.33	0.00	0.58	0.00
CV (%)	2.39	0.02	3.31	0.02	5.98	0.25

Limits of sensitivity

The lower limit of quantification for MPA conjugates using the HPLC-UV assay was arbitrarily defined as 0.5 peak area units for each analyte. Peak areas below 0.5 area units were difficult to measure reproducibly. On this basis, the limits of detection for MPAGlcUA, MPAGlc, AcMPAGlcUA, AcMPAGlc and parent MPA were between 0.04-0.05 μ M.

Linearity of product formation

Linearity of MPAGlcUA, MPAGlc, AcMPAGlcUA, and AcMPAGlc formation with respect to incubation time and enzyme protein concentration was characterized with pooled HLM as the enzyme source. Final incubation conditions (Section 5.2.2) were selected based on a balance between the sensitivity of HPLC quantification at each

Chapter 5: Mycophenolic acid glucosidation

incubation time and protein concentration within the linear range, while maintaining less than 10% utilization of substrate (% conversion). This latter condition is required to ensure that the actual concentration of the substrate present throughout the course of the incubation remains close to the added concentration.

Plots of MPA glycoside peak area vs protein concentration to 1mg/mL and incubation time to 60min were linear for all metabolites, with r^2 values ranging from 0.933 - 0.999. Using a 30min incubation time, MPAGlcUA, MPAGlc, AcMPAGlcUA, and AcMPAGlc formation was linear across the HLM protein concentration range 0.2-1.0mg/mL, at low (0.1mM) and high (1.0mM) MPA concentrations. A protein concentration of 0.2mg/mL was subsequently used to characterize linearity of MPAGlcUA, MPAGlc, AcMPAGlcUA, and AcMPAGlc formation with respect to time at low (0.1mM) and high (1.0mM) MPA concentration. Highest substrate utilization occurred with MPAGlcUA formation but was less than 10% for incubation times to 15min.

Stability of MPA conjugates in incubation samples

In a previous study, AcMPAGlcUA in human plasma was found to undergo hydrolysis at room temperature after 24hr (~40%), or after 30 days at 4 °C or -20 °C (~60% or ~20%, respectively) (Shipkova et al. 2000). Acidified samples with phosphoric acid (pH 2.5) were stable up to 30 days at -20 °C. Due to the unstable nature of acyl glycosides, potassium phosphate buffer at a pH lower than 7.0 (viz. 6.8) was used in all incubations and calibration samples employed in this work to reduce the hydrolysis of AcMPAGlcUA and AcMPAGlc (Miners et al. 1997; Shipkova et al. 2001). Initial experiments confirmed the stability of conjugates formed by incubations of MPA (100, 250, 1000 μ M) and UDP-GlcUA and UDP-Glc (5mM each) with HLM

Chapter 5: Mycophenolic acid glucosidation

as the enzyme source by analyzing conjugates immediately after termination of the reaction, and then 24hr later. MPAGlcUA and MPAGlc peak areas varied between 0.06-0.6% and 0.0-1.5%, respectively, while AcMPAGlcUA, and AcMPAGlc peak areas varied between 4.0-8.3% and 0.0-6.0%, respectively. Similarly, calibration samples were analyzed twice over 2 days; MPAGlcUA, MPAGlc, AcMPAGlcUA, and AcMPAGlc peak areas varied between 0.18-1.9%, 0.6-3.7%, 0.47-4.3% and 1.0-3.0%, respectively. Overall, the results demonstrate that MPAGlcUA, MPAGlc, AcMPAGlcUA, and AcMPAGlc are stable (<10% hydrolysis) over 2 days in incubation and calibration samples. It should be noted, however, that samples were invariably analyzed within 24hr of incubations performed during the course of studies described in this chapter.

5.3.2 Characterization of the kinetics of human liver microsomal MPA glycosidation

MPA glycosidation kinetics in the presence of single and combined cofactors (UDP-Glc and/or UDP-GlcUA)

The kinetics of MPA glycosidation *in vitro* in the presence of single and combined cofactors was investigated as for morphine (Section 3.3.9), but in the absence of BSA. (MPA binding to albumin is very high, resulting in a low unbound fraction in incubations supplemented with BSA. This precludes the addition of BSA to incubations). Michaelis-Menten (hyperbolic) or substrate inhibition kinetics were observed for MPAGlcUA, MPAGlc and AcMPAGlcUA formation by HLM prepared from 4 livers (H10, H12, H13 and H40) in the presence of the individual cofactors (Figure 5.9A-C). MPAGlcUA was the major glycoside formed by HLM followed by AcMPAGlcUA, and MPAGlc. Given the low rate of formation of AcMPAGlc, kinetic parameters for this pathway could not be determined accurately. Rates of formation of the MPA glycosides varied between the four livers, with consistently high activity observed with H12, intermediate activity with H13 and H40, and low activity with H10. Indeed, MPAGlc formation by microsomes from H10 could not be accurately measured in the combined cofactor experiments (Figure 5.9D-F). (Tables in Appendix 2 provide kinetic data for each set of HLM and MPA glycoside in the presence of single and combined cofactors).

In the single cofactor experiments, MPAGlc formation exhibited Michaelis-Menten kinetics with H40 and H12, and weak substrate inhibition kinetics with H13 and H10 ($K_{si} = 452$ and $1,046\mu\text{M}$, respectively). Mean K_m values for each glycoside were similar ($121 - 155\mu\text{M}$; Table 5.2). By contrast, the mean V_{max} values for MPAGlcUA

(5614pmol/min/mg protein) was 4.3- and 7.0-fold higher than the respective values for AcMPAGlcUA and MPAGlc formation. As expected, there was a similar rank order for CL_{int} ; the MPAGlc: AcMPAGlcUA: MPAGlcUA ratio was 1: 1.4: 7.8. Between liver (HLM) variability for each parameter/ pathway combination generally differed less than 2- to 3-fold (Tables 1-3, Appendix 2).

No significant differences were observed in the K_m and V_{max} values for MPA glucuronidation (phenolic and acyl) between the single and combined cofactor (1:1) experiments (Table 5.2). The CL_{int} for MPAGlcUA formation was similarly unchanged compared to the value obtained with UDP-GlcUA alone, although the difference in this parameter for the acyl glucuronidation pathway was statistically significantly different between the single and combined cofactor experiments. In contrast to the glucuronidation pathways, all three kinetic parameters for MPA phenolic glucosidation differed significantly between the single and combined cofactor studies. The use of combined cofactors resulted in an increase in the K_m and decreases in V_{max} and CL_{int} for MPAGlc formation (Table 5.2). The CL_{int} for this pathway was approximately one tenth of the value obtained using UDP-Glc as the sole cofactor, due largely to an approximate 80% reduction in V_{max} . As indicated previously, MPAGlc formation in the presence of combined cofactors was unable to be quantified with microsomes from H10. Hence, the mean kinetic parameters for MPA glucosidation represent data from three livers (H12, H13 and H40).

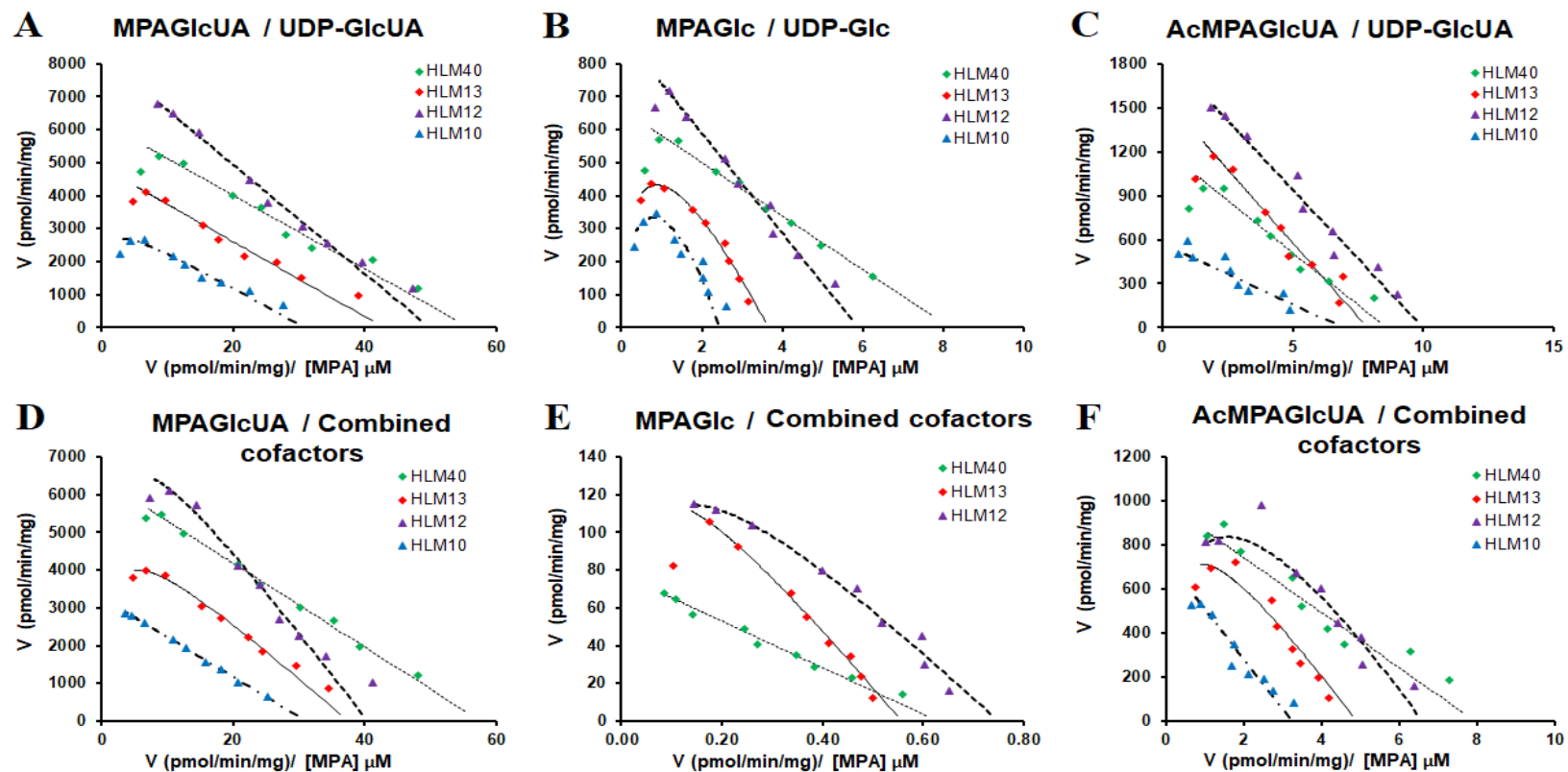


Figure 5. 9: Eadie-Hofstee plots for MPAGlcUA (A and D), MPAGlc (B and E), and AcMPAGlcUA (C and F) formation by microsomes from 4 livers in the presence of UDPGlcUA or UDPGlc separately (5mM each), and combined (1:1), respectively.

Points are experimentally determined values (mean of duplicate experiments). Lines are from fitting with the Michaelis-Menten or substrate inhibition equations.

Table 5. 2: Derived mycophenolic acid (MPA) glycosidation kinetic constants generated using human liver microsomes as the enzyme source.

MPA was used as the variable substrate in the presence of either single or combined cofactors (1:1) (UDP-Glc and UDP-GlcUA; 5mM each). Kinetic constants for MPAGlcUA and AcMPAGlcUA formation were determined for HLM from 4 separate livers in duplicate (i.e. total of 8 estimations), whereas kinetic constants for MPAGlc formation were determined for HLM from 3 separate livers in duplicate (i.e. total of 6 estimations). Data are shown as the mean \pm SD.

Glycoside	Cofactor	Kinetic equation	K_m	V_{max}	CL_{int}
			(μ M)	(pmol/min/mg)	(μ l/min/mg)
MPAGlc [#]	UDP-Glc	MM	155 \pm 72	798 \pm 117	5.82 \pm 2.1
	1:1	MM	236 \pm 75**	144 \pm 58**	0.60 \pm 0.13
MPAGlcUA	UDP-GlcUA	MM	121 \pm 31	5614 \pm 2167	45.5 \pm 9.8
	1:1	MM	148 \pm 55	6110 \pm 2394	41.6 \pm 11.3
AcMPAGlcUA	UDP-GlcUA	MM	154 \pm 54	1316 \pm 564	8.35 \pm 1.3
	1:1	MM	206 \pm 55	1110 \pm 362	5.66 \pm 2.0*

[#]Average of 3 livers (H12, H13, H40); MPAGlc formation by microsomes from H10 was not measurable in the combined cofactor experiments.

Michaelis-Menten kinetics (MM), Substrate Inhibition kinetics (SI); * $p \leq 0.05$ (compared to single cofactor); ** $p \leq 0.01$; *** $p \leq 0.001$

Cofactor (UDP-Glc and UDP-GlcUA) kinetics using pooled human liver microsomes and MPA as the fixed substrate

UDP-Glc and UDP-GlcUA kinetics were characterized with MPA (1mM) as the fixed substrate and pooled HLM as the enzyme source (Figure 5.10). UDP-Glc kinetics were measured with respect to MPAGlc formation, and UDP-GlcUA kinetics with respect to both MPAGlcUA and AcMPAGlcUA formation. All three reactions exhibited negative co-operative kinetics. The mean (\pm SD) S_{50} for UDP-Glc with respect to MPAGlc formation ($13.11 \pm 2.63\text{mM}$) was significantly ($p \leq 0.001$) higher (5.5- and 18.7-fold, respectively) than the mean S_{50} values for UDP-GlcUA measured with respect to AcMPAGlcUA ($2.40 \pm 1.69\text{mM}$) and MPAGlcUA ($0.70 \pm 0.21\text{mM}$) formation (Table 5.3). UDP-GlcUA kinetics, measured with respect to MPAGlcUA formation, exhibited the highest V_{\max} , which was approximately 4.5-fold higher ($p \leq 0.001$) than the respective values obtained from MPAGlc and AcMPAGlcUA formation (Table 5.3). Hence, CL_{int} was also significantly greater for MPAGlcUA formation (with UDP-GlcUA as cofactor; $p \leq 0.001$) than for MPAGlc and AcMPAGlcUA formation (with UDP-Glc and UDP-GlcUA as the respective cofactors). It should be noted that CL_{int} was calculated as V_{\max}/S_{50} (Section 1.3). Although not strictly valid, n is close to 1 (range 0.85 to 0.92) and, therefore, V_{\max}/S_{50} approximates CL_{int} . The ratio of the CL_{int} values (MPAGlc: AcMPAGlcUA: MPAGlcUA) was 1: 5.1: 77.5.

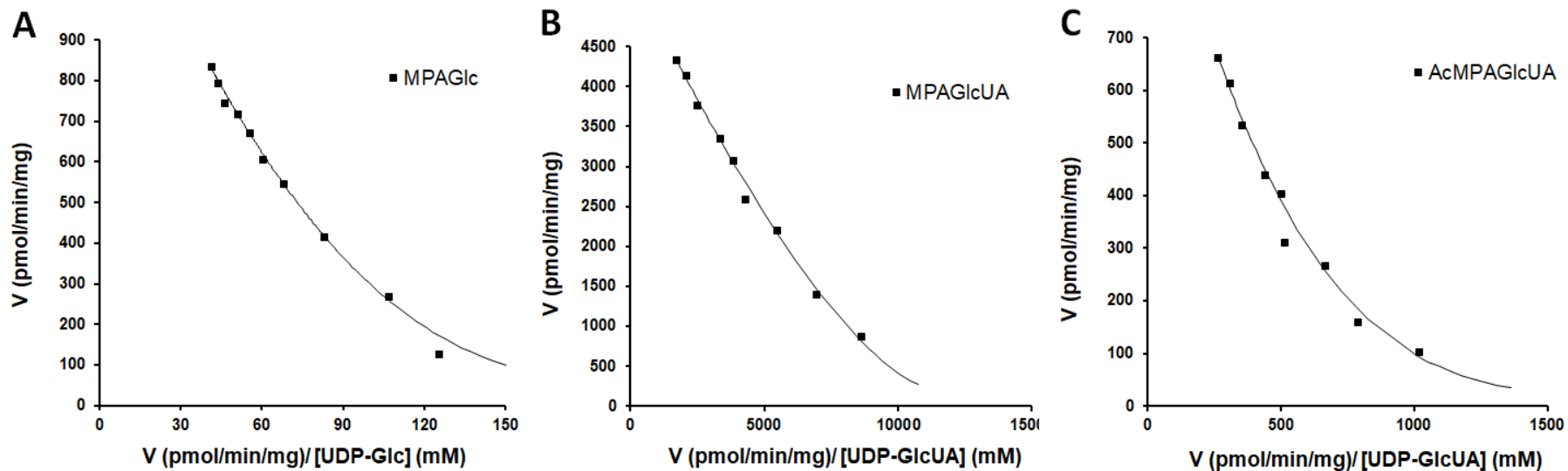


Figure 5. 10: Eadie-Hofstee plots for MPA glycosidation by pooled HLM at a fixed MPA concentration (1mM) with UDP-Glc and UDP-GlcUA as the variable substrates.

MPAGlc formation with UDP-Glc as cofactor (Panel A), MPAGlcUA formation with UDP-GlcUA as cofactor (Panel B) and AcMPAGlcUA formation with UDP-GlcUA as cofactor (Panel C). Points represent mean values of triplicate measurements (n=3). Curves are from fitting with the Hill equation.

Table 5. 3: Derived cofactor kinetic constants for MPA glycosidation generated with cofactor (UDP-Glc or UDP-GlcUA) as the variable substrate.

Data are shown as the mean of triplicate experiments (\pm SD) with pooled HLM.

Cofactor (pathway)	S_{50}	V_{max}	CL_{int}	n
	(mM)	(pmol/min/mg)	(μ l/min/mg)	
UDP-Glc (MPAGlc)	13.11 \pm 2.63	1377 \pm 69	0.11 \pm 0.02	0.89 \pm 0.06
UDP-GlcUA (MPAGlcUA)	0.70 \pm 0.21 ^c	5699 \pm 602 ^c	8.48 \pm 1.66 ^c	0.92 \pm 0.10
UDP-GlcUA (AcMPAGlcUA)	2.40 \pm 1.69 ^c	1276 \pm 450	0.69 \pm 0.35	0.85 \pm 0.14

compared to UDP-Glc (Oneway ANOVA with Bonferroni Post-Hoc Multiple Comparisons):

^a $p \leq 0.05$;

^b $p \leq 0.01$;

^c $p \leq 0.001$;

5.3.3 Cofactor inhibition kinetics

To assess the relative affinities of each cofactor, inhibition kinetics with each cofactor as the co-substrate and the other as the inhibitor were performed at a fixed MPA concentration. As before, low formation of AcMPAGlc resulted in unreliable quantification and hence only the major glycosides of MPA (MPAGlcUA, MPAGlc and AcMPAGlcUA) were measured and analyzed in this study.

Dixon plots for the inhibition of MPAGlc formation by UDP-GlcUA and inhibition of MPAGlcUA and AcMPAGlcUA formation by UDP-Glc at a fixed, saturating MPA concentration (1mM) are shown in Figure 5.11 and derived kinetic data in Table 5.4. UDP-GlcUA competitively inhibited MPAGlc formation with a mean K_i of $353 \pm 55\mu\text{M}$ (mean \pm SD) (Figure 5.11A). Likewise, UDP-Glc was a competitive inhibitor of both MPAGlcUA and AcMPAGlcUA formation. K_i values with respect to MPAGlcUA and AcMPAGlcUA were $25,382 \pm 7,694\mu\text{M}$ (Figure 5.11B) and $5,274 \pm 887\mu\text{M}$ (Figure 5.11C), respectively.

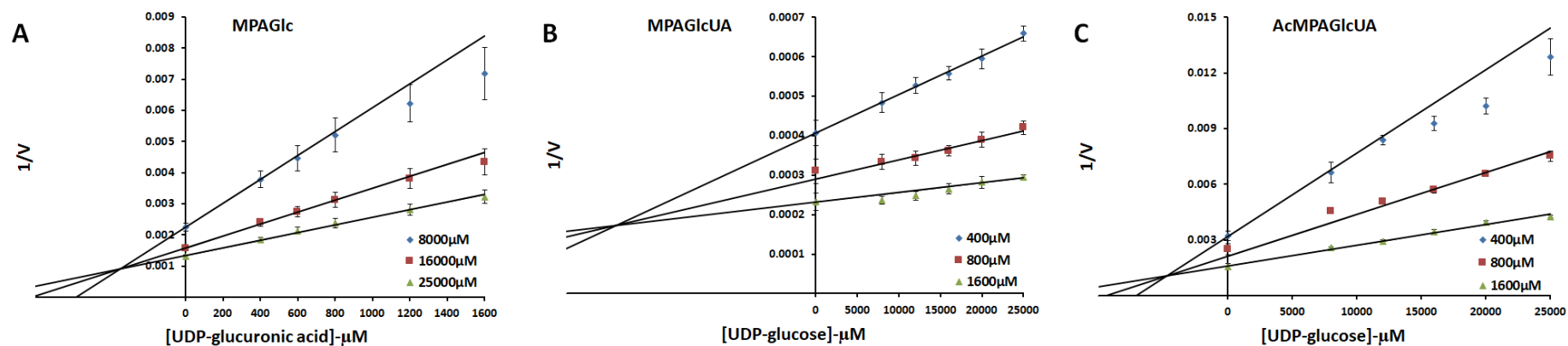


Figure 5. 11: Dixon plots for the inhibition of MPAGlcUA, MPAGlc and AcMPAGlcUA formation by UDP-Glc and UDP-GlcUA at a fixed MPA concentration (1mM) with HLM as the enzyme source.

Panel A: Inhibition of MPAGlc formation by UDP-GlcUA at three (0.8mM (◆), 1.6mM (■), and 2.5mM (▲)) UDP-Glc concentrations. Panel B: Inhibition of MPAGlcUA formation by UDP-Glc at three (0.4mM (◆), 0.8mM (■), and 1.6mM (▲)) UDP-GlcUA concentrations. Panel C: Inhibition of AcMPAGlcUA formation by UDP-Glc at three (0.4mM (◆), 0.8mM (■), and 1.6mM (▲)) UDP-GlcUA concentrations. Points are experimentally determined values (mean of quadruplicate experiments).

Table 5. 4: Derived cofactor inhibitor constants for inhibition of MPAGlcUA, AcMPAGlcUA and MPAGlc formation by UDP-GlcUA and UDP-Glc at a fixed MPA concentration (1mM).

Inhibitor	UDP-Glc		UDP-GlcUA
Glycoside	MPAGlcUA	AcMPAGlcUA	MPAGlc
K_i (μM) \pm SD	25,382 \pm 7,694	5,274 \pm 887	353 \pm 55

K_i : inhibitor constant

5.3.4 Reaction phenotyping of MPA glycosidation

MPA glycosidation by recombinant UGT enzymes expressed in HEK293T cells

Recombinant UGTs were screened for MPA glucuronidation and glucosidation activity at three MPA concentrations (100, 500 and 1500 μ M). Of the hepatically expressed enzymes, UGT1A9 exhibited the highest rate of MPA phenolic glucuronidation and glucosidation (Figure 5.12A and B). The extra-hepatic enzymes UGT 1A7, 1A8 and 1A10 also catalyzed the phenolic glucuronidation and glucosidation of MPA, with rates of glycoside formation similar to those observed for UGT1A9. Lower MPA phenolic glycosidation activity was observed with UGT1A1. UGT1A6 catalyzed the formation of MPAGlcUA, but not MPAGlc. Conversely, UGT2B7 formed MPAGlc, but not MPAGlcUA. UGT2B7 and multiple UGT1A subfamily enzymes (1A1, 1A3, 1A6, 1A8 and 1A10) formed AcMPAGlcUA (Figure 5.12C). Highest activity was observed with UGT1A10 and UGT2B7. Only UGT2B7 catalyzed the acyl glucosidation of MPA (Figure 5.12D).

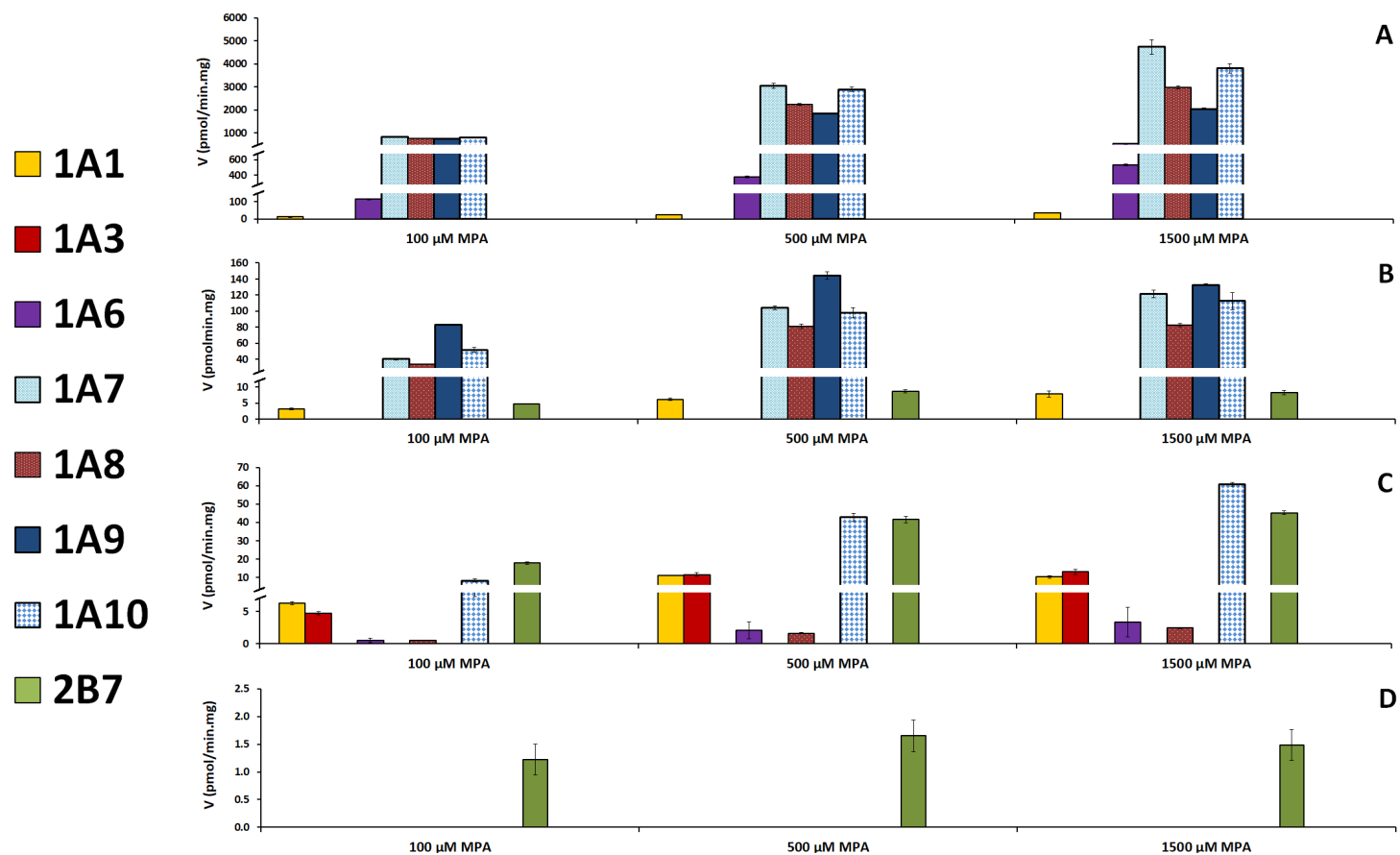


Figure 5. 12: Formation of MPAGlcUA (Panel A), MPAGlc (Panel B), AcMPAGlcUA (Panel C) and AcMPAGlc (Panel D) by recombinant UGT enzymes at MPA concentrations of 100, 500 and 1500μM.

Bars represent the mean of quadruplicate measurements ± SD.

Inhibition of MPAGlcUA, MPAGlc and AcMPAGlcUA formation by UGT enzyme selective inhibitors using human liver microsomes as the enzyme source

As for morphine glycosidation (Section 3.3.2), inhibition studies using pooled HLM (4 livers) as the enzyme source were carried out using UGT selective inhibitors (fluconazole, hecogenin and NFA) to further identify the enzymes involved in the metabolism of MPA (100 μ M). The minor MPA glycoside, AcMPAGlc was not investigated as its formation was too low for accurate quantification, especially in the presence of inhibitors.

NFA is known to inhibit UGT1A9 at low (2.5 μ M) and UGT1A1/UGT2B15 at higher (50-100 μ M) concentrations (Miners et al. 2011). NFA (2.5 μ M) inhibited human liver microsomal MPAGlcUA and MPAGlc formation by 89% and 25%, respectively, but had no effect on AcMPAGlcUA formation. The higher NFA concentration (100 μ M) reduced MPAGlcUA, MPAGlc, and AcMPAGlcUA formation by 99%, 77% and 21%, respectively (Figure 5.13). Hecogenin, an inhibitor of UGT1A4, had little (<12%) effect on the formation of MPAGlcUA, MPAGlc and AcMPAGlcUA by HLM. The UGT2B7/2B4 inhibitor fluconazole (2.5mM) had no effect on MPAGlcUA formation by HLM but reduced MPAGlc and AcMPAGlcUA formation by 29% and 52%, respectively (Figure 5.13). It should be noted that fluconazole (2.5mM) maximally inhibits UGT2B7 catalyzed reactions by ~70% (Uchaipichat et al. 2006b).

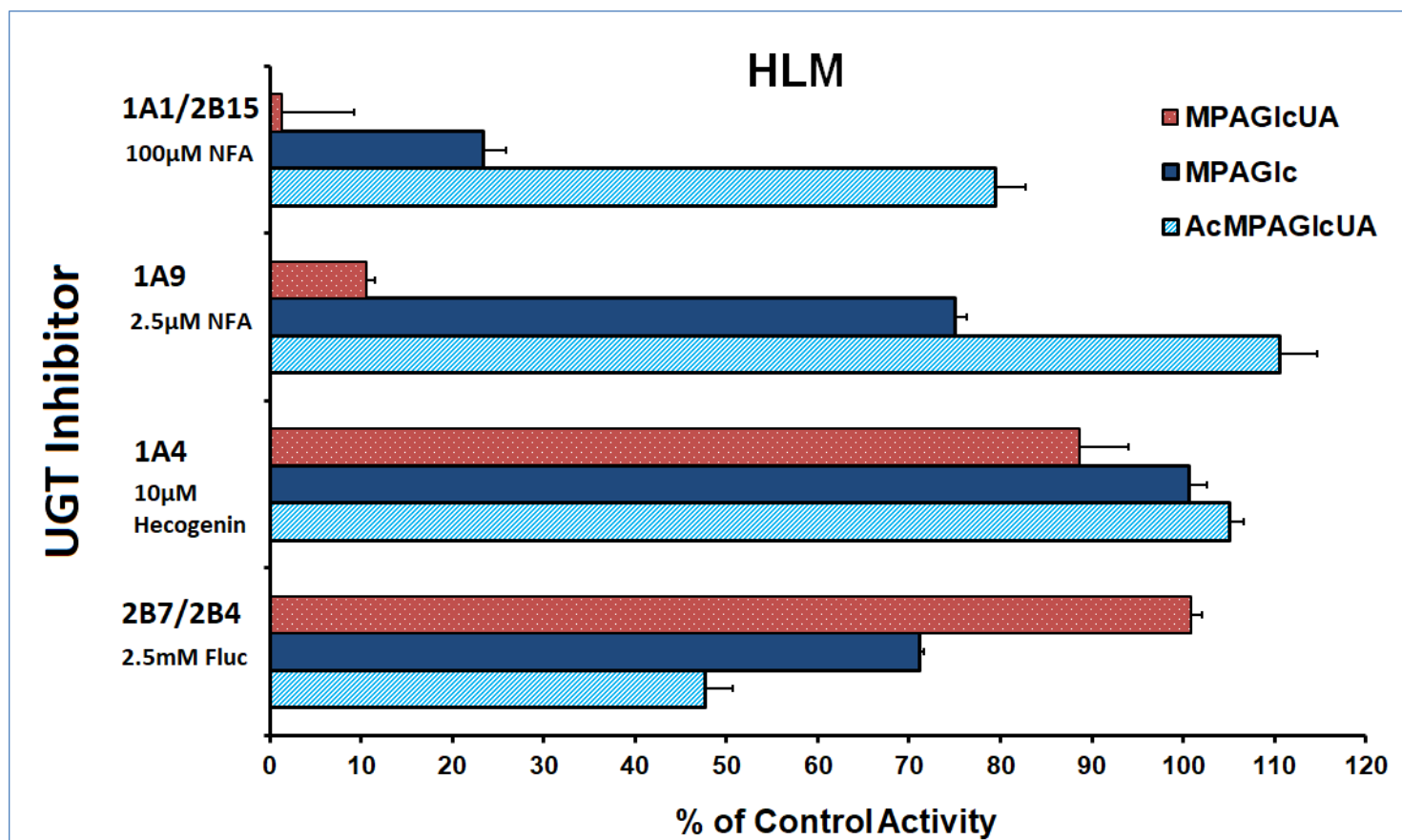


Figure 5. 13: Inhibition of human liver microsomal MPA (100µM) glycoside formation by selective UGT inhibitors: UGT1A9 (NFA, 2.5µM), UGT1A1/ 2B15 (NFA, 100µM), UGT1A4 (hecogenin) and UGT2B7/ 2B4 (fluconazole).

Bars represent the mean of quadruplicate measurements ± SD.

5.4 Discussion

As with morphine (Chapter 3), the kinetics (aglycone and cofactor) of MPA glucosidation and glucuronidation by HLM in the presence of single and combined cofactors (UDP-Glc and UDP-GlcUA) were characterized. Although non-specific binding of MPA (10-1000 μ M) to HLM does not occur (Bowalgaha & Miners 2001; Dostalek et al. 2011), MPA is highly bound (~97-99%) to human serum albumin (HSA) (Bullingham, Nicholls & Kamm 1998; Lipsky 1996; Park 2011; Shaw & Nowak 1995; Staatz & Tett 2007). Hence, incubations of HLM and recombinant protein sources excluded BSA, which is known to enhance the activity of UGT 1A9 and 2B7 *in vitro*, and to a lesser extent UGT 1A1, 1A4, and 1A6 (Chau et al. 2014; Gill, Houston & Galetin 2012; Manevski et al. 2011; Rowland et al. 2006; Rowland et al. 2007; Rowland et al. 2008b). The activities of other UGTs may also be affected by BSA, including UGT 1A7, 1A8, 1A10, 2A1, and 2B15 (Manevski et al. 2013).

It was shown that HLM supplemented with UDP-GlcUA alone formed MPAGlcUA and AcMPAGlcUA. Although incubations of HLM supplemented with UDP-Glc resulted in readily measurable formation of MPAGlc, consistent with previous reports (Picard et al. 2005; Shipkova et al. 2001), AcMPAGlc formation was very low by comparison. In agreement with the data of Shipkova et al. (2001), the rank order of the rate of metabolite formation with HLM as the enzyme source was MPAGlcUA > AcMPAGlcUA > MPAGlc > AcMPAGlc, indicating a lesser role for glucosidation in hepatic MPA metabolism (Appendix 2 and Table 5.2). While Shipkova et al. (2001) reported the acyl glucosidation of MPA by HLM, formation of AcMPAGlc was too low for kinetic analysis. By contrast, Picard et al. (2005) detected the formation of AcMPAGlc in liver, kidney, and intestinal microsomes, although low activity with HIM as the enzyme source precluded kinetic characterization. Formation of all MPA

glycosides has also been reported to be low in HIM compared to liver and kidney microsomes (Bernard & Guillemette 2004; Bowalgaha & Miners 2001; Picard et al. 2005; Shipkova et al. 2001).

Incubations of MPA and UDP-GlcUA alone with HLM as the enzyme source gave a K_m range of 121-148 μ M with respect to MPAGlcUA formation (Table 5.2). This K_m range is consistent with previously published data (Bernard & Guillemette 2004; Miles et al. 2005; Picard et al. 2005), but lower than the K_m range reported (270-351 μ M) by Shipkova et al. (2001) and Bowalgaha and Miners (2001). In contrast, the average K_m for human liver microsomal AcMPAGlcUA formation determined here (154-206 μ M) was lower than all previous reported data (range 370-1,710 μ M) (Picard et al. 2005; Shipkova et al. 2001). The reason for this discrepancy is unknown but may relate to differences in the accuracy of metabolite quantification, study design (e.g. substrate concentration range), and/or data analysis approaches (e.g. graphical vs. computational). K_m values for the formation of MPAGlc by HLM (with UDP-Glc as the sole cofactor) displayed a range of 155-236 μ M, similar to previously reported data (70-380 μ M) (Picard et al. 2005; Shipkova et al. 2001).

In vivo clinical data show approximately 10-fold variability in MPA pharmacokinetic parameters between individuals. The human liver microsomal CL_{int} values for MPA glucosidation and glucuronidation in the presence of single and combined cofactors from this study varied 2 to 3-fold. Clearly, the sample size was small (n=4). Bernard and Guillemette (2004) similarly showed that intrinsic clearance varied about 2-fold between two pooled samples of HLM and 2.5-fold between microsomes from 4 livers. In contrast, variation in other *in vitro* studies with larger numbers of HLM has been

reported to be ~4.7-fold (n=23) and ~4.8-fold (n=50) (Miles et al. 2005; Vietri et al. 2002).

As with morphine, kinetic studies with combined cofactors (1:1) resulted in a statistically significant decrease in MPAGlc formation (Table 5.2). Inclusion of both UDP-Glc and UDP-GlcUA increased the glucuronidation CL_{int} ratio relative to MPAGlc (i.e. MPAGlc: AcMPAGlcUA: MPAGlcUA) from 1: 1.4: 7.8 to 1: 9.4: 69.3. This ~7- to 8-fold increase in the formation of the MPA glucuronides in the combined cofactor experiments was due largely to an 82% decrease in the V_{max} for MPAGlc, similar to observations from the morphine 3-glucosidation studies. These data are consistent with a higher binding affinity of UDP-GlcUA to the UGT enzymes that catalyze MPA glycosidation. The ratio of CL_{int} values for the morphine glycosidation pathways determined in the presence of combined cofactors (UDP-GlcUA and UDP-Glc) was in broad agreement with (relative) urinary glycoside excretion. Quantitative MPA glycoside urinary excretion data are not available. However, Picard et al. (2005) reported AUC_{0-12hr} values for MPA, MPAGlcUA, AcMPAGlcUA and MPAGlc in renal transplant patients. From the published normalized glycoside: MPA ratios, it can be determined that the mean AUC_{0-12hr} values for MPAGlcUA is approximately 440-fold higher than that of MPAGlc, while the AUC_{0-12hr} values of AcMPAGlcUA and AcMPAGlc are similar (ratio 1.15: 1). As noted previously, the ratio of CL_{int} values for MPAGlc, AcMPAGlcUA and MPAGlcUA determined here in the presence of mixed cofactors was approximately 1: 9: 70. Although the *in vitro* data appear to under-estimate MPAGlc formation relative to AcMPAGlcUA and over-estimate MPAGlc formation relative to MPAGlcUA, the data are nevertheless consistent with the observation that MPA glucosidation is a very minor metabolic pathway compared to glucuronidation. It should be noted that AUC values depend on both the formation

and elimination clearances of the metabolite, and this may influence the *in vitro-in vivo* comparison. Moreover, extra-hepatic glycosidation, especially in the kidney (Knights et al. 2016; Margailan et al. 2015a), could contribute to the differences. In this regard, UGT1A9, which is the main UGT enzyme expressed in kidney, contributes to MPAGlcUA formation to a greater extent than MPAGlc formation (Section 5.3.4).

To further explore relative cofactor binding to the human liver microsomal UGT enzymes responsible for MPA glycosidation, UDP-Glc and UDP-GlcUA kinetics with MPA as the (fixed) substrate were determined with HLM as the enzyme source. Negative co-operativity was observed with both cofactors. The mean S_{50} value for UDP-Glc (measured with respect to MPAGlc formation) was 5.5- and 18.7-fold higher than the mean S_{50} values for UDP-GlcUA (measured with respect to the formation of AcMPAGlcUA and MPAGlcUA, respectively). Characterization of cofactor inhibition (UDP-GlcUA and UDP-Glc) with MPA as the fixed substrate and HLM as the enzyme source provided a mean K_i value of 353 μ M for UDP-GlcUA inhibition of MPAGlc formation. By contrast, inhibition of MPAGlcUA and AcMPAGlcUA formation by UDP-Glc was less potent, with respective K_i values of 25,382 μ M and 5,274 μ M. Inhibition was competitive in all cases. Taken together with the results of the single and combined cofactor studies with morphine and MPA as the aglycones, these data are consistent with the hypothesis that UDP-GlcUA has a higher binding affinity for UGT enzymes than does UDP-Glc. Thus, glucuronidation predominates over glucosidation. It is interesting to note that while comparable K_i values (1.39 - 2.49mM) were observed for UDP-Glc inhibition of M3G and M6G formation, this was not the case with UDP-Glc inhibition of MPAGlcUA and AcMPAGlcUA (5-fold difference). This suggests that cofactor binding affinities are enzyme dependent.

Whereas UGT2B7 is responsible for both morphine 3- and 6-glucuronidation, multiple UGT enzymes contribute to MPA phenolic and acyl glycosidation (see subsequent discussion). In this regard, Luukkanen et al. (2005) demonstrated differences in the respective K_m values (52-1256 μ M) of UDP-GlcUA for the various UGT1A sub-family enzymes.

Reaction phenotyping of MPA glycosidation was performed using activity studies with a ‘battery’ of recombinant human UGT enzymes (expressed in HEK293T cells) and by inhibition of human liver microsomal MPA conjugate formation by UGT enzyme selective inhibitors (Miners, Mackenzie & Knights 2010). As described in Section 5.3.4, the highest rate of formation of MPAGlcUA was observed with UGT 1A7, 1A8, 1A9 and 1A10. UGT1A1 and UGT1A6 also catalyzed MPA phenolic glucuronidation. A broadly similar pattern was observed with MPA phenolic glucosidation, except UGT1A6 did not form MPAGlc whereas UGT2B7 did. Multiple UGT enzymes formed the acyl glucuronide of MPA, including UGT1A1, 1A3, 1A6, 1A8, 1A10 and 2B7. Highest activity was observed with the two latter enzymes. By contrast, UGT2B7 was the only enzyme that catalyzed the acyl glucosidation of MPA, although activity was very low (<2pmol/min.mg over the MPA concentration range 100-1500 μ M). It should be noted that UGT 1A6, 1A9 and 1A10 expressed in HEK293T cells are the enzymes that typically exhibit highest glucuronidation activity towards phenols (Uchaipichat et al. 2004).

UGT enzyme-selective inhibition of MPAGlcUA, MPAGlc, and AcMPAGlcUA formation with HLM as the enzyme source demonstrated that the main hepatic enzymes involved in MPA glucuronidation and glucosidation are UGT1A9 and UGT2B7, respectively, with an additional contribution of UGT1A1. Human liver

microsomal MPAGlcUA formation is mediated almost entirely by UGT1A9, with a possible minor contribution (<10%) of UGT1A1 (based on inhibition by NFA, 100 μ M). As indicated previously, fluconazole (2.5mM) maximally inhibits recombinant and human liver microsomal UGT activity by approximately 70% (Uchaipichat et al. 2006a). Thus, the 53% inhibition of AcMPAGlcUA formation by fluconazole indicates that UGT2B7 is the major enzyme responsible for acyl glucuronidation by HLM. The NFA (100 μ M) inhibition data suggests that UGT1A1 also catalyzes AcMPAGlcUA formation by HLM. (It should be noted that, as with MPAGlcUA formation, recombinant UGT2B15 did not catalyze MPA acyl glucuronidation, precluding a significant role of this enzyme in MPA metabolism). As noted previously, recombinant UGT1A3 and UGT1A6 also formed AcMPAGlcUA but no truly selective inhibitors of this enzyme are currently available for reaction phenotyping.

Similar considerations apply to the reaction phenotyping of human liver microsomal MPA phenolic glucosidation. UGT2B7 and UGT1A1 appear to be the major contributors to this pathway, with additional involvement of UGT1A9 (~25%). It should be noted that the inhibition studies were performed at a substrate (MPA) concentration of 100 μ M, based on the range of K_m values for each pathway by HLM (121-153 μ M; Table 5.2). Thus, this substrate concentration (i.e. 100 μ M) will not correspond to the K_m for every UGT enzyme. The contribution of each UGT enzyme will vary depending on the MPA concentration relative to the individual K_m values, and hence absolute contributions of enzymes cannot be made with certainty. The kinetic and reaction phenotyping data confirm that, like morphine glycosidation, MPA glucuronidation and glucosidation occur as complementary metabolic pathways.

However, unlike morphine, the contribution of UGT enzymes to MPA glycosidation differs between pathways.

This is the first study to identify the enzymes involved in MPA glucosidation. As noted in Section 5.1.1, however, several previous studies have investigated MPA glucuronidation by recombinant UGTs (Basu et al. 2004; Bernard & Guillemette 2004; Mojarrabi & Mackenzie 1997; Picard et al. 2005; Shipkova et al. 2001). The results presented here are generally consistent with the published literature relating to MPA phenolic glucuronidation. Almost all studies demonstrate that UGT 1A7, 1A8, 1A9 and 1A10 have the capacity to catalyze MPAGlcUA formation. Most studies additionally suggest a lesser role of UGT1A1 and/or UGT1A6 in MPAGlcUA formation. Of note, however, Shipkova et al. (2001) reported that most UGT1A and 2B subfamily enzymes (UGT 1A1, 1A3, 1A4, 1A6, 1A7, 1A9, 1A10, 2B4, 2B7 and 2B15) all formed MPAGlcUA, with a relatively narrow range of CL_{int} values (0.17-0.54 pmol/min/mg protein). There are also discrepancies between studies that have characterized MPA acyl glucuronidation. Data generated here demonstrated that UGT 1A1, 1A3, 1A6, 1A8, 1A10 and 2B7 catalyzed AcMPAGlcUA formation. Highest activity was observed with UGT1A1 and UGT2B7. By contrast, Picard et al. (2005) reported UGT2B7 and, to a lesser extent UGT1A1 and UGT2B4, formed the acyl glucuronide. In a more limited investigation, Basu et al. (2004) observed AcMPAGlcUA formation by UGT 1A7, 1A8, 1A9 and 1A10. It is noteworthy that the various studies have employed recombinant UGT enzymes expressed in different cell lines (COS1/7, HEK293, Sf9 and *T.ni*). In this regard, the activity of UGT1A10-expressing SupersomesTM is known to be low compared to other expression systems (Troberg et al. 2017). In addition, different analytical techniques which differ in

specificity have been used for glucuronide quantification: HPLC (present study and Shipkova et al. (2001)); LC-MS (Picard et al. 2005); and radiometric TLC (Basu et al. 2004; Mackenzie 2000). Use of the different analytical techniques and expression systems almost certainly contribute to the inter-study variability. These observations further highlight that activity screening studies with recombinant enzymes alone are generally inadequate for reaction phenotyping. At least in the case of hepatic metabolism, selective inhibition of human liver microsomal enzyme activities should additionally be employed to assess the role of individual UGTs in drug glycosidation.

Both the present and previous studies indicate that UGT 1A7, 1A8 and 1A10 contribute to MPA glycosidation. These enzymes are expressed in the gastrointestinal tract (Rowland, Miners & Mackenzie 2013) and could conceivably contribute to gut wall metabolism. This would add another level of complexity to the enterohepatic recycling reported for MPA (see Section 5.1.1) and the impact of genetic polymorphism on MPA elimination. Although reaction phenotyping demonstrated that UGT1A9 is almost exclusively responsible for MPA phenolic glucuronidation, this enzyme plays a lesser role (<50%) in MPA glucosidation. Moreover, MPA data presented here show that glucosidation is a very minor pathway for MPA glycosidation. While genetic polymorphism of UGT1A9 (specifically the Met33Thr substitution) is known to influence MPA clearance via phenolic glucuronidation, any effect of UGT1A9*3 on MPA glucosidation will be inconsequential for MPA elimination.

Chapter 6

Endogenous glucosidation capacity of *Spodoptera frugiperda* (Sf9) and *Trichoplusia ni* (High Five™) cells towards drugs, non-drug xenobiotics and hydroxy steroids

Published in part as: Chau N, Kaya L, Lewis BC, Mackenzie PI, and Miners JO, 2019, 'Drug and chemical glucosidation by Control Supersomes™ and membranes from *Spodoptera frugiperda* (Sf) 9 cells: Implications for the apparent glucuronidation of xenobiotics by UDP-glucuronosyltransferase 1A5', *Drug Metabolism and Disposition*, 47 (3):271-278.

Reproduced with the permission of the American Society for Pharmacology and Experimental Therapeutics.

6.1 Introduction

6.1.1 Expression of recombinant human UGT enzymes in insect cells

Human UDP-glucuronosyltransferase (UGT) enzymes have been heterologously expressed as recombinant proteins in several expression systems, including mammalian (COS, V79, HEK293), baculovirus-infected insect (*Spodoptera frugiperda*, *Trichoplusia ni*), yeast (*Pichia pastoris*, *Saccharomyces cerevisiae*) and bacterial (*Escherichia coli*) cells (Radomska-Pandya, Bratton & Little 2005). Notably, the commercially available products Supersomes™ (Corning®, formerly BD Gentest) and Baculosomes® (ThermoFisher Scientific, formerly PanVera LLC) utilize

the baculovirus-insect expression system with High FiveTM and Sf9 as the respective host cell lines for human UGT protein expression (Peter Maroudas, Corning Incorporated; personal communication and product information, 2013). Control SupersomesTM (c-SUP) do not incorporate the protein of interest, but instead contain the wild-type baculovirus vector (Peter Maroudas, Corning Incorporated; personal communication, 2013). This vector may or may not still contain the *egt* gene that encodes for an ecdysteroid UDP-glucosyltransferase (EGT) protein. As discussed later, the presence of the EGT protein may have implications for studies investigating the metabolism of compounds with ecdysteroid-like structures. Numerous other drug metabolizing enzymes (e.g. CYPs, N-acetyltransferases (NATs), and flavin-containing monooxygenases (FMOs)) have also been expressed in baculovirus-infected insect cells.

With a few exceptions (Oda et al. 2012; Troberg et al. 2017) the increased use of insect cells, such as SupersomesTM and Sf9, for the expression of human UGTs arises from the higher activity observed for most proteins compared to the equivalent proteins expressed in mammalian cells (e.g. HEK293T). However, over time a number of issues relating to the use of UGT enzymes expressed in insect cells have been reported in the literature (Fujiwara, Yoda & Tukey 2018; Knights et al. 2016; Oda et al. 2017; Oda et al. 2012; Troberg et al. 2017; Zhang et al. 2012a). These include the extent and/or size of N-glycans that are attached to the proteins post-translationally which can affect protein structure and function (see later Discussion) and the use of the ‘strong’ baculovirus promoter which, although efficient for protein overexpression, results in significant expression of inactive proteins. The high expression of inactive proteins may be related to ‘sub-optimal’ protein processing during maximal protein biosynthesis (Altmann et al. 1999).

As described in previous Chapters, it is now recognized that numerous human UGT enzymes may utilize UDP-glucose as the cofactor. A number of investigations characterizing xenobiotic glucosidation using commercial Supersomes™ as the enzyme source have encountered unexpected background glucosidation activity in Supersomes™ (c-SUP), presumably due to endogenous insect UDP-glycosyltransferases (Chau et al. 2014; Tang et al. 2003). This clearly poses problems for the reaction phenotyping of drug and chemical glucosidation when recombinant UGTs are used in activity studies. While some studies have acknowledged this problem, it has gone unrecognized in others (Dai et al. 2015; Picard et al. 2005; Shipkova et al. 2001; Toide et al. 2004). The degree of background glucosidation activity will depend on a number of factors, including: the substrate selectivity of the endogenous glucosidating enzyme(s); their level of expression; and substrate binding affinity and turnover.

The demand for biologically active eukaryotic recombinant proteins, combined with technological improvements, has resulted in increased use of the baculovirus-insect cell expression system such that it has now become one of the most widely and routinely used systems for producing recombinant proteins (Griffiths & Page 1997; Kost, Condreay & Jarvis 2005; Unger & Peleg 2012). Recombinant protein production in a eukaryotic expression system tends to be laborious, time-consuming and costly. However, it has certain advantages over other systems such as expression in *Escherichia coli*, which cannot properly express functional human UGTs due to the lack of the post-translational machinery required to correctly fold proteins (Radomska-Pandya, Bratton & Little 2005; Unger & Peleg 2012). The one exception seems to be UGT2B4, which was shown to not be N-glycosylated at its single potential site (Barbier et al. 2000a; Zhang et al. 2012a). Although the post-translational

modification process of insect cells replicates that of mammalian cells reasonably well, post-translational protein glycosylation differs between insect and mammalian cells. Proteins produced from insect cells often demonstrate lower molecular masses due to differences in proteolytic processing, glycosylation site occupancy and glycan structure that can affect thermal stability and enzymatic activity of the recombinant protein to variable extents (Altmann et al. 1999). Additionally, the differences in lipid profiles of the cellular membranes of insect cells compared to mammalian cell lines may influence the function and activities of mammalian proteins expressed in insect cells (Marheineke et al. 1998).

Despite these considerations, baculovirus-infected insect cells generally provide an efficient expression system for eukaryotic proteins. In particular, turn-around time for protein expression is short, the process is easily scaled, and protein yield is relatively high (Altmann et al. 1999). The most common insect cell lines used for recombinant protein production are from the *S. frugiperda* (Sf9 or Sf21) and *Trichoplusia ni* (BTI-TN-5B1-4 or High Five™) lepidopteran species of insects (Fu et al. 2017; Marheineke et al. 1998; Unger & Peleg 2012), more commonly known as the fall army worm and cabbage looper insect, respectively. Sf9 cells are a sub-clone of the Sf21 cell line and were selected for their faster growth rate and higher cell densities compared to Sf21 cells. *Autographa californica* multiple nuclear polyhedrosis virus (AcMNPV), which relies on *S. frugiperda* as its host, is the most common species of baculovirus used for infection (Condreay & Kost 2007). Advantages offered by AcMNPV include: the extremely high transcriptional activity of the AcMNPV polyhedron promoter drives the synthesis of large amounts of the polyhedron protein and therefore also the expression of 'foreign' proteins; the foreign gene products are post-translationally modified to produce biologically active proteins; and, of relevance to cost and

biosafety, insect cells can be grown in serum-free media and the baculovirus cannot replicate in mammalian cells (Altmann et al. 1999; Li et al. 1990).

Nuclear polyhedrosis viruses (NPVs) such as AcMNPV are members of the *Baculoviridae* family of DNA viruses. NPVs contain a single molecule of circular, supercoiled, double stranded (ds) DNA that ranges in size from 90 to over 170 kb in different species of the virus (Rohrmann 1999). The virally encoded ecdysteroid UDP-glucosyltransferase (EGT) from the *egt* gene conjugates ecdysteroids, which are hormones involved in insect larval moulting and pupation, thereby interfering with normal insect host development by prolonging feeding duration and this provides the time for increased yield of virus progeny (O'Reilly 1995; O'Reilly & Miller 1989). Phylogenetic analysis by Hughes (2013) suggests that baculoviral EGTs came into existence about 70 million years ago through horizontal gene transfer of a UDP-glycosyltransferase gene from a lepidopteran host, with its closest relative being the UGT33 and UGT34 families of lepidopteran UDP-glycosyltransferases. EGT is secreted from infected cells in culture and is present in the haemolymph of infected insects (O'Reilly, Brown & Miller 1992). EGT utilizes UDP-Glc and UDP-galactose as cofactors (Evans & O'Reilly 1998; O'Reilly, Brown & Miller 1992), but does not appear to catalyze glucuronidation reactions (O'Reilly & Miller 1989). The EGT protein exhibits substrate selectivity, glucosidating ecdysteroids but apparently not substrates of human UGT enzymes, for example bilirubin, β -estradiol, testosterone, 4-methylumbelliferone and 1-naphthol (O'Reilly & Miller 1989). The ecdysteroids ecdysone, 20-hydroxyecdysone (20-E), 26-hydroxyecdysone and makisterone A are all glucosidated at the C-22 position (O'Reilly et al. 1991; O'Reilly & Miller 1989). In addition, endogenous sources of 26-hydroxyecdysone 22-glucoside have been identified in *Manduca sexta* (tobacco hornworm) and ecdysone 25-glucoside in the

nematode *Parascaris equorum* (O'Reilly et al. 1991; Thompson et al. 1987; Warren et al. 1986), suggesting endogenous glucosidation of ecdysteroids by insect UDP-glycosyltransferases.

As alluded to earlier, insect cells express UDP-glycosyltransferases that primarily utilize UDP-Glc as a cofactor for the detoxification of a diverse range of chemicals (Ahn, Vogel & Heckel 2012; Luque, Okano & O'Reilly 2002; Real, Ferre & Chapa 1991). Important to mammalian UGT topology are two functional motifs; an N-terminal (NT) signal sequence is cleaved upon integration into the ER compartment, while a short transmembrane domain (~20 residues) at the C-terminus (CT) of the protein anchors the enzyme to the membrane (Meech & Mackenzie 1998; Radomska-Pandya et al. 2005). Silkworm and cotton bollworm UDP-glycosyltransferases appear to have similar NT signal sequence and transmembrane domains to human UGTs and are therefore also likely to be anchored to the ER membrane region, unlike the cytosolic plant and bacterial UDP-glycosyltransferases (Ahn et al. 2014; Bock 2015; Huang et al. 2008; Jensen et al. 2011; Kannangara et al. 2017). BmUGT1, a protein cloned from *B. mori*, was expressed in *T. ni* (TN368) cells and its substrate selectivity investigated with UDP-glucose as cofactor. No activity was observed in cell lysate preparations with ecdysone or 20-E, but glucosidation activity was observed with aglycones from several chemical classes including flavonoids, coumarins, xenobiotic phenols, steroids and terpenoids (Luque, Okano & O'Reilly 2002). Interestingly, Luque, Okano and O'Reilly (2002) did not use Sf21 cells for transfection or enzyme assays as they found the cells expressed “*low levels of endogenous UGT activity towards several of the substrates tested*”.

Compared to other ‘detoxification’ gene families (e.g. cytochromes P450, carboxyl/cholinesterases, and glutathione transferases), identification of and biochemical characterization of insect UDP-glycosyltransferases is less advanced (Ahn, Vogel & Heckel 2012; Heidel-Fischer & Vogel 2015; Huang et al. 2008). The sequence identity of *S. frugiperda* and *T. ni* UDP-glycosyltransferases have only recently been determined (Gouin et al. 2017; Herde & Howe 2014). Although studies investigating the substrate selectivities of UDP-glycosyltransferases in other insect species have been conducted, data for *S. frugiperda* and *T. ni* are lacking. Owing to the problems associated with reaction phenotyping of chemical glucosidation by human UGTs expressed in insect cells (Chapter 3), the experiments described in this chapter aimed to characterize the scope and selectivity of drug and chemical glucosidation by these insect cell lines. Aglycones with either a phenolic (1-hydroxypyrene, 1-OHP; 4-methylumbelliferone, 4-MU; MOR; mycophenolic acid, MPA; 1-naphthol, 1-NAP; and 4-nitrophenol, 4-NP), aliphatic alcohol (codeine, COD; 20-hydroxyecdysone, 20-E; 21-hydroxyprogesterone, 21-OHP; phenethyl alcohol, PE; and zidovudine, AZT), acyl (MPA; S-naproxen, S-NAP), or amine (benzocaine, BZC; lamotrigine, LTG; and trifluoperazine, TFP) acceptor functional group were investigated. The chemical structures of the 15 xenobiotics studied are shown in Figure 1; site(s) of conjugation are indicated by arrows. All of these compounds are known to be glucuronidated by HLM and/or recombinant human UGTs (Bowalgaha et al. 2007; Finel et al. 2005; Gaganis et al. 2007; Green & Tephly 1996; Kubota et al. 2007; Raungrut et al. 2010; Rowland et al. 2006; Shipkova et al. 2001; Stone et al. 2003; Uchaipichat et al. 2006a; Uchaipichat et al. 2004). Glucosidation is an incompletely characterized drug metabolizing pathway in humans, although there has been an increase in the appearance of glucosidated compounds in the literature (Chapter 1) and

Chapter 6: Endogenous glucosidation capacity of insect cells

hence, it would be useful to comparatively investigate the endogenous environment of the insect cell lines in which human UGTs have been expressed, and their ability to conjugate known glucuronidated xenobiotics as it potentially impacts drug metabolism studies.

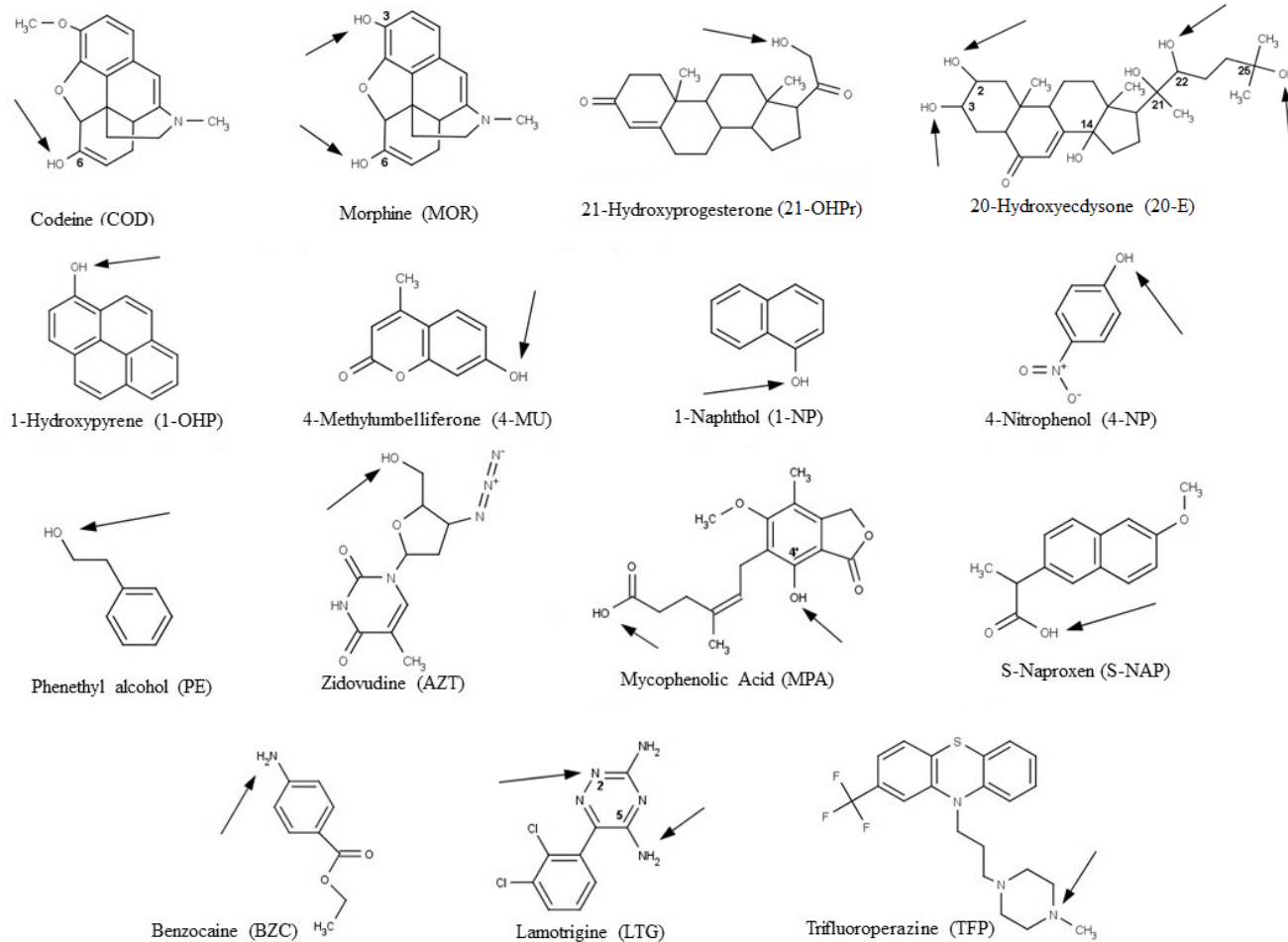


Figure 6. 1: Chemical structures of aglycones used to investigate the glucosidation capacity by Control SupersomesTM (c-SUP) and uninfected *Spodoptera frugiperda* (Sf) 9 cell membranes. Arrows indicate the potential site(s) of glucosidation.

6.1.2 Hypothesis

Endogenous UDP-glycosyltransferases expressed by Sf9 and *T. ni* cells have the ability to glucosidate drugs, non-drug xenobiotics, and endogenous chemicals.

Experimental aims

The overarching aim of the studies described in this Chapter was to characterize the endogenous glucosidation activity of enriched membranes from uninfected *S. frugiperda* (Sf9) and commercially available *T. ni* (c-SUP) cells to assess the implications of endogenous glucosidation for the study of chemical glucosidation by recombinant human UGT enzymes expressed in insect cells. Specific aims were to:

1. Grow and harvest Sf9 insect cells and isolate lysate, and the cytosolic and enriched membrane fractions.
2. Confirm 1-OHP and 20-E glucosidation activity in each cellular/sub-cellular preparation.
3. Develop HPLC assays for the separation and quantification of glucoside conjugates for each aglycone (Figure 6.1) formed by incubations of enriched membranes from uninfected Sf9 cells and commercial c-SUP.
4. Assess the capacity and selectivity of endogenous UDP-glycosyltransferases present in Sf9 enriched membranes and c-SUP towards aglycones with differing acceptor functional groups; namely 1-OHP, 4-MU, MOR, MPA, 1-NAP, 4-NP, COD, 20-E, 21-OHP_r, PE, AZT, S-NAP, BZC, LTG, and TFP.
5. Characterize and compare the kinetics of aglycone glucosidation for selected substrates with Sf9 enriched membranes and c-SUP as the enzyme sources.

6.2 Methods

6.2.1 HPLC and LC-MS equipment, assay development and detection of xenobiotic glucosides

HPLC equipment

Xenobiotic glucoside conjugates were measured by reversed-phase HPLC using an Agilent 1100 series instrument (Agilent Technologies, Sydney, Australia) comprising an auto-injector, a quaternary solvent delivery system and a UV detector (1200 series). Analytes were separated using a variety of columns, depending on the aglycone (Appendix 1).

Development of HPLC (UV or FL) assays for the detection of xenobiotic glucoside and glucuronide conjugates

The chromatography conditions (mobile phase, absorbance wavelength, precipitating agent, retention times for metabolites, detection method, and injection volume) are summarized in Appendix 1. The 15 assays utilized for this work were generally adapted from existing protocols. Where relevant, references for the original protocols are indicated in Appendix 1.

Calibration curves of xenobiotic glycosides

Peaks corresponding to glucoside conjugates were confirmed by co-chromatography with authentic glucoside standards (Table 2.1), where available and from the m/z ratios and fragmentation patterns generated by high resolution LC-MS (see below). Quantification of the glucosides was achieved by reference to standard curves, prepared using either the authentic glucoside conjugate (where available) or the glucuronide when the glucoside conjugate was unavailable (Appendix 1).

Liquid chromatography- mass spectrometry

Glucoside conjugates were additionally separated and detected using a Waters ACQUITY™ Ultra Performance Liquid Chromatography (UPLC) system coupled to a Waters Micromass Q-TOF Premier™ mass spectrometer (Waters Corporation Micromass UK Ltd., Manchester, UK). Analytes were separated on an ACQUITY UPLC® HSST3 column (1.8µm particle size, 2.1×100mm; Waters Corporation, Milford, MA, USA). The mobile phase, delivered at a flow rate of 0.25mL/min, consisted of two solutions (phase A, 100% MS-grade acetonitrile; phase B, 5% acetonitrile in water) mixed according to a gradient timetable. Initial conditions were: 5% phase A - 95% phase B held for 3min followed by a linear gradient over 7min to 60% phase A - 40% phase B, which was held for 0.5min. The total run time, including the return to initial conditions, was 12.5min. The MS operated in positive ion mode with electrospray ionization (ESI+). Time-of-flight data (ToF) data were acquired in selected ion (MS^E) mode, where the first resolving quadrupole acquired mass data from m/z 100 to 1000. Collision cell energy alternated between 2eV and a high energy ramp (3 to 15eV). The cone and desolvation gas flow rates were 50 and 550L/hr, respectively. Desolvation and source temperatures were 250°C and 90°C, respectively, and the capillary and cone voltages were 1,800 and 25V, respectively. MS data were collected as total ion chromatograms, with selected ion (pseudo MRM) data extracted at the [M + H⁺] for each analyte of interest using Waters QuanLynx™ software (Waters Corporation).

6.2.3 Preparation of uninfected Sf9 lysate and membranes

Refer to Section 2.2.2 for the Sf9 cell culturing method.

Sf9 lysate

Lysate was prepared initially to confirm endogenous UDP-glycosyltransferase activity of uninfected Sf9 cells and to also compare activities with membrane fractions. Cells were harvested and washed in phosphate-buffered saline once they had grown to log phase. Cells were subsequently lysed by sonication with eight 1-sec ‘bursts’, each separated by 1min with cooling on ice, using a Vibra Cell VCX 130 Ultrasonics Processor (Sonics and Materials, Newton, CT, USA) and then centrifuged at 12,000g for 1min at 4°C. The supernatant fractions were separated and stored in phosphate buffer (0.1M, pH 7.4) at -80°C until use.

Sf9 membranes

The method employed for the separation of membranes was based on the protocol described in the MSc thesis of Kaya (2011), with minor modification. The procedure, shown in Figure 6.2, was carried out on ice to preserve enzyme activity. Pelleted cells were resuspended in cold deionized water at a concentration of 0.33g cell pellet/mL, and then manually homogenized with 15 strokes in a glass Potter Elvehjem homogenizer. Potassium phosphate buffer (1M, pH 7.4) was added to provide a final concentration of 0.1M. The cell homogenate was then lysed by sonication, as described above for lysate preparation, and the sonicated cells were re-homogenized with another 15 strokes in a glass Potter Elvehjem homogenizer. The cell homogenate was subsequently centrifuged at 10,000g for 10min at 4°C to separate the membrane fraction from cellular debris (nuclear/mitochondrial pellet). This supernatant fraction (S1) was reserved while the pellet (P1) was re-homogenized in half the original volume of 0.1M potassium phosphate buffer (pH 7.4). The homogenate was sonicated as described above and centrifuged at 10,000g for 10min at 4°C. This second pellet (P2)

was discarded, while the supernatant fraction (S2) was combined with the reserved first supernatant fraction (S1) and centrifuged at 105,000g at 4°C for 75min. The pelleted enriched membrane fraction (P3) was resuspended in 1 to 2mL of potassium phosphate buffer (0.1M, pH 7.4), and homogenized briefly (2 -3 strokes) before being stored at -80°C until use.

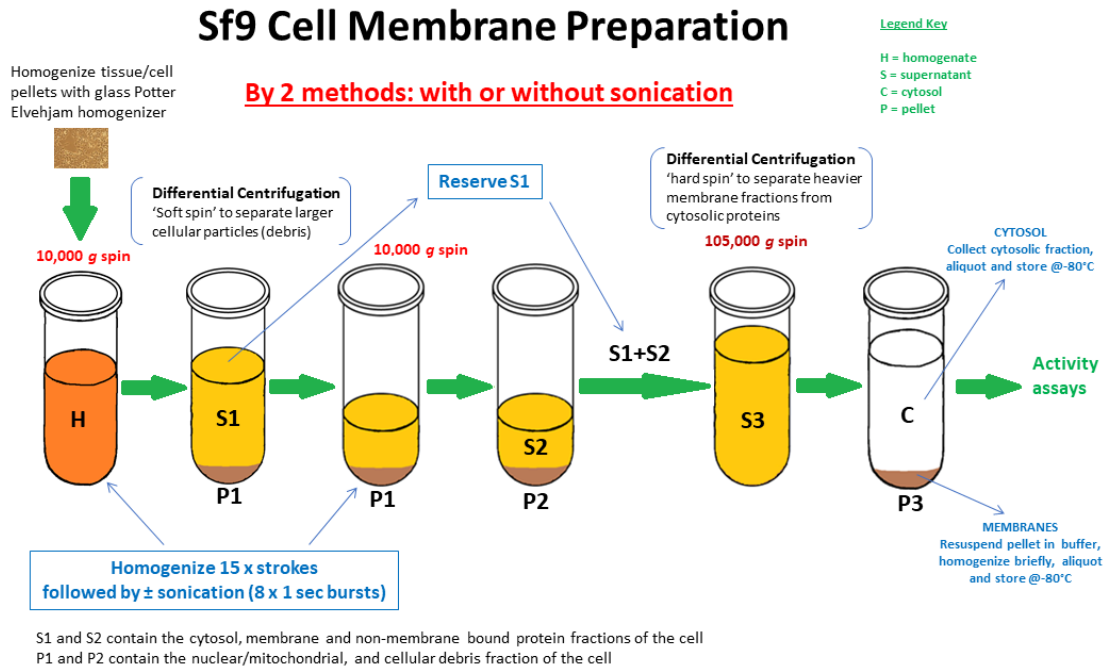


Figure 6. 2: Preparation of Sf9 cell membranes by homogenization and differential centrifugation. Sonication was included as an additional step for lysate preparation to increase protein yield.

Sf9 cell count and viability calculation

Refer to Section 2.2.2.

Sf9 cell seeding density and growth rate

Sf9 cells were seeded at 3×10^5 viable cells/mL (Thermo Fisher Scientific, Sf9 Cells Adapted in Sf-900™ II/III SFM, Publication Number MAN0007364), which approximately doubled to 7.3×10^5 cells/mL over three days. After an additional 48hr

the density reached approximately 2.8×10^6 cells/mL, ready for passaging or harvesting.

Long term storage of Sf9 cell stock and recovery rate

The optimal cell density to store the Sf9 cells long term was found to be 5×10^7 viable cells/mL. This resulted in 72-79% cell viability at the time of cell stock thawing for culturing, and a recovery rate three days later of 82-98% cell viability. This observation was confirmed on three separate occasions by two different researchers. The recovery in terms of amount or density of cells was reproducible (7.6 , 7.3 and 7.7×10^5 cells/mL). By way of example, storage of Sf9 cells at a lower density (1×10^7 viable cells/mL) resulted in 65-87% cell viability at the time of thawing, with no live cells remaining after 24hr. Again, this observation was confirmed on three separate occasions. Media used to freeze cell stocks for storage in liquid nitrogen comprised 60% serum free SFX-Insect medium, 30% FBS and 10% DMSO.

6.2.2 Xenobiotic glucosidation assays

HPLC detection

(i) Sf9 enriched membranes as the enzyme source

Incubations, in a total volume of $200 \mu\text{L}$, contained phosphate buffer (0.1M, pH 7.4 or pH 6.8 for carboxylic acid-containing substrates), MgCl_2 (4mM), Sf9 enriched membranes (0.2mg except for reactions with MPA (0.02mg) and 1-OHP (0.002mg)), substrate, and UDP-Glc (5mM). After a 5min pre-incubation at 37°C in a shaking water bath, reactions were initiated by the addition of UDP-Glc and performed for 2hr (or 1hr for reactions with MPA and 1-OHP). Reactions were terminated by the addition of either perchloric acid (11.6M; $2 \mu\text{L}$), ascorbic acid in methanol (2% w/v; $200 \mu\text{L}$), or acetic acid in methanol (4% v/v; $200 \mu\text{L}$), depending on the substrate (Appendix 1),

and cooling on ice for 10min. Samples were centrifuged (5000g for 10min), and a 5-40 μ L aliquot of the supernatant fraction was analyzed by HPLC. Rates of glucoside formation were measured at four different substrate concentrations with reference to a glucoside or glucuronide standard.

(ii) Control SupersomesTM (c-SUP) as the enzyme source

Experiments utilizing c-SUP as the enzyme source were as described for Sf9 enriched membranes, except the incubation volume was 100 μ L. Reactions were terminated as described for incubations with Sf9 enriched membranes.

(iii) Kinetic studies with Sf9 membranes and c-SUP as the enzyme sources

Incubation conditions for glucosidation kinetic experiments with both c-SUP and Sf9 enriched membranes followed the above protocol with the following changes in protein and incubation time: morphine (MOR; 1mg/mL, 60min), 1-OHP (0.01mg/mL, 15min), MPA (0.1mg/mL, 15min) and 4MU (0.1mg/mL, 30min).

LC-MS detection

LC-MS was performed to confirm the identity of peaks (from the m/z ratio) for glucosides for which no authentic standard was available (viz. S-NAP, AZT, 1-NAP, COD, LTG, TFP, 1-OHP, 20-E). LC-MS was also performed for compounds for which an authentic glucoside standard was available (viz. MPA, MOR, 4-MU, 21-OHP, PE, BZC, 4-NP) for completion. All incubations were performed at least in duplicate. MS studies utilized the above protocol, except all reactions were terminated by the addition of two volumes of MS-grade 4% acetic acid in methanol or 2% ascorbic acid in methanol (BZC glucosidation assay).

6.3 Results

6.3.1 Activity of Sf9 lysate and microsomal fractions

To determine which cell preparation(s) was optimal for measurement of glucosidation activity, lysate, enriched membranes and the cytosolic fraction (0.1mg/mL) were separately screened for activity using 1-OHP (40 μ M) as the probe substrate and an incubation time of 15min. Figure 6.3 shows that membranes yielded 2.06- to 2.77-fold greater 1-OHP glucosidation activity than lysates, depending on whether the membrane fractions were sonicated or not. Very little 1-OHP glucosidation activity (2-8% of lysate activity) remained in the cytosolic fraction, confirming that the enzyme(s) responsible for glucosidation resides in membranes. Although sonication of the membrane fraction resulted in greater (~34%) total glucosidation activity (Figure 6.3), this also carried over into the cytosolic fraction with approximately 12% additional activity compared to no sonication. Membrane and cytosolic fractions (1.0mg/mL) were also incubated with 20-E (10 and 100 μ M) for 2hr; no glucosidation activity was observed for either fractions. Thus, enriched membranes from Sf9 cells were employed in subsequent activity studies.

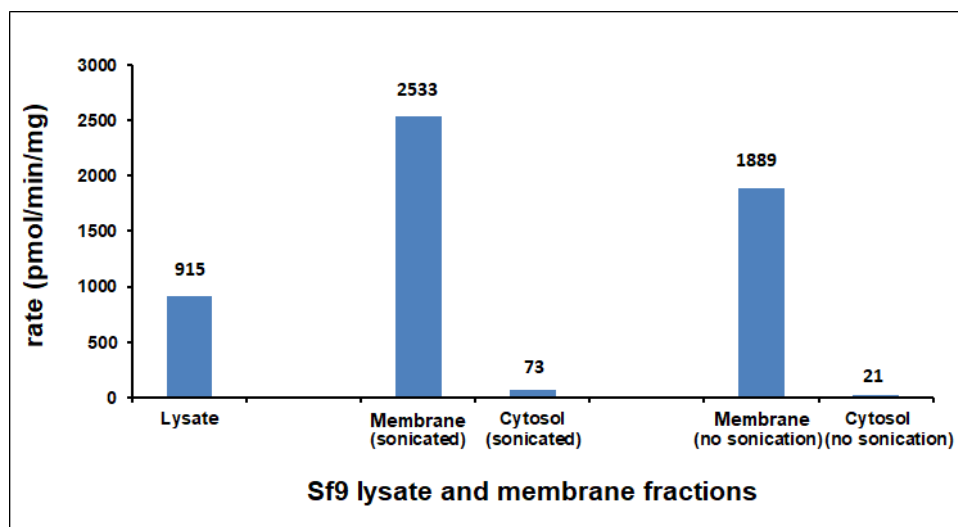


Figure 6. 3: Comparison of the 1-OHP glucosidation activity of Sf9 cell preparations (lysate, membranes and cytosol). The aglycone concentration was 40 μ M.

6.3.2 Xenobiotic glucosidation by Sf9 membranes and c-SUP

Studies were performed to determine the glucosidation capacity and selectivity of Sf9 membranes and c-SUP. Fifteen substrates from chemical classes with differing functional groups (phenolic, aliphatic alcohol, carboxylic acid and amine) were investigated. The activity of each substrate was determined at four concentrations, ranging from 1 – 5000 μ M. In addition to the opioids morphine (MOR) and codeine (COD), a further ten compounds containing a phenolic or aliphatic hydroxyl group were screened for glucosidation by c-SUP and Sf9 membranes with UDP-Glc as cofactor; 1-hydroxypyrene (1-OHP), 4-methylumbelliferone (4-MU), mycophenolic acid (MPA), 1-naphthol (1-NAP), 4-nitrophenol (4-NP), 20-hydroxyecdysone (20-E), 21-hydroxyprogesterone (21-OHPr), phenethyl alcohol (PE), zidovudine (AZT). Two compounds containing a carboxylic acid group, MPA and S-Naproxen (S-NAP), were also evaluated for glucoside conjugate formation, as were three compounds containing an amine group; lamotrigine (LTG), benzocaine (BZC), and trifluoperazine (TFP).

Rates of MOR 3-glucosidation were similar with both Sf9 membranes and c-SUP as the enzyme sources and increased in a concentration dependent manner. MOR was not glucosidated in the 6-position by either Sf9 membranes or c-SUP (Figure 6.4C). In contrast to MOR, which has both phenolic (3-position) and enolic (6-position) hydroxyl groups, codeine has only an enolic hydroxyl group (at the 6-position). Consistent with the lack of MOR 6-glucosidation by c-SUP and Sf9 membranes, codeine was not glucosidated by either enzyme source.

High rates of 1-OHP glucosidation were observed with c-SUP as the enzyme source, with 2- to 20-fold greater activity compared to Sf9 membranes (Figure 6.4A). The increase in 1-OHP glucosidation was concentration dependent for c-SUP across the range (1-25 μ M) investigated, while 1-OHP glucosidation by Sf9 membranes displayed substrate inhibition above 5 μ M. Similarly, rates of 1-NAP glucosidation were higher with c-SUP and increased in a concentration dependent manner (Figure 6.4E). The rate of formation of the phenolic glucoside of MPA by Sf9 membranes was 10.5- to 4-fold higher than by c-SUP (Figure 6.4D). Phenolic glucosidation of MPA by Sf9 membranes approached saturation at the highest aglycone concentrations, whereas MPA glucosidation by c-SUP tended to increase approximately linearly with aglycone concentration. Like MOR, rates of 4-MU and 4-NP glucosidation were similar with both enzyme sources and increased in a concentration dependent manner (Figures 6.4B and F, respectively).

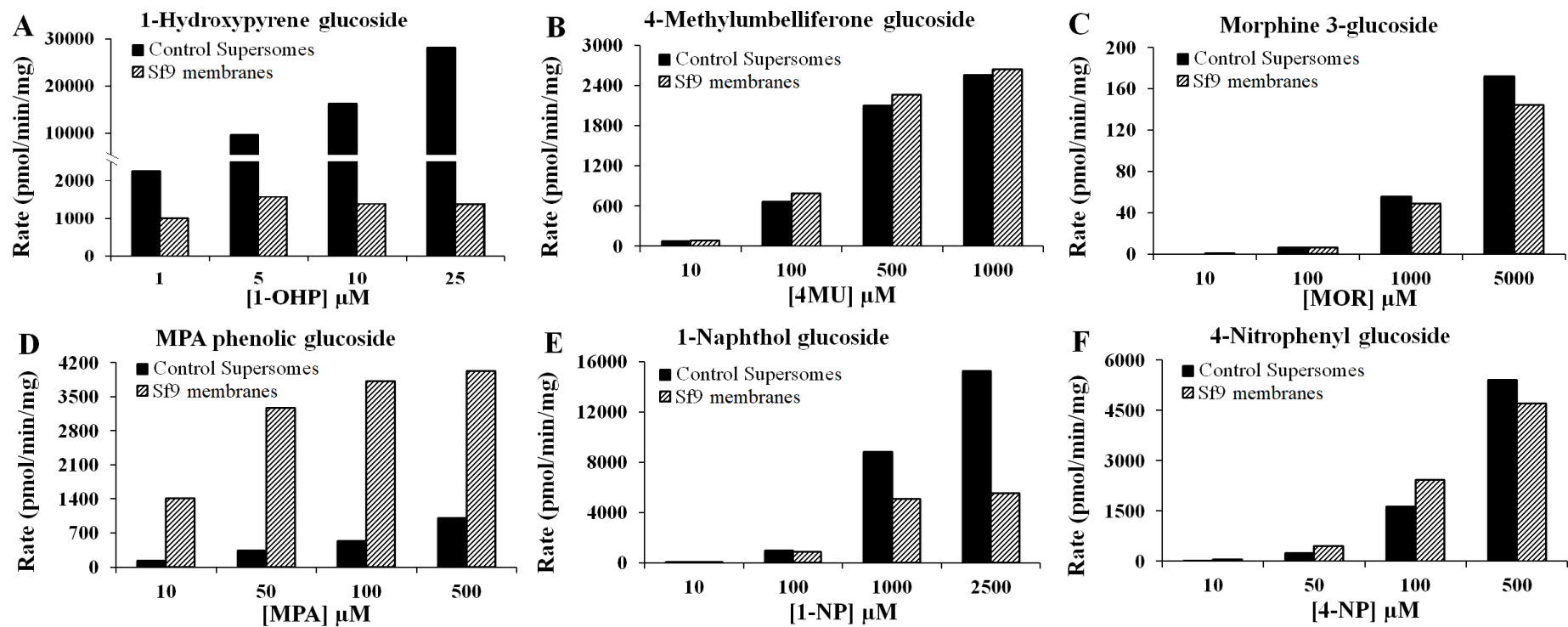


Figure 6. 4: Glucosidation of compounds containing a phenolic hydroxyl group at 4 substrate concentrations by Sf9 cell membranes and c-SUP (Control SupersomesTM): 1-hydroxypyrene (1-OHP) (A), 4-methylumbelliferone (4-MU) (B), morphine (MOR) (C), mycophenolic acid (MPA) (D), 1-naphthol (1-NAP) (E), and 4-nitrophenol (4-NP) (F). Bars represent the mean of duplicate measurements (<10% variance).

21-OHPr exhibited concentration dependent glucosidation activity with both Sf9 membranes and c-SUP, but activity was consistently greater with c-SUP (13.5- to 22.8-fold; Figure 6.5D). Only c-SUP glucosidated the insect hormone 20-E. Three glucoside conjugates were formed; these are referred to as 20-E glucoside 1, 2 and 3 based on the order of elution from the HPLC column (Figure 6.5A, B and C, respectively). The highest rate of formation was observed with glucoside 2, which was approximately 9- to 12-fold greater than the rates of formation of glucosides 1 and 3. Similarly, AZT was glucosidated only by c-SUP (Figure 6.5F). In contrast, PE glucosidation was higher with Sf9 membranes (Figure 6.5E).

Formation of the (minor) acyl glucoside was observed only at the highest MPA concentration (500 μ M) with Sf9 membranes as the enzyme source (cf. Figure 6.6D and 6.4D). Glucosidation of the carboxylic acid-containing compound S-naproxen (S-NAP) and the amines benzocaine (BZC), lamotrigine (LTG), and trifluoperazine (TFP) by c-SUP and Sf9 membranes was additionally investigated (Figure 6.6A-C and E). Rates of S-NAP acyl glucosidation by Sf9 membranes were much higher than by c-SUP (Figure 6.6E). LTG and TFP were both glucosidated by Sf9 membranes, but not by c-SUP (Figure 6.6B and C). However, BZC was glucosidated by both enzyme sources, albeit at a higher rate with Sf9 membranes (Figure 6.6A).

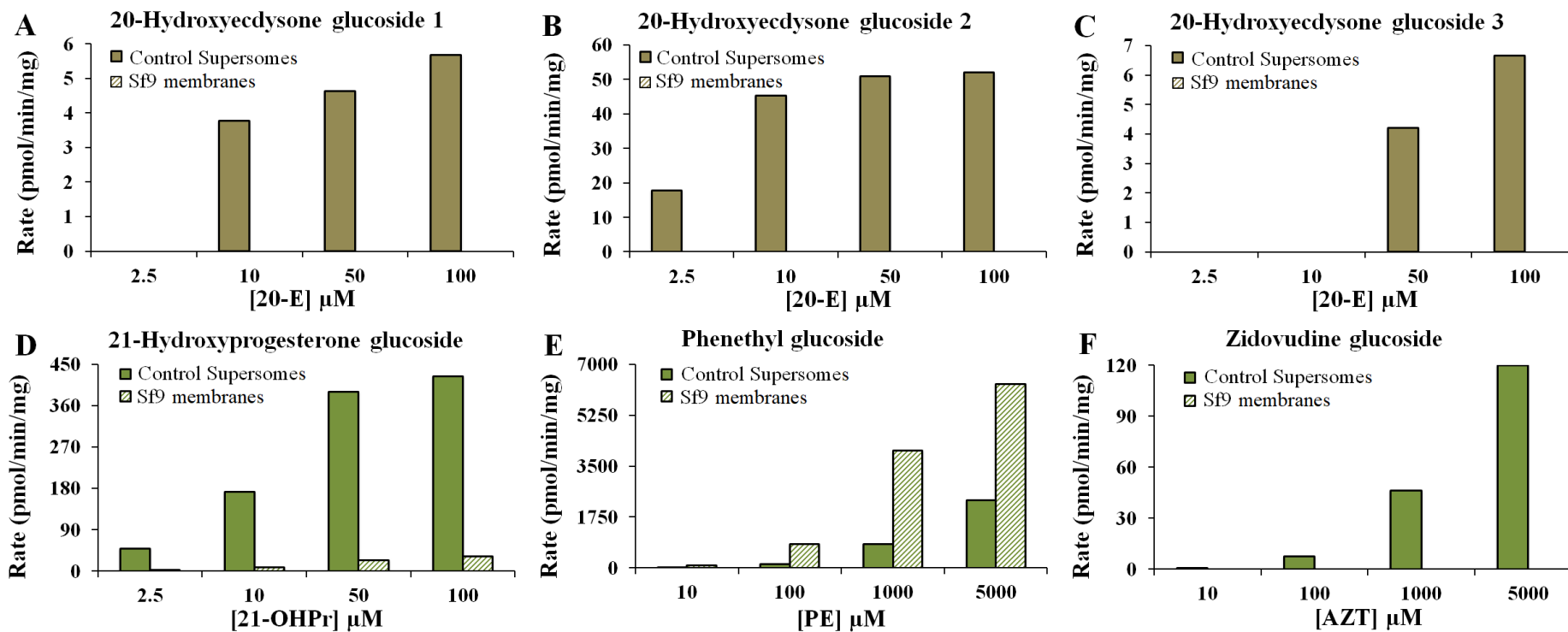


Figure 6. 5: Glucosidation of compounds containing an aliphatic hydroxyl group at 4 substrate concentrations by Sf9 cell membranes and c-SUP (Control Supersomes™): 20-hydroxyecdysone (20-E) (A-C), 21-hydroxyprogesterone (21-OHPr) (D), phenethyl alcohol (PE) (E), and zidovudine (AZT) (F). Bars represent the mean of duplicate measurements (<10% variance).

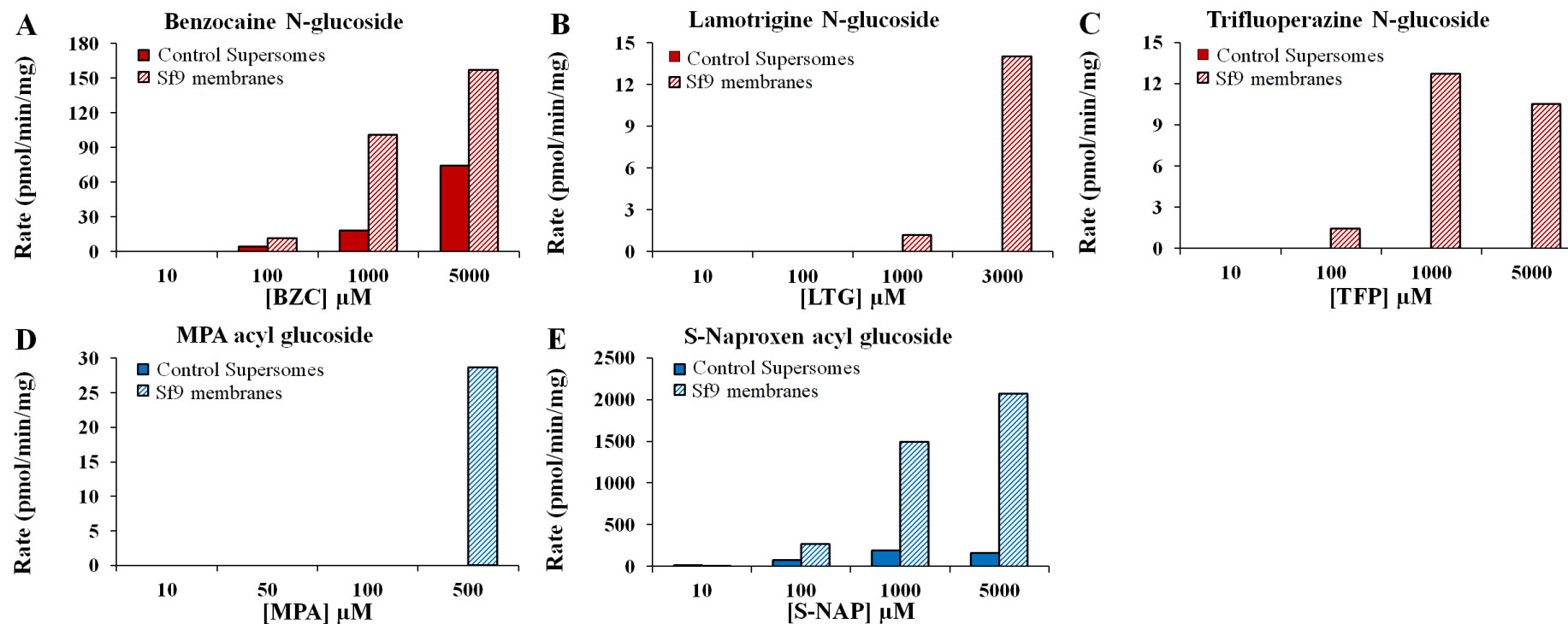


Figure 6. 6: Glucosidation of compounds containing either an amine- or carboxylic acid group at 4 substrate concentrations by Sf9 cell membranes and c-SUP (Control SupersomesTM): benzocaine (BZC) (A), lamotrigine (LTG) (B), trifluoperazine (TFP) (C), mycophenolic acid (MPA) (D), and S-naproxen (S-NAP) (E). Bars represent the mean of duplicate measurements (<10% variance).

6.3.3 Verification of xenobiotic glucoside formation by uninfected Sf9 membranes and c-SUP using mass spectrometry

Peaks corresponding to glucoside conjugates were not observed in chromatograms from experiments performed in the absence of UDP-Glc. As noted in Methods, authentic glucoside conjugates were available for 21-OHPr, 4MU, MPA, 4-NP, BZC and MOR. Glucosidation of these compounds was confirmed by comparison to the retention times of the authentic standards. In addition, the formation of a glucoside conjugate(s) by incubations of Sf9 membranes and c-SUP (supplemented with UDP-Glc) was confirmed for all substrates investigated by high resolution mass spectrometry. Observed and expected m/z values for glucosides are shown in Table 6.1. In addition, fragmentation patterns were consistent with glucoside formation (data not shown). An m/z value corresponding to 4-NP glucoside could not be detected by MS in positive ion mode, even for the authentic standard, despite detection by HPLC and UPLC. However, the fragmentation pattern was consistent with formation of 4-NP glucoside.

Table 6. 1: Observed and expected m/z values (± 0.02 Da) for xenobiotic and steroidal glucosides formed by incubations of Sf9 membranes or c-SUP with UDP-glucose as cofactor.

Xenobiotic		Expected glucoside m/z (+ ion mode)	Observed glucoside m/z (ESI+ mode)	
			Sf9 membranes	c-SUP
Phenols	1-Hydroxypyrene	381.13	381.14	381.13
	4-Methylumbelliferone	339.10	339.08	339.09
	Morphine	448.19	448.18	448.18
	Mycophenolic acid	483.18	483.19	483.19
	1-Naphthol	307.12	307.12	307.13
	4-Nitrophenol	302.09	ND	ND
Aliphatic alcohols	Codeine	462.21	ND	ND
	20-Hydroxyecdysone	643.37	ND	643.39 (1) 643.39 (2) 643.39 (3)
	21-Hydroxyprogesterone	493.27	493.28	493.27
	Phenethyl alcohol	285.13	285.15	285.13
	Zidovudine	430.16	ND	431.16
Amines	Benzocaine	328.13	328.13	328.13
	Lamotrigine	419.07 ^d	419.07 ^d	ND
	Trifluoperazine	571.23	571.22	ND
Carboxylic acids	Mycophenolic acid	483.18	483.19	483.19
	S-Naproxen	410.18 ^a	410.16 ^a	410.18 ^a
		415.13 ^b	415.13 ^b	415.11 ^b
431.11 ^c		431.11 ^c	431.10 ^c	

^a S-naproxen + NH₄ adduct^b S-naproxen + Na adduct^c S-naproxen + K adduct^d Lamotrigine N2-glucoside based on isotopic distribution (Appendix 3)

ND – not detected

6.3.4 Kinetic characterization of MOR, 1-OHP, MPA and 4-MU glucosidation by Sf9 membranes and c-SUP

As described in (Section 3.3), both c-SUP and Supersomes™ expressing UGT2B7 catalyze the 3-glucosidation, but not the 6-glucosidation, of MOR in the presence of UDP-Glc (as cofactor). Thus, in addition to the kinetics of MOR 3-glucosidation by c-SUP (Section 3.3.5), Sf9 membranes were characterized (Figure 6.7A and B, respectively). MOR 3-glucosidation by c-SUP exhibited hyperbolic (Michaelis-Menten) kinetics, whereas negative cooperative kinetics were observed with Sf9 membranes. Respective mean K_m or S_{50} and V_{max} values for MOR 3-glucosidation by c-SUP and Sf9 membranes were 3.4 and 4.4mM, and 266 and 362pmol/min/mg.

To further characterize the glucosidation of hydroxy-containing substrates, the kinetics of 1-OHP (Figure 6.7C and D), MPA (Figure 6.7E and F) and 4-MU (Figure 6.7G and H) glucosidation by c-SUP and Sf9 membranes was investigated. Kinetic parameters given below are the meant \pm standard error of the parameter fit (from model fitting). As with MOR, the kinetic model differed between the two enzyme sources. 1-OHP glucosidation by c-SUP exhibited negative cooperative kinetics ($n = 0.89 \pm 0.01$), but substrate inhibition ($K_{si} = 13.3 \pm 1.9\mu\text{M}$) with Sf9 membranes. Respective mean K_m or S_{50} and V_{max} values for 1-OHP glucosidation by c-SUP and Sf9 membranes were 8.0 ± 0.21 and $1.4 \pm 0.11\mu\text{M}$, and $11,211 \pm 144$ and $2,713 \pm 132\text{pmol/min/mg}$, respectively. MPA phenolic glucosidation by c-SUP and Sf9 membranes were best described by the Michaelis-Menten and substrate inhibition equations, respectively. Mean K_m or S_{50} and V_{max} values for MPA phenolic glucosidation by c-SUP and Sf9 membranes were 165 ± 0.35 and $15.5 \pm 1.1 \mu\text{M}$ ($K_{si} = 2998 \pm 468 \mu\text{M}$), and 916 ± 0.81 and $4,076 \pm 97\text{pmol/min/mg}$, respectively. Unlike the other substrates, 4-MU glucosidation by both c-SUP and Sf9 membranes exhibited negative cooperative

Chapter 6: Endogenous glucosidation capacity of insect cells

kinetics with mean S_{50} , n and V_{\max} values of 282 ± 2.6 and $123 \pm 8.3 \mu\text{M}$, 0.85 ± 0.003 and 0.91 ± 0.03 , and $2,390 \pm 9.3$ and $2,580 \pm 63 \text{pmol/min/mg}$, respectively.

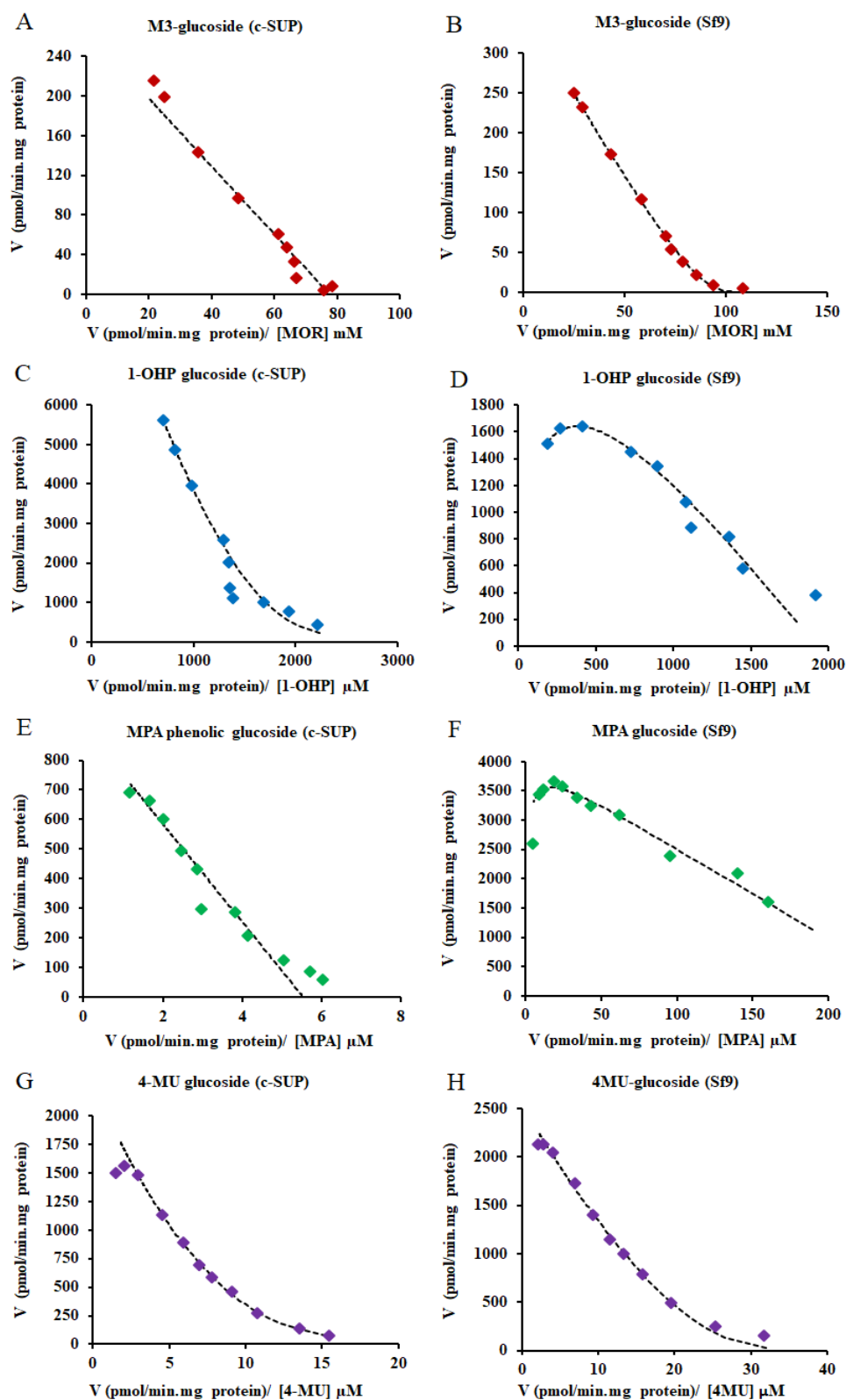


Figure 6. 7: Eadie-Hofstee plots for morphine 3-glucosidation (A and B), 1-hydroxypyrene (1-OHP) (C and D), mycophenolic acid (MPA) (E and F), and 4-methylumbelliferone (4-MU) (G and H) by c-SUP and Sf9 membranes, respectively. Points represent the means of duplicate measurements (<10% variance).

6.4 Discussion

Studies of the biochemical properties of insect UDP-glycosyltransferases have shown that these enzymes typically utilize UDP-Glc as cofactor and are most likely membrane bound like vertebrate UGTs (Ahn 2011; Ahn et al. 2014; Jensen et al. 2011; Kannangara et al. 2017). Insect UDP-glycosyltransferase activity towards a wide variety of plant allelochemicals, ecdysteroid hormones, cuticle tanning precursors, and dietary flavonoids have been detected in body fat, midgut and other tissues (i.e. antenna) suggesting multiple roles in detoxification, olfaction, endobiotic modulation, and sequestration (Ahn 2011; Wang et al. 2018). Sf9 and High FiveTM (c-SUP) insect cell lines from *S. frugiperda* and *T. ni*, respectively, are commonly used commercially and in academia for recombinant protein expression of human drug metabolizing enzymes, including UGTs. This study investigated the potential endogenous glucosidation capacity of Sf9 cells and c-SUP towards several structurally diverse xenobiotics known to be glucuronidated by human UGTs. The addition of an endogenous insect steroid, 20-E, was included for comparison since glucosidation of this compound may be influenced by the absence or presence of the baculovirus expression vector.

As noted above, insect UDP-glycosyltransferases are thought to be membrane bound proteins. The glucosidation activity of Sf9 cell membranes and cytosol were compared to confirm the membrane localization of UDP-glycosyltransferase(s). Activities of membranes and cell lysate (\pm sonication) were additionally investigated to identify the optimal preparation for activity studies. 1-OHP was employed as the substrate, since this compound is efficiently metabolized by Sf9 cell (and c-SUP) UDP-glycosyltransferase(s) (see Results). The rate of 1-OHP glucosidation by enriched Sf9 cell membranes was 35- to 90-fold higher than for the cytosolic fraction. Although

minor cytosolic glucosidation cannot be discounted, it is most likely that the activity observed arises from membrane contamination. Addition of the sonication step increased the 1-OHP glucosidation activity of the membrane fraction by 34%; cytosolic 1-OHP glucosidation also increased. Comparison of the rates of 1-OHP glucosidation by Sf9 cell lysate and membranes showed, not unexpectedly, higher activity of the latter. Thus, subsequent experiments characterizing the scope and selectivity of Sf9 cell UDP-glycosyltransferase(s) employed the enriched membrane fraction (+ sonication) as the enzyme source.

The substrate selectivities of c-SUP and Sf9 membrane UDP-glycosyltransferases were investigated using a series of aglycones with either a phenolic (1-OHP, 4-MU, MOR, MPA, 1-NAP and 4-NP), an aliphatic alcohol (COD, 21-OHPr, PE and AZT), an acyl (MPA and S-NAP) or an amine (BZC, LTG and TFP) acceptor functional group. Differences were observed in the substrate selectivity of the native UDP-glycosyltransferases of c-SUP and Sf9 membranes. Amongst the phenols, rates of 1-OHP and 1-NAP glucosidation were substantially higher with c-SUP, while MPA was preferentially glucosidated by Sf9 membranes. Rates of glucosidation of 4-MU and 4-NP were similar with both enzyme sources. Phenolic compounds, including 1-NAP and 4-NP, have previously been shown to be glucosidated by a silkworm (*B. mori*) UDP-glycosyltransferase (BmUGT) recombinantly expressed in *T. ni* cells (Luque, Okano & O'Reilly 2002). BmUGT also efficiently glucosidated the flavonoids naringenin and quercetin, the phenols *p*-hydroxybiphenyl and umbelliferone, but not scopoletin or 3hydroxy steroids that included ecdysone.

The aliphatic alcohols AZT and 21-OHPr were solely or preferentially glucosidated by c-SUP, while rates of PE glucosidation were higher with Sf9 membranes. Neither

c-SUP nor Sf9 membranes glucosidated MOR and COD at the 6- (enolic) position. Sf9 microsomes glucosidated the carboxylic acid group of MPA and S-NAP, and N-glucosidated BZC, LTG and TFP. By contrast, glucosidation activity of c-SUP was not measurable (MPA, LTG and TFP) or low in comparison to Sf9 membranes (S-NAP and BZC).

Differences in the kinetics of 1-OHP, MPA and MOR (3-position) glucosidation were also observed between the two enzyme sources: 1-OHP, negative cooperative (c-SUP) and substrate inhibition (Sf9); MPA, Michaelis-Menten (c-SUP) and substrate inhibition (Sf9); and MOR, Michaelis-Menten (c-SUP) and substrate inhibition (Sf9). By contrast, 4-MU glucosidation by both enzyme sources exhibited negative cooperative kinetics. When data are considered as intrinsic clearances (calculated as K_m or S_{50} divided by V_{max} ; it should be noted that n values were close to 1 for substrates exhibiting negative cooperative kinetics), ratios (c-SUP/Sf9 membranes) were of a similar order for 1-OHP (0.73), MOR (0.95) and 4-MU (0.40), but considerably lower for MPA (0.02). By way of comparison, the K_m/S_{50} values for MOR 3-glucosidation by c-SUP and Sf9 membranes (3.42 – 4.40mM) were similar to the K_m (5.56mM) reported for MOR 3-glucosidation by human liver microsomes, although the V_{max} was lower (Chau et al. 2014). Notably, 1-OHP was glucosidated very efficiently c-SUP and Sf9 membranes, with respective CL_{int} values of 1,409 and 1,938 $\mu\text{L}/\text{min}\cdot\text{mg}$.

Taken together, the results demonstrate that c-SUP and Sf9 membranes glucosidate drugs and non-drug xenobiotics. However, differences occur between the native UDP-glycosyltransferases of c-SUP and Sf9 membranes. Although neither c-SUP nor Sf9 membranes catalyzed the 6-glucosidation of COD and MOR and CL_{int} ratios were similar for several phenols (1-OHP, MOR and 4-MU), Sf9 membranes preferentially

glucosidated MPA while the aliphatic alcohols 21-OHPr, 20-E, and AZT were glucosidated almost exclusively by c-SUP. Sf9 membranes exclusively or preferentially glucosidated the carboxylic acid- and amine- containing aglycones investigated here. The differences in scope and selectivity of structurally different compounds by Sf9 membranes and c-SUP is not surprising as the literature suggests that exposure to different chemical environments can influence chemical adaptation and hence, the ability to accept and detoxify certain chemical compounds. The enriched membrane fractions from the two different insect cell lines likely represent sources of a combination of UDP-glycosyltransferases, of which the individual enzymes are unknown and uncharacterized. The results presented have indicated that *T. ni* and Sf9 cells express UDP-glycosyltransferase(s) with distinct, but overlapping, substrate selectivities.

No glucoside conjugates were observed when 20-E and UDP-Glc were incubated for 2hr with Sf9 membranes, which suggests that the native UDP-glycosyltransferases from this cell line are not active towards 20-E. The lack of glucosidation activity with 20-E in cytosolic fractions also suggest no virally encoded EGTs were present. This is expected as the Sf9 cells were not transfected (with the baculovirus vector). Unfortunately, cytosolic fractions from Hi-FiveTM cells were not available to compare with c-SUP. As indicated previously, confirmation was provided by the supplier that ‘control’ SupersomesTM (c-SUP) were transfected with the wild-type baculovirus, but not with other genes of interest (i.e. human UGTs). Incubations of 20-E and UDP-Glc with c-SUP as the protein source generated 3 glucoside conjugates. Unlike Sf9 membranes, this suggests that native UDP-glycosyltransferases present in the *T. ni* cells conjugate 20-E, which is consistent with previous reports of endogenous ecdysteroid glucosidation detected by insect cells. However, it cannot be discounted

that soluble EGT proteins are carried over into the membrane fraction during separation.

The formation of multiple glucoside conjugates of 20-E is consistent with the presence of multiple aliphatic hydroxy groups (Figure 6.1). The most likely sites of glucosidation are positions 22, 25, 2 and 3 as they are less sterically hindered than the aliphatic hydroxy groups at positions 14 and 21 (Figure 6.1). Pis et al. (1995) demonstrated that the order of elution of the 20-E derived glucosides on RP-HPLC was: 22-glucoside, 25-glucoside, and co-elution of the 2- and 3-glucosides. Thus, it might be speculated that the peaks observed in chromatograms of incubations of 20-E with c-SUP represent the 2/3-, 22- and 25-glucosides.

S. frugiperda and *T. ni* are polyphagous species and have adapted evolutionarily to be able to digest a variety of host-plants (Gouin et al. 2017; Saremba 2018). *S. frugiperda* is able to feed on approximately 180 different plants from more than 40 plant families and hence is exposed to a wide selection of plant allelochemicals and metabolites (Giraud et al. 2015). The greater number of UDP-glycosyltransferase genes identified in polyphagous herbivore species such as *S. frugiperda* compared to more specialist or monophagous species (i.e. *M. sexta*, *B. mori*, *D. plexippus*, *H. melpomene*) suggest an increased ability to cope with a diverse range of chemicals (Gouin et al. 2017; Heidel-Fischer & Vogel 2015). For example, the honeybee with its highly specialized living environment and diet has only 12 UDP-glycosyltransferase genes and a deficiency in other conjugating enzymes (Ahn, Vogel & Heckel 2012). Gouin et al. (2017) have identified 42 UDP-glycosyltransferase sequences in *S. frugiperda* (in two different strains) and in the species *S. exigua* of the same genus, 32 UDP-glycosyltransferase genes were identified with expression responding to insecticide treatment (Hu et al.

2017). Similarly, 42 UDP-glycosyltransferase genes have been identified in *T. ni* (Herde & Howe 2014). The observed expansion of gene families involved in chemoreception and detoxification in these species is thought to explain their ability to rapidly adapt to insecticide exposure (Fang et al. 2007; Fu et al. 2017).

While it is acknowledged that too few compounds were studied here to establish meaningful structure-function relationships, it is apparent that care is required when investigating drug and chemical glucosidation by recombinant UGT enzymes expressed in insect cells. As discussed in Chapter 3, SupersomesTM expressing UGT2B4, UGT2B7, UGT2B15 and UGT2B17 catalyzed MOR 3-glucosidation, but activity was only apparent for UGT2B7 when the background activity of c-SUP was taken into account. By contrast, HEK293 cells do not express an endogenous UDP-glycosyltransferase capable of glucosidating MOR and other xenobiotics. The data emphasize the requirement for ‘control’ cell lysate/membranes in the investigation of drug and chemical glucosidation (and possibly conjugation with other sugars) by recombinant enzymes expressed in insect cells.

Chapter 7

General Summary and Conclusion

In his review of 1990, Tang noted that glucosidation is a poorly characterized metabolic pathway for drugs and other chemicals. Although there has been an increase in the number of publications investigating drug and chemical glucosidation over the last two decades (Section 1.1.6), glucosidation nevertheless remains a poorly characterized route of drug metabolism compared to glucuronidation. Of note, however, available evidence indicates that UDP-glycosyltransferase enzymes most likely play a pivotal role in drug glucosidation.

Drug metabolism as a discipline plays an important role in drug discovery and development as information gained from these studies are key to further developmental work such as optimization of lead compounds for optimal PK/PD properties, identifying active metabolites, characterizing toxicity and safety profiles, and generating preclinical data to support *in vivo* human dosing predictions (Zhang & Tang 2018). Given the requirement of Regulatory Authorities for the Pharmaceutical Industry (i.e. Therapeutic Goods Administration, Food and Drug Administration, European Medicines Agency) to completely characterize the metabolic pathways of new chemical entities, knowledge of the enzymology of drug glucosidation is important. Moreover, characterization of the role of glucosidation in the metabolism of currently used drugs is important for understanding the role of this pathway as a determinant of drug clearance and response. Both morphine, the most commonly used analgesic for the control of moderate to severe pain, and mycophenolic acid, an immunosuppressant used for the prevention of organ transplant rejection, are known to undergo both glucosidation and glucuronidation in humans. Thus, these drugs were

Chapter 7: Concluding discussion

used as ‘model’ substrates to investigate the enzymology of drug and chemical glucosidation *in vitro* and to test the central hypothesis that human glucosidation and glucuronidation are complementary pathways carried out by common UGT enzymes.

The results presented in Chapter 3 demonstrate that only UGT2B7 glucosidated morphine in addition to catalyzing morphine 3- and 6- glucuronidation as complementary metabolic pathways from reaction phenotyping studies with a panel of recombinant human UGT enzymes expressed in HEK293T cells and UGT enzyme-selective inhibitors with HLM as the enzyme source. Furthermore, while only HEK293T cells expressing UGT2B7 glucosidated morphine, Supersomes™ expressing UGT 2B4, 2B7, 2B15 and 2B17 and Control Supersomes™ (c-SUP) all formed M-3-glucoside. The reason for this and the implications for accurately characterizing human drug glucosidation is discussed further (Chapter 6). Although modest differences in morphine glycosidation was observed with the wild-type UGT2B7 (His268) and UGT2B7*2 (Tyr268), overall, they appear not to affect *in vitro* morphine glucosidation to an appreciable extent, consistent with most previous *in vitro* and *in vivo* observations with morphine glucuronidation. However, this was not the case with whole cell fission yeast biotransformation of ibuprofen to acyl glucoside and glucuronide metabolites (both *R*- and *S*- enantiomers), where the relative formation of these glycosides were dependent on the stereoisomerism of the aglycone and the UGT2B7 variants (Buchheit et al. 2011).

In vitro kinetic data (with HLM and recombinant UGTs) from experiments in the presence of individual cofactors, UDP-Glc and UDP-GlcUA, appear to over-estimate the contribution of glucosidation to morphine elimination, whereas data generated in the presence of both UDP-GlcUA and UDP-Glc (1:1) combined in equimolar

Chapter 7: Concluding discussion

concentrations are more consistent with *in vivo* observations by reducing the V_{\max} of the glucoside significantly (>80%). Hence, for the first time the work here shows that the characterization of complementary pathways by common enzyme(s) should be performed in the presence of both UDP-sugar cofactors. The reason for this over-estimation involves the selective preference for UDP-GlcUA by UGT enzyme(s) as shown by UDP-sugar cofactor inhibition studies in HLM. Therefore, in an *in vivo* or whole cell system such as the fission yeast (Buchheit et al. 2011), this relatively lower formation of drug glucosides compared to glucuronides is not likely due to direct competition for UDP-Glc in the ER pool between UGTs for drug glucosidation and the UDP-glucose glycoprotein glycosyltransferase (UGGT) protein for use in the quality control of protein folding (Meech et al. 2012a). However, the potential for further competition cannot be discounted. Interestingly, evidence suggests endogenous insect UGTs are (ER) membrane bound like human UGTs but in contrast, glucosidation seems to be the major conjugating pathway (Chapter 6).

Firstly, with morphine as the aglycone, kinetics of UDP-GlcUA (with respect to M3G and M6G formation) demonstrated binding with a higher affinity (70-83% lower S_{50}) to UGT2B7 than UDP-Glc. Mutual inhibition of cofactor (UDP-GlcUA and UDP-Glc) binding with HLM as the enzyme source further established that K_i values for UDP-GlcUA inhibition of M-3-glucosidation (0.15 - 0.18mM) were an order of magnitude higher than K_i values for UDP-Glc inhibition of morphine 3- and 6-glucuronidation (1.63 - 2.49mM) in the absence and presence of BSA, resulting in competitive displacement of UDP-Glc. As recommended for characterizing complementary pathways, the kinetic characterization of inhibitors should also be performed in the presence of both UDP-sugars. The measurement of K_i for fluconazole inhibition of

Chapter 7: Concluding discussion

morphine glucosidation in the absence and presence of UDP-GlcUA differed by 50% (increasing from 0.11 to 0.24mM). This unexpected change in K_i reflects the more complex inhibition process that involves both displacement of the aglycone (by fluconazole) and the cofactor (UDP-GlcUA displacement of UDP-Glc).

In addition to morphine, MPA is also known to be both glucuronidated and glucosidated thus, the enzymology of MPA glycosidation was additionally characterized. The results in Chapter 5 demonstrated that in contrast to morphine, MPA acyl and phenolic glucuronidation and glucosidation is complicated with multiple enzymes involved to varying degrees with many hepatic (UGT 1A9, 2B7, 1A1) and extrahepatic (UGT 1A7, 1A8, 1A10) UGTs glucosidating MPA. While UGT1A9 is the major hepatic enzyme involved in MPAGlcUA formation, UGT2B7 is the major hepatic enzyme involved in AcMPAGlcUA formation, and MPAGlc formation is shared between UGT 2B7/1A1/1A9. Similar to morphine, in HLM with MPA as the aglycone, UDP-GlcUA also bound with a higher affinity (82-95% lower S_{50}) than UDP-Glc but the K_i values for UDP-GlcUA inhibition (353 μ M) of MPAGlc formation was not only more than an order of magnitude higher than K_i values for UDP-Glc inhibition of MPAGlcUA and AcMPAGlcUA (5,274 – 25,382 μ M), but which also ranged widely (5-fold difference). This is not surprising given that the reaction phenotyping data verify that many UGT enzymes are involved in MPA glycosidation and this supports the notion that cofactor binding affinities are enzyme dependent.

The molecular basis for selective binding of UDP-GlcUA over UDP-Glc was explored with UGT2B7 as the protein. Structural understanding of the important regions

Chapter 7: Concluding discussion

involved in UDP-Glc and UDP-GlcUA binding was sought by examining the complementary relationship between morphine glucosidation and glucuronidation by UGT2B7 and residues that confer cofactor binding selectivity were identified using automated *in silico* docking with an existing 3-D homology model. Validation of this UGT2B7 model was performed through site-directed mutagenesis and enzyme activity studies. The work here has for the first-time produced homology modelling, mutagenesis and activity data for the binding of UDP-Glc in human UGT2B7. It has highlighted that there are subtle chemical differences behind the binding of UDP-Glc and UDP-GlcUA even though both UDP-Glc and UDP-GlcUA bind within the same domain of the CT of UGT2B7 and binding interactions of the UDP moiety are cofactor independent. Docking data for UDP-Glc was only slightly different to docking results for UDP-GlcUA around the sugar moiety. Docking results showed UDP-GlcUA hydrogen bonding to the NT residue Tyr33, whereas UDP-Glc was more constrained within the CT. The residues involved in the binding of the sugar differed with hydrogen bonding interactions between Asp398 (O6' hydroxyl) and Glu399 (O3' hydroxyl) identified with the glucose moiety, and Asn402 (O6'/carboxylate) and Tyr33 (O2' hydroxyl) with the glucuronic acid moiety. The development of more reliable *in silico* data (i.e. dynamic simulations) for future studies investigating NT selective binding for both acceptor and/ or donor ligands, and to generate experimental hypotheses for experimental validation, relies on the availability of a high-resolution full structure of a human UGT.

As mentioned, studies performed in Chapter 3 demonstrated that morphine glucoside was formed with the insect control cell line (c-SUP). Insect cells are commonly and widely used by academia and industry as hosts for the expression of recombinant human UGTs. Control SupersomesTM (c-SUP) exhibited high M-3-glucosidation

Chapter 7: Concluding discussion

activity but, when corrected for endogenous glucosidation activity, M-3-glucoside formation occurred with just UGT2B7. Further characterization of the endogenous glucosidation activity of enriched membranes from uninfected *S. frugiperda* (Sf9) and commercially available *T. ni* (c-SUP) cells demonstrated that c-SUP and Sf9 membranes glucosidate drugs and non-drug xenobiotics. However, differences occur between the native UDP-glycosyltransferases of c-SUP and Sf9 membranes. Although neither c-SUP nor Sf9 membranes catalyzed the 6-glucosidation of COD and MOR and CL_{int} ratios were similar for several phenols (1-OHP, MOR and 4-MU), Sf9 membranes preferentially glucosidated MPA while the aliphatic alcohols 21-OHP_r, 20-E, and AZT were glucosidated almost exclusively by c-SUP. Sf9 membranes exclusively or preferentially glucosidated the carboxylic acid- and amine- containing aglycones investigated here. The differences in scope and selectivity of structurally different compounds by Sf9 membranes and c-SUP is likely due to the chemically driven genetic adaptation that occurs after exposure to different chemical environments, thus enabling the insects the ability to accept and detoxify a wide variety of chemical compounds. Interestingly, in Chapter 3 kinetic characterization of M-3-glucosidation by c-SUP demonstrated the lack of a ‘BSA effect’; no reduction in K_m was observed as was the case with HLM and SupersomesTM-expressed UGT2B7. This indicates that the activity of the endogenous UDP-glycosyltransferase present in Hi5 cells (used for the generation of SupersomesTM) is not inhibited by long-chain unsaturated fatty acids, presumably because the native UDP-glycosyltransferases in SupersomesTM do not metabolize long-chain unsaturated fatty acids as does human UGT2B7. Hence, overall the studies in Chapters 3 and 6 demonstrate the glucosidating capacity of insect cells and a need for appropriate controls when investigating drug and chemical glucosidation (and possibly conjugation with other sugars) by

Chapter 7: Concluding discussion

recombinant enzymes expressed in insect cells. Although greater glucuronidation activity is sometimes an advantage offered by the SupersomesTM insect expression system, glucosidation cannot be accurately measured using this enzyme source due to native UDP-glycosyltransferase activity. Thus, other expression systems such as HEK293 cells or fission yeast cells are recommended along with appropriate controls (Buchheit et al. 2011).

Since results presented in this thesis support the central hypothesis that glucosidation and glucuronidation occur as complementary metabolic pathways and UGT enzymes catalyze both reactions, it is likely that glucosidation may have been overlooked as a metabolic pathway in the past. In line with recommendations by the Regulatory Authorities for the Pharmaceutical Industry to completely characterize the metabolic pathways of new chemical entities, it would seem reasonable to always investigate a potential role of glucosidation whenever glucuronidation is identified as a metabolic pathway for a drug or other chemical. Furthermore, these studies have shown that it is important to perform combined cofactor studies for characterizing the relative contributions of each pathway to elimination as single cofactor studies over-predict the contribution of glucosidation.

Appendix 1:

Summary Table of HPLC Assay Conditions

Substrate/ metabolite	Reten- tion times (min)	Mobile phase A	Mobile phase B	Precipitant (200 μ L incubation)	Calibration slope and range (μ M)	Detection method	Wave- length (λ) nm	Column	Injection volume (μ L)
AZT ¹	6.16	10mM TEA, pH 2.5 (HClO ₄)	ACN						
GAZT [§]	4.24	95% - 0 min 95% - 3 min 90% - 6 min	5% - 0 min 5% - 3 min 10% - 6 min	2 μ L HClO ₄ (70%)	6.7 (GAZT) (2.5-20)	UV	267	C18 Waters Nova- Pak 4 μ m (3.9 \times 150mm)	15
AZTGlc [†]	3.41	90% - 8 min 95% - 8.1 min	10% - 8 min 5% - 8.1 min						
BZC	10.15	10mM ammonium acetate in water, pH 5.7 (glacial AcOH)	ACN						
BZCGlc [§]	3.69	85% - 0 min 85% - 2 min 70% - 10 min 85% - 15 min	15% - 0 min 15% - 2 min 30% - 10 min 15% - 15 min	200 μ L 2% Ascorbic acid in MeOH	5.55 (BZCGlc) (2-100)	UV	291	C18 Waters Nova- Pak 4 μ m (3.9 \times 150mm)	10
COD ²	4.49	[†] 2mM TEA pH 2.7 (HClO ₄), 10% ACN	ACN						
COD-6-GlcUA [§]	3.32	100% - 0 min 100% - 5.5 min 40% - 5.6 min	0% - 0 min 0% - 5.5 min 60% - 5.6 min	2 μ L HClO ₄ (70%)	5.18 (C6G) (2.5-10)	UV	205	Phenomenex Synergi HydroRP C18 4 μ m (3.0 \times 150mm)	5
COD-6-Glc [†]	ND	40% - 6.4 min 100% - 6.5 min 100% - 15 min	60% - 6.4 min 0% - 6.5 min 0% - 15 min						

Substrate/ metabolite	Reten- tion times (min)	Mobile phase A	Mobile phase B	Precipitant (200 μ L incubation)	Calibration slope and range (μ M)	Detection method	Wave- length (λ) nm	Column	Injection volume (μ L)
20-E ³ 20-EGlc 1 [†] 20-EGlc 2 [†] 20-EGlc 3 [†]	12.50 7.08 8.75 10.54	10mM ammonium acetate in water, pH 5.7 (glacial AcOH) 90% - 0 min 90% - 1 min 85% - 8 min 85% - 13 min 90% - 15min	ACN 10% - 0 min 10% - 1 min 15% - 8 min 15% - 13 min 10% - 15min	2 μ L HClO ₄ (70%)	3.5 (20-E) (2-100)	UV	248	C18 Waters Nova- Pak 4 μ m (3.9 \times 150mm)	5
LTG ⁴ LTG-N2-GlcUA [§] LTG-Glc [†]	10.85 4.68 9.32	25mM phosphate buffer pH 7.4: ACN: TEA (95:5:0.02) 96% - 0 min 96% - 3 min 87% - 7 min 87% - 8 min 50% - 9 min 50% - 11 min 96% - 14 min	ACN 4% - 0 min 4% - 3 min 13% - 7 min 13% - 8 min 50% - 9 min 50% - 11 min 4% - 14 min	2 μ L HClO ₄ (70%)	10.5 (LTG-N2-GlcUA) (2.5-10)	UV	254	Zorbax Eclipse XDB-C8 5 μ m (4.6 \times 150mm)	20
Morphine ⁵ M3G [§] M6G [§] M-3-glucoside [*]	13.6 7.0 10.3 8.5	4mM 1-OSA, 5% ACN, 1% glacial AcOH in water, pH 2.6 96% - 0 min 91% - 10 min 91% - 11 min 75% - 11.1 min 75% - 11.9 min 96% - 12 min 96% - 20min	ACN 4% - 0 min 9% - 10 min 9% - 11 min 25% - 11.1 min 25% - 11.9 min 4% - 12 min 4% - 20min	2 μ L HClO ₄ (70%)	4.19 (M3G) (2-80) 1.90 (M6G) (0.5-16) 4.24 (M3Glucoside) (2-80)	FL	(λ_{ex}) 235 (λ_{em}) 345	C18 Waters Nova- Pak 4 μ m (3.9 \times 150mm) with guard column	10 with needle wash injection (50/50 ACN/water)

Substrate/ metabolite	Reten- tion times (min)	Mobile phase A	Mobile phase B	Precipitant (200µL incubation)	Calibration slope and range (µM)	Detection method	Wave- length (λ) nm	Column	Injection volume (µL)	
MPA ⁶	6.8	10mM ammonium acetate, pH 5.7 (glacial AcOH), 10% ACN in water	ACN	2µL HClO ₄ (70%)	11.23 (MPAGlcUA)	UV	250	C18 Waters Nova- Pak 4µm (3.9×150mm) with guard column	20 with needle wash injection (50/50 ACN/water)	
MPAGlcUA [§]	2.3		95% - 0 min		5% - 0 min					9.99 (MPAGlc)
MPAGlc [§]	4.5		95% - 1 min		5% - 1 min					9.67 (AcMPAGlcUA)
AcMPAGlcUA [§]	5.6		40% - 11 min		60% - 11 min					(all 2.5-25)
AcMPAGlc [§]	7.4	95% - 11.1 min	5% - 11.1 min							
4-MU ⁷	5.8	10mM TEA, pH 2.5 (HClO ₄), 10% ACN in water	ACN	2µL HClO ₄ (70%)	29.45 (4MUGlc)	UV	316	C18 Waters Nova- Pak 4µm (3.9×150mm)	40	
4-MUGlcUA	3.5	96% - 0 min	4% - 0 min		(1-20)					
4-MUGlc [§]	3.35	96% - 3 min	4% - 3 min							
		70% - 3.1 min	30% - 3.1 min							
		70% - 4.1 min	30% - 4.1 min							
		96% - 4.2 min	4% - 4.2 min							
1-NAP ⁸	6.57	10mM TEA, pH 2.5 (HClO ₄), 10% ACN in water	ACN	2µL HClO ₄ (70%)	5.54 (1-NAPGlcUA)	UV	290	C18 Waters Nova- Pak 4µm (3.9×150mm)	20	
1-NAPGlcUA [§]	4.67	86% - 0 min	14% - 0 min		(5-80)					
		86% - 4 min	14% - 4 min							
		36% - 4.1 min	64% - 4.1 min							
		36% - 5 min	64% - 5 min							
1-NAPGlc [†]	3.80	86% - 5.1 min	14% - 5.1 min							

Substrate/ metabolite	Reten- tion times (min)	Mobile phase A	Mobile phase B	Precipitant (200 μ L incubation)	Calibration slope and range (μ M)	Detection method	Wave- length (λ) nm	Column	Injection volume (μ L)		
S-NAP ⁹	10.52	†* 0.12% AcOH in water, 30% ACN		200 μ L 4% AcOH in MeOH	34.6 (S-NAP) (0.5-25)	UV	225	C18 Waters Nova- Pak 4 μ m (3.9 \times 150mm)	30		
S-NAP acyl GlcUA [†]	2.75										
S-NAP acyl Glc [†]	2.68										
4-NP	10.80	10mM ammonium acetate in water, pH 5.7 (glacial AcOH)	ACN	2 μ L HClO ₄ (70%)	2.78 (4-NPGlc)	UV	302	C18 Waters Nova- Pak 4 μ m (3.9 \times 150mm)	5		
4-NPGlc [§]	3.85	90% - 0 min 90% - 2 min 80% - 10 min 90% - 12 min	10% - 0 min 10% - 2 min 20% - 10 min 10% - 12 min		(2-100)						
1-OHP ¹⁰	9.95	1% formic acid, 5% ACN in water, pH 2.1	ACN	200 μ L 4% AcOH in MeOH	297 (1-OHPGlcUA) (1-20)	FL	(λ_{ex}) 242 (λ_{em}) 382	C18 Waters Nova- Pak 4 μ m (3.9 \times 150mm)	5		
1-OHPGlcUA [§]	6.00									77.5% - 0 min 77.5% - 2 min 70% - 2.1 min 70% - 7.5 min 10% - 7.6min 10% - 9 min 77.5% - 9.1min 77.5% - 12 min	22.5% - 0 min 22.5% - 2 min 30% - 2.1 min 30% - 7.5 min 90% - 7.6min 90% - 9 min 22.5% - 9.1min 22.5% - 12 min
1-OHPGlc [†]	5.65										

Substrate/ metabolite	Reten- tion times (min)	Mobile phase A	Mobile phase B	Precipitant (200µL incubation)	Calibration slope and range (µM)	Detection method	Wave- length (λ) nm	Column	Injection volume (µL)
21-OHP 21-OHPGlc [§]	10.45 6.30	10mM ammonium acetate in water, pH 5.7 (glacial AcOH) 75% - 0 min 75% - 2 min 50% - 10 min 75% - 10.1 min	ACN 25% - 0 min 25% - 2 min 50% - 10 min 25% - 10.1 min	2µL HClO ₄ (70%)	5.27 (21-OHPGlc) (2.5-100)	UV	248	C18 Waters Nova- Pak 4µm (3.9×150mm)	20
PE PEGlc [§]	8.05 5.20	10mM ammonium acetate in water, pH 5.7 (glacial AcOH) 87.5% - 0 min 87.5% - 2 min 75% - 10 min 87.5% - 10.1 min	ACN 17.5% - 0 min 17.5% - 2 min 25% - 10 min 17.5% - 10.1 min	2µL HClO ₄ (70%)	2.59 (PEGlc) (10-100)	UV	215	C18 Waters Nova- Pak 4µm (3.9×150mm)	10
TFP ^{1†} TFPGlcUA [†] TFPGlc [†]	9.95 8.99 8.73	0.1% TFA in water 69% - 0 min 52% - 9 min 69% - 9.1 min	0.1% TFA in ACN 31% - 0 min 48% - 9 min 31% - 9.1 min	200µL 4% AcOH in MeOH	35.3 (TFP) (1-10)	UV	256	Beckman ODS 5µm (4.6×250mm)	40

All assays have flow rates of 1.0mL/min unless otherwise indicated (see below).

§ Calibration standard commercially available

* In-house synthesised and validated authentic calibration standard

† No authentic calibration standard commercially available – positive and negative controls (± cofactor, substrate, protein) included with incubations and analysis

*Flow rate 1.5mL/min

†Isocratic mobile phase method

ND = not detected

¹ Adapted from Rowland et al. (2007)

² Raungrut et al. (2010)

³ Adapted from Bowalgaha et al. (2007)

⁴ Rowland et al. (2006)

⁵ Uchaipichat et al. (2011) and Chau et al. (2014)

⁶ Chapter 5 based on adaptations from Korprasertthaworn et al. (2012)

⁷ Lewis et al. (2007)

⁸ Unpublished assay developed in this laboratory adapted from Hanioka et al. (2001a)

⁹ Bowalgaha et al. (2005)

¹⁰ Kaya (2011)

¹¹ Adapted from Uchaipichat et al. (2006a)

Appendix 2:

MPA Kinetic Data for Individual Livers

Tables of derived MPA kinetic data for MPAGlcUA, MPAGlc and AcMPAGlcUA for each liver (H10, H12, H13, H40) and in the presence of single or combined cofactor conditions.

Table 1: Derived MPAGlcUA kinetic constants generated from analysis of individual livers with MPA as the variable substrate in the presence of single cofactor (UDP-GlcUA).

HLM	Model	V_{max}	K_m	K_{si}	Cl_{int}
		pmol/min/mg	μM	μM	$\mu\text{L}/\text{min}/\text{mg}$
40	MM	6238.51	111.54	-	55.93
13	MM	4868.56	113.30	-	42.97
12	MM	8238.46	165.18	-	49.88
10	MM	3112.10	93.69	-	33.22

Table 2: Derived MPAGlc kinetic constants generated from analysis of individual livers with MPA as the variable substrate in the presence of single cofactor (UDP-Glc).

HLM	Model	V_{max}	K_m	K_{si}	CL_{int}
		pmol/min/mg	μM	μM	$\mu\text{L}/\text{min}/\text{mg}$
40	MM	666.29	84.05	-	7.93
13	SI	836.06	228.91	1046.22	3.65
12	MM	891.21	151.22	-	5.89
10	SI	955.18	392.85	452.15	2.43

Table 3: Derived AcMPAGlcUA kinetic constants generated from analysis of individual livers with MPA as the variable substrate in the presence of single cofactor (UDP-GlcUA).

HLM	Model	V_{max}	K_m	K_{si}	CL_{int}
		pmol/min/mg	μ M	μ M	μ L/min/mg
40	MM	1224.14	142.46	-	8.59
13	MM	1583.21	201.26	-	7.87
12	MM	1884.57	188.71	-	9.99
10	MM	573.55	82.66	-	6.94

Table 4: Derived MPAGlcUA kinetic constants generated from analysis of individual livers with MPA as the variable substrate in the presence of combined cofactors (UDP-Glc and UDP-GlcUA in 1:1).

HLM	Model	V_{max}	K_m	K_{si}	Cl_{int}
		pmol/min/mg	μ M	μ M	μ L/min/mg
40	MM	6238.51	111.54	-	55.93
13	MM	4868.56	113.30	-	42.97
12	MM	8238.46	165.18	-	49.88
10	MM	3112.10	93.69	-	33.22

Table 5: Derived MPAGlc kinetic constants generated from analysis of individual livers with MPA as the variable substrate in the presence of combined cofactors (UDP-Glc and UDP-GlcUA in 1:1).

HLM	Model	V_{\max}	K_m	K_{si}	CL_{int}
		pmol/min/mg	μM	μM	$\mu\text{L}/\text{min}/\text{mg}$
40	MM	77.64	158.16	-	0.49
13	SI	171.64	307.61	5092.37	0.56
12	SI	182.31	243.25	2800.67	0.75
10	-	ND	ND	-	-

ND: not determined

Table 6: Derived AcMPAGlcUA kinetic constants generated from analysis of individual livers with MPA as the variable substrate in the presence of combined cofactors (UDP-Glc and UDP-GlcUA in 1:1).

HLM	Model	V_{\max}	K_m	K_{si}	CL_{int}
		pmol/min/mg	μM	μM	$\mu\text{L}/\text{min}/\text{mg}$
40	MM	987.85	124.53	-	7.93
13	SI	1126.91	230.66	2674.17	4.89
12	SI	1593.01	242.03	1166.7	6.58
10	MM	730.81	226.42	-	3.23

Bibliography

Abd Rahman, AN, Tett, SE & Staatz, CE 2013, 'Clinical pharmacokinetics and pharmacodynamics of mycophenolate in patients with autoimmune disease', *Clin Pharmacokinet*, vol. 52, no. 5, pp. 303-331.

Ahmad, B & Powell, JW 1988, 'N1-glucosides as urinary metabolites of sulphadimidine, sulphamerazine and sulphamethoxazole', *Eur J Drug Metab Pharmacokinet*, vol. 13, no. 3, pp. 177-183.

Ahn, SJ 2011, UDP-glycosyltransferases: Comparative genomic analysis in insects and capsaicin glucosylation in *Helicoverpa* spp., Master's, Friedrich Schiller Universität Jena.

Ahn, SJ, Dermauw, W, Wybouw, N, Heckel, DG & Van Leeuwen, T 2014, 'Bacterial origin of a diverse family of UDP-glycosyltransferase genes in the *Tetranychus urticae* genome', *Insect Biochem Mol Biol*, vol. 50, no. pp. 43-57.

Ahn, SJ, Vogel, H & Heckel, DG 2012, 'Comparative analysis of the UDP-glycosyltransferase multigene family in insects', *Insect Biochem Mol Biol*, vol. 42, no. 2, pp. 133-147.

Alary, J, Cravedi, JP, Baradat, M & Carrera, G 1992, 'Mechanism of cadmium-decreased glucuronidation in the rat', *Biochemical Pharmacology*, vol. 44, no. 11, pp. 2139-2147.

Allison, AC, Hovi, T, Watts, RW & Webster, AD 1975, 'Immunological observations on patients with Lesch-Nyhan syndrome, and on the role of de-novo purine synthesis in lymphocyte transformation', *Lancet*, vol. 2, no. 7946, pp. 1179-1183.

Allison, AC, Hovi, T, Watts, RW & Webster, AD 1977, 'The role of de novo purine synthesis in lymphocyte transformation', *Ciba Found Symp*, vol., no. 48, pp. 207-224.

Altmann, F, Staudacher, E, Wilson, IB & Marz, L 1999, 'Insect cells as hosts for the expression of recombinant glycoproteins', *Glycoconj J*, vol. 16, no. 2, pp. 109-123.

Aw, TY & Jones, DP 1982, 'Direct determination of UDP-glucuronic acid in cell extracts by high-performance liquid chromatography', *Analytical Biochemistry*, vol. 127, no. pp. 32-36.

Barbier, O, Girard, C, Breton, R, Belanger, A & Hum, DW 2000a, 'N-glycosylation and residue 96 are involved in the functional properties of UDP-glucuronosyltransferase enzymes', *Biochemistry*, vol. 39, no. 38, pp. 11540-11552.

Barbier, O, Turgeon, D, Girard, C, Green, MD, Tephly, TR, Hum, DW & Belanger, A 2000b, '3'-azido-3'-deoxythymidine (AZT) is glucuronidated by human UDP-glucuronosyltransferase 2B7 (UGT2B7)', *Drug Metab Dispos*, vol. 28, no. 5, pp. 497-502.

- Barcellos, GB, Pauli, I, Caceres, RA, Timmers, LF, Dias, R & de Azevedo, WF, Jr. 2008, 'Molecular modeling as a tool for drug discovery', *Curr Drug Targets*, vol. 9, no. 12, pp. 1084-1091.
- Barnaba, C, Gentry, K, Sumangala, N & Ramamoorthy, A 2017, 'The catalytic function of cytochrome P450 is entwined with its membrane-bound nature', *F1000Research*, vol. 6, no. pp. 662-662.
- Barre, L, Fournel-Gigleux, S, Finel, M, Netter, P, Magdalou, J & Ouzzine, M 2007, 'Substrate specificity of the human UDP-glucuronosyltransferase UGT2B4 and UGT2B7. Identification of a critical aromatic amino acid residue at position 33', *FEBS J*, vol. 274, no. 5, pp. 1256-1264.
- Barta, I, Boros, S., Ambrus, G., Horv, G., Szab, A., Szab, I., Jekkel, A., Knya, A., Mzes, J., Salt, J., Somogyi, G. 2002, *Process for the preparation of mycophenolic acid and derivatives thereof*, Vol. EP 1 216 237 B1, Budapest.
- Basu, NK, Kole, L, Kubota, S & Owens, IS 2004, 'Human UDP-glucuronosyltransferases show atypical metabolism of mycophenolic acid and inhibition by curcumin', *Drug Metab Dispos*, vol. 32, no. 7, pp. 768-773.
- Battaglia, E, Senay, C, Fournel-Gigleux, S, Herber, R, Siest, G & Magdalou, J 1994, 'The chemical modification of human liver UDP-glucuronosyltransferase UGT1*6 reveals the involvement of a carboxyl group in catalysis', *FEBS Lett*, vol. 346, no. 2-3, pp. 146-150.
- Beaulieu, M, Levesque, E, Hum, DW & Belanger, A 1996, 'Isolation and characterization of a novel cDNA encoding a human UDP-glucuronosyltransferase active on C19 steroids', *J Biol Chem*, vol. 271, no. 37, pp. 22855-22862.
- Beaulieu, M, Levesque, E, Hum, DW & Belanger, A 1998, 'Isolation and characterization of a human orphan UDP-glucuronosyltransferase, UGT2B11', *Biochem Biophys Res Commun*, vol. 248, no. 1, pp. 44-50.
- Belfer, I 2013, 'Nature and nurture of human pain', *Scientifica (Cairo)*, vol. 2013, no. pp. 415279.
- Bennett, WM 2003, 'Immunosuppression with mycophenolic acid: one size does not fit all', *J Am Soc Nephrol*, vol. 14, no. 9, pp. 2414-2416.
- Benoit-Biancamano, MO, Connelly, J, Villeneuve, L, Caron, P & Guillemette, C 2009, 'Deferiprone glucuronidation by human tissues and recombinant UDP glucuronosyltransferase 1A6: an in vitro investigation of genetic and splice variants', *Drug Metab Dispos*, vol. 37, no. 2, pp. 322-329.
- Berman, HM, Westbrook, J, Feng, Z, Gilliland, G, Bhat, TN, Weissig, H, Shindyalov, IN & Bourne, PE 2000, 'The Protein Data Bank', *Nucleic Acids Res*, vol. 28, no. 1, pp. 235-242.

Bernard, O & Guillemette, C 2004, 'The main role of UGT1A9 in the hepatic metabolism of mycophenolic acid and the effects of naturally occurring variants', *Drug Metab Dispos*, vol. 32, no. 8, pp. 775-778.

Bernard, O, Tojcic, J, Journault, K, Perusse, L & Guillemette, C 2006, 'Influence of nonsynonymous polymorphisms of UGT1A8 and UGT2B7 metabolizing enzymes on the formation of phenolic and acyl glucuronides of mycophenolic acid', *Drug Metab Dispos*, vol. 34, no. 9, pp. 1539-1545.

Bhasker, CR, McKinnon, W, Stone, A, Lo, ACT, Kubota, T, Ishizaki, T & Miners, JO 2000, 'Genetic polymorphism of UDP-glucuronosyltransferase 2B7 (UGT2B7) at amino acid 268: ethnic diversity of alleles and potential clinical significance', *Pharmacogenetics*, vol. 10, no. 8, pp. 679-685.

Bhatt, DK, Mehrotra, A, Gaedigk, A, Chapa, R, Basit, A, Zhang, H, Choudhari, P, Boberg, M, Pearce, RE, Gaedigk, R, Broeckel, U, Leeder, JS & Prasad, B 2019, 'Age- and Genotype-Dependent Variability in the Protein Abundance and Activity of Six Major Uridine Diphosphate-Glucuronosyltransferases in Human Liver', *Clin Pharmacol Ther*, vol. 105, no. 1, pp. 131-141.

Birkett, DJ 2002, *Pharmacokinetics made easy*, McGraw-Hill Australia Pty Limited, North Ryde NSW.

Birkinshaw, JH, Raistrick, H & Ross, DJ 1952, 'Studies in the biochemistry of micro-organisms. 86. The molecular constitution of mycophenolic acid, a metabolic product of *Penicillium Brevi-compactum* Dierckx. Part III. Further observations on the structural formula for mycophenolic acid', *Biochem J*, vol. 50, no. 5, pp. 630-634.

Boase, S & Miners, JO 2002, 'In vitro-in vivo correlations for drugs eliminated by glucuronidation: Investigations with the model substrate zidovudine', *British Journal of Clinical Pharmacology*, vol. 54, no. 5, pp. 493-503.

Bock, KW 2015, 'The UDP-glycosyltransferase (UGT) superfamily expressed in humans, insects and plants: Animal-plant arms-race and co-evolution', *Biochem Pharmacol*, vol., no. pp.

Bolam, DN, Roberts, S, Proctor, MR, Turkenburg, JP, Dodson, EJ, Martinez-Fleites, C, Yang, M, Davis, BG, Davies, GJ & Gilbert, HJ 2007, 'The crystal structure of two macrolide glycosyltransferases provides a blueprint for host cell antibiotic immunity', *Proc Natl Acad Sci U S A*, vol. 104, no. 13, pp. 5336-5341.

Bosma, PJ, Seppen, J, Goldhoorn, B, Bakker, C, Oude Elferink, RP, Chowdhury, JR, Chowdhury, NR & Jansen, PL 1994, 'Bilirubin UDP-glucuronosyltransferase 1 is the only relevant bilirubin glucuronidating isoform in man', *J Biol Chem*, vol. 269, no. 27, pp. 17960-17964.

Bossuyt, X & Blanckaert, N 1994, 'Carrier-mediated transport of intact UDP-glucuronic acid into the lumen of endoplasmic-reticulum-derived vesicles from rat liver', *Biochemical Journal*, vol. 302, no. Pt 1, pp. 261-269.

Bossuyt, X & Blanckaert, N 1997, 'Carrier-mediated transport of uridine diphosphoglucuronic acid across the endoplasmic reticulum membrane is a prerequisite for UDP-glucuronosyltransferase activity in rat liver', *Biochemical Journal*, vol. 323, no. Pt 3, pp. 645-648.

Bourasset, F & Scherrmann, JM 2006, 'Carrier-mediated processes at several rat brain interfaces determine the neuropharmacokinetics of morphine and morphine-6-beta-D-glucuronide', *Life Sci*, vol. 78, no. 20, pp. 2302-2314.

Bowalgaha, K, Elliot, DJ, Mackenzie, PI, Knights, KM & Miners, JO 2007, 'The glucuronidation of Delta(4)-3-keto C19- and C21-hydroxysteroids by human liver microsomal and recombinant UDP-glucuronosyltransferases (UGTs): 6 alpha- and 21-hydroxyprogesterone are selective substrates for UGT2B7', *Drug Metabolism and Disposition*, vol. 35, no. 3, pp. 363-370.

Bowalgaha, K, Elliot, DJ, Mackenzie, PI, Knights, KM, Swedmark, S & Miners, JO 2005, 'S-Naproxen and desmethylnaproxen glucuronidation by human liver microsomes and recombinant human UDP-glucuronosyltransferases (UGT): role of UGT2B7 in the elimination of naproxen', *British Journal of Clinical Pharmacology*, vol. 60, no. 4, pp. 423-433.

Bowalgaha, K & Miners, JO 2001, 'The glucuronidation of mycophenolic acid by human liver, kidney and jejunum microsomes', *British Journal of Clinical Pharmacology*, vol. 52, no. 5, pp. 605-609.

Bowersox, SS, Lightning, LK, Rao, S, Palme, M, Ellis, D, Coleman, R, Davies, AM, Kumaraswamy, P & Druzgala, P 2011, 'Metabolism and pharmacokinetics of naronapride (ATI-7505), a serotonin 5-HT(4) receptor agonist for gastrointestinal motility disorders', *Drug Metab Dispos*, vol. 39, no. 7, pp. 1170-1180.

Boyd, RA & Lalonde, RL 2007, 'Nontraditional approaches to first-in-human studies to increase efficiency of drug development: will microdose studies make a significant impact?', *Clin Pharmacol Ther*, vol. 81, no. 1, pp. 24-26.

Brazier-Hicks, M, Offen, WA, Gershater, MC, Revett, TJ, Lim, EK, Bowles, DJ, Davies, GJ & Edwards, R 2007, 'Characterization and engineering of the bifunctional N- and O-glucosyltransferase involved in xenobiotic metabolism in plants', *Proc Natl Acad Sci U S A*, vol. 104, no. 51, pp. 20238-20243.

Breton, C & Imberty, A 1999, 'Structure/function studies of glycosyltransferases', *Curr Opin Struct Biol*, vol. 9, no. 5, pp. 563-571.

Breton, C, Mucha, J & Jeanneau, C 2001, 'Structural and functional features of glycosyltransferases', *Biochimie*, vol. 83, no. 8, pp. 713-718.

Breton, C, Snajdrova, L, Jeanneau, C, Koca, J & Imberty, A 2006, 'Structures and mechanisms of glycosyltransferases', *Glycobiology*, vol. 16, no. 2, pp. 29R-37R.

Buchheit, D, Dragan, CA, Schmitt, EI & Bureik, M 2011, 'Production of ibuprofen acyl glucosides by human UGT2B7', *Drug Metab Dispos*, vol. 39, no. 12, pp. 2174-2181.

Buckley, DB & Klaassen, CD 2007, 'Tissue- and Gender-Specific mRNA Expression of UDP-Glucuronosyltransferases (UGTs) in Mice', *Drug Metabolism and Disposition*, vol. 35, no. 1, pp. 121-127.

Bullingham, RES, Nicholls, AJ & Kamm, BR 1998, 'Clinical Pharmacokinetics of Mycophenolate Mofetil', *Clinical Pharmacokinetics*, vol. 34, no. 6, pp. 429-455.

Burchell, B & Blanckaert, N 1984, 'Bilirubin mono- and di-glucuronide formation by purified rat liver microsomal bilirubin UDP-glucuronyltransferase', *Biochemical Journal*, vol. 223, no. 2, pp. 461-465.

Carrupt, PA, Testa, B, Bechalany, A, el Tayar, N, Descas, P & Perrissoud, D 1991, 'Morphine 6-glucuronide and morphine 3-glucuronide as molecular chameleons with unexpected lipophilicity', *J Med Chem*, vol. 34, no. 4, pp. 1272-1275.

Chau, N, Elliot, DJ, Lewis, BC, Burns, K, Johnston, MR, Mackenzie, PI & Miners, JO 2014, 'Morphine glucuronidation and glucosidation represent complementary metabolic pathways that are both catalyzed by UDP-glucuronosyltransferase 2B7: kinetic, inhibition, and molecular modeling studies', *J Pharmacol Exp Ther*, vol. 349, no. 1, pp. 126-137.

Chen, M, LeDuc, B, Kerr, S, Howe, D & Williams, DA 2010, 'Identification of human UGT2B7 as the major isoform involved in the O-glucuronidation of chloramphenicol', *Drug Metab Dispos*, vol. 38, no. 3, pp. 368-375.

Chen, XY, Zhao, LM & Zhong, DF 2003, 'A novel metabolic pathway of morphine: formation of morphine glucosides in cancer patients', *British Journal of Clinical Pharmacology*, vol. 55, no. 6, pp. 570-578.

Christrup, LL 1997, 'Morphine metabolites', *Acta Anaesthesiol Scand*, vol. 41, no. 1 Pt 2, pp. 116-122.

Chu, X, Bleasby, K & Evers, R 2013, 'Species differences in drug transporters and implications for translating preclinical findings to humans', *Expert Opin Drug Metab Toxicol*, vol. 9, no. 3, pp. 237-252.

Chu, X, Liao, M, Shen, H, Yoshida, K, Zur, AA, Arya, V, Galetin, A, Giacomini, KM, Hanna, I, Kusuhara, H, Lai, Y, Rodrigues, D, Sugiyama, Y, Zamek-Gliszczynski, MJ & Zhang, L 2018, 'Clinical Probes and Endogenous Biomarkers as Substrates for Transporter Drug-Drug Interaction Evaluation: Perspectives From the International Transporter Consortium', *Clinical Pharmacology & Therapeutics*, vol. 104, no. 5, pp. 836-864.

Coffman, BL, Kearney, WR, Goldsmith, S, Knosp, BM & Tephly, TR 2003, 'Opioids bind to the amino acids 84 to 118 of UDP-glucuronosyltransferase UGT2B7', *Mol Pharmacol*, vol. 63, no. 2, pp. 283-288.

Coffman, BL, Kearney, WR, Green, MD, Lowery, RG & Tephly, TR 2001, 'Analysis of opioid binding to UDP-glucuronosyltransferase 2B7 fusion proteins using nuclear magnetic resonance spectroscopy', *Mol Pharmacol*, vol. 59, no. 6, pp. 1464-1469.

- Coffman, BL, King, CD, Rios, GR & Tephly, TR 1998, 'The glucuronidation of opioids, other xenobiotics, and androgens by human UGT2B7Y(268) and UGT2B7H(268)', *Drug Metab Dispos*, vol. 26, no. 1, pp. 73-77.
- Coffman, BL, Rios, GR, King, CD & Tephly, TR 1997, 'Human UGT2B7 catalyzes morphine glucuronidation', *Drug Metabolism and Disposition*, vol. 25, no. 1, pp. 1-4.
- Condreay, JP & Kost, TA 2007, 'Baculovirus expression vectors for insect and mammalian cells', *Curr Drug Targets*, vol. 8, no. 10, pp. 1126-1131.
- Court, MH 2005, 'Isoform-selective probe substrates for in vitro studies of human UDP-glucuronosyltransferases', *Methods Enzymol*, vol. 400, no. pp. 104-116.
- Court, MH, Duan, SX, Guillemette, C, Journault, K, Krishnaswamy, S, von Moltke, LL & Greenblatt, DJ 2002, 'Stereoselective Conjugation of Oxazepam by Human UDP-Glucuronosyltransferases (UGTs): *S*-Oxazepam Is Glucuronidated by UGT2B15, While *R*-Oxazepam Is Glucuronidated by UGT2B7 and UGT1A9', *Drug Metabolism and Disposition*, vol. 30, no. 11, pp. 1257-1265.
- Court, MH, Hazarika, S, Krishnaswamy, S, Finel, M & Williams, JA 2008, 'Novel polymorphic human UDP-glucuronosyltransferase 2A3: cloning, functional characterization of enzyme variants, comparative tissue expression, and gene induction', *Mol Pharmacol*, vol. 74, no. 3, pp. 744-754.
- Court, MH, Krishnaswamy, S, Hao, Q, Duan, SX, Patten, CJ, Von Moltke, LL & Greenblatt, DJ 2003, 'Evaluation of 3'-azido-3'-deoxythymidine, morphine, and codeine as probe substrates for UDP-glucuronosyltransferase 2B7 (UGT2B7) in human liver microsomes: Specificity and influence of the UGT2B7*2 polymorphism', *Drug Metabolism and Disposition*, vol. 31, no. 9, pp. 1125-1133.
- Coutinho, PM, Deleury, E, Davies, GJ & Henrissat, B 2003, 'An evolving hierarchical family classification for glycosyltransferases', *J Mol Biol*, vol. 328, no. 2, pp. 307-317.
- Csala, M, Marcolongo, P, Lizák, B, Senesi, S, Margittai, É, Fulceri, R, Magyar, JÉ, Benedetti, A & Bánhegyi, G 2007, 'Transport and transporters in the endoplasmic reticulum', *Biochimica et Biophysica Acta (BBA) - Biomembranes*, vol. 1768, no. 6, pp. 1325-1341.
- Dahmane, E, Boccard, J, Csajka, C, Rudaz, S, Decosterd, L, Genin, E, Duretz, B, Bromirski, M, Zaman, K, Testa, B & Rochat, B 2014, 'Quantitative monitoring of tamoxifen in human plasma extended to 40 metabolites using liquid-chromatography high-resolution mass spectrometry: new investigation capabilities for clinical pharmacology', *Anal Bioanal Chem*, vol. 406, no. 11, pp. 2627-2640.
- Dai, P, Luo, F, Wang, Y, Jiang, H, Wang, L, Zhang, G, Zhu, L, Hu, M, Wang, X, Lu, L & Liu, Z 2015, 'Species- and gender-dependent differences in the glucuronidation of a flavonoid glucoside and its aglycone determined using expressed UGT enzymes and microsomes', *Biopharmaceutics & Drug Disposition*, vol. 36, no. 9, pp. 622-635.

De Gregori, S, De Gregori, M, Ranzani, GN, Allegri, M, Minella, C & Regazzi, M 2012, 'Morphine metabolism, transport and brain disposition', *Metab Brain Dis*, vol. 27, no. 1, pp. 1-5.

de Winter, BCM, Mathot, RAA, Sombogaard, F, Vulto, AG & van Gelder, T 2011, 'Nonlinear Relationship between Mycophenolate Mofetil Dose and Mycophenolic Acid Exposure: Implications for Therapeutic Drug Monitoring', *Clinical Journal of the American Society of Nephrology*, vol. 6, no. 3, pp. 656-663.

Di, L 2014, 'The role of drug metabolizing enzymes in clearance', *Expert Opinion on Drug Metabolism & Toxicology*, vol. 10, no. 3, pp. 379-393.

Dietis, N, Rowbotham, DJ & Lambert, DG 2011, 'Opioid receptor subtypes: fact or artifact?', *BJA: British Journal of Anaesthesia*, vol. 107, no. 1, pp. 8-18.

Dills, RL, Howell, SR & Klaassen, CD 1987, 'Hepatic UDP-glucose and UDP-glucuronic acid synthesis rates in rats during a reduced energy state', *Drug Metab Dispos*, vol. 15, no. 3, pp. 281-288.

Dong, D, Ako, R, Hu, M & Wu, B 2012, 'Understanding substrate selectivity of human UDP-glucuronosyltransferases through QSAR modeling and analysis of homologous enzymes', *Xenobiotica*, vol. 42, no. 8, pp. 808-820.

Dong, Q, Xing, W, Fu, F, Liu, Z, Wang, J, Liang, X, Zhou, X, Yang, Q, Zhang, W, Gao, F, Wang, S & Zhang, H 2016, 'Tetrahydroxystilbene Glucoside Inhibits Excessive Autophagy and Improves Microvascular Endothelial Dysfunction in Prehypertensive Spontaneously Hypertensive Rats', *The American Journal of Chinese Medicine*, vol. 44, no. 07, pp. 1393-1412.

Dostalek, M, Court, MH, Hazarika, S & Akhlaghi, F 2011, 'Diabetes mellitus reduces activity of human UDP-glucuronosyltransferase 2B7 in liver and kidney leading to decreased formation of mycophenolic acid acyl-glucuronide metabolite', *Drug Metab Dispos*, vol. 39, no. 3, pp. 448-455.

Drozdzik, M, Busch, D, Lapczuk, J, Muller, J, Ostrowski, M, Kurzawski, M & Oswald, S 2018, 'Protein Abundance of Clinically Relevant Drug-Metabolizing Enzymes in the Human Liver and Intestine: A Comparative Analysis in Paired Tissue Specimens', *Clin Pharmacol Ther*, vol. 104, no. 3, pp. 515-524.

Dubois, SG, Beaulieu, M, Lévesque, É, Hum, DW & Bélanger, A 1999, 'Alteration of human UDP-glucuronosyltransferase UGT2B17 regio-specificity by a single amino acid substitution' Edited by M. F. Moody', *Journal of Molecular Biology*, vol. 289, no. 1, pp. 29-39.

Due, MR, Piekarz, AD, Wilson, N, Feldman, P, Ripsch, MS, Chavez, S, Yin, H, Khanna, R & White, FA 2012, 'Neuroexcitatory effects of morphine-3-glucuronide are dependent on Toll-like receptor 4 signaling', *J Neuroinflammation*, vol. 9, no. pp. 200.

Duggan, DE, Baldwin, JJ, Arison, BH & Rhodes, RE 1974, 'N-glucoside formation as a detoxification mechanism in mammals', *J Pharmacol Exp Ther*, vol. 190, no. 3, pp. 563-569.

Edmondson, AC, Bedoukian, EC, Deardorff, MA, McDonald-McGinn, DM, Li, X, He, M & Zackai, EH 2017, 'A human case of SLC35A3-related skeletal dysplasia', *Am J Med Genet A*, vol. 173, no. 10, pp. 2758-2762.

Edvardson, S, Ashikov, A, Jalas, C, Sturiale, L, Shaag, A, Fedick, A, Treff, NR, Garozzo, D, Gerardy-Schahn, R & Elpeleg, O 2013, 'Mutations in SLC35A3 cause autism spectrum disorder, epilepsy and arthrogyposis', *Journal of Medical Genetics*, vol. 50, no. 11, pp. 733-739.

Ethell, BT, Anderson, GD & Burchell, B 2003, 'The effect of valproic acid on drug and steroid glucuronidation by expressed human UDP-glucuronosyltransferases', *Biochem Pharmacol*, vol. 65, no. 9, pp. 1441-1449.

Evans, OP & O'Reilly, DR 1998, 'Purification and kinetic analysis of a baculovirus ecdysteroid UDP-glucosyltransferase', *Biochemical Journal*, vol. 330, no. Pt 3, pp. 1265-1270.

Evans, WE & Relling, MV 1999, 'Pharmacogenomics: translating functional genomics into rational therapeutics', *Science*, vol. 286, no. 5439, pp. 487-491.

Fallon, JK, Neubert, H, Hyland, R, Goosen, TC & Smith, PC 2013, 'Targeted Quantitative Proteomics for the Analysis of 14 UGT1As and -2Bs in Human Liver Using NanoUPLC-MS/MS with Selected Reaction Monitoring', *Journal of Proteome Research*, vol. 12, no. 10, pp. 4402-4413.

Fang, X-K, Huang, D-F, Wang, Z-X, Wan, C-L, Sun, T, Xu, W-J, Liu, C-Y, Zhou, P & Qiao, Z-D 2007, 'Identification of the proteins related to cytochrome P450 induced by fenvalerate in a *Trichoplusia ni* cell line', *Cell Biology and Toxicology*, vol. 23, no. 6, pp. 445.

Feng, Y, He, X, Yang, Y, Chao, D, Lazarus, LH & Xia, Y 2012, 'Current Research on Opioid Receptor Function', *Curr Drug Targets*, vol. 13, no. 2, pp. 230-246.

Field, JM, Kudenchuk, PJ, O'Connor, R & VandenHoek, T 2012, *The Textbook of Emergency Cardiovascular Care and CPR*, Wolters Kluwer Health.

Finel, M, Li, X, Gardner-Stephen, D, Bratton, S, Mackenzie, PI & Radominska-Pandya, A 2005, 'Human UDP-Glucuronosyltransferase 1A5: Identification, expression, and activity', *Journal of Pharmacology and Experimental Therapeutics*, vol. 315, no. 3, pp. 1143-1149.

Fisher, MB, Campanale, K, Ackermann, BL, VandenBranden, M & Wrighton, SA 2000, 'In vitro glucuronidation using human liver microsomes and the pore-forming peptide alamethicin', *Drug Metab Dispos*, vol. 28, no. 5, pp. 560-566.

Fladvad, T, Klepstad, P, Langaas, M, Dale, O, Kaasa, S, Caraceni, A & Skorpen, F 2013, 'Variability in UDP-glucuronosyltransferase genes and morphine metabolism: observations from a cross-sectional multicenter study in advanced cancer patients with pain', *Pharmacogenet Genomics*, vol. 23, no. 3, pp. 117-126.

Flores-Diaz, M, Alape-Giron, A, Persson, B, Pollesello, P, Moos, M, von Eichel-Streiber, C, Thelestam, M & Florin, I 1997, 'Cellular UDP-glucose deficiency caused by a single point mutation in the UDP-glucose pyrophosphorylase gene', *Journal of Biological Chemistry*, vol. 272, no. 38, pp. 23784-23791.

Floudas, C, Fung, H, McAllister, S, Monnigmann, M & Rajgaria, R 2006, 'Advances in protein structure prediction and do novo protein design: A review', *Chemical Engineering Science*, vol. 61, no. pp. 966-988.

Foti, RS, Fisher, MB & Lyubimov, AV 2012, 'UDP-Glucuronosyltransferases: Pharmacogenetics, Functional Characterization, and Clinical Relevance', in *Encyclopedia of Drug Metabolism and Interactions*, eds, John Wiley & Sons, Inc.

Frances, B, Gout, R, Monsarrat, B, Cros, J & Zajac, JM 1992, 'Further evidence that morphine-6 beta-glucuronide is a more potent opioid agonist than morphine', *J Pharmacol Exp Ther*, vol. 262, no. 1, pp. 25-31.

Francke, S, Mamidi, RNVS, Solanki, B, Scheers, E, Jadwin, A, Favis, R & Devineni, D 2015, 'In vitro metabolism of canagliflozin in human liver, kidney, intestine microsomes, and recombinant uridine diphosphate glucuronosyltransferases (UGT) and the effect of genetic variability of UGT enzymes on the pharmacokinetics of canagliflozin in humans', *The Journal of Clinical Pharmacology*, vol. 55, no. 9, pp. 1061-1072.

Freeze, HH & Elbein, AD 2009, *Glycosylation Precursors in Essentials of Glycobiology*, eds A Varki, RD Cummings, JD Esko, HH Freeze, P Stanley, CR Bertozzi, GW Hart & ME Etzler, Cold Spring Harbour Laboratory Press, California.

Fremont, JJ, Wang, RW & King, CD 2005, 'Coimmunoprecipitation of UDP-glucuronosyltransferase isoforms and cytochrome P450 3A4', *Mol Pharmacol*, vol. 67, no. 1, pp. 260-262.

Fu, Y, Yang, Y, Zhang, H, Farley, G, Wang, J, Quarles, KA, Weng, Z & Zamore, PD 2017, *The genome of Trichoplusia ni, an agricultural pest and novel model for small RNA biology in bioRxiv*,

Fujita, K, Ando, Y, Yamamoto, W, Miya, T, Endo, H, Sunakawa, Y, Araki, K, Kodama, K, Nagashima, F, Ichikawa, W, Narabayashi, M, Akiyama, Y, Kawara, K, Shiomi, M, Ogata, H, Iwasa, H, Okazaki, Y, Hirose, T & Sasaki, Y 2010, 'Association of UGT2B7 and ABCB1 genotypes with morphine-induced adverse drug reactions in Japanese patients with cancer', *Cancer Chemother Pharmacol*, vol. 65, no. 2, pp. 251-258.

Fujiwara, R & Itoh, T 2014, 'Extensive protein-protein interactions involving UDP-glucuronosyltransferase (UGT) 2B7 in human liver microsomes', *Drug Metab Pharmacokinet*, vol. 29, no. 3, pp. 259-265.

Fujiwara, R, Nakajima, M, Yamamoto, T, Nagao, H & Yokoi, T 2009, 'In silico and in vitro approaches to elucidate the thermal stability of human UDP-glucuronosyltransferase (UGT) 1A9', *Drug Metab Pharmacokinet*, vol. 24, no. 3, pp. 235-244.

Fujiwara, R, Yoda, E & Tukey, RH 2018, 'Species differences in drug glucuronidation: Humanized UDP-glucuronosyltransferase 1 mice and their application for predicting drug glucuronidation and drug-induced toxicity in humans', *Drug Metabolism and Pharmacokinetics*, vol. 33, no. 1, pp. 9-16.

Fujiwara, R, Yokoi, T & Nakajima, M 2016, *Structure and Protein-Protein Interactions of Human UDP-Glucuronosyltransferases*.

Fujiyama, N, Miura, M, Satoh, S, Inoue, K, Kagaya, H, Saito, M, Habuchi, T & Suzuki, T 2009, 'Influence of carboxylesterase 2 genetic polymorphisms on mycophenolic acid pharmacokinetics in Japanese renal transplant recipients', *Xenobiotica*, vol. 39, no. 5, pp. 407-414.

Gaganis, P, Miners, JO, Brennan, JS, Thomas, A & Knights, KM 2007, 'Human renal cortical and medullary UDP-glucuronosyltransferases (UGTs): immunohistochemical localization of UGT2B7 and UGT1A enzymes and kinetic characterization of S-naproxen glucuronidation', *J Pharmacol Exp Ther*, vol. 323, no. 2, pp. 422-430.

Galetin, A, Gertz, M & Houston, JB 2010, 'Contribution of Intestinal Cytochrome P450-Mediated Metabolism to Drug-Drug Inhibition and Induction Interactions', *Drug Metabolism and Pharmacokinetics*, vol. 25, no. 1, pp. 28-47.

Gan, J, Ma, S & Zhang, D 2016, 'Non-cytochrome P450-mediated bioactivation and its toxicological relevance', *Drug Metabolism Reviews*, vol., no. pp. 1-29.

Ghosal, A, Hapangama, N, Yuan, Y, Achanfuo-Yeboah, J, Iannucci, R, Chowdhury, S, Alton, K, Patrick, JE & Zbaida, S 2004, 'Identification of human UDP-glucuronosyltransferase enzyme (s) responsible for the glucuronidation of posaconazole (Noxafil)', *Drug Metabolism and Disposition*, vol. 32, no. 2, pp. 267-271.

Ghosh, D, Griswold, J, Erman, M & Pangborn, W 2010, 'X-ray structure of human aromatase reveals an androgen-specific active site', *J Steroid Biochem Mol Biol*, vol. 118, no. 4-5, pp. 197-202.

Giacomini, KM, Huang, SM, Tweedie, DJ, Benet, LZ, Brouwer, KL, Chu, X, Dahlin, A, Evers, R, Fischer, V, Hillgren, KM, Hoffmaster, KA, Ishikawa, T, Keppler, D, Kim, RB, Lee, CA, Niemi, M, Polli, JW, Sugiyama, Y, Swaan, PW, Ware, JA, Wright, SH, Yee, SW, Zamek-Gliszczynski, MJ & Zhang, L 2010, 'Membrane transporters in drug development', *Nat Rev Drug Discov*, vol. 9, no. 3, pp. 215-236.

Gill, KL, Houston, JB & Galetin, A 2012, 'Characterization of In Vitro Glucuronidation Clearance of a Range of Drugs in Human Kidney Microsomes: Comparison with Liver and Intestinal Glucuronidation and Impact of Albumin', *Drug Metabolism and Disposition*, vol. 40, no. 4, pp. 825-835.

Girard, H, Court, MH, Bernard, O, Fortier, LC, Villeneuve, L, Hao, Q, Greenblatt, DJ, von Moltke, LL, Perused, L & Guillemette, C 2004, 'Identification of common polymorphisms in the promoter of the UGT1A9 gene: evidence that UGT1A9 protein and activity levels are strongly genetically controlled in the liver', *Pharmacogenetics*, vol. 14, no. 8, pp. 501-515.

Giraud, M, Hilliou, F, Fricaux, T, Audant, P, Feyereisen, R & Le Goff, G 2015, 'Cytochrome P450s from the fall armyworm (*Spodoptera frugiperda*): responses to plant allelochemicals and pesticides', *Insect Molecular Biology*, vol. 24, no. 1, pp. 115-128.

Gonzalez, FJ, Coughtrie, M & Tukey, RH 2011, 'Chapter 6: Drug Metabolism', in *Goodman and Gilman's the pharmacological basis of therapeutics*, eds LS Goodman, LL Brunton, B Chabner & BC Knollmann, New York : McGraw-Hill Medical, New York.

Gonzalez, FJ & Nebert, DW 1990, 'Evolution of the P450 gene superfamily: animal-plant 'warfare', molecular drive and human genetic differences in drug oxidation', *Trends Genet*, vol. 6, no. 6, pp. 182-186.

Gouin, A, Bretaudeau, A, Nam, K, Gimenez, S, Aury, J-M, Duvic, B, Hilliou, F, Durand, N, Montagné, N, Darboux, I, Kuwar, S, Chertemps, T, Siaussat, D, Bretschneider, A, Moné, Y, Ahn, S-J, Hänniger, S, Grenet, A-SG, Neunemann, D, Maumus, F, Luyten, I, Labadie, K, Xu, W, Koutroumpa, F, Escoubas, J-M, Llopis, A, Maïbèche-Coisne, M, Salasc, F, Tomar, A, Anderson, AR, Khan, SA, Dumas, P, Orsucci, M, Guy, J, Belser, C, Alberti, A, Noel, B, Couloux, A, Mercier, J, Nidelet, S, Dubois, E, Liu, N-Y, Boulogne, I, Mirabeau, O, Le Goff, G, Gordon, K, Oakeshott, J, Consoli, FL, Volkoff, A-N, Fescemyer, HW, Marden, JH, Luthe, DS, Herrero, S, Heckel, DG, Wincker, P, Kergoat, GJ, Amselem, J, Quesneville, H, Groot, AT, Jacquin-Joly, E, Nègre, N, Lemaitre, C, Legeai, F, d'Alençon, E & Fournier, P 2017, 'Two genomes of highly polyphagous lepidopteran pests (*Spodoptera frugiperda*, Noctuidae) with different host-plant ranges', *Sci Rep*, vol. 7, no. 1, pp. 11816.

Green, MD & Tephly, TR 1996, 'Glucuronidation of amines and hydroxylated xenobiotics and endobiotics catalyzed by expressed human UGT1.4 protein', *Drug Metabolism and Disposition*, vol. 24, no. 3, pp. 356-363.

Griffiths, CM & Page, MJ 1997, 'Chapter 34: Production of heterologous proteins using the baculovirus/insect expression system ', in *Basic Cell Culture Protocols - Methods in Molecular Biology*, eds, Humana Press Inc., Totowa, NJ.

Gu, Y, Tingle, MD & Wilson, WR 2011, 'Glucuronidation of Anticancer Prodrug PR-104A: Species Differences, Identification of Human UDP-Glucuronosyltransferases, and Implications for Therapy', *Journal of Pharmacology and Experimental Therapeutics*, vol. 337, no. 3, pp. 692-702.

Gutstein, HB & Akil, H (eds.) 2006, *Opioid Analgesics*, McGraw Hill Media Publishing Divison, New York.

Ha, S, Walker, D, Shi, Y & Walker, S 2000, 'The 1.9 Å crystal structure of *Escherichia coli* MurG, a membrane-associated glycosyltransferase involved in peptidoglycan biosynthesis', *Protein Sci*, vol. 9, no. 6, pp. 1045-1052.

Hadley, B, Maggioni, A, Ashikov, A, Day, CJ, Haselhorst, T & Tiralongo, J 2014, 'Structure and function of nucleotide sugar transporters: Current progress', *Comput Struct Biotechnol J*, vol. 10, no. 16, pp. 23-32.

Hanahan, D 1985, *DNA Cloning: A Practical Approach*, IRL Press, McLean, Virginia, USA.

Hanioka, N, Jinno, H, Tanaka-Kagawa, T, Nishimura, T & Ando, M 2001a, 'Determination of UDP-glucuronosyltransferase UGT1A6 activity in human and rat liver microsomes by HPLC with UV detection', *J Pharm Biomed Anal*, vol. 25, no. 1, pp. 65-75.

Hanioka, N, Ozawa, S, Jinno, H, Ando, M, Saito, Y & Sawada, J 2001b, 'Human liver UDP-glucuronosyltransferase isoforms involved in the glucuronidation of 7-ethyl-10-hydroxycamptothecin', *Xenobiotica*, vol. 31, no. 10, pp. 687-699.

Hao, D, Xiao, P & Chen, S 2010, 'Phenotype prediction of nonsynonymous single nucleotide polymorphisms in human phase II drug/xenobiotic metabolizing enzymes: perspectives on molecular evolution', *Sci China Life Sci*, vol. 53, no. 10, pp. 1252-1262.

Hara, T, Yamauchi, M, Takahashi, E-i, Hoshino, M, Aoki, K, Ayusawa, D & Kawakita, M 1993, 'The UDP-galactose translocator gene is mapped to band Xp11.23-p11.22 containing the Wiskott-Aldrich syndrome locus', *Somatic Cell and Molecular Genetics*, vol. 19, no. 6, pp. 571-575.

Hara, Y, Nakajima, M, Miyamoto, K & Yokoi, T 2007, 'Morphine glucuronosyltransferase activity in human liver microsomes is inhibited by a variety of drugs that are co-administered with morphine', *Drug Metab Pharmacokinet*, vol. 22, no. 2, pp. 103-112.

Harbourt, DE, Fallon, JK, Ito, S, Baba, T, Ritter, JK, Glish, GL & Smith, PC 2012, 'Quantification of human uridine-diphosphate glucuronosyl transferase 1A isoforms in liver, intestine, and kidney using nanobore liquid chromatography-tandem mass spectrometry', *Anal Chem*, vol. 84, no. 1, pp. 98-105.

Hasselstrom, J & Sawe, J 1993, 'Morphine pharmacokinetics and metabolism in humans. Enterohepatic cycling and relative contribution of metabolites to active opioid concentrations', *Clin Pharmacokinet*, vol. 24, no. 4, pp. 344-354.

Heidel-Fischer, HM & Vogel, H 2015, 'Molecular mechanisms of insect adaptation to plant secondary compounds', *Current Opinion in Insect Science*, vol. 8, no. pp. 8-14.

Herde, M & Howe, GA 2014, 'Host plant-specific remodeling of midgut physiology in the generalist insect herbivore *Trichoplusia ni*', *Insect Biochemistry and Molecular Biology*, vol. 50, no. pp. 58-67.

Higy, M, Junne, T & Spiess, M 2004, 'Topogenesis of Membrane Proteins at the Endoplasmic Reticulum', *Biochemistry*, vol. 43, no. 40, pp. 12716-12722.

Hiraoka, S, Furuichi, T, Nishimura, G, Shibata, S, Yanagishita, M, Rimoin, DL, Superti-Furga, A, Nikkels, PG, Ogawa, M, Katsuyama, K, Toyoda, H, Kinoshita-Toyoda, A, Ishida, N, Isono, K, Sanai, Y, Cohn, DH, Koseki, H & Ikegawa, S 2007, 'Nucleotide-sugar transporter SLC35D1 is critical to chondroitin sulfate synthesis in

cartilage and skeletal development in mouse and human', *Nature Medicine*, vol. 13, no. 11, pp. 1363-1367.

Hirouchi, M, Kusuhara, H, Onuki, R, Ogilvie, BW, Parkinson, A & Sugiyama, Y 2009, 'Construction of triple-transfected cells [organic anion-transporting polypeptide (OATP) 1B1/multidrug resistance-associated protein (MRP) 2/MRP3 and OATP1B1/MRP2/MRP4] for analysis of the sinusoidal function of MRP3 and MRP4', *Drug Metab Dispos*, vol. 37, no. 10, pp. 2103-2111.

Hirschberg, CB, Robbins, PW & Abeijon, C 1998, 'Transporters of nucleotide sugars, ATP, and nucleotide sulfate in the endoplasmic reticulum and Golgi apparatus', *Annu Rev Biochem*, vol. 67, no. pp. 49-69.

Holthe, M, Klepstad, P, Zahlsen, K, Borchgrevink, PC, Hagen, L, Dale, O, Kaasa, S, Krokan, HE & Skorpen, F 2002, 'Morphine glucuronide-to-morphine plasma ratios are unaffected by the UGT2B7 H268Y and UGT1A1*28 polymorphisms in cancer patients on chronic morphine therapy', *Eur J Clin Pharmacol*, vol. 58, no. 5, pp. 353-356.

Holthe, M, Rakvag, TN, Klepstad, P, Idle, JR, Kaasa, S, Krokan, HE & Skorpen, F 2003, 'Sequence variations in the UDP-glucuronosyltransferase 2B7 (UGT2B7) gene: identification of 10 novel single nucleotide polymorphisms (SNPs) and analysis of their relevance to morphine glucuronidation in cancer patients', *Pharmacogenomics J*, vol. 3, no. 1, pp. 17-26.

Houston, JB & Aleksandra, G 2008, 'Methods for Predicting In Vivo Pharmacokinetics Using Data from In Vitro Assays', *Current Drug Metabolism*, vol. 9, no. 9, pp. 940-951.

Houston, JB & Kenworthy, KE 2000, 'In vitro-in vivo scaling of CYP kinetic data not consistent with the classical Michaelis-Menten model', *Drug Metabolism and Disposition*, vol. 28, no. 3, pp. 246-254.

Houston, JB, Kenworthy, KE & Galetin, A (eds.) 2003, *Typical and atypical enzyme kinetics*, Fontis Media S.A., Lausanne.

Hu, B, Zhang, S-H, Ren, M-M, Tian, X-R, Wei, Q, Mburu, DK & Su, J-Y 2017, 'The expression of *Spodoptera exigua* P450 and UGT genes: tissue specificity and response to insecticides', *Insect Science*, vol., no. pp. n/a-n/a.

Hu, Y, Chen, L, Ha, S, Gross, B, Falcone, B, Walker, D, Mokhtarzadeh, M & Walker, S 2003, 'Crystal structure of the MurG:UDP-GlcNAc complex reveals common structural principles of a superfamily of glycosyltransferases', *Proc Natl Acad Sci U S A*, vol. 100, no. 3, pp. 845-849.

Hu, Y & Walker, S 2002, 'Remarkable structural similarities between diverse glycosyltransferases', *Chem Biol*, vol. 9, no. 12, pp. 1287-1296.

Huang, FF, Chai, CL, Zhang, Z, Liu, ZH, Dai, FY, Lu, C & Xiang, ZH 2008, 'The UDP-glucosyltransferase multigene family in *Bombyx mori*', *BMC Genomics*, vol. 9, no. pp. 563.

- Hughes, AL 2013, 'Origin of Ecdysteroid UDP-glycosyltransferases of Baculoviruses through Horizontal Gene Transfer from Lepidoptera', *Coevolution*, vol. 1, no. 1, pp. 1-7.
- Hutchinson, MR, Zhang, Y, Shridhar, M, Evans, JH, Buchanan, MM, Zhao, TX, Slivka, PF, Coats, BD, Rezvani, N, Wieseler, J, Hughes, TS, Landgraf, KE, Chan, S, Fong, S, Phipps, S, Falke, JJ, Leinwand, LA, Maier, SF, Yin, H, Rice, KC & Watkins, LR 2010, 'Evidence that opioids may have toll-like receptor 4 and MD-2 effects', *Brain Behav Immun*, vol. 24, no. 1, pp. 83-95.
- Ieiri, I, Nishimura, C, Maeda, K, Sasaki, T, Kimura, M, Chiyoda, T, Hirota, T, Irie, S, Shimizu, H, Noguchi, T, Yoshida, K & Sugiyama, Y 2011, 'Pharmacokinetic and pharmacogenomic profiles of telmisartan after the oral microdose and therapeutic dose', *Pharmacogenetics and Genomics*, vol. 21, no. 8, pp. 495-505.
- Ikushiro, S, Emi, Y & Iyanagi, T 1997, 'Protein-protein interactions between UDP-glucuronosyltransferase isozymes in rat hepatic microsomes', *Biochemistry*, vol. 36, no. 23, pp. 7154-7161.
- Innocenti, F, Iyer, L, Ramirez, J, Green, MD & Ratain, MJ 2001, 'Epirubicin glucuronidation is catalyzed by human UDP-glucuronosyltransferase 2B7', *Drug Metab Dispos*, vol. 29, no. 5, pp. 686-692.
- Ishida, N, Kuba, T, Aoki, K, Miyatake, S, Kawakita, M & Sanai, Y 2005, 'Identification and characterization of human Golgi nucleotide sugar transporter SLC35D2, a novel member of the SLC35 nucleotide sugar transporter family', *Genomics*, vol. 85, no. 1, pp. 106-116.
- Iswandana, R, Irianti, MI, Oosterhuis, D, Hofker, HS, Merema, MT, de Jager, MH, Mutsaers, HAM & Olinga, P 2018, 'Regional Differences in Human Intestinal Drug Metabolism', *Drug Metab Dispos*, vol. 46, no. 12, pp. 1879-1885.
- Jain, AN 1996, 'Scoring noncovalent protein-ligand interactions: a continuous differentiable function tuned to compute binding affinities', *J Comput Aided Mol Des*, vol. 10, no. 5, pp. 427-440.
- Jain, AN 2003, 'Surflex: fully automatic flexible molecular docking using a molecular similarity-based search engine', *J Med Chem*, vol. 46, no. 4, pp. 499-511.
- Järvinen, E, Troberg, J, Kidron, H & Finel, M 2017, 'Selectivity in the Efflux of Glucuronides by Human Transporters: MRP4 Is Highly Active toward 4-Methylumbelliferone and 1-Naphthol Glucuronides, while MRP3 Exhibits Stereoselective Propranolol Glucuronide Transport', *Mol Pharm*, vol. 14, no. 10, pp. 3299-3311.
- Jennings, AL, Davies, AN, Higgins, JP, Gibbs, JS & Broadley, KE 2002, 'A systematic review of the use of opioids in the management of dyspnoea', *Thorax*, vol. 57, no. 11, pp. 939-944.

Jensen, NB, Zagrobelny, M, Hjerno, K, Olsen, CE, Houghton-Larsen, J, Borch, J, Moller, BL & Bak, S 2011, 'Convergent evolution in biosynthesis of cyanogenic defence compounds in plants and insects', *Nat Commun*, vol. 2, no. pp. 273.

Jeong, E-S, Kim, Y-W, Kim, H-J, Shin, H-J, Shin, J-G, Kim, KH, Chi, YH, Paik, SH & Kim, D-H 2015, 'Glucuronidation of fimasartan, a new angiotensin receptor antagonist, is mainly mediated by UGT1A3', *Xenobiotica*, vol. 45, no. 1, pp. 10-18.

Jin, CJ, Miners, JO, Lillywhite, KJ & Mackenzie, PI 1993, 'Complementary Deoxyribonucleic-Acid Cloning and Expression of a Human Liver Uridine Diphosphate-Glucuronosyltransferase Glucuronidating Carboxylic Acid-Containing Drugs', *Journal of Pharmacology and Experimental Therapeutics*, vol. 264, no. 1, pp. 475-479.

Johnson, EF & Stout, CD 2005, 'Structural diversity of human xenobiotic-metabolizing cytochrome P450 monooxygenases', *Biochemical and Biophysical Research Communications*, vol. 338, no. 1, pp. 331-336.

Johnson, EF & Stout, CD 2013, 'Structural diversity of eukaryotic membrane cytochrome p450s', *J Biol Chem*, vol. 288, no. 24, pp. 17082-17090.

Jones, EL, Epinette, WW, Hackney, VC, Menendez, L & Frost, P 1975, 'Treatment Of Psoriasis With Oral Mycophenolic Acid', *Journal of Investigative Dermatology*, vol. 65, no. 6, pp. 537-542.

Joseph, PD, Guengerich, FP & Miners, JO 2005, "Phase I and Phase II" Drug Metabolism: Terminology that we Should Phase Out?', *Drug Metabolism Reviews*, vol. 37, no. 4, pp. 575-580.

Jude, AR, Little, JM, Bull, AW, Podgorski, I & Radomska-Pandya, A 2001a, '13-Hydroxy- and 13-Oxo-octadecadienoic acids: Novel Substrates for Human UDP-Glucuronosyltransferases', *Drug Metabolism and Disposition*, vol. 29, no. 5, pp. 652-655.

Jude, AR, Little, JM, Czernik, PJ, Tephly, TR, Grant, DF & Radomska-Pandya, A 2001b, 'Glucuronidation of linoleic acid diols by human microsomal and recombinant UDP-glucuronosyltransferases: identification of UGT2B7 as the major isoform involved', *Arch Biochem Biophys*, vol. 389, no. 2, pp. 176-186.

Jude, AR, Little, JM, Freeman, JP, Evans, JE, Radomska-Pandya, A & Grant, DF 2000, 'Linoleic acid diols are novel substrates for human UDP-glucuronosyltransferases', *Arch Biochem Biophys*, vol. 380, no. 2, pp. 294-302.

Kaivosaaari, S, Finel, M & Koskinen, M 2011, 'N-glucuronidation of drugs and other xenobiotics by human and animal UDP-glucuronosyltransferases', *Xenobiotica*, vol. 41, no. 8, pp. 652-669.

Kallionpaa, RA, Jarvinen, E & Finel, M 2015, 'Glucuronidation of estrone and 16alpha-hydroxyestrone by human UGT enzymes: The key roles of UGT1A10 and UGT2B7', *J Steroid Biochem Mol Biol*, vol. 154, no. pp. 104-111.

Kang, SP, Ramirez, J, House, L, Zhang, W, Mirkov, S, Liu, W, Haverfield, E & Ratain, MJ 2010, 'A pharmacogenetic study of vorinostat glucuronidation', *Pharmacogenet Genomics*, vol. 20, no. 10, pp. 638-641.

Kannangara, R, Siukstaite, L, Borch-Jensen, J, Madsen, B, Kongstad, KT, Staerk, D, Bennedsen, M, Okkels, FT, Rasmussen, SA, Larsen, TO, Frandsen, RJN & Møller, BL 2017, 'Characterization of a membrane-bound C-glucosyltransferase responsible for carminic acid biosynthesis in *Dactylopius coccus* Costa', *Nature Communications*, vol. 8, no. 1, pp. 1987.

Kanoh, H, Tada, M, Uesawa, Y & Mohri, K 2011, 'Buclome N-Glucuronide Formation: Species Differences and Identification of Human UDP-Glucuronosyltransferase Isoforms', *Pharmacology & Pharmacy*, vol. 2, no. 4, pp. 361-369.

Kassahun, K, McIntosh, I, Cui, D, Hreniuk, D, Merschman, S, Lasseter, K, Azrolan, N, Iwamoto, M, Wagner, JA & Wenning, LA 2007, 'Metabolism and Disposition in Humans of Raltegravir (MK-0518), an Anti-AIDS Drug Targeting the Human Immunodeficiency Virus 1 Integrase Enzyme', *Drug Metabolism and Disposition*, vol. 35, no. 9, pp. 1657-1663.

Kaya, L 2011, Functional characterization of human UDP-glucuronosyltransferase 1A5 (UGT1A5): Expression systems and structure-function, Flinders University.

Kemp, DC, Fan, PW & Stevens, JC 2002, 'Characterization of raloxifene glucuronidation in vitro: contribution of intestinal metabolism to presystemic clearance', *Drug Metab Dispos*, vol. 30, no. 6, pp. 694-700.

Kerdpin, O, Elliot, DJ, Mackenzie, PI & Miners, JO 2006, 'Sulfinpyrazone C-glucuronidation is catalyzed selectively by human UDP-glucuronosyltransferase 1A9', *Drug Metab Dispos*, vol. 34, no. 12, pp. 1950-1953.

Kerdpin, O, Knights, KM, Elliot, DJ & Miners, JO 2008, 'In vitro characterisation of human renal and hepatic frusemide glucuronidation and identification of the UDP-glucuronosyltransferase enzymes involved in this pathway', *Biochemical Pharmacology*, vol. 76, no. 2, pp. 249-257.

Kerdpin, O, Mackenzie, PI, Bowalgaha, K, Finel, M & Miners, JO 2009, 'Influence of N-Terminal Domain Histidine and Proline Residues on the Substrate Selectivities of Human UDP-Glucuronosyltransferase 1A1, 1A6, 1A9, 2B7, and 2B10', *Drug Metabolism and Disposition*, vol. 37, no. 9, pp. 1948-1955.

Kiang, TK, Ensom, MH & Chang, TK 2005, 'UDP-glucuronosyltransferases and clinical drug-drug interactions', *Pharmacol Ther*, vol. 106, no. 1, pp. 97-132.

Kida, Y, Ohgiya, S, Mihara, K & Sakaguchi, M 1998, 'Membrane Topology of NADPH-Cytochrome P450 Reductase on the Endoplasmic Reticulum', *Archives of Biochemistry and Biophysics*, vol. 351, no. 2, pp. 175-179.

Kimizu, T, Takahashi, Y, Oboshi, T, Horino, A, Koike, T, Yoshitomi, S, Mori, T, Yamaguchi, T, Ikeda, H, Okamoto, N, Nakashima, M, Saitsu, H, Kato, M, Matsumoto,

N & Imai, K 2017, 'A case of early onset epileptic encephalopathy with de novo mutation in SLC35A2: Clinical features and treatment for epilepsy', *Brain Dev*, vol. 39, no. 3, pp. 256-260.

Kimura, Y 2003, 'Prevention of Cancer Chemotherapy Drug-Induced Adverse Reaction, Antitumor and Antimetastatic Activities by Natural Products', in *Studies in Natural Products Chemistry*, eds A-u Rahman, Elsevier.

King, CD, Rios, GR, Assouline, JA & Tephly, TR 1999, 'Expression of UDP-glucuronosyltransferases (UGTs) 2B7 and 1A6 in the human brain and identification of 5-hydroxytryptamine as a substrate', *Arch Biochem Biophys*, vol. 365, no. 1, pp. 156-162.

Knights, KM, Spencer, SM, Fallon, JK, Chau, N, Smith, PC & Miners, JO 2016, 'Scaling factors for the in vitro–in vivo extrapolation (IV–IVE) of renal drug and xenobiotic glucuronidation clearance', *British Journal of Clinical Pharmacology*, vol. 81, no. 6, pp. 1153-1164.

Knights, KM, Winner, LK, Elliot, DJ, Bowalgaha, K & Miners, JO 2009, 'Aldosterone glucuronidation by human liver and kidney microsomes and recombinant UDP-glucuronosyltransferases: inhibition by NSAIDs', *Br J Clin Pharmacol*, vol. 68, no. 3, pp. 402-412.

Kodera, H, Nakamura, K, Osaka, H, Maegaki, Y, Haginoya, K, Mizumoto, S, Kato, M, Okamoto, N, Iai, M, Kondo, Y, Nishiyama, K, Tsurusaki, Y, Nakashima, M, Miyake, N, Hayasaka, K, Sugahara, K, Yuasa, I, Wada, Y, Matsumoto, N & Saitsu, H 2013, 'De novo mutations in SLC35A2 encoding a UDP-galactose transporter cause early-onset epileptic encephalopathy', *Hum Mutat*, vol. 34, no. 12, pp. 1708-1714.

Korprasertthaworn, P, Rowland, A, Lewis, BC, Mackenzie, PI, Yoovathaworn, K & Miners, JO 2012, 'Effects of amino acid substitutions at positions 33 and 37 on UDP-glucuronosyltransferase 1A9 (UGT1A9) activity and substrate selectivity', *Biochem Pharmacol*, vol. 84, no. 11, pp. 1511-1521.

Kost, TA, Condreay, JP & Jarvis, DL 2005, 'Baculovirus as versatile vectors for protein expression in insect and mammalian cells', *Nat Biotechnol*, vol. 23, no. 5, pp. 567-575.

Krishnaswamy, S, Duan, SX, Von Moltke, LL, Greenblatt, DJ & Court, MH 2003, 'Validation of serotonin (5-hydroxytryptamine) as an in vitro substrate probe for human UDP-glucuronosyltransferase (UGT) 1A6', *Drug Metab Dispos*, vol. 31, no. 1, pp. 133-139.

Kubota, T, Lewis, BC, Elliot, DJ, Mackenzie, PI & Miners, JO 2007, 'Critical roles of residues 36 and 40 in the phenol and tertiary amine aglycone substrate selectivities of UDP-glucuronosyltransferases 1A3 and 1A4', *Molecular Pharmacology*, vol. 72, no. 4, pp. 1054-1062.

Kuehl, GE, Lampe, JW, Potter, JD & Bigler, J 2005, 'Glucuronidation of nonsteroidal anti-inflammatory drugs: Identifying the enzymes responsible in human liver microsomes', *Drug Metabolism and Disposition*, vol. 33, no. 7, pp. 1027-1035.

Kumamoto, K, Goto, Y, Sekikawa, K, Takenoshita, S, Ishida, N, Kawakita, M & Kannagi, R 2001, 'Increased expression of UDP-galactose transporter messenger RNA in human colon cancer tissues and its implication in synthesis of Thomsen-Friedenreich antigen and sialyl Lewis A/X determinants', *Cancer Res*, vol. 61, no. 11, pp. 4620-4627.

Kurkela, M, Hirvonen, J, Kostianen, R & Finel, M 2004, 'The interactions between the N-terminal and C-terminal domains of the human UDP-glucuronosyltransferases are partly isoform-specific, and may involve both monomers', *Biochem Pharmacol*, vol. 68, no. 12, pp. 2443-2450.

Kuypers, DR, Le Meur, Y, Cantarovich, M, Tredger, MJ, Tett, SE, Cattaneo, D, Tonshoff, B, Holt, DW, Chapman, J, Gelder, T & Transplantation Society Consensus Group on, TDMoMPA 2010, 'Consensus report on therapeutic drug monitoring of mycophenolic acid in solid organ transplantation', *Clin J Am Soc Nephrol*, vol. 5, no. 2, pp. 341-358.

Kuypers, DR, Naesens, M, Vermeire, S & Vanrenterghem, Y 2005, 'The impact of uridine diphosphate-glucuronosyltransferase 1A9 (UGT1A9) gene promoter region single-nucleotide polymorphisms T-275A and C-2152T on early mycophenolic acid dose-interval exposure in de novo renal allograft recipients', *Clin Pharmacol Ther*, vol. 78, no. 4, pp. 351-361.

Laakkonen, L & Finel, M 2010, 'A Molecular Model of the Human UDP-Glucuronosyltransferase 1A1, Its Membrane Orientation, and the Interactions between Different Parts of the Enzyme', *Molecular Pharmacology*, vol. 77, no. 6, pp. 931-939.

Laemmli, UK 1970, 'Cleavage of Structural Proteins during Assembly of Head of Bacteriophage-T4', *Nature*, vol. 227, no. 5259, pp. 680-&.

Lairson, LL, Henrissat, B, Davies, GJ & Withers, SG 2008, 'Glycosyltransferases: structures, functions, and mechanisms', *Annu Rev Biochem*, vol. 77, no. pp. 521-555.

Lapham, K, Bauman, J, Walsky, R, Niosi, M, Orozco, C, Bourcier, K, Giddens, G, Obach, R & Hyland, R 2012, *Digoxin and tranilast identified as novel isoform selective inhibitors of human UDP glucuronosyltransferase 1A9 activity. in Drug Metab Rev*, Vol. 44,

Larkin, MA, Blackshields, G, Brown, NP, Chenna, R, McGettigan, PA, McWilliam, H, Valentin, F, Wallace, IM, Wilm, A, Lopez, R, Thompson, JD, Gibson, TJ & Higgins, DG 2007, 'Clustal W and Clustal X version 2.0', *Bioinformatics*, vol. 23, no. 21, pp. 2947-2948.

Lee, WA, Gu, L, Miksztal, AR, Chu, N, Leung, K & Nelson, PH 1990, 'Bioavailability improvement of mycophenolic acid through amino ester derivatization', *Pharm Res*, vol. 7, no. 2, pp. 161-166.

Lepine, J, Bernard, O, Plante, M, Tetu, B, Pelletier, G, Labrie, F, Belanger, A & Guillemette, C 2004, 'Specificity and regioselectivity of the conjugation of estradiol, estrone, and their catecholestrogen and methoxyestrogen metabolites by human

uridine diphospho-glucuronosyltransferases expressed in endometrium', *J Clin Endocrinol Metab*, vol. 89, no. 10, pp. 5222-5232.

Levesque, E, Beaulieu, M, Green, MD, Tephly, TR, Belanger, A & Hum, DW 1997, 'Isolation and characterization of UGT2B15(Y85): a UDP-glucuronosyltransferase encoded by a polymorphic gene', *Pharmacogenetics*, vol. 7, no. 4, pp. 317-325.

Levesque, E, Beaulieu, M, Hum, DW & Belanger, A 1999, 'Characterization and substrate specificity of UGT2B4 (E458): a UDP-glucuronosyltransferase encoded by a polymorphic gene', *Pharmacogenetics*, vol. 9, no. 2, pp. 207-216.

Levesque, E, Delage, R, Benoit-Biancamano, MO, Caron, P, Bernard, O, Couture, F & Guillemette, C 2007, 'The impact of UGT1A8, UGT1A9, and UGT2B7 genetic polymorphisms on the pharmacokinetic profile of mycophenolic acid after a single oral dose in healthy volunteers', *Clin Pharmacol Ther*, vol. 81, no. 3, pp. 392-400.

Levesque, E, Turgeon, D, Carrier, JS, Montminy, V, Beaulieu, M & Belanger, A 2001, 'Isolation and characterization of the UGT2B28 cDNA encoding a novel human steroid conjugating UDP-glucuronosyltransferase', *Biochemistry*, vol. 40, no. 13, pp. 3869-3881.

Lewis, BC, Mackenzie, PI, Elliot, DJ, Burchell, B, Bhasker, CR & Miners, JO 2007, 'Amino terminal domains of human UDP-glucuronosyltransferases (UGT) 2B7 and 2B15 associated with substrate selectivity and autoactivation', *Biochemical Pharmacology*, vol. 73, no. 9, pp. 1463-1473.

Lewis, BC, Mackenzie, PI & Miners, JO 2011, 'Homodimerization of UDP-glucuronosyltransferase 2B7 (UGT2B7) and identification of a putative dimerization domain by protein homology modeling', *Biochem Pharmacol*, vol. 82, no. 12, pp. 2016-2023.

Lewis, SS, Hutchinson, MR, Rezvani, N, Loram, LC, Zhang, Y, Maier, SF, Rice, KC & Watkins, LR 2010, 'Evidence that intrathecal morphine-3-glucuronide may cause pain enhancement via toll-like receptor 4/MD-2 and interleukin-1beta', *Neuroscience*, vol. 165, no. 2, pp. 569-583.

Li, C & Wu, Q 2007, 'Adaptive evolution of multiple-variable exons and structural diversity of drug-metabolizing enzymes', *BMC Evol Biol*, vol. 7, no. pp. 69.

Li, D, Fournel-Gigleux, S, Barre, L, Mulliert, G, Netter, P, Magdalou, J & Ouzzine, M 2007, 'Identification of aspartic acid and histidine residues mediating the reaction mechanism and the substrate specificity of the human UDP-glucuronosyltransferases 1A', *J Biol Chem*, vol. 282, no. 50, pp. 36514-36524.

Li, JA, Happ, B, Schetter, C, Oellig, C, Hauser, C, Kuroda, K, Knebel-Morsdorf, D, Klenk, HD & Doerfler, W 1990, 'The expression of the Autographa californica nuclear polyhedrosis virus genome in insect cells', *Vet Microbiol*, vol. 23, no. 1-4, pp. 73-78.

Li, X, Bratton, S & Radominska-Pandya, A 2007, 'Human UGT1A8 and UGT1A10 mRNA are expressed in primary human hepatocytes', *Drug Metab Pharmacokinet*, vol. 22, no. 3, pp. 152-161.

- Lin, JH & Wong, BK 2002, 'Complexities of glucuronidation affecting in vitro in vivo extrapolation', *Curr Drug Metab*, vol. 3, no. 6, pp. 623-646.
- Linnet, K 2002, 'Glucuronidation of olanzapine by cDNA-expressed human UDP-glucuronosyltransferases and human liver microsomes', *Hum Psychopharmacol*, vol. 17, no. 5, pp. 233-238.
- Linster, CL & Van Schaftingen, E 2003, 'Rapid stimulation of free glucuronate formation by non-glucuronidable xenobiotics in isolated rat hepatocytes', *Journal of Biological Chemistry*, vol. 278, no. 38, pp. 36328-36333.
- Lipsky, JJ 1996, 'Mycophenolate mofetil', *The Lancet*, vol. 348, no. 9038, pp. 1357-1359.
- Liu, Y & Coughtrie, MWH 2017, 'Revisiting the Latency of Uridine Diphosphate-Glucuronosyltransferases (UGTs)—How Does the Endoplasmic Reticulum Membrane Influence Their Function?', *Pharmaceutics*, vol. 9, no. 3, pp. 32.
- Lizák, B, Csala, M, Benedetti, A & Bánhegyi, G 2008, 'The translocon and the non-specific transport of small molecules in the endoplasmic reticulum (Review)', *Molecular Membrane Biology*, vol. 25, no. 2, pp. 95-101.
- Locuson, CW & Tracy, TS 2007, 'Comparative modelling of the human UDP-glucuronosyltransferases: Insights into structure and mechanism', *Xenobiotica*, vol. 37, no. 2, pp. 155-168.
- Lotsch, J & Geisslinger, G 2005, 'Are mu-opioid receptor polymorphisms important for clinical opioid therapy?', *Trends Mol Med*, vol. 11, no. 2, pp. 82-89.
- Lotsch, J, Geisslinger, G & Tegeder, I 2009, 'Genetic modulation of the pharmacological treatment of pain', *Pharmacol Ther*, vol. 124, no. 2, pp. 168-184.
- Lowry, OH, Rosebrough, NJ, Farr, AL & Randall, RJ 1951, 'Protein Measurement with the Folin Phenol Reagent', *Journal of Biological Chemistry*, vol. 193, no. 1, pp. 265-275.
- Lu, D, Dong, D, Xie, Q, Li, Z & Wu, B 2018, 'Disposition of mianserin and cyclizine in UGT2B10-overexpressing HEK293 cells: Identification of UGT2B10 as a novel N-glycosidation enzyme and BCRP as an N-glycoside transporter', *Drug Metab Dispos*, vol., no. pp.
- Lühn, K, Wild, MK, Eckhardt, M, Gerardy-Schahn, R & Vestweber, D 2001, 'The gene defective in leukocyte adhesion deficiency II encodes a putative GDP-fucose transporter', *Nature Genetics*, vol. 28, no. pp. 69.
- Luque, T, Okano, K & O'Reilly, DR 2002, 'Characterization of a novel silkworm (*Bombyx mori*) phenol UDP-glucosyltransferase', *Eur J Biochem*, vol. 269, no. 3, pp. 819-825.
- Luukkanen, L, Taskinen, J, Kurkela, M, Kostianen, R, Hirvonen, J & Finel, M 2005, 'Kinetic characterization of the 1A subfamily of recombinant human UDP-glucuronosyltransferases', *Drug Metab Dispos*, vol. 33, no. 7, pp. 1017-1026.

Ma, J, Zheng, L, Deng, T, Li, C-L, He, Y-S, Li, H-J & Li, P 2013, 'Stilbene glucoside inhibits the glucuronidation of emodin in rats through the down-regulation of UDP-glucuronosyltransferases 1A8: Application to a drug–drug interaction study in Radix Polygoni Multiflori', *Journal of Ethnopharmacology*, vol. 147, no. 2, pp. 335-340.

Ma, L, Sun, J, Peng, Y, Zhang, R, Shao, F, Hu, X, Zhu, J, Wang, X, Cheng, X, Zhu, Y, Wan, P, Feng, D, Wu, H & Wang, G 2012, 'Glucuronidation of edaravone by human liver and kidney microsomes: biphasic kinetics and identification of UGT1A9 as the major UDP-glucuronosyltransferase isoform', *Drug Metab Dispos*, vol. 40, no. 4, pp. 734-741.

Mackenzie, P, Little, JM & Radominska-Pandya, A 2003, 'Glucosidation of hyodeoxycholic acid by UDP-glucuronosyltransferase 2B7', *Biochemical Pharmacology*, vol. 65, no. 3, pp. 417-421.

Mackenzie, PI 1990, 'Expression of chimeric cDNAs in cell culture defines a region of UDP glucuronosyltransferase involved in substrate selection', *J Biol Chem*, vol. 265, no. 6, pp. 3432-3435.

Mackenzie, PI 2000, 'Identification of uridine diphosphate glucuronosyltransferases involved in the metabolism and clearance of mycophenolic acid', *Therapeutic Drug Monitoring*, vol. 22, no. 1, pp. 10-13.

Mackenzie, PI, Bock, KW, Burchell, B, Guillemette, C, Ikushiro, S, Iyanagi, T, Miners, JO, Owens, IS & Nebert, DW 2005, 'Nomenclature update for the mammalian UDP glycosyltransferase (UGT) gene superfamily', *Pharmacogenetics and Genomics*, vol. 15, no. 10, pp. 677-685.

Mackenzie, PI, Gardner-Stephen, DA & Miners, JO 2010, 'Chapter 4.20 - UDP-Glucuronosyltransferases', in *Comprehensive Toxicology (Second Edition)*, eds CA McQueen, Elsevier, Oxford.

Mackenzie, PI, Owens, IS, Burchell, B, Bock, KW, Bairoch, A, Belanger, A, FournelGigleux, S, Green, M, Hum, DW, Iyanagi, T, Lancet, D, Louisot, P, Magdalou, J, Chowdhury, JR, Ritter, JK, Schachter, H, Tephly, TR, Tipton, KF & Nebert, DW 1997, 'The UDP glycosyltransferase gene superfamily: Recommended nomenclature update based on evolutionary divergence', *Pharmacogenetics*, vol. 7, no. 4, pp. 255-269.

Mackenzie, PI, Rogers, A, Elliot, DJ, Chau, N, Hulin, JA, Miners, JO & Meech, R 2011, 'The Novel UDP Glycosyltransferase 3A2: Cloning, Catalytic Properties, and Tissue Distribution', *Molecular Pharmacology*, vol. 79, no. 3, pp. 472-478.

Mackenzie, PI, Rogers, A, Treloar, J, Jorgensen, BR, Miners, JO & Meech, R 2008, 'Identification of UDP Glycosyltransferase 3A1 as a UDP N-Acetylglucosaminyltransferase', *Journal of Biological Chemistry*, vol. 283, no. 52, pp. 36205-36210.

Madadi, P, Ross, CJ, Hayden, MR, Carleton, BC, Gaedigk, A, Leeder, JS & Koren, G 2009, 'Pharmacogenetics of neonatal opioid toxicity following maternal use of codeine

during breastfeeding: a case-control study', *Clin Pharmacol Ther*, vol. 85, no. 1, pp. 31-35.

Magdalou, J, Fournel-Gigleux, S & Ouzzine, M 2010, 'Insights on membrane topology and structure/function of UDP-glucuronosyltransferases', *Drug Metabolism Reviews*, vol. 42, no. 1, pp. 159-166.

Manevski, N, Moreolo, PS, Yli-Kauhaluoma, J & Finel, M 2011, 'Bovine serum albumin decreases Km values of human UDP-glucuronosyltransferases 1A9 and 2B7 and increases Vmax values of UGT1A9', *Drug Metab Dispos*, vol. 39, no. 11, pp. 2117-2129.

Manevski, N, Troberg, J, Svaluto-Moreolo, P, Dziedzic, K, Yli-Kauhaluoma, J & Finel, M 2013, 'Albumin stimulates the activity of the human UDP-glucuronosyltransferases 1A7, 1A8, 1A10, 2A1 and 2B15, but the effects are enzyme and substrate dependent', *Plos One*, vol. 8, no. 1, pp. e54767.

Manevski, N, Yli-Kauhaluoma, J & Finel, M 2012, 'UDP-glucuronic acid binds first and the aglycone substrate binds second to form a ternary complex in UGT1A9-catalyzed reactions, in both the presence and absence of bovine serum albumin', *Drug Metab Dispos*, vol. 40, no. 11, pp. 2192-2203.

Mano, Y, Usui, T & Kamimura, H 2006, 'Identification of human UDP-glucuronosyltransferase responsible for the glucuronidation of niflumic acid in human liver', *Pharm Res*, vol. 23, no. 7, pp. 1502-1508.

Mano, Y, Usui, T & Kamimura, H 2007, 'The UDP-Glucuronosyltransferase 2B7 Isozyme Is Responsible for Gemfibrozil Glucuronidation in the Human Liver', *Drug Metabolism and Disposition*, vol. 35, no. 11, pp. 2040-2044.

Marciniak, S & Perry, GH 2017, 'Harnessing ancient genomes to study the history of human adaptation', *Nature Reviews Genetics*, vol. 18, no. pp. 659.

Margaillan, G, Rouleau, M, Fallon, JK, Caron, P, Villeneuve, L, Turcotte, V, Smith, PC, Joy, MS & Guillemette, C 2015a, 'Quantitative Profiling of Human Renal UDP-glucuronosyltransferases and Glucuronidation Activity: A Comparison of Normal and Tumoral Kidney Tissues', *Drug Metabolism and Disposition*, vol. 43, no. 4, pp. 611-619.

Margaillan, G, Rouleau, M, Klein, K, Fallon, JK, Caron, P, Villeneuve, L, Smith, PC, Zanger, UM & Guillemette, C 2015b, 'Multiplexed Targeted Quantitative Proteomics Predicts Hepatic Glucuronidation Potential', *Drug Metabolism and Disposition*, vol. 43, no. 9, pp. 1331-1335.

Marheineke, K, Grunewald, S, Christie, W & Reilander, H 1998, 'Lipid composition of *Spodoptera frugiperda* (Sf9) and *Trichoplusia ni* (Tn) insect cells used for baculovirus infection', *FEBS Lett*, vol. 441, no. 1, pp. 49-52.

Marschall, HU, Matern, H, Wietholtz, H, Egestad, B, Matern, S & Sjovall, J 1992, 'Bile acid N-acetylglucosaminidation. In vivo and in vitro evidence for a selective

conjugation reaction of 7 beta-hydroxylated bile acids in humans', *J Clin Invest*, vol. 89, no. 6, pp. 1981-1987.

Martineau, I, Tchernof, A & Bélanger, A 2004, 'Amino acid residue Ile211 is essential for the enzymatic activity of human UDP-Glucuronosyltransferase 1A10 (UGT1A10)', *Drug Metabolism and Disposition*, vol. 32, no. 4, pp. 455-459.

Matsubara, K, Fukushima, S, Akane, A, Kobayashi, S & Shiono, H 1992, 'Increased urinary morphine, codeine and tetrahydropapaveroline in parkinsonian patient undergoing L-3,4-dihydroxyphenylalanine therapy: a possible biosynthetic pathway of morphine from L-3,4-dihydroxyphenylalanine in humans', *Journal of Pharmacology and Experimental Therapeutics*, vol. 260, no. 3, pp. 974-978.

McGurk, KA, Brierley, CH & Burchell, B 1998, 'Drug Glucuronidation by Human Renal UDP-Glucuronosyltransferases', *Biochemical Pharmacology*, vol. 55, no. 7, pp. 1005-1012.

McLure, JA, Birkett, DJ, Elliot, DJ, Williams, JA, Rowland, A & Miners, JO 2011, 'Application of the fluorescent probe 1-anilinonaphthalene-8-sulfonate to the measurement of the nonspecific binding of drugs to human liver microsomes', *Drug Metab Dispos*, vol. 39, no. 9, pp. 1711-1717.

McLure, JA, Miners, JO & Birkett, DJ 2000, 'Nonspecific binding of drugs to human liver microsomes', *Br J Clin Pharmacol*, vol. 49, no. 5, pp. 453-461.

Meech, R, Hu, DG, McKinnon, RA, Mubarakah, SN, Haines, AZ, Nair, PC, Rowland, A & Mackenzie, PI 2019, 'The UDP-Glycosyltransferase (UGT) Superfamily: New Members, New Functions, and Novel Paradigms', *Physiol Rev*, vol. 99, no. 2, pp. 1153-1222.

Meech, R & Mackenzie, PI 1997a, 'Structure and function of uridine diphosphate glucuronosyltransferases', *Clin Exp Pharmacol Physiol*, vol. 24, no. 12, pp. 907-915.

Meech, R & Mackenzie, PI 1997b, 'UDP-glucuronosyltransferase, the role of the amino terminus in dimerization', *J Biol Chem*, vol. 272, no. 43, pp. 26913-26917.

Meech, R & Mackenzie, PI 1998, 'Determinants of UDP glucuronosyltransferase membrane association and residency in the endoplasmic reticulum', *Arch Biochem Biophys*, vol. 356, no. 1, pp. 77-85.

Meech, R & Mackenzie, PI 2010, 'UGT3A: novel UDP-glycosyltransferases of the UGT superfamily', *Drug Metabolism Reviews*, vol. 42, no. 1, pp. 45-54.

Meech, R, Miners, JO, Lewis, BC & Mackenzie, PI 2012a, 'The glycosidation of xenobiotics and endogenous compounds: versatility and redundancy in the UDP glycosyltransferase superfamily', *Pharmacol Ther*, vol. 134, no. 2, pp. 200-218.

Meech, R, Mubarakah, N, Shivasami, A, Rogers, A, Nair, PC, Hu, DG, McKinnon, RA & Mackenzie, PI 2015, 'A Novel Function for UDP Glycosyltransferase 8: Galactosidation of Bile Acids', *Molecular Pharmacology*, vol. 87, no. 3, pp. 442-450.

Meech, R, Rogers, A, Zhuang, LZ, Lewis, BC, Miners, JO & Mackenzie, PI 2012b, 'Identification of Residues That Confer Sugar Selectivity to UDP-Glycosyltransferase 3A (UGT3A) Enzymes', *Journal of Biological Chemistry*, vol. 287, no. 29, pp. 24122-24130.

Mikus, G, Bochner, F, Eichelbaum, M, Horak, P, Somogyi, AA & Spector, S 1994, 'Endogenous codeine and morphine in poor and extensive metabolisers of the CYP2D6 (debrisoquine/sparteine) polymorphism', *J Pharmacol Exp Ther*, vol. 268, no. 2, pp. 546-551.

Miles, KK, Stern, ST, Smith, PC, Kessler, FK, Ali, S & Ritter, JK 2005, 'An investigation of human and rat liver microsomal mycophenolic acid glucuronidation: evidence for a principal role of UGT1A enzymes and species differences in UGT1A specificity', *Drug Metab Dispos*, vol. 33, no. 10, pp. 1513-1520.

Miley, MJ, Zielinska, AK, Keenan, JE, Bratton, SM, Radomska-Pandya, A & Redinbo, MR 2007, 'Crystal structure of the cofactor-binding domain of the human phase II drug-metabolism enzyme UDP-glucuronosyltransferase 2B7', *Journal of Molecular Biology*, vol. 369, no. 2, pp. 498-511.

Milne, RW, Nation, RL & Somogyi, AA 1996, 'The disposition of morphine and its 3- and 6-glucuronide metabolites in humans and animals, and the importance of the metabolites to the pharmacological effects of morphine', *Drug Metab Rev*, vol. 28, no. 3, pp. 345-472.

Miners, JO, Bowalgaha, K, Elliot, DJ, Baranczewski, P & Knights, KM 2011, 'Characterization of niflumic acid as a selective inhibitor of human liver microsomal UDP-glucuronosyltransferase 1A9: application to the reaction phenotyping of acetaminophen glucuronidation', *Drug Metab Dispos*, vol. 39, no. 4, pp. 644-652.

Miners, JO, Chau, N, Rowland, A, Burns, K, McKinnon, RA, Mackenzie, PI, Tucker, GT, Knights, KM & Kichenadasse, G 2017, 'Inhibition of human UDP-glucuronosyltransferase enzymes by lapatinib, pazopanib, regorafenib and sorafenib: Implications for hyperbilirubinemia', *Biochemical Pharmacology*, vol. 129, no. pp. 85-95.

Miners, JO, Knights, KM, Houston, JB & Mackenzie, PI 2006, 'In vitro-in vivo correlation for drugs and other compounds eliminated by glucuronidation in humans: pitfalls and promises', *Biochem Pharmacol*, vol. 71, no. 11, pp. 1531-1539.

Miners, JO & Mackenzie, PI 1991, 'Drug glucuronidation in humans', *Pharmacol Ther*, vol. 51, no. 3, pp. 347-369.

Miners, JO, Mackenzie, PI & Knights, KM 2010, 'The prediction of drug-glucuronidation parameters in humans: UDP-glucuronosyltransferase enzyme-selective substrate and inhibitor probes for reaction phenotyping and in vitro-in vivo extrapolation of drug clearance and drug-drug interaction potential', *Drug Metab Rev*, vol. 42, no. 1, pp. 196-208.

Miners, JO, Polasek, TM, Mackenzie, PI & Knights, KM 2010, 'The In Vitro Characterization of Inhibitory Drug-Drug Interactions Involving UDP-

Glucuronosyltransferase', in *Enzyme- and Transporter-Based Drug-Drug Interactions: Progress and Future Challenges*, eds SK Pang, DA Rodrigues & MR Peter, Springer New York, New York, NY.

Miners, JO, Smith, PA, Sorich, MJ, McKinnon, RA & Mackenzie, PI 2004, 'Predicting human drug glucuronidation parameters: Application of in vitro and in silico modeling approaches', *Annual Review of Pharmacology and Toxicology*, vol. 44, no. pp. 1-25.

Miners, JO, Valente, L, Lillywhite, KJ, Mackenzie, PI, Burchell, B, Baguley, BC & Kestell, P 1997, 'Preclinical prediction of factors influencing the elimination of 5,6-dimethylxanthenone-4-acetic acid, a new anticancer drug', *Cancer Res*, vol. 57, no. 2, pp. 284-289.

Mojarrabi, B & Mackenzie, PI 1997, 'The human UDP glucuronosyltransferase, UGT1A10, glucuronidates mycophenolic acid', *Biochem Biophys Res Commun*, vol. 238, no. 3, pp. 775-778.

Morrish, GA, Foster, DJR & Somogyi, AA 2006, 'Differential in vitro inhibition of M3G and M6G formation from morphine by (R)- and (S)-methadone and structurally related opioids', *British Journal of Clinical Pharmacology*, vol. 61, no. 3, pp. 326-335.

Mulichak, AM, Losey, HC, Lu, W, Wawrzak, Z, Walsh, CT & Garavito, RM 2003, 'Structure of the TDP-epi-vancosaminyltransferase GtfA from the chloroeremomycin biosynthetic pathway', *Proc Natl Acad Sci U S A*, vol. 100, no. 16, pp. 9238-9243.

Nagashima, S, Hirotsu, M & Yoshikawa, T 2000, 'Purification and characterization of UDP-glucuronate: baicalein 7-O-glucuronosyltransferase from *Scutellaria baicalensis* Georgi. cell suspension cultures', *Phytochemistry*, vol. 53, no. 5, pp. 533-538.

Nair, PC, McKinnon, RA & Miners, JO 2016, 'Cytochrome P450 structure-function: insights from molecular dynamics simulations', *Drug Metab Rev*, vol. 48, no. 3, pp. 434-452.

Nair, PC, Meech, R, Mackenzie, PI, McKinnon, RA & Miners, JO 2015, 'Insights into the UDP-sugar selectivities of human UDP-glycosyltransferases (UGT): a molecular modeling perspective', *Drug Metab Rev*, vol., no. pp. 1-11.

Nakamura, K, Hirayama-Kurogi, M, Ito, S, Kuno, T, Yoneyama, T, Obuchi, W, Terasaki, T & Ohtsuki, S 2016, 'Large-scale multiplex absolute protein quantification of drug-metabolizing enzymes and transporters in human intestine, liver, and kidney microsomes by SWATH-MS: Comparison with MRM/SRM and HR-MRM/PRM', *PROTEOMICS*, vol. 16, no. 15-16, pp. 2106-2117.

Nakazawa, T, Miyata, K, Omura, K, Iwanaga, T & Nagata, O 2006, 'Metabolic profile of FYX-051 (4-(5-pyridin-4-yl-1h-[1,2,4]triazol-3-yl)pyridine-2-carbonitrile) in the rat, dog, monkey, and human: identification of N-glucuronides and N-glucosides', *Drug Metab Dispos*, vol. 34, no. 11, pp. 1880-1886.

Nebert, DW & Gonzalez, FJ 1987, 'P450 genes: structure, evolution, and regulation', *Annu Rev Biochem*, vol. 56, no. pp. 945-993.

- Neighbors, SM & Soine, WH 1995, 'Identification of phenobarbital N-glucuronides as urinary metabolites of phenobarbital in mice', *Drug Metab Dispos*, vol. 23, no. 5, pp. 548-552.
- Ng, BG, Asteggiano, CG, Kircher, M, Buckingham, KJ, Raymond, K, Nickerson, DA, Shendure, J, Bamshad, MJ, Ensslen, M & Freeze, HH 2017, 'Encephalopathy caused by novel mutations in the CMP-sialic acid transporter, SLC35A1', *Am J Med Genet A*, vol. 173, no. 11, pp. 2906-2911.
- Nishimura, M, Suzuki, S, Satoh, T & Naito, S 2009, 'Tissue-Specific mRNA Expression Profiles of Human Solute Carrier 35 Transporters', *Drug Metabolism and Pharmacokinetics*, vol. 24, no. 1, pp. 91-99.
- Nishiyama, T, Kobori, T, Arai, K, Ogura, K, Ohnuma, T, Ishii, K, Hayashi, K & Hiratsuka, A 2006, 'Identification of human UDP-glucuronosyltransferase isoform(s) responsible for the C-glucuronidation of phenylbutazone', *Arch Biochem Biophys*, vol. 454, no. 1, pp. 72-79.
- Noguchi, A, Horikawa, M, Fukui, Y, Fukuchi-Mizutani, M, Iuchi-Okada, A, Ishiguro, M, Kiso, Y, Nakayama, T & Ono, E 2009, 'Local Differentiation of Sugar Donor Specificity of Flavonoid Glycosyltransferase in Lamiales', *The Plant Cell*, vol. 21, no. 5, pp. 1556-1572.
- O'Reilly, DR 1995, 'Baculovirus-encoded ecdysteroid UDP-glucosyltransferases', *Insect Biochemistry and Molecular Biology*, vol. 25, no. 5, pp. 541-550.
- O'Reilly, DR, Brown, MR & Miller, LK 1992, 'Alteration of ecdysteroid metabolism due to baculovirus infection of the fall armyworm *Spodoptera frugiperda*: Host ecdysteroids are conjugated with galactose', *Insect Biochemistry and Molecular Biology*, vol. 22, no. 4, pp. 313-320.
- O'Reilly, DR, Howarth, OW, Rees, HH & Miller, LK 1991, 'Structure of the ecdysone glucoside formed by a baculovirus ecdysteroid UDP-glucosyltransferase', *Insect Biochemistry*, vol. 21, no. 7, pp. 795-801.
- O'Reilly, DR & Miller, LK 1989, 'A baculovirus blocks insect molting by producing ecdysteroid UDP-glucosyl transferase', *Science*, vol. 245, no. 4922, pp. 1110-1112.
- Obach, RS 2013, 'Pharmacologically Active Drug Metabolites: Impact on Drug Discovery and Pharmacotherapy', *Pharmacological Reviews*, vol. 65, no. 2, pp. 578-640.
- Obach, RS, Reed-Hagen, AE, Krueger, SS, Obach, BJ, O'Connell, TN, Zandi, KS, Miller, S & Coe, JW 2006, 'Metabolism and disposition of varenicline, a selective alpha 4 beta 2 acetylcholine receptor partial agonist, in vivo and in vitro', *Drug Metabolism and Disposition*, vol. 34, no. 1, pp. 121-130.
- Oda, S, Kato, Y, Hatakeyama, M, Iwamura, A, Fukami, T, Kume, T, Yokoi, T & Nakajima, M 2017, 'Evaluation of Expression and Glycosylation Status of UGT1A10 in Supersomes and Intestinal Epithelial Cells with a Novel Specific UGT1A10

Monoclonal Antibody', *Drug Metabolism and Disposition*, vol. 45, no. 9, pp. 1027-1034.

Oda, S, Nakajima, M, Hatakeyama, M, Fukami, T & Yokoi, T 2012, 'Preparation of a Specific Monoclonal Antibody against Human UDP-Glucuronosyltransferase (UGT) 1A9 and Evaluation of UGT1A9 Protein Levels in Human Tissues', *Drug Metabolism and Disposition*, vol. 40, no. 8, pp. 1620-1627.

Offen, W, Martinez-Fleites, C, Yang, M, Kiat-Lim, E, Davis, BG, Tarling, CA, Ford, CM, Bowles, DJ & Davies, GJ 2006, 'Structure of a flavonoid glucosyltransferase reveals the basis for plant natural product modification', *EMBO J*, vol. 25, no. 6, pp. 1396-1405.

Ohno, S, Kawana, K & Nakajin, S 2008, 'Contribution of UDP-glucuronosyltransferase 1A1 and 1A8 to morphine-6-glucuronidation and its kinetic properties', *Drug Metab Dispos*, vol. 36, no. 4, pp. 688-694.

Ohno, S & Nakajin, S 2009, 'Determination of mRNA expression of human UDP-glucuronosyltransferases and application for localization in various human tissues by real-time reverse transcriptase-polymerase chain reaction', *Drug Metab Dispos*, vol. 37, no. 1, pp. 32-40.

Ohno, S & Nakajin, S 2011, 'Quantitative Analysis of UGT2B28 mRNA Expression by Real-Time RT-PCR and Application to Human Tissue Distribution Study', *Drug Metabolism Letters*, vol. 5, no. 3, pp. 202-208.

Ohtsuki, S & Terasaki, T 2007, 'Contribution of carrier-mediated transport systems to the blood-brain barrier as a supporting and protecting interface for the brain; importance for CNS drug discovery and development', *Pharm Res*, vol. 24, no. 9, pp. 1745-1758.

Operana, TN & Tukey, RH 2007, 'Oligomerization of the UDP-glucuronosyltransferase 1A proteins: homo- and heterodimerization analysis by fluorescence resonance energy transfer and co-immunoprecipitation', *J Biol Chem*, vol. 282, no. 7, pp. 4821-4829.

Osborne, R, Joel, S, Trew, D & Slevin, M 1990, 'Morphine and metabolite behavior after different routes of morphine administration: demonstration of the importance of the active metabolite morphine-6-glucuronide', *Clin Pharmacol Ther*, vol. 47, no. 1, pp. 12-19.

Osmani, SA, Bak, S, Imberty, A, Olsen, CE & Moller, BL 2008, 'Catalytic key amino acids and UDP-sugar donor specificity of a plant glucuronosyltransferase, UGT94B1: molecular modeling substantiated by site-specific mutagenesis and biochemical analyses', *Plant Physiol*, vol. 148, no. 3, pp. 1295-1308.

Osmani, SA, Bak, S & Moller, BL 2009, 'Substrate specificity of plant UDP-dependent glycosyltransferases predicted from crystal structures and homology modeling', *Phytochemistry*, vol. 70, no. 3, pp. 325-347.

Ouzzine, M, Gulberti, S, Ramalanjaona, N, Magdalou, J & Fournel-Gigleux, S 2014, 'The UDP-glucuronosyltransferases of the blood-brain barrier: their role in drug metabolism and detoxication', *Front Cell Neurosci*, vol. 8, no. pp. 349.

Ouzzine, M, Magdalou, J, Burchell, B & Fournel-Gigleux, S 1999, 'An internal signal sequence mediates the targeting and retention of the human UDP-glucuronosyltransferase 1A6 to the endoplasmic reticulum', *J Biol Chem*, vol. 274, no. 44, pp. 31401-31409.

Owens, DK & McIntosh, CA 2009, 'Identification, recombinant expression, and biochemical characterization of a flavonol 3-O-glucosyltransferase clone from *Citrus paradisi*', *Phytochemistry*, vol. 70, no. 11-12, pp. 1382-1391.

Owens, IS & Ritter, JK 1995, 'Gene structure at the human UGT1 locus creates diversity in isozyme structure, substrate specificity, and regulation', *Prog Nucleic Acid Res Mol Biol*, vol. 51, no. pp. 305-338.

Paibir, SG, Soine, WH, Thomas, DF & Fisher, RA 2004, 'Phenobarbital N-glucosylation by human liver microsomes', *Eur J Drug Metab Pharmacokinet*, vol. 29, no. 1, pp. 51-59.

Palmer, T 1995, *Understanding Enzymes*, Prentice Hall Ellis Horwood, Sydney.

Paquette, S, Moller, BL & Bak, S 2003, 'On the origin of family 1 plant glycosyltransferases', *Phytochemistry*, vol. 62, no. 3, pp. 399-413.

Pardridge, WM 2012, 'Drug transport across the blood-brain barrier', *J Cereb Blood Flow Metab*, vol. 32, no. 11, pp. 1959-1972.

Park, H 2011, 'The Emergence of Mycophenolate Mofetil in Dermatology: From Its Roots in the World of Organ Transplantation to its Versatile Role in the Dermatology Treatment Room', *The Journal of Clinical and Aesthetic Dermatology*, vol. 4, no. 1, pp. 18-27.

Park, WB, Choe, PG, Song, KH, Jeon, JH, Park, SW, Kim, HB, Kim, NJ, Oh, MD & Choe, KW 2010, 'Genetic factors influencing severe atazanavir-associated hyperbilirubinemia in a population with low UDP-glucuronosyltransferase 1A1*28 allele frequency', *Clin Infect Dis*, vol. 51, no. 1, pp. 101-106.

Pasternak, G & Pan, Y-X 2011, 'Mu opioid receptors in pain management', *Acta Anaesthesiologica Taiwanica*, vol. 49, no. 1, pp. 21-25.

Patana, AS, Kurkela, M, Finel, M & Goldman, A 2008, 'Mutation analysis in UGT1A9 suggests a relationship between substrate and catalytic residues in UDP-glucuronosyltransferases', *Protein Eng Des Sel*, vol. 21, no. 9, pp. 537-543.

Patana, AS, Kurkela, M, Goldman, A & Finel, M 2007, 'The human UDP-glucuronosyltransferase: identification of key residues within the nucleotide-sugar binding site', *Mol Pharmacol*, vol. 72, no. 3, pp. 604-611.

Patel, CG, Ogasawara, K & Akhlaghi, F 2013, 'Mycophenolic acid glucuronide is transported by multidrug resistance-associated protein 2 and this transport is not

inhibited by cyclosporine, tacrolimus or sirolimus', *Xenobiotica*, vol. 43, no. 3, pp. 229-235.

Pattanawongsa, A, Chau, N, Rowland, A & Miners, JO 2015, 'Inhibition of Human UDP-Glucuronosyltransferase Enzymes by Canagliflozin and Dapagliflozin: Implications for Drug-Drug Interactions', *Drug Metab Dispos*, vol. 43, no. 10, pp. 1468-1476.

Pattanawongsa, A, Nair, PC, Rowland, A & Miners, JO 2016, 'Human UDP-Glucuronosyltransferase (UGT) 2B10: Validation of Cotinine as a Selective Probe Substrate, Inhibition by UGT Enzyme-Selective Inhibitors and Antidepressant and Antipsychotic Drugs, and Structural Determinants of Enzyme Inhibition', *Drug Metabolism and Disposition*, vol. 44, no. 3, pp. 378-388.

Pedersen, LC, Darden, TA & Negishi, M 2002, 'Crystal structure of beta 1,3-glucuronyltransferase I in complex with active donor substrate UDP-GlcUA', *J Biol Chem*, vol. 277, no. 24, pp. 21869-21873.

Peer, CJ, Sissung, TM, Kim, A, Jain, L, Woo, S, Gardner, ER, Kirkland, CT, Troutman, SM, English, BC, Richardson, ED, Federspiel, J, Venzon, D, Dahut, W, Kohn, E, Kummur, S, Yarchoan, R, Giaccone, G, Widemann, B & Figg, WD 2012, 'Sorafenib is an inhibitor of UGT1A1 but is metabolized by UGT1A9: implications of genetic variants on pharmacokinetics and hyperbilirubinemia', *Clin Cancer Res*, vol. 18, no. 7, pp. 2099-2107.

Picard, N, Cresteil, T, Premaud, A & Marquet, P 2004, 'Characterization of a phase I metabolite of mycophenolic acid produced by CYP3A4/5', *Therapeutic Drug Monitoring*, vol. 26, no. 6, pp. 600-608.

Picard, N, Ratanasavanh, D, Premaud, A, Le Meur, Y & Marquet, P 2005, 'Identification of the UDP-glucuronosyltransferase isoforms involved in mycophenolic acid phase II metabolism', *Drug Metabolism and Disposition*, vol. 33, no. 1, pp. 139-146.

Pis, J, Girault, JP, Grau, V & Lafont, R 1995, 'Analysis of Ecdysteroid Conjugates - Chromatographic Characterization of Sulfates, Phosphates and Glucosides', *European Journal of Entomology*, vol. 92, no. 1, pp. 41-50.

Poeaknapo, C, Schmidt, J, Brandsch, M, Dräger, B & Zenk, MH 2004, 'Endogenous formation of morphine in human cells', *Proceedings of the National Academy of Sciences of the United States of America*, vol. 101, no. 39, pp. 14091-14096.

Powell, MJD 1977, 'Restart procedures for the conjugate gradient method', *Mathematical Programming*, vol. 12, no. 1, pp. 241-254.

Qi, YL, Liao, F, Zhao, CQ, Lin, YD & Zuo, MX 2005, 'Cytotoxicity, apoptosis induction, and mitotic arrest by a novel podophyllotoxin glucoside, 4DPG, in tumor cells', *Acta Pharmacol Sin*, vol. 26, no. 8, pp. 1000-1008.

Qu, X, Swanson, R, Day, R & Tsai, J 2009, 'A guide to template based structure prediction', *Curr Protein Pept Sci*, vol. 10, no. 3, pp. 270-285.

Radomska-Pandya, A, Bratton, S & Little, JM 2005, 'A historical overview of the heterologous expression of mammalian UDP-glucuronosyltransferase isoforms over the past twenty years', *Current Drug Metabolism*, vol. 6, no. 2, pp. 141-160.

Radomska-Pandya, A, Bratton, SM, Redinbo, MR & Miley, MJ 2010, 'The crystal structure of human UDP-glucuronosyltransferase 2B7 C-terminal end is the first mammalian UGT target to be revealed: the significance for human UGTs from both the 1A and 2B families', *Drug Metab Rev*, vol. 42, no. 1, pp. 133-144.

Radomska-Pandya, A, Czernik, PJ, Little, JM, Battaglia, E & Mackenzie, PI 1999, 'Structural and functional studies of UDP-glucuronosyltransferases', *Drug Metab Rev*, vol. 31, no. 4, pp. 817-899.

Radomska-Pandya, A, Little, JM, Pandya, JT, Tephly, TR, King, CD, Barone, GW & Raufman, J-P 1998, 'UDP-glucuronosyltransferases in human intestinal mucosa', *Biochimica et Biophysica Acta (BBA) - Lipids and Lipid Metabolism*, vol. 1394, no. 2, pp. 199-208.

Radomska-Pandya, A, Ouzzine, M, Fournel-Gigleux, S & Magdalou, J 2005, 'Structure of UDP-glucuronosyltransferases in membranes', *Methods Enzymol*, vol. 400, no. pp. 116-147.

Radomska-Pandya, A, Pokrovskaya, ID, Xu, J, Little, JM, Jude, AR, Kurten, RC & Czernik, PJ 2002, 'Nuclear UDP-Glucuronosyltransferases: Identification of UGT2B7 and UGT1A6 in Human Liver Nuclear Membranes', *Archives of Biochemistry and Biophysics*, vol. 399, no. 1, pp. 37-48.

Radomska, A, Little, J, Pyrek, JS, Drake, RR, Igari, Y, Fournel-Gigleux, S, Magdalou, J, Burchell, B, Elbein, AD, Siest, G & et al. 1993, 'A novel UDP-Glc-specific glucosyltransferase catalyzing the biosynthesis of 6-O-glucosides of bile acids in human liver microsomes', *J Biol Chem*, vol. 268, no. 20, pp. 15127-15135.

Raungrut, P, Uchaipichat, V, Elliot, DJ, Janchawee, B, Somogyi, AA & Miners, JO 2010, 'In Vitro-In Vivo Extrapolation Predicts Drug-Drug Interactions Arising from Inhibition of Codeine Glucuronidation by Dextropropoxyphene, Fluconazole, Ketoconazole, and Methadone in Humans', *Journal of Pharmacology and Experimental Therapeutics*, vol. 334, no. 2, pp. 609-618.

Rawlins, MD 1974, 'Variability in Response to Drugs', *British Medical Journal*, vol. 4, no. 5936, pp. 91-94.

Real, MD, Ferre, J & Chapa, FJ 1991, 'UDP-glucosyltransferase activity toward exogenous substrates in *Drosophila melanogaster*', *Anal Biochem*, vol. 194, no. 2, pp. 349-352.

Reddy, CS, Vijayasathy, K, Srinivas, E, Sastry, GM & Sastry, GN 2006, 'Homology modeling of membrane proteins: a critical assessment', *Comput Biol Chem*, vol. 30, no. 2, pp. 120-126.

Riemersma, M, Sandrock, J, Boltje, TJ, Bull, C, Heise, T, Ashikov, A, Adema, GJ, van Bokhoven, H & Lefeber, DJ 2015, 'Disease mutations in CMP-sialic acid

transporter SLC35A1 result in abnormal alpha-dystroglycan O-mannosylation, independent from sialic acid', *Hum Mol Genet*, vol. 24, no. 8, pp. 2241-2246.

Ritter, JK 2007, 'Intestinal UGTs as potential modifiers of pharmacokinetics and biological responses to drugs and xenobiotics', *Expert Opin Drug Metab Toxicol*, vol. 3, no. 1, pp. 93-107.

Ritter, JK, Chen, F, Sheen, YY, Lubet, RA & Owens, IS 1992, 'Two human liver cDNAs encode UDP-glucuronosyltransferases with 2 log differences in activity toward parallel substrates including hyodeoxycholic acid and certain estrogen derivatives', *Biochemistry*, vol. 31, no. 13, pp. 3409-3414.

Roberts, MS, Magnusson, BM, Burczynski, FJ & Weiss, M 2002, 'Enterohepatic circulation: physiological, pharmacokinetic and clinical implications', *Clin Pharmacokinet*, vol. 41, no. 10, pp. 751-790.

Rohrmann, GF 1999, 'Baculoviruses (Baculoviridae) - Nucleopolyhedrovirus', in *Encyclopedia of Virology (Second Edition)*, eds RG Webster, Elsevier, Oxford.

Ross, J, Li, Y, Lim, E & Bowles, DJ 2001, 'Higher plant glycosyltransferases', *Genome Biol*, vol. 2, no. 2, pp. REVIEWS3004.

Rouleau, M, Audet-Delage, Y, Desjardins, S, Rouleau, M, Girard-Bock, C & Guillemette, C 2017, 'Endogenous Protein Interactome of Human UDP-Glucuronosyltransferases Exposed by Untargeted Proteomics', *Front Pharmacol*, vol. 8, no. pp. 23.

Rowland, A, Elliot, DJ, Knights, KM, Mackenzie, PI & Miners, JO 2008a, 'The "albumin effect" and in vitro-in vivo extrapolation: sequestration of long-chain unsaturated fatty acids enhances phenytoin hydroxylation by human liver microsomal and recombinant cytochrome P450 2C9', *Drug Metab Dispos*, vol. 36, no. 5, pp. 870-877.

Rowland, A, Elliot, DJ, Williams, JA, MacKenzie, PI, Dickinson, RG & Miners, JO 2006, 'In vitro characterization of lamotrigine N2-glucuronidation and the lamotrigine-valproic acid interaction', *Drug Metabolism and Disposition*, vol. 34, no. 6, pp. 1055-1062.

Rowland, A, Gaganis, P, Elliot, DJ, Mackenzie, PI, Knights, KM & Miners, JO 2007, 'Binding of inhibitory fatty acids is responsible for the enhancement of UDP-glucuronosyltransferase 2B7 activity by albumin: implications for in vitro-in vivo extrapolation', *J Pharmacol Exp Ther*, vol. 321, no. 1, pp. 137-147.

Rowland, A, Knights, KM, Mackenzie, PI & Miners, JO 2008b, 'The "albumin effect" and drug glucuronidation: bovine serum albumin and fatty acid-free human serum albumin enhance the glucuronidation of UDP-glucuronosyltransferase (UGT) 1A9 substrates but not UGT1A1 and UGT1A6 activities', *Drug Metab Dispos*, vol. 36, no. 6, pp. 1056-1062.

- Rowland, A, Mackenzie, PI & Miners, JO 2015, 'Transporter-mediated uptake of UDP-glucuronic acid by human liver microsomes: assay conditions, kinetics, and inhibition', *Drug Metab Dispos*, vol. 43, no. 1, pp. 147-153.
- Rowland, A, Miners, JO & Mackenzie, PI 2013, 'The UDP-glucuronosyltransferases: their role in drug metabolism and detoxification', *Int J Biochem Cell Biol*, vol. 45, no. 6, pp. 1121-1132.
- Ruppert, J, Welch, W & Jain, AN 1997, 'Automatic identification and representation of protein binding sites for molecular docking', *Protein Sci*, vol. 6, no. 3, pp. 524-533.
- Sahai, J, Gallicano, K, Pakuts, A & Cameron, DW 1994, 'Effect of fluconazole on zidovudine pharmacokinetics in patients infected with human immunodeficiency virus', *J Infect Dis*, vol. 169, no. 5, pp. 1103-1107.
- Sallustio, BC 2008, 'Glucuronidation-Dependent Toxicity and Bioactivation', in *Advances in Molecular Toxicology*, eds JC Fishbein, Elsevier, Hungary.
- Sambrook, J & Russell, DW 2001, *Molecular cloning: A laboratory handbook.*, Cold Spring Harbor Press, New York.
- Saremba, B 2018, Nicotine metabolism in the cabbage looper *Trichoplusia ni* (Hübner), Master's, The University of British Columbia.
- Savage, RE, Tyler, AN, Miao, XS & Chan, TC 2008, 'Identification of a novel glucosylsulfate conjugate as a metabolite of 3,4-dihydro-2,2-dimethyl-2H-naphtho[1,2-b]pyran-5,6-dione (ARQ 501, beta-lapachone) in mammals', *Drug Metab Dispos*, vol. 36, no. 4, pp. 753-758.
- Sawada, S, Suzuki, H, Ichimaida, F, Yamaguchi, MA, Iwashita, T, Fukui, Y, Hemmi, H, Nishino, T & Nakayama, T 2005, 'UDP-glucuronic acid:anthocyanin glucuronosyltransferase from red daisy (*Bellis perennis*) flowers. Enzymology and phylogenetics of a novel glucuronosyltransferase involved in flower pigment biosynthesis', *J Biol Chem*, vol. 280, no. 2, pp. 899-906.
- Sawchuk, RJ & Elmquist, WF 2000, 'Microdialysis in the study of drug transporters in the CNS', *Adv Drug Deliv Rev*, vol. 45, no. 2-3, pp. 295-307.
- Sawyer, MB, Innocenti, F, Das, S, Cheng, C, Ramirez, J, Pantle-Fisher, FH, Wright, C, Badner, J, Pei, D, Boyett, JM, Cook, E, Jr. & Ratain, MJ 2003, 'A pharmacogenetic study of uridine diphosphate-glucuronosyltransferase 2B7 in patients receiving morphine', *Clin Pharmacol Ther*, vol. 73, no. 6, pp. 566-574.
- Schutz, E, Shipkova, M, Armstrong, VW, Wieland, E & Oellerich, M 1999, 'Identification of a pharmacologically active metabolite of mycophenolic acid in plasma of transplant recipients treated with mycophenolate mofetil', *Clin Chem*, vol. 45, no. 3, pp. 419-422.
- Sear, JW, Hand, CW, Moore, RA & McQuay, HJ 1989, 'Studies on morphine disposition: Influence of general anaesthesia on plasma concentrations of morphine and its metabolites', *British Journal of Anaesthesia*, vol. 62, no. 1, pp. 22-27.

Segel, IH 1993, *Enzyme Kinetics: Behavior and Analysis of Rapid Equilibrium and Steady-State Enzyme Systems*, Wiley-Interscience, New York.

Senafi, SB, Clarke, DJ & Burchell, B 1994, 'Investigation of the Substrate-Specificity of a Cloned Expressed Human Bilirubin Udp-Glucuronosyltransferase - Udp-Sugar Specificity and Involvement in Steroid and Xenobiotic Glucuronidation', *Biochemical Journal*, vol. 303, no. pp. 233-240.

Senay, C, Ouzzine, M, Battaglia, E, Pless, D, Cano, V, Burchell, B, Radominska, A, Magdalou, J & Fournel-Gigleux, S 1997, 'Arginine 52 and histidine 54 located in a conserved amino-terminal hydrophobic region (LX2-R52-G-H54-X3-V-L) are important amino acids for the functional and structural integrity of the human liver UDP-glucuronosyltransferase UGT1*6', *Mol Pharmacol*, vol. 51, no. 3, pp. 406-413.

Sesma, JI, Esther, CR, Jr., Kreda, SM, Jones, L, O'Neal, W, Nishihara, S, Nicholas, RA & Lazarowski, ER 2009, 'Endoplasmic reticulum/golgi nucleotide sugar transporters contribute to the cellular release of UDP-sugar signaling molecules', *J Biol Chem*, vol. 284, no. 18, pp. 12572-12583.

Shao, H, He, X, Achnine, L, Blount, JW, Dixon, RA & Wang, X 2005, 'Crystal structures of a multifunctional triterpene/flavonoid glycosyltransferase from *Medicago truncatula*', *Plant Cell*, vol. 17, no. 11, pp. 3141-3154.

Shaw, LM, Figurski, M, Milone, MC, Trofe, J & Bloom, RD 2007, 'Therapeutic Drug Monitoring of Mycophenolic Acid', *Clinical Journal of the American Society of Nephrology*, vol. 2, no. 5, pp. 1062-1072.

Shaw, LM, Korecka, M, Venkataramanan, R, Goldberg, L, Bloom, R & Brayman, KL 2003, 'Mycophenolic acid pharmacodynamics and pharmacokinetics provide a basis for rational monitoring strategies', *Am J Transplant*, vol. 3, no. 5, pp. 534-542.

Shaw, LM & Nowak, I 1995, 'Mycophenolic acid: measurement and relationship to pharmacologic effects', *Therapeutic Drug Monitoring*, vol. 17, no. 6, pp. 685-689.

Sherwin, CM, Fukuda, T, Brunner, HI, Goebel, J & Vinks, AA 2011a, 'The evolution of population pharmacokinetic models to describe the enterohepatic recycling of mycophenolic acid in solid organ transplantation and autoimmune disease', *Clin Pharmacokinet*, vol. 50, no. 1, pp. 1-24.

Sherwin, CM, Sagcal-Gironella, AC, Fukuda, T, Brunner, HI & Vinks, AA 2011b, 'Development of population PK model with enterohepatic circulation for mycophenolic acid in patients with childhood-onset systemic lupus erythematosus', *Br J Clin Pharmacol*, vol. 73, no. 5, pp. 727-740.

Shimizu, T, Okamoto, I, Tamura, K, Satoh, T, Miyazaki, M, Akashi, Y, Ozaki, T, Fukuoka, M & Nakagawa, K 2010, 'Phase I clinical and pharmacokinetic study of the glucose-conjugated cytotoxic agent D-19575 (glufosfamide) in patients with solid tumors', *Cancer Chemother Pharmacol*, vol. 65, no. 2, pp. 243-250.

Shipkova, M, Armstrong, VW, Wieland, E, Niedmann, PD, Schutz, E, Brenner-Weiss, G, Voihsel, M, Braun, F & Oellerich, M 1999a, 'Identification of glucoside and

carboxyl-linked glucuronide conjugates of mycophenolic acid in plasma of transplant recipients treated with mycophenolate mofetil', *Br J Pharmacol*, vol. 126, no. 5, pp. 1075-1082.

Shipkova, M, Schutz, E, Armstrong, VW, Niedmann, PD, Oellerich, M & Wieland, E 2000, 'Determination of the acyl glucuronide metabolite of mycophenolic acid in human plasma by HPLC and Emit', *Clin Chem*, vol. 46, no. 3, pp. 365-372.

Shipkova, M, Schutz, E, Armstrong, VW, Niedmann, PD, Wieland, E & Oellerich, M 1999b, 'Overestimation of mycophenolic acid by EMIT correlates with MPA metabolite', *Transplant Proc*, vol. 31, no. 1-2, pp. 1135-1137.

Shipkova, M, Strassburg, CP, Braun, F, Streit, F, Grone, HJ, Armstrong, VW, Tukey, RH, Oellerich, M & Wieland, E 2001, 'Glucuronide and glucoside conjugation of mycophenolic acid by human liver, kidney and intestinal microsomes', *British Journal of Pharmacology*, vol. 132, no. 5, pp. 1027-1034.

Siegel, DH, Shieh, JTC, Kwon, E-k, Baselga, E, Blei, F, Cordisco, M, Dobyns, WB, Duffy, KJ, Garzon, MC, Gibbs, DL, Grimmer, JF, Hayflick, SJ, Krol, AL, Kwok, P-Y, Lorier, R, Matter, A, McWeeney, S, Metry, D, Mitchell, S, Pope, E, Santoro, JL, Stevenson, DA, Bayrak-Toydemir, P, Wilmot, B, Worthey, EA, Frieden, IJ, Drolet, BA & Broeckel, U 2013, 'Copy Number Variation Analysis in 98 Individuals with PHACE Syndrome', *Journal of Investigative Dermatology*, vol. 133, no. 3, pp. 677-684.

Sintchak, MD, Fleming, MA, Futer, O, Raybuck, SA, Chambers, SP, Caron, PR, Murcko, MA & Wilson, KP 1996, 'Structure and Mechanism of Inosine Monophosphate Dehydrogenase in Complex with the Immunosuppressant Mycophenolic Acid', *Cell*, vol. 85, no. 6, pp. 921-930.

Slovak, JE, Mealey, K & Court, MH 2017, 'Comparative metabolism of mycophenolic acid by glucuronic acid and glucose conjugation in human, dog, and cat liver microsomes', *Journal of Veterinary Pharmacology and Therapeutics*, vol. 40, no. 2, pp. 123-129.

Smith, MT 2000, 'Neuroexcitatory effects of morphine and hydromorphone: evidence implicating the 3-glucuronide metabolites', *Clin Exp Pharmacol Physiol*, vol. 27, no. 7, pp. 524-528.

Sneitz, N, Court, MH, Zhang, X, Laajanen, K, Yee, KK, Dalton, P, Ding, X & Finel, M 2009, 'Human UDP-glucuronosyltransferase UGT2A2: cDNA construction, expression, and functional characterization in comparison with UGT2A1 and UGT2A3', *Pharmacogenet Genomics*, vol. 19, no. 12, pp. 923-934.

Somogyi, AA, Barratt, DT & Collier, JK 2007, 'Pharmacogenetics of opioids', *Clin Pharmacol Ther*, vol. 81, no. 3, pp. 429-444.

Song, Z 2013, 'Roles of the nucleotide sugar transporters (SLC35 family) in health and disease', *Mol Aspects Med*, vol. 34, no. 2-3, pp. 590-600.

Sorich, MJ, Miners, JO, McKinnon, RA & Smith, PA 2004, 'Multiple pharmacophores for the investigation of human UDP-glucuronosyltransferase isoform substrate selectivity', *Mol Pharmacol*, vol. 65, no. 2, pp. 301-308.

Sosicka, P, Maszczak-Seneczko, D, Bazan, B, Shauchuk, Y, Kaczmarek, B & Olczak, M 2017, 'An insight into the orphan nucleotide sugar transporter SLC35A4', *Biochimica et Biophysica Acta (BBA) - Molecular Cell Research*, vol. 1864, no. 5, pp. 825-838.

Spiro, RG 2002, 'Protein glycosylation: nature, distribution, enzymatic formation, and disease implications of glycopeptide bonds', *Glycobiology*, vol. 12, no. 4, pp. 43R-56R.

Staatz, CE & Tett, SE 2007, 'Clinical pharmacokinetics and pharmacodynamics of mycophenolate in solid organ transplant recipients', *Clin Pharmacokinet*, vol. 46, no. 1, pp. 13-58.

Stachulski, AV, Scheinmann, F, Ferguson, JR, Law, JL, Lumbard, KW, Hopkins, P, Patel, N, Clarke, S, Gloyne, A & Joel, SP 2003, 'Structure-activity relationships of some opiate glycosides', *Bioorganic & Medicinal Chemistry Letters*, vol. 13, no. 6, pp. 1207-1214.

Starlard-Davenport, A, Xiong, Y, Bratton, S, Gallus-Zawada, A, Finel, M & Radomska-Pandya, A 2007, 'Phenylalanine⁹⁰ and phenylalanine⁹³ are crucial amino acids within the estrogen binding site of the human UDP-glucuronosyltransferase 1A10', *Steroids*, vol. 72, no. 1, pp. 85-94.

Stefano, GB, Goumon, Y, Casares, F, Cadet, P, Fricchione, GL, Rialas, C, Peter, D, Sonetti, D, Guarna, M, Welters, ID & Bianchi, E 2000, 'Endogenous morphine', *Trends in Neurosciences*, vol. 23, no. 9, pp. 436-442.

Sten, T, Bichlmaier, I, Kuuranne, T, Leinonen, A, Yli-Kauhaluoma, J & Finel, M 2009, 'UDP-glucuronosyltransferases (UGTs) 2B7 and UGT2B17 display converse specificity in testosterone and epitestosterone glucuronidation, whereas UGT2A1 conjugates both androgens similarly', *Drug Metab Dispos*, vol. 37, no. 2, pp. 417-423.

Stingl, JC, Bartels, H, Viviani, R, Lehmann, ML & Brockmöller, J 2014, 'Relevance of UDP-glucuronosyltransferase polymorphisms for drug dosing: A quantitative systematic review', *Pharmacology & Therapeutics*, vol. 141, no. 1, pp. 92-116.

Stone, AN, Mackenzie, PI, Galetin, A, Houston, JB & Miners, JO 2003, 'Isoform selectivity and kinetics of morphine 3-and 6-glucuronidation by human UDP-glucuronosyltransferases: Evidence for atypical glucuronidation kinetics by UGT2B7', *Drug Metabolism and Disposition*, vol. 31, no. 9, pp. 1086-1089.

Suda, T, Kamiyama, S, Suzuki, M, Kikuchi, N, Nakayama, K, Narimatsu, H, Jigami, Y, Aoki, T & Nishihara, S 2004, 'Molecular cloning and characterization of a human multisubstrate specific nucleotide-sugar transporter homologous to *Drosophila* fringe connection', *J Biol Chem*, vol. 279, no. 25, pp. 26469-26474.

- Takaoka, Y, Ohta, M, Takeuchi, A, Miura, K, Matsuo, M, Sakaeda, T, Sugano, A & Nishio, H 2010, 'Ligand orientation governs conjugation capacity of UDP-glucuronosyltransferase 1A1', *J Biochem*, vol. 148, no. 1, pp. 25-28.
- Takeda, S, Kitajima, Y, Ishii, Y, Nishimura, Y, Mackenzie, PI, Oguri, K & Yamada, H 2006, 'Inhibition of UDP-glucuronosyltransferase 2b7-catalyzed morphine glucuronidation by ketoconazole: dual mechanisms involving a novel noncompetitive mode', *Drug Metab Dispos*, vol. 34, no. 8, pp. 1277-1282.
- Tang, BK 1990, 'Drug glucosidation', *Pharmacol Ther*, vol. 46, no. 1, pp. 53-56.
- Tang, BK, Inaba, T & Kalow, W 1975, 'N-Hydroxyamobarbital: The second major metabolite of amobarbital in man', *Drug Metabolism and Disposition*, vol. 3, no. 6, pp. 479-486.
- Tang, BK, Kalow, W & Grey, AA 1978, 'Amobarbital metabolism in man: N-glucoside formation', *Res Commun Chem Pathol Pharmacol*, vol. 21, no. 1, pp. 45-53.
- Tang, BK, Kalow, W & Grey, AA 1979, 'Metabolic fate of phenobarbital in man. N-Glucoside formation', *Drug Metab Dispos*, vol. 7, no. 5, pp. 315-318.
- Tang, CY, Hochman, JH, Ma, B, Subramanian, R & Vyas, KP 2003, 'Acyl glucuronidation and glucosidation of a new and selective endothelin ETA receptor antagonist in human liver microsomes', *Drug Metabolism and Disposition*, vol. 31, no. 1, pp. 37-45.
- Tang, CY & Ma, B 2005, 'Glycosidation of an endothelin ETA receptor antagonist and diclofenac in human liver microsomes: Aglycone-dependent UDP-sugar selectivity', *Drug Metabolism and Disposition*, vol. 33, no. 12, pp. 1796-1802.
- Thomas, PD & Kejariwal, A 2004, 'Coding single-nucleotide polymorphisms associated with complex vs. Mendelian disease: evolutionary evidence for differences in molecular effects', *Proc Natl Acad Sci U S A*, vol. 101, no. 43, pp. 15398-15403.
- Thompson, MJ, Feldlaufer, MF, Lozano, R, Rees, HH, Lusby, WR, Svoboda, JA & Wilzer, KR 1987, 'Metabolism of 26-[14C]hydroxyecdysone 26-phosphate in the tobacco hornworm, *Manduca sexta* L., to a new ecdysteroid conjugate: 26-[14C]hydroxyecdysone 22-glucoside', *Archives of Insect Biochemistry and Physiology*, vol. 4, no. 1, pp. 1-15.
- Tjornelund, J, Hansen, SH & Cornett, C 1989, 'New metabolites of the drug 5-aminosalicylic acid. I: N-beta-D-glucopyranosyl-5-aminosalicylic acid', *Xenobiotica*, vol. 19, no. 8, pp. 891-899.
- Toide, K, Terauchi, Y, Fujii, T, Yamazaki, H & Kamataki, T 2004, 'Uridine diphosphate sugar-selective conjugation of an aldose reductase inhibitor (AS-3201) by UDP-glucuronosyltransferase 2B subfamily in human liver microsomes', *Biochemical Pharmacology*, vol. 67, no. 7, pp. 1269-1278.
- Tojicic, J, Benoit-Biancamano, MO, Court, MH, Straka, RJ, Caron, P & Guillemette, C 2009, 'In vitro glucuronidation of fenofibric acid by human UDP-

glucuronosyltransferases and liver microsomes', *Drug Metab Dispos*, vol. 37, no. 11, pp. 2236-2243.

Toyama, K, Uchida, N, Ishizuka, H, Sambe, T & Kobayashi, S 2015, 'Single-dose evaluation of safety, tolerability and pharmacokinetics of newly formulated hydromorphone immediate-release and hydrophilic matrix extended-release tablets in healthy Japanese subjects without co-administration of an opioid antagonist', *J Clin Pharmacol*, vol. 55, no. 9, pp. 975-984.

Tredger, JM & Brown, NW 2006, 'Mycophenolate: better value through monitoring?', *Transplantation*, vol. 81, no. 4, pp. 507-508.

Tripathi, SP, Bhadauriya, A, Patil, A & Sangamwar, AT 2013, 'Substrate selectivity of human intestinal UDP-glucuronosyltransferases (UGTs): in silico and in vitro insights', *Drug Metabolism Reviews*, vol. 45, no. 2, pp. 231-252.

Tripos™ 2010a, *BioPolymer™ Manual SYBYL-X 1.1*, Tripos, L.P., St. Louis, MO.

Tripos™ 2010b, *Chapter 2: Force Fields within SYBYL Force Field Manual SYBYL-X 1.1*, Tripos, L.P., St. Louis, MO.

Tripos™ 2010c, *Chapter 3.2: The Surflex-Dock Method Docking Suite Manual SYBYL-X 1.1*, Tripos, L.P., St. Louis, MO.

Tripos™ 2010d, *Chapter 5.2: Minimization Methods Force Field Manual SYBYL-X 1.1*, Tripos, L.P., St. Louis, MO.

Troberg, J, Jarvinen, E, Ge, GB, Yang, L & Finel, M 2017, 'UGT1A10 Is a High Activity and Important Extrahepatic Enzyme: Why Has Its Role in Intestinal Glucuronidation Been Frequently Underestimated?', *Mol Pharm*, vol. 14, no. 9, pp. 2875-2883.

Tsoutsikos, P, Miners, JO, Stapleton, A, Thomas, A, Sallustio, BC & Knights, KM 2004, 'Evidence that unsaturated fatty acids are potent inhibitors of renal UDP-glucuronosyltransferases (UGT): kinetic studies using human kidney cortical microsomes and recombinant UGT1A9 and UGT2B7', *Biochem Pharmacol*, vol. 67, no. 1, pp. 191-199.

Tukey, RH & Strassburg, CP 2000, 'Human UDP-glucuronosyltransferases: metabolism, expression, and disease', *Annu Rev Pharmacol Toxicol*, vol. 40, no. pp. 581-616.

Turgeon, D, Carrier, J-Sb, Lévesque, Er, Hum, DW & Bélanger, A 2001, 'Relative Enzymatic Activity, Protein Stability, and Tissue Distribution of Human Steroid-Metabolizing UGT2B Subfamily Members**This work was supported by the Medical Research Council of Canada, the Fonds de la Recherche en Santé du Québec, and Endorecherche', *Endocrinology*, vol. 142, no. 2, pp. 778-787.

Turgeon, D, Chouinard, S, Belanger, P, Picard, S, Labbe, JF, Borgeat, P & Belanger, A 2003, 'Glucuronidation of arachidonic and linoleic acid metabolites by human UDP-glucuronosyltransferases', *J Lipid Res*, vol. 44, no. 6, pp. 1182-1191.

Turner, RM, Park, BK & Pirmohamed, M 2015, 'Parsing interindividual drug variability: an emerging role for systems pharmacology', *Wiley Interdisciplinary Reviews. Systems Biology and Medicine*, vol. 7, no. 4, pp. 221-241.

Uchaipichat, V, Galetin, A, Houston, JB, Mackenzie, PI, Williams, JA & Miners, JO 2008, 'Kinetic modeling of the interactions between 4-methylumbelliferone, 1-naphthol, and zidovudine glucuronidation by udp-glucuronosyltransferase 2B7 (UGT2B7) provides evidence for multiple substrate binding and effector sites', *Mol Pharmacol*, vol. 74, no. 4, pp. 1152-1162.

Uchaipichat, V, Mackenzie, PI, Elliot, DJ & Miners, JO 2006a, 'Selectivity of substrate (trifluoperazine) and inhibitor (amitriptyline, androsterone, canrenoic acid, hecogenin, phenylbutazone, quinidine, quinine, and sulfinpyrazone) "probes" for human udp-glucuronosyltransferases', *Drug Metab Dispos*, vol. 34, no. 3, pp. 449-456.

Uchaipichat, V, Mackenzie, PI, Guo, XH, Gardner-Stephen, D, Galetin, A, Houston, JB & Miners, JO 2004, 'Human UDP-glucuronosyltransferases: Isoform selectivity and kinetics of 4-methylumbelliferone and 1-naphthol glucuronidation, effects of organic solvents, and inhibition by diclofenac and probenecid', *Drug Metabolism and Disposition*, vol. 32, no. 4, pp. 413-423.

Uchaipichat, V, Raungrut, P, Chau, N, Janchawee, B, Evans, AM & Miners, JO 2011, 'Effects of Ketamine on Human UDP-Glucuronosyltransferases In Vitro Predict Potential Drug-Drug Interactions Arising from Ketamine Inhibition of Codeine and Morphine Glucuronidation', *Drug Metabolism and Disposition*, vol. 39, no. 8, pp. 1324-1328.

Uchaipichat, V, Winner, LK, Mackenzie, PI, Elliot, DJ, Williams, JA & Miners, JO 2006b, 'Quantitative prediction of in vivo inhibitory interactions involving glucuronidated drugs from in vitro data: the effect of fluconazole on zidovudine glucuronidation', *British Journal of Clinical Pharmacology*, vol. 61, no. 4, pp. 427-439.

Unger, T & Peleg, Y 2012, 'Recombinant protein expression in the baculovirus-infected insect cell system', *Methods Mol Biol*, vol. 800, no. pp. 187-199.

van Gelder, T, Berden, JH & Berger, SP 2015, 'To TDM or not to TDM in lupus nephritis patients treated with MMF?', *Nephrol Dial Transplant*, vol. 30, no. 4, pp. 560-564.

van Schaik, RHN, van Agteren, M, de Fijter, JW, Hartmann, A, Schmidt, J, Budde, K, Kuypers, D, Le Meur, Y, van der Werf, M, Mamelok, R & van Gelder, T 2009, 'UGT1A9 -275T>A/-2152C>T Polymorphisms Correlate With Low MPA Exposure and Acute Rejection in MMF/Tacrolimus-Treated Kidney Transplant Patients', *Clinical Pharmacology & Therapeutics*, vol. 86, no. 3, pp. 319-327.

Vietri, M, Pietrabissa, A, Mosca, F & Pacifici, GM 2002, 'Inhibition of mycophenolic acid glucuronidation by niflumic acid in human liver microsomes', *Eur J Clin Pharmacol*, vol. 58, no. 2, pp. 93-97.

Walsky, RL, Bauman, JN, Bourcier, K, Giddens, G, Lapham, K, Negahban, A, Ryder, TF, Obach, RS, Hyland, R & Goosen, TC 2012, 'Optimized assays for human UDP-glucuronosyltransferase (UGT) activities: altered alamethicin concentration and utility to screen for UGT inhibitors', *Drug Metab Dispos*, vol. 40, no. 5, pp. 1051-1065.

Walters, WP, Green, J, Weiss, JR & Murcko, MA 2011, 'What do medicinal chemists actually make? A 50-year retrospective', *J Med Chem*, vol. 54, no. 19, pp. 6405-6416.

Wang, H, Yuan, L & Zeng, S 2011, 'Characterizing the effect of UDP-glucuronosyltransferase (UGT) 2B7 and UGT1A9 genetic polymorphisms on enantioselective glucuronidation of flurbiprofen', *Biochem Pharmacol*, vol. 82, no. 11, pp. 1757-1763.

Wang, S, Liu, Y, Zhou, JJ, Yi, JK, Pan, Y, Wang, J, Zhang, XX, Wang, JX, Yang, S & Xi, JH 2018, 'Identification and tissue expression profiling of candidate UDP-glycosyltransferase genes expressed in *Holotrichia parallela motschulsky* antennae', *Bulletin of Entomological Research*, vol., no. pp. 1-10.

Wang, T, Gu, J, Wu, P-F, Wang, F, Xiong, Z, Yang, Y-J, Wu, W-N, Dong, L-D & Chen, J-G 2009, 'Protection by tetrahydroxystilbene glucoside against cerebral ischemia: involvement of JNK, SIRT1, and NF- κ B pathways and inhibition of intracellular ROS/RNS generation', *Free Radical Biology and Medicine*, vol. 47, no. 3, pp. 229-240.

Wang, X 2009, 'Structure, mechanism and engineering of plant natural product glycosyltransferases', *FEBS Lett*, vol. 583, no. 20, pp. 3303-3309.

Warren, JT, Steiner, B, Dorn, A, Pak, M & Gilbert, LI 1986, 'Metabolism of Ecdysteroids During the Embryogenesis of *Manduca Sexta*', *Journal of Liquid Chromatography*, vol. 9, no. 8, pp. 1759-1782.

Watanabe, Y, Nakajima, M, Ohashi, N, Kume, T & Yokoi, T 2003, 'Glucuronidation of Etoposide in Human Liver Microsomes Is Specifically Catalyzed by UDP-Glucuronosyltransferase 1A1', *Drug Metabolism and Disposition*, vol. 31, no. 5, pp. 589-595.

Welch, W, Ruppert, J & Jain, AN 1996, 'Hammerhead: fast, fully automated docking of flexible ligands to protein binding sites', *Chem Biol*, vol. 3, no. 6, pp. 449-462.

Westley, IS, Brogan, LR, Morris, RG, Evans, AM & Sallustio, BC 2006, 'Role of Mrp2 in the hepatic disposition of mycophenolic acid and its glucuronide metabolites: effect of cyclosporine', *Drug Metab Dispos*, vol. 34, no. 2, pp. 261-266.

Wex, B, Safi, RM, Antonios, G, Zgheib, PZ, Awad, DB, Kobeissy, FH, Mahfouz, RA, El-Sabban, MM & Yazbek, SN 2018, 'SLC35B4, an Inhibitor of Gluconeogenesis, Responds to Glucose Stimulation and Downregulates Hsp60 among Other Proteins in HepG2 Liver Cell Lines', *Molecules*, vol. 23, no. 6, pp.

Weyrich, LS, Duchene, S, Soubrier, J, Arriola, L, Llamas, B, Breen, J, Morris, AG, Alt, KW, Caramelli, D, Dresely, V, Farrell, M, Farrer, AG, Francken, M, Gully, N, Haak, W, Hardy, K, Harvati, K, Held, P, Holmes, EC, Kaidonis, J, Lalueza-Fox, C, de

la Rasilla, M, Rosas, A, Semal, P, Soltysiak, A, Townsend, G, Usai, D, Wahl, J, Huson, DH, Dobney, K & Cooper, A 2017, 'Neanderthal behaviour, diet, and disease inferred from ancient DNA in dental calculus', *Nature*, vol. 544, no. pp. 357.

Wietholtz, H, Marschall, HU, Reuschenbach, R, Matern, H & Matern, S 1991, 'Urinary excretion of bile acid glucosides and glucuronides in extrahepatic cholestasis', *Hepatology*, vol. 13, no. 4, pp. 656-662.

Wilkinson, GR 2005, 'Drug Metabolism and Variability among Patients in Drug Response', *New England Journal of Medicine*, vol. 352, no. 21, pp. 2211-2221.

Williams, JA, Hyland, R, Jones, BC, Smith, DA, Hurst, S, Goosen, TC, Peterkin, V, Koup, JR & Ball, SE 2004, 'Drug-drug interactions for UDP-Glucuronosyltransferase substrates: A pharmacokinetic explanation for typically observed low exposure (AUC_i/AUC) ratios', *Drug Metabolism and Disposition*, vol. 32, no. 11, pp. 1201-1208.

Wilson, JF, Weale, ME, Smith, AC, Gratrix, F, Fletcher, B, Thomas, MG, Bradman, N & Goldstein, DB 2001, 'Population genetic structure of variable drug response', *Nature Genetics*, vol. 29, no. pp. 265.

Xiong, Y, Bernardi, D, Bratton, S, Ward, MD, Battaglia, E, Finel, M, Drake, RR & Radomska-Pandya, A 2006, 'Phenylalanine 90 and 93 Are Localized within the Phenol Binding Site of Human UDP-Glucuronosyltransferase 1A10 as Determined by Photoaffinity Labeling, Mass Spectrometry, and Site-Directed Mutagenesis', *Biochemistry*, vol. 45, no. 7, pp. 2322-2332.

Xiong, Y, Patana, AS, Miley, MJ, Zielinska, AK, Bratton, SM, Miller, GP, Goldman, A, Finel, M, Redinbo, MR & Radomska-Pandya, A 2008, 'The first aspartic acid of the DQxD motif for human UDP-glucuronosyltransferase 1A10 interacts with UDP-glucuronic acid during catalysis', *Drug Metab Dispos*, vol. 36, no. 3, pp. 517-522.

Yang, F, Machalz, D, Wang, S, Li, Z, Wolber, G & Bureik, M 2018, 'A common polymorphic variant of UGT1A5 displays increased activity due to optimized cofactor binding', *FEBS Lett*, vol., no. pp.

You, M, Yue, Z, He, W, Yang, X, Yang, G, Xie, M, Zhan, D, Baxter, SW, Vasseur, L, Gurr, GM, Douglas, CJ, Bai, J, Wang, P, Cui, K, Huang, S, Li, X, Zhou, Q, Wu, Z, Chen, Q, Liu, C, Wang, B, Li, X, Xu, X, Lu, C, Hu, M, Davey, JW, Smith, SM, Chen, M, Xia, X, Tang, W, Ke, F, Zheng, D, Hu, Y, Song, F, You, Y, Ma, X, Peng, L, Zheng, Y, Liang, Y, Chen, Y, Yu, L, Zhang, Y, Liu, Y, Li, G, Fang, L, Li, J, Zhou, X, Luo, Y, Gou, C, Wang, J, Wang, J, Yang, H & Wang, J 2013, 'A heterozygous moth genome provides insights into herbivory and detoxification', *Nature Genetics*, vol. 45, no. pp. 220.

Yu, Q, Jiang, L-L, Luo, N, Fan, Y-X, Ma, J, Li, P & Li, H-J 2017, 'Enhanced absorption and inhibited metabolism of emodin by 2, 3, 5, 4'-tetrahydroxystilbene-2-O-β-D-glucopyranoside: Possible mechanisms for *Polygoni Multiflori Radix*-induced liver injury', *Chinese Journal of Natural Medicines*, vol. 15, no. 6, pp. 451-457.

Yuan, L-M, Gao, Z-Z, Sun, H-Y, Qian, S-N, Xiao, Y-S, Sun, L-L & Zeng, S 2016, 'Inter-isoform Hetero-dimerization of Human UDP-Glucuronosyltransferases (UGTs) 1A1, 1A9, and 2B7 and Impacts on Glucuronidation Activity', *Sci Rep*, vol. 6, no. pp. 34450-34450.

Yuan, L, Qian, S, Xiao, Y, Sun, H & Zeng, S 2015, 'Homo- and hetero-dimerization of human UDP-glucuronosyltransferase 2B7 (UGT2B7) wild type and its allelic variants affect zidovudine glucuronidation activity', *Biochemical Pharmacology*, vol. 95, no. 1, pp. 58-70.

Zamek-Gliszczyński, MJ, Taub, ME, Chothe, PP, Chu, X, Giacomini, KM, Kim, RB, Ray, AS, Stocker, SL, Unadkat, JD, Wittwer, MB, Xia, C, Yee, SW, Zhang, L, Zhang, Y & International Transporter, C 2018, 'Transporters in Drug Development: 2018 ITC Recommendations for Transporters of Emerging Clinical Importance', *Clin Pharmacol Ther*, vol. 104, no. 5, pp. 890-899.

Zhang, HB, Patana, AS, Mackenzie, PI, Ikushiro, S, Goldman, A & Finel, M 2012a, 'Human UDP-Glucuronosyltransferase Expression in Insect Cells: Ratio of Active to Inactive Recombinant Proteins and the Effects of a C-Terminal His-Tag on Glucuronidation Kinetics', *Drug Metabolism and Disposition*, vol. 40, no. 10, pp. 1935-1944.

Zhang, M, Yu, L-m, Zhao, H, Zhou, X-x, Yang, Q, Song, F, Yan, L, Zhai, M-e, Li, B-y, Zhang, B, Jin, Z-x, Duan, W-x & Wang, S-w 2017, '2,3,5,4'-Tetrahydroxystilbene-2-O- β -D-glucoside protects murine hearts against ischemia/reperfusion injury by activating Notch1/Hes1 signaling and attenuating endoplasmic reticulum stress', *Acta Pharmacologica Sinica*, vol. 38, no. 3, pp. 317-330.

Zhang, QY, Jiang, M, Zhao, CQ, Yu, M, Zhang, H, Ding, YJ & Zhai, YG 2005, 'Apoptosis induced by one new podophyllotoxin glucoside in human carcinoma cells', *Toxicology*, vol. 212, no. 1, pp. 46-53.

Zhang, W, Chen, XF, Huang, YJ, Chen, QQ, Bao, YJ & Zhu, W 2012b, '2,3,4',5-Tetrahydroxystilbene-2-O-beta-D-glucoside inhibits angiotensin II-induced cardiac fibroblast proliferation via suppression of the reactive oxygen species-extracellular signal-regulated kinase 1/2 pathway', *Clin Exp Pharmacol Physiol*, vol. 39, no. 5, pp. 429-437.

Zhang, W, Wang, CH, Li, F & Zhu, WZ 2008, '2,3,4',5-Tetrahydroxystilbene-2-O-beta-D-glucoside suppresses matrix metalloproteinase expression and inflammation in atherosclerotic rats', *Clin Exp Pharmacol Physiol*, vol. 35, no. 3, pp. 310-316.

Zhang, Y, Han, Y-H, Putluru, SP, Matta, MK, Kole, P, Mandlekar, S, Furlong, MT, Liu, T, Iyer, RA, Marathe, P, Yang, Z, Lai, Y & Rodrigues, AD 2016, 'Diclofenac and Its Acyl Glucuronide: Determination of In Vivo Exposure in Human Subjects and Characterization as Human Drug Transporter Substrates In Vitro', *Drug Metabolism and Disposition*, vol. 44, no. 3, pp. 320-328.

Zhang, Z & Tang, W 2018, 'Drug metabolism in drug discovery and development', *Acta pharmaceutica Sinica. B*, vol. 8, no. 5, pp. 721-732.

Zhao, J, Liang, Y, Song, F, Xu, S, Nian, L, Zhou, X & Wang, S 2016, 'TSG attenuates LPC-induced endothelial cells inflammatory damage through notch signaling inhibition', *IUBMB Life*, vol. 68, no. 1, pp. 37-50.

Zhao, J, Xu, S, Song, F, Nian, L, Zhou, X & Wang, S 2014, '2,3,5,4'-tetrahydroxystilbene-2-O-beta-D-glucoside protects human umbilical vein endothelial cells against lysophosphatidylcholine-induced apoptosis by upregulating superoxide dismutase and glutathione peroxidase', *IUBMB Life*, vol. 66, no. 10, pp. 711-722.

Zheng, L, Baumann, U & Reymond, JL 2004, 'An efficient one-step site-directed and site-saturation mutagenesis protocol', *Nucleic Acids Res*, vol. 32, no. 14, pp. e115.

Zhou, J & Miners, JO 2014, 'Enzyme Kinetics of Uridine Diphosphate Glucuronosyltransferases (UGTs)', in *Enzyme Kinetics in Drug Metabolism: Fundamentals and Applications*, eds S Nagar, UA Argikar & DJ Tweedie, Springer, New York.

Zhu, B, Bush, D, Doss, GA, Vincent, S, Franklin, RB & Xu, S 2008, 'Characterization of 1'-hydroxymidazolam glucuronidation in human liver microsomes', *Drug Metab Dispos*, vol. 36, no. 2, pp. 331-338.

Zhu, W, Bilfinger, TV, Baggerman, G, Goumon, Y & Stefano, GB 2001, 'Presence of endogenous morphine and morphine 6 glucuronide in human heart tissue', *Int J Mol Med*, vol. 7, no. 4, pp. 419-422.

Zientek, MA & Youdim, K 2015, 'Reaction phenotyping: advances in the experimental strategies used to characterize the contribution of drug-metabolizing enzymes', *Drug Metab Dispos*, vol. 43, no. 1, pp. 163-181.